

Development of Thermal-Insulating Soilcrete using Laboratory Jet Grouting Setup

by

Babak Nikbakhtan

A thesis submitted in partial fulfillment of the requirements for the degree of

Doctor of Philosophy

in

Mining Engineering

Department of Civil and Environmental Engineering
University of Alberta

© Babak Nikbakhtan, 2015

ABSTRACT

One of the most effective ways to lower the energy used to heat or cool residential and commercial buildings is Underground Thermal Energy Storage (UTES) systems. These systems store thermal energy in underground enclosures (borefield) where it can be used when it is needed. UTES systems significantly improve energy efficiency. This results in decreasing usage of fossil fuels and fewer greenhouse gas emissions into the atmosphere. In most UTES systems, the top portion of the borefield is insulated to prevent heat from escaping. However, most of the time, there is no insulation on the sides and bottom of the borefield area. This can reduce the UTES systems' performance when the surrounding ground does not have desirable thermal properties and underground water flow conditions.

The current research focuses on the Southwood UTES project in Edmonton, Alberta, Canada. A 67-meters core logging was confirmed a coal layer at 30 to 50 meters beneath the borefield. That layer prevents heat from escaping from the borefield underneath. However, there is no insulating element around the perimeter. Hence, a proposal was made to develop new insulating material to create thermal-insulating elements for underground enclosures that will keep the heat inside the enclosure from escaping and will increase the efficiency of the UTES systems.

In order to inject the thermal-insulating material into the soil structure, an appropriate ground modification method is required. During past two decades, jet grouting has been introduced as one of the most effective methods for ground modification. Developments during the past decade have progressed to where jet grouting is now a suitable substitution for common grouting methods in cohesive soils. Therefore, the jet grouting technique was chosen to inject the thermal-insulating grout into the soil and modify its thermal properties.

The understanding of jet grouting process is very limited because of its complex operations. It is difficult to predict or precisely control the quality of the jet grouting product, soilcrete. In most cases, to evaluate the performance of the jet grouting operation on a particular soil type, it is necessary to conduct trial jet grouting in the field. Trial jet grouting takes place at a temporary location that has the same geotechnical properties as the main jobsite. It involves grouting more than one column using different operational parameters. After jet grouting, test columns are dug out for visual inspections and desired tests. In the trial jet grouting method, finding a location that is similar to the jobsite is not always possible. It can be time-consuming and expensive, and not even lead to desired results. Thus, it was proposed to design and manufacture a laboratory jet grouting setup with almost the same performance ability as the field equipment but with a reduced footprint and cost. To verify and validate the success of the proposed design, thermal-insulating grout was developed in the laboratory. Then, based on the theoretical definition of the jet grouting process, soilcrete specimens were hand-mixed and cast in the laboratory. Physical, mechanical, and thermal properties of the specimens were calculated using laboratory tests. The results were verified based on the literature values. After the a suitable thermal-insulating grout mixture was developed and the manufacturing laboratory jet grouting setup was completed, an actual jet grouting test was performed on the reconstructed in-situ soil formation in the jet grouting tank. This test was performed to validate the laboratory results obtained from hand-mixed specimens. Also, the capability of the manufactured jet grouting setup and actual laboratory jet grouting experiment results were verified with well-documented literature about jet grouting projects. The results revealed tremendous improvements in thermal and strength properties of the soilcrete compared to the in-situ soil, as well as a successful performance of the laboratory jet grouting setup.

PREFACE

This thesis is an original work by Babak Nikbakhtan. However, the core logging data and determination of soil thermal properties using the Thermal Constants Analyzer TPS 1500 comes from research that I participated in, and which was led by Dr. Derek Apel at the University of Alberta. The laboratory jet grouting setup described in Chapter four was designed by me, with the assistance of Dr. Apel, engineers at the John Brooks Company Ltd (JBCL), and machine shop technicians at the University of Alberta. All other engineering aspects of manufacturing and selection of parts were contracted by JBCL.

The experimental laboratory tests and data analysis in Chapter five, jet grouting test using laboratory jet grouting setup and data analysis in Chapter six, and concluding analysis in Chapter seven are all my original work, as well as the literature reviews in Chapter two and Chapter three. My colleague, John Lee, a MSc student of Dr. Apel, helped me during preparation of reconstructed soil in the jet grouting tank.

Two papers were published from Chapter three of this thesis as: “Jet grouting: mathematical model to predict soilcrete column diameter – part I”, B. Nikbakhtan, D. Apel, K. Ahangari, *International Journal of Mining and Mineral Engineering*, Vol. 6, No. 1, 2015, 46-56; and “Jet grouting: using artificial neural networks to predict soilcrete column diameter – part II”, B. Nikbakhtan, D. Apel, K. Ahangari, *International Journal of Mining and Mineral Engineering*, Vol. 6, No. 1, 2015, 57-71. These papers came to conclusion about the limitations of current methods in predicting soilcrete properties. To overcome those limitations, a proposal was made to design and manufacture a laboratory jet grouting setup. Other three papers have been submitted to different journals as follows. “Physical modeling of jet grouting in the laboratory,” from Chapter four; “Introduction of thermal-insulating grout mixture for jet grouting application,” from Chapter five; and “Development of thermal-insulating soilcrete using laboratory jet grouting setup,” from Chapter six. In all of the above papers, I was responsible for the data collection and analysis as well as the manuscript composition. Dr. Apel assisted me with the data collection and contributed to manuscript edits. Dr. Ahangari was the supervisory author and was involved with manuscript edits.

This Thesis is dedicated:

To my wonderful family, Hakimeh and Nader
Who have always supported me

To my lovely wife, Niousha
Who have been great a source of motivation

To my brother, Siamak
Who has stood by me all the time

To Niousha's family
For their support and patience

ACKNOWLEDGEMENTS

First, I sincerely give my greatest thanks and express my deepest appreciation to my supervisor, Professor Derek Apel, for his continuous help and valuable friendship through my entire PhD program. His support and encouragement always helped me to overcome difficulties during my research. I would like to extend my gratitude to all of my advisory committee members for their precious time and comments in my Doctoral exam: Dr. Ergun Kuru, Dr. Yashar Pourrahimian, Dr. Hassan Dehghanpour, Dr. Les Sudak, and Dr. Piotr Szmigiel; as well as my previous Doctoral candidacy exam committee members: Dr. Yashar Pourrahimian, Dr. Tayfun Babadaghli, Dr. Jeff Boisvert, and Dr. Lijun Deng. Your comments are much appreciated.

The majority of my research consisted of experimental work that involved the help of many staff at the University of Alberta. My deepest appreciation extends to Christine Hereygers (geotechnical lab technician), Robert Anusic and Lucas Duerksen (Mining lab technicians), and Rizaldy Mariano (concrete lab technician) for their supportive actions during all the experimental laboratory tests. I acknowledge my colleagues: John Lee, for his great contribution during my sample preparations; and Muhammad Mamun and Dr. Wei Victor Liu, for introducing me to the usage of the transient plane source (TPS) device. I am also grateful to the Department of Civil and Environmental Engineering at the University of Alberta, for providing me with research and teaching assistance during my graduate studies. My gratitude also goes to all of my friends in Edmonton for their support.

I would like to thank my parents, Hakimeh and Nader, and my brother, Siamak, for their unconditional support and love through all these years. They have been very strong to let me slip away to pursue my PhD adventure. I also would like to thank my wife's family for their support and patience. Finally, my greatest and grateful words are dedicated to the person who has believed in me and has chosen to spend her life with me, Niousha. Her endless love and patience have been always a great help.

TABLE OF CONTENTS

ABSTRACT	
PREFACE	
ACKNOWLEDGEMENTS	
TABLE OF CONTENTS	
LIST OF TABLES	
LIST OF FIGURES	
LIST OF APPENDICES	
LIST OF EQUATIONS	
LIST OF ABBREVIATIONS	
LIST OF NOMENCLATURE	
Chapter 1 INTRODUCTION	1
1-1. Underground thermal energy storage.....	2
1-2. Statement of the problem I.....	2
1-3. Jet Grouting.....	3
1-4. Statement of the problem II.....	4
1-5. Definition of the problem.....	5
1-6. Objectives of the study.....	6
1-7. Scope and limitations of the work.....	6
1-8. Research methodology	7
1-9. Thesis outline	7
Chapter 2 UNDERGROUND THERMAL ENERGY STORAGE	9
2-1. Introduction	10
2-2. UTES projects in Alberta, Canada	12
2-3. Thermal-insulating concept of BTES.....	14
2-4. Thermal-insulating material	15
2-5. Conclusion.....	16
Chapter 3 JET GROUTING.....	21
3-1. Introduction	22
3-2. Jet grouting.....	23
3-3. Definition of terms	25

3-4.	Jet grouting construction process	27
3-5.	Jet grouting systems	28
3.5.1.	Single fluid system, F1	28
3.5.2.	Double fluid system, F2	28
3.5.3.	Triple fluid system, F3	29
3.5.4.	Recent developments of jet grouting systems.....	30
3.5.4.1.	Super soil stabilization management method.....	30
3.5.4.2.	Sacrificial casing	30
3.5.4.3.	Super jet grouting.....	31
3.5.4.4.	Super-midi jet grouting	31
3.5.4.5.	Cross jetting (X-Jet).....	31
3-6.	Current methods to evaluate jet grouting operations	32
3-7.	Important parameters in jet grouting.....	35
3-8.	Effect of different parameters on soilcrete diameter	36
3.8.1.	Nozzles, rotating and lifting speed.....	36
3.8.2.	Jetting pressure and flow rate	38
3.8.3.	Soil properties	39
3-9.	Jet grouting operation design procedure	39
3.9.1.	Methods to calculate soilcrete diameter.....	41
3.9.1.1.	Specific energy.....	41
3.9.1.2.	Other empirical methods	45
3.9.2.	Methods to calculate soilcrete strength.....	56
3.9.3.	Composition of soilcrete vs its diameter and strength	62
3-10.	Conclusion	68
Chapter 4 LABORATORY JET GROUTING SETUP		111
4-1.	Introduction	112
4-2.	Jet grouting laboratory experiment design	114
4-3.	High pressure pumping plant	116
4-4.	Nozzles.....	123
4-5.	Vertical motion mechanism	126
4-6.	Rotation motion mechanism	127

4-7. Jet grouting mixing tank.....	127
4-8. Control panel.....	128
Chapter 5 DEVELOPMENT OF THERMAL-INSULATING GROUT	171
5-1. Introduction.....	172
5-2. Soil properties' test results and discussions.....	172
5.2.1. Particle-size analysis.....	174
5.2.2. Test for soil constants (Atterberg limits).....	174
5.2.3. Soil classification.....	176
5.2.4. Specific gravity.....	176
5.2.5. Compaction test.....	177
5.2.6. Unconfined compressive strength.....	178
5.2.7. Modulus of elasticity.....	180
5.2.8. Thermal properties.....	180
5-3. Thermal-insulating grout mixtures.....	187
5-4. Soilcrete and grout test results and discussions.....	192
5.4.1. Unit weight of grout and soilcrete mixes.....	192
5.4.2. Expansion and bleeding test of fresh grout mixes.....	192
5.4.3. Marsh funnel viscosity test of fresh grout mixes.....	193
5.4.4. Density, absorption, and voids of hardened soilcrete mixes.....	194
5.4.5. Unconfined compressive strength of cylindrical soilcrete.....	195
5.4.6. Modulus of elasticity of cylindrical soilcrete.....	196
5.4.7. Splitting tensile strength of cylindrical soilcrete mixes.....	197
5.4.8. Moisture content of hardened soilcrete mixes.....	198
5.4.9. Thermal properties of hardened soilcrete mixes.....	198
5.4.9.1. Thermal conductivity.....	199
5.4.9.2. Volumetric heat capacity.....	199
5.4.9.3. Specific heat capacity.....	200
5.4.9.4. Heat diffusivity.....	201
5-5. Conclusions.....	202
Chapter 6 LABORATORY JET GROUTING EXPERIMENT	264
6-1. Introduction.....	265

6-2. Reconstructing the in-situ soil	265
6-3. Reconstructed soil test results and discussion.....	266
6-4. Implementation of the laboratory jet grouting	269
6-5. Soilcrete and grout test results and discussion.....	271
6.5.1. Mechanical properties of thermal-insulating grout.....	271
6.5.2. Mechanical properties of soilcrete	271
6.5.3. Thermal properties of soilcrete	273
6-6. Conclusions	274
Chapter 7 CONCLUSION	296
7-1. Research summary	297
7-2. Conclusions	298
7-3. Contributions.....	299
7-4. Availability of similar equipment around the world	300
7-5. Recommendations for future research.....	300
BIBLIOGRAPHY	304

LIST OF TABLES

Table 2-1 Thermal energy storage projects in European countries	17
Table 2-2 Mixing proportions of experimental shotcrete	17
Table 2-3 Testing results of insulating shotcrete	17
Table 3-1 Operational parameters of jet grouting systems and soilcrete properties	70
Table 3-2 Triple fluid jet grouting equipment	70
Table 3-3 Super jet grouting, Super-Midi jet grouting, and X-jet grouting specifications.....	71
Table 3-4 Sampling and testing methods of soilcrete properties quality control	71
Table 3-5 Effect of jet grouting different parameters on soilcrete diameter and strength	71
Table 3-6 The most well documented jet grouting projects	72
Table 3-7 Soilcrete column diameter in different systems	74
Table 3-8 Jet grouting systems advantages and disadvantages	74
Table 3-9 UCS of soilcrete	74
Table 3-10 Compare between physical and mechanical properties of soil and soilcrete	75
Table 3-11 Effective column diameter and operational parameters double fluid granular soil..	75
Table 3-12 Effective column diameter and operational parameters double fluid cohesive soil...	75
Table 3-13 Effective column diameter and operational parameters triple fluid granular soil	75
Table 3-14 Effective column diameter and operational parameters triple fluid cohesive soil	75
Table 3-15 Effective column diameter and operational parameters for super-jet granular soil ...	76
Table 3-16 Effective column diameter and operational parameters for super-jet cohesive soil...	76
Table 4-1 Jet grouting equipment quotes.....	129
Table 4-2 Water jet applications	129
Table 4-3 Specifications of designed nozzles	130
Table 4-4 Nozzle performance in different pressure	130
Table 5-1 Minimum requirement for mass of test specimen, and balance readability	206
Table 5-2 UCS of specimens with different moisture contents	206
Table 5-3 Modulus of elasticity of specimens with different moisture contents	206
Table 5-4 Thermal properties of the given soil in the experiments using empirical methods....	206
Table 5-5 Results of thermal test on soil core samples.....	207
Table 5-6 Proportions of the aggregates	207
Table 5-7 Final proportions of aggregates in the soilcrete body	208
Table 5-8 Unit weight of grout and soilcrete mixes	208
Table 5-9 Expansion and bleed water of grout mixes.....	208
Table 5-10 Marsh Funnel Viscosity test results.....	208
Table 5-11 Density and voids of hardened soilcrete specimens	208
Table 5-12 UCS test results	209
Table 5-13 Modulus of elasticity of soilcrete in different mixes.....	209
Table 5-14 Splitting tensile strength test results	209
Table 5-15 Moisture content of each mix during time	209
Table 5-16 Thermal properties of aggregates	210

Table 5-17 Thermal properties of soilcrete mixes	210
Table 6-1 Minimum time required for failure in direct shear test	278
Table 6-2 Direct shear test results on reconstructed soil specimens.....	278
Table 6-3 Water pump performance test	278
Table 6-4 Grout pump performance test.....	278
Table 6-5 Vertical motion calibration.....	278
Table 6-6 Rotational motion calibration.....	278
Table 6-7 Jet grouting operational parameters.....	278
Table 6-8 56 day old thermal-insulating grout samples.....	279
Table 6-9 UCS, E, and STS of 56 day hardened soilcrete.....	279
Table 6-10 Direct shear test results on dry soilcrete specimens	279
Table 6-11 Direct shear test results on wet soilcrete specimens.....	279
Table 6-12 Thermal properties of soilcrete specimens in both dry and wet condition.....	279
Table 6-13 Thermal conductivity of insulating shotcrete developed by.....	280
Table 6-14 Variation of important soilcrete properties.....	279
Table 6-15 Improvement percentage of soilcrete properties versus in-situ soil	280
Table 6-16 Recommended safety factor to calculate actual soilcrete properties.....	280

LIST OF FIGURES

Figure 2-1 The schematic of BTES system	18
Figure 2-2 Plan view of the borefield	18
Figure 2-3 A BTES borehole with a single U-tube.....	18
Figure 2-4 Actual condition of BTES in DLSC project	19
Figure 2-5 Net annual thermal energy balance	19
Figure 2-6 Conceptual BTES system with thermal-insulating enclosure.....	20
Figure 3-1 Historical development of jet grouting method	77
Figure 3-2 Jet grouting workability area.....	77
Figure 3-3 Application limits for grouting techniques	77
Figure 3-4 Jet grouting v.s. low pressure conventional grouting.....	78
Figure 3-5 Jet grouting applications	78
Figure 3-6 Jet grouting applications	79
Figure 3-7 Construction sequence of jet grouting.....	79
Figure 3-8 Soilcrete different geometries	79
Figure 3-9 Different soil erodibility characteristics.....	80
Figure 3-10 Single jet grouting system, F1.....	80
Figure 3-11 Double fluid jet grouting system, F2.....	80
Figure 3-12 Triple fluid jet grouting system, F3.....	81
Figure 3-13 Super jet grouting system.....	81
Figure 3-14 Soilcrete columns in clayey soil formed by super jet grouting.....	81
Figure 3-15 Soilcrete columns in sandy soil formed by super jet grouting.....	82
Figure 3-16 Schematic and dimensions of X-Jet grouting system	82
Figure 3-17 X-Jet grouting and type of soilcrete column forming	83
Figure 3-18 Comparison of jet velocity in X-Jet and single nozzle jet	83
Figure 3-19 New hydraulic measuring device	83
Figure 3-20 Scheme of column diameter measurement	84
Figure 3-21 Effect of nozzle shape on jet performance.....	85
Figure 3-22 Relationship between potential core length and straight length.....	86
Figure 3-23 Relationship between core length and narrowing angle	86
Figure 3-24 Relationship between cutting distance and number of passes in sand.....	86
Figure 3-25 Relationship between cutting distance and rotation speed in sand	87
Figure 3-26 Optimal repetition frequency of eroding jet.....	87
Figure 3-27 Lifting methods	87
Figure 3-28 Relationship between column diameter and duration of jet grouting	88
Figure 3-29 Relationship between soilcrete diameter and lifting rate	88
Figure 3-30 Relationship between soilcrete diameter and rotational speed	88
Figure 3-31 Relationship between soilcrete diameter and pressure.....	89
Figure 3-32 Relation between eroding distance and jet pressure	89
Figure 3-33 Relationships of dynamic pressure rates and distance from nozzle.....	89

Figure 3-34 Jet axial pressure of water jet versus cutting distance from nozzle outlet	90
Figure 3-35 Relationship between water pressure and air flow rate with eroding distance	90
Figure 3-36 Relationship between grout pressure and soilcrete diameter	91
Figure 3-37 Column diameter ranges against soil type	91
Figure 3-38 Column diameter ranges in granular soils against SPT blow count.....	91
Figure 3-39 Column diameter ranges in fine-grained soils	92
Figure 3-40 Soilcrete diameter vs N_{spt} in different soil types and jet grouting systems	92
Figure 3-41 A typical jet grouting project procedure	92
Figure 3-42 Applicability of the three main JG systems for cohesive and granular soils	93
Figure 3-43 Soilcrete diameter vs N_{spt} for different jet grouting systems.....	93
Figure 3-44 Compressive strength of soilcrete	93
Figure 3-45 Development of soilcrete strength with time	94
Figure 3-46 UCS of soilcrete based on soil types.....	94
Figure 3-47 Relationship between specific energy per column meter and column diameter	94
Figure 3-48 Correlation between total energy and minimum diameter of soilcrete	95
Figure 3-49 Comparison of energy at the nozzle and at the pump	95
Figure 3-50 Specific jet grouting energy against soilcrete diameter	95
Figure 3-51 Cutting distance vs jet fluid energy.....	96
Figure 3-52 Time versus distance for nine pressure-flow rate combinations.....	96
Figure 3-53 The distances reached for different combinations of pressure and flow rate.....	97
Figure 3-54 Soilcrete diameter relationship with lifting speed for different energy levels	97
Figure 3-55 Plots of diameter versus lift speed for different values of E	98
Figure 3-56 Relationship between jet grout column diameter and withdrawal rate	98
Figure 3-57 Estimation of soilcrete column diameter.....	99
Figure 3-58 Relation between c/w ratio and diameter	99
Figure 3-59 Relation between grout pressure and diameter	100
Figure 3-60 Relation between withdrawal and rotational speed with diameter.....	100
Figure 3-61 Structure of two-layered ANN model	100
Figure 3-62 Strength gain trends.....	101
Figure 3-63 Relationship between UCS and total water-cement ratio	101
Figure 3-64 Soilcrete columns and block samples	102
Figure 3-65 Relation between grout flow and average uniaxial compressive strength	102
Figure 3-66 Relation between grout pressure and average uniaxial compressive strength	102
Figure 3-67 Vertical section of the boreholes.....	103
Figure 3-68 Relation between c/w ratio with UCS.....	103
Figure 3-69 Relation between grout pressure with UCS	103
Figure 3-70 Relation between withdrawal and rotational speed with UCS.....	104
Figure 4-1 Equipment required to perform jet grouting treatment	131
Figure 4-2 Agitator and mixing unit to mix the grout	131
Figure 4-3 Water high pressure pump	131

Figure 4-4 Grout high pressure pump.....	132
Figure 4-5 Air compressors	132
Figure 4-6 Control panel of jet grouting operational parameters	132
Figure 4-7 Water, grout and air swivel jointed to the rod.....	133
Figure 4-8 Triple-duck cross section of triple fluid jet grouting rod	133
Figure 4-9 Triple fluid jet grouting monitor	133
Figure 4-10 Water, air, and grout nozzles in triple fluid monitor.....	134
Figure 4-11 Plan view of laboratory experiment	135
Figure 4-12 Front view of laboratory experiment.....	136
Figure 4-13 Flow variation for different plunger numbers.....	137
Figure 4-14 Water pump and motor.....	138
Figure 4-15 Water jetting plant.....	138
Figure 4-16 Grout pump and motor	139
Figure 4-17 Grout jetting and mixing plant	139
Figure 4-18 Flow meters in grout and water line.....	140
Figure 4-19 Pressure gauges on top of the frame before rotary union.....	140
Figure 4-20 Grout mixing plant	140
Figure 4-21 Optimal nozzle design.....	141
Figure 4-22 Nozzle design for jet grouting.....	141
Figure 4-23 Designed nozzles with bigger orifices	141
Figure 4-24 Nozzle geometry	141
Figure 4-25 PW nozzles with smaller orifice sizes.....	142
Figure 4-26 Uni-Guide assembly and steel cable of vertical motion.....	142
Figure 4-27 Rotational and vertical motion	143
Figure 4-28 Vertical motion motor	143
Figure 4-29 Vertical motion motor position and orientation	144
Figure 4-30 Rotary union assembly	144
Figure 4-31 V-belt mechanism for rotational motion	145
Figure 4-32 Jet grouting mixing tank.....	146
Figure 4-33 Jet grouting mixing tank Cap	147
Figure 4-34 Modeling of casing on the cap of the jet grouting mixing tank	147
Figure 4-35 Control panel box of laboratory jet grouting setup	148
Figure 5-1 Delivered cores samples from GSS Geothermal Ltd	211
Figure 5-2 Extracted soil sample from core barrels.....	211
Figure 5-3 Rock crusher machine	211
Figure 5-4 Maximum particle size of soil after crushing.....	211
Figure 5-5 Rock grinder machine	212
Figure 5-6 Maximum particle size passes sieve No.4 after grinding.....	212
Figure 5-7 Mixing all grinded soil samples together	212
Figure 5-8 Hydrometer test on portion smaller than sieve No. 10.....	212

Figure 5-9 Distribution of Particle-Size Analysis.....	213
Figure 5-10 Atterberg limits	213
Figure 5-11 Liquid limit test.....	214
Figure 5-12 Flow curve for liquid limit determination.....	214
Figure 5-13 Plasticity chart.....	215
Figure 5-14 Flowchart group names for inorganic silty and clayey soils.....	215
Figure 5-15 Specific gravity test.....	216
Figure 5-16 Principles of compaction.....	216
Figure 5-17 Standard Proctor test equipment	216
Figure 5-18 Compacted soil samples.....	217
Figure 5-19 Standard Proctor compaction test results for the soil samples.....	217
Figure 5-20 Pushing Shelby tubes through remolded soil samples	217
Figure 5-21 Shelby tubes inside the remolded soil samples	218
Figure 5-22 Extracting soil samples from Shelby tubes	218
Figure 5-23 Soil sample for UCS test.....	218
Figure 5-24 Unconfined Compression Strength test.....	218
Figure 5-25 Cross-sectional area correction determination.....	219
Figure 5-26 Failure of specimens under UCS tests for 10.82%, 12.5%, and 14.92%.....	219
Figure 5-27 Failure of specimens under UCS test for 17.49%, 20.36%.....	219
Figure 5-28 UCS of soil specimens versus moisture content	220
Figure 5-29 Average stress-strain curves for different moisture contents.....	220
Figure 5-30 Modulus of elasticity of soil specimens with different moisture contents.....	220
Figure 5-31 Heat flow through an element of soil	221
Figure 5-32 Thermal properties and water content for standard soils	221
Figure 5-33 TPS 1500 setup in the laboratory	222
Figure 5-34 Sample preparation.....	222
Figure 5-35 Variation of thermal conductivity with depth	222
Figure 5-36 Variation of specific heat capacity with depth.....	223
Figure 5-37 Variation of heat diffusivity with depth	223
Figure 5-38 Vertical profile of heat conductivity based on laboratory and field thermal tests ..	224
Figure 5-39 Grain size distribution of various cement	225
Figure 5-40 Grain size distribution of ELP.....	225
Figure 5-41 Grinding the top and bottom of the specimens	226
Figure 5-42 Density of fresh grout and soilcrete specimens with different mixtures of ELP	226
Figure 5-43 Density of fresh grout and soilcrete mixes during curing time.....	226
Figure 5-44 Relationship between density of fresh grout and its bleeding in all mixes.....	227
Figure 5-45 Relationship between fresh grout density and Marsh Funnel Viscosity.....	227
Figure 5-46 56-day volume of permeable pore spaces in different soilcrete mixes	227
Figure 5-47 Relationship between volume of permeable pore spaces versus 28-day density....	228
Figure 5-48 UCS test on soilcrete samples	228

Figure 5-49 UCS of soilcrete specimens with different mixtures of ELP material	228
Figure 5-50 UCS of soilcrete specimens during curing times	229
Figure 5-51 UCS reduction with respect to controlling mix 1.....	229
Figure 5-52 UCS improvement percentage with respect to in-situ soil strength.....	230
Figure 5-53 Progression of soilcrete mixes during curing time and in-situ soil strength.....	231
Figure 5-54 28-day UCS of soilcrete mixes versus 28-day density.....	232
Figure 5-55 28-day UCS of soilcrete mixes versus voids.....	232
Figure 5-56 Modulus of elasticity of soilcrete specimens with different mixtures of ELP	233
Figure 5-57 Relationship between 28-day density and 28-day modulus of elasticity	233
Figure 5-58 Relationship between 28-day UCS and E of soilcrete mixes.....	234
Figure 5-59 Relationship between E and UCS of soilcrete mixes in all ages.....	234
Figure 5-60 Relationship between 28-day E and voids of soilcrete mixes.....	235
Figure 5-61 Splitting tensile strength of soilcrete specimens with different mixtures of ELP ...	235
Figure 5-62 Relationship between 28-day STS and 28-day density of soilcrete mixes	236
Figure 5-63 Relationship between 28-day STS and 28-day UCS of soilcrete mixes	236
Figure 5-64 Relationship between STS and UCS of soilcrete mixes in all ages	237
Figure 5-65 Relationship between 28-day STS and 28-day E of soilcrete mixes	237
Figure 5-66 Relationship between 28-day STS and voids of soilcrete mixes	238
Figure 5-67 Moisture content of soilcrete mixes in different curing times	238
Figure 5-68 Relationship between 28-day moisture content and 28-day density	238
Figure 5-69 Relationship between 28-day moisture content and 28-day UCS	239
Figure 5-70 Relationship between 28-day moisture content and 28-day E	239
Figure 5-71 Relationship between 28-day moisture content and 28-day STS	240
Figure 5-72 Relationship between 28-day moisture content and voids	240
Figure 5-73 Soilcrete samples for thermal properties test	240
Figure 5-74 Thermal conductivity of soilcrete mixes with increasing ELP material	241
Figure 5-75 Thermal conductivity reduction with respect to controlling mix 1 and soil	241
Figure 5-76 Relationship between thermal conductivity and moisture content of soilcrete.....	242
Figure 5-77 Thermal conductivity reduction from wet to oven-dried condition.....	242
Figure 5-78 Relationship between thermal conductivity and 28-day density of soilcrete.....	243
Figure 5-79 Relationship between thermal conductivity and voids of soilcrete.....	243
Figure 5-80 Volumetric heat capacity of soilcrete mixes with increasing ELP material	244
Figure 5-81 Improvement percentage of volumetric heat capacity of soilcrete mixes.....	244
Figure 5-82 Relationship between volumetric heat capacity and moisture content of soilcrete	245
Figure 5-83 Relationship between volumetric heat capacity and 28-day density of soilcrete....	245
Figure 5-84 Relationship between volumetric heat capacity and voids of soilcrete.....	246
Figure 5-85 Specific heat capacity of soilcrete mixes with increasing ELP.....	246
Figure 5-86 Specific heat capacity improvement percentage in all mixes	246
Figure 5-87 Heat diffusivity of soilcrete mixes with increasing ELP material	247
Figure 5-88 Heat diffusivity improvement percentage in all mixes	247

Figure 5-89 Relationship between heat diffusivity and moisture content of soilcrete mixes	247
Figure 5-90 Relationship between heat diffusivity and 28-day density of soilcrete mixes	248
Figure 5-91 Relationship between heat diffusivity and voids of soilcrete mixes	248
Figure 6-1 In-situ cores used to create reconstructed soil in laboratory	281
Figure 6-2 Excluding coal layers during crushing in-situ core samples	281
Figure 6-3 Crushed in-situ soil	282
Figure 6-4 Conditioning oven dried and crushed soil with its in-situ moisture content.....	282
Figure 6-5 Jet grouting tank wrapped with thick plastic.....	282
Figure 6-6 Compacting soil in different layers in jet grouting tank	283
Figure 6-7 Extracting soil samples from reconstructed and compacted soil	283
Figure 6-8 Reconstructed soil with a center jetting hole in jet grouting tank.....	283
Figure 6-9 Uniaxial compression strength on reconstructed soil specimens.....	284
Figure 6-10 Mohr's failure envelope and Mohr-Coulomb failure envelope	284
Figure 6-11 Schematic drawing of direct shear apparatus.....	285
Figure 6-12 Direct shear test on reconstructed soil specimens.....	285
Figure 6-13 Shear stress versus shear displacement in direct shear test on reconstructed soil ..	286
Figure 6-14 shear stress vs normal stress in direct shear test on reconstructed soil	286
Figure 6-15 Laboratory jet grouting operation	287
Figure 6-16 Soilcrete mixture in laboratory jet grouting tank	287
Figure 6-17 Cores extracted from soilcrete body in jet grouting tank	288
Figure 6-18 UCS of 56 day hardened thermal-insulating grout	288
Figure 6-19 Unconfined compressive strength test on soilcrete cores	289
Figure 6-20 STS test on soilcrete cores	289
Figure 6-21 UCS of soilcrete and grout versus soil.....	289
Figure 6-22 Modulus of elasticity of soilcrete and grout versus soil.....	290
Figure 6-23 Direct shear test on soilcrete cores.....	290
Figure 6-24 Shear stress versus shear displacement in direct shear test on soilcrete dry	291
Figure 6-25 shear stress vs normal stress in direct shear test on soilcrete dry.....	291
Figure 6-26 Shear stress versus shear displacement in direct shear test on soilcrete wet	292
Figure 6-27 shear stress vs normal stress in direct shear test on soilcrete wet	292
Figure 6-28 Shear displacement versus change in height of the soilcrete dry.....	293
Figure 6-29 Cohesion of soil versus soilcrete in wet and dry condition.....	293
Figure 6-30 Friction angle of soil versus soilcrete in wet and dry condition	294
Figure 6-31 Thermal conductivity of soil versus soilcrete in wet and dry condition	294
Figure 6-32 Volumetric heat capacity of soil versus soilcrete in wet and dry condition.....	295
Figure 6-33 Thermal diffusivity of soil versus soilcrete in wet and dry condition.....	295
Figure 7-1 Los Frailes tailing dam failure	303

LIST OF APPENDICES

Appendix 3-1 Jet grouting different applications	105
Appendix 3-2 Jet grouting different applications	106
Appendix 3-3 Application of triple fluid jet grouting in cut-off walls	107
Appendix 3-4 Jet grouting applications	108
Appendix 3-5 Differences between SSS-MAN method and other three jet grouting methods ..	109
Appendix 3-6 Construction steps of SSS-MAN jet grouting method.....	110
Appendix 4-1 Water pump data sheet.....	149
Appendix 4-2 Water pump motor data sheet	151
Appendix 4-3 Pressure relief valve of water pump data sheet.....	152
Appendix 4-4 Water and grout pump motor VFD data sheet.....	153
Appendix 4-5 Grout pump data sheet	155
Appendix 4-6 Grout pump motor data sheet.....	157
Appendix 4-7 Pressure relief valve of grout pump data sheet	158
Appendix 4-8 Grout mixer data sheet.....	159
Appendix 4-9 Flow meter data sheet	160
Appendix 4-10 An example of head loss calculation	162
Appendix 4-11 PW series nozzle data sheet	163
Appendix 4-12 Vertical motion gear motor data sheet.....	165
Appendix 4-13 DC speed controller data sheet	166
Appendix 4-14 Uni-Guide vertical motion data sheet	167
Appendix 4-15 Rotary union data sheet.....	168
Appendix 4-16 Rotational motion gear motor data sheet	169
Appendix 4-17 Electrical configuration of the laboratory jet grouting experiment	170
Appendix 5-1 Vertical profile and core logging data sheet	249
Appendix 5-2 Unit conversion information.....	254
Appendix 5-3 Thermal conductivity of unfrozen silt and clay soils.....	255
Appendix 5-4 Thermal conductivity of frozen silt and clay soils.....	255
Appendix 5-5 Average thermal conductivity of unfrozen silt and clay soils	256
Appendix 5-6 Average thermal conductivity of frozen silt and clay soils	256
Appendix 5-7 Thermal conductivity of unfrozen sandy soils	257
Appendix 5-8 Thermal conductivity of frozen sandy soils.....	257
Appendix 5-9 Average thermal conductivity of unfrozen sandy soils	258
Appendix 5-10 Average thermal conductivity of frozen sandy soils	258
Appendix 5-11 Stress to strain curve of mix 1 soilcrete	259
Appendix 5-12 Stress to strain curve of mix 2 soilcrete	260
Appendix 5-13 Stress to strain curve of mix 3 soilcrete	261
Appendix 5-14 Stress to strain curve of mix 4 soilcrete	262
Appendix 5-15 Stress to strain curve of mix 5 soilcrete	263

LIST OF EQUATIONS

Equation 3-1 41
Equation 3-2 41
Equation 3-3 41
Equation 3-4 42
Equation 3-5 42
Equation 3-6 43
Equation 3-7 43
Equation 3-8 43
Equation 3-9 43
Equation 3-10 44
Equation 3-11 44
Equation 3-12 45
Equation 3-13 45
Equation 3-14 46
Equation 3-15 46
Equation 3-16 47
Equation 3-17 47
Equation 3-18 47
Equation 3-19 48
Equation 3-20 48
Equation 3-21 49
Equation 3-22 49
Equation 3-23 50
Equation 3-24 50
Equation 3-25 51
Equation 3-26 52
Equation 3-27 52
Equation 3-28 52
Equation 3-29 53
Equation 3-30 53
Equation 3-31 53
Equation 3-32 53
Equation 3-33 55
Equation 3-34 55
Equation 3-35 55
Equation 3-36 56
Equation 3-37 56
Equation 3-38 56
Equation 3-39 57

Equation 3-40.....	58
Equation 3-41.....	58
Equation 3-42.....	58
Equation 3-43.....	59
Equation 3-44.....	59
Equation 3-45.....	59
Equation 3-46.....	61
Equation 3-47.....	61
Equation 3-48.....	61
Equation 3-49.....	62
Equation 3-50.....	62
Equation 3-51.....	62
Equation 3-52.....	63
Equation 3-53.....	63
Equation 3-54.....	63
Equation 3-55.....	64
Equation 3-56.....	64
Equation 3-57.....	64
Equation 3-58.....	64
Equation 3-59.....	64
Equation 3-60.....	65
Equation 3-61.....	65
Equation 3-62.....	65
Equation 3-63.....	66
Equation 3-64.....	66
Equation 3-65.....	66
Equation 3-66.....	66
Equation 3-67.....	67
Equation 4-1.....	117
Equation 4-2.....	117
Equation 4-3.....	117
Equation 4-4.....	118
Equation 4-5.....	118
Equation 4-6.....	118
Equation 4-7.....	119
Equation 4-8.....	119
Equation 4-9.....	120
Equation 4-10.....	120
Equation 4-11.....	120
Equation 4-12.....	121

Equation 4-13.....	122
Equation 4-14.....	125
Equation 4-15.....	126
Equation 5-1.....	173
Equation 5-2.....	174
Equation 5-3.....	174
Equation 5-4.....	176
Equation 5-5.....	177
Equation 5-6.....	178
Equation 5-7.....	178
Equation 5-8.....	179
Equation 5-9.....	179
Equation 5-10.....	179
Equation 5-11.....	180
Equation 5-12.....	181
Equation 5-13.....	181
Equation 5-14.....	182
Equation 5-15.....	182
Equation 5-16.....	183
Equation 5-17.....	183
Equation 5-18.....	183
Equation 5-19.....	184
Equation 5-20.....	184
Equation 5-21.....	184
Equation 5-22.....	184
Equation 5-23.....	184
Equation 5-24.....	184
Equation 5-25.....	184
Equation 5-26.....	186
Equation 5-27.....	188
Equation 5-28.....	192
Equation 5-29.....	193
Equation 5-30.....	193
Equation 5-31.....	194
Equation 5-32.....	194
Equation 5-33.....	194
Equation 5-34.....	194
Equation 5-35.....	195
Equation 5-36.....	195
Equation 5-37.....	195

Equation 5-38.....	197
Equation 6-1.....	267
Equation 6-2.....	267
Equation 6-3.....	268
Equation 6-4.....	268
Equation 6-5.....	268
Equation 6-6.....	276
Equation 6-7.....	276

LIST OF ABBREVIATIONS

AASHTO	American Association of State Highway and Transportation Officials
ANN	Artificial Neural Network
ATES	Aquifer Thermal Energy Storage
BTES	Borehole Thermal Energy Storage
CCP	Chemical Churning Pile
CJG	Column Jet Grout
DLSC	Drake Landing Solar Community
ELP	Expanded Lightweight Perlite
GHG	Greenhouse Gas
JBCL	John Brooks Company Limited
JG	Jet Grout
JSG	Jumbo Special Grout
LL	Liquid Limit
MFV	Marsh Funnel Viscosity
MIT	Massachusetts Institute of Technology
NC	Normally Consolidated clay
OC	Over-Consolidated clay
PI	Plastic Index
PL	Plastic Limit
rpm	Round per Minute
SPT	Standard Penetration Test
SSD	Sum of Squared-Deviations
SSS-MAN	Super Soil Stabilization Management Method
STS	Splitting Tensile Strength
UCS	Unconfined Compression Strength
UCSC	Unified Soil Classification System
USBM	U.S. Bureau of Mines
UTES	Underground Thermal Energy Storage
VFD	Variable frequency drive
VSD	Variable speed drive

LIST OF NOMENCLATURE

CHAPTER THREE

In General:

q_u	unconfined compression strength
S_u	undrained shear strength,
v_t	withdrawal rate
D	soilcrete column diameter
E	modulus Elasticity
Esc	specific energy per cubic meter of column
Esl	specific energy per lineal meter of column
N or Nspt	standard penetration test blow count value
Np	number of nozzles
p	mean ejection pressure
P	mean power delivered by fluid exiting the nozzle
Q	rate of fluid ejection
Rs	rotational speed
S	cross sectional area of the column
T	specific injection time
w/c	water to cement ratio
Δt	duration of jetting
Δz	lifting step

In Equation 3-1 to Equation 3-4:

E_{sa}	specific energy of the compressed air
E_{sg}	specific energy of the grout
E_{st}	specific energy of jet grouting system
E_{sw}	specific energy of water
v_t	withdrawal rate
Pa	compressed air pressure
Pg	grout pressure
Pw	water pressure
Qa	compressed air flow rate
Qg	grout flow rate
Qw	water flow rate

In Equation 3-5:

E_p	specific energy of jet grouting system
p	grout pressure
Q	grout flow rate
v	monitor lifting rate

In Equation 3-6 to Equation 3-9:

A_n	cross-sectional area of the nozzle
E_n	jetting energy at the nozzle
v_n	grout velocity at the nozzles
ρ_g	grout density
d	diameter of nozzles
L	unit length of the column
m	grout mass delivered in the time Δt corresponding to treatment length L
M	number of nozzles
n	number of nozzles
Q	grout flow rate
v	monitor lifting rate
Δt	time corresponding to treatment length L

In Equation 3-10:

E_s	jetting energy per unit of column diameter
D	soilcrete diameter

In Equation 3-11:

E_j	jet grouting specific energy
P_w & P_g	water and grout pressures
Q_w & Q_g	water and grout flow rates
V_t	withdrawal rate

In Equation 3-12:

L	distance from nozzle to the measurement point
P	dynamic pressure of water jet
Q	discharge flow rate of water jet
T	jetting time

In Equation 3-13 and Equation 3-14:

D	soilcrete column
E	the volume of cut per minute
L	lift speed

In Equation 3-15:

P_{grout}	discharge pressure
v_n	tangential velocity at a nozzle outlet
FR	flow rate
K	constant related with jetting liquid
N	represent the number of passes
R	column radius

In Equation 3-16:

V_j	injected grout volume per unit length
D	soilcrete diameter
n	initial soil porosity
α	coefficients of percentage of grout retained by the subsoil
β	percentage of soil removed by jet action

In Equation 3-17 to Equation 3-19:

d_0	nozzle diameter
L_m	the radius of influence
R_m	the external radius of the monitor
R_s	the rotational speed
v_0	initial jet velocity
V_n	the nozzle movement velocity
ρ_f	density of injected fluid
K	a coefficient of the ground from field data
N	the number of repetition
P	the jetting pressure
Q	the jetting flow rate
α	empirical coefficients from field data
β	empirical coefficients from field data
γ	empirical coefficients from field data
δ	empirical coefficients from field data

In Equation 3-20 to Equation 3-22:

d_m	diameter of jetting monitor
d_n	nozzle diameter
l_j	maximum jet cutting distance from nozzle
N_c	bearing capacity term corresponding to failure condition at jet tip
P_i	pressure at nozzle inlet
P_s	ambient pressure at nozzle outlet
q_{bu}	ultimate soil bearing resistance
s_u	undrained shear strength
u_0	velocity of ambient medium
V_0	exit velocity of central jet
D	diameter of jetting column

In Equation 3-23 and Equation 3-24:

c' and ϕ'	effective cohesion and friction angle of the soil, respectively
c_u	undrained soil cohesion
D_{grout}	nozzles diameter
v_0	initial speed of the jet threads (immediately after thenozzle)
v_x	mean velocity of the jet at distance x
v_{xmax}	represent the respective maximum velocity
γ_f	unit weight of the injected fluid
σ_z	initial vertical overburden stress
Ω_s and Ω_c	a parameter accounting for energy dissipation of the injected fluid on granular and cohesive soils
g	gravitational acceleration
N	turbulent kinematic viscosity ration of injected uid and water
Λ	a coefficient related with the nozzle shape

In Equation 3-25 to Equation 3-28:

D_h	hydraulic diameter of the backflow cross-section
P_p	pressure loss due to friction in borehole
P_p	pressure loss due to friction in borehole
R_1	column size determined from zero effective stress
R_2	the column size determined from pressure losses in backflow
R_2	the column size determined from pressure losses in backflow
v_0	initial jet velocity at nozzle exit
v_L	critical jet velocity

v_{sp}	backflow velocity of the spoil material
x_c	length of the initial region
ρ_f	density of injected fluid
σ'_h	horizontal effective stress
ΔP_s	pressure loss per unit length of flow due to friction in ground
ΔP_s	pressure loss per unit length of flow due to friction in ground
ΔP	pressure drop due to friction
L	length of the backflow

In Equation 3-29 to Equation 3-31:

A and B	empirical coefficients dependent on the properties of the soil
c	cohesion of the soil
D	Soilcrete diameter
P	the injection pressure
Q	the flow rate
V	the rate of ascent of the monitor

In Equation 3-32:

d_0	rod diameter
D_{grout}	nozzle diameter
p_a	atmospheric pressure
b	a parameter related to the soil characteristics
FR	flow rate of the fluid injected
M	number of nozzle of the rod
R	radius of the soilcrete column
UCS	UCS of soilcrete

In Equation 3-33 to Equation 3-35:

C_g	soil conductivity
D_{10}	diameter corresponding to 10% finer in particle-size distribution curve
D_{60}	diameter corresponding to 60% finer in particle-size distribution curve
D_{90}	diameter corresponding to 90% finer in particle-size distribution curve
G_R	soil groutability ratio
L_g	lifting speed
P_a	air pressure
P_g	grout pressure
P_w	water pressure

R_g	rotating speed
γ_g	grout density
c	cohesion
D	diameter of the soilcrete
k	soil permeability

In Equation 3-36 and Equation 3-37:

c	cohesion
σ_c	Unconfined Compressive Strength
σ_t	Brazilian indirect tensile strength
φ	friction angle

In Equation 3-38:

A_w	Cement content percent by mass
$q_u(t_0)$	Unconfined compressive strength at t_0 days
$q_u(t)$	Unconfined compressive strength at t days
K	480 A_w for granular soils and 70 A_w for fine grain soil
t	Curing time

In Equation 3-39:

τ_0	28-day shear strength obtained by direct shear test with zero normal stress
UCS	28-day unconfined compressive strength

In Equation 3-40 and Equation 3-41:

UCS_0	experimental constant
γ_d	dry unit weight
m and n	experimental constants.
S/C	soil/cement ratio
W/C	water/cement ratio

In Equation 3-42:

A	a coefficient related to the type of clay, liquidity index and age of the mixture
B	an empirical constant which is independent of the type of clay
W_c/C	the soil-water/cement ratio

In Equation 3-43:

m_c	weight of cement in dry state
-------	-------------------------------

m_w weight of water in soilcrete including water in the original soil and grout
 R_m water/cement ratio

In Equation 3-44:

UCS_{14} UCS at 14-days curing time with initial water content as much as soil liquid limit
 UCS_t UCS at age t (days)
 a and b a coefficient for inland clays

In Equation 3-45:

$UCS_{(\frac{W_c}{C})_1,t}$ UCS at $(\frac{W_c}{C})_1$ for the curing period of t days
 $UCS_{(\frac{W_c}{C})_2,28}$ UCS at $(\frac{W_c}{C})_2$ for the reference curing period of 28 days
 W_c water content
 C cement content
 LI liquidity index
 t curing period in days

In Equation 3-46:

D_u degree of mixing uniformity
 N_1 number of collected samples
 N_2 number of samples with an pH value higher than critical value

In Equation 3-47:

f_{cm} 28 days strength of the mixture
 $f_{cm}(t)$ strength at age t
 a a coefficient for concrete and soilcrete
 s a coefficient related with cement type
 t age of the mixture

In Equation 3-48:

E_{cm} 28 days stiffness of the mixture
 $E_{cm}(t)$ stiffness at age t
 a and b coefficients to be adjusted using jet grouting data
 s a coefficient related with cement type
 t age of the mixture

In Equation 3-49:

E_{c0}	was determined for each formulation based on 28 days stiffness
$E_{ci}(t)$	stiffness at age t
f_{cm}	28 days stiffness of the mixture
f_{cm0}	10 MPa
α_E	a coefficient depends on type of aggregate
a, b and c	coefficients to be adjusted
s	a coefficient related with cement type
t	age of the mixture

In Equation 3-50 to Equation 3-52:

γ_{sc}	unit weight of soilcrete
C	total mass of cement in the soilcrete
R	long term strength
S	mass of soil solids
W	total mass of water in the soilcrete

In Equation 3-53 to Equation 3-55:

G_C	absolute specific gravity of cement
G_S	absolute specific gravity of soil particles
γ_b	bulk density
C	cement contained in the volume of the treated soil
R	Unconfined compressive strength of soilcrete at 120-days
S	dry soil contained in the volume of the treated soil
W	total water contained in the volume of the treated soil

In Equation 3-56:

ρ_c	density of cement
ρ_g	density of grout
ρ_w	density of water
W	water/cement ratio

In Equation 3-57 to Equation 3-61:

Q_g	flow rate of grout delivery
V_{cl}	volume of soilcrete column
V_g	volume of grout for forming the column
V_s	volume of soil

V_{sr}	volume of soil subject to removal during formation of the column
w_0	volume moisture content of soil (in completely saturated soil $n=w_0$)
γ_c	density of cement
$A = V_g/V_s$	weight content of cement (C) in a unit volume of soilcrete column
d	drill hole diameter
D	soilcrete diameter
H	length of the column which the grout is delivered
n	undisturbed porosity
v	speed of longitudinal (withdrawal speed or lifting rate)
w/c	water/cement ratio of the grout

In Equation 3-62 to Equation 3-66:

$\left(\frac{c}{w}\right)^e$	cement/water ratio of the ejected cutting
$\left(\frac{w}{c}\right)^{grout}$	water/cement ratio of injected grout
G_c	3.0 specific gravity of cement injected
G_s	specific gravity of the soil
$Q^{ejected}$	flow rate of ejected cuttings
$Q^{injected\ grout}$	flow rate of injected grout
q_u	compressive strength of hardened soilcrete
W_{cement}^c	weight of cement in column
W_{soil}^c	weight of soil in column
W_t^c	total weight of column
W_{water}^c	weight of water in column
γ_t^c	total unit weight of soilcrete column
$\gamma_t^{in-situ}$	total unit weight of soilcrete column
γ_t^o	density of the out flow
γ_w	unit weight of water
ΔZ	height of soilcrete column
D	soilcrete column diameter
L	lifting rate of monitor through height of ΔZ
w	in-situ water content

In Equation 3-67:

n	original soil porosity
V	soilcrete column volume per unit length
V_j	volume of injected grout per length of treatment.

α	volumetric percentage of grout retained by the subsoil
β	volumetric percentage of soil removed by the jet action
δ	percentage of pores filled with grout

CHAPTER FOUR

In Equation 4-1 and Equation 4-2:

p	operation pressure
P	power output from the plunger pump
Q	flow rate

In Equation 4-3:

P_{in}	power input to the pump
η	efficiency of the pump
P	power output from the pump

In Equation 4-4 to Equation 4-8:

D_H	pipe diameter
L_H	pipe length
ρ_w	density of water
Δp	pressure loss in the pipe
f	friction factor
Q	flow rate
Re	Reynolds number
v	flow velocity in the pipe
μ	dynamic viscosity of water

In Equation 4-9 to Equation 4-14:

c_d	an efficiency parameter
P_i	available pressure at the nozzles
P_o	total pressure at nozzle outlet
P_{static}	hydrostatic pressure in borehole
v_o	jet velocity
ρ_{slurry}	slurry density in borehole
ρ_w	mass density of water
g	acceleration due to gravity
h	depth of the nozzle
P	operating pressure ($P_i - P_o$)

B multiplying factor

In Equation 4-15:

F_R reaction force
 \dot{I}_j jet impulse flow
 v_j jet velocity
 ρ_w density of the water
 \dot{m} water mass flow rate
 P operating pressure
 Q flow rate

CHAPTER FIVE

In Equation 5-1:

M_c mass of container
 $M_{c ds}$ mass of container and oven dry specimen
 $M_{c ms}$ mass of container and moist specimen
 M_s mass of oven dry specimen
 M_w mass of water
 w water content

In Equation 5-2 and Equation 5-3:

C_c coefficient of Gradation
 C_u uniformity Coefficient
 D_{10} effective Size
 D_{30} diameter corresponding to 30% finer in particle-size distribution curve
 D_{60} diameter corresponding to 60% finer in particle-size distribution curve

In Equation 5-4:

M_1 mass of pycnometer and water
 M_2 mass of pycnometer and water and soil solids
 M_s mass of oven dried soil solids
 ρ_s density of soil solids
 ρ_w density of water

In Equation 5-5 to Equation 5-7:

G_s specific gravity of soil solids
 $V_{(m)}$ volume of mold

w_{sat}	water content for complete saturation
γ_d	dry unit weight of soil
γ_w	unit weight of water at 20°C
W	weight of the compacted soil in the mold

In Equation 5-8 to Equation 5-10:

A_0	initial cross-sectional area of specimen
q_u	unconfined compression strength
s_u	undrained shear strength
σ_1	major principle stress is
σ_3	confining pressure
A	corrected cross-sectional area of specimen
ϵ	axial strain for a given axial force

In Equation 5-11 to Equation 5-25:

C_s, C_w, C_a	heat capacities per unit volume of soil solids, water, and air, respectively
C_U and C_F	volumetric heat capacity of unfrozen and frozen
T_1	temperature of end face
T_2	initial temperature
x_s, x_w, x_a	solid, water, and air compositions in unit volume of soil, respectively
γ_d	dry unit weight of the soil
γ_w	unit weight of water
ΔT	change in temperature
A	cross-sectional of soil
C	heat capacity per unit volume
c	specific heat capacity
k	heat conductivity
l	length of soil element
m	mass of substance acting as environment
q	heat flow
Q	quantity of heat
w	water content
α	heat diffusivity
ρ	density

In Equation 5-26:

t_{tot}	total measurement time for the transient recording
------------------	--

k	a typical value in hot-disc measurements
α	thermal diffusivity of the specimen material

In Equation 5-27 and Equation 5-28:

M_c	mass of the measure filled with freshly mixed grout or soilcrete
M_m	mass of the measure
V_m	volume of measure
ρ_c	density of cement grains
ρ_g	density of grout
ρ_w	density of water
w	water cement ratio
ρ	fresh unit weight of grout

In Equation 5-29 and Equation 5-30:

V_1	volume of sample at beginning of test
V_2	volume of sample at prescribed intervals, measured at upper surface of water layer
V_g	volume of grout portion of sample at prescribed intervals, at upper surface of grout

In Equation 5-31 to Equation 5-37:

g_1	bulk density, dry
g_2	apparent density
A	mass of oven-dried sample in air
B	mass of surface-dry sample in air after immersion
C	mass of surface-dry sample in air after immersion and boiling
D	apparent mass of sample in water after immersion and boiling
ρ	density of water

In Equation 5-38:

d	diameter of specimen
l	length of specimen
P	maximum applied load
T	splitting tensile strength

CHAPTER SIX

d_f	estimate relative lateral displacement at failure
R_d	displacement rate
t_f	total estimated elapsed time to failure

τ_f	shear stress on the failure plane
$N_{S.v.A}$	improvement percentage of soil particular property relative to the same property of actual soilcrete
$N_{S.v.H}$	improvement percentage of soil particular property relative to the same property of hand-mixed soilcrete
c	cohesion
θ	particular property of soil or soilcrete in both wet and dry condition
σ	normal stress on the failure plane
φ	angle of internal friction
β	field factor of safety for each particular property

Chapter 1 INTRODUCTION

This chapter includes a general overview of the research. First, it explains an overall definition of both Underground Thermal Energy Storage and Jet Grouting systems. Then it discusses the definition of the problem, objectives of the study, scope and limitation of the work, the research methodology, and the thesis outline.

1-1. Underground thermal energy storage

In developed economies, buildings account for 40% of energy consumption and greenhouse gas (GHG) emission. More than half of the building energy (55%) is used for heating and cooling. Increased concerns about global warming have led environmental, political, and business leaders to look for new ways to reduce GHGs such as carbon dioxide. The development of an efficient and renewable energy supply such as a thermal energy storage system can be a solution for the demand to simultaneously reduce GHG emissions. The thermal energy storage system stores the energy, which can be either heat or cold, in the ground to be used at a later time. One of the most common thermal energy storage systems is a seasonal thermal energy storage system which stores a large volume of energy to meet a seasonal load (Gaine and Duffy 2010). Seasonal thermal energy storage systems usually store energy underground and are known as Underground Thermal Energy Storage (UTES). Borehole Thermal Energy Storage (BTES) is a common practice of UTES. It is a closed loop system which includes many vertical boreholes placed 50 to 200 meters below the ground. In this method, the ground itself is the storage medium. Energy is carried out from the energy source into the ground, using single or multiple U-tubes which are inserted into boreholes to deliver/absorb the heat using fluids into/from the ground. The best ground conditions for BTES methods are high thermal conductivity with low groundwater flow (Roth and Brodrick 2009). The performance of BTES systems depend on various operational and geometrical parameters such as operation schedules, injection temperature, injection-production rate, geometrical configuration of the borehole, permeability of the ground, and thermal properties of the ground (K. S. Lee 2008). In the current study, thermal properties of the ground were investigated in order to increase the performance of the BTES systems.

1-2. Statement of the problem I

In most BTES systems, the top portion of the borefield is covered with sand, polystyrene insulation layers, waterproof membrane, and soil to insulate the borefield area and reduce the amount of heat that can escape. However, most of the time, there is no insulation on the sides and bottom of the BTES (Mcclenahan et al. 2006), which can reduce the performance when the surrounding ground does not have desirable heat conductivity properties and underground water flow conditions. Therefore, regardless of the energy source, the entire perimeter, top surface, and

bottom of the BTES must be insulated to reduce the amount of heat that can escape. Using different insulation layers may reduce the amount of energy escaping from BTES.

Some places, such as many areas in Alberta, Canada, can also use underground coal seams to their advantage. For instance, many areas in Edmonton, Alberta, have coal seams located at depths between 10 to 100 meters. Since coal is an excellent insulator, ensuring that the insulating enclosure is at the same depth as the coal layer will ensure that the entire borefield is insulated. GSS Geothermal Ltd., in cooperation with the University of Alberta in Edmonton, has worked on the Southwood 19-acre townhome rental community project in southeast Edmonton, aiming to increase the underground energy reservation and optimize the boreholes design. In the Southwood project, the coal layer is located between 30 to 50 meters beneath the BTES, which can prevent heat from escaping from the bottom. However, there are no insulation layers to insulate the perimeter of the borefield. Hence, the development of new thermal-insulating material and elements was proposed in the current research to create a thermal-insulating enclosure around the BTES borefield, which will keep the heat inside the enclosure from escaping and increase the efficiency of the UTES systems. It is essential to use an appropriate ground modification technique to inject the newly developed thermal-insulating material into the soil structure and create the thermal-insulating elements. Thus, it was proposed that the outside walls of the BTES borefield should be insulated by modifying the soil's thermal-insulating properties using jet grouting technology and thermal-insulating grouts.

1-3. Jet Grouting

The jet grouting method uses high velocity hydraulic energy to erode the soil, which is the first step in the process. After that, excavated soil grains are removed from the borehole and replaced with reinforced material, such as cement and grout, to form a solidified in-situ element known as soilcrete. In this method, the grouting fluid or water is forced through a small nozzle by pumping pressure to create high velocity energy to overcome the soil strength and erode it (Schaefer 1997). Generally, jet grouting can be done with three different systems based on the number of fluids used in process. These systems are known as single fluid, double fluid, and triple fluid. The triple fluid system, which is being used in this study, is the most complicated method and uses three tubes to separately carry water, grout, and air. In the triple fluid system, more soils are excavated and it is possible to fully replace the soil with grout (HBI et al. 1994). The system is

the most effective ground modification method for cohesive soils. It is also more controllable and safer for sensitive structures than the single fluid system (Brill, Burke, and Ringen 2003).

After selecting the jet grouting system, the design of the jet grouting operational parameters is based on the previous experiences. The way in which these parameters and the soil properties influence the soilcrete properties is uncertain (Li and Hu 2010). These uncertainties may increase the overall cost and risk of the project. In many cases, they may limit the use of jet grouting. Many researchers and jet grouting experts have attempted to evaluate the effects of different parameters on soilcrete properties. They have also calculated some structural, physical, and/or mechanical properties of soilcrete. However, these approaches are scarce and have serious limitations. It is common to determine soilcrete properties using field trial jet grouting. Trial jet grouting takes place at a temporary location that has the same geotechnical properties as the main jobsite. It involves grouting more than one (but usually fewer than 10) columns using different operational parameters. The test columns are dug out after curing. Their specific properties, based on the project requirement, are measured. Finally, based on the in-situ trial test results, the actual operational parameters are suggested to reach the desired soilcrete properties in the main jobsite.

1-4. Statement of the problem II

Generally, field trial jet grouting is necessary in order to properly design soilcrete properties (Tinoco 2012; Warner 2004). But this approach is expensive, time-consuming and site-dependent. More importantly, it does not always lead to desirable results. Although many researchers have been studying the design of soilcrete properties, no reliable and accurate measuring system exists that is accepted by all (Brill, Burke, and Ringen 2003). Most researchers have studied soilcrete diameter and very few have reported soilcrete mechanical properties. Also no attempt has been made to study the thermal properties of soilcrete.

Another factor that makes this method more attractive is the shortage of a good ground condition. Given the fast growth of urbanization and industrialization, as well as rapid developments of municipal construction in major Alberta cities such as Edmonton and Calgary, every available patch of ground may in use for construction purposes (S. Y. Liu et al. 2008). This decreases the availability of areas with good ground and soil conditions. Sometimes structures must be built on peaty and weak soils. In such cases, jet grouting can be used to improve the

engineering properties of the soil (J. L. Wang, Wang, and Wang 2009). To date, the jet grouting technique has been used mostly in large-scale projects, but by introducing relatively less expensive equipment with low maintenance costs and high reliability, jet grouting is going to spread into small projects. Its ability in underpinning foundations even near buried utility lines without the need to excavate makes the method ideal for providing ground improvements in municipal areas (Bedenis, Jedele, and Maranowski 2005). However, it is hard to find a particular ground condition that is the same as the main jobsite in municipal areas. Also, the presence of surrounding buildings and underground utilities makes trial jet grouting impossible (Haider and Byle 2000).

1-5. Definition of the problem

The literature review shows that jet grouting has rarely been used to improve the thermal-insulating properties of soils. It was proposed to use expanded lightweight perlite (ELP) to develop thermal-insulating grout, which produces an optimal thermal-insulating soilcrete that can be used in jet grouting. The improvement criteria were developed based on a comparison of the thermal and strength properties of the thermal-insulating soilcrete compared to the in-situ soil. Using the ELP material as grout aggregates may reduce the thermal conductivity as well as the strength of the in-situ soil. It is important not to compromise the in-situ strength properties of the soil by addition the ELP material.

The only and best way to predict the thermal-insulating properties of soilcrete is to perform trial jet grouting in a laboratory, using actual jet grouting parameters and equipment, to simulate the operation on a particular soil. However, the actual field jet grouting equipment is huge and very expensive to use in a laboratory environment. To date, no laboratory setup is available for measuring and designing the parameters of double and triple fluid jet grouting, which are the most complicated and efficient systems. Therefore, it was proposed to design and manufacture a laboratory jet grouting setup with almost the same performance ability as the field equipment but with a reduced footprint and cost. This setup simulates, in a laboratory, the entire process of the jet grouting system. All operational parameters can be taken into account. Also, the groutability of the developed thermal-insulating grout mixture can be observed using a laboratory jet grouting setup. In the current research, a modified triple fluid jet grouting system is built to study the thermal and mechanical properties of the soilcrete in cohesive soil.

1-6. Objectives of the study

Based on the problem definition, the following are the most important objectives of the current study:

- 1) Studying the effect of different parameters and empirical methods to calculate the soilcrete properties based on well-documented literature.
- 2) Designing and manufacturing the laboratory jet grouting setup based on the actual field jet grouting equipment and procedure.
- 3) Developing an optimal grout mixture with optimal soilcrete thermal, physical, and mechanical properties by hand-mixing different grout mixtures and ELP with a particular soil from the Southwood UTES project in Edmonton, Alberta.
- 4) Developing mathematical correlations to predict the properties of the soilcrete based on the results of the hand-mixing soilcrete laboratory experiment.
- 5) Implementing the laboratory jet grouting operation using the optimal grout mixture to validate the laboratory results obtained from hand-mixed soilcrete and study the effect of ELP material on actual soilcrete properties as well as evaluating the performance of the laboratory jet grouting setup on the soil.

1-7. Scope and limitations of the work

The laboratory equipment for the triple fluid jet grouting system was designed and manufactured to simulate, as much as possible, the actual process of jet grouting. In the triple fluid jet grouting system, the main task of shrouded-air around the water jet is to enhance the jetting action to improve the erosion distance, which consequently increases the soilcrete diameter. The presence of air bubbles in the soilcrete structure will have a negative effect on the soilcretes' mechanical properties. Also, mixing the grout with ELP material may reduce the mechanical properties while increasing the air voids throughout the soilcrete. Therefore, it is expected that the reduction in the mechanical properties will be an issue.

On the other hand, there are many constraints regarding the size of the laboratory jet grouting mixing tank. If a large diameter tank is manufactured, more soil is required to fill it. This will increase the weight of the tank. There is no need to build a soilcrete specimen with a large diameter in the laboratory experiment. Moreover, it would be very expensive to manufacture a coaxial water conduit shrouded with air. To make the procedure more practical, simplify the manufacturing process for the equipment and nozzles, and keep expenses as low as possible, compressed air was not used in the laboratory setup.

1-8. Research methodology

To verify and validate the success of the proposed design, thermal-insulating grout was developed in the laboratory using three different aggregates of water, cement, and ELP material. Then, based on the theoretical definition of the jet grouting process, soilcrete specimens were hand-mixed and cast with appropriate proportions of the grout mixture and soil. Physical, mechanical, and thermal properties of the specimens were calculated using laboratory tests. The results were verified based on the literature values and findings. After a suitable thermal-insulating grout mixture was developed and the manufacturing laboratory jet grouting setup completed, an actual jet grouting test was performed on the reconstructed in-situ soil formation in the jet grouting tank. The optimal jet grouting operational parameters were used to create the actual thermal-insulating soilcrete. This test was performed to validate the laboratory results obtained from hand-mixed specimens. Also, the capability of the manufactured jet grouting setup and actual laboratory jet grouting experiment results were verified with well-documented literature about jet grouting projects.

1-9. Thesis outline

This thesis consists of seven chapters. Each is briefly introduced as follows.

Chapter Two: This chapter reviews the UTES technique and discusses two ongoing projects in Alberta. It also explains the thermal-insulating concept of the Southwood UTES project in Edmonton

Chapter Three: This chapter discusses the basics and historical development of the jet grouting method. It also includes a literature review of all important jet grouting operational and soil parameters that affect soilcrete properties. The last part of the chapter presents a design approach of the jet grouting operation as well as some empirical and theoretical methods in order to understand and address the jet grouting process properly and predict the soilcrete properties. It is hoped that this will help the jet grouting specialists to use these methods to initially evaluate their projects.

Chapter Four: This chapter looks at the design procedure of the laboratory jet grouting setup, which simulates the entire jet grouting process. The laboratory jet grouting setup will be used to study the effect of jet grouting on the thermal and mechanical properties of a particular soil condition from the Edmonton area.

Chapter Five: This chapter discusses the development of thermal-insulating grout for a jet grouting operation. Based on theoretical values obtained from literature about the jet grouting technique, five different grout mixtures were developed and hand-mixed with in-situ soil samples obtained from a particular project in Edmonton, Alberta, Canada. Many laboratory geotechnical tests were carried out on hand-mixed soilcrete samples to find an optimal mixture, which resulted in better thermal, physical, and mechanical properties of soilcrete.

Chapter Six: This chapter examines the reconstruction procedure of the in-situ soil in the jet grouting tank. It also discusses implementation steps of the laboratory jet grouting operation after the development of the most suitable thermal-insulating grout mixture and the completion of the manufacturing laboratory jet grouting setup. Also, the capability of the manufactured jet grouting setup and the actual laboratory jet grouting experiment results were verified with well-documented literature about jet grouting projects.

Chapter Seven: This chapter contains the summary of the research and its contributions, as well as concluding statements and recommendations for future research in both jet grouting technique and its thermal-insulating concept.

Chapter 2 UNDERGROUND THERMAL ENERGY STORAGE

This chapter reviews the underground thermal energy storage (UTES) technique and discusses two ongoing projects in Alberta. It also explains the thermal-insulating concept of the Southwood UTES project in Edmonton

2-1. Introduction

Reducing carbon emissions in buildings and lowering required energy costs for heating and air conditioning are a high priority internationally. Developing an efficient and renewable energy supply such as a thermal energy storage system can be a solution for energy demands, as it can simultaneously reduce greenhouse gas (GHG) emissions (Gaine and Duffy 2010). In other words, one of the effective ways to lower the energy used to heat or cool residential and commercial buildings is by using a thermal energy storage system (Lamarche and Beauchamp 2007a). Thermal energy storage systems have been known to provide economic and environmental solutions to energy problems (K. S. Lee 2008). These systems provide significant improvement in energy efficiency, which results in decreasing usage of fossil fuels. Consequently, carbon dioxide emissions to the atmosphere can be reduced considerably (H. Wang and Qi 2008). Although the high initial capital cost of every energy efficient system is a disadvantage, by increasing a building's energy efficiency, the operating costs over the system's lifetime will be lower than costs of a conventional non-energy efficient system (Gaine and Duffy 2010).

A thermal energy storage system stores energy (either heat or cold) in the ground to be used at a later time. The two most common types of thermal energy storage systems are the diurnal system and the annual or seasonal thermal energy system. Diurnal systems store heat during the night so that it can be used during the day. Seasonal thermal energy systems require a large volume of energy to meet the seasonal load (Gaine and Duffy 2010). These energy sources, which can be used by a seasonal thermal energy system, are solar thermal (typically low-temperature collectors), industrial waste heat, excess heat from district energy systems, snow and ice, and seawater (Roth and Brodrick 2009). Seasonal thermal energy systems usually store energy underground and are known as Underground Thermal Energy Storage (UTES). The UTES systems are preferred because there is no need for a floor area; the ground has a constant mean temperature compared with ambient air and is capable of holding the energy relatively constant during the year compared to other methods such as above ground tanks. UTES systems are unobtrusive, which improves their overall performance and reduces operating costs. In recent years, UTES systems have been known as the cleanest, most energy efficient and cost-effective methods for space heating residential and commercial buildings (Lamarche and Beauchamp 2007b). There are two methods of UTES systems: aquifer thermal energy storage (ATES) and

borehole thermal energy storage (BTES). In the ATES method, underground water is used to store the energy and wells are used to pump the water in and out to store or extract the energy. The BTES method, which is the focus of the current study, is a closed loop system which includes many vertical boreholes placed 50 to 200 meters below the ground. In this method, the ground itself is the storage medium. Most of the BTES systems have almost the same components. Figure 2-1 shows an example of major components of a BTES project in the Drake landing solar community (DLSC) in Alberta, Canada. In that particular project, solar panels were used to collect the energy and store it underground. The major components of each BTES system can be divided into energy source (solar in the DLSC project), energy center, borefield, district heating system, and consumers (houses). Energy is carried out from the energy source (solar collection panels) to the energy center. In the energy center, thermal energy is transferred to water in short-term thermal storage tanks. During the summer, the energy of the heated water from the storage tanks is transferred and stored in the borefield. To maximize the horizontal stratification of heat transfer during the storage, heated water flows from the center of the borefield and passes through the borehole to the outside (Figure 2-2) (Mcclenahan et al. 2006). A single or multiple U-tube(s) is inserted into the boreholes to deliver/absorb the heat, using fluids into/from the ground (Figure 2-3). The pipes act as a huge heat exchanger with the ground. After the boreholes are drilled and the pipes inserted, the boreholes are back-filled with high thermal conductivity material, which helps the heat transfer between the pipes and the ground. With this method, by having a large number of boreholes, a significant storage of the thermal energy is possible. This energy can be used for space heating in large communities or commercial buildings. The thermal properties of ground and underground water flow conditions are significant in this method (Gaine and Duffy 2010). The best ground conditions for BTES methods are high thermal conductivity with low underground water flow (Roth and Brodrick 2009). Any BTES needs to be fully charged with thermal energy. After that, the optimum performance will be achieved. Initial heat transferred into the soil is used to increase the ground temperature above its initial temperature ($5 - 10^{\circ}\text{C}$) (W. P. Wong et al.). The initial cost of boreholes in the ground is the most significant obstacle to the growth of this method. However, this cost will become lower as the cost of energy increases and the method will be in more demand in the near future (Lamarche and Beauchamp 2007a). It is important to simulate the BTES system's performance and analyze its life cycle to justify investment, mainly when the

size of the system increases (Sepehri 2011). The performance of BTES systems depends on various operational and geometrical parameters such as operation schedules, injection temperature, injection-production rate, geometrical configuration of the borehole, and the permeability and thermal properties of the ground (K. S. Lee 2008). Thermal properties that should be considered for the feasibility study of BTES systems are the thermal conductivity of the ground, initial undisturbed ground temperature, thermal diffusivity, and specific heat capacity.

2-2. UTES projects in Alberta, Canada

Most populated cities in Canada receive significantly more sun exposure during the year than countries such as Germany, Italy, and Japan, where the use of solar energy is becoming common. Table 2-1 illustrates the number of thermal energy storage projects in European countries. Southern Alberta receives slightly less sun exposure than states such as Arizona, but a very small portion of sun exposure energy is used for space heating in Alberta. Also, due to Canada's geographic location, the major amount of sun exposure is received during the summer. During the winter, when the need for space heating is at its peak, sun exposure is relatively low. The significant difference in Alberta between the space heating demand in the summer and winter suggests that the UTES option is a more reliable method to store energy underground. The following two projects are discussed to show the importance of the UTES systems.

The first large-scale solar BTES system in Canada, which is also the largest of its kind in North America, is located in the town of Okotoks, 15 minutes south of Calgary, Alberta, in the DLSC project. The heat energy of the sun is collected by solar panels during the summer and then stored and reused as energy to space-heat 52 modern detached homes during the following winter. The project uses 144 boreholes that are 35 meters long and 150 millimeters in diameter. The borefield is used to store heat at temperatures of up to 80°C from solar collectors (Gaine and Duffy 2010; W. P. Wong et al.). Figure 2-4 shows the actual condition of the BTES recorded on July 27, 2015. Based on the design, a typical new house uses 126 GJ of natural gas per year (100 GJ for space-heat and 26 GJ for domestic hot water) and emits 6.3 tonnes of GHG. It also uses 8760 kWh of electricity per year. In Alberta, most electricity generation is coal-fired. Hence, generating 8760 kWh of electricity emits 6.8 tonnes of GHG. Therefore, a new house emits almost 13 tonnes per year of GHG. Using solar energy and a BTES system, each DLSC house

should save 110.8 GJ of natural gas and 630 kWh of electricity each year (taking into consideration pumping system energy). The gas and electrical savings for each new house reduce 5.8 tonnes of GHG per year, or 43%. Thus, when all houses are occupied and the BTES is fully charged, the total reduction of GHG for the community should be 300 tonnes per year (McClenahan et al. 2006).

The second project studied in this thesis is the redevelopment of Southwood, which is a 19-acre townhome rental community in southeast Edmonton, designed to provide affordable living for families and seniors. The project was proposed by GSS Geothermal Ltd¹. to use natural gas cogenerates to generate electricity and heat during winter months for the community. The cogeneration devices can be used in residential and commercial buildings to improve electricity generation efficiency and, hence, reduce overall energy costs. When electricity is generated, so is a huge amount of heat. That heat is a valuable byproduct which can be collected and used for space-heating and domestic hot water. During the summer, the amount of generated heat is even more than that of demanded heat. The excess heat can be stored underground with a BTES system and then used in the winter. In other words, the electrical output from a cogeneration power plant to meet a community's electrical demand will result in a seasonal and annual thermal imbalance. BTES can control the imbalance by storing and transferring the excess heat underground (GSS 2012). Figure 2-5 illustrates an example of the net annual thermal energy balance of a building's heat requirements. In the figure, the building's heating requirement is determined synthetically. It is also assumed that a cogeneration device is implemented to provide a constant 10 kWh of thermal energy over the entire year. In the figure at any hour, if the net thermal balance is positive, an excess of heat is generated by the cogeneration device and must be injected underground. If the net thermal balance is negative, there is an insufficient amount of heat available from the cogeneration device and either a BTES heat pump or an auxiliary heater must be used to make up the deficit and keep the building warm (Roppelt 2011). Hence, in this project, the source of BTES energy will be the excess heat generated by cogeneration devices used to produce electricity. The Southwood energy system will produce electricity and heat during the year with low costs. Decreasing the carbon dioxide emission up to 60% in new buildings, reducing the use of primary energy, and increasing the use of renewable energy sources are the direct benefits of the project (Kantrowitz and McFaralane 2012). Reducing

¹ <http://www.groundsourcesolutions.com>

transportation energy, traffic, and accident risk are the indirect benefits (Laloui, Nuth, and Vulliet 2006).

2-3. Thermal-insulating concept of BTES

In most BTES systems, the top portion of the borefield is covered with sand, polystyrene insulation layers, a waterproof membrane, and soil to insulate the borefield area and reduce the amount of heat that escapes. However, most of the time, there is no insulation on the sides and bottom of the BTES (Mcclenahan et al. 2006). This can reduce the BTES performance when the surrounding ground does not have desirable heat conductivity properties and underground water flow conditions¹. Regardless of the energy source, the entire perimeter, top surface, and bottom of the BTES must be insulated to reduce the amount of energy that escapes. When the energy source is the excessive heat of an industrial activity, the matter of heat that escapes is more important. This is because natural gas is being used to produce the excessive heat, even if that excessive heat is a byproduct.

In the DLSC project, there are no insulation layers on the sides and bottom of the BTES. Therefore, of 1950 GJ and 2100 GJ of energy in BTES, only 750 GJ and 1000 GJ can be recovered, respectively. This means that 61% and 53% of the energy is lost from the BTES (W. P. Wong et al.; Mcclenahan et al. 2006). Using different insulation layers may reduce the amount of the escaped energy from BTES. Additionally, some areas in Alberta can use coal seams to their advantage. Many areas in Edmonton have a thin coal seam located at depths between 10 to 100 meters. Since coal is an excellent insulator², creating the insulating enclosure to the depth of the coal layer would also insulate the heat storage system at the bottom of the storage enclosure. In the Southwood project, the coal layer is located 30 to 50 meters beneath the BTES, which can prevent heat from escaping from the bottom. However, there are neither insulation layers nor any concepts to insulate the perimeter of the borefield to decrease the energy escape. More importantly, the source of energy is excessive heat from an industrial activity, and it is critical to prevent that heat from being wasted. The author proposes a concept of creating an insulated enclosure around the BTES area, which will prevent the stored heat from escaping into

¹ It is desirable for the ground to have high heat conductivity in order to charge the BTES borefield with thermal energy. This helps heat to transfer fast from vertical boreholes through the soil. However, high heat conductivity may have a negative effect on the injected heat that escapes from the perimeter of the borefield area.

² Average thermal conductivity, volumetric heat capacity, specific heat capacity, heat diffusivity, and density of coal are 0.2 W/m.K, 1.95 MJ/m³.K, 1300 J/kg.K, 0.1 mm²/sec, and 1500 kg/m³, respectively.

the surrounding environment. It is proposed that the walls of the borefield be insulated by modifying the soil's thermal properties by using jet grouting technology and thermal-insulating grouts (Figure 2-6).

2-4. Thermal-insulating material

Insulation has been considered the most cost-effective technique of energy conservation to prevent carbon dioxide abatement (W. V. Liu 2013). Insulating concrete mixtures were originally developed for use as the insulation layers on the rock surfaces of deep and hot underground mines. Bottomley (1985) stated that fully and partially insulating can reduce the geothermal heat load by 50 to 70% and 25 to 40%, respectively. The United States bureau of mines (USBM) proposed an idea about a new type of shotcrete for the thermal insulation of deep underground mines. The new shotcrete uses expanded lightweight perlite (ELP) in the mixture. It performed well in both the rock support aspect and insulating layer (USBM 1994). The research was abandoned due to the sudden closure of the USBM in 1995. W. V. Liu (2013) conducted research regarding the development of insulating shotcrete for applications in underground tunnels. He replaced the sand aggregate of the shotcrete with the following volumes of ELP aggregate: 0, 25, 50, 75, and 100%. Table 2-2 illustrates all mix proportions. The results (Table 2-3) showed that increasing the amount of ELP weakened the shotcrete's mechanical properties, but improved the thermal properties.

To improve the understanding of thermal insulating material, it is important to understand the composition of ELP. Raw perlite is a natural siliceous volcanic rock which contains 2 to 5% water in the amorphous and glassy form of magma (Kramar and Bindiganavile 2010). In temperatures above 870°C, raw perlite undergoes substantial volume expansion (four to 20 times). After the water evaporates, porous ELP is produced (Ciullo 1996). ELP has been widely used in concrete and mortar applications because of its lightweight and good performance in thermal and acoustical insulation, as well as fire protection (W. V. Liu 2013). It has been used as an aggregate in the concrete field since the early 1940s, to manufacture lightweight structures and slabs. For this use, ELP is mixed with other aggregates to obtain sufficient strength and thermal insulation properties (Brouk 1949). Not only does ELP have no toxicity (Sakai, T. & Nagao 1985), it is widely used in fire retardants to reduce the flammability of other material (Kasai et al. 1979). Moreover, because of its low bulk density (about 71 kg/m³) (W. V. Liu,

Apel, and Bindiganavile 2011), the cost of ELP in volume is very low (Bolen 2004). Therefore, there is no restriction regarding its use in jet grouting operations. The only condition is that the thermal, physical, and mechanical properties of the soilcrete have to be studied after mixing. To have better thermal properties, lightweight aggregates described in (ASTM:C332-09 2009) can be used.

2-5. Conclusion

The development of new thermal-insulating material and elements was proposed to create a thermal-insulating enclosure around the BTES borefield, which will keep the heat inside the enclosure from escaping and increase the efficiency of the UTES systems. It is proposed that the walls of the borefield be insulated by modifying the soil's thermal properties by using jet grouting technology and thermal-insulating grouts. The desired impact of the current research is that the efficiency of the UTES systems will be greatly improved, making these systems more desirable in many areas. The systems can capture heat at times where it is not needed, and harvest the energy when it is. This technology will reduce Canada's reliance on fossil fuels and reduce its carbon footprint.

Table 2-1 Thermal energy storage projects in European countries (“Underground Thermal Energy Storage for Efficient Heating and Cooling of Buildings” 2013)

	Belgium	Denmark	Germany	Netherland	Spain	Sweden	United kingdom
GSHP	••	•••	••••	•••	•	••••	••
ATES	••	••	•	••••	-	•••	•
BTES	•	-	•••	••	-	••••	•
	•	Few applications		•••	Many applications		
	••	Some applications		••••	Very many applications		

Table 2-2 Mixing proportions of experimental shotcrete (W. V. Liu 2013)

Mix number	P0	P25	P50	P75	P100
Replacement percentage (%)	0	25	50	75	100
Cement (kg/m ³)	519.5	519.5	519.5	519.5	519.5
Water/Cement	0.45	0.45	0.45	0.45	0.45
Water(kg/m ³)	233.8	233.8	233.8	233.8	233.8
Sand (kg/m ³)(Oven-dry)	1623.5	1217.6	811.7	405.9	0.0
ELP (kg/m ³)(Oven-dry)	0.0	17.3	34.6	52.0	69.3

Table 2-3 Testing results of insulating shotcrete (W. V. Liu 2013)

ELP replacement percentage	0	25	50	75	100
Fresh concrete density (kg/m ³)	2192.7	2101.2	1929.7	1698.0	1397.8
Hardened density (kg/m ³)	2303.0	2151.5	1989.9	1757.6	1444.4
Oven-dry density (kg/m ³)	2139.2	1974.6	1844.8	1525.3	1169.1
1st day UCS (MPa)	12.32	11.35	11.80	10.98	7.71
3rd day UCS (MPa)	27.31	22.19	22.41	16.40	11.50
7th day UCS (MPa)	33.86	27.95	28.56	22.08	13.50
28th day UCS (MPa)	43.78	40.70	32.96	22.64	16.87
1st day STS (MPa)	1.46	1.28	1.49	1.46	1.32
3rd day STS (MPa)	2.86	2.14	2.85	2.28	2.07
7th day STS (MPa)	3.15	2.92	3.18	2.35	2.24
28th day STS (MPa)	4.33	4.08	3.87	2.73	2.32
Air-dry samples moisture content (%)	7.58	8.87	12.18	17.86	27.96
Air-dry (48hrs) thermal conductivity (W/(m · K))	2.5164	2.0696	1.7532	1.1565	0.6852
Air-dry (48hrs) thermal diffusivity (mm ² /s)	1.1562	0.8487	0.5587	0.4701	0.2682
Air-dry (48hrs) volumetric heat capacity (MJ/(m ³ · K))	2.1764	2.4385	3.1378	2.4602	2.5544
Oven-dry (48hrs) thermal conductivity (W/(m · K))	1.8313	1.4450	1.1830	0.7351	0.3799
Oven-dry (48hrs) thermal diffusivity (mm ² /s)	0.9977	0.9363	0.6584	0.6141	0.3438
Oven-dry (48hrs) volumetric heat capacity (MJ/(m ³ · K))	1.8354	1.5433	1.7968	1.1972	1.1050

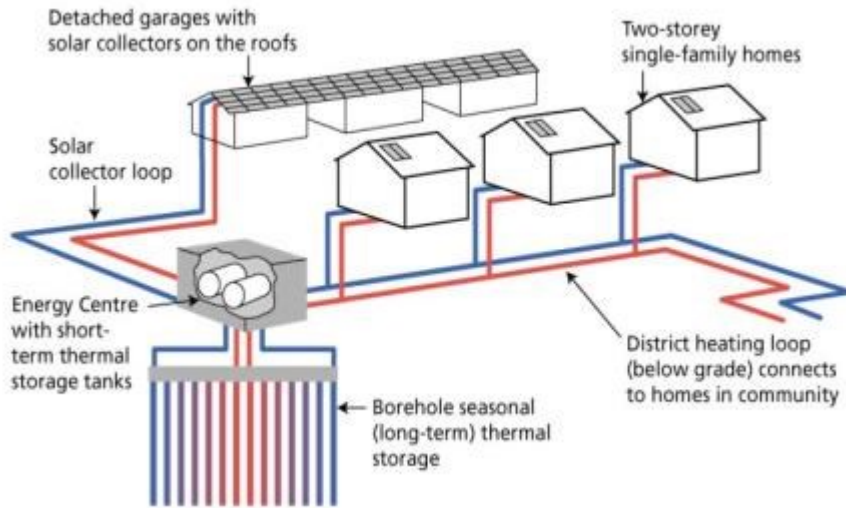


Figure 2-1 The schematic of BTES system (Mcclenahan et al. 2006)

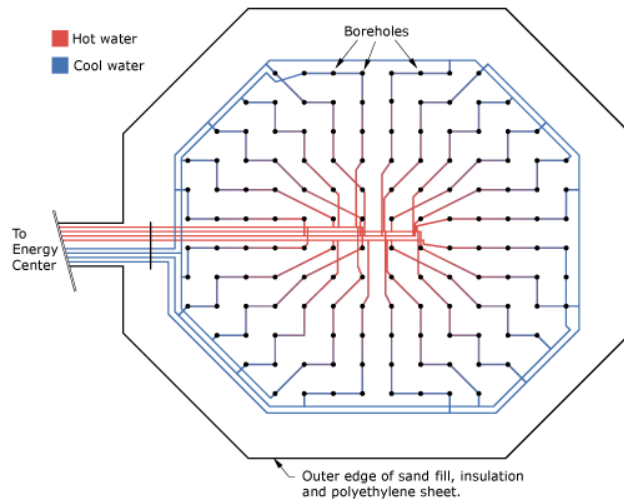


Figure 2-2 Plan view of the borefield (Mcclenahan et al. 2006)

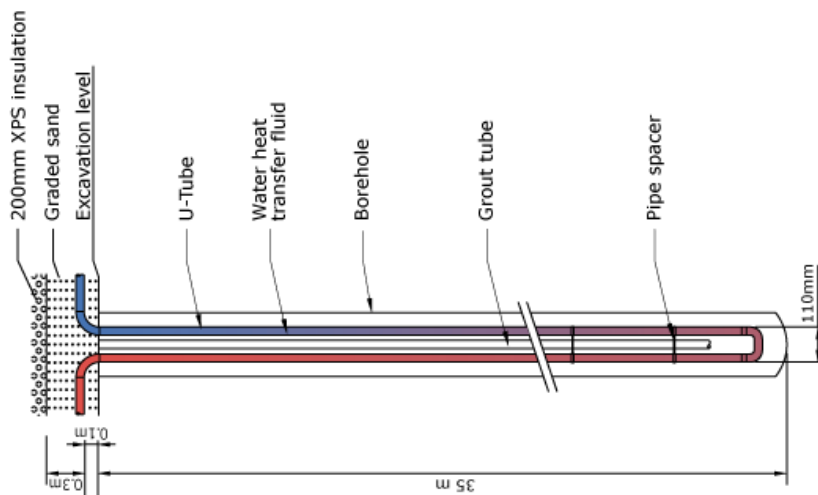


Figure 2-3 A BTES borehole with a single U-tube (Mcclenahan et al. 2006)

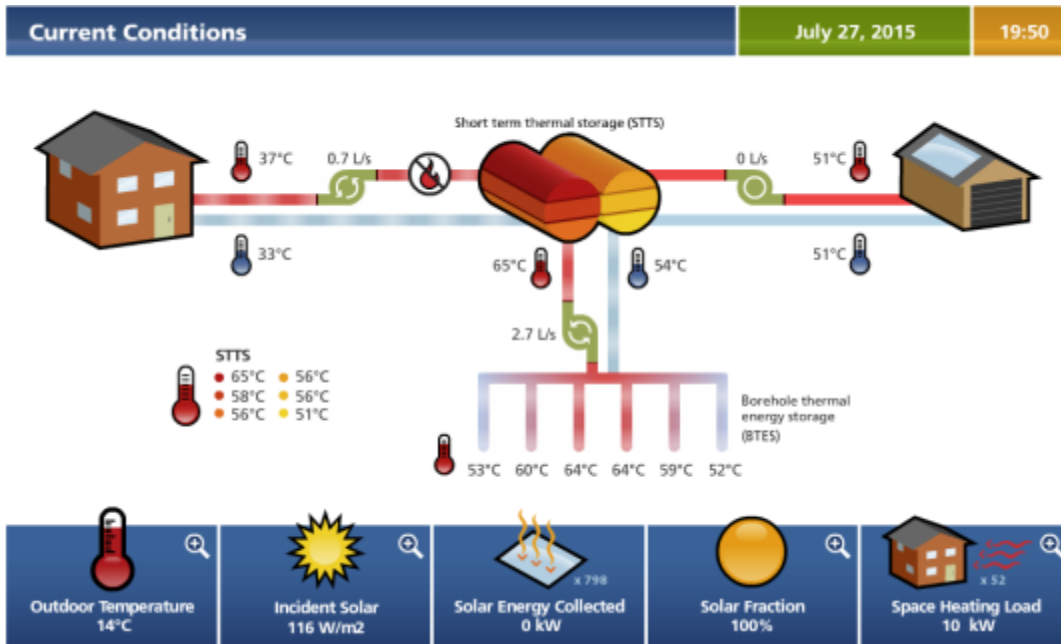


Figure 2-4 Actual condition of BTES in DLSC project (DLSC 2015)

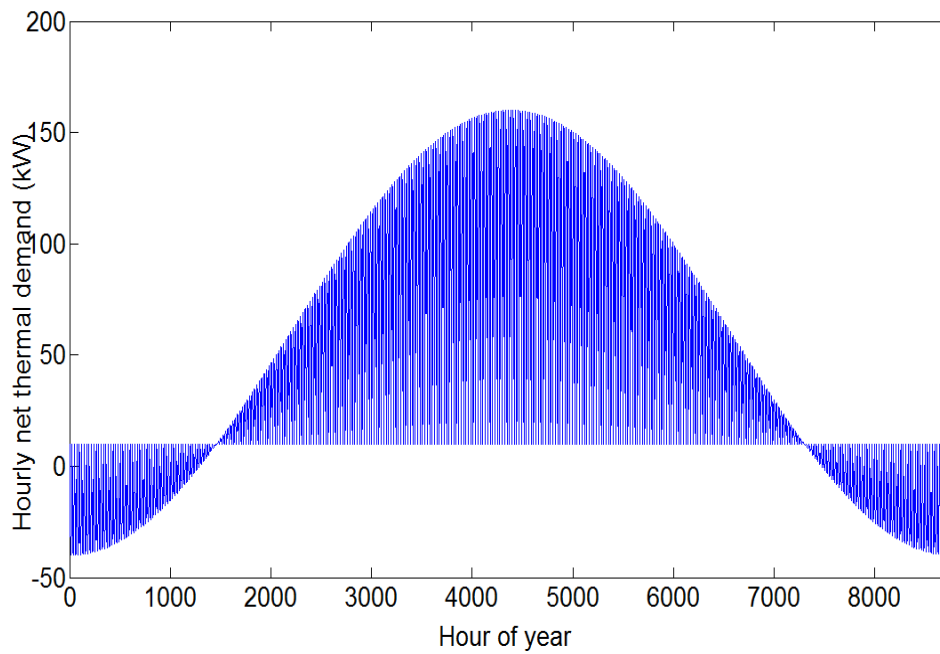


Figure 2-5 Net annual thermal energy balance (Roppelt 2011)

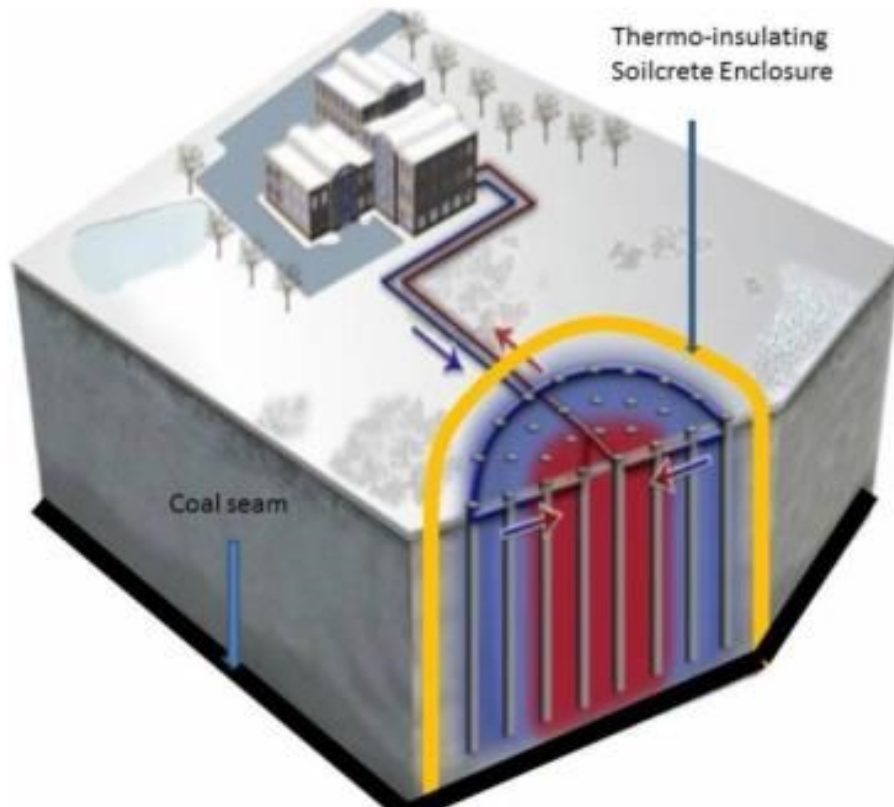


Figure 2-6 Conceptual BTES system with thermal-insulating enclosure

Chapter 3 JET GROUTING

This chapter discusses the basics and historical development of the jet grouting method. It also includes a literature review of all important jet grouting operational and soil parameters that affect soilcrete properties.

The last part of the chapter presents a design approach of the jet grouting operation as well as some empirical and theoretical methods in order to understand and address the jet grouting process properly and predict the soilcrete properties. It is hoped that this will help the jet grouting specialists to use these methods to initially evaluate their projects.

3-1. Introduction

Soft ground includes soils with a high amount of fine particles such as silt or clay with high moisture content, peat foundations, and loose sandy deposits near underground water tables (Kamon and Bergado 1992). In soft clay soils, undrained shear strength, S_u , or unconfined compression strength (UCS), q_u , is used to assess ground softness. Standard penetration test (SPT) N-values are used to assess ground consistency and its relative density (Bergado et al. 1996). Since past two decades, soil modification techniques reached a new level of accuracy in geotechnical engineering, and are now systematically considered a solution to ground improvement, reinforcement, and treatment problems involving poor or unstable soil conditions or soft ground (Schaefer 1997).

Today, instead of using expensive, deep foundations to remove or replace deep layers of fill or soft or loose soil, more economical in-situ ground improvement methods are used in most cases to mitigate undesirable conditions. Ground reinforcement methods can use structural benefits from the construction of elements in the ground without improvement of surrounding soil. Furthermore, soil treatment is accomplished by adding some non-soil material into the soil or subjecting it to different physical and mechanical situations to improve its properties. Some common additives are bentonite, fly ash, cement, sand, lime, or combinations thereof. Soil treatment methods are used to strengthen the soil, decrease the compressibility/swell potential, reduce permeability and heave/settlement, shorten construction times and costs, and assist in environmental mitigation efforts such as encapsulating waste material and groundwater (Schaefer 1997).

For shallow applications, the in-situ soil can be excavated and mixed with the admixtures and placed at a project location using conventional earth-moving equipment; however for deep foundations, all admixtures are placed directly into the in-situ soil using specialized equipment such as jet grouting to form columnar or wall-shaped structures. The type of admixture used to treat the soil can be decided depending on the particular project, cost, improvement purposes, availability of admixture, site accessibility, and time of construction. The physical and mechanical characteristics of the soil must be well understood. These characteristics include grain size distribution, moisture content, plasticity, density, and strength. The characteristics of the admixture, similarly, must be well known.

3-2. Jet grouting

Flowing water energy has a long history. Hydraulic energy was used to mine valuable deposits in ancient Egypt (Summers 1995). It was used during the Gold Rush in the 19th century and in Japan in the 1960s to erode soil and create soil-cement elements. High pressure jets are widely used in industry, but most significantly in civil and mining engineering, where high velocity jets are used to cut in-situ soil structures for ground modification (Ji 2008).

The development of jet grouting is well summarized by Kauschinger, Perry, and Hankour (1992) and Bruce (1994). In the early 1960s, the Yamakado brothers started to use water jets to cut the soil and mix it with cement. The chemical churning pile (CCP) method was developed by Nakanishi in early 1970s and was improved to the jumbo special grout (JSG) method. In the CCP method, chemical grout, which was later replaced with cement grout, was injected from nozzles placed at the bottom of a single monitor rod. During the jetting, the monitor was rotated to create a soilcrete. The only difference between CCP and JSG is that in the JSG method, compressed air is used as well as cement grout. The jet grout (JG) method was developed by Yahiro of the Kajima Corp in the early 1970s and later improved into the column jet grout (CJG) method. In both the JG and CJG methods, a triple fluid rod was used to deliver water, air, and cement grout fluids underground. In the JG method, the rod only moved in one direction without rotating. However, the rod was rotated in the CJG method during withdrawal to create soilcrete columns (Yahiro and Yoshida 1973; Ji 2008) Figure 3-1 illustrates the historical development of jet grouting.

The jet grouting method uses high velocity hydraulic energy to erode soil. The excavated soil grains are removed from the borehole and replaced with reinforced material such as cement or grout to form a solidified in-situ element known as soilcrete. There has been widespread discussion that jet grouting is simply a high pressure grouting system. This description is incorrect, although grouting fluid or water is forced through a small nozzle by using high pressure pumps to create high velocity energy to overcome the soil strength and erode it (Schaefer 1997). Jet grouting provides huge advantages over other ground treatment and reinforcement methods. It can be used on a wide range of soil types and ground conditions for different mining and civil engineering applications, including sensitive projects that require high quality control and personal safety (Figure 3-2 and Figure 3-3). Other advantages of the method are that soilcrete properties such as strength, permeability, and/or thermal conductivity can be

designed; there are no harmful vibrations; it can be used in limited working spaces; it is reliable; it is relatively less costly; it is quick; it is very effective for underpinning buried active utilities; it is insensitive to soils with low permeability such as those that contain a high percentage of clay; there is less danger of the soil fracturing or heaving because the jetting ambience is open to atmosphere via borehole annulus; it uses an automated implementation process; it is easy to install; it can be done from horizontal to vertical directions; it is able to bypass obstacles and buried utility lines; it increases the lateral compaction of the surrounding soil; it increases the frictional resistance of the surrounding soil and soilcrete column; it reduces permeability; it controls the depth of installation; all work is done in-situ from the surface; and it results in minimum settlement which means it will not disturb nearby historic or sensitive structures (Vardar et al. 2005; Plescan and Rotaru 2010; “Difficult Foundation Problems Solved by Jet Grouting”; Brill, Burke, and Ringen 2003).

Jet grouting has been used in various applications such as slope stabilization, ground water cutoff, soil bearing capacity increase, underground structures support, soil liquefaction prevention, and permeability decrease (JJGA 2005). It is a suitable substitution for common ground modification methods such as chemical injection, trenching, piling systems, and using compressed air with a freezing method in tunnel building. It can be used to create a watertight diaphragm, stabilize excavation and gradients, construct a retaining wall, establish piles, and stabilize walls and tunnel fronts. Figure 3-4 illustrates a comparison of jet grouting and conventional low pressure grouting methods which have been used in ground improvement; however the usage of conventional grouting is limited to restricted soils with certain void and pore spaces where the soil structure remains unchanged (Foundations 2012). A list of jet grouting main applications appears below and is shown in Figure 3-5 and Figure 3-6, and Appendix 3-1 and Appendix 3-2 (B Nikbakhtan 2007; B. Nikbakhtan, Aghababaei, and Pourrahimian 2007; B. Nikbakhtan and Ahangari 2010; B. Nikbakhtan, Apel, and Ahangari 2014a; B. Nikbakhtan, Apel, and Ahangari 2014b; B Nikbakhtan et al. 2009; B Nikbakhtan, Ahangari, and Rahmani 2010; B Nikbakhtan and Ghoshtasbi 2008; B Nikbakhtan and Osanloo 2009; B Nikbakhtan and Pourrahimian 2006; B Nikbakhtan and Pourrahimian 2007; B Nikbakhtan, Pourrahimian, and Aghababaei 2007a; B Nikbakhtan, Pourrahimian, and Aghababaei 2007b; Babak Nikbakhtan and Nikbakhtan 2008; S. Nikbakhtan, Nikbakhtan, and Rahmani 2008; Houlsby 1990; I. K. Mihalidis 1999; R. Essler and Yoshida 2004).

Groundwater control: flow prevention either into the base of excavation or the sides of it, ground water control during tunneling, and reducing or preventing water seepage through dams.

Movement control: stabilization of ground and prevention of structure movement during excavation or tunneling, supporting roof and sides of tunnel during excavation and in the long term after construction, and increasing the bearing capacity of piles and walls to withstand against the lateral movement.

Support: underpinning buildings, ground improvement, converting weak material to high strength material, and transferring foundation load from weak material to competent material.

Environmental: creating lateral and vertical walls to prevent contaminant material flow.

Jet grouting offers great flexibility for working conditions in selected intervals of soil layers or at very great depths. This flexibility is possible because of the creation of small boreholes that go from horizontal to vertical with minimum disturbance to sensitive structures. Such flexibility makes jet grouting an ideal ground improvement/reinforcement/treatment method in urban areas (Ji 2008) and has led to its increased use over the past decade (Alsayedahmad 1992).

3-3. Definition of terms

Some important terms pertaining to jet grouting equipment and procedure are defined as follows (ASCE 2009; BSEN12716:2001 2001):

“Jet grouting: an in-situ injection technique employed with specialized equipment that includes grout pump(s), grout mixer, drill rig, drill rods and injection monitor with horizontal radial nozzles delivering high velocity fluids to erode, mix, and stabilize in-situ soils using engineered grout slurry.

Horizontal jet grouting: Treatment performed from horizontal or sub-horizontal borehole (within +/- 20 degrees of the horizontal plane).

Jet grouting rig: rotary rig able to automatically regulate the rotation and translation of the jet grouting string and tool.

Jet grouting string: jointed rods, with single, double or triple inner conduits which convey the jet grouting fluid(s) to the monitor.

Monitor: a single, double, or triple fluid drill pipe attached to the end of a drilling string and designed to deliver one to three elements of the jet grouting process, typically air, water, and grout. The monitor has one or more injection points (nozzles).

Nozzle: a specially manufactured device fitted into the monitor and designed to transform the high pressure fluid flow in the string into the high speed jet directed at the soil.

Soil-cement (Soilcrete): mixture of grout slurry and in-situ soils formed by the jet grouting process.

Jet grouting operational parameters: pressure of the fluid(s) within the jet grouting string, flow rate of the fluid(s), grout composition, rotational speed of the jet grouting string, and rate of withdrawal or insertion of the jet grouting string.

Pre-jetting, pre-cutting, or pre-washing: the method by which the jet grouting of an element is facilitated by a preliminary disaggregation phase consisting of jetting with water and/or other fluids.

Radius of influence: effective distance of disaggregation of soil by the jet, measured from the axis of the monitor.

Spoil return: all materials including but not limited to liquids, semi-solids, and solids, which are discharged via the annulus of the jet grouting borehole above the ground surface as a result of jet grouting.”

3-4. Jet grouting construction process

Generally all jet grouting systems have the same construction procedure. First, the equipment is set up on location with a designated drilling angle. Then, a borehole with a diameter of 100 to 150 millimeters is drilled to the bottom of the designated depth using rotary methods (Schaefer 1997). Mud or casing can be used to stabilize the borehole wall during drilling. Other methods can also be used to overcome the drilling difficulties. These methods include pre-drilling, injecting high flow and/or high pressure drill fluid, and attaching a Down-The-Hole hammer beneath the monitor (Schaefer 1997). If casing is used, there must be a sufficient distance between the bottom of the casing and nozzles so that the casing does not interfere with the jet grouting process (Ji 2008). After drilling, the monitor is lowered to the bottom of the borehole, where jet grouting starts. During jet grouting, the monitor is lifted up and, if required, rotated uniformly to the designated depth (Schaefer 1997) (Figure 3-7). Figure 3-8 illustrates jet grouting's ability to build different geometries of soilcrete columns based the need and the system used (Schaefer 1997; HBI 2004).

Usually, the borehole diameter is larger than the monitor. The annular space between the monitor and borehole is used to return spoil (or excavated) material to the ground surface. Spoil material flow-out should be smooth and continuous during the jetting to prevent excessive pressure buildup. Otherwise, uplift velocity will not be great enough to exhaust these particles to the ground surface and annulus plugging can happen. Annulus plugging will act as passive pressure against the soil and may cause ground hydrofracturing, poor soilcrete quality and geometry, and/or ground surface heaving (Schaefer 1997; Ji 2008). Different soils have different erodibility (Figure 3-9). For instance, cohesionless soils are easy to cut and erode since they have moisture only as a binder, whereas clays are difficult to erode since they have cohesion. Therefore, they are generally eroded in chunk pieces which are larger than the size of a grain of sand. Different techniques can be used to improve the spoil material return. These techniques include casing the borehole to decrease friction between the spoil material and borehole, using a multi-direction set of nozzles, pre-cutting, injecting air to lift up the slurry material, and/or making multiple cutting lifts (Brill, Burke, and Ringen 2003; Schaefer 1997).

3-5. Jet grouting systems

Jet grouting has two different forms: mix in-place, and excavation/replacement. The forms can be made using three jet grouting systems (single fluid, double fluid, and triple fluid) based on the number of the fluids used in process. The operational parameters vary with the jet grouting systems and consequently the soilcrete properties are different in each system (HBI et al. 1994) (Table 3-1). The definition of each system is provided in the following sections (Alsayedahmad 1992; HBI 2004; Ji 2008).

3.5.1. Single fluid system, F1

This system is the simplest. It was introduced by Yahiro in the early 1970's. Only one fluid, such as grout, is injected into the soil structure with high pressure (Figure 3-10). The injected high velocity grout slurry approximately 200 m/sec (650 ft/sec) partially erodes the soil structure and mixes with coarser material while the finer materials are washed out of the borehole during monitor withdrawal. This system is not very effective in cohesive soils. The soilcrete diameter can reach 0.6 to 1.2 meter in gravelly soils. In loose, silty, and sandy soils larger diameters can be reached. The most important applications of this system are cutoff walls in porous soil, soil consolidation for the tunnel roof, and bottom bracing for deep trenches in soft soils, anchors, and sealing applications.

3.5.2. Double fluid system, F2

This method represents a major improvement in the single fluid system by introducing a shrouded-air jet around the grout (Figure 3-11). Two coaxial conduits are used. These were introduced by Yahiro in the early 1970s. The inside conduit is grout while the space between the conduits is air, which encircles the grout in order to separate the grout from the slurry and keep the soil from falling into the jet stream. This will increase the cutting distance and therefore increase the soilcrete diameter. The presence of the air also helps the airlifting process of the spoil material return; however, this will cause the soilcrete to have a high air content, which will decrease its strength. Grout is both the cutting and mixing medium. This system is more effective than the single fluid system in cohesive soils. The most important applications of this method are in soil stabilization, underpinning, panel cutoff walls, and bottom bracing for deep trenches in soft soils.

3.5.3. Triple fluid system, F3

This system is the most complicated and uses three tubes to carry water, grout, and air, separately (Figure 3-12). It was used for the first time by (Yahiro and Yoshida 1973). A high pressure water jet with a velocity of up to 300 m/s and a coaxial air jet are used to totally break up the soil structure at an upper elevation and wash out the finer material up to the ground surface. At the same time, low pressure grout is replaced with soil material at lower elevations after soil erosion. In this method, more soils are excavated and full replacement of soil with grout is possible (HBI et al. 1994). The soilcrete diameter in this system is larger than other methods (Table 3-1). This method is the most effective for cohesive soils. It is more controllable and safer for sensitive structures than the single fluid system (Brill, Burke, and Ringen 2003). The applications are in underpinning and excavation support, horizontal slab/ground water control, panel cutoff walls, sealing applications, and most fine-grained soil stabilization.

When the triple fluid system is used for excavation and replacement, most of the soil is replaced with cementations material and mixed with the remaining soil. In other words, triple fluid jet grouting is a partial soil replacement technique with cementations material, in which the primary aspect is to modify engineering properties of the soil such as decreasing permeability and thermal conductivity, and increasing strength (Alsayyedahmad 1992). The parameters that should be assigned in a single fluid system are grout pressure and flow rate, number and dimensions of grout nozzles, water/cement ratio, withdrawal, and rotational speed. In the double fluid system, in addition to single fluid parameters, it is necessary to assign the air pressure and flow rate, and number and dimension of air nozzles. In the triple fluid system, in addition to single and double fluid parameters, it is necessary to assign water pressure and flow rate, and the number and dimension of water nozzles (HBI et al. 1994).

Yahiro et al. (1975) have studied the advantages of the triple fluid jet grouting system over other systems. In their study, they explained the difference between water jet and water-air jet cutting efficiency and the description of the cutoff wall construction. They also introduced other useful applications for the triple fluid system (Appendix 3-3). They concluded that the cutting action of the water-air jet in the soil is related to the complicated function of many parameters of the soil and water-air jet. They also reported that the axial dynamic pressure of water is the most important parameter, which controls the water-air jet's ability to cut the soil. Increasing the encircled air pressure around the water jet can increase the cutting efficiency. Table 3-2

illustrates the necessary equipment for the triple fluid jet grouting system. The results from Yahiro et al. (1975) showed that constructing cut-off walls to prevent groundwater flow in sand, clay, and silt layers was almost completely effective; in transitional areas between consolidated and unconsolidated soils, the effect was good; and in sandy-gravel soils, the effect was not so good. It is important to note that, the permeability of soilcrete decreased from 1/100 to 1/10,000 to its original value depending on different soil types (Alsayyedahmad 1992).

Yahiro, Yoshida, and Nishi (1982) have divided the mechanism of ground improvement into three categories of reduction of buoyancy by dewatering, vibration, and consolidation. Based on their research, they concluded that these mechanisms might not always solve ground improvement problems, and that the triple fluid jet grouting system is better able to solve such problems (Appendix 3-4).

3.5.4. Recent developments of jet grouting systems

Over time, the jet grouting technique has been improved to overcome different field difficulties. Some of the improvements are discussed in the following sections (Table 3-3) (Schaefer 1997; HBI 2004; Ji 2008; X-Jet 2002; Superjet 2004).

3.5.4.1. Super soil stabilization management method

Miki and Nakanishi (1984) developed a new jet grouting method, the super soil stabilization management method (SSS-MAN-Method). Construction steps and a comparison to different jet grouting systems are shown in Appendix 3-5 and Appendix 3-6. In this method, after drilling a hole to the specified depth, the rotary water jet is lowered to the bottom of the hole and cuts the surrounding soil. The soil is removed through the withdrawal of the monitor, leaving a large space. The dimension is measured by supersonic wave techniques, after which the space is filled with grout. The authors were able to produce columns that were four meters and 2.5 meters in diameter in sandy and clayey soils, respectively.

3.5.4.2. Sacrificial casing

In this method a pre-installed thin wall PVC casing is used to aid in controlling spoil return (Viner and Wooden 1990). The PVC casing is weakly grouted in a pre-drilled hole. During jet

grouting, the PVC casing is blasted into small pieces by a cutting jet while acting as a stable borehole to help to ease spoil return.

3.5.4.3. Super jet grouting

This method was developed by Yoshida in the early 1990s and is used in soft soils where soil stabilization is necessary (Figure 3-13). It was modified from the double fluid system, and uses a triple fluid system rod. Erosion energy is boosted by increasing the grout velocity. The system is used not only for grouting but also for drilling. The water jet is first injected as drilling fluid while the monitor is lowered. After the designated depth is reached, the water jet injection is stopped and the grout jet shrouded with air is injected while the monitor is lifted (Ji 2008). This method uses opposing nozzles with a high sophisticated jetting monitor. Using a very slow rotation and lifting speed, the diameter of soilcrete can reach three to 5.5 meters (Figure 3-14 and Figure 3-15). This method is more effective for mass stabilization of soil and can be used in the following applications: horizontal slab/ground water control, stabilization of liquefiable strata, panel cutoff walls, structural support across excavation walls, and stabilization of soft soil for microtunneling (HBI 2004). This development of this method is regarded as the most significant advancement of the jet grouting technique (Brill, Burke, and Ringen 2003).

3.5.4.4. Super-midi jet grouting

This method is a small version of super jet grouting. Unlike super jet grouting, the system uses a double fluid monitor. It is self-drilling and does not need any other equipment for drilling. It is used when super jet grouting is not available due to space constraints. The grout flow rate in super jet grouting and super-midi jet grouting is 50 to 80% more than that in the double fluid jet grouting system (Boehm and Posey 2003).

3.5.4.5. Cross jetting (X-Jet)

This method was developed to allow for better control of soilcrete's quality and geometry (M. Shibazaki, Yoshida, and Matsumoto 1996). Figure 3-16 and Figure 3-17 illustrate the schematics of the X-Jet grouting system and formed soilcrete columns, respectively. A pair of water/air nozzles is designed to intersect at a designated point at which the fluid energy dissipates quickly. With a slow withdrawal and rotational rate, a controlled shape of soilcrete is eroded

(Figure 3-18). The grouting material is injected at the lower depth of the crossing nozzles (Ji 2008).

3-6. Current methods to evaluate jet grouting operations

Although jet grouting has been very useful in civil engineering and in the mining industry, from the geotechnical and ground modification perspective, the understanding of the process is very limited because of its complex and underground operations. There is great uncertainty regarding soilcrete creation and its engineering properties. It is difficult to predict or precisely control the quality of soilcrete.

Soilcrete's structural, physical, mechanical, and/or thermal properties may change for many reasons along the axis (Flora, Lignola, and Manfredi 2007). For instance, in vertical jet grouting with a given jet energy (i.e., constant jet grouting operational parameters), the soilcrete diameter decreases as the soil strength and depth increase (P Croce and Flora 2000; HBI et al. 1994). In the same manner, for any given grout pressure and withdrawal rate, jet grouted volume and consequently soilcrete diameter decrease as the clay content increases (D. a. Bruce, 1994). Depending on the soil type, the variation can differ. Another variation may occur when soil properties change suddenly along the jet grouting axis (Figure 3-4). For instance, the variation can be critical when soil properties change from soft layers to a harder matrix, which will cause a sharp reduction in the soilcrete diameter. Poh and Wong (2001) reported trial jet grouting experiment results showing that using the same jet grouting operational parameters (or the same jetting energy) along two different soft-to-medium stiff marine clay layers failed to form the soilcrete columns in the medium layer. Hence, another set of operational parameters with more jetting energy per unit lift of monitor should be used to form proper soilcrete columns in a medium stiff clayey layer. Paolo Croce et al. (2004) have shown that unit weight and UCS increase with depth. Meyers et al. (2003) theoretically calculated that the UCS of soilcrete is 3,500 kPa. However, after testing, many of the samples failed at the strength below the required minimum value, which indicates that using only the developed equations may not be enough to predict various soilcrete properties. Soilcrete properties vary along the radius of the soilcrete and these variations are very difficult to understand. In small diameter soilcretes, such as one-meter column, these variations are negligible, but in large diameter soilcretes ranging from two to three meters, these variations should be properly addressed.

The degree of success in a jet grouting operation from the perspective of soilcrete structural, physical, mechanical, and/or thermal properties depends significantly on the soil characteristics and jet grouting operating parameters. These parameters can make the soilcrete body heterogeneous instead of perfectly cylindrical with the same particular properties along the axis and/or radius. These uncertainties will increase the overall cost of the project and might limit the use of jet grouting in many cases (Ji 2008; Flora, Lignola, and Manfredi 2007). This issue, together with the lack of precise knowledge about the effect of depth on the properties of the soilcrete, leads to designs that are either over-conservative or unsafe. However, geotechnical companies must understand the jet grouting process and ensure the success of the operation.

Although increasing knowledge about the jet grouting technique over the past decades has made it easier to choose appropriate systems to complete particular project goals, only experienced specialists can decide what type of system should be used to produce a particular type of soilcrete (Schaefer 1997). It is important, but also complicated, to estimate the operational parameters to produce a particular soilcrete. The influence of these parameters and soil properties on the soilcrete properties is still not clear (Li and Hu 2010). The process is less complicated if a project was done using the same jet grouting system at a jobsite with the same geotechnical properties. In such cases, it is possible to empirically estimate some operational parameters from past projects (Schaefer 1997; B. Nikbakhtan, Apel, and Ahangari 2014a; B. Nikbakhtan, Apel, and Ahangari 2014b; B. Nikbakhtan and Ahangari 2010; B. Nikbakhtan and Osanloo 2009). However, for the new projects with different jet grouting systems, soil types, and goals, the uncertainty remains. A common way to determine soilcrete properties with different operational parameters is to perform in-situ trial jet grouting in a temporary jobsite with the same geotechnical soil properties as the main jobsite. This is called Quality Assurance. During the in-situ trial stage, jet grouting is done on several columns in a field that has the same soil type as the main jobsite. Various operational parameters are used in this stage. The test columns are dug out after several days and their particular properties, based on the project goals, are measured. Finally, based on the in-situ trial test results, the actual operational parameters are suggested to reach the desired soilcrete properties at the main jobsite. The trial jet grouting can be used to verify many considerations based on the project purposes. These considerations include measuring the effectiveness of the system in achieving the specified criteria; measuring the treatment effectiveness in terms of physical, mechanical, and/or thermal properties of the

soilcrete; providing information about operational parameters to achieve a specific column diameter; monitoring ground movement caused by jet grouting; investigating effective ways to prevent grout intrusion to adjacent utilities and structures; measuring the effectiveness of spoil material return; investigating noise and vibration emissions within the ground and adjacent structures; and providing valuable information about the operation costs (“Victoria Station Upgrade Supplementary Environmental Statement: Technical Appendix G – Jet Grouting Trials Report” 2008; Collotta, Frediani, and Manassero 2004).

Many researchers have attempted to extract empirical relationships from trial test results to predict the soilcrete properties at the main jobsite. In the main jobsite, after determining the operational parameters, all parameters should be consistent and controlled during jet grouting in a particular section. Then, the quality of the soilcrete must be controlled through direct and indirect in-situ measurements at the main jobsite. This process is called Quality Control (B Nikbakhtan, Ahangari, and Rahmani 2010). The quality control measurements can vary relative to the particular goals of projects. Table 3-4 illustrates the sampling and testing methods of soilcrete properties for different goals. In many cases, the operational parameters must be optimized based on the results of quality control measurements. Some novel quality control techniques of the soilcrete diameter are discussed in the following section.

Passlick and Doerendahl (2006) suggested a new quality control method using a hydraulic mechanical device to measure the soilcrete diameter at the main job site. This method has been able to mechanically measure the diameter of 2.6 meters at a depth of 37 meters (Figure 3-19). Gemmi et al. (2003) proposed using an electrotomography investigation, one of many types of geophysical investigations, to evaluate the effectiveness and quality of jet grouting work in underpinning projects. They also explained that the reliability of the method can be variable based on the distance of electrodes from the soilcrete. Schorr et al. (2007) proposed using a wave-based analysis approach to measure the soilcrete column diameter in combination with the trial method. A. Malinin et al. (2010) proposed another mechanical way to measure the soilcrete diameter after the jet grouting but before the hardening of the soilcrete (Figure 3-20). This device is limited to measuring the diameter of soilcrete only to a depth of one meter. Another limitation with the device is that if the soil type is not clay, it is difficult to recognize the soilcrete boundary with in-situ soil.

3-7. Important parameters in jet grouting

The most important soilcrete properties when designing and evaluating a jet grouting operation are structural, physical, mechanical, and thermal. These include diameter, permeability, strength, and heat conductivity. By being able to determine the diameter of soilcrete, the number of required columns and their spacing for activities such as cut-off walls, soil improvement and slope stability can be calculated, and the volume of required grout can be estimated. In the same manner, by being able to calculate the strength of the soilcrete, the number of columns for applications such as excavation support, underpinning, and ground reinforcement can be calculated. By being able to calculate the thermal and permeability properties of the soilcrete, the number of columns and their spacing/overlapping can be estimated, and the improvement percent can be calculated at the design stage.

Theoretically, parameters affecting soilcrete properties are jet grouting operational parameters, geotechnical specifications of the soil, and grout type. These parameters are discussed in the following sections. Bergado et al. 1996 stated that the most important parameters affecting the design of jet grouting are soil type, mixture influx between soil and grout, existing jet energy from the nozzle, grout flow rate, rotating speed and lifting speed. Yahiro et al. (1982) carried out research to investigate the way in which these parameters affect the diameter and strength of soilcrete in the field (Table 3-5). Results showed that it is possible to achieve a maximum soilcrete diameter of 3.5 meters and 2.5 meters in sandy soils and clay soils, respectively. They also noted that even if the in-situ soil had SPT test N-values less than 10 blows/ft, the soilcrete produced a strength of 30 (2942) to 50 (4903) kg/cm² (kPa) and 13 (1275) to 50 (4903) kg/cm² (kPa) in sandy and clay soils, respectively (Alsayedahmad 1992). Carter and Webber (2007) mentioned that soilcrete properties are influenced by pressure, nozzle diameter, grout density, grout internal friction/cohesion, and nozzle flow turbulence. All affect the total energy transferred to erode the soil. The density of the grout/soil mixture; the cohesive strength of the soil, rocks and debris; and the rate of movement of the jet through the soil also affect the volume of soil influenced by the jet. Regarding the main soil properties which affect the soilcrete, various suggestions have been made. The conclusion is that the following three soil variables influence soilcrete diameter: grading, relative density, and undrained shear strength (P Croce and Flora 2000). Nikbakhtan and Ahangari (2010) stated that soilcrete strength and diameter depend on jet grouting parameters such as grout pressure, withdrawal and rotational speed, number and

diameter of nozzles, water to cement (w/c) ratio, and in-situ soil properties. B. Nikbakhtan et al. (2014a), (2014b) divided those important parameters into two main categories. The first group includes grout density and operational parameters of the jet grouting system, such as water pressure, grout pressure, air pressure, lifting speed, and rotating speed. The second group includes geotechnical properties of the in-situ soil, such as soil permeability, cohesion, soil conductivity and soil groutability ratio. B. Nikbakhtan et al. (2014a), (2014b) also explained that water, grout, and air pressure and the soil permeability coefficient, soil conductivity coefficient, and groutability rate directly impact the soilcrete column diameter. Other parameters such as lifting speed, rotating speed, grout density and cohesion have a reverse relationship relative to soilcrete diameter changes.

The dependency of soilcrete properties on an extensive number of operational parameters and soil characteristics makes trial jet grouting necessary to achieve optimized soilcrete and operation results (Warner 2004). So far, many research projects have been carried out to understand the effect of important operational parameters and soil geotechnical characteristics on soilcrete properties. However, most of the studies have focused on predicting mainly soilcrete diameter and, sometimes, its mechanical properties such as UCS. Very few attempts have been made to study the thermal properties of soilcrete. It is clear that although the effect of the different parameters can be the same in different soil conditions, the actual numeric results can be totally different. Based on the author's knowledge, no project was designed based on other previous project results, even if projects had similar soil properties. However, empirical relationships can give an initial idea about soilcrete properties. Table 3-6 summarizes all previous well-documented jet grouting literature. The following sections summarize the effect of different parameters on soilcrete properties and all empirical relationships to calculate soilcrete diameter, strength, composition, and the specific energy of the jet grouting system.

3-8. Effect of different parameters on soilcrete diameter

3.8.1. Nozzles, rotating and lifting speed

Nozzles are the most important parts of the jet grouting procedure. Their shape, dimension and accuracy can influence the quality of the soilcrete. Generally, nozzle design is based on Leach and Walker (1966) for rock cutting using a water jet in air (Chu Eu Ho 2005). Figure 3-21 (a) shows the effect of the narrowing angle of the nozzles on the dynamic pressure of the jet. The

narrowing angle of 13 degrees provides the best performance. Figure 3-21 (b) shows that for a fixed cone angle of 13 degrees, the best performance of the jetting can be achieved when a certain straight portion of the nozzle is three times at which the nozzle diameter at its exit. For jet grouting applications, Mitsuhiro Shibazaki (2003) recommended that a nozzle with a narrowing angle of 13 degrees and a certain straight portion of 2.5 to 3 times the diameter provides the best performance (Figure 3-22 and Figure 3-23). Nozzles should also be accurately finished from inside, outside, and the exit point to be able to create a focused jet to erode the soil (Mitsuhiro Shibazaki 2003).

H. Yoshida et al. (1991) studied the effect of the number of nozzles (N_p) and rotational speed (R_s) on cutting distance using a silty sand soil with N_{SPT} 3 to 6 blows per 300 millimeters. Figure 3-24 and Figure 3-25 show that for a given jetting energy, the cutting distance increases with the number of jet nozzles and decreases when the jet rotational speed increases. Figure 3-24 also shows that 10 passes is the optimum number of nozzles, and after that the increasing rate of cutting distance diminishes. H. Yoshida et al. (1991) also emphasized that to have the minimum number of passes (N_p) within a given lifting step (Δz), the withdrawal rate (v_t) has to be selected in such a way that the duration of jetting (Δt) is matched with the rotational speed (R_s), i.e., $\Delta t = N_p/R_s = \Delta z/v_t$ (Chu Eu Ho 2005). M. Shibazaki et al. (1996) also suggested that to reach an optimal cutting, operational parameters should be designed based on the rotational speed of 10 rpm with impact frequency limited to within 10 passes.

The optimal repetition frequency of the eroding jet is shown in Figure 3-26, based on experimental results. It is clear that frequency in excess of five increases the column's diameter. Figure 3-27 illustrates two different steady and incremental withdrawal (or lifting) methods. With steady withdrawal, it is not possible to withdraw the jetting rod in steps to provide enough time for rotation. Based on experimental results, a five-centimeter lift for up to two meters in diameter and a 10 centimeter lift for more than four meters in diameter have been suggested as optional increments (R. Essler and Yoshida 2004).

M. Shibazaki et al. (1996) carried out a field test in silty sand (N_{SPT} 10 to 15 blows per 300 millimeters) to demonstrate the relationship between pullout time (the time of jetting required for soil cutting in each lift step) and soilcrete diameter. The results Figure 3-28 show that in the maximum duration ($t = t_0$), the largest column diameter with an average diameter 5.7 meters can be obtained. In each lifting step of Δz , the time Δt for cutting the soil can be calculated

by $\Delta t = \Delta z/v_t$, where v_t is the withdrawal rate of the monitor. A. Malinin et al. (2010) carried out experimental jet grouting research on three different soils: cohesive soil, non-cohesive soil, and soil with low cohesion. The results show that when the rod-lifting time increases, so does the soilcrete diameter (Figure 3-29). Also, when the rotational rate of a particular speed increases, so does the diameter of the soilcrete; however, after that speed, the diameter decreases when the rotational rate increases (Figure 3-30).

3.8.2. Jetting pressure and flow rate

Pressure and flow rate control jetting energy and jetting energy controls different properties of the soilcrete such as diameter (Ji 2008; Kauschinger, Perry, and Hankour 1992). The withdrawal rate, rotational speed and number of the nozzles determine the exposure time of the soil being eroded (Brill, Burke, and Ringen 2003; Ji 2008). Increasing the pressure up to a practical limit of 60 MPa can increase the soilcrete diameter (Mussger, Koinig, and Reischl 1987); however, to erode the soil, dynamic jetting energy must be greater than a critical pressure, which is equal to soil compressive strength (Brill, Burke, and Ringen 2003). If the jetting energy is lower than the critical energy, the exposure time of the jetting can still increase the erosion distance to a limit (S. N. P. Coulter 2004). Mitsuhiro Shibazaki (2003) reported that at more than five repetitions of rotation, the diameter did not increase significantly on loose sands.

During jet grouting, the eroding distance radically increases as the water jet pressure exceeds the UCS of the soil. The relationship between the eroding distance and water jet pressure is shown in Figure 3-31 and Figure 3-32. It is possible to erode the same distance with lower pressure but a long period of jet exposure on the soil face will be needed (R. Essler and Yoshida 2004).

The water jet eroding distance varies among different media. Figure 3-33 illustrates the eroding distance of a water jet in air, water, and water with shrouded-air. The figure shows that the air shroud around the water jet increases the eroding distance. However, to increase this effectiveness, the air shroud velocity should be higher than half the sonic velocity to ensure the thickness of one millimeter (Tinoco 2012; R. Essler and Yoshida 2004).

Yahiro and Yoshida (1973) evaluated several factors influencing the cutting distance efficiency of jet grouting in different soil types to compare the capability of a high pressure water jet in a triple fluid system with a grout jet in a single fluid system. The results show that the triple fluid system is more efficient and capable of cutting in sand, silt, and soft rock. Yahiro and Yoshida

(1973) investigated the effect of the air jet surrounding the water jet in the triple fluid jet grouting system. The result is presented in Figure 3-34. Their research showed that compared to the original soil, the compressive strength and permeability of the soilcrete increases and decreases, respectively (Alsayyedahmad 1992). Figure 3-35 shows the effect of the shrouded-air flow rate and dynamic pressure with the eroding distance. The relationship between grout pressure and soilcrete diameter in two different soft clay and sandy soils is shown in Figure 3-36.

3.8.3. Soil properties

The grading, relative density, and undrained shear strength (S_u) of soil can influence the soilcrete diameter (P Croce and Flora 2000). Relative density can be estimated by an SPT blow count (N). Some publications have indicated that the diameter decreases with decreasing soil grain size (Figure 3-37) (Bell 1993; Botto 1985) and increasing N and S_u (Figure 3-38 and Figure 3-39) (Miki and Nakanishi 1984; Tornaghi 1989).

Figure 3-43 illustrates the relationship between the soilcrete column and soil N_{spt} value as a function of the jet grouting systems. Figure 3-40 shows the relationship between the soilcrete diameter and soil N_{spt} value as a function of the different soil types and jet grouting systems.

3-9. Jet grouting operation design procedure

Figure 3-41 presents an overall procedure of the jet grouting operation design and implementation. It is important to understand the soilcrete properties before formulating hand-mixed soilcrete in a laboratory. This can be achieved by reviewing a comprehensive literature report of different theoretical and empirical relationships derived to calculate soilcrete properties. The design procedure of the jet grouting operation, as well as different methods to calculate soilcrete properties and jet grouting operational parameters, are discussed in the following section. It is hoped that this may help jet grouting specialists to use these methods to initially evaluate their projects.

- 1) Figure 3-2 and Figure 3-3 can be used to give an idea about how jet grouting performs compared to other grouting methods in different soil types. It is clear that jet grouting is the best option in silt and clay soils.

- 2) To select which jet grouting system is suitable for a particular project, it is important to take into account the primary factors: soil properties and the main goal of jet grouting operations. Each system has its own advantages and disadvantages and each system should be used based on the project requirements and ability of the system. The main aspects of each system, including their main operation parameters, advantages, and soilcrete properties, are presented in Table 3-1, Table 3-3, Table 3-7, Table 3-8, and Figure 3-42. Figure 3-43 and Table 3-1 give estimates about soilcrete strength and its diameter in different jet grouting systems.
- 3) Different operational parameters and soil types may affect the soilcrete diameter and strength. Table 3-5 presents the effect of operational parameters on the diameter and strength of the soilcrete in both sandy and clay soils. Figure 3-21 to Figure 3-40 and Figure 3-42 and Figure 3-43 present the effect of jet grouting operational parameters, nozzle configuration, and soil properties on soilcrete diameter. Figure 3-44 through Figure 3-46 and Table 3-9 and Table 3-10 present different soilcrete strength values in different soil types.
- 4) Based on jet grouting operational parameters and soil properties, the different theoretical and empirical methods described in following three sections (3.9.1, 3.9.2, and 3.9.3) should be used to calculate soilcrete diameter, strength, and composition relative to particular project goals.
- 5) Laboratory formulation experiments should be conducted with hand-mixed soilcrete samples to verify the values estimated by theoretical and empirical relationships.
- 6) Trial jet grouting test columns should be implemented in the field or by using a laboratory setup to validate hand-mixed experiment results from the laboratory and estimate operational parameter values for the main jet grouting operation in the field.
- 7) During the main jet grouting operation in the field, all operational parameters must be controlled and monitored. Also, different types of tests must be conducted on the

soilcrete to identify the properties during jet grouting and after the soilcrete has hardened, to calibrate trial jet grouting results (Table 3-4).

3.9.1. Methods to calculate soilcrete diameter

JJGA, (2005) proposed a comprehensive guideline for operational parameters and soilcrete diameter values for double fluid, triple fluid, and super jet grouting systems (Chu Eu Ho 2005). The values are presented in Table 3-11 to Table 3-16. Other methods to calculate soilcrete diameter are discussed in the following sections.

3.9.1.1. Specific energy

Tornaghi (1989) proposed that specific energy of compressed air can be expressed using the dimensional equation shown below:

Equation 3-1

$$E_{sa} \left(\text{in } \frac{\text{MJ}}{\text{m}} \right) = \frac{0.035 Q_a \left[\frac{\text{l}}{\text{min}} \right] \times \{ (10 P_a [\text{MPa}])^{0.29} - 1 \}}{v_t \left[\frac{\text{cm}}{\text{min}} \right]}$$

Therefore, specific jet energy can be calculated in each of single, double, and triple fluid systems using the equations below (Chu Eu Ho 2005).

In a single fluid jet grouting system:

Equation 3-2

$$E_{sg} = \frac{P_g Q_g}{v_t}$$

In a double fluid jet grouting system:

Equation 3-3

$$E_{st} = E_{sg} + E_{sa}$$

In a triple fluid jet grouting system:

Equation 3-4

$$E_{st} = E_{sw} + E_{sa}, \quad E_{sw} = \frac{P_w Q_w}{v_t}$$

De Paoli et al. (1989) developed a relationship between jet grouting specific energy and soilcrete diameter shown in Figure 3-47, where the specific energy per lineal meter of a column is $E_{sl} = P \times T$ (MJ/m); specific energy per cubic meter of a column is $E_{sc} = P \times T/S$ (MJ/m³); where P is the mean power delivered by fluid exiting the nozzle, expressed by the product $Q \times p$; Q is the rate of fluid ejection (m³/sec); p is the mean ejection pressure (MPa); T is the specific injection time (sec/m); and S is the cross sectional area of the column (m²).

Groppo Sembenelli and Sembenelli (1999) developed a relationship between total specific energy (grout and air) and the minimum diameter of soilcrete (Figure 3-48). Figure 3-48 shows that the correlation is different for different jobsites.

P Croce and Flora (2000) stated that among several empirical relationships which do not seem to have physical meaning, one relationship proposed by Tornaghi (1989) is notable. The relationship correlates soilcrete column diameter with jetting energy per unit of column diameter. Equation 3-5 calculates the energy at pump (E_p).

Equation 3-5

$$E_p = \frac{p \times Q}{v}$$

Where,
p: grout pressure
Q: grout flow rate
v: monitor lifting rate

P. Croce and Flora (2000) proposed an approach to design the jet grouting column diameter. This approach is based on the jetting energy at the nozzles (E_n), not at the pump, in order to account for the pressure loss through circuit lines and nozzle. However, this approach provides no insight

into the mechanism of jet grouting. The authors suggested that energy losses in the jetting system could be as large as 20% (Figure 3-49). Generally, for the unit length of column L:

Equation 3-6

$$E_n = \frac{m \times v_n^2}{2 \times L}$$

Equation 3-7

$$m = \rho_g \times Q \times \Delta t$$

Expressing v_n as a ratio between Q and the overall nozzle cross-section.

Equation 3-8

$$E_n = \frac{8 \times \rho_g \times Q^3}{\pi^2 \times M^2 \times d^4 \times v}$$

Where,

- E_n : jetting energy at the nozzle
- m: grout mass delivered in the time Δt corresponding to treatment length L
- v_n : grout velocity at the nozzles
- ρ_g : grout density
- Q: grout flow rate
- M: number of nozzles
- d: diameter of nozzles
- v: monitor lifting rate

Equation 3-9

$$v_n = (Q/n)/A_n$$

Where,

- n: number of nozzles
- A_n : cross-sectional area of the nozzle ($= \frac{1}{4} \pi d_n^2$)

Equation 3-8 has advantages over the current definition of the jetting energy (Equation 3-5) because it is accounting for grout density and nozzle diameter (which can be changed from case to case) rather than for grout pressure (which is almost constant).

I K Mihalis et al. (2004) derived a relationship between specific jet grouting energy E_s and soilcrete diameter based on Equation 3-10 (Figure 3-50). Based on their results, the successful execution of different jet grouting systems can be done within the following specific energy ranges: single fluid jet grouting 17 MJ/m and 30 MJ/m; double fluid jet grouting 40 MJ/m and 80 MJ/m; triple fluid jet grouting: not exceeding approximately 130 MJ/m. However D. a. Bruce (1994) stated that the typical range of specific energy for double and triple fluid jet grouting is 8 to 110 MJ/m and 9 to 200 MJ/m, respectively.

Equation 3-10

$$E_s = 0.0101 \times D^{2.02}$$

T. S. Lee et al. (2005) drew a relationship between jet grouting specific energy and jet grouting operational parameters using the equation below. For simplicity of calculation, the contribution of the compressed air is neglected.

Equation 3-11

$$E_j \left(\frac{\text{MJ}}{\text{m}} \right) = \frac{P_w Q_w + P_g Q_g}{V_t}$$

Where P_w & P_g = water and grout pressures in MPa
 Q_w & Q_g = water and grout flow rates in m^3/hour
 V_t = withdrawal rate (meter/hour)

Tsuboi et al. (2007) developed a relationship between cutting distance and jet grouting specific energy (Figure 3-51).

3.9.1.2. Other empirical methods

Without considering any type of soil or jet grouting system, Kanematsu (1980) proposed that the soilcrete diameter is around 300 times of nozzle diameter (in meters).

H. Yoshida et al. (1989) conducted an investigation the effect that water jet pressure and flow rate factors have on the time and cutting distance of the jet through loose sandy soil. Three pressure values of 3800, 5200, and 6600 psi were used with three flow rates of 75, 150, and 300 l/min. They used a steel tank with eight vibration sensors attached to the steel net. The time was recorded using the vibration caused by the water jet. Figure 3-52 illustrates the relationship between nine pressure-flow rate combinations. Based on the figure, the equation below was derived to correlate the relationship between cutting distance, pressure, flow rate, and time.

Equation 3-12

$$T = 31.2 \times L^{2.21} \times P^{-1.72} \times Q^{-1.88}$$

Where: T = jetting time (sec),
L = distance from nozzle to the measurement point (cm),
P = dynamic pressure of water jet (MPa), and
Q = discharge flow rate of water jet (lit/min).

Equation 3-12 shows that the flow rate influence on the cutting distance is much greater than the pressure. Equation 3-12 can be used to calculate the cutting distance for any pressure and flow rate with known time (Figure 3-53). H. Yoshida et al. (1989) also found that by doubling the jetting energy, the cutting distance and area increase by a factor of 1.8 and 3.24, respectively. Energy increase can be achieved by increasing P and/or Q; however an increase in Q has a greater effect on the increase of the cutting distance.

R. D. Essler (1995) emphasized that soilcrete diameter depends on both the input jetting energy and the ability of the ground to be eroded. Equation 3-13 was suggested to calculate jetting's volume of soil cut per minute.

Equation 3-13

$$E = 7.85 \times L \times D^2$$

Where, E: the volume of cut per minute (liter)
 L: lift speed (cm/min)
 D: soilcrete column (m)

For a given energy and the same soil type, the soilcrete diameter has the below (Equation 3-14) relationship with the withdrawal rate. This relationship is shown in Figure 3-56. Figure 3-54 shows this relationship for different values of E. In all cases, E is relative to the site and specific energy. Only experience allows the jet grout designer to estimate E for a particular soil type. However, implementing a number of trial jet grouting columns with varying withdrawal rates can develop the same curve presented in Figure 3-55.

Equation 3-14

$$D = \text{constant} \times \sqrt[2]{L}$$

M. Shibazaki and Yoshida (1997) carried out an experiment using a triple fluid jet grouting system to build columns with diameters more than five meters, and proposed an empirical relationship to predict the soilcrete diameter based on the experimental results.

Equation 3-15

$$R = (4.95 \times K \times P_{\text{grout}}^{-1.4} \times FR^{-1.6} \times N^{-0.2} \times v_n^{-0.3}) - 0.7$$

Where, R: column radius (m)
 K: a constant related to jetting liquid (2.5 for cement slurry and 1.0 for water)
 P_{grout} : discharge pressure (kg/cm²)
 FR: flow rate (l/min)
 N: represents the number of passes
 v_n : tangential velocity at a nozzle outlet (m/s)

M. Shibazaki and Yoshida (1997) also proposed the ranges of parameters on which Equation 3-15 can rely, which are:

$$200 \leq P_{\text{grout}} \leq 500 \text{ kgf/cm}^2; 70 \leq \text{FR} \leq 300 \text{ l/min}; 1 \leq N \leq 20; 0.1 \leq v_n \leq 0.2 \text{ m/s}.$$

P. Croce & Flora (1998) proposed the equation shown below to calculate the soilcrete diameter created by single fluid jet grouting in pyroclastic soils.

Equation 3-16

$$D = 2 \times \left(\frac{\alpha \cdot V_j}{\pi[1 - (1 - \beta) \times (1 - n)]} \right)^{0.5}$$

Where, V_j : injected grout volume per unit length
 n : initial soil porosity
 α, β : coefficients related to percentage of grout retained by the subsoil and the percentage of soil removed by jet action, respectively.

Mitsuhiro Shibazaki (2003) proposed an empirical equation, Equation 3-17, to calculate soilcrete diameter. The experiment was performed under a jetting pressure of 30MPa and a flow rate of 0.3 m³/min in loose sandy soil.

Equation 3-17

$$L_m = K \times P^\alpha \times Q^\beta \times N^\gamma / V_n^\delta$$

Equation 3-18

$$V_n = R_m \times R_s / 60$$

Where, L_m : the radius of influence, m
 K : a coefficient of the ground from field data, dimensionless = 0.315
 P : the jetting pressure, MPa
 Q : the jetting flow rate, m³/min
 N : the number of repetitions, dimensionless
 V_n : the nozzle movement velocity, m/s
 α : empirical coefficients from field data, dimensionless = 0.003

β : empirical coefficients from field data, dimensionless = 2.186

γ : empirical coefficients from field data, dimensionless = 0.135

δ : empirical coefficients from field data, dimensionless = 0.198

R_m : the external radius of the monitor, m

R_s : the rotational speed, rpm

Equation 3-17 shows the effect of the different parameters on soilcrete diameter. It can be understood that flow rate has the biggest influence on diameter. Theoretically doubling the flow rate can increase the diameter 355% (Ji 2008). Value K is based on the soil type and may vary from one site to another. Therefore, an in-situ trial test must be carried out to calibrate this value; direct calculating of the diameter may lead to inaccurate results. If jet pressure and flow rate are expressed in terms of the nozzle diameter and jet velocity, Equation 3-17 can be rewritten as Equation 3-19 (Ji 2008).

Equation 3-19

$$L_m = 0.124 \times \rho_f \times d_0^{4.372} \times v_0^{2.192} \times N^{0.135} / V_n^{0.198}$$

Where,

d_0 : nozzle diameter

v_0 : initial jet velocity

ρ_f : density of injected fluid

Chu E Ho (2007) and Chu E Ho (2005) described a mathematical model for a single fluid system of the jet grouting process using physical modeling of jet grouting, fundamental theories of jet hydrodynamics, and soil mechanics. He proposed to calculate the erosion distance using Equation 3-20 and Equation 3-21. The equations showed good results for clays, silty clays and cemented silts, however the results for silty sands were conservative.

Equation 3-20

$$\frac{l_j}{d_n} = 6.25 \sqrt{\frac{(P_i - P_s)}{q_{bu}}}$$

Equation 3-21

$$D = 2l_j + d_m$$

Where,

- l_j : maximum jet cutting distance from nozzle
- d_m : diameter of jetting monitor
- D: diameter of jetting column
- d_n : nozzle diameter
- P_i : pressure at nozzle inlet
- P_s : ambient pressure at nozzle outlet
- q_{bu} : ultimate soil bearing resistance = $N_c S_u$
- s_u : undrained shear strength
- N_c : bearing capacity term corresponding to failure condition at jet tip (=2.4 for cohesive soil)

To measure the undrained shear strength, the direct measurement methods are more amenable than the indirect methods such as the plasticity index and liquidity index. However for medium stiff to stiff cohesion soil, undrained shear strength can be calculated using $S_u(\text{kPa}) = 4.4N$, where N is the standard penetration blowcount (SPT). Soil bearing resistance of cohesionless soils in jet excavation is about $q_{bu} = 12N$.

Equation 3-20 has been derived based on a single fluid jet grouting system. However, Chu E Ho (2011) and Chu E Ho (2009) has extended his research to derive another equation for a triple fluid jet grouting system to calculate the cutting distance of a high velocity water jet shrouded with compressed air jet. Equation 3-22 is proposed to calculate the cutting distance of triple fluid jet grouting in cohesive soils where the ultimate bearing resistance of soil is $q_{bu} = 2.4S_u$.

Equation 3-22

$$\frac{l_j}{d_n} = 6.25(1 + M) \sqrt{\frac{(P_i - P_s)}{q_{bu}}}$$

Where, $M = 3\lambda$, value M should be calibrated using a full-scale trial jet grouting test. It has been found to be 1.6 for normally consolidated marine clay

$$\lambda = u_0/V_0$$

u_0 : velocity of ambient medium

V_0 : exit velocity of central jet

Modoni et al. (2006) proposed a complete theoretical model to calculate the radius of the soilcrete in three different soil types, namely granular soils including gravels and sands and cohesive or clayey soils. They assumed that jet propagation is taking place in two steps: one from the nozzle to the soil face, which is the space between the monitor and the soil; and one through the soil skeleton. Based on their model, the maximum radius of soilcrete created by the single fluid jet grouting system in granular (gravel and sand) and cohesive (clay) soils can be calculated using Equation 3-23 and Equation 3-24, respectively. For a detailed description of assumptions and considerations, it is recommended to refer to the original publication (Modoni, Croce, and Mongiovi 2006).

Equation 3-23

$$R = \frac{2 \times v_0 \times \Lambda \times C \times D_{\text{grout}}}{\sqrt{\frac{\Omega_s \cdot g \cdot N}{\gamma_f} \times \frac{c' + \sigma_z \cdot \tan(\varphi')}{1 + \Omega_s \cdot \left[\frac{\tan(\varphi')}{2} \right]}}}$$

Equation 3-24

$$R = \frac{2 \times v_0 \times \Lambda \times C \times D_{\text{grout}}}{\sqrt{\frac{\Omega_c \cdot g \cdot N \cdot c_u}{\gamma_f}}}$$

Where, v_0 : initial speed of the jet threads (immediately after the nozzle)

Λ : a coefficient (experimentally quantified) related to the nozzle shape that affect the attenuation of the fluid velocity along the jet axis (x)

$C = \sqrt{\xi}/2$ where $\xi = v_x/v_{x\text{max}}$ which represent a fraction of the maximum velocity of the jet at distance x from the nozzle

v_x : mean velocity of the jet at distance x

$v_{x\max}$: represent the respective maximum velocity

D_{grout} : nozzle diameter

Ω_s and Ω_c : dimensionless parameter accounting for energy dissipation of the injected fluid on granular and cohesive soils respectively

g : gravitational acceleration

N : turbulent kinematic viscosity ration of injected uid and water ($N = \epsilon_f / \epsilon_w$)

γ_f : unit weight of the injected fluid

c' and ϕ' : effective cohesion and friction angle of the soil, respectively

c_u : undrained soil cohesion

σ_z : initial vertical overburden stress

Ji (2008) carried out a limited width tank experiment on sandy soil to understand the mechanism of interaction between injected fluid and soil through visual observation in the single fluid jet grouting system. The existence of both seepage and erosion at the jet/soil interface and the defined influence radius as the movement of erosion front was reported. Hydrodynamic characteristics of the jet and effect of spoil backflow, as well as the effect of other parameters such as surrounding fluid properties, nozzle diameter and flow conditions, were taken into consideration. In these models, the interaction of jet/soil at their interface was taken into account as an important parameter to define the cutting distance. It is assumed that the soil fails where the jet pressure overcomes the soil strength, and therefore the radius of influence is the distance where jet pressure becomes equal to soil resistance. Ji (2008) proposed that there were two factors that control the ultimate eroding distance of the jet. One is soil resistance against the jet represented by horizontal effective stress, and the second is the frictional loss of the backflow. Two limiting conditions were imposed to predict the soilcrete diameter (Figure 3-57). The smaller number is determined as the column diameter.

Equation 3-25

$$\sigma'_h = \frac{1}{2} \rho_f v_L^2 \quad \text{or} \quad v_L = \sqrt{\frac{2\sigma'_h}{\rho_f}}$$

Equation 3-26

$$\frac{\Delta P}{L} = \frac{32\mu_{sp}v_{sp}}{D_h^2}$$

Equation 3-27

$$R_1 = \frac{v_0 x_c}{v_L} = \frac{v_0 x_c}{\sqrt{\frac{2\sigma'_h}{\rho_f}}}$$

Equation 3-28

$$(P_p + \Delta P_s R_2) - \frac{1}{2} \rho_f \left(\frac{v_0 x_c}{R_2} \right)^2 = 0$$

Where,

σ'_h : horizontal effective stress, Pa

v_L : critical jet velocity, m/s

ρ_f : density of injected fluid, kg/m³

ΔP : pressure drop due to friction, Pa

L: length of the backflow, m

v_{sp} : backflow velocity of the spoil material, m/s

D_h : hydraulic diameter of the backflow cross-section, m

v_0 : initial jet velocity at nozzle exit, m/s

x_c : length of the initial region, m

R_1 : column size determined from zero effective stress, m

P_p : pressure loss due to friction in borehole, Pa

ΔP_s : pressure loss per unit length of flow due to friction in ground, Pa

R_2 : the column size determined from pressure losses in backflow, m

Carletto (2009) observed that soilcrete diameter is affected by both the jet grouting energy and soil resistance, and tried to simplify the equations of Modoni et al. (2006). The manuscript was written in Italian and it is recommended to refer to the original publication for a detailed description of the theory.

Nikbakhtan and Ahangari (2010) developed empirical relationships between soilcrete diameter with withdrawal and rotational speed, w/c ratio, and grout pressure. Figure 3-58, Figure 3-59, and Figure 3-60 show that with increasing grout pressure and w/c ratio, the diameter increases logarithmically; and with increasing withdrawal and rotational speed, the diameter decreases. They also concluded that diameter is more sensitive to w/c ratio than other parameters.

A. G. Malinin and Gladkov (2011) developed the Ischebek relationship to calculate the soilcrete diameter based on the operational parameters (Equation 3-29).

Equation 3-29

$$D = \sqrt[A]{\frac{PQ}{BV}}$$

Where, P: the injection pressure in MPa,
 Q: the flow rate in m³/sec,
 V: the rate of ascent of the monitor in m/sec,
 A and B: empirical coefficients dependent on the properties of the soil.

Equation 3-30

$$A(c) = 5.7 \times c^{-0.25}$$

Equation 3-31

$$B(c) = 11.2 \times c^{0.4}$$

Where, c: cohesion of the soil in kPa.

Z. F. Wang et al. (2012) developed a relationship (Equation 3-32) between important jet grouting parameters and soil properties to calculate soilcrete diameter based on the kinematic flow theory.

Equation 3-32

$$R = \frac{d_0}{2} + b \cdot \frac{4FR}{M\pi D_{grout} \sqrt{UCS/p_a}}$$

Where,

- R: radius of the soilcrete column
- d_0 : rod diameter
- FR: flow rate of the fluid injected
- M: number of nozzle on the rod
- D_{grout} : nozzle diameter
- UCS: UCS of soilcrete
- p_a : atmospheric pressure
- b: a parameter related to the soil characteristics, (=1.2 to 2.0 for very soft clay; 0.75 to 1.4 for clay silt; 0.25 to 0.75 for sand)

Equation 3-32 shows that soilcrete diameter is related to its strength which means this approach can be used after the creation of the soilcrete column and when the UCS of the soilcrete column is known.

Tinoco, Gomes Correia, and Cortez (2011a), Tinoco (2012), Tinoco, Gomes Correia, and Cortez (2012), and Tinoco, Gomes Correia, and Cortez (2011b) proposed a new approach to predict UCS, diameter, and deformability properties of soilcrete based on data mining techniques. They showed that data-driven models are able to learn the complex relationships between soilcrete properties and other important factors. Based on their analysis, it can be concluded that the method is highly related to the data used to train the model. Their results precisely show in some cases that the prediction was less accurate which can be explained by the fact that the database included just a few records in that particular range of data. Also the applicability of the model was not assessed in the real jet grouting project.

B. Nikbakhtan et al. (2014a) proposed a mathematical model based on the sum of squared-deviations (SSD) method to estimate the diameter of soilcrete created by the triple fluid system jet grouting. Before using any mathematical models, they divided those important parameters into two main categories. The first group includes operational parameters such as water pressure (P_w), grout pressure (P_g), air pressure (P_a), lifting speed (L_g), rotating speed (R_g) and grout density (γ_g). The second group includes physical and mechanical properties of the in-situ soil such as soil permeability (k), cohesion (c), soil conductivity (C_g) and soil groutability ratio (G_R). Equation 3-33 was proposed to calculate the diameter of soilcrete. B. Nikbakhtan et al. (2014a) also mentioned that water pressure, grout pressure, air pressure, soil permeability

coefficient, soil conductivity coefficient and groutability rate have direct impact on the soilcrete column diameter. They also pointed out that other parameters such as lifting speed, rotating speed, grout density and cohesion have a reverse relationship with soilcrete diameter changes.

Equation 3-33

$$D = A. (L_s^{-1})^a. (R_s^{-1})^b. (P_w)^c. (P_a)^d. (P_g)^e. (\gamma_g^{-1})^f. (K)^g. (C^{-1})^h. (G_R)^i. (C_g)^j$$

Equation 3-34

$$C_g = \frac{(D_{10})^2}{D_{90} \times D_{60}}$$

Equation 3-35

$$G_R = \frac{D_{10}}{d_{100 \text{ cement}}}$$

Where D is diameter (cm) of the soilcrete and A, a, b, c, d, e, f, g, h, i and j are 7.459×10^{-10} , -0.1353, 0.3363, 0.4678, -0.2914, -0.0138, -2.1720, -0.0275, 1.6572, 3.2038, and -1.8489, respectively. According to the results, Equation 3-33 can predict the diameters with an error range of 3 to 20%; however the theoretical assumptions will be in agreement with the mathematical relationship when all power coefficients are positive but a, d, e, f, g, and j coefficients are negative. Although a, d, e, and g are small and can be neglected, there is still an issue with the f and j, which means the relationship between soil conductivity and grout density does not match the literature and field observations. B. Nikbakhtan et al. (2014a) have concluded that mathematical modeling might have shortcomings preventing it from fitting a perfect relationship for all parameters.

B. Nikbakhtan, Apel, and Ahangari (2014a) attempted to estimate the diameter of soilcrete using artificial neural network (ANN) methods and develop optimal neural network models to reduce, as much as possible, the need for trial jet grouting (Figure 3-61). A precise set of data from reliable resources and literature was collected to create a database with a wide range of input parameters to train the ANN model. They designed and tested 125 ANN models with different numbers of hidden layers, nodes in each layer, and training epochs. It was observed that with

increasing the number of the hidden layers and neurons, the ANN model fits much better with the training data. However, this may overfit the model. Results revealed that the ANN model was very successful in learning the complex relationships between the operational parameters and soilcrete diameter. The optimum model was able to predict the theoretical diameter of the soilcrete with an error rate of 10%. However, it was concluded that the prediction result can be highly related to the data used to train the model.

3.9.2. Methods to calculate soilcrete strength

The mechanical properties of soilcrete have generally been evaluated with the UCS test, and seldom with the direct shear (Mongiovi, Croce, and Zaninetti 1991; P. Croce et al. 1994), and/or triaxial test (P. Croce and Flora 1998). Expected soilcrete uniaxial compressive strength is summarized in Table 3-9 from different publications.

Nishimatsu (1972) developed the relationships shown below to obtain cohesion (c) and friction angles (ϕ) from UCS for soilcrete.

Equation 3-36

$$c = \frac{\sigma_c \sigma_t}{2[\sigma_t(\sigma_c - 3\sigma_t)]^{0.5}}$$

Equation 3-37

$$\tan\phi = \frac{\sigma_c^2 - 4c^2}{4\sigma_c \times c}$$

Where, σ_c : UCS
 σ_t : brazilian indirect tensile strength

Unconfined compressive strength of the soil increases with increasing cement content (J.K Mitchell, Veng, and Monismith 1974):

Equation 3-38

$$q_u = q_u(t_0) + K \log t/t_0$$

Where: $q_u(t)$ = Unconfined compressive strength at t days, kPa
 $q_u(t_0)$ = Unconfined compressive strength at t_0 days, kPa
 A_w = Cement content percent by mass,
 K = 480 A_w for granular soils and 70 A_w for fine grain soil
 t = Curing time

Satio, Kawasaki, Niia, Babasaki, and Miyata (1980) calculated the shear strength of the soilcrete using the equation below:

Equation 3-39

$$\tau_o = 0.53 + 0.37(\text{UCS}) - 0.0014(\text{UCS})^2, \quad \left(\text{UCS} \leq 60 \frac{\text{kg}}{\text{cm}^2} \right)$$

Where, τ_o : 28-day shear strength (kg/cm^2) obtained by direct shear test with zero normal stress

UCS: 28-day unconfined compressive strength (kg/cm^2)

Andromalos and Gazaway (1989) presented a case history of jet grouting on silty fine-to-medium sand soils with standard penetration test N-values of 10 to 40 to evaluate different grout mixes to determine the diameter of soilcrete columns. Laboratory results of compressive strength versus specimen age with two different w/c ratios of 1.5:1 and 2:1 and two different lifting speeds of 0.6 and 1.0 ft/min are presented in Figure 3-62. Figure 3-62 shows that lower w/c ratio and lifting speed produce higher compressive strength.

D.A. Bruce & Bruce (2003) reported that tensile strength of soilcrete is between 8 to 14% of its UCS.

J. A. B. Tinoco (2012) summarized the equations below to calculate the UCS of soilcrete based on different parameters:

- 1) P. Croce & Flora (1998) carried out a single fluid jet grouting test on pyroclastic soil with w/c ratio of one and grouting pressure of 45 MPa and withdrawal step of 40mm. They

correlated the UCS of soilcrete with its dry unit weight ($\gamma_d, \text{kg/m}^3$). Equation 3-40 ($R^2 = 0.70$) presents the correlation .

Equation 3-40

$$\text{UCS} = 2933 \times \gamma_d - 32427$$

- 2) F. H. Lee et al. (2005) proposed Equation 3-41 to calculate soilcrete strength in cohesive soil for a given type of cement.

Equation 3-41

$$\text{UCS} = \text{UCS}_0 \times \frac{e^{m \times (S/C)}}{(W/C)^n}$$

Where, W/C: water/cement ratio
 S/C: soil/cement ratio
 UCS_0 (KPa), m and n are experimental constants.

- 3) Narendra et al. (2006) proposed Equation 3-42 to calculate the strength of soilcrete particularly in a laboratory:

Equation 3-42

$$\text{UCS} = \frac{A}{B \frac{W_c}{C}}$$

Where, A: a coefficient related to the type of clay, liquidity index and age of the mixture
 W_c/C : the soil-water/cement ratio
 B: an empirical constant which is independent of the type of clay (1.22 to 1.24)

- 4) S. Y. Liu et al. (2008) introduced the total w/c ratio (R_m) which is in good correlation with the UCS of marine clay stabilized with cement (Figure 3-63), and is defined as Equation 3-43.

Equation 3-43

$$R_m = \frac{m_w}{m_c}$$

Where, m_w : weight of water in soilcrete including water in the original soil and grout
 m_c : weight of cement in dry state

S. Y. Liu et al. (2008) also summarized the following relationships proposed by other authors to predict the UCS of the soilcrete:

- 1) Nagaraj and Miura (1996): calculated UCS of four different inland clays with different liquid limits.

Equation 3-44

$$\frac{UCS_t}{UCS_{14}} = a + b \cdot \ln(t)$$

Where, UCS_t : UCS at age t (days)
 UCS_{14} : UCS at 14-days curing time with initial water content as much as liquid limit of soil
 $a = -0.20$ for inland clays (and 0.190 for Ariake clays based on (Yamadera, Nagaraj, and Miura 1997))
 $b = 0.458$ for inland clays (and 0.299 for Ariake clays based on (Yamadera, Nagaraj, and Miura 1997))

- 2) (Horpibulsuk, Miura, and Nagaraj 2003):

Equation 3-45

$$\frac{UCS_{(\frac{W_c}{C})_{1,t}}}{UCS_{(\frac{W_c}{C})_{2,28}}} = \begin{cases} 1.24 [(\frac{W_c}{C})_2 - (\frac{W_c}{C})_1] \times (0.038 + 0.281 \cdot \ln(t)), & LI = 1.0 \sim 2.5 \\ 1.24 [(\frac{W_c}{C})_2 - (\frac{W_c}{C})_1] \times (-0.216 + 0.342 \cdot \ln(t)), & LI > 2.5 \end{cases}$$

Where, t: curing period in days
 $UCS_{(\frac{w_c}{c})_1,t}$: UCS at $(\frac{w_c}{c})_1$ for the curing period of t days
 W_c : water content
 C: cement content
 $UCS_{(\frac{w_c}{c})_2,28}$: UCS at $(\frac{w_c}{c})_2$ for the reference curing period of 28 days
 LI: liquidity index

Nikbakhtan and Osanloo (2009) discussed the effects of grout pressure and grout flow on soil and soilcrete properties. They carried out trial jet grouting on six columns using the triple fluid system. After 32 days, the perimeter of columns was dug out to evaluate soilcrete diameters and properties using laboratory uniaxial compressive, triaxial compressive, direct shear, brazilian, and Schmidt hammer tests (Figure 3-64). According to the laboratory results, by increasing grout pressure and flow rate, the UCS of soilcrete increases logarithmically (Figure 3-65 and Figure 3-66). The results are presented in Table 3-10.

Nikbakhtan and Ahangari (2010) developed empirical relationships between soilcrete UCS and its diameter with withdrawal and rotational speed, w/c ratio, and grout pressure. For this purpose, three 5.0m-depth columns with various operational parameters were jet grouted in fine-grained clayey soil (Figure 3-67). To evaluate the effect of specific operational parameters on soilcrete properties, all other parameters such as air pressure, airflow, water pressure, water flow, and number and diameter of nozzles were held constant, and then the grout pressure, w/c ratio, withdrawal, and rotational speeds were changed. After the trial jet grouting, the perimeter of the columns was dug out to measure the diameter of the columns. Also, the samples were taken for laboratory UCS tests. The results showed that increasing grout pressure and w/c ratio increases the UCS logarithmically (Figure 3-68 and Figure 3-69). Also, increasing the withdrawal and rotational speed, decreases the UCS (Figure 3-70). Nikbakhtan and Ahangari also concluded that the UCS of soilcrete is more sensitive to w/c ratio than other parameters.

S. L. Shen et al. (2010) suggested multiplying the degree of mixing uniformity (D_u) with strength from a standard laboratory mixing test to calculate the strength of the soilcrete. The degree of mixing uniformity is calculated using Equation 3-46 (adopted from (Tinoco 2012)).

Equation 3-46

$$D_u = \frac{N_1}{N_2} \times 100\%$$

Where, N_1 : number of collected samples
 N_2 : number of samples with an pH value higher than critical value.

In addition to all empirical relationships to calculate the UCS of the soilcrete, Tinoco (2012) summarized two EC2 (CEN 2004) and MC90 (CEB-FIP 1991) regulations to calculate mechanical properties of the concrete.

- 1) Based on EC2 (CEN 2004), the strength of concrete and its stiffness are calculated using Equation 3-47 and Equation 3-48.

Equation 3-47

$$f_{cm}(t) = e^{\left(s \cdot \left[1 - \left(\frac{28}{t}\right)^a\right]\right)} \cdot f_{cm}$$

Where, $f_{cm}(t)$: strength at age t
 f_{cm} : 28-day strength of the mixture
s: a coefficient related to cement type
t: age of the mixture
a = 1/2 for concrete (the same number can be adapted to soilcrete)

Equation 3-48

$$E_{cm}(t) = \left(e^{\left(s \cdot \left[1 - \left(\frac{28}{t}\right)^a\right]\right)} \right)^b \cdot E_{cm}$$

Where, $E_{cm}(t)$: stiffness at age t
 E_{cm} : 28-day stiffness of the mixture
s: a coefficient related to cement type
t: age of the mixture

a and b: coefficients to be adjusted using JG data

- 2) Based on MC90 (CEB-FIP 1991) concrete stiffness can be calculated using Equation 3-49.

Equation 3-49

$$E_{ci}(t) = \left(e^{(s \cdot [1 - (\frac{28}{t})^a])} \right)^b \cdot \alpha_E \cdot E_{c0} \cdot \left(\frac{f_{cm}}{f_{cm0}} \right)^c$$

Where, $E_{ci}(t)$: stiffness at age t
s: a coefficient related to cement type
t: age of the mixture
 α_E : a coefficient depends on type of aggregate (=0.99 for soil clay)
 $f_{cm0} = 10$ MPa
 f_{cm} : 28-day stiffness of the mixture
 E_{c0} : was determined for each formulation based on 28-day stiffness
a, b and c: coefficients to be adjusted

3.9.3. Composition of soilcrete vs its diameter and strength

Aschieri, Jamiolkowski, and Tornaghi (1983) suggested a formula to estimate the unit weight of the soilcrete γ_{sc} using a cement/water ratio (C/W) and soil/water ratio (S/W) based on the 100 jet grouting cored samples, in which the specific gravity of in situ soil and cement particles was assumed to be 2.75 and 3.06, respectively. Another statistical relationship between C/W and the long-term strength of soilcrete R was suggested (Alsayyedahmad 1992).

Equation 3-50

$$\gamma_{sc} = \frac{1 + S/W + C/W}{0.1 + 0.37(S/W) + 0.33(C/W)}$$

Equation 3-51

$$C/W = R^{1/2}$$

Where S = mass of soil solids,
 W = total mass of water in the soilcrete,
 C = total mass of cement in the soilcrete, and
 R = long term strength in kPa.

With substituting Equation 3-51 into Equation 3-50:

Equation 3-52

$$\gamma_{sc} = \frac{1 + S/W + 0.447(R^{1/2})}{0.1 + 0.37(S/W) + 0.15(R^{1/2})}$$

De Paoli et al. (1989) calculated the composition of the jet grouted soil in terms of the cement (C), dry soil (S), and total water (W) contained in the volume of the treated soil, according to the general expression of bulk density (Equation 3-53) in which assumes full saturation and strength (R) mainly depends on the c/w ratio.

Equation 3-53

$$\gamma_b = \frac{1 + \frac{C}{W} + \frac{S}{W}}{1 + \frac{\bar{W}}{G_C} + \frac{\bar{W}}{G_S}}$$

Where, G_C: absolute specific gravity of cement
 G_S: absolute specific gravity of soil particles

The UCS of soilcrete for cement/peaty soil mixes at 120-days can be calculated using Equation 3-54.

Equation 3-54

$$R = 15 \times \left(\frac{C}{W}\right)^3, (\text{MPa})$$

Equation 3-55

$$\frac{C}{W} = 0.405 \times R^{1/3}$$

P. Croce, Chisari, and Merletti (1990) calculated the density of water-cement (grout) mix based on Equation 3-56.

Equation 3-56

$$\rho_g = \frac{1 + W}{1/\rho_c + W/\rho_w}$$

Where, ρ_g : density of grout (=1500 kg/m³ for typical grout type)
 ρ_c : density of cement (=3150 kg/m³ for typical grout type)
 ρ_w : density of water (=1000 kg/m³ for typical grout type)
W: water/cement ratio (=1 for typical grout type)

Khasin (1996) developed a series of equations to calculate the composition of the soilcrete column and its diameter.

Equation 3-57

$$V_{sr} = V_{cl} \left(1 - \frac{1}{A - n + w_0 + 1} \right)$$

Equation 3-58

$$V_g = V_{cl} \left(\frac{A}{A - n + w_0 + 1} \right)$$

Equation 3-59

$$Q_g = V_{cl} \left(\frac{V}{H} \right) \left(\frac{A}{A - n + w_0 + 1} \right)$$

Equation 3-60

$$A = \frac{C(1 - n + w_0)(1/\gamma_c + w/c)}{1 - C(1/\gamma_c + w/c)}$$

Equation 3-61

$$d = D \sqrt{1 - \frac{1}{A - n + w_0 + 1}}$$

Where,

- V_{sr} : volume of soil subject to removal during formation of the column
- V_g : volume of grout for forming the column
- Q_g : flow rate of grout delivery
- V_{cl} : volume of soilcrete column
- $A = V_g/V_s$: weight content of cement (C) in a unit volume of soilcrete column
- V_s : volume of soil
- n : undisturbed porosity
- w_0 : volume moisture content of soil (in completely saturated soil $n=w_0$)
- v : speed of longitudinal (withdrawal speed or lifting rate)
- H : length of the column which the grout is delivered
- γ_c : density of cement
- w/c : water/cement ratio of the grout
- d : drill hole diameter
- D : soilcrete diameter

Kauschinger et al. (1992) proposed equations for single fluid jet grouting to calculate the diameter of the soilcrete based on the mass balance theory.

Equation 3-62

$$D = \sqrt{\frac{W_t^c}{\frac{\pi}{4} \times \Delta Z \times \gamma_t^c}}$$

Equation 3-63

$$W_t^c = W_{\text{cement}}^c + W_{\text{water}}^c + W_{\text{soil}}^c$$

Equation 3-64

$$W_{\text{soil}}^c = \left(\frac{\pi D^2}{4} \Delta Z \right) \left(\frac{\gamma_t^{\text{in situ}}}{1+w} \right) - \left(\frac{\gamma_t^o(\gamma_w)}{1 + \frac{\left(\frac{C}{W}\right)^e}{\left(\frac{S}{W}\right)^e} + \frac{1}{\left(\frac{S}{W}\right)^e}} \right) \left(\frac{Q^{\text{ejected}} \times \Delta Z}{L} \right)$$

Equation 3-65

$$W_{\text{cement}}^c = \left(\frac{G_c(\gamma_w)}{1 + G_c \left(\frac{W}{C}\right)^{\text{grout}}} \right) \left(\frac{Q^{\text{injected grout}} \Delta Z}{L} \right) - \left(\frac{\gamma_t^o(\gamma_w)}{1 + \frac{\left(\frac{S}{W}\right)^e}{\left(\frac{C}{W}\right)^e} + \frac{1}{\left(\frac{C}{W}\right)^e}} \right) \left(\frac{Q^{\text{ejected}} \Delta Z}{L} \right)$$

Equation 3-66

$$W_{\text{water}}^c = \left(\frac{w\pi D^2}{4} \right) (\Delta Z) \left(\frac{\gamma_t^{\text{in situ}}}{1+w} \right) + \left(\frac{W}{C} \right)^{\text{grout}} \left(\frac{G_c \gamma_w}{1 + G_c \left(\frac{W}{C}\right)^{\text{grout}}} \right) \left(\frac{Q^{\text{injected grout}} \Delta Z}{L} \right) - \left(\frac{\gamma_t^o(\gamma_w)}{1 + \left(\frac{C}{W}\right)^e + \left(\frac{S}{W}\right)^e} \right) \left(\frac{Q^{\text{ejected}} \Delta Z}{L} \right)$$

Where,

D: soilcrete column diameter

W_t^c : total weight of column

W_{cement}^c : weight of cement in column

W_{water}^c : weight of water in column

W_{soil}^c : weight of soil in column

ΔZ : height of soilcrete column

γ_t^c : total unit weight of soilcrete column

w: in-situ water content

$\gamma_t^{\text{in situ}}$: total unit weight of soilcrete column

L: lifting rate of monitor through height of ΔZ

$Q^{\text{injected grout}}$: flow rate of injected grout

G_c : 3.0 specific gravity of cement injected

$\left(\frac{W}{C}\right)^{\text{grout}}$: water/cement ratio of injected grout

γ_w : unit weight of water

γ_t^0 : density of the outflow

G_s : specific gravity of the soil

$\left(\frac{C}{W}\right)^e$: cement/water ratio of the ejected cutting (for sandy gravel soil it is equal to

$0.135q_u^{1/2}$

q_u : compressive strength of hardened soilcrete (kg/cm^2)

Q^{ejected} : flow rate of ejected cuttings

The composition of the soilcrete depends on the soil type and jet grouting system used. An accurate analytical calculation of exact soilcrete composition is not possible in practice because of the complex process of jet erosion, mixing, replacement, filling of pore spaces, and jet grouting parameters (P Croce and Flora 2000). On other hand, during the jet grouting there is also always a spoil material with unknown compositions (S. N. P. Coulter 2004). P Croce & Flora (2000) proposed Equation 3-67 to calculate the composition of the soilcrete based on conservation of the mass. The equation only calculates the composition of the cured soilcrete and thus does not consider any volume change due to bleed of water or contraction during the hardening.

Equation 3-67

$$V = \frac{\alpha}{\delta(n + \beta - n\beta)} V_j$$

Where,

V: soilcrete column volume per unit length

α : volumetric percentage of grout retained by the subsoil

δ : percentage of pores filled with grout (excluding the jet grouting in clean gravels, the pores can be assumed completely filled with grout $\delta=1$)

- β : volumetric percentage of soil removed by the jet action
- n: original soil porosity
- V_j : volume of injected grout per length of treatment.

(Kauschinger et al. 1992) suggested that the spoil material return, including grouted soil, ranged from 0 to 80% of injected grout volume. Generally, the percentage of spoil return is less than 50 with a typical value of 30. P Croce and Flora (2000) stated that complete retention, which means 0% outflow, could be expected in clean gravels where grout can permeate through the soil voids. They also reported that the grout volume was 60 to 80% of the total soilcrete column volume in the single fluid jet grouting system. With complete mixing ($\beta=1-\alpha$) within the column with original soil porosity of 0.35, 70 to 80% of the grout volume is retained. Complete mixing means the percent of grout retained within the column is equal to the percent of the soil retained in the column. P Croce and Flora (2000) also found that in single fluid jet grouting on sandy gravel and silt sand, the percentage of soil removal (β) varies between 30 to 60, and the percentage of grout retained (α) varies between 65 to 90.

3-10. Conclusion

Jet grouting method uses a high velocity hydraulic energy to first erode the soil and then replace it with different cementitious material based on a particular project goal. It can be used on a wide range of soil types and ground conditions for different mining and civil engineering applications. The method offers great flexibility for working conditions in selected intervals of soil layers or at very great depths. Such flexibility makes jet grouting an ideal ground modification technique. However, the understanding of the process is very limited because of its complex operation where jet erosion, mixing, replacement, and filling of pore spaces are all taking place at the same time. There is also always a spoil material return with unknown proportions of grout and soil. Properties and compositions of the soilcrete depend on the soil type and jet grouting operational parameters used. Hence, in practice, it is not possible to accurately calculate the exact soilcrete composition as well as its diameter and engineering properties. To understand and address the jet grouting process properly, the effect of different parameters on soilcrete properties have been discussed. A design approach of the jet grouting operation as well as some empirical and theoretical methods have also been presented. It is hoped that this will help the jet grouting

specialists to use these methods to initially evaluate their projects. It is important to emphasize that those methods are site-dependent and involve many limitations. It is strongly recommended to carry out laboratory formulation experiments with hand-mixed soilcrete samples to verify the values estimated by theoretical and empirical relationships. Trial jet grouting test columns should also be implemented in the field or by using a laboratory setup to validate hand-mixed experiment results and estimate operational parameter values for the main jet grouting operation in the field.

Table 3-1 Operational parameters of jet grouting systems and soilcrete properties (D. a. Bruce, 1994)

Jet Grouting Parameters		Single	Double	Triple
Pressure, MPa	Water Jet	N.A.	N.A.	30~55
	Grout jet	30~55	30~55	1~4
	Air Jet	N.A.	0.7~1.7	0.7~1.7
Flow, Lit/min	Water Jet	N.A.	N.A.	70~100
	Grout jet	60~150	100~150	150~250
	Air Jet	N.A.	1~3	1~3
Nozzles, mm	Water Jet	PW	PW	1.8~2.6
	Grout jet	1.8~3	2.4~3.4	3.5~6
Number of water nozzles		N.A.	N.A.	1~2
Number of grout nozzles		2-6	1-2	1
Water/Cement ratio of grout		0.8~2		
Cement content in soilcrete, Kg/m ³		400~1000	150~550	150~650
Rotating speed of monitor, rpm		10~30	10~30	3~8
Lifting speed of monitor, min/m		3~8	3~10	10~25
Diameter of Soilcrete, m	Coarse grain soil	0.5~1	1~2	1.5~3
	Fine grain soil	0.4~0.8	1~1.5	1~2
Resistance of Soilcrete, MPa	Sandy soil	10~30	7.5~15	10~20
	Clayey soil	1.5~10	1.5~5	1.5~7.5

Table 3-2 Triple fluid jet grouting equipment (Yahiro, Yoshida, and Nishi 1975)

Machine	Specification
Guide-hole drilling machine	Boring machine and auger chosen based on soil type.
High-pressure water pump	Plunger pump Outlet pressure: 200 ~ 700 kg/cm ² Discharge: 50 ~ 70 l/min
Air compressor	Outlet pressure: more than 3 kg/cm ² Discharge: more than 1 m ³ /min
Grout pump	Outlet pressure: less than 10 kg/cm ² Discharge: 100 ~ 150 l/min
Monitor	Triple pipe (water, air, and grout) Water jet nozzle diameter: 1.6 ~ 2.0mm Air nozzle: 1 ~ 2mm loop nozzle
Lift apparatus for monitor	Boring machine, Truck crane Uplift speed: 5 ~ 200 cm/min
other	Grout mixer, sand pump, air hose, casing pipe, water tank

Table 3-3 Super jet grouting, Super-Midi jet grouting, and X-jet grouting specifications (X-Jet 2002; Superjet 2004; Ji 2008)

Method	Super jet (Superjet 2004)	Super jet –Midi (Superjet 2004)	X-Jet (X-Jet 2002)
System	Modified double fluid system		Triple fluid
Injection direction	Two opposite direction		Cross-injection
Tube configuration	Triple rod	Double rod	Triple rod
Tube diameter (cm)	14.2	9.0	9.0
Drill hole diameter (cm)	25.0 ~ 35.0	15.0 ~ 25.0	14.2
Water pressure (MPa)	N.A.		40
Water flow rate (l/min)	N.A.		180
Air pressure (MPa)	0.7 ~ 1.05		0.6 ~ 1.05
Air flow rate (m ³ /min)	>10		6 ± 2
Grout pressure (MPa)	30		4 ± 1
Grout flow rate (l/min)	300×2=600	200×2=400	190 ~ 250 ¹
Withdrawal rate (min/m)	16	12	8, 16, 24 ²
Diameter (m)	5.0	3.5	2.5
Grouting depth (m)	30 (maximum 65)		60

Table 3-4 Sampling and testing methods of soilcrete properties quality control (Schaefer 1997)

Requirement	Sample Method(s)	Test Methods
Strength	Wet grab (in-situ) cast in to molds Cast in place plastic pipe retrieved after cure Core drilling	Unconfined Compression Triaxial Tension Spiriting tensile strength Direct Shear CPT (in-situ) if soft enough
Permeability	As above plus: Cast-in-Place Piezometer Drilled and cast Piezometer	Permeameter Rising or Falling Head (in-situ) Packer Testing

Table 3-5 Effect of jet grouting different parameters on soilcrete diameter and strength (Yahiro, Yoshida, and Nishi 1982)

Parameter	Sandy soil		Clayey soil	
	diameter	strength	diameter	Strength
Water pressure	Increase	N.A.	Increase	N.A.
Water flow	Increase	N.A.	Increase	N.A.
Grout pressure	None	N.A.	Increase	N.A.
Grout flow	None	Increase	Increase	Increase
Rotation speed	Increase	N.A.	Decrease	N.A.
Lifting speed	Decrease	N.A.	Decrease	N.A.

¹ depending on soil condition

Table 3-6 The most well documented jet grouting projects

Application	Related literature projects and research works
Acceptance and use of high-pressure water and jet grouting technique	(K.B. Andromalos and Gazawy 1986; Godfrey and JR 1987; Munfakh 1987; Gosaburo 1985; Pettit and Wooden 1988; B Nikbakhtan, Ahangari, and Rahmani 2010; B Nikbakhtan et al. 2009; S. Nikbakhtan, Nikbakhtan, and Rahmani 2008; B Nikbakhtan and Ghoshtasbi 2008; B Nikbakhtan and Pourrahimian 2006; B Nikbakhtan and Pourrahimian 2007; Guatteri; HBI et al. 1994; Tarricone 1994; Kenneth B Andromalos and Bahner 2003; “Victoria Station Upgrade Supplementary Environmental Statement: Technical Appendix G – Jet Grouting Trials Report” 2008; “GeoEng Consultants”; Kazemian and Huat 2009; Lunardi 1997; Tsuboi et al. 2007; Hong et al. 2002; Day, Zarlinski, and Jacobson 1997; Ganeshan and Yang 2009; Kwong, Sandefur, and Hashiro 2010; Mcgonagle et al. 2011; Lloret et al. 1991; Oteo and Sopena 1991; Li and Hu 2010; Passlick and Doerendahl 2006; Lai et al. 2010; Shao and Ivanetich 2010; I. H. Wong and Poh 2000; Cristelo, Glendinning, and Pinto 2011; Plescan and Rotaru 2010; J. L. Wang, Wang, and Wang 2009; Martin Ii et al. 2004; HBI 2004; G.K. Burke, Peterson, and Smith; Kazemian et al. 2010; “Specialist Grouting”; George K Burke 2004; Brill, Burke, and Ringen 2003; Duzceer and Gokalp 2003; Durgunoglu, Kulac, Yilmaz, et al. 2003; Pinto et al. 2003; Durgunoglu, Kulac, Oruc, et al. 2003; Foundations 2012; “Jet Grouting”; Keller; R. D. Essler 1995; Morey and Harris 1995; G K Burke, Cacoilo, and Chadwick 2000; Kazemian and Huat 2010; Khasin 1996; Olgun and Martin 2008; Y. S. Fang et al. 2006; J P Welsh 1998; Spagnoli 2008; Gemmi, Morelli, and Bares 2003; J.G. Wang et al. 1999; A. G. Malinin and Malinin 2007; R. Essler and Yoshida 2004; Saurer and Lesnik 2011; Lawrence and Gruner 1999; Kauschinger, Perry, and Hankour 1992)
Excavation Support Underpinning Structure Support	(Soranzo and Mazzalai 1986; G.K. Burke, Heller, and Johnsen 1989; Kenneth B Andromalos and Gazaway 1989; Babak Nikbakhtan and Nikbakhtan 2008; B. Nikbakhtan, Aghababaei, and Pourrahimian 2007; B Nikbakhtan, Pourrahimian, and Aghababaei 2007a; B Nikbakhtan, Pourrahimian, and Aghababaei 2007b; Guatteri; Pettit and Wooden 1988; Rosenbaum 1989; George K Burke, Johnsen, and Heller 1989; Kauschinger and Welsh 1989; “Lake Placid’s Luge Run Undergoes Jet Grouting” 1990; Viner and Wooden 1990; G.K. Burke and Meffe 1991; Joseph p. Welsh and Burke 1991; Parry-Davies et al. 1992; Kauschinger, Perry, and Hankour 1992; Koelling and Ringen 1992; Flick et al. 1992; G.K. Burke and Brill 1992; Moseley 1993; Scarborough, Boehm, and Brill 1993; HBI et al. 1994; Tarricone 1994; G. k. Burke and Koelling 1995; C. e. Ho 1995; Drooff, Furth, and Scarborough 1995; Pearlman 1998; Sheen 2001; C E Ho, Lim, and Tan 2002; Arora and Kinley 2011; Klein, Andromalos, and Trimble 2006; Haider and Byle 2000; Saglamer et al. 2002; Wei; Boehm 2004; J. Davie et al. 2003; Dash, Lee, and Anderson 2003; Rollins et al. 2010; C E Ho and Hu 2006; T. Hurley and Crockford 2010; J G Wang et al. 1998; Chu Eu Ho, Lim, and Tan 2005; Chu Eu Ho and Tan 2003; Meyers, Myers, and Petrasic 2003; Yilmaz et al. 2008; Alzamora, Wayne, and Han; C. e. Ho 2010; Boehm and Posey 2003; Senapathy, Davie, and Bohem 2003; Yang, Tan, and Leung 2011)
Cutoff walls and Groundwater Control	(B Nikbakhtan 2007; Guatteri; Pettit and Wooden 1988; Garner et al. 1989; Joseph p. Welsh and Burke 1991; Miyasaka 1992; Steiner, Schneider, and Cartus 1992; Koelling and Ringen 1992; G. k. Burke 1992; Moseley 1993; G. k. Burke and Brill 1993; HBI et al. 1994; Tarricone 1994; Joseph P Welsh and Burke 1995; G. k. Burke 1995; G. k. Burke and Koelling 1995; Tanaka and Yokoyama 2006; Cong-jiao, Shi-bao, and Feng-shan 2011; Poh and Wong 2001; Gropo Sembenelli and Sembenelli 1999; G K Burke 2007; Lewis and Taube 2003; Ayoubian and Nasri 2004; T. Hurley and Crockford 2010; P Croce and Modoni 2007)

<p style="text-align: center;">Tunneling Ground Stabilization Ground movement control</p>	<p>(Mussger, Koinig, and Reischl 1987; Langbehn 1986; Donald A Bruce, Boley, and Gallavresi 1987; Guatteri; Pettit and Wooden 1988; De Paoli, Tornaghi, and Bruce 1989; Stella et al. 1990; Viner and Wooden 1990; GALLAVRESI 1992; Flick et al. 1992; Moseley 1993; HBI et al. 1994; “Safety Issue Boosts Record Soft Ground Jet Grouting Job” 1994; Tarricone 1994; Edgerton, Berti, and Wong 1995; C. e. Ho 1995; Atwood and Lambrechts 1995; Raines and Honke 1996; S L Shen et al. 2009; Flora, Lignola, and Manfredi 2007; Raju and Yandamuri 2010; Vardar et al. 2005; Samtani and Alexander 2005; Vià, Marotta, and Peach 2005; Furth, Gordon, and Dobbels 2003; Yoshitake et al. 2004; J. R. Davie et al. 2003; T. M. Hurley 2004; Gazzarrini, Kokan, and Jungaro 2005; T. S. Lee, Murray, and Kiese 2005; Tonon 2011; YuLiang et al. 2011; Chen, Lim, and Furuhashi 2011; S. Coulter and Martin 2006; I K Mihalis, Tsiambaos, and Anagnostopoulos 2004; Morey and Campo 1999; Chu E Ho 2011; S Coulter and Martin 2006; Pichler et al. 2004; Palla and Leitner 2009; Pichler et al. 2003; Mustapha and Ramdan 2008; Senapathy, Davie, and Bohem 2003; Franz and Camper 2003; Gens et al. 2006; Massoudi 2008; Yourman, Jr., Diaz, and Gilbert 2006; Lignola, Flora, and Manfredi 2008; Hashimoto, Ye, and Ye 2009; Guatteri et al. 2009; Kochen 1992; Steven Coulter and Martin 2004; Paolo Croce, Modoni, and Russo 2004; Shirlaw 2003; Kwong and Francis 2003; Berry et al. 1988)</p>
<p style="text-align: center;">Piling Anchoring</p>	<p>(Pettit and Wooden 1988; “Process and Device for the Decontamination of Contaminated Sites”; HBI et al. 1994; Tarricone 1994; Lianwei and Guangyong 2011; Pearlman 1998; Rollins, Adsero, and Brown 2009; Hsieh, Wang, and Ou 2003; Bedenis, Jedele, and Maranowski 2005; Brengola and Roberts 2003; Padura et al. 2009; Kenneth B Andromalos and Gazaway 1989; Muller 2003; Smith and Borden, roy 2007)</p>
<p style="text-align: center;">Environmental Applications Contamination Control</p>	<p>(Gazaway and Jasperse 1992; “Process and Device for the Decontamination of Contaminated Sites”; Flick et al. 1992; G. k. Burke 1992; HBI et al. 1994; Tarricone 1994; G. k. Burke 1995; Burson et al. 1997; Loomis and Jessmore 2003; Suer et al. 2009; Carter and Webber 2007)</p>
<p style="text-align: center;">Study on effect of the different operational parameters, soil type, and jet grouting systems on soilcrete properties</p>	<p>(Yahiro and Yoshida 1973; Yahiro and Yoshida 1974; Yahiro, Yoshida, and Nishi 1975; Broid et al.; J.K. Mitchell 1981; M. Shibazaki and Ohta 1982; Yahiro, Yoshida, and Nishi 1982; Aschieri, Jamiołkowski, and Tornaghi 1983; Baumann 1984; Miki and Nakanishi 1984; Greenwood 1987; De Paoli, Tornaghi, and Bruce 1989; H. Yoshida et al. 1989; B. Nikbakhtan and Ahangari 2010; B Nikbakhtan and Osanloo 2009; B. Nikbakhtan, Apel, and Ahangari 2014a; B. Nikbakhtan, Apel, and Ahangari 2014b; van hoesen 1992; Harris, Wooden, and Motl 1992; Jongpradist et al. 2010; F. H. Lee et al. 2005; Pavlovic et al. 2010a; Pavlovic et al. 2010b; Osborne and Chiat 2010; C. E. Ho, Tan, and Lim 2001; P. Croce, Flora, and Modoni 2001; Ozgurel and Vipulanandan 2005; Spagnoli 2008; Chu Eu Ho 2009; Dabbagh, Gonzalez, and Pena 2002; A. Malinin, Gladkov, and Malinin 2010; Schorr, Traegner, and Micciche 2007; Mitsuhiro Shibazaki 2003; Collotta, Frediani, and Manassero 2004; Mitsuhiro Shibazaki, Yokoo, and Yoshida 2003; Tinoco, Gomes Correia, and Cortez 2011a; Stark et al. 2009; Hiroshi Yoshida et al. 2007; A. G. Malinin and Gladkov 2011; Chernyakov 2009; P Croce and Modoni 2007; Modoni, Croce, and Mongiovi 2006; P Croce and Flora 2000; Mondoni, Croce, and Mongiovi 2008; Morey and Campo 1999; Brandstatter, Lackner, and Mang 2005; S Coulter and Martin 2006; Yung-Show, Liao, and Ta-King 1994; Tinoco, Gomes Correia, and Cortez 2011b; Stavridakis 2006; Carroll et al. 2004; Y.-S. Fang, Liao, and Sze 1994; Mitsuhiro Shibazaki et al. 2005; Y.-S. Fang, Kuo, and Wang 2004; Bzówka 2004)</p>
<p style="text-align: center;">Jet grouting guidelines</p>	<p>(“GeoEng Consultants”; ASCE 2009; “Application of Ground Improvement : Jet Grouting”; BSEN12716:2001 2001; Druss 2003; Casagrande 2012)</p>

Table 3-7 Soilcrete column diameter in different systems (George K Burke 2004)

System	Soft Clays	Silts	Sands
Single Fluid	1.5 – 3.0ft 0.4 – 0.9m	2.0 – 3.5ft 0.6 – 1.1m	2.5-2.4ft 0.8 – 1.2m
Double Fluid	3.0 – 6.0ft 0.9 – 1.8m	3.0 – 6.0ft 0.9 – 1.8m	4.0 – 7.0ft 1.2 – 2.1m
Super Jet	10.0 – 14.0ft 3.0 – 4.3m	11.0 – 15.0ft 3.3 – 4.6m	11.5 – 16ft 3.5 – 5.0m
Triple Fluid	3.0 – 4.0ft 0.9 – 1.2m	3.0 – 4.5ft 0.9 – 1.4m	3.0 – 6.0ft 0.9 – 2.5m
X-Jet	7.5ft 2.3 m	7.5ft 2.3m	7.5ft 2.3m

Table 3-8 Jet grouting systems advantages and disadvantages (George K Burke 2004)

System	Advantages	Disadvantages
Single Fluid	-Simplest system and equipment -Good to seal vertical joints -Good in cohesionless soil	-Smallest geometry created -Hardest to control heave -Difficult to control quality in cohesive soils
Double Fluid	-Most utilized system -Availability of equipment and tooling -High energy, good geometry achieved -Most experience -Often most economical	-Very difficult to control heave in cohesive soils -Spoil handling can be difficult -Not usually considered for underpinning
Triple Fluid	-Most controllable system -Highest quality in difficult soils -Best underpinning system -Easiest to control spoil and heave	-Complex system and equipment -Requires significant experience
Super Jet	-Lowest cost per volume treated -Best mixing achieved	-Requires special equipment and tooling -Difficult to control heave in cohesive soils -Spoil handling difficult -Cannot work near surface without support -Highest logistical problems
X-Jet	-Confidence of geometry -Controllable materials cost -Best for soft cohesive soils	-Very specialized equipment that requires daily calibration -Limited experience available

Table 3-9 UCS of soilcrete, adopted from (Carreto 2000; Tinoco 2012; P Croce and Flora 2000)

Author/Data	$\frac{w}{c}$	Soil Type - UCS (MPa)				
		Organic clay	Clay	Silt	Sand	Gravel
Welsh and Burke (1991)	-	-	1 to 5	1 to 5	5 to 11	5 to 11
Baumann (1984)	1:1.5	-	-	6 to 10	10 to 14	12 to 18
	1:1.0	-	-	3 to 5	5 to 7	6 to 10
Paviani (1989)	-	-	1 to 5	1 to 5	8 to 10	20 to 40
Teixeira et al. (1987)	-	0.5 to 2.5	1.5 to 3.5	2 to 4.5	2.5 to 8	-
JJGA (1995)	-	0.3	1	1 to 3	-	-
Guatteri et al. (1994)	-	-	0.5 to 4	1.5 to 5	3 to 8	-
(Bell 1993)	-	-	0.5 to 8	4 to 18	5 to >25	5 to >30
(Miki 1985)	-	-	<5	5 to 10		
(M. Shibazaki 1991)	-	-	10	30		
(B Nikbakhtan and Osanloo 2009)	-	-	2.4		-	-
(B. Nikbakhtan and Ahangari 2010)	-	-	0.9 to 3.3		-	-

Table 3-10 Compare between physical and mechanical properties of soil and soilcrete (B Nikbakhtan and Osanloo 2009)

	Before jet grouting	After jet grouting
UCS (MPa)	0.025-0.05	2.4
C (KPa)	40	770
ϕ (degree)	0	25
Water content (%)	38	50-75
σ_t (KPa)	3.75-7.5	645

Table 3-11 Effective column diameter and operational parameters for double fluid system in granular soil (JJGA 2005) (adopted from (Chu Eu Ho 2005))

SPT N value (bellows/0.3m)	N<10	10<N<20	20<N<30	30<N<35	35<N<40	40<N<50
Diameter (m) 0<Z<25m	2.0	1.8	1.6	1.4	1.2	1.0
Withdrawal rate (min/m)	40	35	30	26	21	17
Grout flow rate (l/min)	60					
Grout pressure (bars)	200					
Air pressure (bars)	7					

Table 3-12 Effective column diameter and operational parameters for double fluid system in cohesive soil (JJGA 2005) (adopted from (Chu Eu Ho 2005))

SPT N value (bellows/0.3m)	Hammer weight	0<N<1	1<N<2	2<N<3	3<N<4
Diameter (m) 0<Z<25m	2.0	1.8	1.6	1.4	1.2
Withdrawal rate (min/m)	30	27	23	20	16
Grout flow rate (l/min)	60				
Grout pressure (bars)	200				
Air pressure (bars)	7				

Table 3-13 Effective column diameter and operational parameters for triple fluid system in granular soil (JJGA 2005) (adopted from (Chu Eu Ho 2005))

SPT N value (bellows/0.3m)	N<30	30<N<50	50<N<100	100<N<150	150<N<175	175<N<200
Diameter(m) 0<Z<30m	2.0	2.0	1.8	1.6	1.4	1.2
Diameter(m)30<Z<40m	1.8	1.8	1.6	1.4	1.2	1.0
Withdrawal (min/m)	16	20		25		
Grout flow rate (l/min)	180			140		
Grout pressure (bars)	20 to 50					
Water flow rate (l/min)	70					
Water pressure (bar)	400					
Air pressure (bars)	7					

Table 3-14 Effective column diameter and operational parameters for triple fluid system in cohesive soil (JJGA 2005) (adopted from (Chu Eu Ho 2005))

SPT N value (bellows/0.3m)	N<3	3<N<5	5<N<7	7<N<9
Diameter (m) 0<Z<30m	2.0	1.8	1.6	1.2
Diameter (m) 30<Z<40m	1.8	1.6	1.4	1.0
Withdrawal rate (min/m)	20		25	
Grout flow rate (l/min)	180		140	
Grout pressure (bars)	20 to 50			
Water flow rate (l/min)	70			
Water pressure (bar)	400			
Air pressure (bars)	7			

Table 3-15 Effective column diameter and operational parameters for super-jet system in granular soil (JJGA 2005)
(adopted from (Chu Eu Ho 2005))

SPT N value (bellows/0.3m)	N<50	50<N<100	N<50	50<N<100
Diameter (m) 0<Z<20m	3.5	3.2	5.0	4.5
Diameter (m) Z>20m	3.2	2.8	4.5	4.0
Withdrawal rate (min/m)	12		16	
Grout flow rate (l/min)	400		600	
Grout pressure (bars)	300			
Air pressure (bars)	7			

Table 3-16 Effective column diameter and operational parameters for super-jet system in cohesive soil (JJGA 2005)
(adopted from (Chu Eu Ho 2005))

SPT N value (bellows/0.3m)	N<3	3<N<5	N<3	3<N<5
Diameter (m) 0<Z<20m	3.5	3.2	5.0	4.5
Diameter (m) Z>20m	3.2	2.8	4.5	4.0
Withdrawal rate (min/m)	12		16	
Grout flow rate (l/min)	400		600	
Grout pressure (bars)	300			
Air pressure (bars)	7			

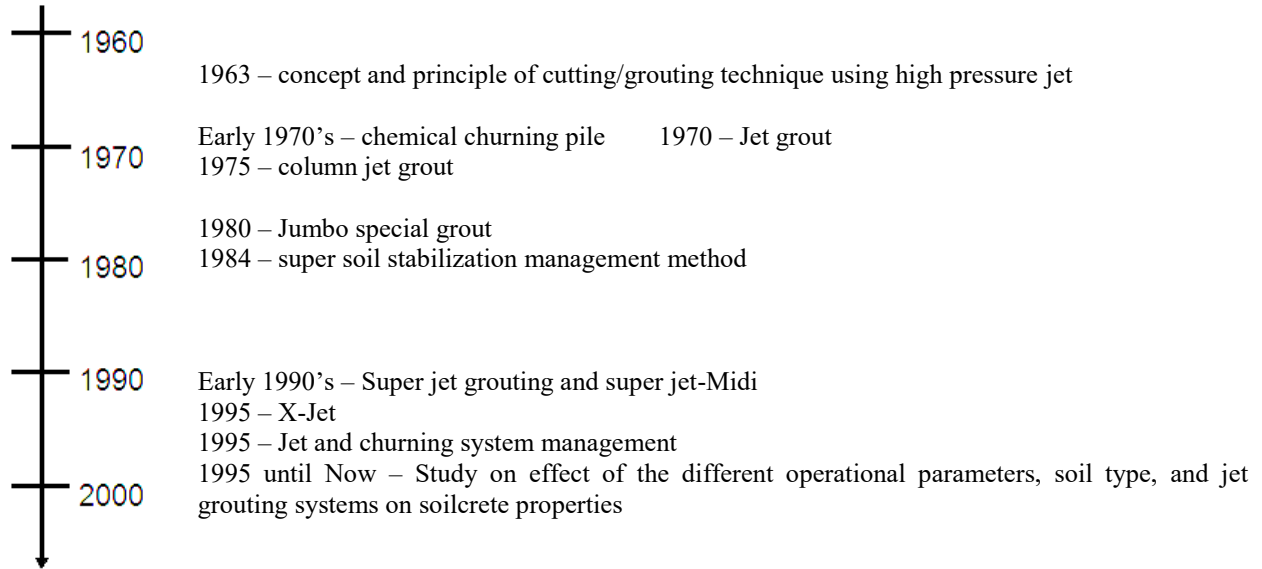


Figure 3-1 Historical development of jet grouting method (Ji 2008)

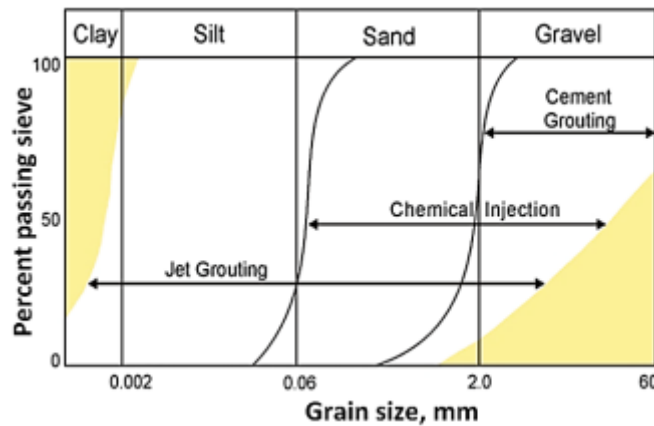


Figure 3-2 Jet grouting workability area (HBI, 2004)

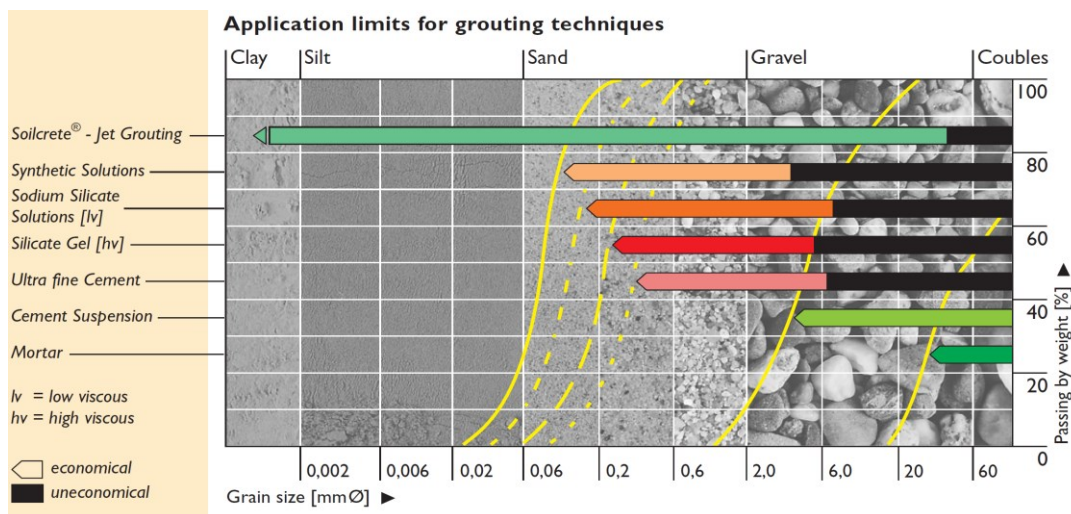


Figure 3-3 Application limits for grouting techniques (“Specialist Grouting”, “The soilcrete - jet grouting process”)



Figure 3-4 Jet grouting (left) v.s. low pressure conventional grouting (right) (Foundations 2012)

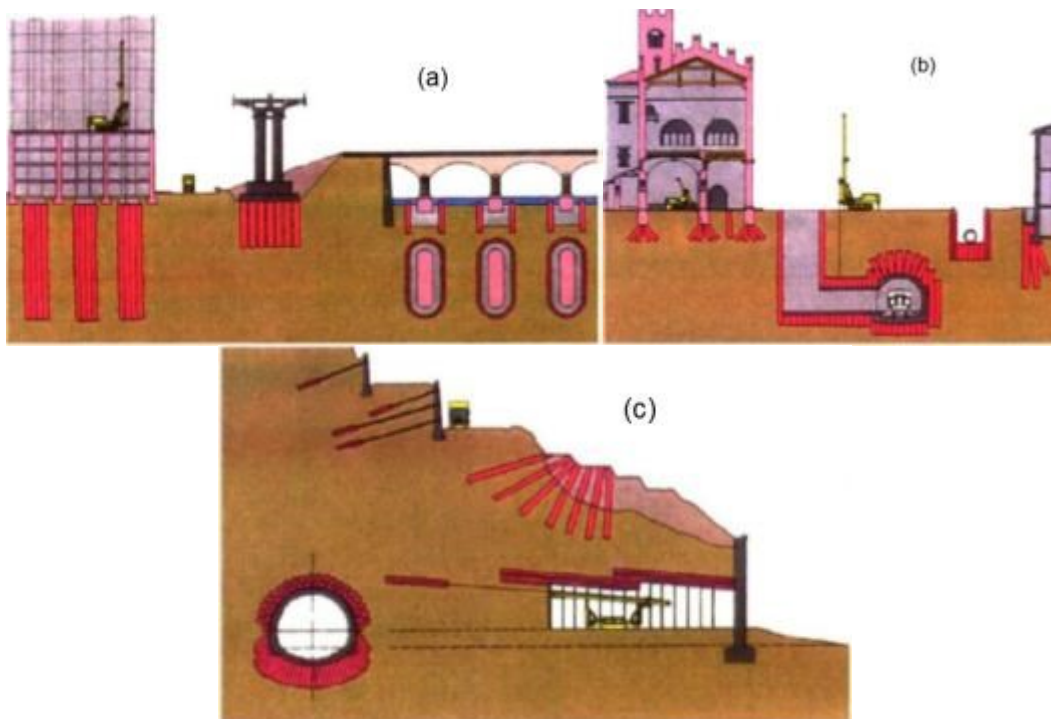


Figure 3-5 Jet grouting applications: (a) foundations and cofferdams; (b) underpinning, excavations, shafts, soft ground tunneling; (c) anchorages, slope stabilization, NATM tunneling (“Trevi Brochure” 2010)

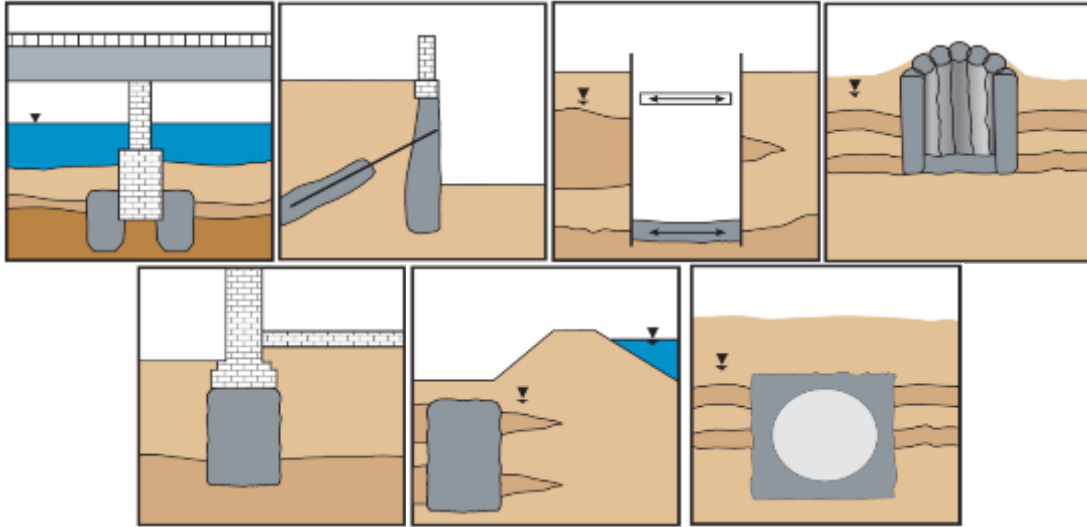


Figure 3-6 Jet grouting applications (HBI 2004)

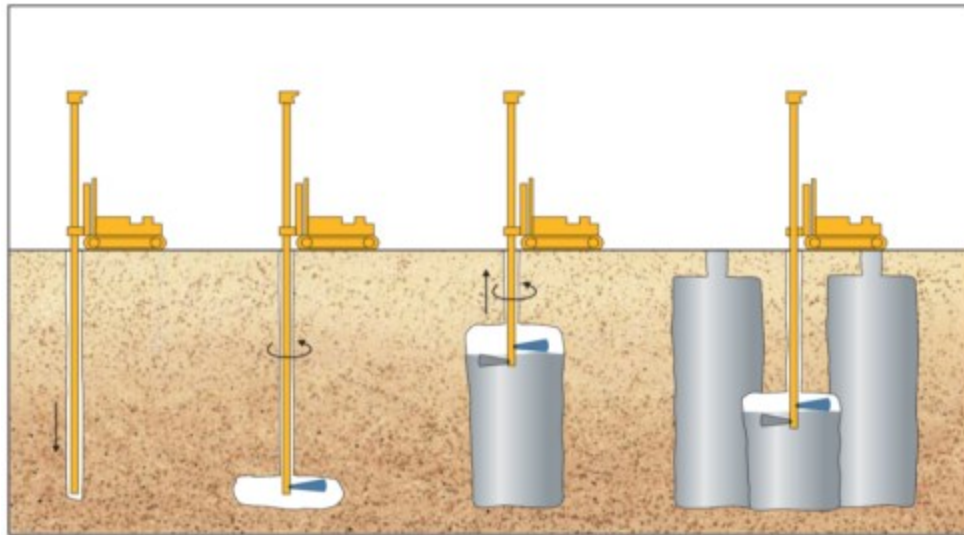


Figure 3-7 Construction sequence of jet grouting (HBI 2004)

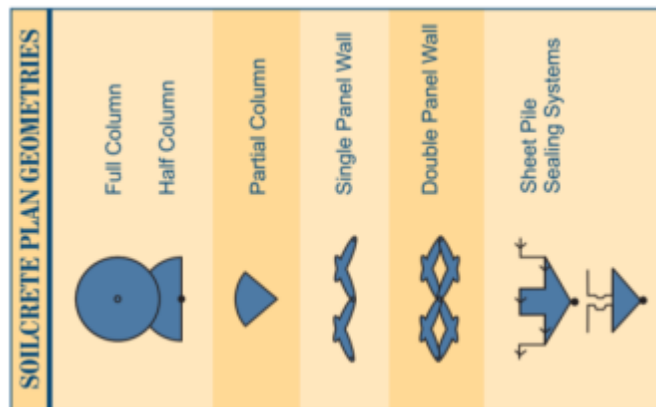


Figure 3-8 Soilcrete different geometries (HBI 2004; Schaefer 1997)

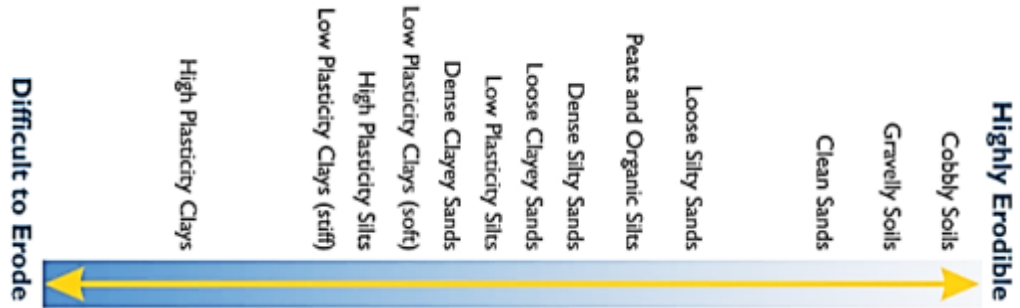


Figure 3-9 Different soil erodibility characteristics (Schaefer 1997; HBI 2004)

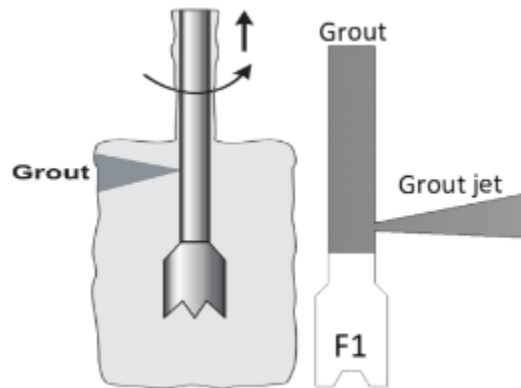


Figure 3-10 Single jet grouting system, F1 (HBI 2004; B Nikbakhtan 2007; B. Nikbakhtan, Aghababaei, and Pourrahimian 2007; B Nikbakhtan and Ghoshtasbi 2008; B Nikbakhtan and Osanloo 2009; B Nikbakhtan and Pourrahimian 2006)

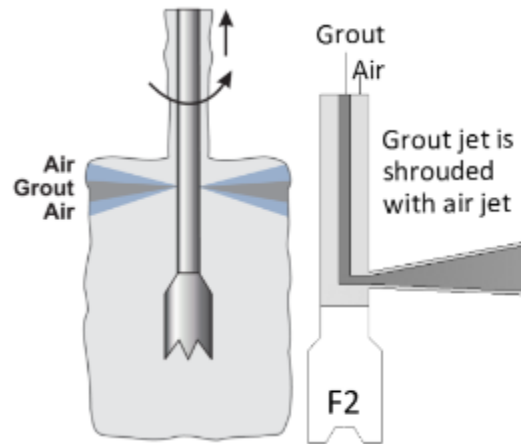


Figure 3-11 Double fluid jet grouting system, F2 (HBI 2004; B Nikbakhtan 2007; B. Nikbakhtan, Aghababaei, and Pourrahimian 2007; B Nikbakhtan and Ghoshtasbi 2008; B Nikbakhtan and Osanloo 2009; B Nikbakhtan and Pourrahimian 2006)

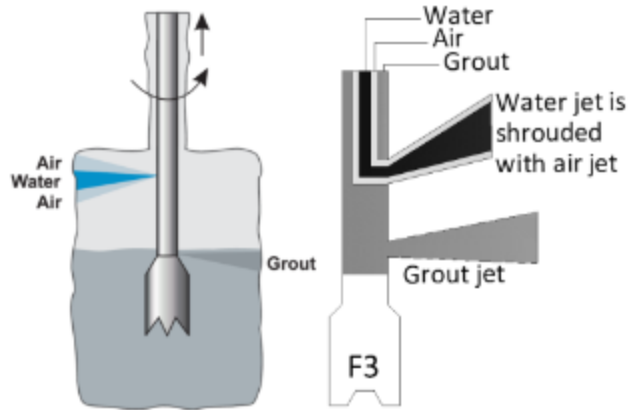


Figure 3-12 Triple fluid jet grouting system, F3 (HBI 2004; B Nikbakhtan 2007; B. Nikbakhtan, Aghababaei, and Pourrahimian 2007; B Nikbakhtan and Ghoshtasbi 2008; B Nikbakhtan and Osanloo 2009; B Nikbakhtan and Pourrahimian 2006)

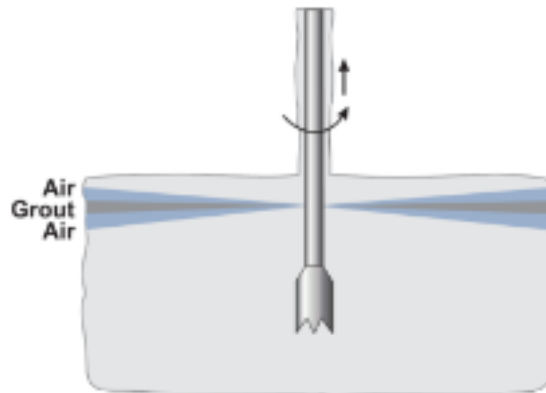


Figure 3-13 Super jet grouting system (HBI 2004)



Figure 3-14 Soilcrete columns in clayey soil formed by super jet grouting (Superjet 2004)



Figure 3-15 Soilcrete columns in sandy soil formed by super jet grouting (Superjet 2004)

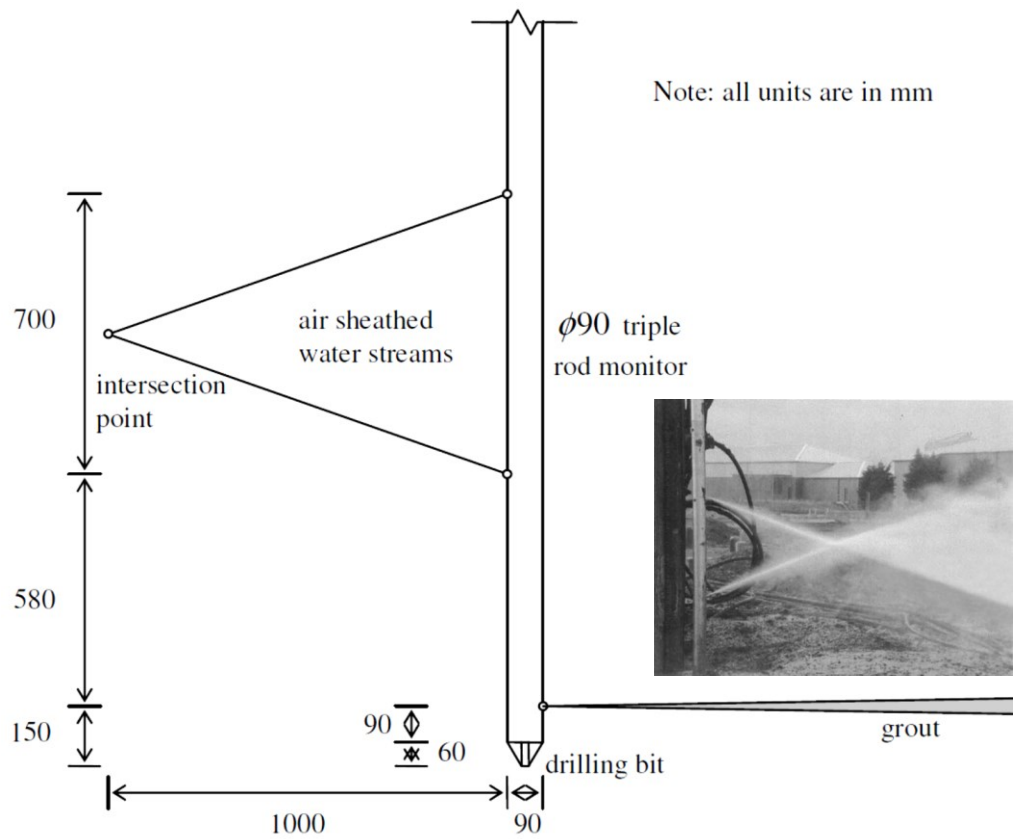


Figure 3-16 Schematic and dimensions of X-Jet grouting system (Ji 2008)

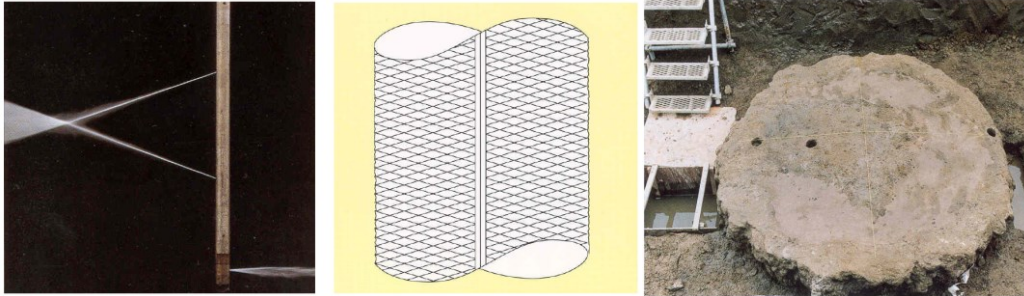


Figure 3-17 X-Jet grouting and type of soilcrete column forming (X-Jet 2002)

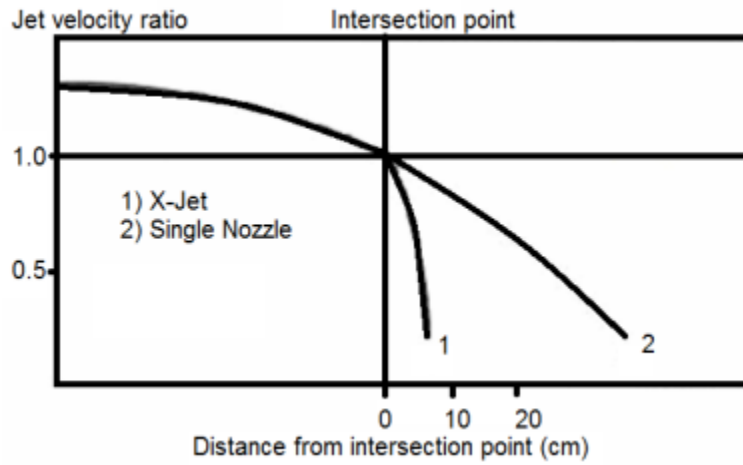


Figure 3-18 Comparison of jet velocity in X-Jet and single nozzle jet (X-Jet 2002)



Figure 3-19 New hydraulic measuring device (Passlick and Doerendahl 2006)

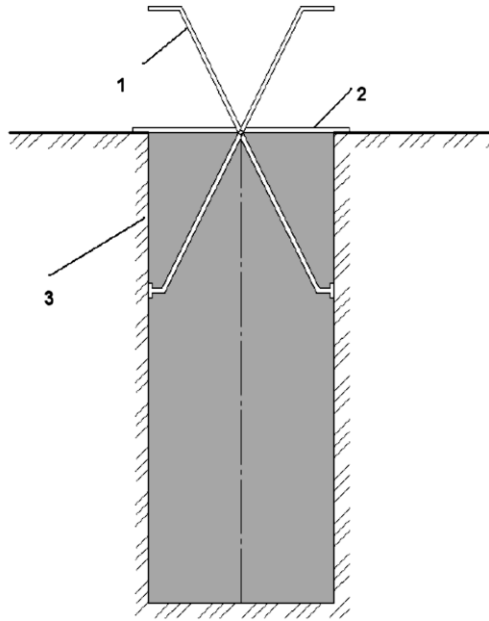


Figure 3-20 Scheme of column diameter measurement; 1) measuring device; 2) holder; 3) soilcrete column wall (A. Malinin, Gladkov, and Malinin 2010)

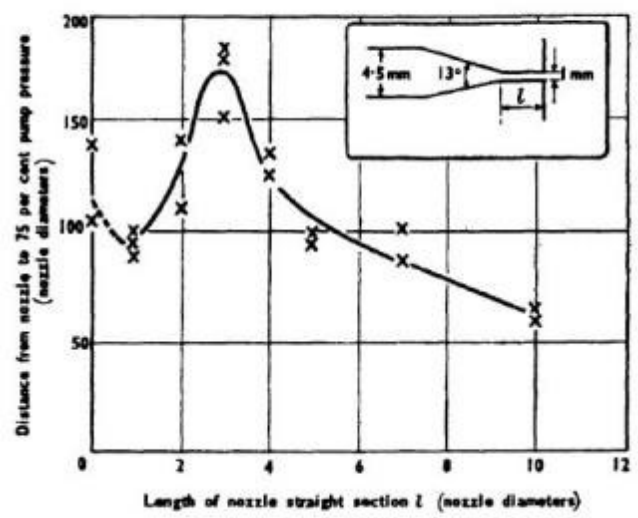
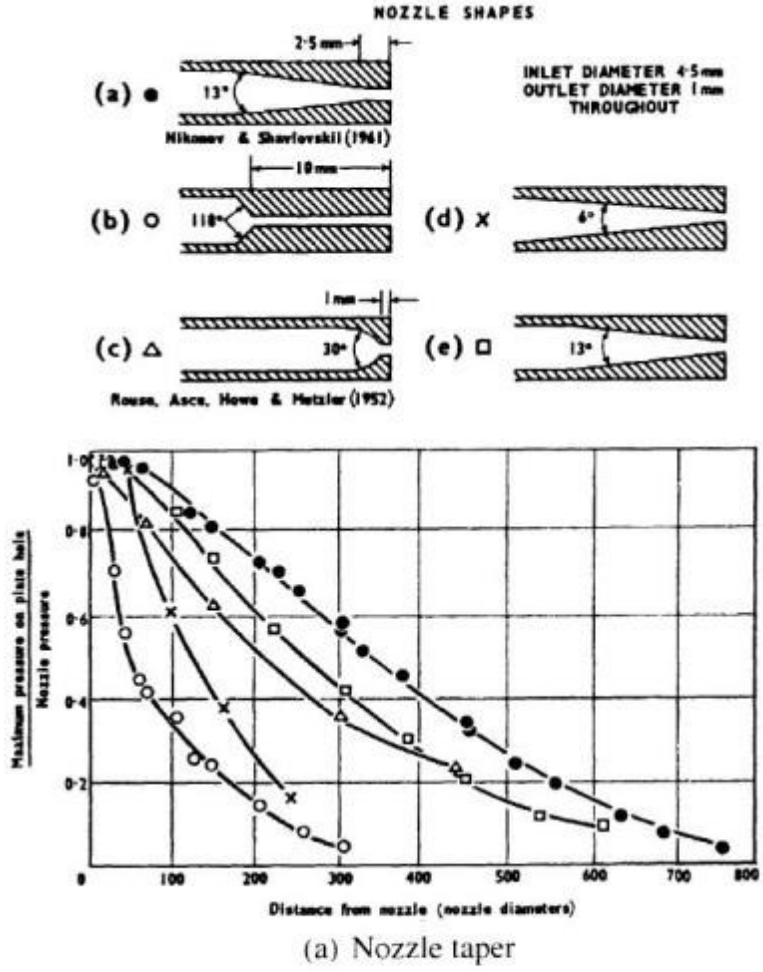


Figure 3-21 Effect of nozzle shape on jet performance (Leach and Walker 1966) (adopted from (Chu Eu Ho 2005))

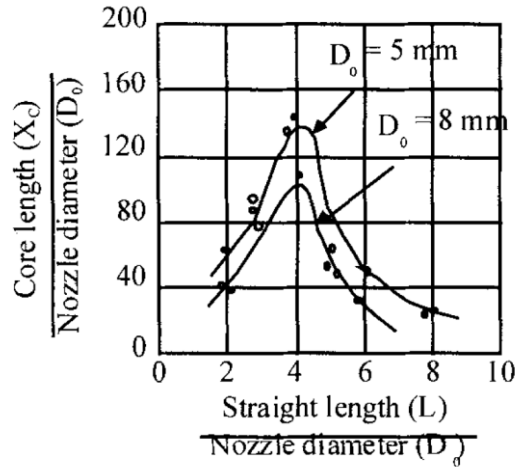


Figure 3-22 Relationship between potential core length and straight length (Mitsuhiro Shibazaki 2003)

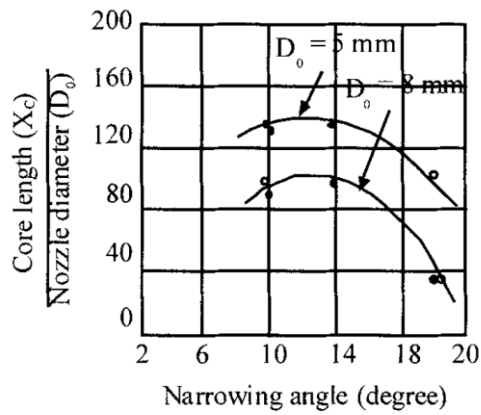


Figure 3-23 Relationship between core length and narrowing angle (Mitsuhiro Shibazaki 2003)

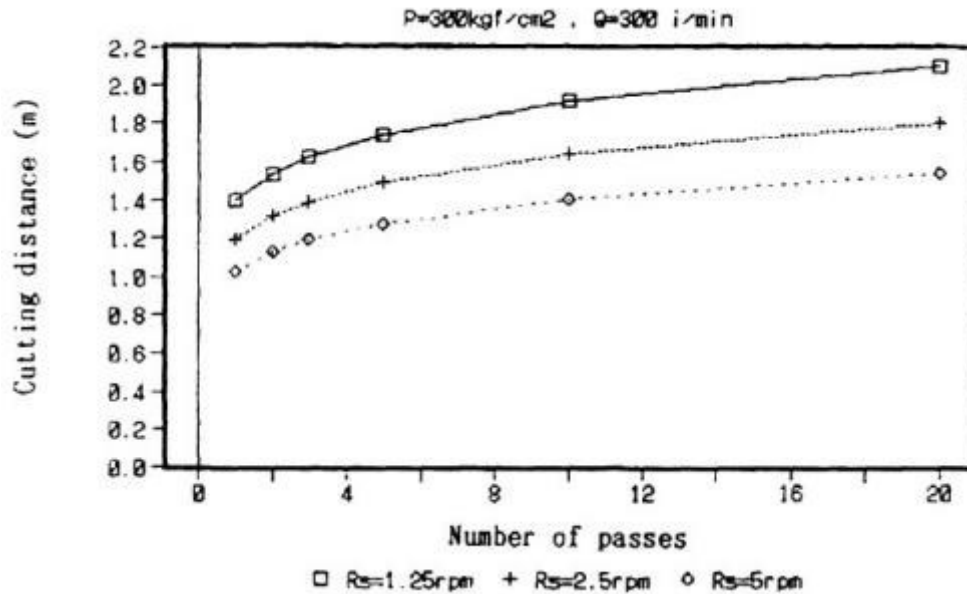


Figure 3-24 Relationship between cutting distance and number of passes in sand (H. Yoshida et al. 1991) (adopted from (Chu Eu Ho 2005))

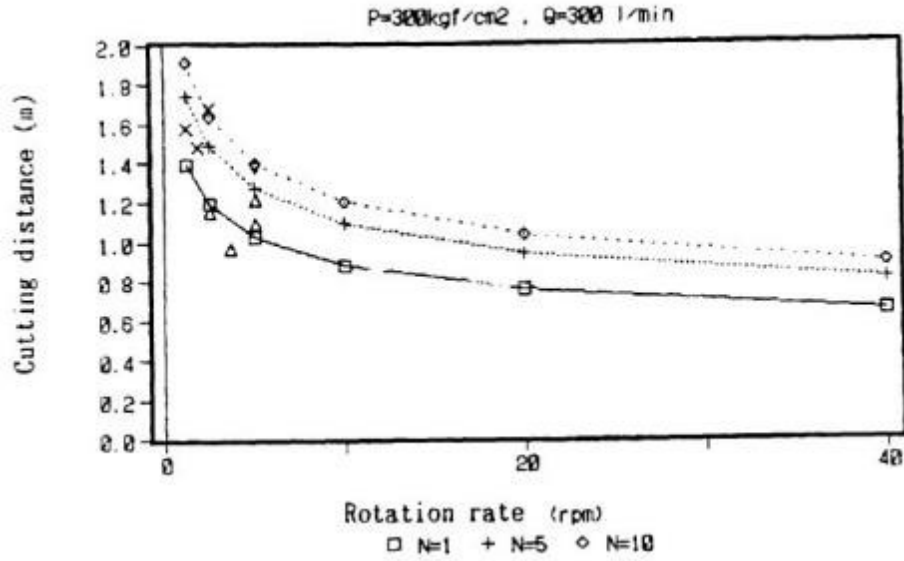


Figure 3-25 Relationship between cutting distance and rotation speed in sand (H. Yoshida et al. 1991) (adopted from (Chu Eu Ho 2005))

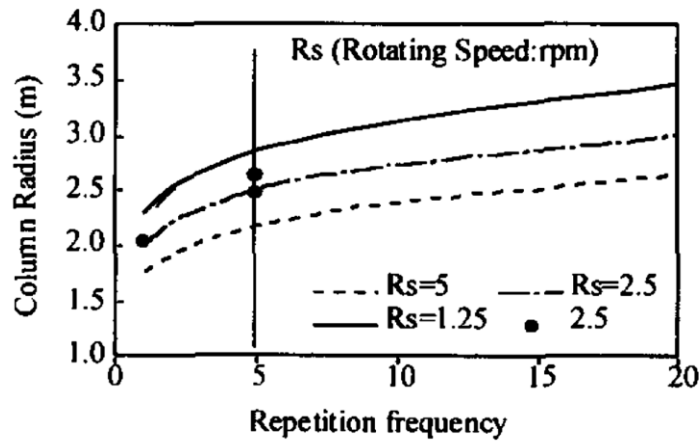


Figure 3-26 Optimal repetition frequency of eroding jet (R. Essler and Yoshida 2004)

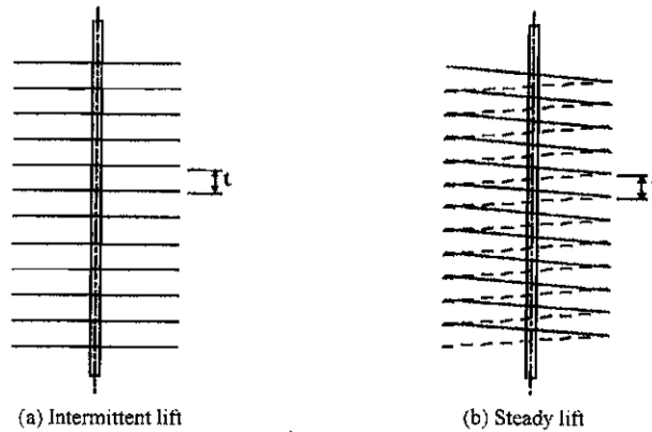
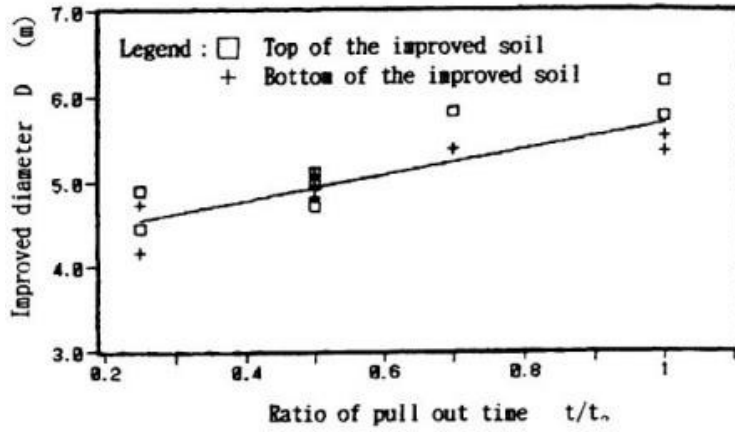


Figure 3-27 Lifting methods (R. Essler and Yoshida 2004)



Soil is silty sand with SPT. $N = 10$ to 15 blows/300mm
 $P = 300$ bar. $Q = 300$ l/min
 t_0 = Longest duration of jetting adopted in the trials
 t = Reduced duration of jetting ($t < t_0$)

Figure 3-28 Relationship between column diameter and duration of jet grouting (M. Shibazaki, Yoshida, and Matsumoto 1996) (adopted from (Chu Eu Ho 2005))

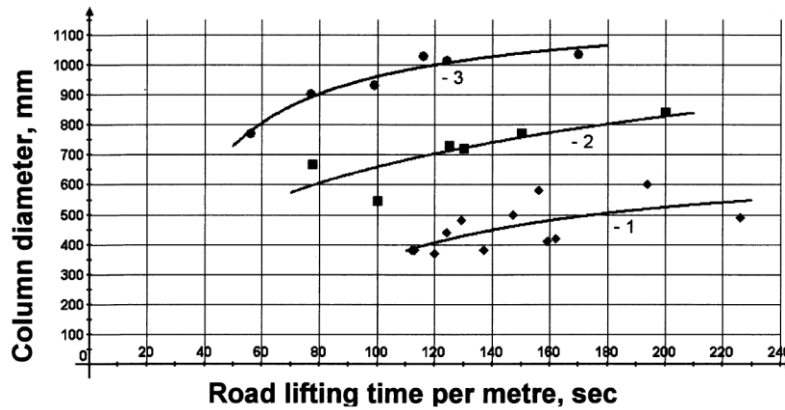


Figure 3-29 Relationship between soilcrete diameter and lifting rate; 1) cohesive soil $c = 47$ kPa; 2) soil with low cohesion $c = 7$ kPa; 3) non-cohesive soil $c = 1$ kPa (A. Malinin, Gladkov, and Malinin 2010)

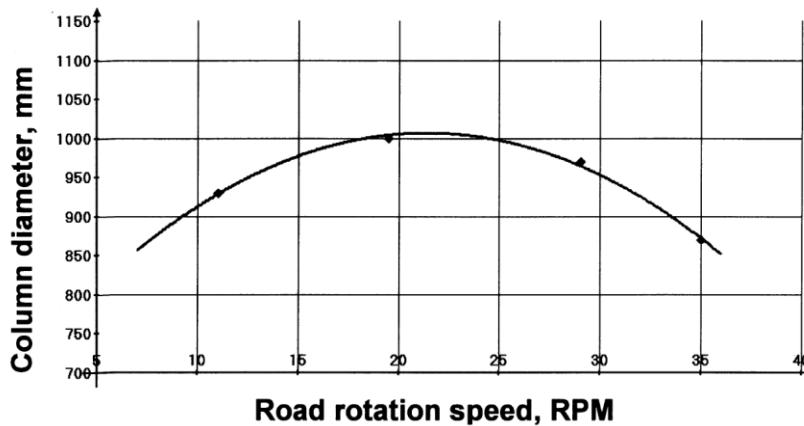


Figure 3-30 Relationship between soilcrete diameter and rotational speed (A. Malinin, Gladkov, and Malinin 2010)

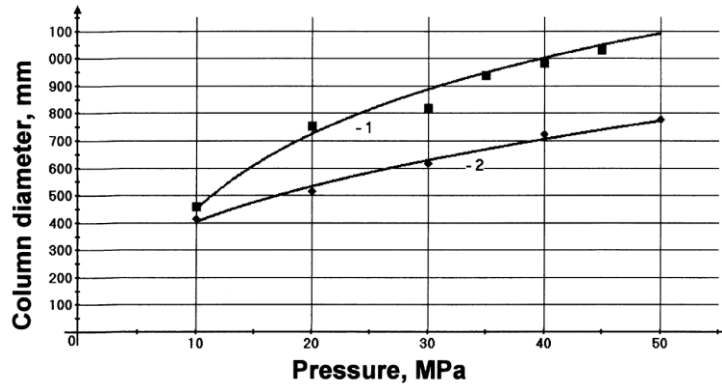


Figure 3-31 Relationship between soilcrete diameter and pressure; 1) non-cohesive soil $c = 1\text{ kPa}$; 2) soil with low cohesion $c = 7\text{ kPa}$ (A. Malinin, Gladkov, and Malinin 2010)

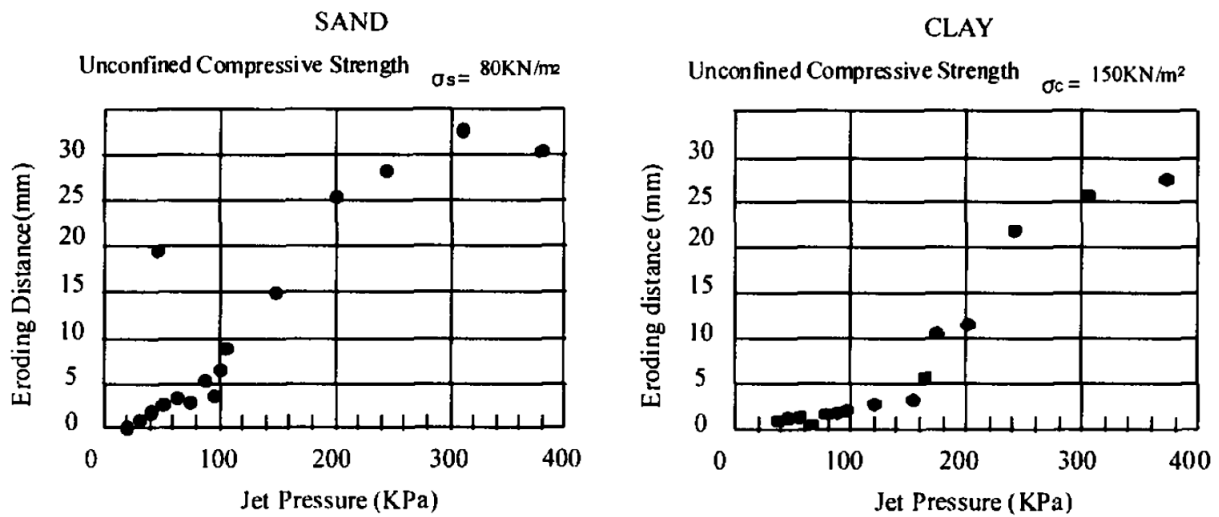


Figure 3-32 Relation between eroding distance and jet pressure (R. Essler and Yoshida 2004)

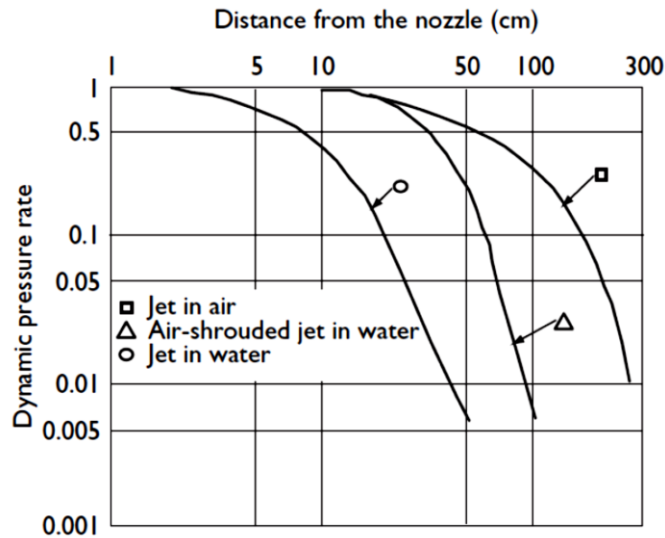


Figure 3-33 Relationships of dynamic pressure rates and distance from nozzle in various media (R. Essler and Yoshida 2004)

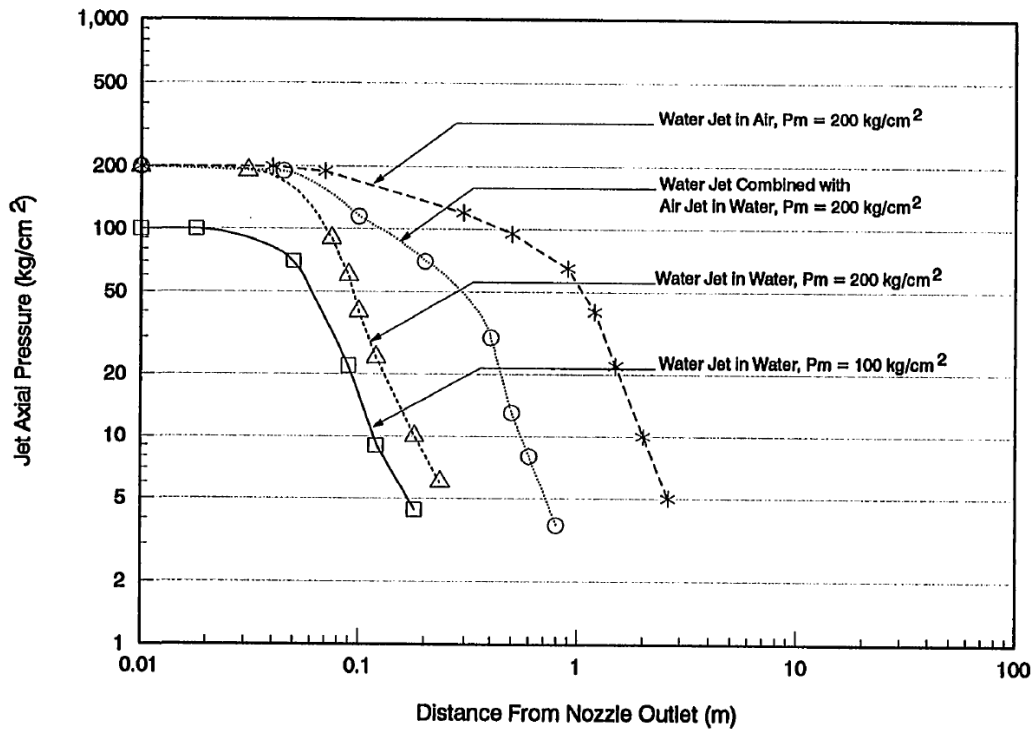


Figure 3-34 Jet axial pressure of water jet versus cutting distance from nozzle outlet (Yahiro and Yoshida 1973)

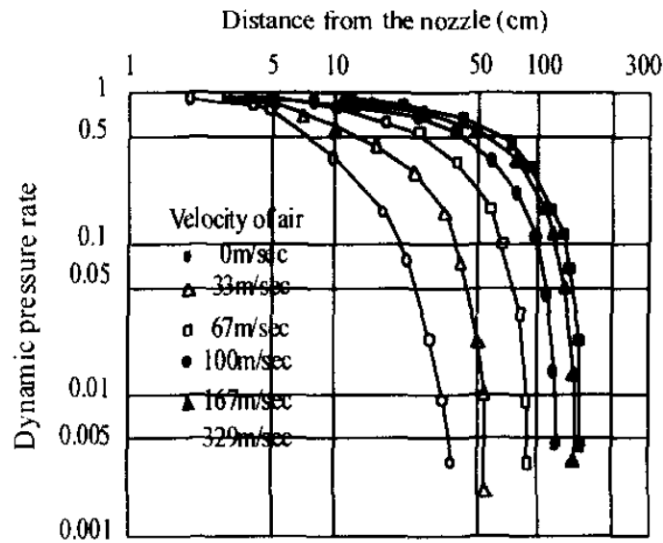


Figure 3-35 Relationship between water pressure and air flow rate with eroding distance (R. Essler and Yoshida 2004)

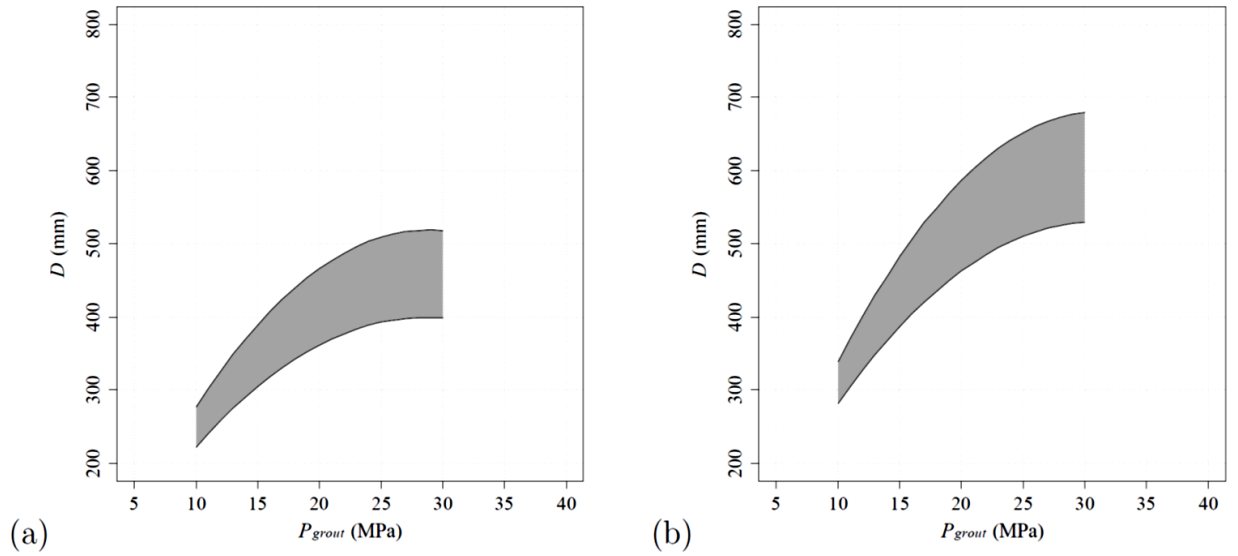


Figure 3-36 Relationship between grout pressure and soilcrete diameter (D); a) soft clay, b) sandy soil medium dense (Langbehn 1986) (adopted from (Tinoco 2012))

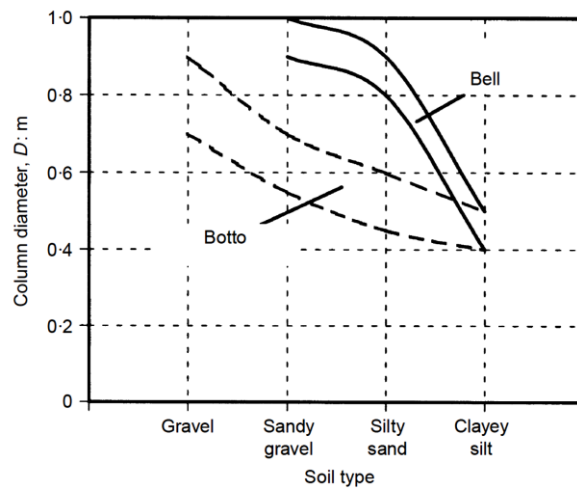


Figure 3-37 Column diameter ranges against soil type (Bell 1993; Botto 1985) (adopted from (P Croce and Flora 2000))

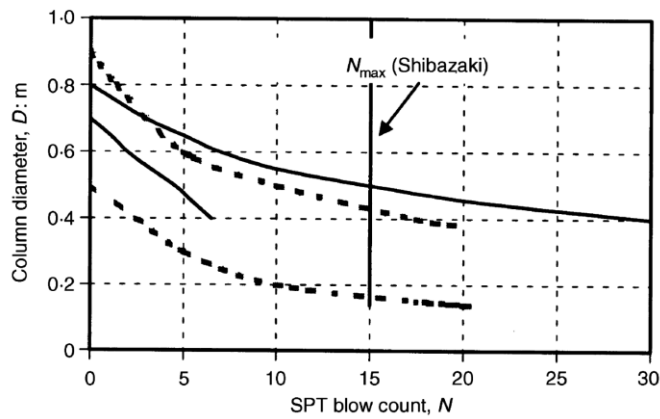


Figure 3-38 Column diameter ranges in granular soils against SPT blow count (Miki and Nakanishi 1984; Tornaghi 1989; M. Shibazaki 1991) (adopted from (P Croce and Flora 2000))

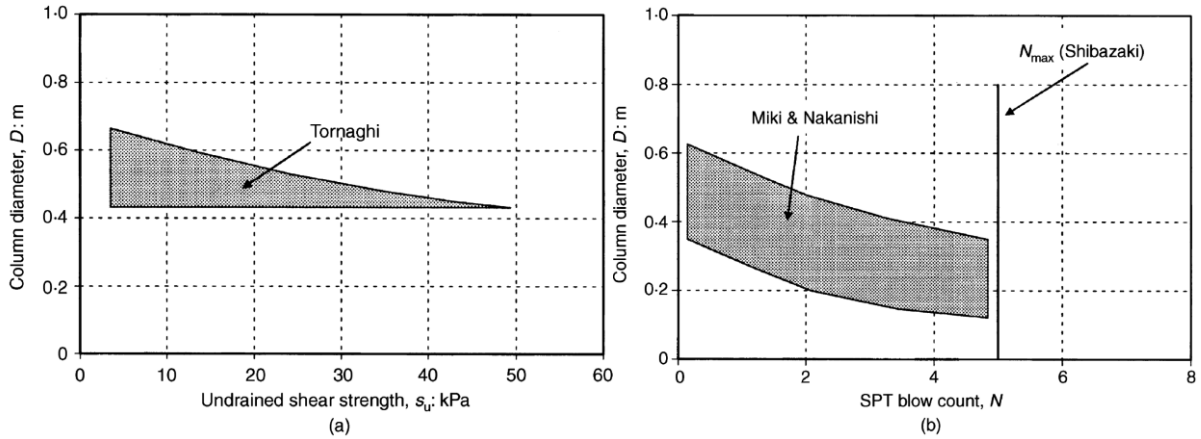


Figure 3-39 Column diameter ranges in fine-grained soils: (a) against undrained shear strength (Tornaghi 1989); (b) against SPT blow count (Miki and Nakanishi 1984; M. Shibazaki 1991) (adopted from (P Croce and Flora 2000))

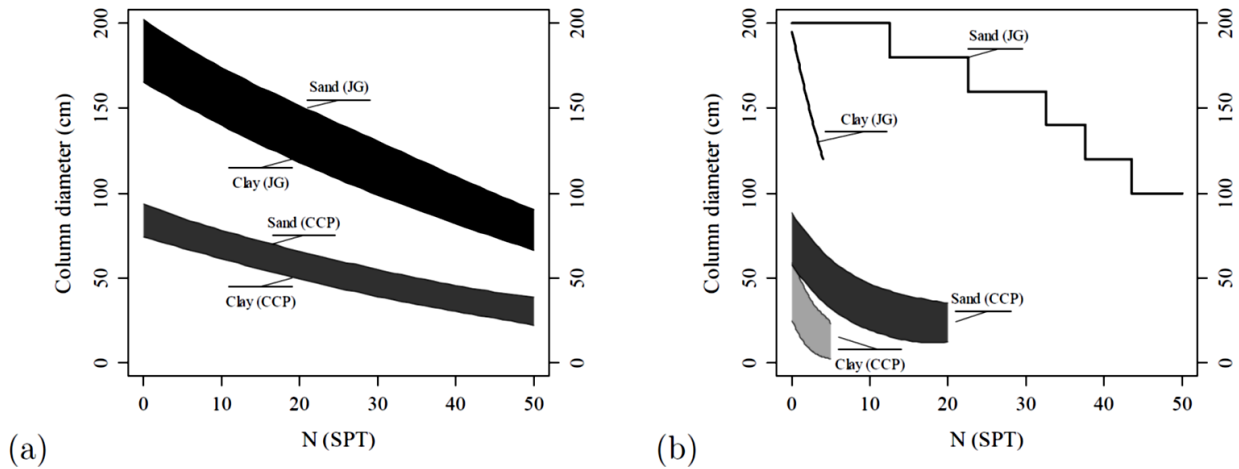


Figure 3-40 Soilcrete diameter vs N_{spt} in different soil types and jet grouting systems, a) according to Brazilian practice (NOVATECNICA, 2003), b) proposed by (Miki & Nakanishi, 1984) and (Abramento, Koshima, & Zirlis, 1998) (CCP: single fluid system, JG: double fluid system)

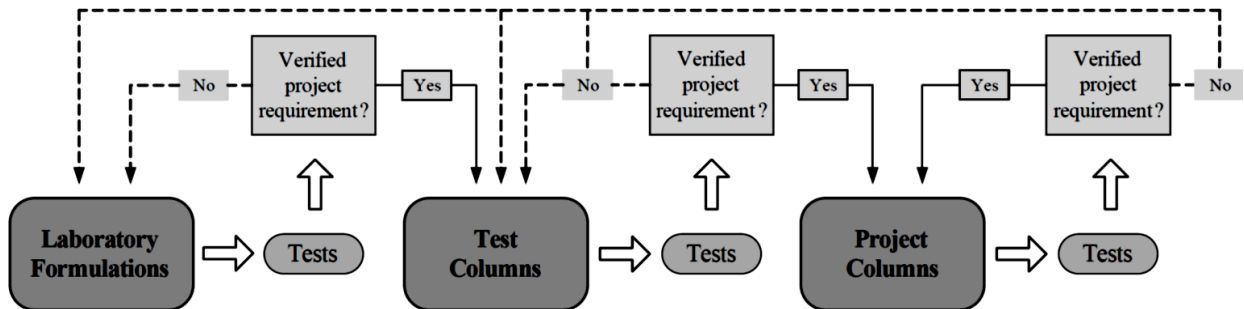


Figure 3-41 A typical jet grouting project procedure (Tinoco 2012)

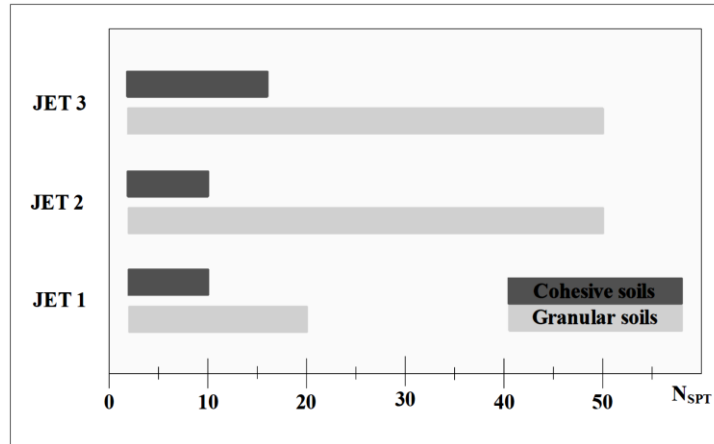


Figure 3-42 Applicability of the three main JG systems for cohesive and granular soils (Tinoco 2012)

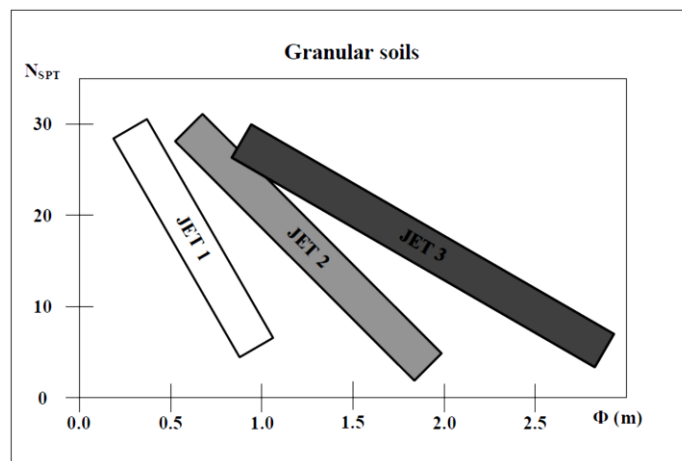
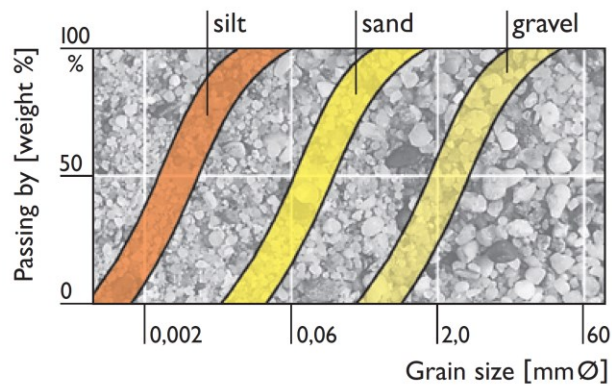


Figure 3-43 Soilcrete diameter vs N_{spt} for different jet grouting systems (Jet1: single fluid system, Jet2: double fluid system, Jet3: triple fluid system) (Tinoco 2012)



Type of soil	silt	sand	gravel
Compressive strength [N/mm ²]	≤ 5	≤ 10	< 25

Figure 3-44 Compressive strength of soilcrete (Keller; “Specialist Grouting”)

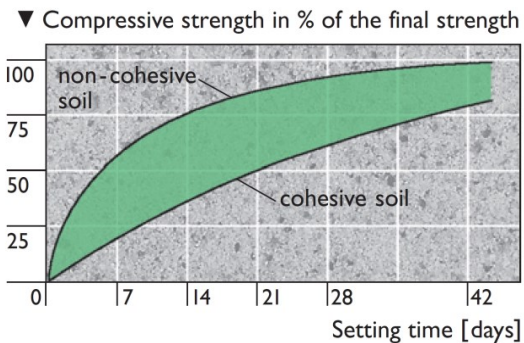


Figure 3-45 Development of soilcrete strength with time (Keller; “Specialist Grouting”)

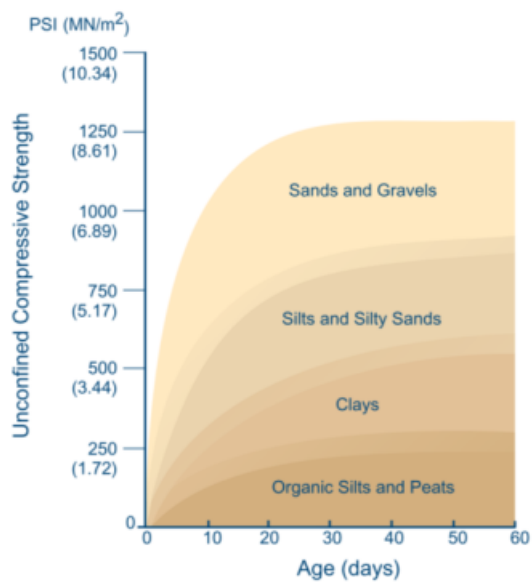


Figure 3-46 UCS of soilcrete based on soil types

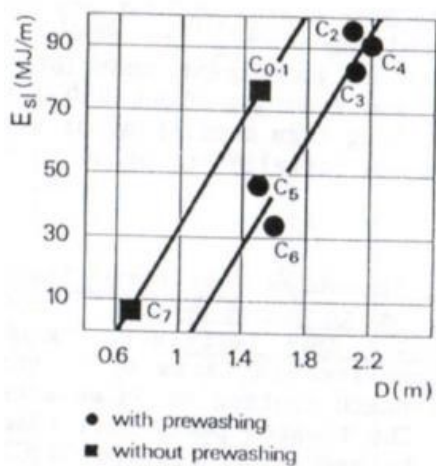


Figure 3-47 Relationship between specific energy per column meter (E_{sl}) and column diameter (D) (De Paoli, Tornaghi, and Bruce 1989)

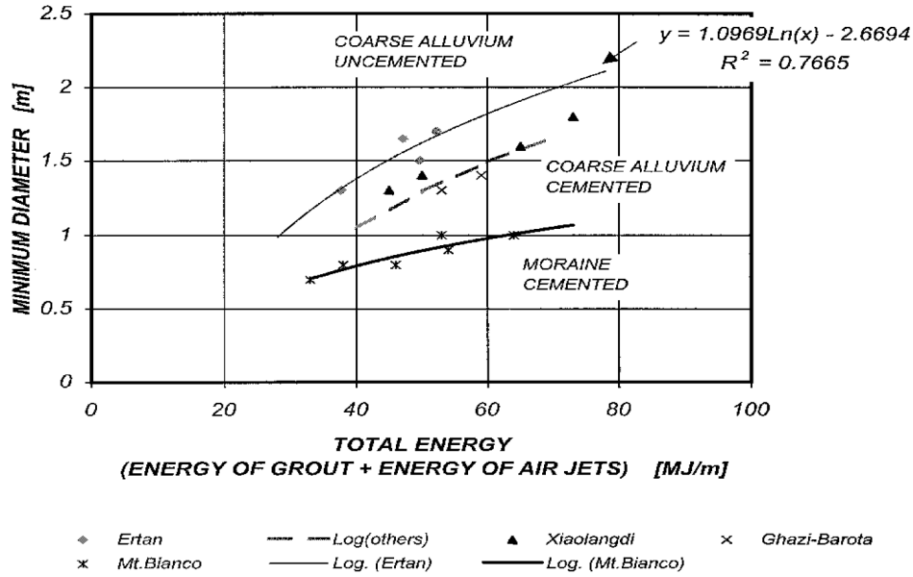


Figure 3-48 Correlation between total energy and minimum diameter of soilcrete from full-scale tests carried out at Ertan [results from similar tests at Xiaolangdi (Yellow River), Ghazi (Indus), and Mt. Bianco (Italy) Also shown for comparison] (Groppo Sembenelli and Sembenelli 1999)

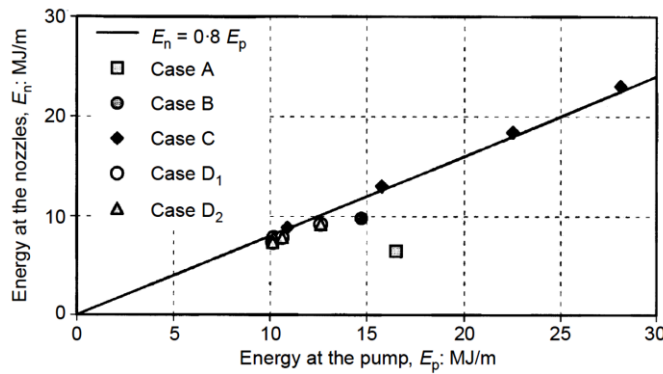


Figure 3-49 Comparison of energy at the nozzle and at the pump (P Croce and Flora 2000)

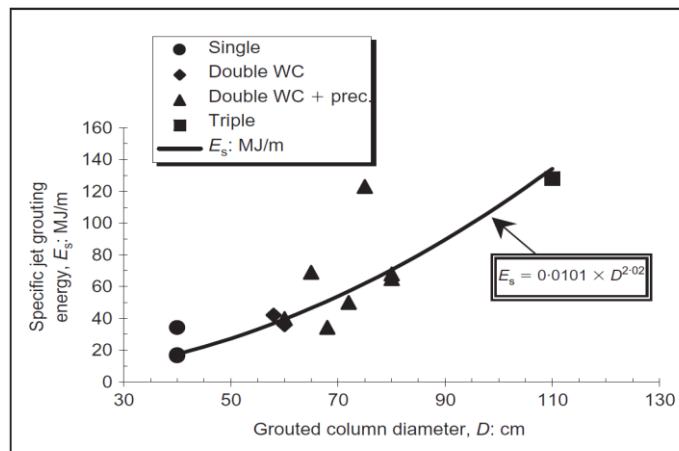
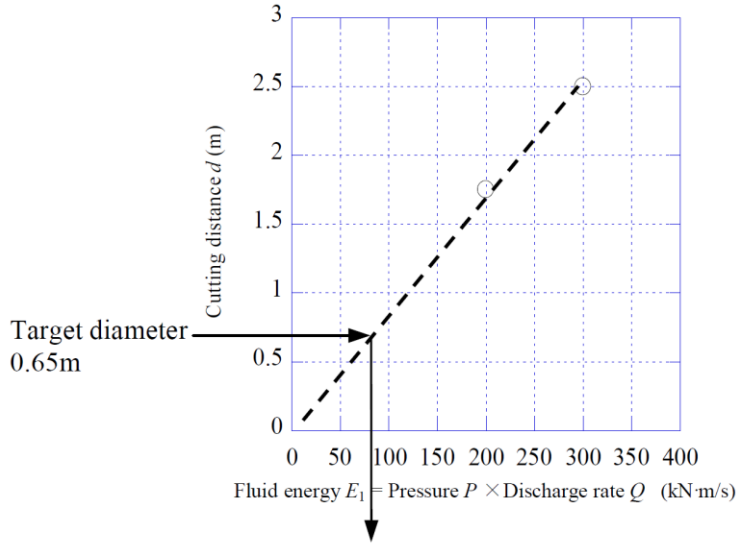


Figure 3-50 Specific jet grouting energy against soilcrete diameter (I K Mihalís, Tsiambaos, and Anagnostopoulos 2004)



Fluid energy $E_1 = \text{Pressure } P \times \text{Discharge rate } Q = 80$ (kN·m/s)
 Figure 3-51 Cutting distance vs jet fluid energy (Tsuboi et al. 2007)

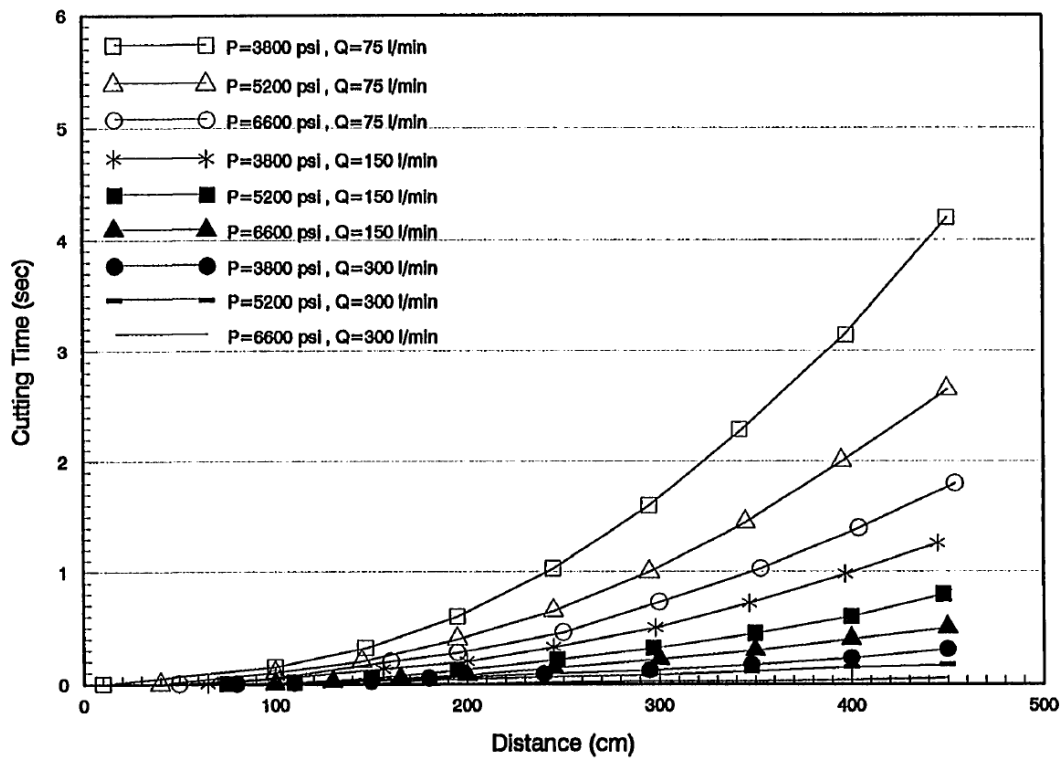


Figure 3-52 Time versus distance for nine pressure-flow rate combinations (H. Yoshida et al. 1989)

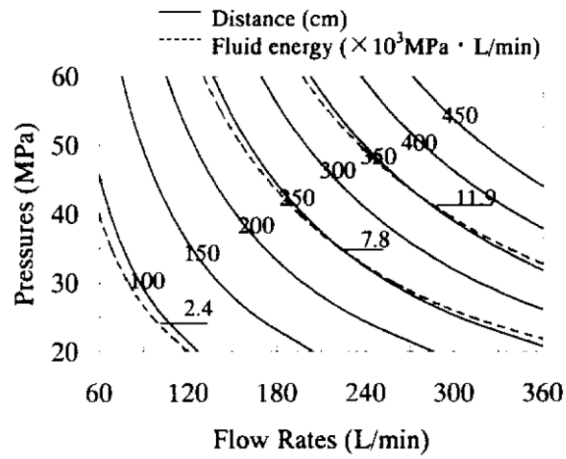


Figure 3-53 The distances reached for different combinations of pressure and flow rate, and constant hydraulic energy (H. Yoshida et al. 1989)

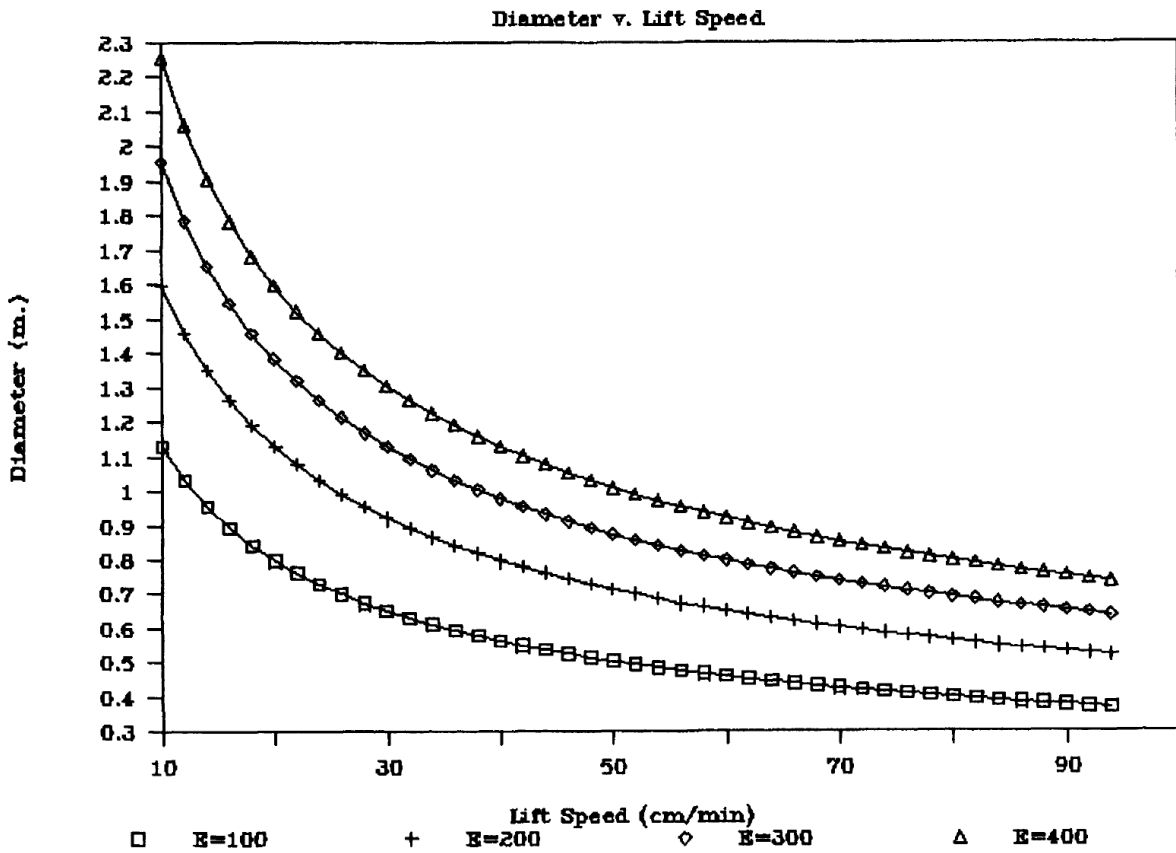


Figure 3-54 Soilcrete diameter relationship with lifting speed for different energy levels (R. D. Essler 1995)

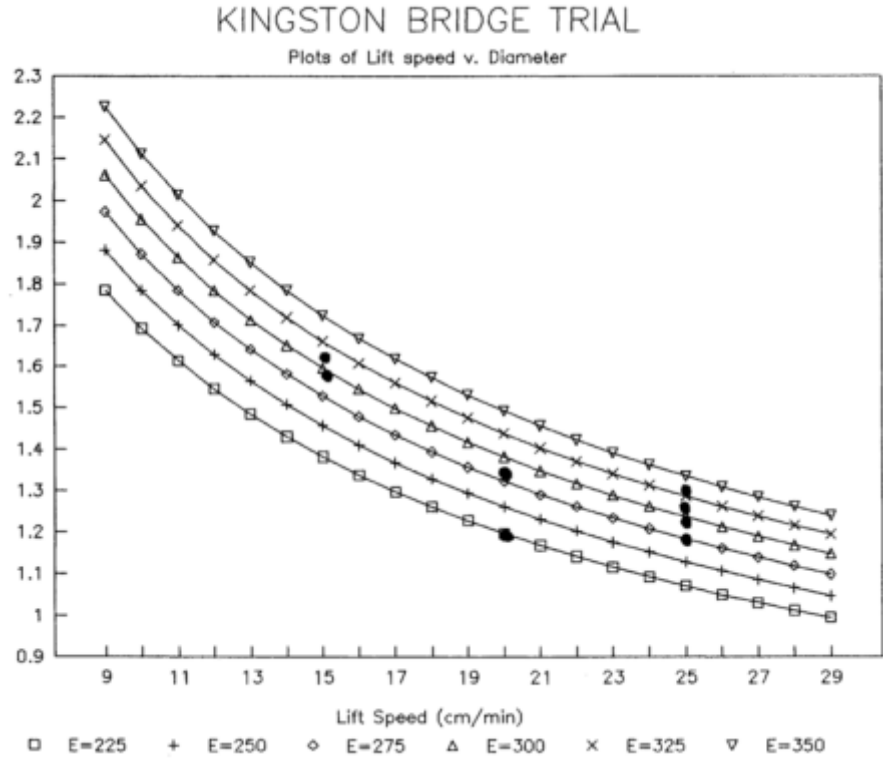


Figure 3-55 Plots of diameter versus lift speed for different values of E (liter/min) (R. D. Essler 1995)

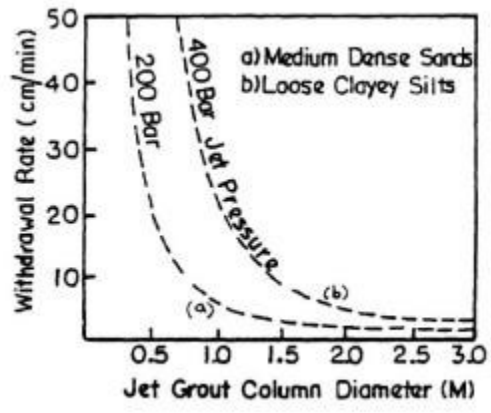


Figure 3-56 Relationship between jet grout column diameter and withdrawal rate (Coomber 1985) (adopted from (Chu Eu Ho 2005))

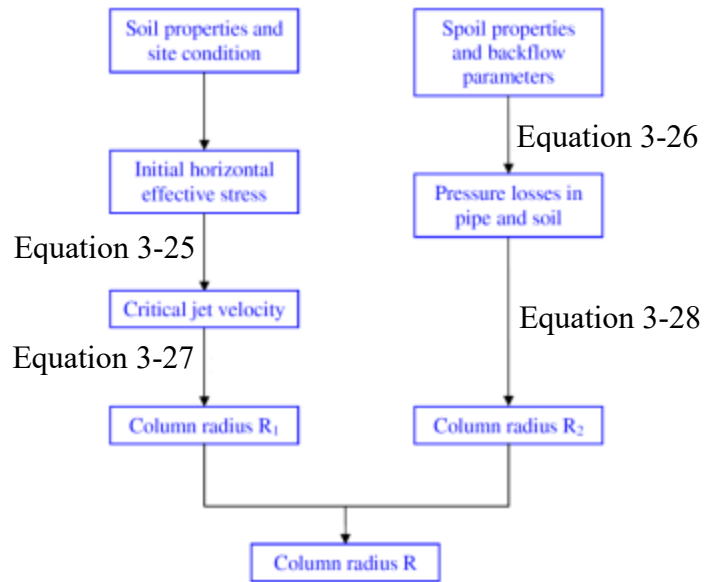


Figure 3-57 Estimation of soilcrete column diameter (Ji 2008)

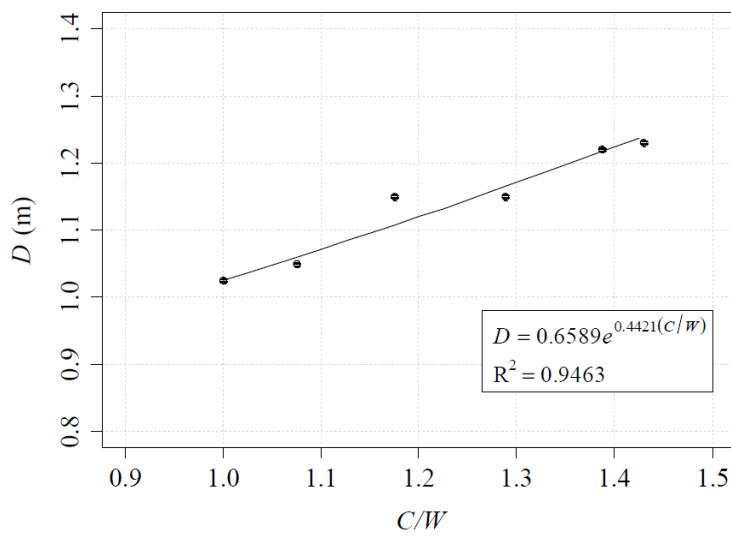


Figure 3-58 Relation between c/w ratio and diameter (B. Nikbakhtan and Ahangari 2010)

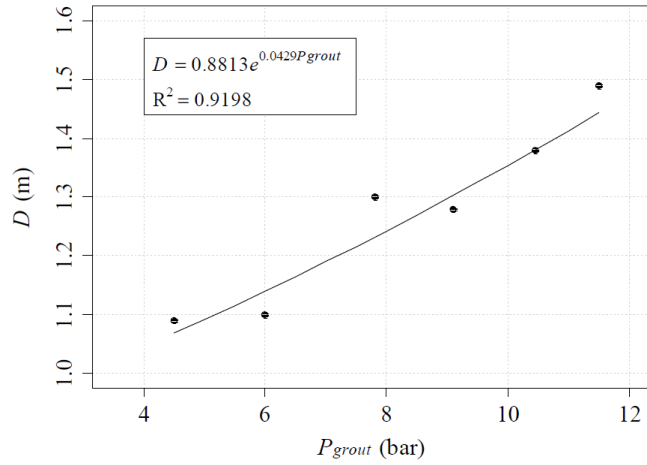


Figure 3-59 Relation between grout pressure and diameter (B. Nikbakhtan and Ahangari 2010)

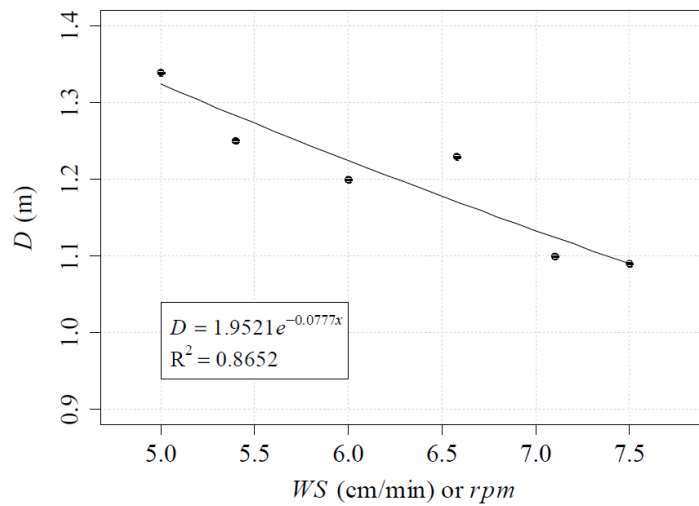


Figure 3-60 Relation between withdrawal and rotational speed with diameter (B. Nikbakhtan and Ahangari 2010)

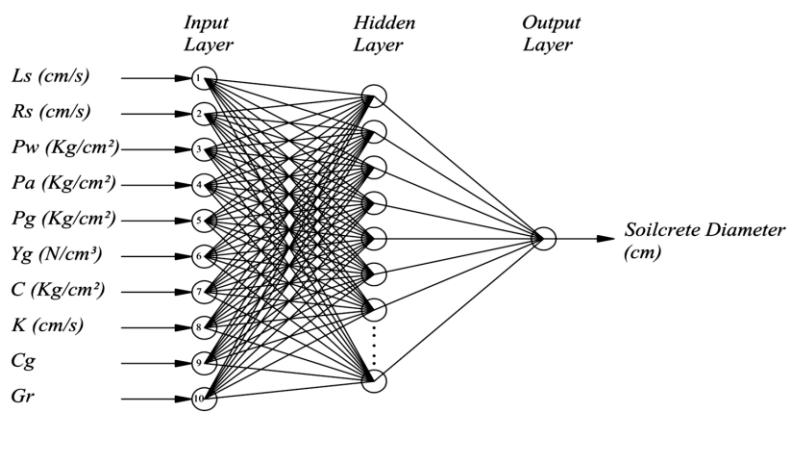


Figure 3-61 Structure of two-layered ANN model (B. Nikbakhtan, Apel, and Ahangari 2014a)

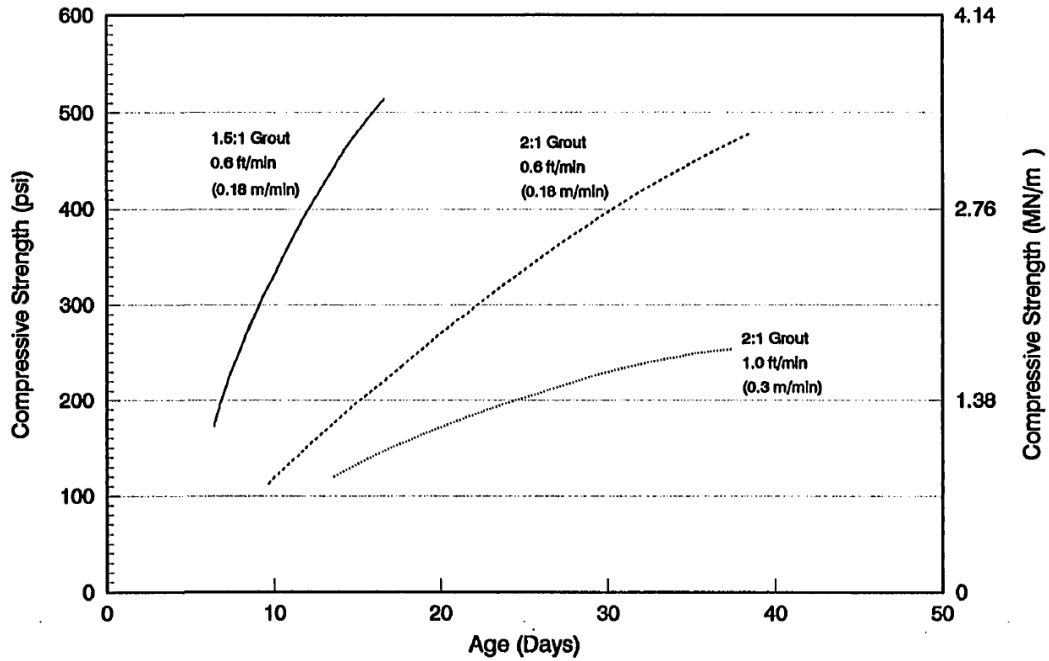


Figure 3-62 Strength gain trends (K.B. Andromalos and Gazawy 1986)

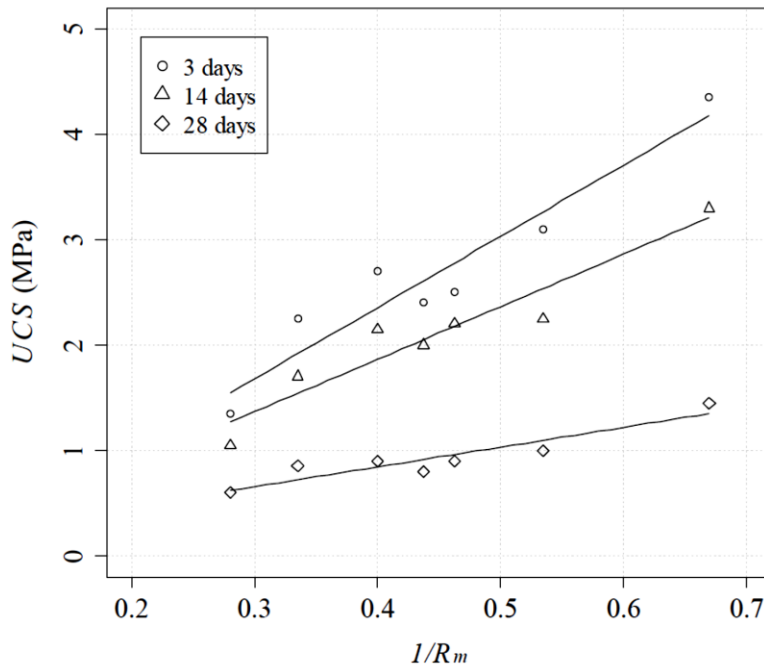


Figure 3-63 Relationship between UCS and total water-cement ratio (S. Y. Liu et al. 2008) (adopted from (Tinoco 2012)).



Figure 3-64 Soilcrete columns and block samples (B Nikbakhtan and Osanloo 2009)

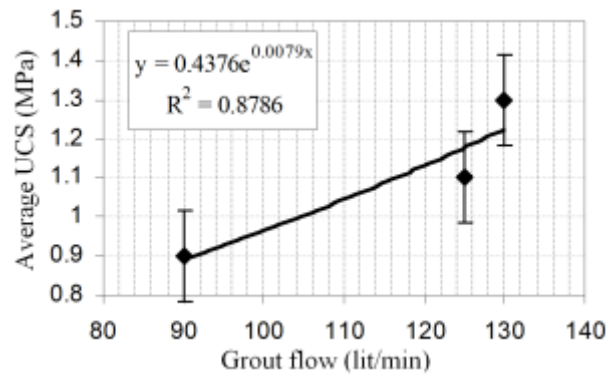


Figure 3-65 Relation between grout flow and average uniaxial compressive strength (B Nikbakhtan and Osanloo 2009)

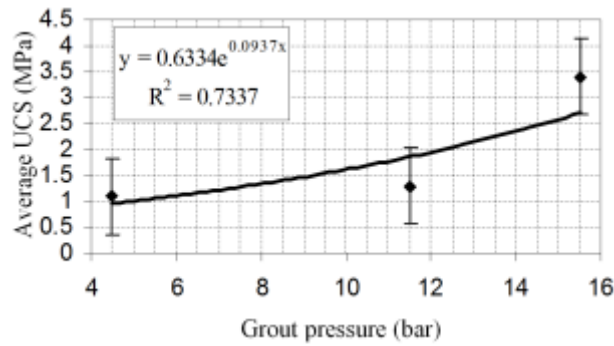


Figure 3-66 Relation between grout pressure and average uniaxial compressive strength (B Nikbakhtan and Osanloo 2009)

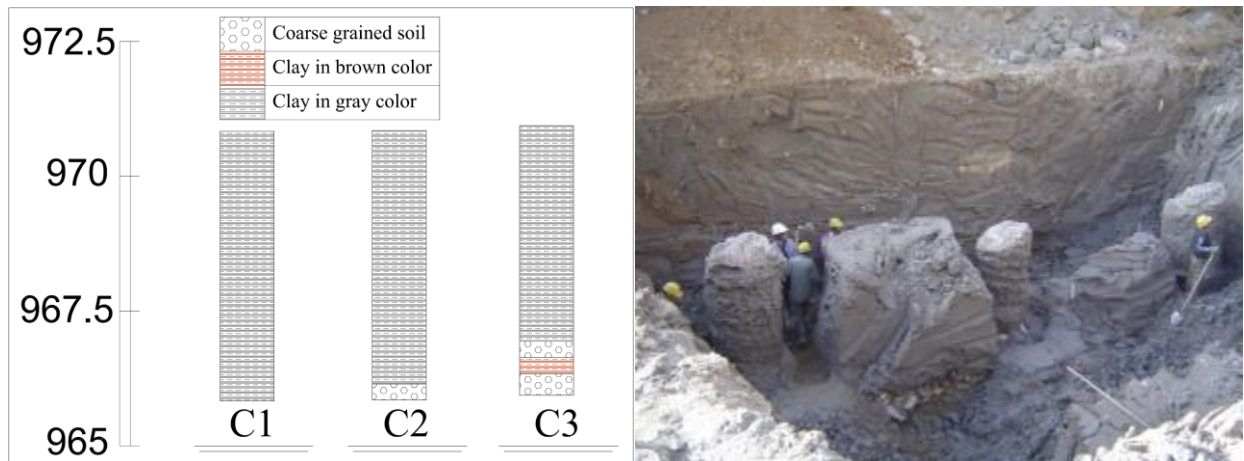


Figure 3-67 Vertical section of the boreholes (B. Nikbakhtan and Ahangari 2010)

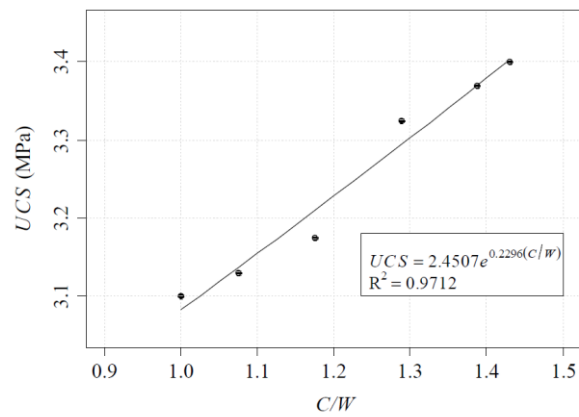


Figure 3-68 Relation between c/w ratio with UCS (B. Nikbakhtan and Ahangari 2010)

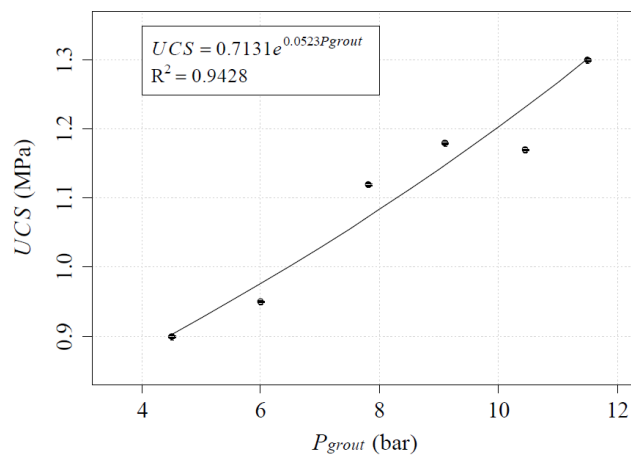


Figure 3-69 Relation between grout pressure with UCS (B. Nikbakhtan and Ahangari 2010)

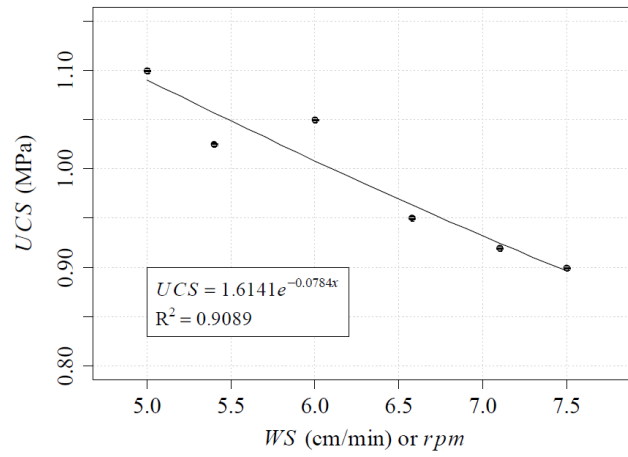
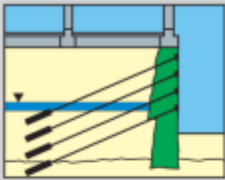


Figure 3-70 Relation between withdrawal and rotational speed with UCS (B. Nikbakhtan and Ahangari 2010)

Appendix 3-1 Jet grouting different applications (1/2) (Keller)

Underpinning



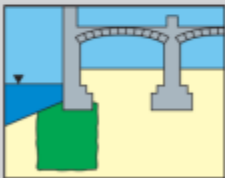
Underpinning by means of low deformation gravity walls sometimes also used as a ground water seepage barrier, may be safely constructed even from confined working areas.

Tunnel protection



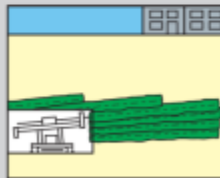
Soilcrete tunnel protection is mainly constructed in loose soils below or close to endangered structures, sometimes with the aim of reducing the groundwater ingress into the tunnel excavation.

Foundation restoration



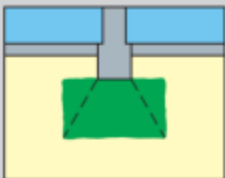
Historical buildings may be endangered in the event of settlements occurring. Soilcrete provides a safe foundation with the maximum structural protection.

Soilcrete - Horizontal



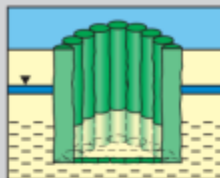
Horizontal Soilcrete columns protect tunnel drives in loose soil formations. They are constructed from working faces and are horizontal or slightly inclined.

Foundation modification



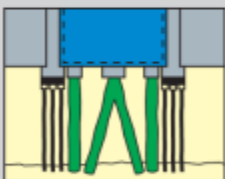
Changes in utilisations or modifications of buildings often require an enlargement or alteration of the foundation. Soilcrete is an economical and flexible solution for this task.

Shaft supports



Shafts with intersecting Soilcrete columns are constructed if a vibration free installation is required and/or the shafts enter into ground water bearing strata.

Deep foundation



Soilcrete is used for new foundations which require special care in view of nearby existing structures such as historical buildings or computer centres.

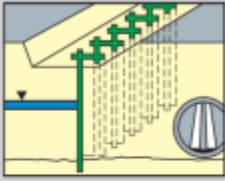
Earthpressure relief



Structures exposed to earth pressures, such as historical walls, abutments, avalanche galleries, steep slopes protections or quay walls may be relieved by the addition of or connection to a statically calculated backup Soilcrete body.

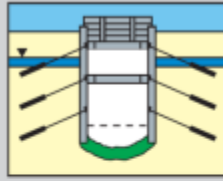
Appendix 3-2 Jet grouting different applications (2/2) (Keller)

Panel walls



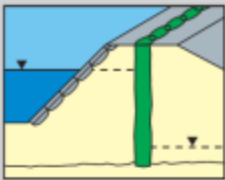
Soilcrete panel walls to cut off ground water are used below roads and buildings, for crossing pipelines and to subdivide building pits into different excavation sections. According to the sealing requirements single or multiple panels may be constructed.

Vault slabs



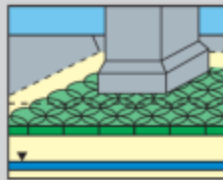
For small building pits and shafts with reduced width Soilcrete slabs are used as prevention against the water uplift pressure, reducing the required depth of slabs normally required to resist the hydrostatic uplift.

Column walls



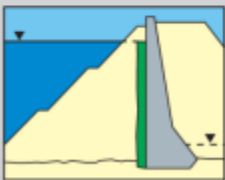
In the event of higher mechanical strain by shearforce, danger of undermining or of a high impermeability requirements, cut off walls of intersecting Soilcrete columns may be constructed.

Sealing cover



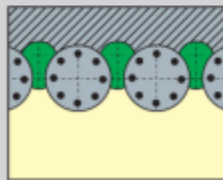
The Soilcrete cover protects the groundwater below buildings against affects from construction activities and old toxic waste deposits.

Dam sealing



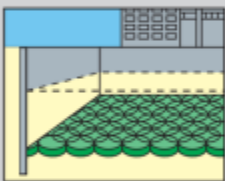
Soilcrete may be used to repair dam cores or enlarge cut-off walls in or below dams.

Joint sealing



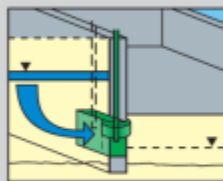
For sealing of joints between piles, sheet piles or other construction parts in the ground the Soilcrete wing-jet is applied.

Sealing slabs



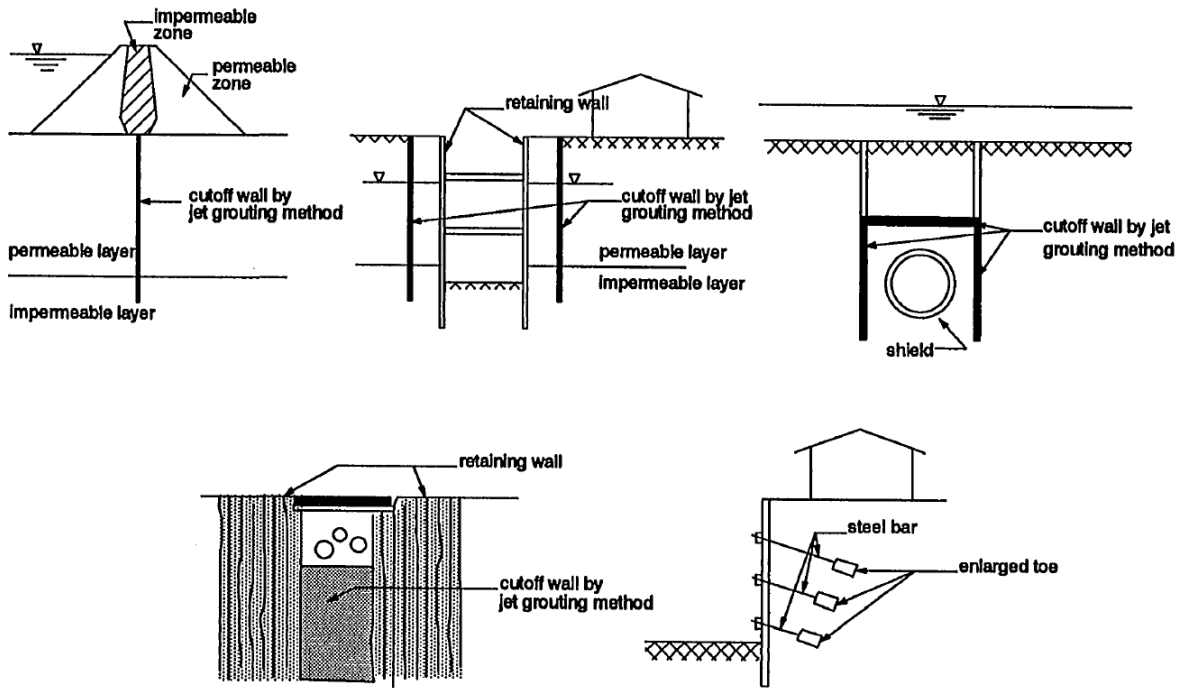
Soilcrete sealing slabs are constructed by means of overlapping columns within an uplift proof depth. The sealing slabs may be connected to any kind of vertical sealing systems.

Groundwater exits

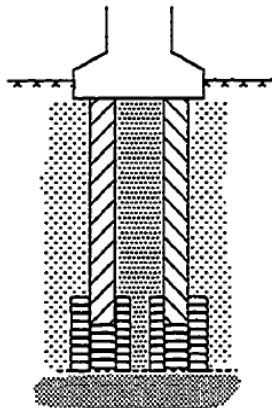


Sealing walls are often used as temporary ground water barriers. The reinstatement of the permeability may be reached using the Soilcrete process to wash out the binder material from predetermined sections.

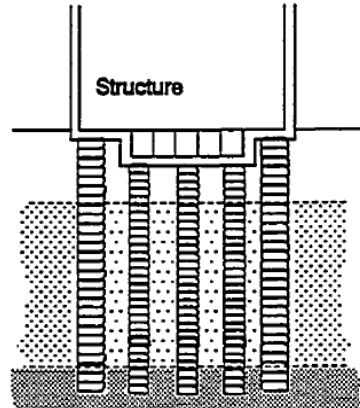
Appendix 3-3 Application of triple fluid jet grouting in cut-off walls (Yahiro et al., 1975)



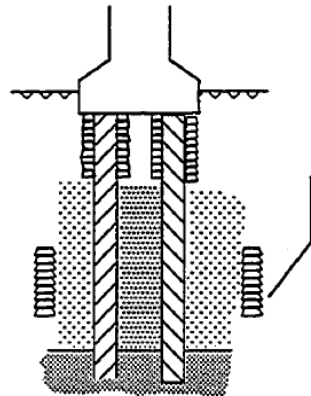
Appendix 3-4 Jet grouting applications (Yahiro et al., 1982)



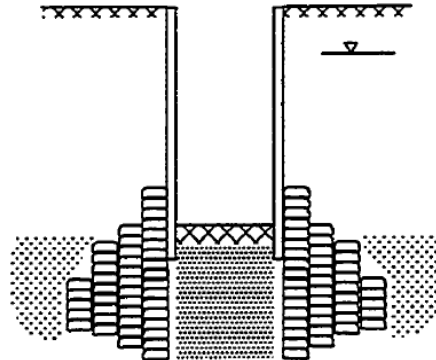
Improvement of bearing layer for piers or existing piles



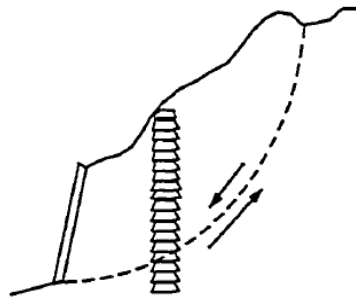
Improvement of ground under the existing structure



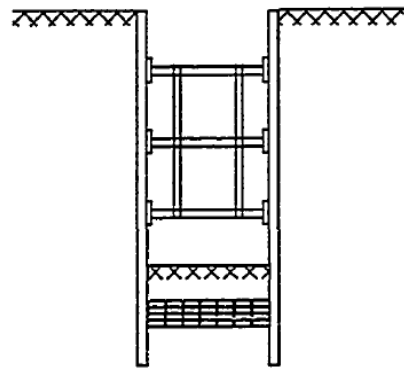
Improvement of resistance capacity of piers and existing piles against horizontal forces



Reduction of uplift



Prevention of slope failure

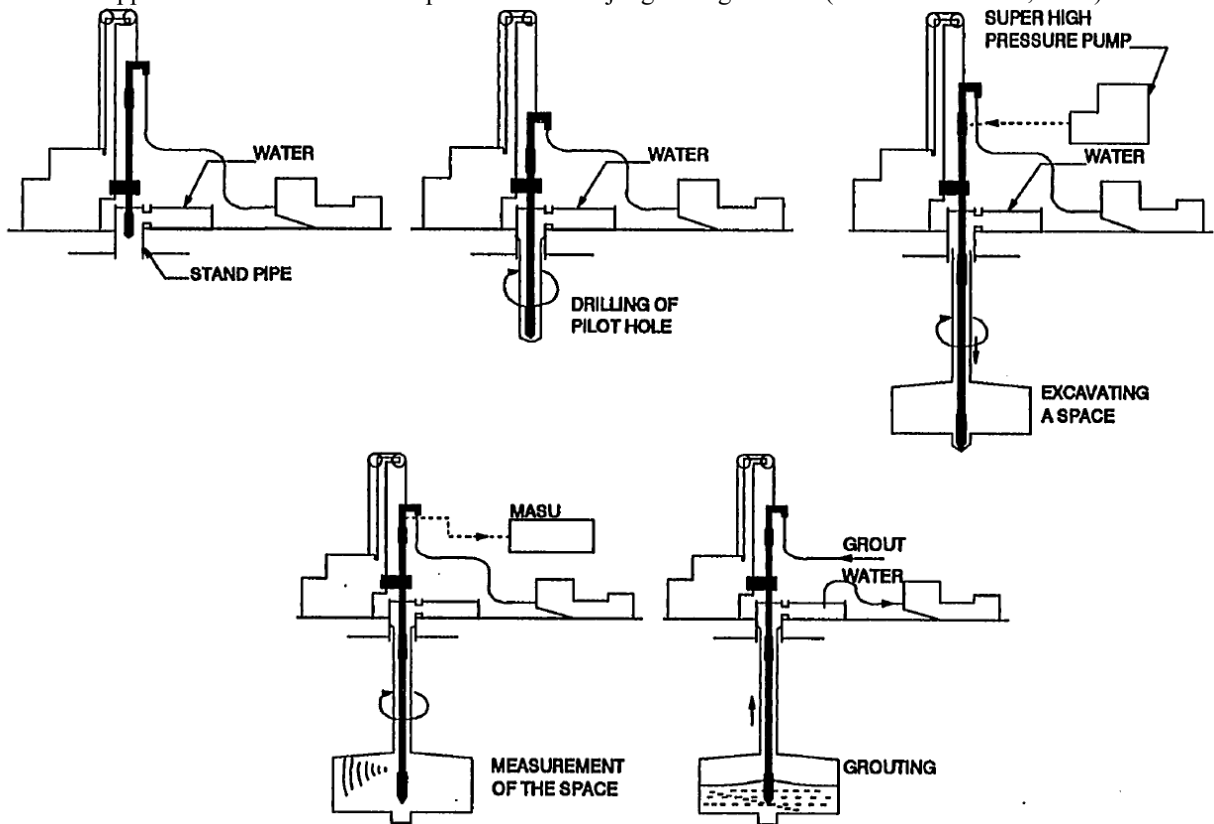


Soil Improvement below excavated bottom

Appendix 3-5 Differences between SSS-MAN method and other three jet grouting methods(Miki & Nakanishi, 1984)

Method	Chemical churning pile method (CCP): a mixing method using a high speed grout jet	Jumbo Jet Special Grout (JSG): a mixing method using a high speed grout jet enveloped by an air jet	Column Jet Grout (CJG): a partial replacement method using a high speed water jet enveloped by air jet	Super Soil Stabilization Management method (SSS-MAN): reverse type replacement method using a high speed water jet enveloped by air jet
Schematic diagram	<p>0.3-0.5 m Effective Dia.</p>	<p>0.6-2.0 m Effective Dia.</p>	<p>1.5-3.0 m Effective Dia.</p>	<p>2.0-4.0 m Effective Dia.</p>
Outline of the method	Uplift of a rotating horizontal grout jet with a super high pressure (20MPa) mixes in-situ soil with grout and produces a cylindrical solidified body	Uplift of a rotating high speed horizontal grout jet enveloped by air jet mixes in-situ soil with the grout and produces a large size cylindrical solidified body	Lifting of a rotating high pressure water jet enveloped by an air jet cut in-situ soil, which is partially removed by the uplift flow of the air and water. The excavation is filled with grout continuously supplied from a rod to produce a cylindrical solidified body	A pilot hole is drilled by reverse circulation, then a rotation super high pressure (60MPa) water jet enveloped by air jet is lowered removing the cut soil through the reverse rod to produce an excavation which is filled with grout after confirmation of the size
Soil type	Cohesive soil (N<5), sandy soil (N<15)	Cohesive soil, sandy soil, gravelly soil	Cohesive soil, sandy soil, gravelly soil	Cohesive soil, sand soil, gravelly soil
Important efficiency	An improved diameter of 300-500mm with a relatively uniform strength with uniformity are attainable	An improved diameter of 800-2000mm and a high strength with uniformity are attainable	An improved diameter of 1500-3000mm and a high strength with uniformity are attainable	A large cylindrical solidified body with a diameter of 2000-4000mm is attainable. Concrete, clay, cement mortar, etc can be used as grout. The diameter of a body can be confirmed on the ground

Appendix 3-6 Construction steps of SSS-MAN jet grouting method (Miki & Nakanishi, 1984)



Chapter 4 LABORATORY JET GROUTING SETUP

This chapter looks at the design procedure of the laboratory jet grouting setup, which simulates the entire jet grouting process. The laboratory jet grouting setup will be used to study the effect of jet grouting on the thermal and mechanical properties of a particular soil condition from the Edmonton area.

4-1. Introduction

Due to the complexity of a number of parameters' effects on soilcrete properties and the heterogeneity of the soil profile, designing soilcrete properties has been a huge challenge and complex task (Tinoco 2012). Many companies and researchers have been investigating how to (1) explain different jet grouting systems, jet grouting case histories in different projects, and modifications of jet grouting systems based on a particular project requirement (Alsayedahmad 1992); and (2) ways to evaluate the effect of different operational parameters, soil types, and jet grouting systems on soilcrete properties. However, no reliable and accurate method exists to be accepted by everyone (Brill, Burke, and Ringen 2003). Many different methods have been discussed to calculate and measure soilcrete properties in Chapter three, but those methods are rare and site-dependent, and involve many limitations in terms of jet grouting systems, soil types, and jet grouting operational parameters. The methods can be over-conservative and may affect project financials and the quality of the soilcrete. Generally, empirical relationships and methods ignore the effect of soil strength and hydrodynamic properties of the jet (Chu Eu Ho 2005). The theoretical calculations have not been experimentally verified yet, and using such approaches may lead the project to undesired results. In the past 10 years, very few researchers have tried to make a physical model of jet grouting in a laboratory to explain the process in more detail (Chu Eu Ho 2005; Ji 2008). Only a single fluid jet grouting with lower grout pressure and flow rate than actual values was used, and in that case, it was used to evaluate only the soilcrete diameter. Physical, mechanical, and thermal properties of the soilcrete have not been studied under the physical modeling of the jet grouting process. Recently, a few researchers have taken a novel approach to data mining to train an artificial neural network model with previous data from different jobsites and conditions. The goal was to predict the soilcrete properties in a new jobsite with totally different conditions (B. Nikbakhtan, Apel, and Ahangari 2014a; B. Nikbakhtan, Apel, and Ahangari 2014b; Tinoco 2012; Tinoco, Gomes Correia, and Cortez 2011a; Tinoco, Gomes Correia, and Cortez 2011b; Tinoco, Gomes Correia, and Cortez 2012). These approaches depend significantly on the data used to train the model. Therefore, during the prediction, if there is a huge variance in jet grouting operational parameters, soil conditions, and grout type between the previous and current data, the prediction will not be precise enough to rely on. The trial jet grouting approach is expensive, time-consuming and site-dependent, which means there is no

chance to modify operational parameters when new ground conditions are encountered. As a result, the approach may not always lead to desirable results.

Also, due to the very fast growth of urbanization and industrialization, every piece of ground may be required for construction purposes (S. Y. Liu et al. 2008). With the rapid development of high-rise and municipal construction such as subways, tunnels, and basements in the major Alberta cities of Edmonton and Calgary, the availability of areas with good ground and soil conditions decreases. Sometimes structures must be built on peaty and weak soils. In such situations, it is important to ensure safe and prompt ground conditions for construction. The main goal of jet grouting is to improve physical, mechanical, and/or thermal properties of a wide range of soils, which consequently reduces ground settlement, deformation, permeability, and heat and energy loss in different projects (J. L. Wang, Wang, and Wang 2009). Although the jet grouting technique has been used for large-scale projects in the past, with the introduction of relatively inexpensive equipment with low maintenance costs and high reliability, its use in small projects has increased. Its ability to underpin deep foundations, even near active buried utility lines under safe conditions, without needing to open excavations, makes the method a highly desirable ground improvement technique for use in municipal areas (Bedenis, Jedele, and Maranowski 2005). Implementing trial jet grouting and finding a particular ground condition with the same properties as a major jobsite in a municipal area with limited working space is impossible and impractical because of the presence of surrounding structures and underground utilities (Haider and Byle 2000). The need to precisely evaluate jet grouting performance and soilcrete properties before an actual project remains crucial.

The best way to evaluate jet grouting performance and soilcrete properties is to conduct a laboratory experiment simulation of jet grouting in a particular soil condition with actual jet grouting parameters and equipment (Ji 2008). However, actual jet grouting equipment is too big to be used in a laboratory. A decision was made for this project to design and build laboratory jet grouting equipment that would have almost the same ability as actual field equipment but with a reduced footprint and cost. To the author's knowledge, to date, no laboratory setup is available for evaluating double and triple fluid jet grouting, which are the most complicated and efficient jet grouting methods. Constructing a complete physical model of the jet grouting system simulates the entire process in a laboratory environment where all parameters can be taken into account together. In the current dissertation, the triple fluid jet grouting system will be modeled

to study the thermal and mechanical properties of the soilcrete in cohesive soil. An advantage of choosing cohesive material is that the hydraulic conductivity of the cohesive soil is low. There is no bleeding or permeation into the surrounding area (Chu Eu Ho 2005) so the boundary of jet grouting can be precisely determined.

4-2. Jet grouting laboratory experiment design

Figure 4-1 shows the necessary equipment to implement the jet grouting technique in the field. It includes five major parts: (1) cement bins; (2) batching plant, which includes water tanks (Figure 4-2); (3) high pressure water (Figure 4-3) and grout (Figure 4-4) pumps with air compressors (Figure 4-5); (4) panel control board of jet grouting operational parameters (Figure 4-6); (5) drilling rig, which includes jetting rod (Figure 4-8) and monitor (Figure 4-9), withdrawal and rotating motions, nozzles (Figure 4-10), swivels (Figure 4-7) to separate grout-air in a double fluid system and to separate grout-air-water in a triple fluid system, and high pressure hoses (Lunardi 1997). The jetting rod and monitor in the double and triple fluid system have a coaxial and triple-duct to allow the separate flow of air-grout and air-grout-water, respectively. On the jetting monitor there is a nozzle for air, grout, and water.

Based on the actual jet grouting equipment and procedure, laboratory equipment for the triple fluid jet grouting system has been designed to simulate the actual process as much as possible. However, as discussed in Chapter three, the main task of shrouded-air is to help the jetting action to be more effective in improving the erosion distance and consequently the diameter of the soilcrete. The presence of air bubbles in the soilcrete structure will have a negative effect on the soilcretes' mechanical properties. Also, mixing the grout with expanded lightweight perlite (ELP) may reduce the mechanical properties while increasing the air voids throughout the soilcrete. Therefore it is expected that the reduction in the mechanical properties will be an issue. On the other hand, there are many constraints regarding the size of the laboratory jet grouting mixing tank. If a large diameter tank is manufactured, more soil is required to fill the tank. This will increase the weight of the tank. Also, there is no need to build a very large diameter of soilcrete specimens in the laboratory experiment. Moreover it would be very expensive to manufacture a coaxial water duct shrouded with air. Hence, compressed air will not be used in order to make the procedure more practical and simplify the process of manufacturing the equipment and nozzles, and also to keep the expenses as low as possible.

Laboratory equipment contains eight main components: a high-pressure pumping plant, grout mixer plant, water and grout swivel and rotary union, jetting monitor and nozzles, high-pressure hoses, rotating and withdrawal systems, relief valve, and mixing tank. Because this is a relatively large project for a laboratory, many price quotes regarding pumps, withdrawal and rotating mechanisms, swivels, nozzles, and manufacturing of the test tank were requested from specialists in the United States, Canada, and Japan (Table 4-1). The cost of the actual triple fluid jet grouting system is \$417,979.45CAD, according to a well-known jet grouting specialist (YBM Co. Ltd). Based on experience, quote estimates, feasibility, accessibility, and technical and economic factors, the John Brooks Company Ltd (JBCL) was chosen to manufacture the equipment. Although the author created an initial design, a complete design was finalized after numerous meetings with JBCL engineers and University of Alberta Machine Shop technicians. The overall cost of the manufacturing was expected to be around 30,000.00 CAD. Engineering aspects of manufacturing and the selection of parts such as pumps and cavitation effects and head loss, motors, nozzles, rods, couplings, and electrical designs, were done by JBCL and are not the focus of the dissertation.

The laboratory jet grouting experiment was designed with two positive displacement diaphragm pumps to pump high pressure water (up to 2500 psi) and the grout mixture (up to 300 psi) into two separate solid stream nozzles. The nozzles were connected to the end of the piping assembly, a so-called monitor, to simultaneously rotate and rise vertically along a linear slide track. The laboratory experiment was designed in such a way that the speed of each pump can be controlled through variable frequency drives (VFD) to control the flow rate. Pressure delivered to each nozzle can be controlled by adjusting the pressure relief valves installed on the discharge of each pump. The rotating and lifting speed of the nozzles can be adjusted through a variable speed controller drive (VSD). The flow and pressure can also be adjusted by using nozzles of different shapes. The laboratory experiment can be specifically used for to test the effects of several adjustable operating parameters on soilcrete properties. The major components of the laboratory experiment are: a model D04 pump with 7.5-horsepower, 1750 rpm, and 208-230 volts motor (water); a 7.5-horsepower NEMA VFD; a model M03 pump with one-horsepower, 1750 rpm, and 208-230 volts motor (grout); a one-horsepower NEMA VFD; two pressure relief valves; a polyethylene water supply tank (65 US gallons); a polyethylene grout supply tank (65 US gallons); a mixer with 1/2-horsepower motor (mounted above grout tank); a jetting tank with

custom cover (42 inches diameter and 40 inches height); a 1/4-horsepower 90 VDC motor with winding spool for vertical motion; a VSD speed controller for vertical motion; a 1/4-horsepower 90 VDC motor with sheaves for rotational motion; a VSD speed controller for rotational motion; a flow meter calibrated for water; a flow meter calibrated for grout mixture; a two-port rotary union with 1/2-inch NPT connections; a rotating assembly; two 1.5 mm custom spray nozzles; two 2.5 mm custom spray nozzles; a PW1/4M0004 model solid stream nozzle; and a PW1/4M0003 model solid stream nozzle. The final plan and front view of the laboratory experiment are illustrated in Figure 4-11 and Figure 4-12. The following sections explain the design criteria of each component in more detail.

4-3. High pressure pumping plant

The main components of the water jet application are the water storage tank, pump, delivery pipe, control valve, relief valve, and nozzles (Ji 2008). The water passes through the pump and is pressurized into the delivery pipe and then into the nozzles. The nozzles have a smaller orifice diameter than the pipes; thus the velocity of water is being accelerated to pass the nozzles. At the same time, the control valve controls the amount of water that flows toward the nozzles. The relief valve is designed for safety reasons, to divert extra water to the storage tank to prevent any water build-up. Any water jet application shall be designed based on a particular task. Table 4-2 illustrates some examples of water jet applications.

The selection of the water and grout pump shall be based on the application and amount of energy needed. A high flow rate means more energy can be delivered and is beneficial for more applications. However, the rate must be carefully chosen based on many factors of a particular task; otherwise, it can raise the operational cost and volume of water usage. Generally, pumps are divided into positive displacement and hydraulic intensifiers. Positive displacement or plunger pumps are piston-driven mechanisms, which can be used with low to intermediate pressure. This means that the flow rate and pressure are in the ranges of 70 to 2000 bar and 10 to 2000 L/min (Labus 2001; Vijay 2001). Applications such as cleaning, mining, material cutting, hydro-demolition, and jet grouting use the same flow rate and pressure. The plunger pump was used in this laboratory experiment. If the pump runs with same speed, the flow rate and pressure are consistent. However, the plunger diameter can be modified to produce different flow rates and pressures. Based on the number of plungers, there is a variation in the flow rate

(Figure 4-13). The amount of variation becomes smaller with a higher number of plungers. A three-plunger or triplex pump is the most common (Ji 2008), and was used in the current laboratory experiment. The power output of plunger pumps is calculated using Equation 4-1:

Equation 4-1

$$P = Q \times p$$

Where, P: power output from the plunger pump (Watt)
Q: flow rate (m³/s)
p: operation pressure (Pa)

Power output can be expressed as kW with Equation 4-2:

Equation 4-2

$$P = 0.00167 \times Q \times p$$

Where: P: power output from the plunger pump (kW)
Q: flow rate (Lit/min)
p: operation pressure (bar)

The internal leakage and friction of the plunger pump can cause some drop in output pressure; thus, the efficiency of plunger pump calculated using Equation 4-3 is always less than one and is typically between 85 and 92 % (Ji 2008).

Equation 4-3

$$\eta = \frac{P}{P_{in}} \times 100\%$$

Where, η : efficiency of the pump, %
P: power output from the pump, Watt
 P_{in} : power input to the pump, Watt

Another pressure/head loss occurs when pressurized water is delivered through the pipes to reach the nozzles. Basically, this is the major head loss. The selection of pipe material and size shall be done carefully in consideration of the flow rate and operating pressure. However a safety factor of 2.5 must be always considered for the bursting pressure of pipes based on maximum operation pressure (WJA 2002). For any straight portion of pipe, head loss is considered as mechanical energy converts to internal energy. In laminar flow ($Re < 2000$) and turbulent flow ($Re > 3000$), the conversion is caused by the viscous resistance to flow, and dissipation of the turbulence energy, respectively. Head loss in a pipe is calculated using Equation 4-4 (Ji 2008).

Equation 4-4

$$\Delta p = f \cdot \frac{\rho_w \cdot v^2}{2} \cdot \frac{L_H}{D_H}$$

Where, Δp : pressure loss in the pipe, Pa
 f : friction factor, dimensionless
 ρ_w : density of water, kg/m^3
 v : flow velocity in the pipe, m/s
 L_H : pipe length, m
 D_H : pipe diameter, m

For laminar flow:

Equation 4-5

$$f = \frac{64}{Re}$$

Equation 4-6

$$Re = \frac{\rho_w \cdot D_H \cdot v}{\mu}$$

Where, Re : Reynolds number

μ : dynamic viscosity of water, Pascal. sec ($\frac{\text{kg}}{\text{m}} \cdot \text{s}$)

For turbulent flow, a value of f can be calculated from the Moody diagram which plots f against the Reynolds number. However, there are some empirical equations to calculate this value. Equation 4-7 can be used for most commercial high water pressure applications for Re ranging from 4,000 to 100,000.

Equation 4-7

$$\frac{\Delta p}{L_H} = \frac{712 \times Q^2}{D_H^5 \times Re^{0.25}}$$

Where, Δp : pressure loss in the pipe, bar

Q : flow rate, m

ρ_w : density of water, kg/m^3

L_H : pipe length, m

D_H : pipe diameter, m

Re : Reynolds number, dimensionless and for water = $21115 \times \frac{Q}{D_H}$

Equation 4-8 can be derived by substituting Re in Equation 4-7. Pressure loss is highly pipe diameter-dependent, which means that with a small increase in the pipe diameter, the head loss will decrease (Ji 2008). However, head loss is dependent on pipe length as well. Thus, to reduce the head loss, a pipe with a large internal diameter and short length is recommended. Head loss also occurs in fitting and valves. The value for such losses can be found in the manufacturer's guide for fittings and valves. However, Momber (1998a) stated that the pressure loss for any pipe fitting is equivalent to three meters of pipe length of the same diameter.

Equation 4-8

$$\frac{\Delta p}{L_H} = \frac{59.1 \times Q^{1.75}}{D_H^{4.75}}$$

In field operations, typically very high capacity pumps operate at a pressure between 2900 to 8700 psi (20 to 60 MPa), to produce high flow rates of 17 to 48 gpm US (70-180 lit/min). The fluid velocity is typically between 200 to 350 m/sec. Regarding the selection of the water and grout pumps, all head losses must be calculated and taken into consideration. P Croce and Flora (2000) stated that a reduction factor of $\alpha = 0.8$ can be applied to pump pressure to account for all head losses in the line and nozzles. Available pressure at the nozzles (P_i) can be defined as follows:

Equation 4-9

$$P_i = \alpha P_{\text{pump}}$$

There is another hydrostatic pressure in the borehole at the nozzle outlet caused by slurry and is given by:

Equation 4-10

$$P_{\text{static}} = \rho_{\text{slurry}}gh$$

Where, ρ_{slurry} : slurry density in borehole
 g : acceleration due to gravity
 h : depth of the nozzle

C. E. Ho (2008) stated that additional pressure is needed to keep the upward flow of the slurry in the borehole and can be accounted for by applying a multiplying factor of $\beta > 0$. Total pressure at nozzle outlet (P_o) can be expressed as follows.

Equation 4-11

$$P_o = (1 + \beta)P_{\text{static}}$$

However, in a normal jetting condition, P_i is several orders of magnitude higher than P_o . Thus, the jet penetration distance is independent from the value of β .

In the current laboratory experiment, due to the high volume of containment that will be produced and issues with disposal, it is not practical to use such a high flow rate as a field operation. However, an attempt was made to use the maximum possible pressure and flow rate in the laboratory experiment, taking into consideration the current facilities, feasibilities, and budget. For the water pump, a high pressure triple-plunger electrical pump (D/G-04-X) with a 7/8-inch (22.22mm) shaft diameter was chosen (Figure 4-14 and Figure 4-15). The maximum pressure and flow rate of the pump at a maximum speed of 1790 rpm is 2500 psi (170 bars) and 2.9 gpm US (11.0 lit/min). Based on the manufacturer's guidelines (Equation 4-12), a 7.5-HP TEFC three-phase AC motor was chosen to drive the pump. A VFD MA7200 was used for precise speed and torque control of the water pump, to be able to produce different pressures and flow rates. The inlet of the water pump was linked with a storage water polyethylene tank with a capacity of 65 US gallons using an SS flex house with a one-inch diameter. For a safety control, the outlet pipe from the pump was linked with a high pressure relief valve with a 3/4-inch diameter set to 2500 psi, which was connected to a circulate pipe that leads back to the water tank. All specifications of the water pump and motor, relief valve and VFD are shown in Appendix 4-1 to Appendix 4-4.

Equation 4-12

$$\text{electric motor HP} = \frac{6 \times \text{rpm}}{63000} + \frac{\text{gpm} \times \text{psi}}{1460 - \left(\frac{\text{psi} - 500}{20}\right)}$$

For the grout pump, an intermediate pressure triple-plunger electrical pump (D/G-03-X) with a 7/8-inch (22.22mm) shaft diameter was chosen (Figure 4-16 and Figure 4-17). The maximum pressure and flow rate of the pump at a maximum speed of 1750 rpm is 250 psi (17 bars) and 3.0 gpm US (11.3 lit/min). Based on the manufacturer's guidelines, (Equation 4-13) a 1-HP TEFC three-phase AC motor was chosen to drive the pump. A VFD MA7200 was used for precise speed and torque control of the grout pump to be able to produce different pressures and flow rates. The inlet of the grout pump has been linked with a storage grout polyethylene tank with a capacity of 65 US gallons using an SS flex house with a two-inch diameter. For a safety control, the outlet pipe from the pump was linked with a high pressure relief valve with a 3/4-inch

diameter set to 500 psi, which was connected to a circulate pipe back that leads back to the grout tank.

Equation 4-13

$$\text{electric motor HP} = \frac{6 \times \text{rpm}}{63000} + \frac{\text{gpm} \times \text{psi}}{1460}$$

To mix the water and cement in the grout tank, a Neptune mixer with 1/2-HP motor with 32 inches of shaft length and a 5/8-inch shaft diameter was chosen and mounted on a steel frame on top of the grout tank. In addition, two flow meters and pressure gauges were designed and placed in both the water and grout lines to monitor both the flow and pressure after the fluid was pressurized (Figure 4-18). Another two pressure gauges were placed on top of the rod before the rotary union to measure fluid pressures before they pass through the monitor to reach the nozzles (Figure 4-19). The maximum working pressure of the water and grout pressure gauges is 3000 psi and 600 psi, respectively. The water and grout flow meters were designed for 1-cps liquid with 1/4-inch diameter and 10-cps liquid with 1/2-inch diameter, respectively, with accuracy of 2% and maximum line pressure of 3000 psi (Figure 4-20).

All specifications of the grout pump and motor, mixer, relief valve and VFD are shown in Appendix 4-4 to Appendix 4-9.

To calculate the head loss, the dynamic viscosity of the fluid is required. The viscosity is known for the water, but has to be measured for the grout. To confirm the reduction factor of $\alpha = 0.8$, head/pressure loss was calculated for the water line using a Pressure Drop open source calculator. To make this calculation, the whole piping assembly line from the water and grout pumps through to the nozzles was taken into consideration as follows.

Water pump	Grout pump
	Steel nipple adapter, 3/8 inch * 1½ inch, 3000 psi
Steel nipple pipe ½ inch diameter 6 inch, 3000 psi	Steel reducer coupling, 3/8 inch to ½ inch, 3000psi
	Steel nipple pipe ½ inch diameter 6 inch, 3000 psi
Tee ½ inch * ½ inch * ¼ inch, 3000 psi	Tee ½ inch * ½ inch * ¼ inch, 3000 psi
Pressure gauge	Pressure gauge

Adapter, ½ inch to ¾ inch, 3000 psi
 Relief valve, ¾ inch diameter
 Reducer bushing, ½ inch to ¾ inch
 Black pipe, ½ inch * 72 inch, 6000 psi
 Reducer coupling steel, ½ inch to ¼ inch, 3000psi
 Steel pipe, ¼ inch * 4 inch, 3000 psi
 Flow meter
 Steel pipe, ¼ inch * 4 inch, 3000 psi
 Reducer coupling steel, ½ inch to ¼ inch, 3000psi
 Steel pipe, ½ inch * 14 inch, 3000 psi
 Elbow
 Vertical steel pipe, ½ inch * 120 inch, 3000 psi
 Black hose, ½ inch * 36 inch, 6000 psi
 Tee ½ inch * ½ inch * ¼ inch, 3000 psi
 Pressure gauge
 Black hose, ½ inch * 4 inch, 3000 psi
 Rotary union
 Black hose, ½ inch * 72 inch, 3000 psi
 Elbow, ½ inch to 1 inch, 4000 psi
 Steel pipe, 1 inch * 50 inch, 3000 psi
 Reducer coupling, 1 inch * ½ inch
 Elbow steel, ½ inch, 4000 psi
 Elbow steel, ½ inch, 4000 psi
 Elbow steel, ½ inch, 4000 psi
 Nozzle

Adapter, ½ inch to ¾ inch, 3000 psi
 Relief valve, ¾ inch diameter
 Reducer bushing, ½ inch to ¾ inch
 Black pipe, ½ inch * 72 inch, 6000 psi
 Tee ½ inch * ½ inch, 3000 psi
 Steel pipe, ½ inch * 4 inch, 3000 psi
 Flow meter
 Steel pipe, ½ inch * 14 inch, 3000 psi
 Elbow steel, ½ inch, 4000 psi
 Vertical steel pipe, ½ inch * 120 inch, 3000 psi
 Black hose, ½ inch * 36 inch, 6000 psi
 Tee ½ inch * ½ inch * ¼ inch, 3000 psi
 Pressure gauge
 Steel pipe, ½ inch * 16 inch, 3000 psi
 Rotary union
 Black hose, ½ inch * 72 inch, 3000 psi
 Elbow, ½ inch to 1 inch, 4000 psi
 Steel pipe, 1 inch * 50 inch, 3000 psi
 Reducer coupling, 1 inch * ½ inch
 Elbow steel, ½ inch, 4000 psi
 Elbow steel, ½ inch, 4000 psi
 Elbow steel, ½ inch, 4000 psi
 Nozzle

The overall head loss in the water line under a maximum flow rate was around 11 psi, which is around a 1/2-percent of the total pressure. Appendix 4-10 shows an example of the head loss calculations. Although the head loss can be considerably higher in the grout line because of grout high dynamic viscosity, head loss can be neglected because in the laboratory experiment, all pipes are short. However, as explained before, two pressure gauges were installed on top of the supporting frame to monitor the actual fluid pressures right before the fluid passes the rotary union towards the nozzles (Figure 4-19). The measured pressure on the gauges was taken into account as actual jetting pressures.

4-4. Nozzles

Even though nozzles are the smallest part of the jet grouting system, they are the most important (Labus 2001) and control the pressure distribution and pattern of the jetting, which determines

the system's effectiveness (Kee and Kurko 1972). The water is pressurized in the pump and pushed towards the lines to pass out of the nozzle orifice. For a given flow rate, the size and geometry of the orifice control the velocity of water leaving the nozzle (Ji 2008). As discussed earlier, the entry angle, length of the straight exit section, and surface roughness of nozzles are the most important issues in the nozzle design (Vijay 2001). Nikonov and Shavlovsky (1961) and Summers (1995) suggested a nozzle design in Figure 4-21, which can produce a more coherent jet stream than other designs. Frank et al. (1972) stated that a nozzle with an internal angle of 11 degrees and a straight section of a three-nozzle diameter is optimal.

For jet grouting applications, a nozzle with a narrowing angle of 13 degrees and a certain straight portion of 2.5 to three times the diameter has the best performance (Mitsuhiro Shibasaki 2003). Figure 4-22 shows a recommendation of the Japanese jet grouting association regarding nozzle design. In addition to nozzle design, a good flow condition before the nozzle is required to have an effective jetting. Nikonov and Shavlovsky (1961) and Vijay (2001) suggested using a large circular inlet pipe with a diameter of nine to 10 times the nozzle diameter and a straight length of 40 to 50 times the inlet pipe diameter before the nozzle can minimize fluid turbulence. However, due to space constraints, these conditions are not possible in most jet grouting applications.

The surface roughness of nozzles also affects the jetting performance. Barker and Selberg (1978) observed that a smooth finish of nozzles helps to produce a more coherent jetting stream over a longer distance. Electroformed nickel nozzles were generally better than brass and carbide nozzles. Roughness on the internal surface should not exceed 2.5×10^{-4} millimeters.

The nozzle orifice size is also important in the effectiveness of the jetting system. For a given flow rate, any reduction in a nozzle outlet orifice will increase the jetting velocity, and consequently operational pressure to push the fluid will increase. Ji (2008) stated that a 10% reduction in nozzle diameter leads to a 23% increase in jetting velocity and a 52% increase in dynamic pressure, which means that a more powerful pump is required to drive the fluid.

The exit velocity of cutting water (v_0) with a nozzle pressure of P_i is given by Equation 4-14 (Momber 1998b). c_d is a dimensionless coefficient that accounts for transforming the potential energy into kinetic energy. It depends on the nozzle design and pump pressure. Its value is between 0.6 for poor nozzle design and 0.95 for good design (Summers 1995).

Equation 4-14

$$v_0 = c_d \sqrt{\frac{2P}{\rho_w}}$$

Where, v_0 : jet velocity, m/s
 ρ_w : mass density of water, kg/m³
 c_d : an efficiency parameter, dimensionless
P: operating pressure ($P_i - P_0$), Pa

The flow rate is equal to the nozzle area multiplied by the jet velocity. Based on the maximum flow rate of the cutting water jet ($Q_w = 11$ l/min) and the maximum computed water jet exit velocity ($v_0 = 200$ m/s) at maximum water pressure, the water nozzle diameter was estimated to be about one millimeter. Also, based on the maximum flow rate of the grout jet ($Q_g = 11.3$ l/min) and the average computed grout jet velocity based on the different mixtures ($v_0 = 50$ m/s) at maximum grout pressure, the grout nozzle diameter was estimated to be about two millimeters.

All jetting lines from the output of the pumps into the pressure gauges through the relief valves and the flow meters were 1/2-inch black hoses with a maximum operating pressure of 6000 psi. From the flow meters to the top of the supporting frame where the jetting lines were connected to the rotary union, steel pipes with a 1/2- inch diameter and maximum working pressure of 3000 psi were used. To meet the criteria of having a large pipe diameter of nine to 10 times the nozzle diameter for the nozzle with a one to 2.5 millimeters diameter, steel pipes with one-inch diameter and maximum working pressure of 3000 psi from the rotary union to nozzles were chosen to reduce the turbulence flow as much as possible. However, since the fluid is injected horizontally and the monitor was placed vertically, it was not possible to have a straight section of 40 to 50 times the pipe diameter before the nozzle.

Four carbon steel nozzles were designed and manufactured for water and grout lines (Figure 4-23). Figure 4-24 and Table 4-3 show the specifications of the nozzles. All of the nozzles have a convergence angle of 13 degrees. Based on previous studies (Ji 2008), the cone section length where the fluid is accelerated through the orifice was determined to be seven times

the nozzle diameter, D , ($L_2 = 7D$), and the straight section before the orifice was considered to be four times the nozzle diameter ($L_3 = 4D$). Another two PW nozzles with smaller orifice sizes were chosen for water (030) and grout (040) lines (Figure 4-25). Table 4-4 shows the performance of these two nozzles under different pressures. All specifications of the PW series of nozzles are shown in Appendix 4-11. In the experiment, one pair of nozzles was used in jet grouting based on its performance on a particular soil condition.

Jet velocity can also produce reaction force; however, one of the advantages of a water jet is that the reaction force is relatively low, even in high pressure operations. Reaction force can be calculated using the impulse law of flow continuity as shown in Equation 4-15 (Momber 1998a). The reaction force for a water jet with pressure of 400 bar and a flow rate of 20 L/min is only 94N.

Equation 4-15

$$F_R = \dot{I}_j = \dot{m} \cdot v_j = (\rho_w \cdot Q) \cdot \sqrt{\frac{2P}{\rho_w}} = Q \cdot \sqrt{2P \cdot \rho_w}$$

Where,

- F_R : reaction force, N
- \dot{I}_j : jet impulse flow, N
- \dot{m} : water mass flow rate, kg/s
- v_j : jet velocity, m/s
- ρ_w : density of the water, kg/m³
- Q : flow rate, m³/s
- P : operating pressure, Pa

4-5. Vertical motion mechanism

To have a very smooth vertical movement, both solid pipes (monitor) were mounted on a uni-guide track with a two-piece aluminum design. The result is a unique assembly that eliminates tolerance stack-up, and dampens the shock loads. The maximum static load capacity of the uni-guide is 1000 lbs. After mounting the monitor on the uni-guide, the whole system was attached to a 1/4-HP gear motor with a maximum of 8 rpm using a swivel and a 25ft 3/16-inch steel cable

with a maximum working load of 800 lbs to produce vertical movement on the monitor (Figure 4-26 and Figure 4-27). Appendix 4-12 illustrates the specifications of the gear motor. The gear motor was connected with a VSD to control the speed of the motor, which consequently controlled the withdrawal rate. The design specification of the VSD unit is presented in Appendix 4-13.

The motor and winding spool must be securely anchored to the floor or a heavily weighted skid to provide sufficient counterweight for the rotating and lifting assembly (Figure 4-28). JBCL suggests that the motor should be oriented so that the winding spool is pointing forward and is positioned more than halfway to the front from the back of the frame. This will encourage the cable to wind properly onto the spool rather than bunching up at the far end (Figure 4-29). Appendix 4-14 illustrates the Uni-Guide vertical motion data sheet.

4-6. Rotation motion mechanism

To separate the water and grout lines, a rotary union was used. All piping assembly from the pumps' side was connected to a two-passage rotary union where separate rotations of the monitor and rod pipes are possible, while the piping assembly on the pump hand side is constant (Figure 4-30). The specification of the rotary union is shown in Appendix 4-15. To rotate the monitors on the rotary union, the V-belt mechanism was used with a connection to a 1/4 HP gear motor (Figure 4-31). Appendix 4-16 illustrates the specifications of the gear motor. The gear motor was connected to a VSD to control the speed of the motor, which consequently controlled the rotation speed. The design specification of VSD unit is presented in Appendix 4-13.

4-7. Jet grouting mixing tank

A custom-made jet grouting tank that is 42 inches in diameter and 40 inches high was designed based on the laboratory feasibilities and the nature of jet grouting (Figure 3-32). As discussed previously, cohesionless soils are easy to cut and erode because they have only moisture as a binder and nothing else. However, clays are difficult to erode because they have cohesion. Clays are generally eroded in chunk pieces, which are larger than the size of a grain of sand. Since uplift velocity is not great enough to exhaust these particles to the ground surface, annulus plugging can occur. To prevent this, casing was modeled on the cap of the tank to accelerate the outflow of the spoil material. The casing was connected to the spoil material-collecting drums

(Figure 4-33 and Figure 4-34). Four holes were designed on the perimeter of the tank to allow the entry of compressed air and simplify the procedure to demold the hardened soilcrete after the jet grouting process. After the jet grouting, all of the bolts can be removed from the bottom of the tank. Using the other four chain hooks around the tank, the whole tank can be removed and the hardened soilcrete will be left on the bottom of the tank for further investigation.

4-8. Control panel

A control panel was designed to control all jet grouting operational parameters at the same time using all VFD for the water and grout pump, speed controller for vertical and rotational motions, and mixer motor and emergency stops for each motor (Figure 4-35). The electrical configuration of the system was designed by JBCL and is shown in Appendix 4-17.

Table 4-1 Jet grouting equipment quotes

Company Components		Equipment Type						
		Field	Laboratory					
		YBM CO., LTD	John Brooks CO., LTD	Different Companies and Manufacturers				
Water pump		\$84,554.00	\$4,931.00	\$58,000.00 ¹	\$4,795.00 ²	\$3,851.00 ³	\$72,873.00 ⁴	
Grout pump		\$43,539.00		\$22,283.91 ⁵			\$24,314.00 ⁶	
Jet Grout Machine	Electrical	\$141,344.00	\$2,933.00	\$2,933.00 ⁷				
	Rotation mechanism		Rotation swivel	\$1,380.00 ⁸	\$2,285.00 ⁹			
			Gear-motor & other parts	\$3,967.00	\$3,967.00 ¹⁰			
	Vertical motion mechanism		\$1,875.05	\$4,398.00 ¹¹				
	Wooden frame		\$1,106.00	\$1,106.00 ¹²				
	Nozzles		\$25,320.00	\$2,064.00	\$2,064.00 ¹³			
Mixing plant/Mixer		\$103,484.00	\$6,860.55	\$39,300.00 ¹⁴				
Water, grout, test & disposal tank & pipes		\$4,391.00						
Spare parts for pumps & J.G. tools		\$7,131.00						\$1,610.00
Shipping and insurance		\$8,216.45	-	-	-	-	-	
TOTAL (CAD)		\$417,979.45	\$26,726.60	\$137,946.91	\$84,741.91	\$83,797.91	\$154,850.00	

Table 4-2 Water jet applications (Summers 1995) (adopted from (Ji 2008))

Application	Operational Pressure (bar)	Flow Rate (L /min)
Car Washes & Cleaning	70	20
Coal & Rock Mining	70	4000
Industrial Cleaning	140~1400	20
Mining & Demolition	700~1000	40~200
Industrial Machining	2000~4000	4
Impulse Fragmentation	2000~7000	40~80
Special Applications	>70000	Varied flow

¹ Con-Tech Systems LTD.

² Renown Industries LTD.

³ Rotating Right INC.

⁴ TDH Fluid Systems INC.

⁵ Wajax industrial components LP

⁶ TDH Fluid Systems INC.

⁷ Assumption: the same as the John Brooks Co., LTD

⁸ Rotary Systems, Inc.

⁹ Dynamic Sealing Technologies, Inc.

¹⁰ Assumption: the same as the John Brooks Co., LTD

¹¹ Newmark Systems, Inc.

¹² Assumption: the same as the John Brooks Co., LTD

¹³ Assumption: the same as the John Brooks Co., LTD

¹⁴ Con-Tech Systems LTD.

¹⁵ Assumption: the same as the John Brooks Co., LTD

Table 4-3 Specifications of designed nozzles (mm)

Fluid	D	T	D ₀	T ₀	L ₁	L ₂	L ₃	L ₄	L ₁ + L ₂ + L ₃	B
water	1.5	7.5	3.89	6.30	16.5	10.5	6	15	33	13
	2.5	7	6.49	5.01	5.5	17.5	10			
grout	1.5	7.5	3.89	6.30	16.5	10.5	6			
	2.5	7	6.49	5.01	5.5	17.5	10			

Table 4-4 Nozzle performance in different pressure

Nozzle size	Orifice Dia., mm	GPM @ PSI										
		100	200	250	400	600	800	1000	2000	3000	4000	5000
030	1.09	0.47	0.67	0.75	0.95	1.16	1.34	1.5	2.12	2.6	3.00	3.35
040	1.32	0.63	0.89	1.00	1.30	1.55	1.79	2.00	2.83	3.46	4.00	4.47

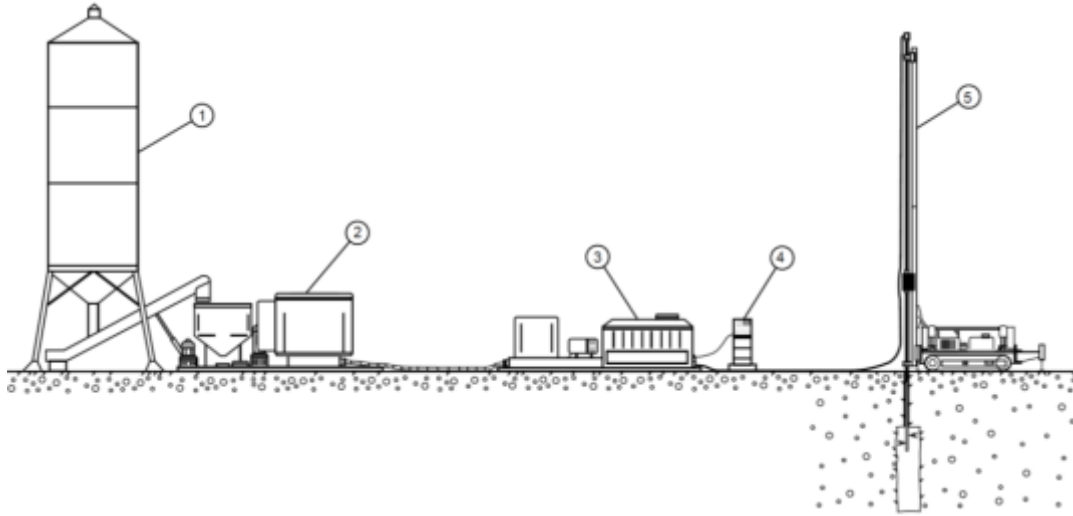


Figure 4-1 Equipment required to perform jet grouting treatment (Lunardi 1997)



Figure 4-2 Agitator and mixing unit to mix the grout; internal diameter 96cm; depth 90cm



Figure 4-3 Water high pressure pump; maximum pressure: 50MPa and maximum flow rate: 70lit/min



Figure 4-4 Grout high pressure pump



Figure 4-5 Air compressors



Figure 4-6 Control panel of jet grouting operational parameters



Figure 4-7 Water, grout and air swivel jointed to the rod



Figure 4-8 Triple-duck cross section of triple fluid jet grouting rod



Figure 4-9 Triple fluid jet grouting monitor



Figure 4-10 Water, air, and grout nozzles in triple fluid monitor

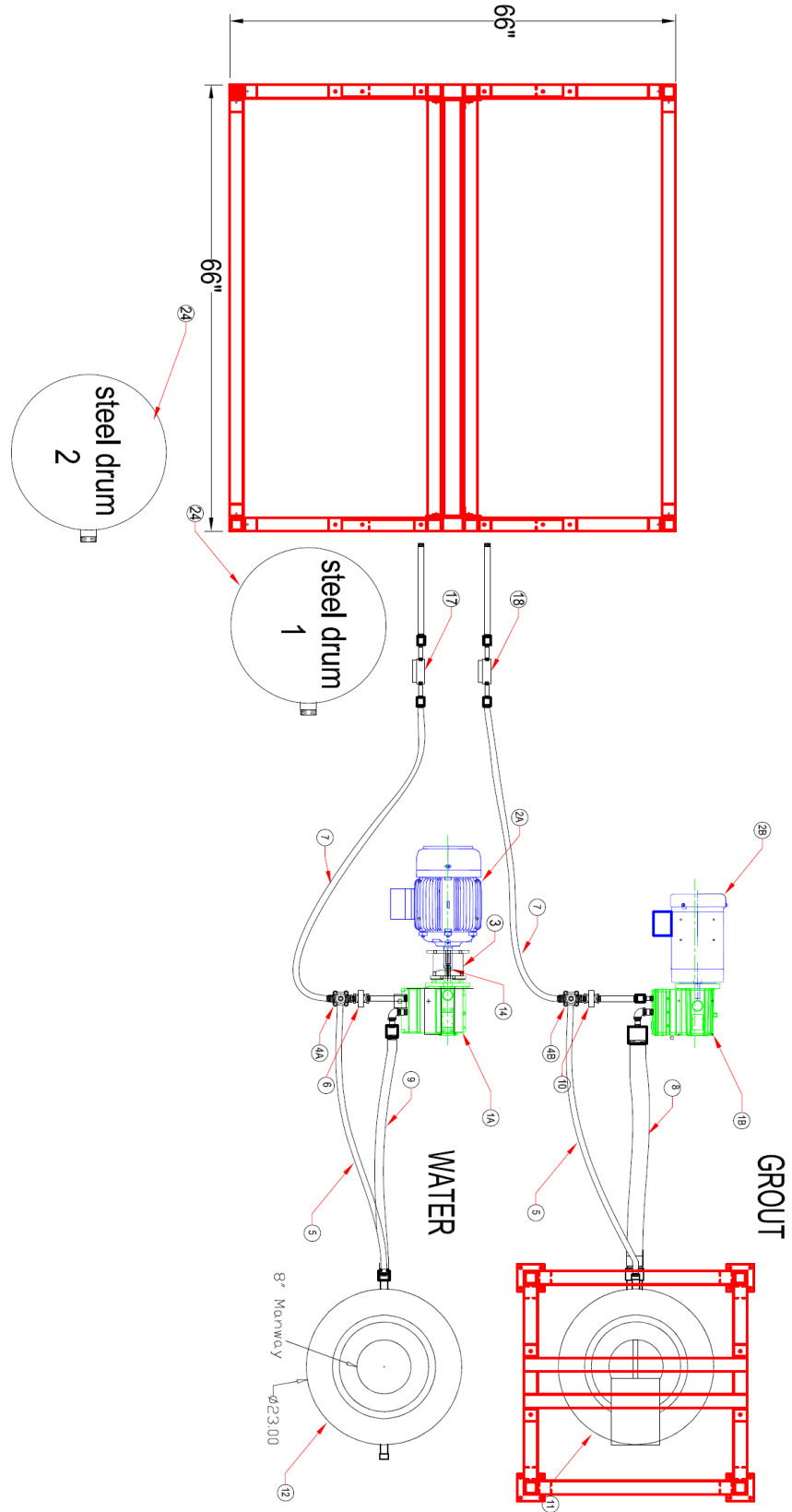


Figure 4-11 Plan view of laboratory experiment

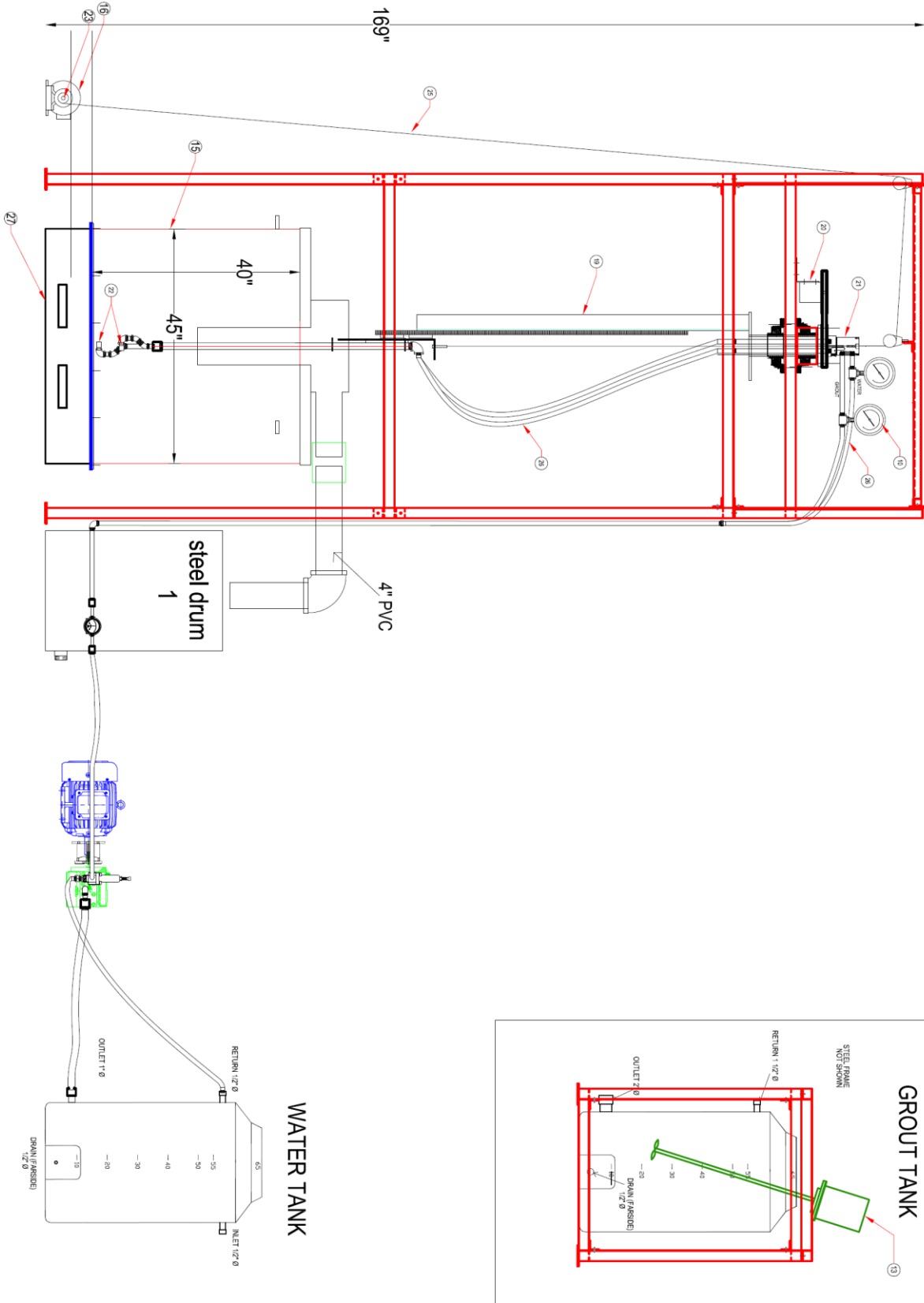


Figure 4-12 Front view of laboratory experiment

- 1A) Water pump (DO4XABTHFEHG)
- 2A) 7.5HP TEFC motor (PDH7/504TE2N)
- 1B) Grout pump (M03XKBTHFEHA)
- 2B) 1HP TEFC motor (CEM3546)
- 3) Hydrocell coupling (A04-022-1202)
- 4A) Relief valve for water pump (C62ABBSSEF)
- 4B) Relief valve for grout pump (C22AABASSEF)
- 5) ½ inch diameter hoses × 72 inches long with coupling (S3330278 109-08LMLM/72" with 0808-08-08)
- 6) 3000 psi pressure gauge (025FF03000EX)
- 7) ½ inch diameter hoses × 144 inches long (S3330278 109-08LMLM/144")
- 8) 2" × 36" SS flex hose (HOSE2-77012)
- 9) 1" × 36" SS flex hose (HOSE1-77012)
- 10) 600 psi Pressure gauge (025FF00300)
- 11) SS65 Tank (SS65-Grout Tank)
- 12) SS65 Tank (SS65-Water Tank)
- 13) B3.0 Mixer (B3.0)
- 14) M38 Shaft coupling (A04-038-1203)
- 15) Custom tank (Q12-1339-R4)
- 16) 1/4HP 90VDC motor (10870000)
- 17) Water flowmeter 1 cps liquid ¼ inch diameter (2221FGS-1E-2.5B-C-0-5-W)
- 18) Grout flowmeter 10 cps liquid ¼ inch diameter (2321FGS1E25BC0663GPMS)
- 19) Rotating and lifting assembly (S1920 Rotating Assembly)
- 20) 1/4 HP 90 VDC motor (M1135042)
- 21) ½"2 port rotary union (12-N-23212)
- 22) Nozzles (Nozzles-77012)
- 23) Spool mounted to motor shaft (2IN Winding Spool)
- 24) Steel drum (10758)
- 25) Steel cable (25FT×3/16 INWSWIVEL HOOK)
- 26) ½ inch diameter hoses × 60 inches long with coupling (S3330278 109-08LMLM/60" with 0808-08-08)
- 27) Wooden skid 48" × 48" × 8.5" (S1920 SUPPORT SKID)

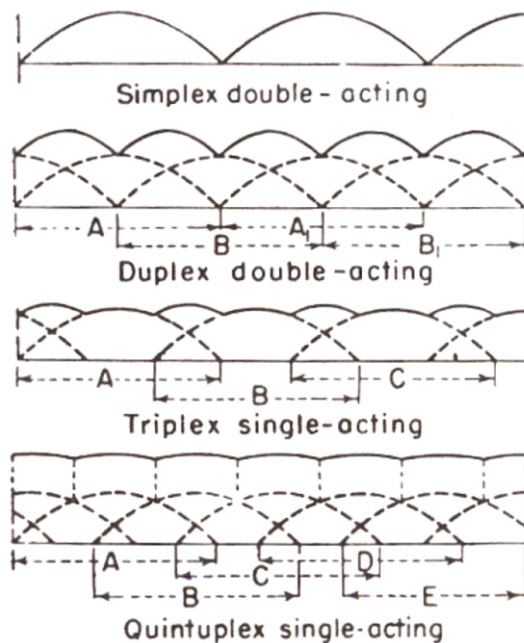


Figure 4-13 Flow variation for different plunger numbers (Gronauer 1972) (adopted from (Ji 2008))

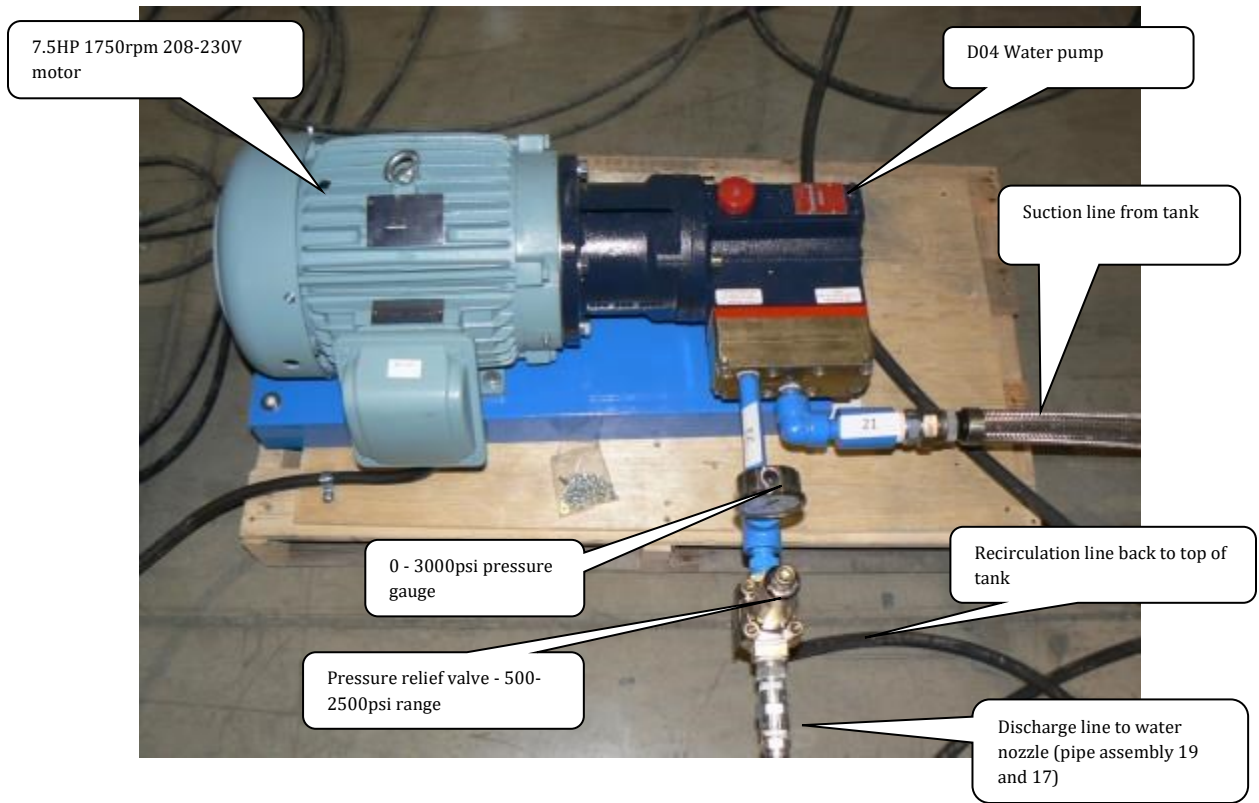


Figure 4-14 Water pump and motor



Figure 4-15 Water jetting plant

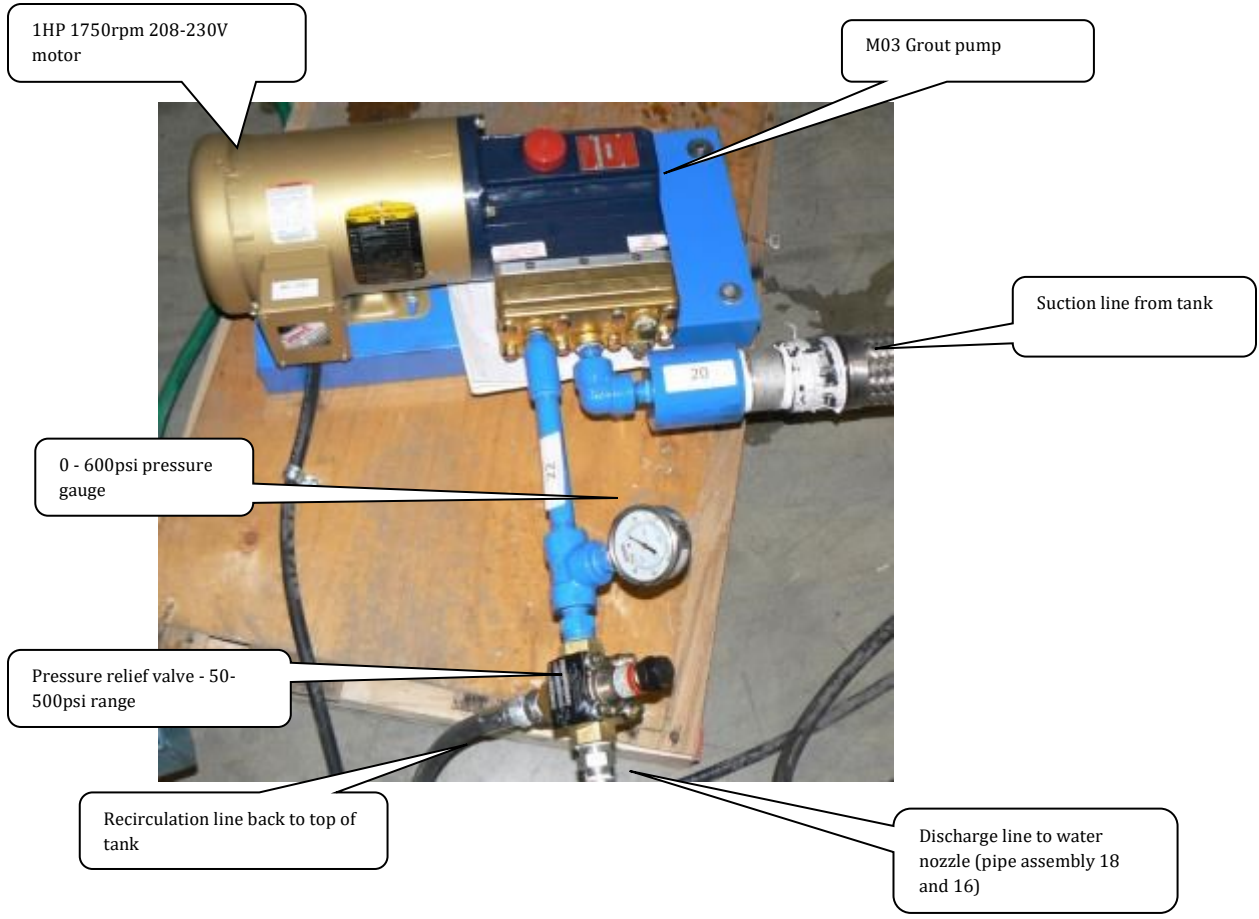


Figure 4-16 Grout pump and motor



Figure 4-17 Grout jetting and mixing plant



Figure 4-18 Flow meters in grout and water line



Figure 4-19 Pressure gauges on top of the frame before rotary union



Figure 4-20 Grout mixing plant

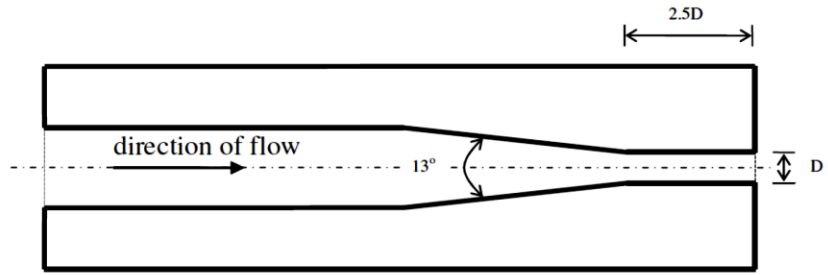


Figure 4-21 Optimal nozzle design (Ji 2008)

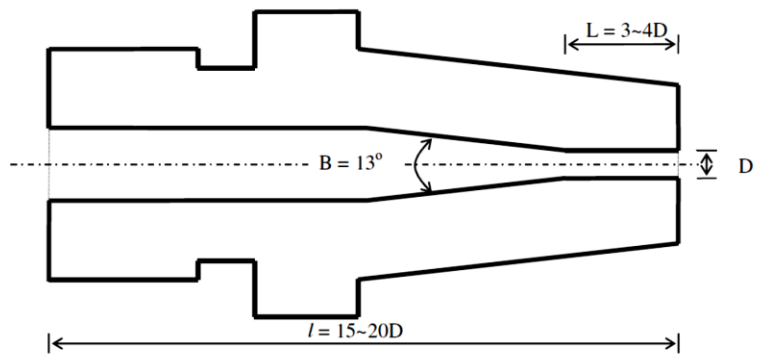


Figure 4-22 Nozzle design for jet grouting (JJGA 2005)



Figure 4-23 Designed nozzles with bigger orifices

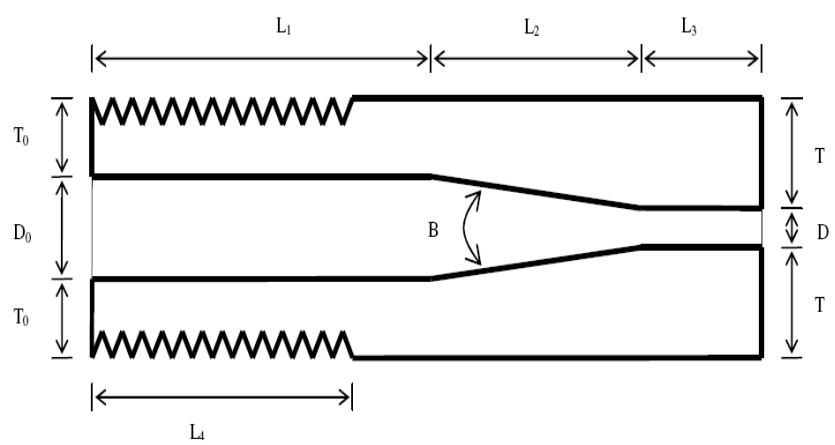


Figure 4-24 Nozzle geometry (Ji 2008)



Figure 4-25 PW nozzles with smaller orifice sizes



Figure 4-26 Uni-Guide assembly and steel cable of vertical motion

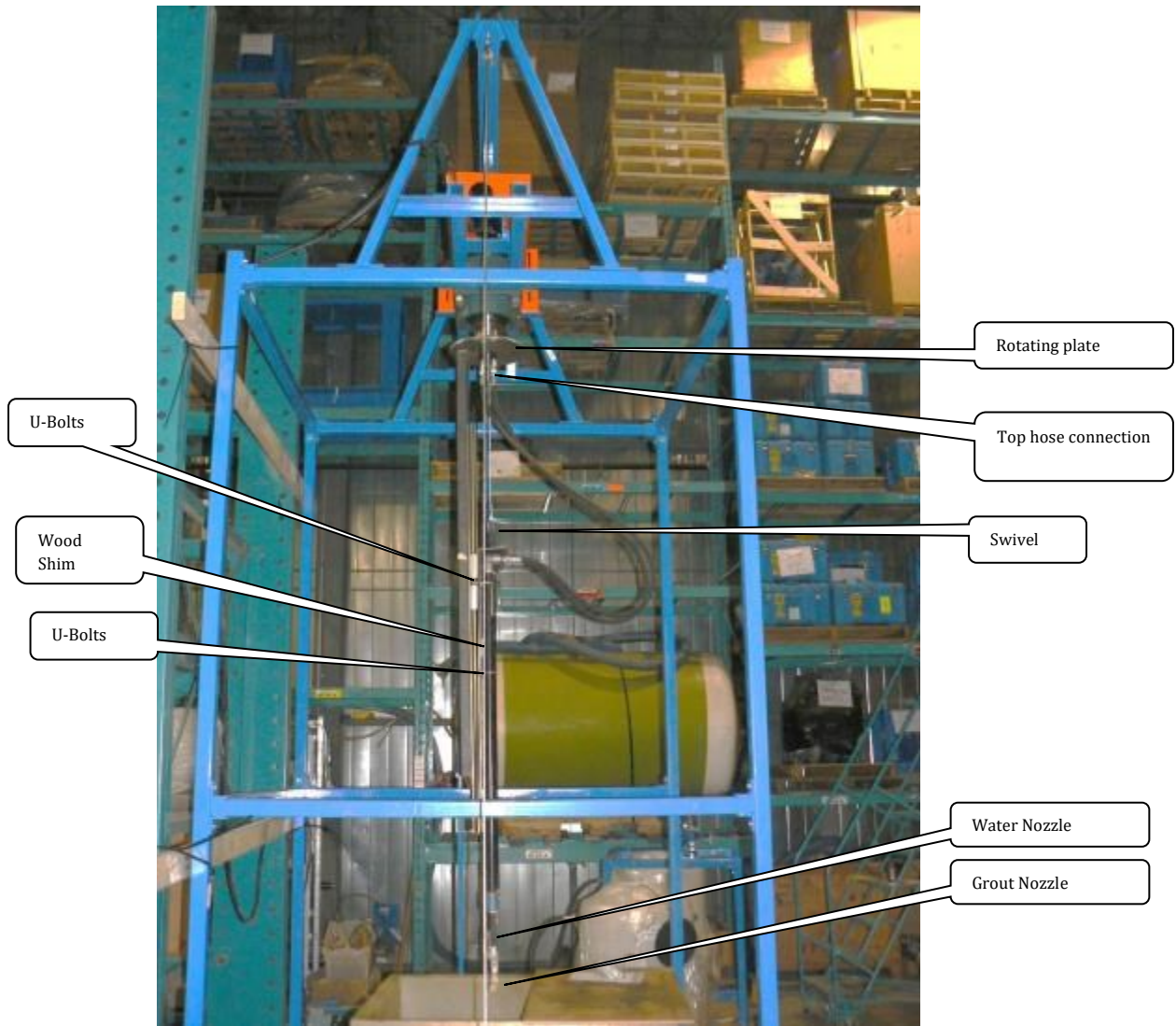


Figure 4-27 Rotational and vertical motion



Figure 4-28 Vertical motion motor



Front of Support Frame

Vertical Motion Motor and Winding Spool position and orientation

Figure 4-29 Vertical motion motor position and orientation

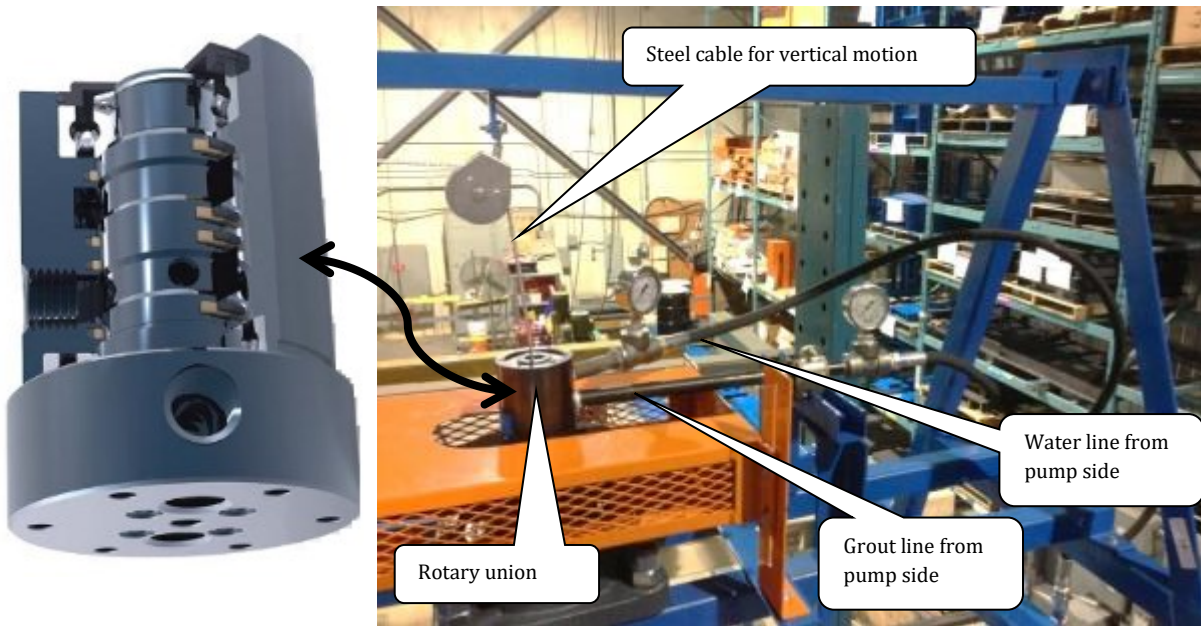


Figure 4-30 Rotary union assembly

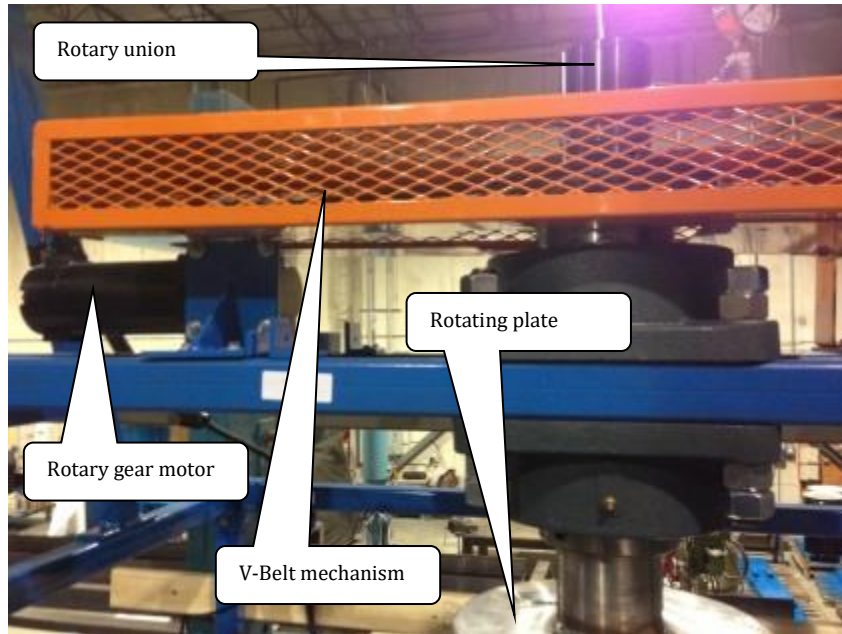
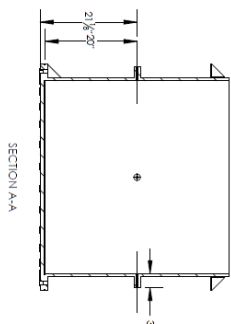
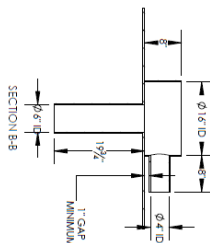
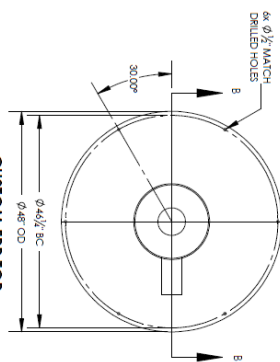
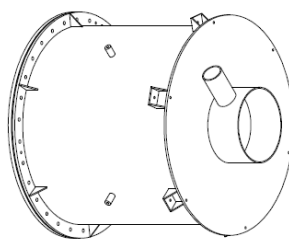
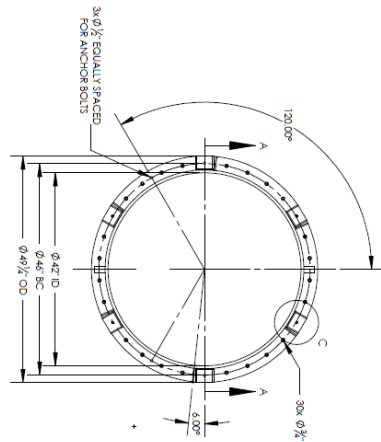


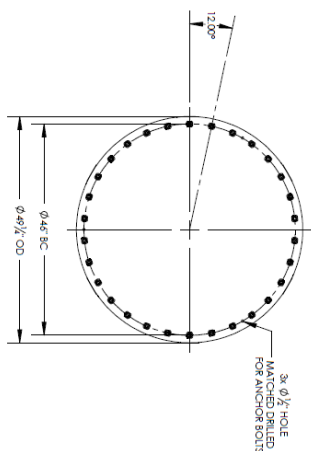
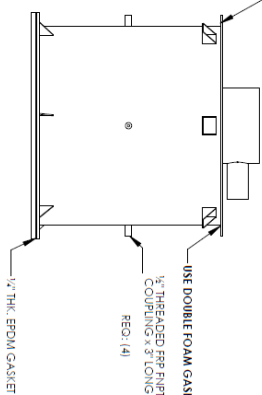
Figure 4-31 V-belt mechanism for rotational motion

THIS DRAWING AND ALL INFORMATION THEREON IS THE PROPERTY OF FILAMAT COMPOSITES INC. IS CONFIDENTIAL AND MUST NOT BE MADE PUBLIC OR COPIED. THIS DRAWING IS LOANED SUBJECT TO RETURN ON DEMAND AND IS NOT BE USED DIRECTLY OR INDIRECTLY IN ANY WAY DETRIMENTAL TO THE INTERESTS OF FILAMAT COMPOSITES INC. ALL COPYRIGHT AND PATENT RIGHTS RESERVED.

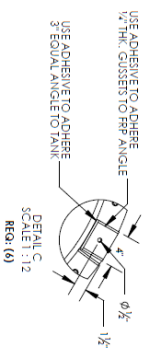
NOTES: -TANK CANNOT BE PRESSURIZED
-FRP ANGLES MAY BE USED AS LIFTING LUGS
BUT NEED TO USE A MINIMUM OF 3 TO LIFT



DO NOT STRAP TOP TO TANK



BOTTOM VIEW ON BASEPLATE



UNLESS OTHERWISE SPECIFIED
DIMENSIONS ARE IN INCHES
DIMENSIONS ARE TO FACE UNLESS NOTED OTHERWISE
DIMENSIONS ARE TO FACE UNLESS NOTED OTHERWISE
DIMENSIONS ARE TO FACE UNLESS NOTED OTHERWISE

TITLE		NAME		DATE		SIZE		DWG. NO.		SHEET		WEIGHT		REV.	
42" X 40" HIGH FRP FLANGE BASED TANK		AL		10/11/12			B		SB-12-2050	1	OF 1			0	
DRAWN	CHECKED	APPROVED		SCALE: 1:22		SHEET: 1 OF 1		WEIGHT:		REV: 0					

Figure 4-32 Jet grouting mixing tank

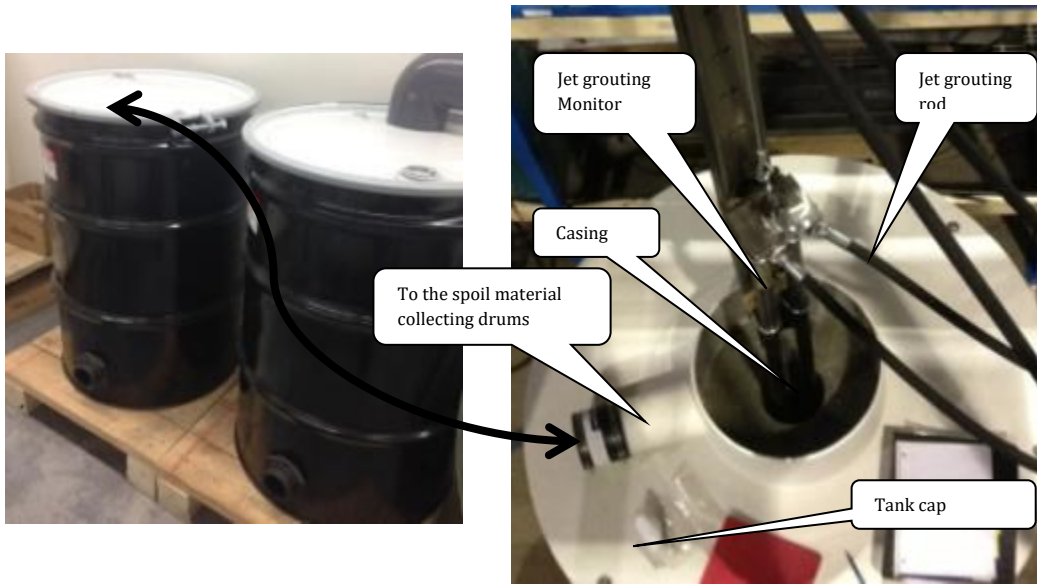


Figure 4-33 Jet grouting mixing tank Cap



Figure 4-34 Modeling of casing on the cap of the jet grouting mixing tank

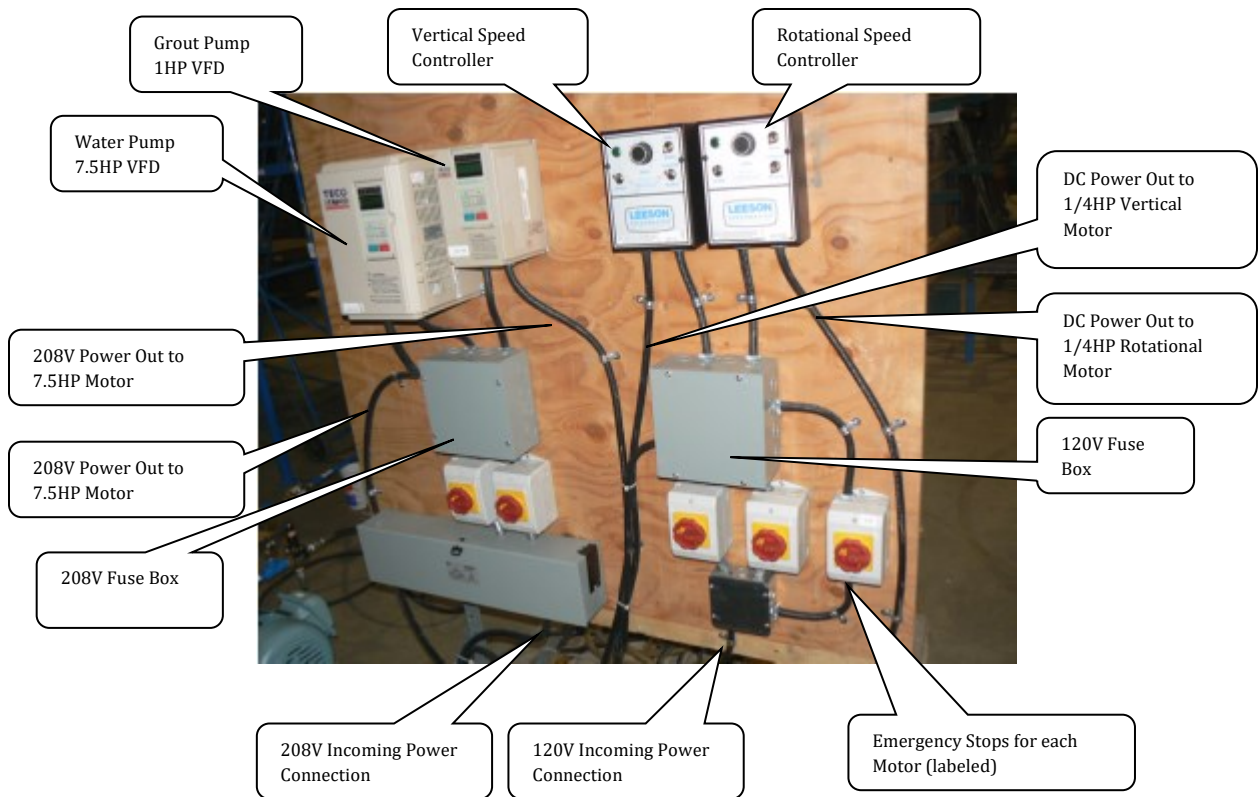


Figure 4-35 Control panel box of laboratory jet grouting setup

D/G-04 Series Performance

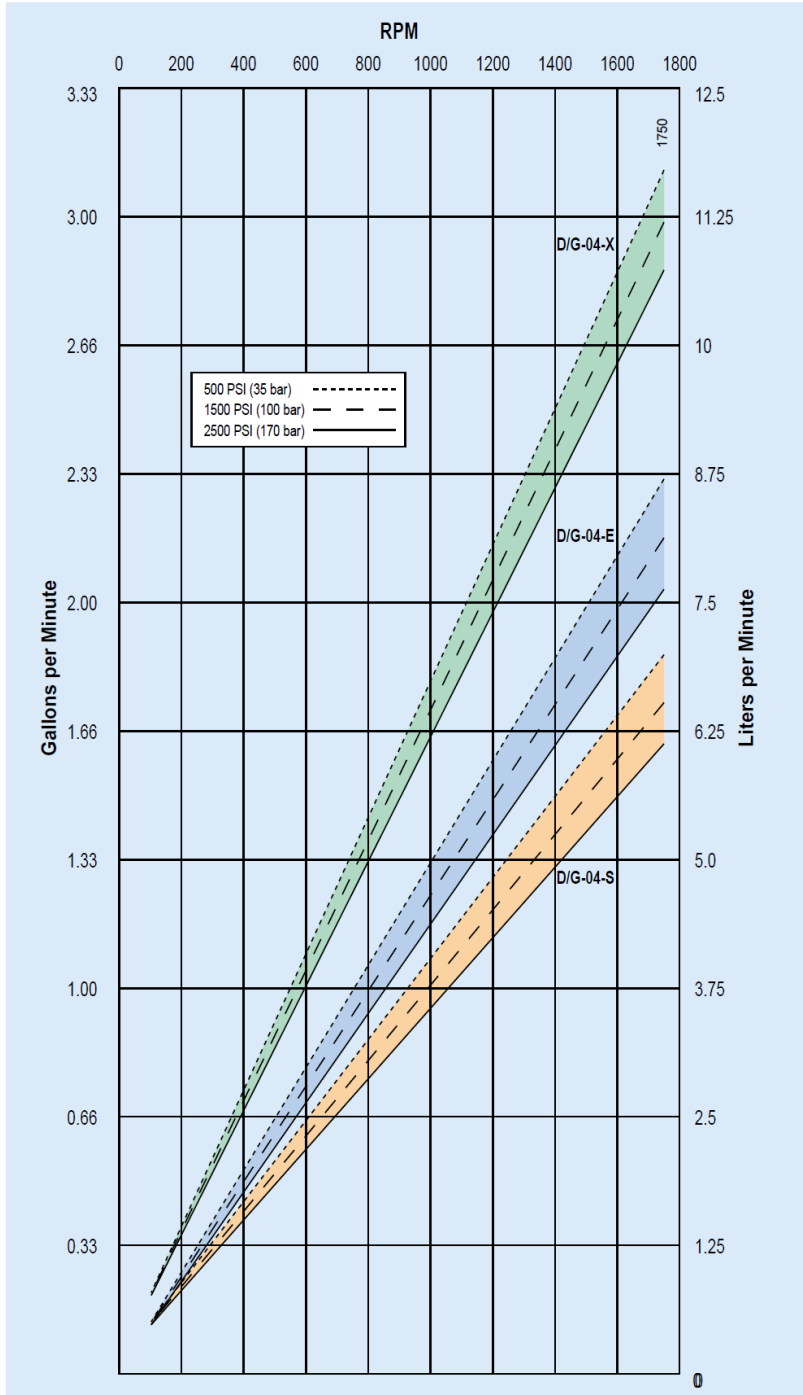
flow

model	max flow		max input
	gpm	l/min	rpm
D/G-04-X	2.9	11.0	1750
D/G-04-E	2.1	7.8	1750
D-/G04-S	1.6	6.1	1750

pressure

Maximum Inlet Pressure:
500 psi (35 bar)

Pressure Variable To:
2500 psi (170 bar)



Calculating Required Horsepower (kW)**

$$\frac{6 \times \text{rpm}}{63,000} + \frac{\text{gpm} \times \text{psi}}{1,460 - \left(\frac{\text{psi}-500}{20}\right)} = \text{electric motor HP}$$

$$\frac{6 \times \text{rpm}}{84,428} + \frac{\text{lpm} \times \text{bar}}{511 - \left(\frac{\text{bar}-35}{4}\right)} = \text{electric motor kW}$$

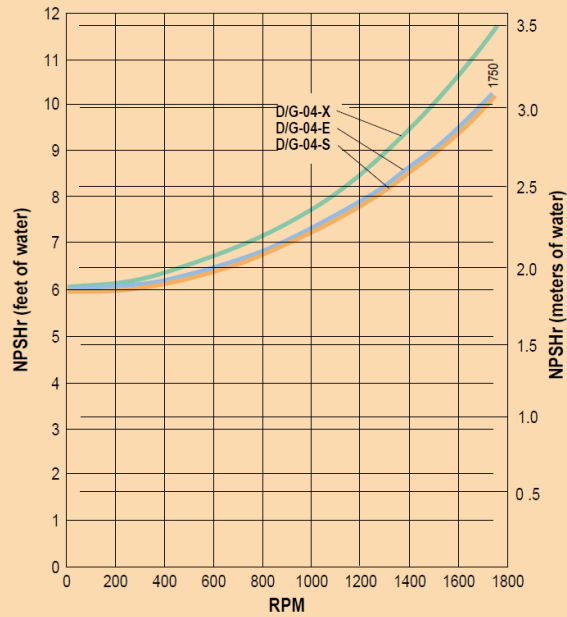
**rpm equals pump shaft rpm. HP/kW is required application power. Use caution when sizing motors with variable speed drives.

D/G-04 Series Specifications

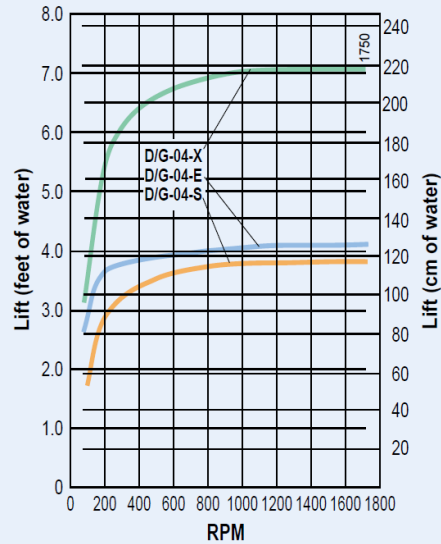
Max Pressure	2500 psi (170 bar)		
Capacity @ Max Pressure	rpm	gpm	l/min
D/G-04-X	1750	2.9	11.0
D/G-04-E	1750	2.1	7.8
D/G-04-S	1750	1.6	6.1
Delivery @ Max Pressure	revs/gal		
	500 psi	1500 psi	2500 psi
D/G-04-X	565	583	603
D/G-04-E	761	795	833
D/G-04-S	921	972	1093
	revs/liter		
	35 bar	100bar	170 bar
D/G-04-X	149	154	159
D/G-04-E	201	211	224
D/G-04-S	244	257	287
Max Inlet Pressure	500 psi (35 bar)		
Max Temperature	250°F (121°C) – Consult factory for correct component selection for temperatures above 160°F (71°C)		
Inlet Port	D-04: 1/2 inch NPT; G-04: 1/2 inch BSPT		
Discharge Port	D-04: 1/2 inch NPT; G-04: 1/2 inch BSPT		
Shaft Diameter	7/8 inch (22.22 mm)		
Shaft Rotation	Bi-directional		
Bearings	Ball bearings		
Oil Capacity	1.1 U.S. quart (1.05 liters), see Accessories Section for oil selection and specification.		
Weight	37 lbs (16.8 kg)		




Refer to installation guidelines and design considerations for additional information.

Net Positive Suction Head (NPSHr)



Dry Lift



MOTOR TYPE: AEHH8N		CATALOG No: PDH7/504TE2N		ISSUED: July 9, 2010		
NAMEPLATE INFORMATION						
HP	Pole	RPM	Frame	Voltage	Hz	Phase
7.5	4	1755	213T	460	60	3
Enclosure	Ins. Class	Service Factor	Time Rating	NEMA Design	Rated Amb.	Rated Altitude
TEFC	F	1.15	Continuous	B	-40 to 40 C ⁰	<3300 ft
TYPICAL PERFORMANCE						
Efficiency (%)				Power Factor (%)		
Full Load		3/4 Load	1/2 Load	Full Load	3/4 Load	1/2 Load
Nom.	Min.					
91.7	90.2	91.0	89.5	86.5	82.0	72.0
Torque				Currents (A)		
Full Load lb -ft	Locked Rotor % FLT	Pull up %FLT	Break Down %FLT	No Load	Full Load	Locked Rotor
22.4	250	155	270	2.8	8.9	64.0
NEMA KVA Code	Inertia WR ²			Safe Stall Time (s)		Noise Level Sound Press. dB(A)
	Rotor lb-ft ²	NEMA Load lb-ft ²	Max. Allowable lb-ft ²	Cold	Hot	
H	0.848	39.00	110.00	29.0	20.0	60.0
VFD DUTY INFORMATION						
Speed Range				VFD		S.F.
Constant Torque	Variable Torque	Constant Power		Carrier	Type	
10 : 1	20 : 1	60-120Hz		≤ 3kHz	VPWM or CPWM	1.0 ONLY
ADDITIONAL INFORMATION						
Bearings		Appro. Weight lbs	CSA Certified			
DE	NDE		Class I, Div. 2, Groups B, C & D		T3B	
6308ZZ	6306ZZ	171	Class I, Zone II, Groups IIB+H2, IIB & IIA		T3B	
Issued By :	<i>George Kang</i>					

C62/63/64 Series Specifications

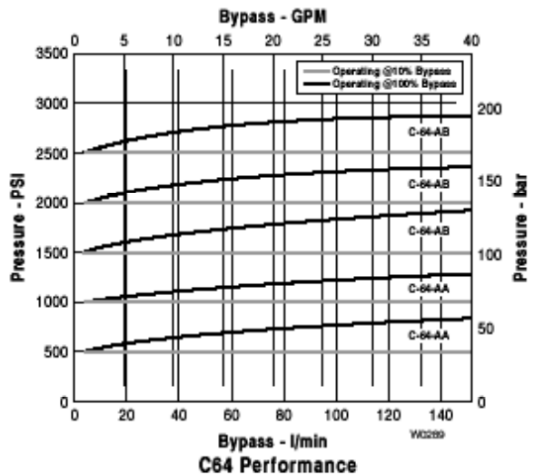
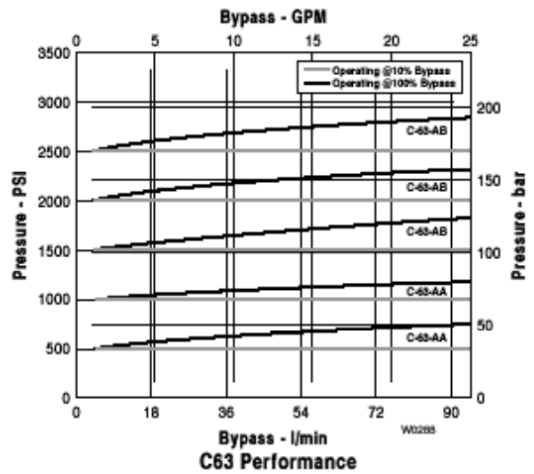
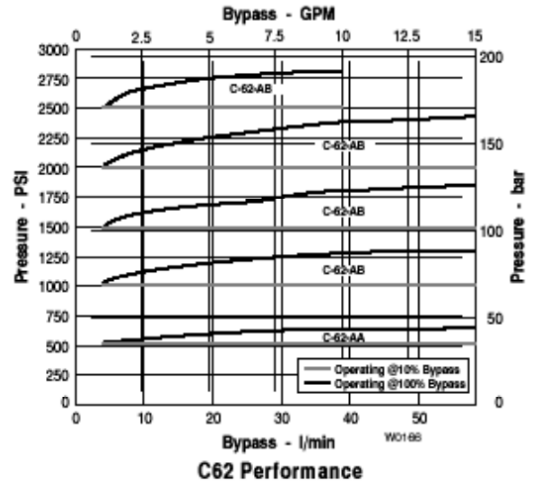
Capacity	Maximum		Minimum	
	gpm	l/min	gpm	l/min
C62-A/D	14	53	1	3.8
C63-A/D	25	94	1	3.8
C64-A/D	40	151	1	3.8

Pressure Range	Model Configuration Suffix	
	A	B
psi		
C62-A	75-500	500-2500
C63-A	75-1000	1000-2500
C64-A	75-1000	1000-2500
bar		
C62-D	5-35	35-172
C63-D	5-69	69-172
C64-D	5-69	69-172

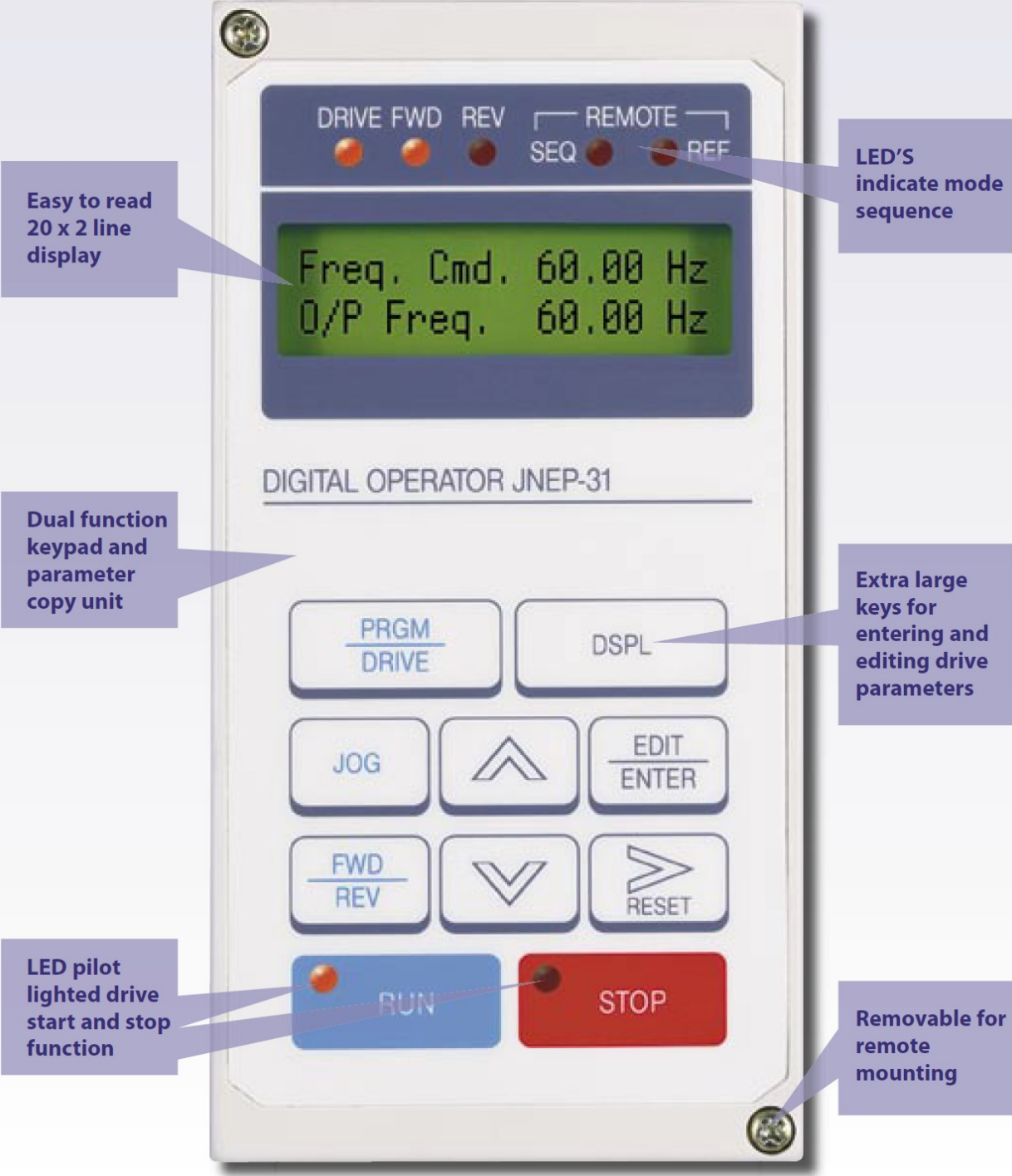
Max Temperature	200°F
------------------------	-------

Inlet and Outlet Ports	
C62-A	3/4" NPT
C63-A	1" NPT
C64-A	1-1/4" NPT
C62-D	3/4" BSPT
C63-D	1" BSPT
C64-D	1-1/4" BSPT

Weight	
C62-A/D	4 lbs (1.8 kg)
C63-A/D	6.2 lbs (2.8 kg)
C64-A/D	7.2 lbs (3.3 kg)



Digital Operator



Features and Benefits

- **Sensorless Vector** – The MA7200 has precise speed and torque control for the most demanding system performance and simple set-up through an auto-tuning function. It can be operated in sensorless vector or V/Hz mode to match the user's specific application.
- **Graphical LCD Operator** - The MA7200 offers easily read parameters and status in plain English text on a 2 line by 20 character lighted LCD, eliminating the need to memorize parameters - the user can set up the drive without an instruction manual! Straight forward monitoring of drive status through the operator is also available, which simplifies set-up and troubleshooting.
- **Parameter Copy** - No extra hardware is required on this drive. The copy feature is included as standard in the keypad. Simple cloning of the drive program is available, making it perfect for the OEM.
- **Flexible Input/Output Options** - The MA7200 offers Sink or Source Selectable Digital Inputs - 4 Preset, 4 User Programmable, 16 Preset Speeds, 2 Analog Inputs, 2 Analog Outputs, 3 Multi-Function Output Contacts - 1 Form C Relay, 1 Form A Relay, and 1 Open Collector Output.
- **Built-in PID Control** - The MA7200 has scalable PID feedback for accurate system regulation.
- **Powerful Programming Options** - The MA7200 allows the user to set up basic parameters for simple tasks or take advantage of advanced features for demanding applications.
- **Simple PLC** - The MA7200 can set custom run patterns for multiple machine cycles.
- **Communications** - The MA7200 has Modbus RTU as a standard. The user can control, program and monitor the drive(s) over an Industrial Network. Other protocols are also available.
- **PG Interface Built-in** - The MA7200 has Speed Control Accuracy of 0.1% .
- **User Selectable V/F Curves + S Curve area available.**
- **Motor/Drive Systems** - Pair the MA7200 with a TECO-Westinghouse motor for single source reliability.

D/G-03 Series Performance

flow

model*	max flow		max input
	gpm	l/min	rpm
D/G-03-X	3.0	11.3	1750
D/G-03-E	2.2	8.3	1750
D/G-03-S	1.8	6.8	1750
D/G-03-B	1.1	4.2	1750
D/G-03-G	0.5	1.9	1750

pressure

Maximum Inlet Pressure:
250 psi (17 bar)

Pressure Variable To:

Metallic Heads:
 D/G-03-X: 1000 psi (69 bar)
 D/G-03-E: 1200 psi (83 bar)
 D/G-03-S: 1200 psi (83 bar)
 D/G-03-B: 1200 psi (83 bar)
 D/G-03-G: 1200 psi (83 bar)

Non-Metallic Heads:
 All Models: 250 psi (17 bar)

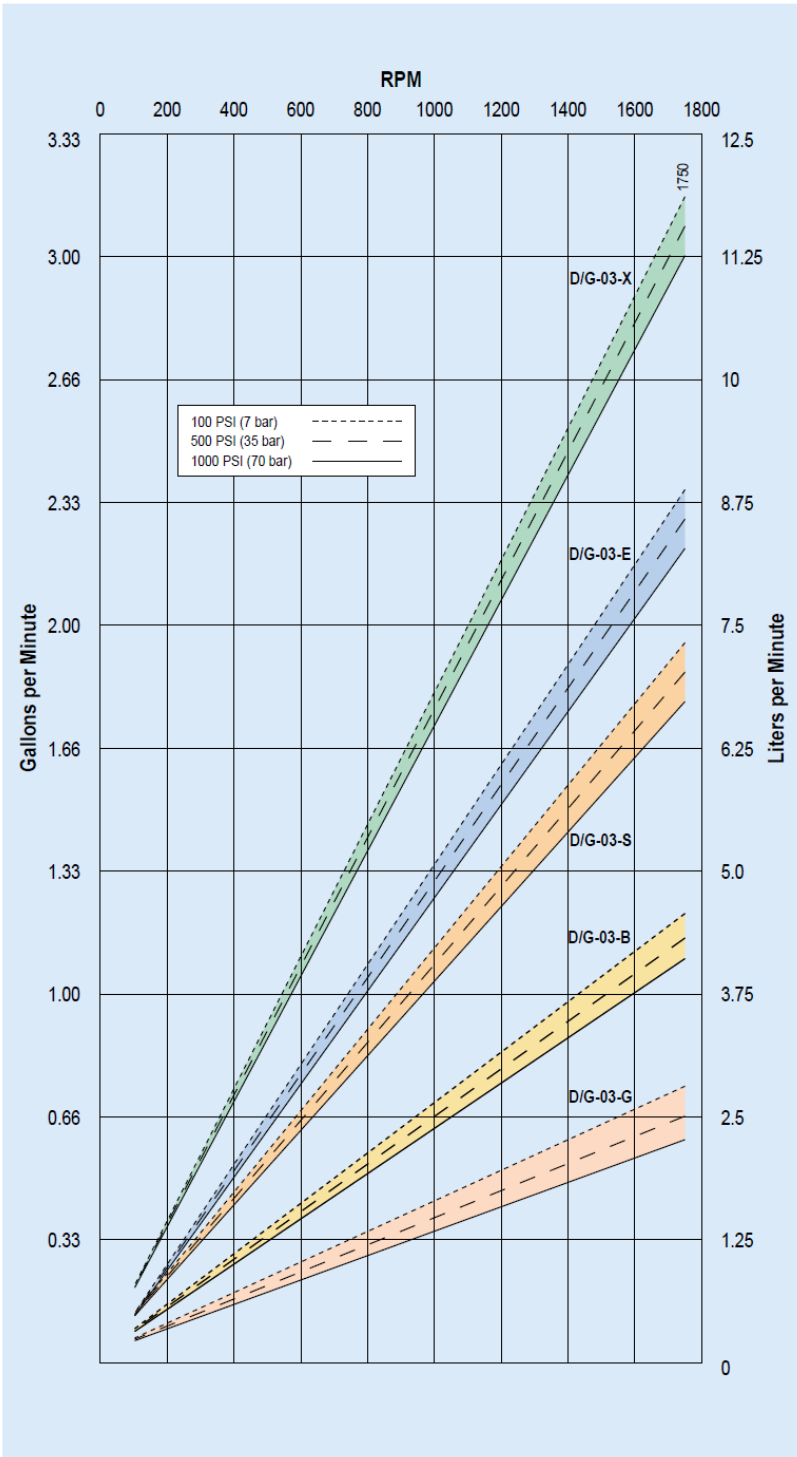
*** Note**
 Performance and specification ratings apply to all configurations unless specifically noted otherwise.

Calculating Required Horsepower (kW)**

$$\frac{6 \times \text{rpm}}{63,000} + \frac{\text{gpm} \times \text{psi}}{1,460} = \text{electric motor HP}$$

$$\frac{6 \times \text{rpm}}{84,428} + \frac{\text{lpm} \times \text{bar}}{511} = \text{electric motor kW}$$

**rpm equals pump shaft rpm. HP/kW is required application power. Use caution when sizing motors with variable speed drives.



D/G-03 Series Specifications

Max Pressure*

Metallic Heads:	D/G-03-X: 1000 psi (69 bar)
	D/G-03-S, E, B, G: 1200 psi (83 bar)
Non-Metallic Heads:	All models: 250 psi (17.3 bar)

Maximum Capacity*

	rpm	gpm	l/min
D/G-03-X	1750	3.0	11.3
D/G-03-E	1750	2.2	8.3
D/G-03-S	1750	1.8	6.8
D/G-03-B	1750	1.1	4.2
D/G-03-G	1750	0.5	1.9

Delivery @ Max Pressure*

	revs/gal	revs/liter
D/G-03-X	584	155
D/G-03-E	795	204
D/G-03-S	972	258
D/G-03-B	1591	415
D/G-03-G	3500	906

Max Inlet Pressure

250 psi (17.3 bar)

Max Temperature

Metallic Heads:	250°F (121°C) – Consult factory for correct component selection for temperatures above 160°F (71°C)
	Non-Metallic Heads:
	140°F (60°C)

Inlet Port

D-03, M-03, M-23: 1/2 inch NPT
G-03, G-13: 1/2 inch BSPT

Discharge Port

D-03, M-03, M-23: 3/8 inch NPT
G-03, G-13: 3/8 inch BSPT

Shaft Diameter

D/G-03: 7/8 inch (22.22 mm) shaft-driven
M-03: 5/8 inch hollow shaft for NEMA 56C C-Face motor
G-13: 24 mm hollow shaft for IEC 90 B5 Flange motor
M-23: 20 mm hollow shaft for use with Honda engine

Shaft Rotation

Bi-directional

Bearings

Ball bearings

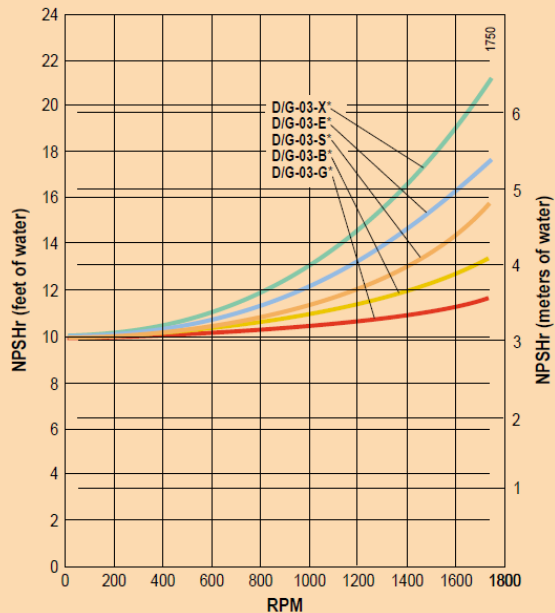
Oil Capacity

1 US quart (0.95 liters), see Accessories Section for oil selection and specification.

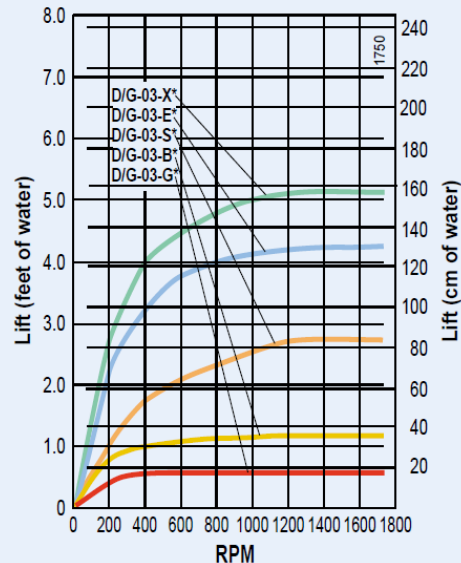
Weight

Metallic Heads:	28 lbs (12.7 kg)
Non-Metallic Heads:	19 lbs (8.6 kg)

Net Positive Suction Head (NPSHr)



Dry Lift



* Note

Performance and specification ratings apply to all configurations unless specifically noted otherwise.

Refer to installation guidelines and design considerations for additional information.

Appendix 4-6 Grout pump motor data sheet

BALDOR • RELIANCE Product Information Packet: CEM3546 - 1HP, 1760RPM, 3PH, 60HZ, 56C, 3519M, TEFC, F1, N

Part Detail									
Revision:	D	Status:		PRD/A	Change #:		Proprietary:	No	
Type:	AC	Prod. Type:	3519M		Elec. Spec:	35WGM492	CD Diagram:		
Enclosure:	TEFC	Mfg Plant:			Mech. Spec:	35A012	Layout:		
Frame:	56C	Mounting:	F1		Poles:	04	Created Date:	08-04-2010	
Base:	RG	Rotation:	RS		Insulation:	F	Eft. Date:	07-15-2011	
Leads:	9#18	Literature:			Elec. Diagram:		Replaced By:		
Nameplate NP1259L									
CAT.NO.		CEM3546							
SPEC.		35A012M492G1							
HP		1							
VOLTS		208-230/460							
AMP		3.1-3/1.5							
RPM		1760							
FRAME		56C			HZ	60	PH	3	
SER.F.		1.15			CODE	L	DES	B	CL
NEMA-NOM-EFF		85.5			PF	71			F
RATING		40C AMB-CONT							
CC					USABLE AT 208V	3.1			
DE		6205			ODE	6203			
ENCL		TEFC			SN				

C22/23/24 Series Valves



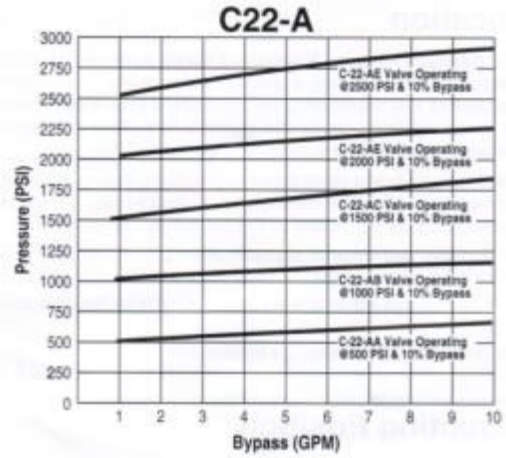
Capacity	Maximum		Minimum	
	gpm	l/min	gpm	l/min
C22-A/D	10	37.8	3	11.3
C23-A/D	20	75.7	3	11.3
C24-A/D	40	151.4	5	18.9

Pressure Range	Model Configuration			
	AA	AB	AC	AE
psi				
C22-A	75-500	500-1000	1000-1500	1500-2500
C23-A	75-500	500-1000	1000-1500	—
C24-A	75-500	500-1000	1000-1500	—
bar				
C22-D	5-34.5	34.5-69	69-103	103-172
C23-D	5-34.5	34.5-69	69-103	—
C24-D	5-34.5	34.5-69	69-103	—

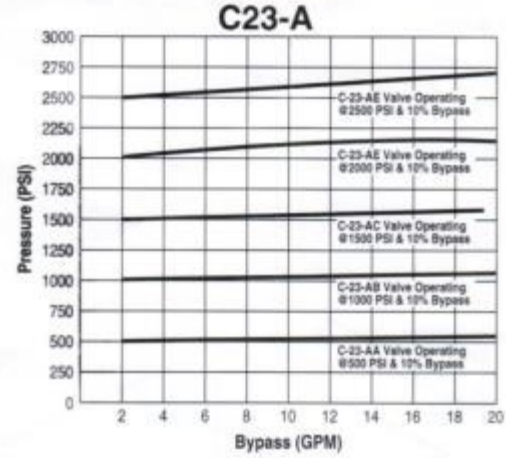
Max Temperature	200°F
Inlet and Outlet Ports	
C22-A	3/4" NPT
C23-A	1" NPT
C24-A	1-1/4" NPT
C22-D	3/4" BSPT
C23-D	1" BSPT
C24-D	1-1/4" BSPT

Weight	
C22-A/D	3 lbs (1.3 kg)
C23-A/D	6 lbs (2.7 kg)
C24-A/D	10 lbs (4.5 kg)

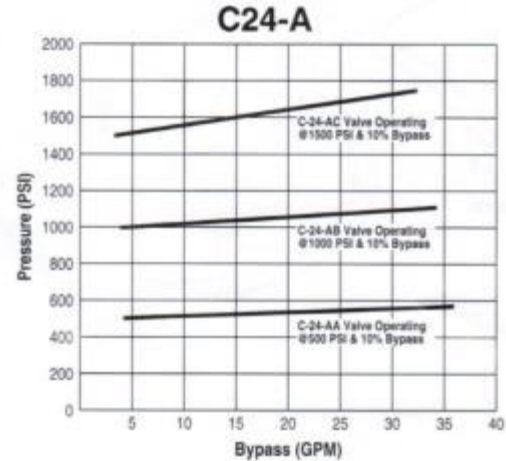
C22



C23



C24



Series A and B Economy Batch Mixer, 1750 rpm Direct Drive Clamp Mount

Neptune's economy line of small direct drive mixers for small batches of low viscosity fluids.

Features

- Universal motor mount accepts 48 and 56 frame foot mounted motors.
- Motors are available in TEFEC or explosion-proof enclosures. Air motors also available.
- Off-the-shelf delivery. Shaft and Prop 316SS.
- PVC coating available.
- Clamp adjusts to any angle.

Model Number	Standard Motor Description	Shaft Length	Shaft Diameter
Totally-enclosed fan-cooled (TEFC)			
A-1.0	1/4 HP-1-115	32"	1/2"
B-1.0	1/4 HP-1-115/230	32"	1/2"
B-2.0	1/3 HP-1-115/230	32"	1/2"
B-3.0	1/2 HP-1-115/230	32"	3/8"
B-3.2	1/2 HP-3-230/460	32"	3/8"

Explosion-proof class 1 group D (EP)

B-3.1	1/2 HP-1-115/230	32"	3/8"
-------	------------------	-----	------

Air motor

B-4.0	1/4 HP to 1/2 HP AIR	35"	3/8"
-------	----------------------	-----	------

To develop

1/4 HP at 1725 RPM requires 10 CFM at 45 PSI; 1/3 HP at 1725 RPM requires 14 CFM at 60 PSI; 1/2 HP at 1725 RPM requires 18 CFM at 80 PSI.

MODEL
B-1.0



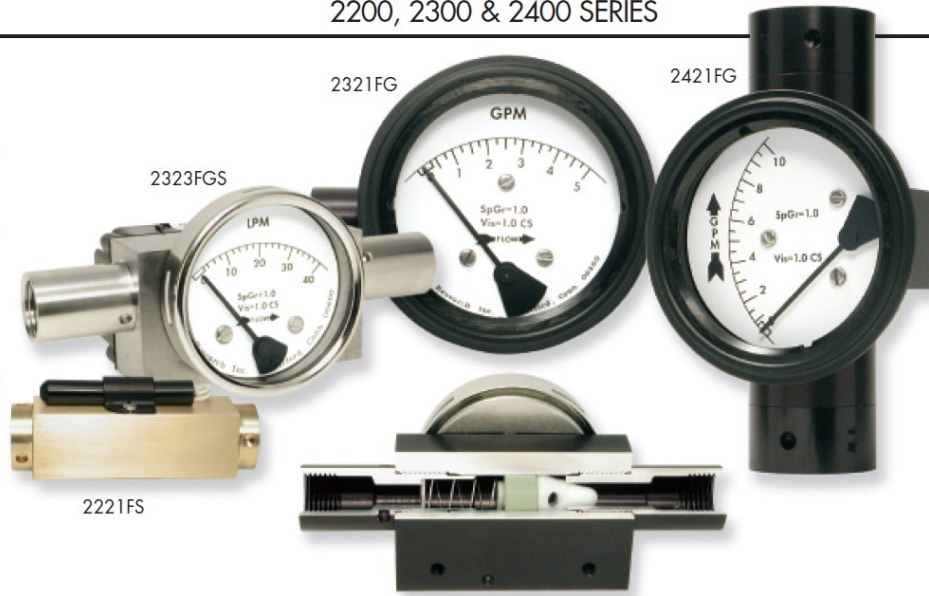
MODEL
B-4.0



**0-1 to 0-30 GPM
1.5-10 to 1-100 SCFM**
Variable-Area Flow
for Liquids or Gases

Features

- Large, easy-to-read dial
- Rugged, high line pressure design
- Vertical or horizontal mounting



Our variable-area flowmeters are designed for liquid or gas applications where rotameters often fall short. These models have large dials with bold markings and characters that are easy to read from a distance. They also handle high line pressures and can be mounted in any orientation.

Like rotameters, they are mounted directly in the flow stream, but with bodies machined from solid blocks of metal, they handle high-pressure applications of up to 5000 psi (vs 150 psi for rotameters). This makes them a natural for hydraulic systems.

The variable-area sensor, a movable Delrin cone (2200 & 2300) or Teflon cone (2400), rests in a precision orifice.

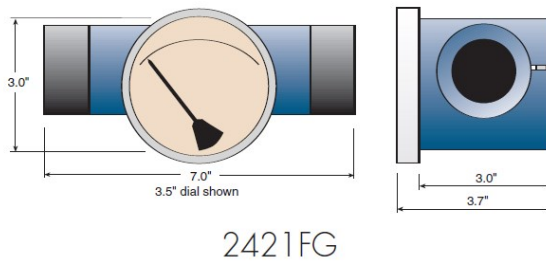
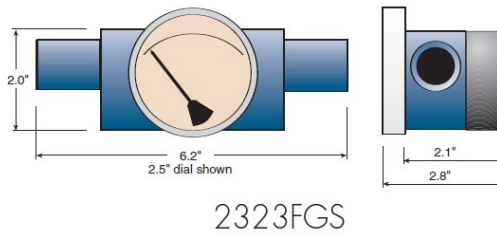
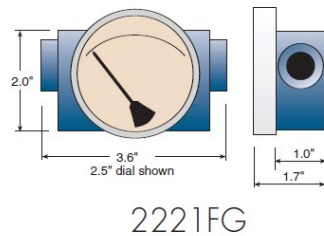
Fluid flow causes the sensor to move from the orifice and against a stainless steel spring while the flow rate is indicated on an easy-to-read dial face.

We offer them with pressure bodies (and wetted parts) of aluminum, stainless steel or brass. A variety of dial sizes are available, from 2.5 inch to 4.5 inch.

Choose from a wide selection of dial, porting, seal and calibration options. Switches, relays and transmitters are available with the dial or as stand-alone instruments. More details on these models can be found on our flow introduction pages 16-19. Electrical details are on pages 26-27.

Dimensions

Detailed drawings on website.



Specifications (Detailed Specification Sheets on Website)

Model	Flow range	Porting	Maximum line press./temp.	Accuracy (F.S./repeatability)	Turndown*	Electrical Available**
2221FG/FGS/FS	<u>Liquids</u> 0-1 to 0-5 GPM (0-4 to 0-18 LPM) <u>Air & Gas</u> 1.5-10 to 3-25 SCFM (40-280 to 75-700 SLPM)	1/4" NPT	3000 psig (200 bar) 200°F (93°C)	<u>Liquids</u> 2%/1% <u>Air & Gas</u> 5%/1%	10:1	1 or 2 switches
2223FGS/FS/FGT/FT	<u>Liquids</u> 0-1 to 0-5 GPM (0-4 to 0-18 LPM) <u>Air & Gas</u> 1.5-10 to 3-25 SCFM (40-280 to 75-700 SLPM)	1/4" NPT	5000 psig (200 bar) 200°F (93°C)	<u>Liquids</u> 2%/1% <u>Air & Gas</u> 5%/1%	10:1	1 or 2 switches 1 relay transmitter NEMA 4X Class 1-Div. 2
2321FG/FGS/FS	<u>Liquids</u> 0-1 to 0-10 GPM (0-4 to 0-18 LPM) <u>Air & Gas</u> 4-30 to 10-100 SCFM (100 to 850 SLPM)	1/2" NPT	3000 psig (200 bar) 200°F (93°C)	<u>Liquids</u> 2%/1% <u>Air & Gas</u> 5%/1%	10:1	1 or 2 switches
2323FGS/FS/FGT/FT	<u>Liquids</u> 0-1 to 0-10 GPM (0-3.8 to 0-38 LPM) <u>Air & Gas</u> 4-30 to 10-100 SCFM (100-850 SLPM)	1/2" NPT	5000 psig (340 bar) 200°F (93°C)	<u>Liquids</u> 2%/1% <u>Air & Gas</u> 5%/1%	10:1	1 or 2 switches 1 relay transmitter NEMA 4X Class 1-Div. 2
2421FG/FGS/FS	<u>Liquids Only</u> 0-10 to 0-30 GPM (0-36 to 0-110 LPM)	1" NPT	1500 psig (100 bar) 200°F (93°C)	2%/1%	10:1	1 or 2 switches
2423FGS/FS	<u>Liquids Only</u> 0-10 to 0-30 GPM (0-36 to 0-110 LPM)	1" NPT	1500 psig (100 bar) 200°F (93°C)	2%/1%	10:1	1 or 2 switches 1 relay NEMA 4X

F=Flow G=Gauge S=Switch T=Transmitter

*Turndown results in 1st mark at approximately 10% of full scale

**NEMA 4X switch models have a 1/2 inch NPT conduit port as standard. A DIN 43650A-PG11 with mating connector is optional, rated IP65 & NEMA 4X

How to Order

Select from each of the applicable categories to construct a model number. Use the model number when ordering or obtaining additional information and pricing from Orange Research or your local distributor.

Reordering? You must supply the Part Number from your instrument label.

Sample Model Number
2221FGS - 1A - 2.5B - A 0-1 GPM-W, 5T

2221FGS	1A	2.5B	A	0-1 GPM	W	5T
Model	Flow Body	Dial Case	Electrical	Range	Calibration	Options (more on pg. X)
2221FG	1A = aluminum	2.5B = 2.5" basic	A = SPST, N.O.	<u>Liquid</u>	W = std. calibr. -water	5 = plastic lens
2221FGS	1C = 316 SS	3.5B = 3.5" basic	B = SPST, N.C.	0-1, 0-2, 0-3, 04,	O = std. calibr. -oil	6 = liquid fill (glycerine)
2221FS	1E = brass	4.5B = 4.5" basic	C = SPDT	0-5, 0-8, 0-10, 0-15,	A = std. calibr. -air	8 = reverse flow
2223FGS		<i>Change "B" to "F" above for flanged dial case</i>	A-A = 2 ea. -A	0-20, 0-25, 0-30	S = special calibr.*	9 = vertical flow (specify direction - up or downward)
2223FS			B-B = 2 ea. -B	GPM	*Liquids: must specify specific gravity and viscosity	Special Seals (Buna-N standard):
2321FG			C-C = 2 ea. -C	<u>Air & Gas</u>	*Gas: must specify gas, pressure and temperature	T = Teflon
2321FGS			R2 = relay	2220 Series:	See std. calibration conditions page 18	V = Viton
2321FS			T2 - transmitter	1.5-10, 2-15, 3-20,		
2323FGS				3-25 SCFM		
2323FS				2320 Series:		
<i>More models above</i>				4-30, 4-40, 5-50,		
				5-75, 10-100 SCFM		

Pressure Drop Online-Calculator

Calculation output

Flow medium:	Water 20 °C / liquid
Volume flow::	11 l/min
Weight density:	998.206 kg/m ³
Dynamic Viscosity:	1001.61 10 ⁻⁶ kg/ms
Element of pipe:	circular
Dimensions of element:	Diameter of pipe D: 12.7 mm Length of pipe L: 0.2032 m
Velocity of flow:	4.75 ft./s
Reynolds number:	18318
Velocity of flow 2:	-
Reynolds number 2:	-
Flow:	turbulent
Absolute roughness:	0.0016 mm
Pipe friction number:	0.03
Resistance coefficient:	0.43
Resist.coeff.branching pipe:	-
Press.drop branch.pipe:	-
Pressure drop:	9.33 lbw./sq.ft. 0.06 psi

Appendix 4-11 PW series nozzle data sheet

Components Section - Nozzle Volume Chart

A commonly used standard for nozzle size is the “nozzle number” which is equivalent to the nozzle capacity in GPM at a specific PSI. Spray angle does not effect nozzle volume.

Table with columns for Nozzle Size, Orifice Diameter, and Flow rate (GPM) at Pressure (PSI) from 5 to 9000 PSI. The table lists various nozzle sizes and their corresponding flow rates across a range of pressures.

Components Section - Nozzles



1/4, 1/8 and QC Nozzles

ORDERING INFORMATION				
QC connection	PW	QC	00 15, 25 or 40	orifice size as shown above
¼ npt connection	PW	1/4M		
¼ fpt connection	PW	1/4W		
1/8 npt connection	PW	1/8M		



QC Nozzle



1/4 M Nozzle



1/4 F Nozzle

- Hardened Stainless steel orifice in a stainless steel housing
- ¼ inch mpt threading, 1/8 mpt threading, ¼ fpt thatreading or QC connection
- 5000 psi maximum pressure
- QC nozzles color coded based on orifice size.
- Available in 0° (red), 15° (yellow), 25° (green), and 40° (white) spray angle.

Orifice size	GPM @ PSI				
	1000	2000	3000	4000	5000
020	1.00	1.41	1.73	2.00	2.24
025	1.25	1.77	2.17	2.50	2.80
030	1.50	2.12	2.60	3.00	3.35
032	1.63	2.30	2.81	3.25	3.63
035	1.75	2.47	3.03	3.50	3.91
037	1.88	2.65	3.25	3.75	4.17
040	2.00	2.83	3.46	4.00	4.47
045	2.25	3.18	3.90	4.50	5.03
050	2.50	3.54	4.33	5.00	5.59
055	2.75	3.89	4.76	5.50	6.15
060	3.00	4.24	5.20	6.00	6.71
070	3.50	4.95	6.06	7.00	7.83
075	3.75	5.30	6.50	7.50	8.39
080	4.00	5.66	6.93	8.00	8.94
085	4.25	6.01	7.36	8.50	9.50
090	4.50	6.36	7.79	9.00	10.06
100	5.00	7.07	8.66	10.00	11.18

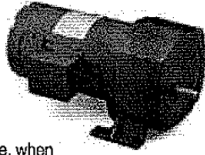
LEESON **FHP DC GEARMOTORS**
PARALLEL SHAFT GEARMOTORS

SCR RATED:
105-1112 In-Lbs Torque
LOW VOLTAGE:
320-1087 In-Lbs Torque

Electrical Specifications:

SCR Rated Gearmotors

SCR rated, permanent magnet DC gearmotors. Totally enclosed for continuous duty, general purpose applications. All have constant torque throughout the 60:1 speed range, when powered by a full-wave, unfiltered SCR-type adjustable speed control having a typical form factor of 1.3 to 1.4.



Low Voltage Gearmotors

Totally enclosed, permanent magnet DC gearmotors, performance matched for continuous duty. Motors are designed for battery power or can be used with a low voltage controller with form factor up to 1.05.

Mechanical Specifications:

Gearbox has rugged aluminum die cast housing, for maximum gear and bearing support. Precision machined gearing, hardened for maximum load capability. All gearing designed and rated to AGMA Class 9 standards and to withstand momentary shock overload of 200%. Oversized output bearings for greater overhung load capacity and longer life. High-carbon alloy output shaft provides maximum strength and rigidity. All needle bearing journals are precision-ground after heat treating, to provide maximum finish and fit. Heavy-duty industrial oil seals help keep lubricant in and dirt out. Gears and bearings are splash lubricated with permanent, heavy-duty gear oil. Conduit box is included as standard.

Application Notes:

These gearmotors are designed for mounting at any angle, but shaft-up with motor below gearhead is not recommended. Overhung load capacities shown are at center of output shaft.

P1100 DC gearmotors have the same mounting dimensions as Bison 483 gearmotors and many Dayton gearmotors. The motor's stall torque exceeds recommended full load torques. A current limiting device such as an SCR control should be used to prevent damage.

For additional information, see Bulletin 1830.

P1100 SERIES DC • SCR RATED
FRACTIONAL HP • PARALLEL SHAFT • TOTALLY ENCLOSED
1.0 SERVICE FACTOR

Output RPM	F.L. Torque (Lb.In.)	Input HP	Catalogue Number	Type & Frame	Ratio to 1	Arm Volts DC	F.L. Amps DC	Overhung Load (lbs.)	DIMENSIONS XL Inches	XH Inches
8	1087	1/4	108700	P1103-48	212	90	2.7	700	14.24	12.74
12	1030	1/4	108701	P1103-48	143	90	2.7	700	14.24	12.74
18	750	1/4	108702	P1103-48	95	90	2.7	700	14.24	12.74
42	353	1/4	108703	P1102-48	42	90	2.7	650	14.24	12.74
60	238	1/4	108704	P1102-48	29	90	2.7	625	14.24	12.74
92	160	1/4	108705	P1102-48	19	90	2.7	575	14.24	12.74
135	105	1/4	108706	P1102-48	13	90	2.7	525	14.24	12.74
18	1112	1/2	108707**	P1103-48	95	90	5.0	700	16.49	14.99
33	822	1/2	108708**	P1103-48	53	90	5.0	650	16.49	14.99
42	705	1/2	108709**	P1102-48	42	90	5.0	650	16.49	14.99
60	476	1/2	108710**	P1102-48	29	90	5.0	625	16.49	14.99
92	320	1/2	108711**	P1102-48	19	90	5.0	575	16.49	14.99
135	210	1/2	108712**	P1102-48	13	90	5.0	525	16.49	14.99

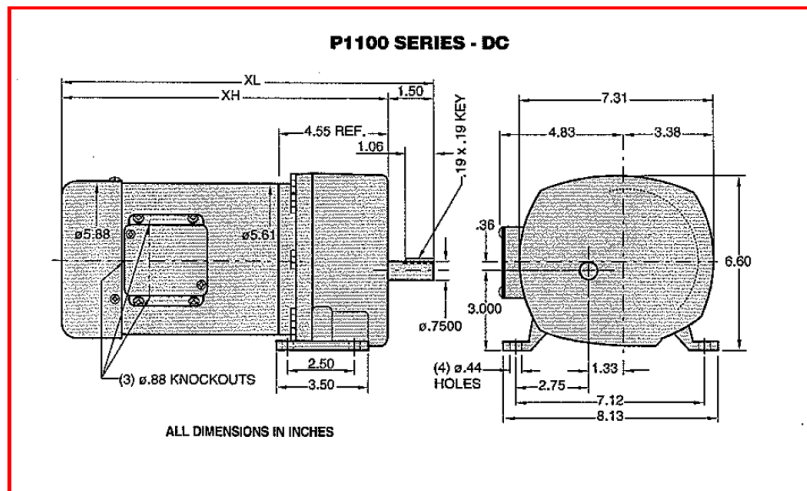
** TEFC enclosure.

P1100 SERIES DC • LOW VOLTAGE (12V)
FRACTIONAL HP • PARALLEL SHAFT • TOTALLY ENCLOSED
1.0 SERVICE FACTOR

Output RPM	F.L. Torque (Lb.In.)	Input HP	Catalogue Number	Type & Frame	Ratio to 1	Arm Volts DC	F.L. Amps DC	Overhung Load (lbs.)	DIMENSIONS XL Inches	XH Inches
8	1087	1/4	108729	P1103-48	212	12	21.0	700	13.74	12.24
60	238	1/4	108730	P1102-48	29	12	21.0	625	13.74	12.24
42	705	1/2	108731**	P1102-48	42	12	40.0	650	15.99	14.49
92	320	1/2	108732**	P1102-48	19	12	40.0	575	15.99	14.49

** TEFC enclosure.

BISON/DAYTON
DIRECT INTERCHANGE





DC ADJUSTABLE SPEED DRIVES SCR CONTROLS



LEESON Speedmaster® DC controls are general purpose drives designed for use with permanent magnet type direct current motors. NEMA 1 enclosed drives are suitable for most industrial applications, with the NEMA 4X enclosures best suited for washdown or outdoor installations or for extremely dusty applications. Chassis only units are available for building into equipment, machinery or existing enclosures. Most controls have a dual voltage switch allowing the control to be used on 115 or 230 volt, single phase, 50/60 Hertz service. However, the proper voltage motor should be selected for use with the power supply input, i.e., 90 volt DC motors for 115 volt input or 180 volt motors for 230 volt input service. Installation and adjustment instructions are included.

SCR/Thyristor drives are available in unidirectional and electro-mechanical type reversing styles for NEMA frame ratings and sub-fractional HP sizes.

The MM23000D Difference

The MM23000D Series SCR drives are dual voltage (115 or 230 VAC) and in the industry standard "MM" footprint (3.58" x 4.30"). NEMA 1 and 4X enclosures round out the MM23000D family.

This series is more resilient to vibration and comes with another feature, a user-selectable inhibit circuit. The user can adjust the function of the inhibit with jumper pins. The MM23000D Series drives can inhibit with either open or closed contacts. They can also inhibit either minimum set speed or stop.

All MM23000D Series drives come with LEDs to let the user know when the power is on (green) or if the motor has reached the current limit (red). For applications that require control of a DC motor in the 1/20 to 2 HP range, the MM23000D is an excellent solution.

Features:

- **Industry Standard Footprint:** Full wave, single quadrant SCR drives in the industry standard "MM" footprint (3.58" x 4.30").
- **Enclosures Available:** MM23000D Series is available in a NEMA 1 enclosure for simple mounting and user operation, or 4X enclosure for more industrial applications.
- **Separate Calibrations:** Calibration trimmer pots for: minimum speed, maximum speed, current limit, acceleration, deceleration, and IR compensation.
- **Multiple LED Indicators:** LEDs indicating current limit (red) and power (green).
- **Speed Regulation:** Speed regulation maintains speed within 1% of the base speed within a speed range of 60:1.
- **Adjustable Inhibit:** Open or close contacts to stop or rotate motor at a minimum speed.

CHASSIS MOUNT • EC2

Everything needed for driving a 90VDC brush motor with no frills. Features small footprint but standard mounting, 1% speed regulation, user easily sets min/max speed, IR comp, current limit and accel/decel. Requires a speed reference signal from a wired 10K OHM potentiometer or a 0-6VDC isolated signal. Stop/start is available through inhibit terminals causing motor to coast to a stop; opening terminals causes the motor to accelerate to set speed.

Typical applications: Conveyors, Materials Handling, Packaging/Sorting/Printing and other OEM machinery.



HP Range 115 VAC	Output Amps	Catalogue Number	List Price	Disc. Sym.	App. Wgt.
1/8 to 1/2	5*	EC2	\$89	A	1
1/4 to 1	10	EC2 (with heatsink)	141	A	1

* For 3/4 and 1HP - 115V or 1.5 and 2HP - 230V Heat Sink #223-0159 required.

CHASSIS MOUNT with speed pot

115 VAC	HP Range 230 VAC	Output Amps	Catalogue Number	List Price	Disc. Sym.	App. Wgt.
1/20 to 1/8	1/20 to 1/4	1.5	MM23012D	\$195	A	1
1/8 to 1	1/4 to 2	10*	MM23002D	184	A	1
1/8 to 1	1/4 to 2	10*	MM23001C*	184	A	1
Heat Sink*			223-0159	52	A	1

* Heat Sink #223-0159 required above 5 amps.

* Has field supply for shunt wound motor control.

NEMA 1

115 VAC	HP Range 230 VAC	Output Amps	Catalogue Number	List Price	Disc. Sym.	App. Wgt.
1/20 to 1/8	1/20 to 1/8	1.5	MM23112D	\$369	A	5
1/8 to 1	1/4 to 2	10 +	MM23102D	372	A	5
Heat Sink+			223-0174	75	A	1

+ Heat Sink #223-0174 required above 5 amps.

NEMA 1 • REVERSING

115 VAC	HP Range 230 VAC	Output Amps	Catalogue Number	List Price	Disc. Sym.	App. Wgt.
1/20 to 1/8	1/10 to 1/4	1.5	MM23212D	\$477	A	5
1/8 to 1+	1/4 to 2*	10	MM23202D	510	A	5
Heat Sink+			223-0174	75	A	1

+ For 3/4 and 1HP - 115V or 1.5 and 2HP - 230V Heat Sink #223-0174 required.

NEMA 4X

115 VAC	HP Range 230 VAC	Output Amps	Catalogue Number	List Price	Disc. Sym.	App. Wgt.
1/8 to 1	1/4 to 2	10	174102*	\$397	A	6
1/20 to 1/8	1/10 to 1/4	1.5	MM23412D	489	A	7
1/8 to 1	1/4 to 2	10	MM23402D	499	A	7
1.5	3	15	174709	1359	A	8

* Plastic enclosure

NEMA 4X • REVERSING

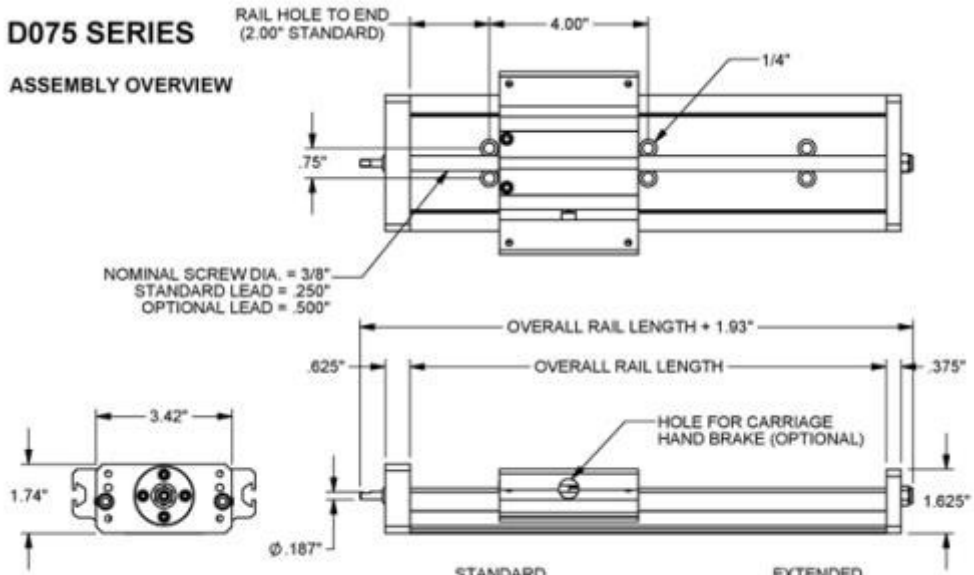
115 VAC	HP Range 230 VAC	Output Amps	Catalogue Number	List Price	Disc. Sym.	App. Wgt.
1/8 to 1	1/4 to 2	10	174107**	\$514	A	7

** Plastic enclosure - Drive does not have dynamic braking. Motor must be at zero speed before reversing.

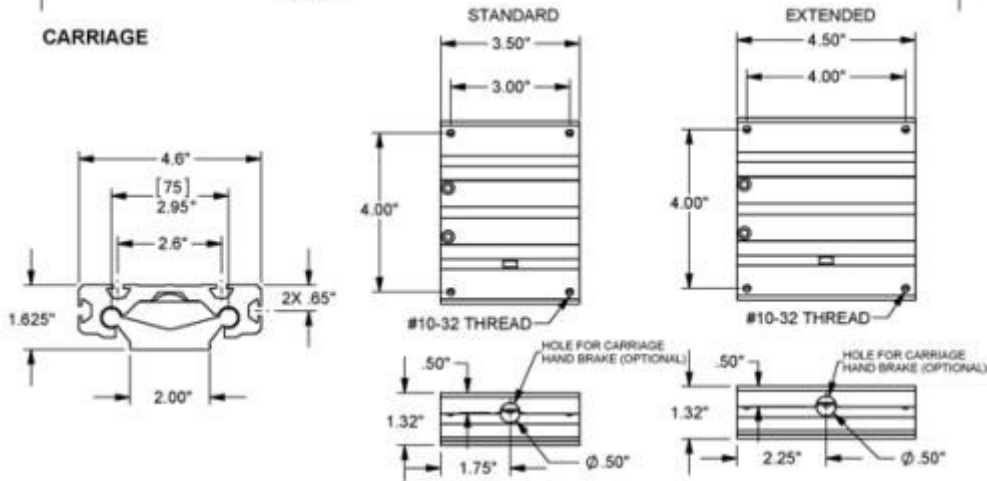
Appendix 4-14 Uni-Guide vertical motion data sheet

D075 SERIES

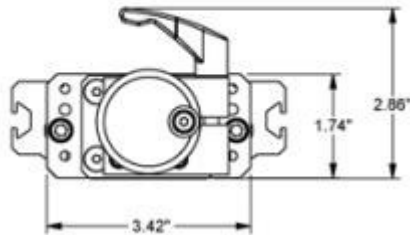
ASSEMBLY OVERVIEW



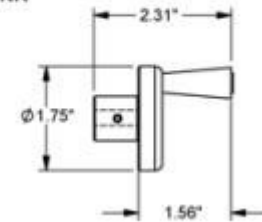
CARRIAGE



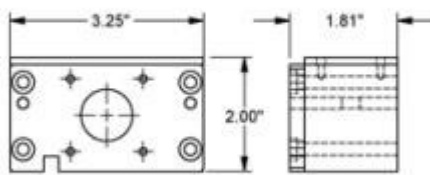
HAND BRAKE



HAND CRANK

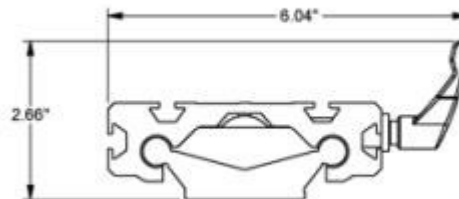


MOTOR MOUNT ATTACHMENT

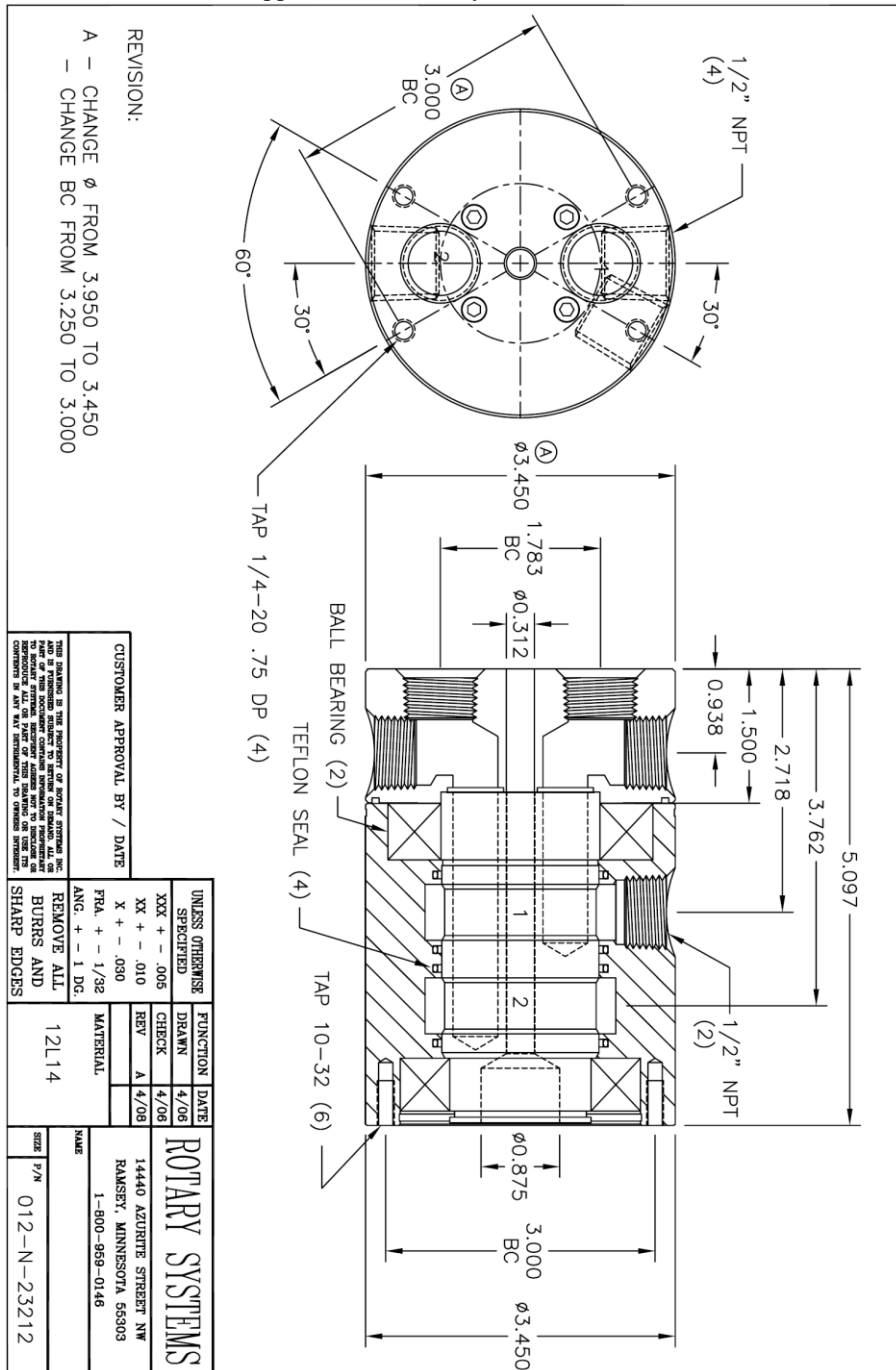


NEMA 17 MOUNTING

CARRIAGE HAND BRAKE



Appendix 4-15 Rotary union data sheet

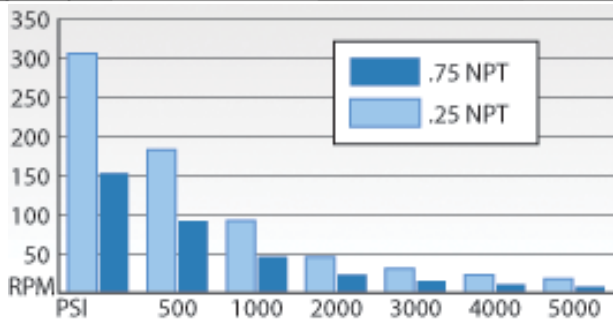


REVISION:
 A - CHANGE ϕ FROM 3.950 TO 3.450
 - CHANGE BC FROM 3.250 TO 3.000

CUSTOMER APPROVAL BY / DATE

THIS DRAWING IS THE PROPERTY OF ROTARY SYSTEMS INC. AND IS PROVIDED SUBJECT TO PATENT AND TRADEMARK RIGHTS. NO PART OF THIS DRAWING IS TO BE REPRODUCED OR TRANSMITTED IN ANY FORM OR BY ANY MEANS, ELECTRONIC OR MECHANICAL, INCLUDING PHOTOCOPYING, RECORDING, OR BY ANY INFORMATION STORAGE AND RETRIEVAL SYSTEM, WITHOUT THE WRITTEN PERMISSION OF ROTARY SYSTEMS INC. ANY VIOLATION OF THIS NOTICE IS SUBJECT TO LEGAL ACTION.

UNLESS OTHERWISE SPECIFIED	FUNCTION	DATE	ROTARY SYSTEMS
XXX + - .005	DRAWN	4/08	14440 AZURITE STREET NW
XX + - .010	CHECK	4/08	RAMSEY, MINNESOTA 55303
X + - .030	REV	A 4/08	1-800-869-0146
FRA. + - 1/32	MATERIAL		
ANG. + - 1 DG.			
REMOVE ALL BURNS AND SHARP EDGES			
	12L14		
	SIZE P/N		
	012-N-23212		



SUB-FHP DC GEARMOTORS
RIGHT ANGLE SHAFT GEARMOTORS



SCR RATED:
5-135 In-Lbs Torque
LOW VOLTAGE:
25-135 In-Lbs Torque

Electrical Specifications:
SCR Rated Gearmotors

Totally enclosed right-angle gearmotors, performance matched for continuous service over a 60:1 speed range. All have constant torque throughout the range when powered by a full-wave, unfiltered SCR-type 115 volt input adjustable speed control having a typical form factor of 1.3 to 1.4. Also available as factory options are motors for low voltage input and with double output shafts.

Low Voltage Gearmotors

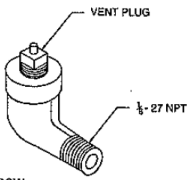
Totally enclosed, permanent magnet DC gearmotors, performance matched for continuous duty. Motors are designed for battery power or can be used with a low voltage controller with form factor up to 1.05.

Mechanical Specifications:

This worm-type right-angle gearing features hardened, steel worm with bronze worm wheel for long life and quiet operation. Precision machined aluminum housings are used. Gearbox has all ball bearings. The housing is sealed and lubrication is permanent with an oil bath. The output shaft is field interchangeable from left hand style to right hand style by reassembly.

Application Notes:

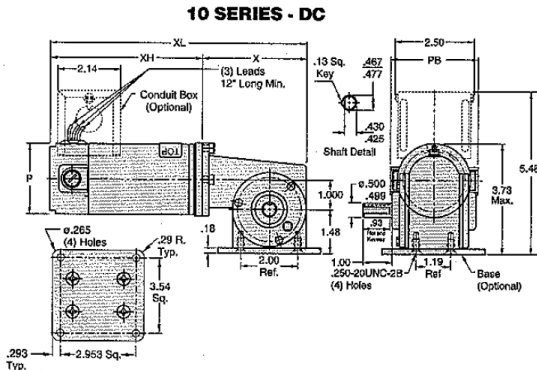
For optimum seal life, these right-angle gearmotors have a lubrication breather positioned for horizontal mounting. For other mountings, the breather-plug must be reoriented by using a 90° NPT taper pipe elbow (see drawing). Elbow not available from LEESON. Vent plug is available (Part #M1900177_01). However, the motor portion of the gearmotor should never be mounted below the gearhead.



Overhung load capacities shown are at center of output shaft. Conduit box *not* supplied with motor. See page 171 for optional conduit box and optional base kit. See page 205 for cross reference data between LEESON and other gearmotors.

For additional information on LEESON gearmotors, see Bulletin 1830.

BODINE/DAYTON
DIRECT INTERCHANGE

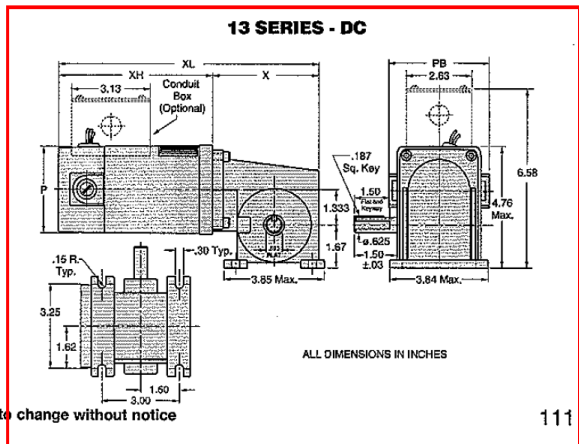


RIGHT-ANGLE DC • SCR RATED
TENV • 1.0 SERVICE FACTOR

Output RPM	F.L. Torque (In.-Lbs.)	Input HP	Catalogue Number	Gearmotor Type & Frame	Ratio to 1	Arm Volts DC	Full Load Amps. DC	Overhung Load (lbs.)	DIMENSIONS				
									P	PB	X Inches	XL	XH
42	22	1/17	M1115018	10F60-25D	60	90	1.00	185	2.50	3.00	3.60	8.79	5.19
62	19	1/17	M1115019	10F40-25D	40	90	1.00	185	2.50	3.00	3.60	8.79	5.19
125	16	1/17	M1115020	10F20-25D	20	90	1.00	185	2.50	3.00	3.60	8.79	5.19
250	10	1/17	M1115021	10F10-25D	10	90	1.00	185	2.50	3.00	3.60	8.79	5.19
500	5	1/17	M1115022	10F05-25D	5	90	1.00	185	2.50	3.00	3.60	8.79	5.19
42	30	1/12	M1135053	13F60-34A	60	180	0.53	235	3.38	4.00	4.50	9.64	5.14
62	35	1/12	M1135054	13F40-34A	40	180	0.53	235	3.38	4.00	4.50	9.64	5.14
125	18	1/12	M1135055	13F20-34A	20	180	0.53	235	3.38	4.00	4.50	9.64	5.14
250	10	1/12	M1135056	13F10-34A	10	180	0.53	235	3.38	4.00	4.50	9.64	5.14
500	5	1/12	M1135057	13F05-34A	5	180	0.53	235	3.38	4.00	4.50	9.64	5.14
42	80	3/8	M1135069	13F60-34C	60	90	1.40	235	3.38	4.00	4.50	10.64	6.14
62	70	1/2	M1135038	13F40-34C	40	90	1.40	235	3.38	4.00	4.50	10.64	6.14
62	70	1/2	M1135058	13F40-34C	40	180	0.70	235	3.38	4.00	4.50	10.64	6.14
125	45	1/2	M1135039	13F20-34C	20	90	1.40	235	3.38	4.00	4.50	10.64	6.14
125	45	1/2	M1135059	13F20-34C	20	180	0.70	235	3.38	4.00	4.50	10.64	6.14
250	25	1/2	M1135040	13F10-34C	10	90	1.40	235	3.38	4.00	4.50	10.64	6.14
250	25	1/2	M1135060	13F10-34C	10	180	0.70	235	3.38	4.00	4.50	10.64	6.14
500	13	1/2	M1135041	13F05-34C	5	90	1.40	235	3.38	4.00	4.50	10.64	6.14
500	13	1/2	M1135061	13F05-34C	5	180	0.70	235	3.38	4.00	4.50	10.64	6.14
62	135	1/4	M1135042	13F40-34G	40	90	2.30	235	3.38	4.00	4.50	12.64	8.14
62	135	1/4	M1135062	13F40-34G	40	180	1.30	235	3.38	4.00	4.50	12.64	8.14
83	125	1/4	M1135043	13F30-34G	30	90	2.30	235	3.38	4.00	4.50	12.64	8.14
83	125	1/4	M1135063	13F30-34G	30	180	1.30	235	3.38	4.00	4.50	12.64	8.14
125	90	1/4	M1135044	13F20-34G	20	90	2.30	235	3.38	4.00	4.50	12.64	8.14
125	90	1/4	M1135064	13F20-34G	20	180	1.30	235	3.38	4.00	4.50	12.64	8.14
250	50	1/4	M1135045	13F10-34G	10	90	2.30	235	3.38	4.00	4.50	12.64	8.14
250	50	1/4	M1135065	13F10-34G	10	180	1.30	235	3.38	4.00	4.50	12.64	8.14
500	30	1/4	M1135046	13F05-34G	5	90	2.30	235	3.38	4.00	4.50	12.64	8.14
500	30	1/4	M1135066	13F05-34G	5	180	1.30	235	3.38	4.00	4.50	12.64	8.14

RIGHT-ANGLE DC • LOW VOLTAGE (12V)
TENV • 1.0 SERVICE FACTOR

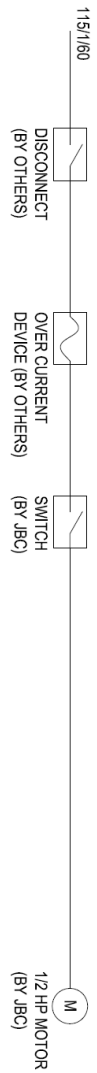
Output RPM	F.L. Torque (In.-Lbs.)	Input HP	Catalogue Number	Gearmotor Type & Frame	Ratio to 1	Arm Volts DC	Full Load Amps. DC	Overhung Load (lbs.)	DIMENSIONS				
									P	PB	X Inches	XL	XH
42	80	1/8	M1135249	13F60-34	60	12	11.0	235	3.38	4.21	4.50	10.39	5.89
250	25	1/8	M1135250	13F10-34	10	12	11.0	235	3.38	4.21	4.50	10.39	5.89
62	135	1/4	M1135251	13F40-34	40	12	21.0	235	3.38	4.21	4.50	12.64	8.14
125	90	1/4	M1135252	13F20-34	20	12	21.0	235	3.38	4.21	4.50	12.64	8.14



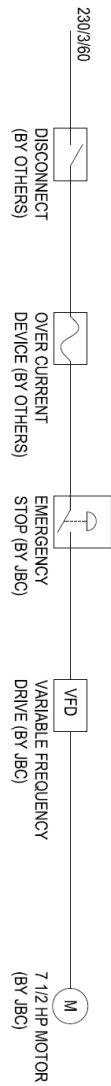
Specifications are subject to change without notice

ELECTRICAL - SINGLE LINE DIAGRAMS (all wiring by others)

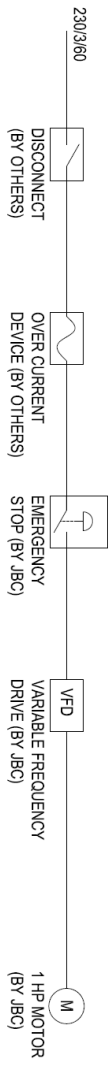
MIXER



WATER PUMP



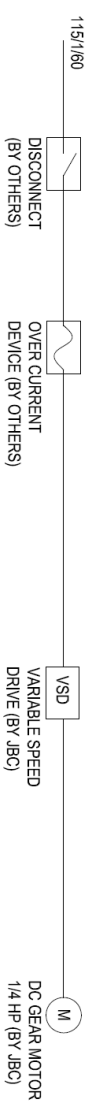
GROUT PUMP



ROTATIONAL MECHANISM



VERTICAL MECHANISM



Chapter 5 DEVELOPMENT OF THERMAL-INSULATING GROUT

This chapter discusses the development of thermal-insulating grout for a jet grouting operation. Based on theoretical values obtained from literature about the jet grouting technique, five different grout mixtures were developed and hand-mixed with in-situ soil samples obtained from a particular project in Edmonton, Alberta, Canada. Many laboratory geotechnical tests were carried out on hand-mixed soilcrete samples to find an optimal mixture, which resulted in better thermal, physical, and mechanical properties of soilcrete.

5-1. Introduction

Insulating concrete mixtures with expanded lightweight perlite (ELP) have been used in different thermal insulating projects in hot deep mines and underground structures. ELP can also be used to develop a new thermal-insulation grout mixture for jet grouting.

GSS Geothermal Ltd., in cooperation with the University of Alberta in Edmonton, Canada, has worked on the Southwood 19-acre townhome rental community project in southeast Edmonton, aiming to increase the underground energy reservation and optimize the boreholes design. The current research focused in part on this project. GSS Geothermal Ltd. provided soil cores from a 67-meter-deep vertical borehole. Figure 5-1 shows the cores, which are covered by a plastic seal and protected by PVC barrels. To carry out jet grouting on any type of soil, a good knowledge of the soil's thermal, physical, and mechanical properties is fundamental. Therefore, before jet grouting, the logging of cores was done to record the core size, geology, locations, and other engineering properties. Appendix 5-1 shows the logging data sheet. To direct further research, laboratory and in-situ investigations were conducted to identify the soil properties, focusing on the physical, mechanical, and thermal properties. After identifying soil properties, a number of grout and soil mixtures were created in the laboratory to determine the initial physical, mechanical, and thermal properties of hand-mixed soilcrete and to prepare a guideline regarding actual characteristics of soilcrete created by the laboratory jet grouting setup.

5-2. Soil properties' test results and discussions

Based on the core logging information, the soil type in elevation ranged from five to 15 meters consisted entirely of clay with a few uneven sand layers; the only core barrels in that interval were used to hand-mixed the soilcrete samples. To identify the engineering properties of the soil, the following laboratory tests were carried out on core samples: moisture content (ASTM:D2216-10 2010); particle-size analysis (ASTM:D421-85 2007; ASTM:D422-63 2007); specific gravity (ASTM:D854-10 2010); unit weight (ASTM:D7263-09 2009); Atterberg limits (ASTM:D421-85 2007; ASTM:D4318-10 2010); engineering soil classification (ASTM:D2487-11 2011); compaction test (ASTM:D698-12 2012); and unconfined compressive strength (UCS) test (ASTM:D5102-09 2009; ASTM:D2166/D2166M-13 2013); modulus of elasticity; and thermal property test.

First, the in-situ moisture content of soil in four different sections of 273 to 300, 480 to 540, 540 to 600, and 600 inches was measured to be 15.5%. Method B was used from ASTM:D2216-10 (2010) based on significant digits reported and the size of the specimen (mass) required. In this method, the water content by mass is recorded to the nearest 0.1%. Taking into consideration Table 5-1, and the particle size distribution of the soil sample, which passes through the No. 4 sieve, three 100-g specimens of soil samples were tested for each of the core barrels. Moisture content was calculated using Equation 5-1.

Equation 5-1

$$w = \frac{M_{cms} - M_{cds}}{M_{cds} - M_c} \times 100 = \frac{M_w}{M_s} \times 100$$

Where,

w: water content, %,

M_{cms} : mass of container and moist specimen, g

M_{cds} : mass of container and oven-dried specimen, g

M_c : mass of container, g

M_w : mass of water ($M_w = M_{cms} - M_{cds}$), g

M_s : mass of oven dry specimen ($M_s = M_{cds} - M_c$), g

After measuring and calculating the in-situ water content, all of the soil samples were extruded from the core barrels (Figure 5-2) and oven-dried. After samples had dried for 24 hours, a rock crusher was used to crush all of the samples (Figure 5-3) into a maximum of two centimeters particle sizes (Figure 5-4). The samples were then ground (Figure 5-5) to reduce the maximum particle size to pass through the No. 4 sieve (Figure 5-6). The reason for oven drying the samples before crushing them is to prevent the wet clay samples from clogging the crusher jaws. After grinding, all soil samples were mixed together based on the ASTM:D75/D75M-09 (2009) and ASTM:C702/C702M-11(2011) to produce a uniform soil for laboratory tests and soilcrete mixes (Figure 5-7). This method provides a procedure by which a large sample obtained in the field or one produced in the laboratory can be reduced to a convenient size for conducting any specific laboratory test in a way that even smaller portions of test sample are representative of the whole sample.

5.2.1. Particle-size analysis

Particles larger than 75 μm (retained on sieve No. 200) were analyzed with mechanical sieving, while for material finer than what can fit through a No. 200 sieve, a sedimentation process with a hydrometer was used. Two portions of soil samples were chosen from the total mixed sample (Figure 5-7) to carry out the test. The selected samples were sieved on a No. 10 sieve to separate the fraction smaller than what can pass through the No. 10 sieve. Because all soil samples were finer than the No. 4 sieve, there was no need to sieve the retained portion on either the No. 10 or No. 4 sieve. For this test, material passing a No. 10 sieve is required in the amount of 115-g for sandy soil or 65-g of either silt or clay soils. First, the hydrometer test was done on a fraction smaller than a No. 10 sieve (Figure 5-8). Then, all the suspension was washed on the No. 200 sieve until the wash water was clear. The fraction retained on the No. 200 sieve was oven dried. The mechanical sieve was carried out on the sample using No. 4, 10, 20, 40, 60, 100, and 200 sieves. Figure 5-9 shows the distribution of particle size analysis. This curve can also be used to compare different granular soils with the defining three parameters of Effective Size (D_{10}), Uniformity Coefficient (C_u), and Coefficient of Gradation (C_c) where:

Equation 5-2

$$C_c = \frac{(D_{30})^2}{D_{10} * D_{60}}$$

Equation 5-3

$$C_u = \frac{D_{60}}{D_{10}}$$

Where, D_{30} : diameter corresponding to 30% finer in particle-size distribution curve
 D_{60} : diameter corresponding to 60% finer in particle-size distribution curve

5.2.2. Test for soil constants (Atterberg limits)

Clay minerals are cohesive because of their nature of water absorption. When they appear in fine-grained soil structures, soils can be remolded in the presence of moisture. At very low moisture content, these soils behave like brittle material. When the moisture content grows high,

soil behaves like a liquid. In short, there are four stages for soil: solid, semisolid, plastic, and liquid (Figure 5-10). In the early 1900s, Albert Mauritz Atterberg developed a method to determine the behavior and consistency of fine-grained soils based on the water content (Das 2008). The moisture content, in percentages, at which the transition from solid into semi-solid, semi-solid into plastic, and plastic into liquid state takes place, is defined as the shrinkage limit, plastic limit (PL), and liquid limit (LL), respectively.

To test the soil constants (ASTM:D421-85 2007), material passing through a No. 40 sieve is required in a total amount of 220-g allocated as follows: LL 100-g; PL 15-g; centrifuge moisture equivalent 10-g; volumetric shrinkage 30-g; and check tests 65-g. In this laboratory experiment, only LL and PL were considered. Based on ASTM:D4318-10 (2010), six and three samples were chosen for LL and PL, respectively, and sieved on a No. 10 sieve. The passing fraction was sieved on a No. 40 sieve to determine the LL and PL. A wet preparation method was used to prepare the test specimen and method. A multipoint test was used to determine the values. The multipoint method is more precise and should be used in most cases. Different moisture contents were added to six samples of the LL test to adjust the moisture content of the soil required to close the 12.7 mm distance of groove in the soil path inside the brass cap with blows of 15 to 35 (Figure 5-11). The moisture content of the soil, by percentage, was plotted with the corresponding number of blows in a semi-logarithmic graph. The moisture content referred to as 25 blows on the flow curve gives the liquid limit, which is 36.4 for the experimental soil samples (Figure 5-12). The plastic limit is defined as the moisture content, in percent, at which a 3.2 mm specimen of rolled soil crumbles (Das 2008). For the given soil samples, PL was determined to be 19.57%. The plastic index (PI), which is the difference of the liquid limit and plastic limit, is calculated as 16.83 %. The plastic index can be used to provide a great deal of information about the nature of the cohesive soils. Casagrande in 1932 developed a plasticity chart for a wide range of soils (Figure 5-13). The important features of the chart are the A-Line and the U-Line. The A-Line separates inorganic silts from inorganic clays and the U-Line is approximately the upper limit of the relationship of the plasticity index to the liquid limit for any type of soil found so far (Das 2008). Based on the plasticity index, the given soil samples fall into the Inorganic Clays of Medium Plasticity group.

5.2.3. Soil classification

To express specifications of soils with a united language, soil classification systems have been developed. Soils with the same properties are classified in the same group and sub-grouped based on their engineering properties. Two elaborate classification systems, the American Association of State Highway and Transportation Officials (AASHTO) and the Unified Soil Classification System (USCS), have been approved by many engineers. In both methods, the particle-size distribution and plasticity of soils have been used as classification parameters. The AASHTO is used more in highway departments; however, the USCS is more accepted among geotechnical engineers (Das 2008). Therefore, the USCS method was used in this research to classify the soil. Based on the USCS, soils with particles less than 50% passing through a No. 200 sieve are coarse-grained soils and those with 50% or more passing through a No. 200 sieve are fine-grained soils. As shown in Figure 5-14, the particle-size distribution and plasticity parameters, the tested soil in the laboratory falls into the Sandy Lean Clay (CL) group.

5.2.4. Specific gravity

The specific gravity of soil solids is one of the important parameters used in various calculations. The specific gravity of most minerals is between 2.6 and 2.9. This value for light-colored sands made mostly from quartz is about 2.65; for clayey and silty soils it can vary between 2.6 and 2.9. Since the given soil sample has solids that pass through the No. 4 sieve, the ASTM:D854-10 (2010) was used to determine the specific gravity of this material. Two samples were prepared (Figure 5-15) using the wet preparation method. The specific gravity of soil solids was calculated to be 2.7 (Equation 5-4).

Equation 5-4

$$G_s = \frac{\rho_s}{\rho_w} = \frac{M_s \times \rho_w @ T^{\circ}C}{(M_1 - M_2 + M_s) \times \rho_w @ 20^{\circ}C}$$

Where,
 M_s : mass of oven dried soil solids
 M_1 : mass of pycnometer and water
 M_2 : mass of pycnometer and water and soil solids
 ρ_w : density of water

ρ_s : density of soil solids

5.2.5. Compaction test

Generally, compaction is densification of soil by removing air with mechanical energy to increase the unit weight in the construction of highway embankments, earth dams and many other engineering structures. The degree of compaction is measured by dry unit weight. During the compaction process, water is added into the soil as a softening agent, which results in the soil particles slipping over each other to move into a densely packed position. The dry unit weight initially increases when the water content increases during the compaction; however, at a certain point, any increase in the moisture content will decrease the dry unit weight (Figure 5-16). This happens because added water takes up the space that would be occupied with solid soil particles. The moisture content at which the maximum dry unit weight is reached is called the optimum moisture content (Das 2008). To measure the optimum water content of the given soil samples, a proctor compaction Test was used (ASTM:D698-12 2012). Taking into consideration the particle-size analysis, Method A with a four-inch diameter mold with a volume of 943.3 cm³ was chosen. During compaction, the mold was attached to its base and an extension attached to its top. Based on previous experience, five different water contents were added to five soil samples and then compacted into the mold in three equal layers using a 2.5 kg hammer with a drop distance of 304.8 mm, which delivers 25 blows per layer (Figure 5-17). Three trials were done for each moisture content (15 tests in total) and average values were considered after the test (Figure 5-18). For each sample, the moist unit weight was calculated using Equation 5-5. After measuring the moisture content (w) of each sample, the dry unit weight was calculated using Equation 5-6.

Equation 5-5

$$\gamma = \frac{W}{V_{(m)}}$$

Where, W : weight of the compacted soil in the mold
 $V_{(m)}$: volume of mold

Equation 5-6

$$\gamma_d = \frac{\gamma}{1 + \frac{w(\%)}{100}}$$

The theoretical maximum dry unit weight can be also calculated when there is no air in void spaces with full saturation of 100% (Das 2008; ASTM:D698-12 2012). Equation 5-7 was used, taking into consideration the dry unit weight, to calculate the plotting points of the 100% saturation curve (zero air voids curve).

Equation 5-7

$$w_{\text{sat}} = \frac{(\gamma_w)(G_s) - \gamma_d}{(\gamma_d)(G_s)} \times 100\%$$

Where, w_{sat} : water content for complete saturation
 γ_w : unit weight of water at 20°C
 γ_d : dry unit weight of soil
 G_s : specific gravity of soil solids

The calculated dry unit weight is plotted with the corresponding water content to determine the maximum dry unit weight and optimum moisture content (Figure 5-19). The maximum dry unit weight and optimum moisture content are calculated as 1785 kg/m³ and 14.75%, respectively. The dry unit weight at the initial water content of 15.5% is also 1785 kg/m³.

5.2.6. Unconfined compressive strength

After completing the compaction tests on all 15 samples, remolded samples with different moisture contents were used to determine the UCS of the soil sample. The procedure began with pushing 1½ inch diameter Shelby tubes inside the remolded samples to get at least two soil cores from the samples (Figure 5-20). After pushing the Shelby tubes (Figure 5-21), the cores were extruded from the tubes (Figure 5-22) and stored in a moisture-constant room at a temperature of 23 ± 2°C for the UCS test (Figure 5-23).

In the UCS test, confining pressure σ_3 is zero and an axial load is applied to the specimen to cause failure. At failure, total minor principle stress is zero and major principle stress is σ_1 and since the undrained shear strength is independent of confining pressure, it is equal to one-half of the UCS (Figure 5-24) (Das 2008).

Equation 5-8

$$\tau_f = s_u = \frac{\sigma_1}{2} = \frac{q_u}{2} = c_u$$

Method A of the ASTM:D5102-09 (2009) test method was used to determine the UCS of remolded specimens having height-to-diameter ratios between 2.00 and 2.50. Based on the type of failure in each specimen, an original cross-section of the specimen was corrected as follows: if the diameter of the specimen after the test did not change, it meant a brittle failure occurred and there was no need for an original cross-section correction; if a radial deformation occurred but the specimen still had a cylindrical shape, it meant that a cylindrical shape failure occurred and the cross-sectional area had to be corrected using Equation 5-9; if a radial deformation increased during the test, and the specimen assumed a barrel shape, then Equation 5-10 was used to correct the cross-sectional area (Das 2008).

Equation 5-9

$$A = \frac{A_0}{1 - \frac{\epsilon}{100}}$$

Equation 5-10

$$A = \frac{A_0}{1 - \frac{0.6\epsilon}{100}}$$

Where, A: corrected cross-sectional area of specimen
 A₀: initial cross-sectional area of specimen
 ϵ : axial strain for a given axial force

During the test of the specimen with a moisture content of 10.82%, the compression machine failed and no data was recovered for axial displacement and loads. Specimens with 12.5% moisture content had a cylindrical shape failure and specimens with 14.92%, 17.49% and 20.36% moisture content had barrel shape failures (Figure 5-26 and Figure 5-27). Table 5-2 and Figure 5-28 show the values of the UCS for each specimen. The UCS increases with increasing moisture content up to the optimum moisture content. After that point, it decreases as the moisture content increases. The UCS of in-situ soil with an in-situ moisture content of 15.5% is equal to 370 kPa (Figure 5-28).

5.2.7. Modulus of elasticity

The modulus of elasticity (E) of soil specimens was calculated based on the UCS test results. For this purpose during compression, the axial displacement was measured as well to be able to calculate the E. The stress-to-strain curve is shown in Figure 5-29. The average slope of the stress-to-strain curve was used as the E (Table 5-3). The E at 15.5% moisture content was calculated to be 48 kPa. Figure 5-30 shows a strong relationship between the values of E for each specimen versus moisture contents. With an increase of moisture content, the E decreases.

5.2.8. Thermal properties

Thermal properties of soils are important in many engineering projects where heat transfer takes place through soil structure. Thermal conductivity of soils is defined as the amount of heat passing in unit time through a unit cross-section of soil under a unit temperature gradient which is applied in the direction of the heat flow. Figure 5-31 illustrates a schematic view of the heat flow through a cross-sectional area of soil. Based on the figure, the thermal conductivity is defined as Equation 5-11 (Farouki 1986)¹.

Equation 5-11

$$k = \frac{q}{\frac{A(T_2 - T_1)}{l}}$$

¹ The unit now normally used for k in soil studies is W/m.K. A British Thermal Unit (BTU) is amount of the energy needed to cool or heat one pound of water by one degree Fahrenheit at a constant pressure of one atm (Appendix 5-2)

Where, k: heat conductivity
 A: cross-sectional of soil
 q: heat flow
 T₂: initial temperature
 T₁: temperature of end face
 l: length of soil element

The definition of heat conductivity applies for a steady condition where temperature at a point does not change with time. However, if the temperature changes with time, it means that the soil itself is gaining or losing heat. For instance, if the temperature is decreasing with time, some of the heat is absorbed by the soil to increase the temperature, and the rest of the heat is transferred. So the term “heat capacity per unit volume¹ (C) of soil” is defined as heat energy required to increase the temperature of the unit volume by 1°C. The heat capacity is the product of mass specific heat² (c, cal/g°C) and density (ρ, g/cm³) (Equation 5-12) (Farouki 1986).

Equation 5-12

$$C = c \cdot \rho$$

Specific heat capacity is a measurable physical quantity of heat required to increase the temperature of unit mass for 1 Kelvin (Equation 5-13).

Equation 5-13

$$Q = m \cdot c \cdot \Delta T$$

Where, Q: quantity of heat (J)
 m: mass of substance acting as environment (kg)
 c: specific heat capacity (J/kg.K)
 ΔT: change in temperature (K)

¹ Volumetric heat capacity

² Specific heat capacity

Generally, water, air, and soil solids appeared in soil structure. Thus, for a unit volume of soil, heat capacity is calculated using Equation 5-14.

Equation 5-14

$$C = x_s C_s + x_w C_w + x_a C_a$$

Where, x_s , x_w , and x_a : solid, water, and air compositions in a unit volume of soil, respectively

C_s , C_w , and C_a : heat capacities per unit volume of soil solids, water, and air, respectively ($C_w@4^\circ\text{C} = 4.20 \text{ MJ/m}^3 \cdot \text{K}$).

When there is an unsteady state condition, thermal properties and behavior of soil are governed with both heat conductivity and heat capacity. Thus, the term “heat diffusivity” (α) is defined as Equation 5-15 (Farouki 1986). Thermal conductivity governs when conditions are in a steady state. However, thermal diffusivity applies when the temperature changes and conditions are not in a steady state.

Equation 5-15

$$\alpha = \frac{k}{C}$$

A higher value of heat diffusivity means that the soil is capable of rapid and considerable change in temperature. Frozen soils have more thermal conductivity than unfrozen soils. Also ice has a lower heat capacity than liquid water¹; for a given soil, the thermal diffusivity in frozen soil is greater than in unfrozen. As a result, temperature in a frozen soil can change rapidly and the variation is greater. The two materials can have different heat conductivities but the same diffusivities (Farouki 1986).

In determining the thermal properties of soils, the most common method has been that of Kersten (1949). Based on this method, Sanger (1968) has proposed a chart (Figure 5-32) to determine the thermal properties of unfrozen and frozen soils for known water content in ground freezing

¹ Ice has thermal diffusivity eight time greater than liquid water

construction (Farouki). The soils are divided into two groups: one for coarse and one for fine. The difference in thermal properties has to do with the quartz content. In the current laboratory experiment, empirical equations were initially considered to determine the thermal properties of the given soil specimens. Laboratory measurements and in-situ field test were then conducted for a complete assessment of the thermal properties.

Equation 5-16 and Equation 5-17 give the volumetric heat capacity of unfrozen (C_U) and frozen (C_F) soils, respectively (Farouki 1986).

Equation 5-16

$$C_U = \frac{\gamma_d}{\gamma_w} \left(0.18 + 1.0 \frac{w}{100} \right) C_w$$

Equation 5-17

$$C_F = \frac{\gamma_d}{\gamma_w} \left(0.18 + 0.5 \frac{w}{100} \right) C_w$$

Where, γ_d : dry unit weight of the soil
 γ_w : unit weight of water
 w : water content

Kersten has proposed a different series of equations to estimate the heat conductivity of unfrozen (+4°C) and frozen (-4°C) soils in terms of the water content ($w\%$) and dry unit weight (γ_d). For fine soil containing 50% or more silt-clay, Equation 5-18 and Equation 5-19 give k in Btu in./ft² hr °F for unfrozen and frozen silt-clay soils, respectively, where γ_d is in lb/ft³. These equations are presented in Appendix 5-3 and Appendix 5-4. Equation 5-20 and Equation 5-21 give k in W/mK for unfrozen and frozen silt-clay soils, respectively, where γ_d is in g/cm³ (Appendix 5-5 and Appendix 5-6). These equations have a deviation less than 25% from measured thermal conductivities for given soils and are applicable for water content of 7% and greater (Das 2008).

Equation 5-18

$$k = [0.9 \log w - 0.2] 10^{0.01 \gamma_d}$$

Equation 5-19

$$k = 0.01(10)^{0.022\gamma_d} + 0.085(10)^{0.008\gamma_d} w$$

Equation 5-20

$$k = 0.1442[0.9\log w - 0.2]10^{0.6243\gamma_d}$$

Equation 5-21

$$k = 0.001442(10)^{1.373\gamma_d} + 0.01226(10)^{0.4994\gamma_d} w$$

For coarse soils with water content of 1% or more, Equation 5-22 and Equation 5-23 give k in Btu in./ft² hr °F for unfrozen and frozen soils, respectively, where γ_d is in lb/ft³. These equations are presented in Appendix 5-7 and Appendix 5-8. Equation 5-24 and Equation 5-25 give k in W/mK for unfrozen and frozen soils, respectively, where γ_d is in g/cm³ (Appendix 5-9 and Appendix 5-10). These equations have a deviation of less than 25% from measured thermal conductivities for given coarse-grained soils. However, in some cases where coarse-grained soil contains 31% silt-clay, the equations have calculated 50% more values more than measured values. Thus, the equations apply for soils with a very low amount (less than 20 %) of silt-clay (Das 2008).

Equation 5-22

$$k = [0.7\log w + 0.4]10^{0.01\gamma_d}$$

Equation 5-23

$$k = 0.076(10)^{0.013\gamma_d} + 0.032(10)^{0.0146\gamma_d} w$$

Equation 5-24

$$k = 0.1442[0.7\log w + 0.4]10^{0.6243\gamma_d}$$

Equation 5-25

$$k = 0.01096(10)^{0.8116\gamma_d} + 0.00461(10)^{0.9115\gamma_d} w$$

Taking into consideration of the dry unit weight of 1785 kg/m^3 at the initial moisture content of 15.5% and using Figure 5-32, Equation 5-15, Equation 5-16, Equation 5-18 and Equation 5-20, the average values of thermal properties of soil samples used in the laboratory experiment are presented in Table 5-4.

For a complete assessment of thermal properties, laboratory methods shall be done to measure the thermal properties of the soil specimen using two different steady state and transient test methods. In the steady state method, the sample should be in a steady state condition when measurements are being taken, which takes a considerable amount of time. However, in the transient method, the soil temperature varies with time, and measurements can be made very quickly. This method is more versatile than the steady state method (Farouki 1986). In current laboratory experiments, the thermal properties were tested by the Thermal Constants Analyzer TPS 1500, which uses the transient plane heat source method described by (ISO22007-2 2008) that is based on a three-dimensional non-steady state heat conduction in the sample. This method is suitable for homogenous material with isotropic or anisotropic properties and a uniaxial body with a heat conductivity range of $0.01 \text{ Watt/m.K} < \lambda < 500 \text{ Watt/m.K}$, a thermal diffusivity range of $5 \times 10^{-8} \text{ m}^2/\text{s} \leq \alpha \leq 10^{-4} \text{ m}^2/\text{s}$, temperatures in the approximate range of $50 \text{ K} < T < 1000 \text{ K}$, and a specific heat capacity per unit volume in the approximate range of $0.2 \text{ MJ/m}^3\text{K} < C < 5 \text{ MJ/m}^3\text{K}$. The laboratory TPS 1500 device is the product of Thermtest Inc. and can rapidly measure the thermal properties of the material within 20 to 1280 seconds with accuracy better than 5%, and reproducibility better than 1%. Figure 5-33 shows the equipment (SMPE 2012a; SMPE 2012b).

From cylindrical soil core barrels, nicely consolidated sections were chosen and sliced into two or more pieces using a hand saw and/or electrical chop saw with a clamp. The sections were cut to a thickness between 25 and 40 mm (Figure 5-34). In this method, the specimen thickness had to be larger than the penetration depth, Δp_{prob} , which is defined as “how far into the specimen, in the direction of heat flow, a heat wave has travelled” (ISO22007-2 2008). Penetration depth is calculated using Equation 5-26. The surface of the samples were ground enough to ensure good thermal contact between the 6.403 mm radius Kapton probe and sample. The output power and the measuring time were calibrated by several comparative tests. Using calibration numbers, the

initial estimation of heat diffusivity and Equation 5-26, the penetration depth was between 20 and 25 mm, which is smaller than the specimen thicknesses.

Equation 5-26

$$\Delta p_{\text{prob}} = k\sqrt{\alpha \cdot t_{\text{tot}}}$$

Where, t_{tot} : total measurement time for the transient recording
 α : thermal diffusivity of the specimen material
 k : a typical value in hot-disc measurements ($\kappa = 2$), depend on sensitivity of the temperature recordings

Table 5-5 demonstrates the laboratory results of the thermal properties' test on the whole length of the core barrel sample. Figure 5-35, Figure 5-36, and Figure 5-37 illustrate the variation of thermal conductivity, volumetric heat capacity, and heat diffusivity values with depth. From the given figures, it can be concluded that thermal properties are not depth-dependent.

Considering the reference values of thermal conductivity for clay material, typical values are commonly in the range of 0.15 to 2.5 W/m.K ((Tarnawski and Leong 2000) and Table 5-4). As seen in Figure 5-35, the values tested are well within this range. However, the calculated volumetric heat capacity and thermal diffusivity values (Table 5-4) are not quite in the same range as the laboratory tests (Figure 5-36 and Figure 5-37). An in-situ field test was proposed to make sure all laboratory results were correct and reliable. For this purpose, GSS Geothermal Ltd. performed a field thermal test in the same borehole in which the soil core barrel was drilled. Figure 5-38 illustrates the results of the in-situ test, including laboratory results, with the mineralogy of the jobsite. An error with 6% of the value is shown on the vertical profile, which is the maximum error of the machine. Laboratory and field results have, overall, the same shape. However, even taking the error into consideration, laboratory results stand away from the in-situ test results. This can be explained in two ways: first, the resolution of the laboratory test is different from that of the in-situ test, which means that in the laboratory test, only point values are being measured, whereas in the field test, relative values of about one meter resolution are being measured. The second reason has to do with the nature of both tests. The results from the laboratory tests are mostly lower than those from the field. In laboratory tests, to have an

appropriate contact between the probe and soil samples, the surfaces of the sliced samples were ground. However, in the field test, the borehole was fitted with a pipe to carry water up and down its length. Then the borehole was grouted to provide a contact surface and secure the pipe. The thermal conductivity of the grout is 1.8 W/mK which is higher than most of the laboratory test results. The thermal conductivity of the grout was detected by the machine, which resulted in the high values of the field test.

As pointed out earlier, only soil specimens from five to 15 meters depth of the core barrel were chosen and crushed and then mixed together to be used in the laboratory experiment. The average value of laboratory (1.10W/mK) and in-situ (1.71W/mK) heat conductivity tests in the specified depth range was considered to be the average soil thermal conductivity (1.41W/mK). Volumetric thermal capacity and thermal diffusivity of the given soil were considered to be 0.83 MJ/m³K and 1.56 mm²/s, respectively.

5-3. Thermal-insulating grout mixtures

For more than two centuries, grout mixtures have been used to modify soil and rock properties by filling voids and cracks. Grouts can range from very low viscosity to very thick mixtures of water and solid material. Most of the time, the most important characteristics of grouts are pumpability and flowability. A grout with a flowable mixture of solids and water is called a suspended solids grout. A variety of materials such as bentonite, cement, fly ash, lime, or combinations thereof can be added to the grout to change its physical and mechanical properties. The admixture used to treat the soil can be chosen depending on the particular project, degree of improvement needed, cost, availability, site accessibility, and time of construction.

Cement is generally the best admixture to be mixed with soil because of its availability, lower cost, and relatively high strength as compared to other types of admixtures. Soil treated with cement has been used in highways, railroads, and airport construction since Portland cement was invented in 1824. The raw materials used to manufacture Portland cement are limestone, quartz sand, clay, and iron, which supply the necessary ingredients of lime, silica, alumina, and iron. After mixing a proper proportion, the raw materials are pulverized and fired, resulting in cement clinkers. Clinkers are finely ground and mixed with up to 5% gypsum to produce the final product. There are four different types of Portland cement, but only type I (ordinary Portland cement) and type II (high early strength cement) are used in grouting. Type II generally has finer

material than type I. Type II provides more reactive surface area, and therefore more rapid setting. Figure 5-39 illustrates the particle size of different cements. The ability of Portland cement to penetrate into the voids and cracks of soils and rocks is called groutability and is defined as a ratio of the smallest opening size to the largest cement particle size. The groutability must be at least more than three in order to permit grouting to work properly. Viscosity is another important factor in grout's ability to penetrate a formation. A small amount of water must be mixed with cement to make thick grout (mortar), which can only penetrate into large voids for a short distance under high pressure. The amount of water mixed with cement is usually expressed as the water cement ratio (w/c). Generally, in grouting, a ratio of one is the thickest mix and a ratio of five to six is the thinnest. In thin grouts, the solid material tends to settle quickly to the bottom of the grout tanks. This can be prevented by evenly mixing the grout using an agitator. However, solids can still settle on the bottom of a pump, pipes, valves, fittings, or event fissures which are being treated. To keep the cement particles suspended in the grout, bentonite is used in the grout mixture in a proportion of up to 5% of the cement weight.

The initial set time for the cement mixture for structural purposes is one to two hours, but in thin grouts, that time is extended to 18 to 24 hours (Karol 2003). Mixing soil with cement grout will increase the strength and durability of the soil and decrease the compressibility and swelling potential. In the triple fluid of jet grouting, the soil formation is initially destroyed and eroded by high water pressure and then grout is injected into the formation. Taking this into consideration, the w/c ratio of one was chosen for all grout mixtures in the current experiment. The grout density should be checked after the material has been batched. Cement should be mixed by weight. Water should be mixed by weight or volume. The density of grout, ρ_g , is related to the w/c ratio as shown in Equation 5-27 (Jefferis 1994). Equation 5-27 is the same as Equation 3-56 discussed in Chapter three. The current laboratory experiment used Type GU Portland cement (CSA:A23.1-09/A23.2-09 2009) with a bulk density of 1505 kg/m³.

Equation 5-27

$$\rho_g = \frac{1 + w}{\frac{w}{\rho_w} + \frac{1}{\rho_c}}$$

Where, w: water cement ratio

ρ_c : density of cement grains, (typically 3150 kg/m^3 , $G_{s,\text{cement solids}} = 3.15$)

ρ_w : density of water

ELP has been widely used as a lightweight aggregate in concrete and mortar applications since the 1940s because of its lightweight aspects and good performance in thermal and acoustical insulation and fire protection. It is also widely used in fire retardants to reduce flammability. In the current laboratory experiment, ELP was chosen for the development of a new type of isolating grout. It was obtained from a local supplier and has a bulk density of 71.49 kg/m^3 and water absorption of 100%. The grain size distribution of the ELP is shown in Figure 5-40. The thermal conductivity of the ELP is around 0.04 W/m.K .

As discussed previously, due to the complexity of the jet grouting operation, the designing and calculating proportions of cementitious material (cement and ELP), water, soil, and jet grouting parameters have been the most important and difficult part of the laboratory experiments. A back-analysis calculation method was considered to calculate the proportions of each aggregate. Generally, 29 cylindrical specimens, with heights of 150 mm and diameters of 75 mm, were required for each of the five batches (total 145 specimens) to accomplish all laboratory tests. The arrangement of the design is described as follows:

- 1) ELP/cement ratio was considered by weight. Water/cementitious material ratio by weight and volume were considered to be one. Jet grouting water/grout ratio and soilcrete grout/soil ratio were considered by volume since the unit weight of the soilcrete and grout were not known and measured at the time of the designing.
- 2) Regarding jet grouting parameters based on the discussion in Chapter three, the volumetric percentage of grout retained by subsoil, α , and volumetric percentage of soil removed by jet grouting, β , were considered 80%, and 50%, respectively which means the ratio of grout/soil was 8:5 in the soilcrete body. Also based on the flow rates of water and grout in triple fluid jet grouting system in different projects, the volume of water to grout was considered to be 40%.

- 3) Five different proportions of ELP were replaced with cement by weight. Those proportions are: 0.0%, 15%, 30%, 50%, and 70%.
- 4) Based on 29 specimens, a total of 19 liters of soilcrete was required for each of the five batches. If average initial unit weight of soilcrete is assumed 1800 kg/m^3 , 33 kg of soilcrete was required.
- 5) The volume of soil and grout was calculated.
- 6) The water required for the soil to reach its in-situ water content was calculated based on the calculated soil mass.
- 7) The volume of jet grouting additional water was calculated based on the previously calculated volume of the grout.
- 8) The amount of water and cementitious material for all grout mixes was calculated by volume, based on the water/cementitious material ratio of one.
- 9) The weight of cementitious material was calculated in mix No.1 and since this mix had zero amount of ELP, the weight of cementitious material was equal to weight of cement.
- 10) The weight of cementitious material was kept constant in all mixes which was equal to weight of cement in mix No.1.
- 11) The weight of cement and ELP were calculated with replacing cement with different amounts of ELP, by weight.

Table 5-6 and Table 5-7 show the proportions of the aggregates for each of five mixes and final proportions of each aggregate in the soilcrete, respectively. Five different batches of grout and soilcrete mixes were prepared in the laboratory experiment. The mixing procedures were divided into two different steps. The first step was preparing the grout and the second was preparing the

soilcrete mixes. In grout mixes, water was placed in the tank and the drill mixer was started. Then, the cement and ELP were added in that order. The ELP was pre-soaked in water so that its water absorption did not affect the water/cement ratio of the grout mixes. The cementitious materials (cement and ELP) were mixed for five minutes with water to obtain the desired consistency. After preparing grout mixes, fresh unit weight (ASTM:C138/C138M-13 2013), bleeding and expansion (ASTM:C940-10a 2010), and Marsh funnel viscosity (MFV) (ASTM:C939-10 2010; ASTM:D6910/D6910M-09 2009) tests were conducted on the grout specimens. In the second step, soilcrete mixing (ASTM:C192/C192M-13 2013), soil was placed into the mixer and conditioned to its in-situ water content. Then, jet grouting water was added into the soil in the mixer. Finally, the grout mix was poured into the mixer. When all the ingredients were in the mixer, the soilcrete was mixed for 3 min followed by a 3 min rest, followed by a 2 min final mixing. After the mixing, a unit weight (ASTM:C138/C138M-13 2013) test was conducted on freshly mixed soilcrete samples and the mixture was poured into cylinders with a 75 mm diameter and 150 mm height and left for 48 hours to harden enough for demolding. After demolding, the specimens were placed in a moist room at 23.0 ± 2.0 C to be cured for further testing on thermal and physical properties (ASTM:C642-13 2013), UCS (ASTM:C39/C39M-12a 2012), E (ASTM:C469/C469M-10 2010), and splitting tensile (STS) strength (ASTM:C496/C496-11 2011). All laboratory tests were conducted on the third, seventh, and 28th day¹ in two different conditions of wet and dry. The wet condition means that each sample was left in the moisture room for any particular period of time after demolding. The dry condition means that after being in the moisture room for a particular period of time, the samples were oven-dried for 24 hours at 110°C and then tested. The oven-dried condition is a situation in which the heat has already been injected into the borefield area in the underground heat storage system. It is necessary to understand the dry condition in order to investigate the effect of heat injected into the borefield area on thermal, physical and mechanical properties of the soilcrete mixes. Since perlite was used in the aggregates, the top surface of the samples was very rough. Before conducting any of the aforementioned tests, the top and bottom of all specimens were

¹ One-day age samples were so weak and fragile that it was not possible to demold them. Therefore they were left for 48 hours in the cylinders to be hardened enough before demolding. Also, 14-day tests could not be done on specimens, since all laboratories and hydraulic pumps of the university were closed because of January holidays.

ground to a smooth surface (Figure 5-41). The description and results of each test are discussed in the following sections.

5-4. Soilcrete and grout test results and discussions

5.4.1. Unit weight of grout and soilcrete mixes

Unit weight is mass per unit volume. After batching the grout and soilcrete mixes, the fresh material was poured into a known volume and measured and weighed. Then, the fresh unit weight, ρ , of samples was calculated using Equation 5-28 (ASTM:C138/C138M-13 2013).

Equation 5-28

$$\rho = \frac{M_c - M_m}{V_m}$$

Where, M_c : mass of the measure filled with freshly mixed grout or soilcrete
 M_m : mass of the measure
 V_m : volume of measure

The density of hardened soilcrete samples was also measured and calculated within three, seven, and 28 days of when the samples were cast. Table 5-8 presents the results. Figure 5-42 shows that all densities have a decreasing trend when the amount of ELP increases, which occurs because of ELP's porous structure and much lower bulk density. Figure 5-43 shows the density changes during the curing time of the soilcrete mixes. It has been observed that density remains almost the same after the seventh day of curing.

5.4.2. Expansion and bleeding test of fresh grout mixes

The amount of expansion and accumulation of bleed water in freshly mixed grout was measured (ASTM:C940-10a 2010). In this test, 1000 ml of freshly mixed grout were placed in a graduated cylinder to monitor the change in total volume and accumulation of bleed water. Volume measurement was recorded three minutes after the mixing in 15 min intervals for first 60 min and thereafter hourly intervals were recorded until two measurements became the same. The expansion and bleed water were calculated using Equation 5-29 and Equation 5-30. Table 5-9

shows the maximum expansion and bleed water values of all five grout mixes. Figure 5-44 shows the relationship between the density of fresh grout and its bleeding. Fresh grout density decreases and the percentage of bleeding increases as the amount of ELP is increased.

Equation 5-29

$$\text{Expansion, \%} = \frac{V_g - V_1}{V_1} \times 100$$

Equation 5-30

$$\text{Bleeding, \%} = \frac{V_2 - V_g}{V_1} \times 100$$

Where, V_g : volume of grout portion of sample at prescribed intervals, at upper surface of grout, mL
 V_1 : volume of sample at beginning of test, mL
 V_2 : volume of sample at prescribed intervals, measured at upper surface of water layer, mL

5.4.3. Marsh funnel viscosity test of fresh grout mixes

The Marsh funnel viscosity test is usually an indirect measurement of the viscosity of clay slurries (ASTM:D6910/D6910M-09 2009). The flow cone test can also be used in the laboratory and field to determine the time flux of a specified volume of grout through a standardized flow cone. The flow cone test has been used mostly for neat grouts containing materials that pass through the No. 8 sieve (2.36 mm) (ASTM:C939-10 2010). However, based on Figure 5-40, the perlite material contains particles larger than sieve No. 8. Therefore, the Marsh funnel test was used in the laboratory experiments to provide information about the effect of ELP on the viscosity of the grout mixtures. MFV is defined as “the time in seconds required for 946 mL of slurry to flow into a graduated cup from a funnel (known as a Marsh funnel) with specific dimensions” (ASTM:D6910/D6910M-09 2009). The MFV is not a true viscosity and is only an apparent value of the relative sense. Table 5-10 illustrates the test result. A higher value of MFV means high viscosity. Low values mean slurries with lower viscosity. Table 5-10 shows that

increasing the replacement ratio of ELP with cement decreases the viscosity of the grout. Figure 5-45 shows a strong linear relationship between fresh grout density and the MFV.

5.4.4. Density, absorption, and voids of hardened soilcrete mixes

The ASTM:C642-13 (2013) test method was used to determine density, percent absorption, and percent voids in 56-day-old hardened soilcretes. These values are useful in the development of data required for mass and volume conversion of the soilcrete, and are calculated in Table 5-11 and Figure 5-46 using Equation 5-31 to Equation 5-37. Figure 5-47 illustrates a strong relationship between 28-day-old oven-dried and wet density of all soilcrete mixes versus their volume of permeable pore spaces. As the amount of ELP increases, the bulk density and volume of permeable pore spaces of soilcrete mixes decreases and increases, respectively.

Equation 5-31

$$\text{Absorption after immersion, \%} = \left[\frac{(B - A)}{A} \right] \times 100$$

Equation 5-32

$$\text{Absorption after immersion and boiling, \%} = \left[\frac{(C - A)}{A} \right] \times 100$$

Equation 5-33

$$\text{Bulk density, dry} = \left[\frac{A}{(C - D)} \right] \times \rho = g_1$$

Equation 5-34

$$\text{Bulk density}^1 \text{ after immersion} = \left[\frac{B}{(C - D)} \right] \times \rho$$

¹ Bulk density is the property of powders, granules, and other divided solids and is defined as the mass of material particles divided by total volume of their occupancy. It is not intrinsic property of material and can change based on how the material is handled.

Equation 5-35

$$\text{Bulk density after immersion and boiling} = \left[\frac{C}{(C - D)} \right] \times \rho$$

Equation 5-36

$$\text{Apparent density} = \left[\frac{A}{(A - D)} \right] \times \rho = g_2$$

Equation 5-37

$$\text{Volume of permeable pore space (voids), \%} = \left[\frac{g_2 - g_1}{g_2} \right] \times 100 = \left[\frac{(C - A)}{(C - D)} \right] \times 100$$

Where,

A: mass of oven-dried sample in air, g

B: mass of surface-dried sample in air after immersion, g

C: mass of surface-dried sample in air after immersion and boiling, g

D: apparent mass of sample in water after immersion and boiling, g

g_1 : bulk density, dry, Mg/m³

g_2 : apparent density, Mg/m³

ρ : density of water = 1 Mg/m³ = 1 g/cm³

5.4.5. Unconfined compressive strength of cylindrical soilcrete

Based on the results of the density test on hardened soilcrete samples (Table 5-8 and Table 5-11), the ASTM:C39/C39M-12a (2012) test method was used to determine the UCS of the cylindrical soilcrete samples that had a density in excess of 800 kg/m³. Samples were tested with a loading rate of 0.25 ± 0.05 MPa/s in three different time frames: three, seven, and 28 days after casting. As explained previously, tests were done in two different conditions of wet and dry. Table 5-12 and Figure 5-48 illustrate the results of the tests. Figure 5-49 shows that UCS decreases as the amount of ELP increases. Also, Figure 5-50 shows that for each mix, the UCS increased with curing times from day three to day 28. Figure 5-51 shows the reduction percentage of 28-day UCS in all mixes with respect to control Mix 1. The overall reduction is due to the weak porous microstructure of ELP, which increases porosity and reduces the density of the soilcrete and consequently decreases the UCS. Figure 5-52 shows a 28-day UCS improvement and reduction

percentage of each mix with respect to in-situ soil strength (370 kPa). Except for Mix 5, all soilcrete mixes achieved higher values of strength than the in-situ soil after 28 days. For example, Mix 3 achieved a value of UCS that is almost 435% higher than that of the in-situ soil 28 days after mixing. As previously discussed, during the jet grouting operation, the whole structure of the soil is initially weakened and excavated and then replaced with cementitious material; this means the UCS of soilcrete columns can be even less than that in the in-situ soil during the first days of curing. However, to prevent any settlement or collapse of the ground surface, it is important to maintain the strength of the soilcrete so that it is as strong as or stronger than the in-situ soil, even during the first days of curing. Figure 5-53 shows the UCS progression of soilcrete mixes during curing. The UCS of mixes 4 and 5 is less than that in the in-situ soil during the first seven days of curing after the mixing process. However, mixes 1, 2 and 3 have higher UCS values than the in-situ soil, even after three days of curing. Figure 5-54 demonstrates a strong relationship between the 28-day-old UCS of soilcrete mixes and their densities. UCS decreases with decreasing density. Figure 5-55 presents a strong relationship between 28-day UCS versus voids of soilcrete mixes. As the specimen voids increase, UCS decreases.

5.4.6. Modulus of elasticity of cylindrical soilcrete

The E of hardened soilcrete cylinders was calculated based on the UCS test using (ASTM:C496/C496-11 2011). For this purpose, the longitudinal displacement of soilcrete samples was measured during the compression test. Stress-to-strain curves are presented in Appendix 5-11 to Appendix 5-15. The average slope of the stress-to-strain curve was considered as E (Table 5-13). As with the UCS, the E of soilcrete mixes decreases as the amount of the ELP increases (Figure 5-56). Figure 5-57 shows a good relationship between 28-day densities of soilcrete mixes with their corresponding E. Figure 5-58 shows a perfect linear relationship between 28-day UCS and the E of soilcrete mixes. The regression between UCS and E of all mixes with different ages is also reasonable (Figure 5-59). Figure 5-60 presents a strong relationship between the 28-day E versus voids of soilcrete mixes. It is clear that with increasing voids of the specimen, E decreases.

5.4.7. Splitting tensile strength of cylindrical soilcrete mixes

The STS method is used to evaluate the shear resistance of lightweight concrete. The ASTM:C496/C496-11 (2011) test method was used to apply a diametral compressive load along the length of the soilcrete cylindrical specimen at a rate of 11.6 to 23 KPa/s until failure occurs. The loading causes tensile and compressive stresses on a plane on which the load is applied, and in an area immediately around the applied load, respectively. In such a situation, tensile failure occurs instead of compression, because the areas of applied load are in a triaxial compression state, allowing them to withstand much higher compressive stresses than occur in a uniaxial compression strength test. The specimen's STS is calculated using Equation 5-38. The results of the test are shown in Table 5-14.

Equation 5-38

$$T = \frac{2P}{\pi ld}$$

Where, T: splitting tensile strength, MPa
 P: maximum applied load, N
 l: length of specimen, mm
 d: diameter of specimen, mm

Generally, STS values of all mixes showed trends similar to UCS with respect to increasing ELP, which means STS decreased with an increasing amount of ELP (Figure 5-61). Also for each mix, STS increased with curing times from the third day to the 28th day. Figure 5-62 presents a good relationship between 28-day STS and the density of soilcrete specimens. It is clear that as density increases, so does STS. Figure 5-63 shows a perfect power regression for the 28-day wet and oven-dried STS and UCS. This regression is still reasonable for all mixes with different ages (Figure 5-64). This proves that both UCS and STS strength gain rates are similar during the curing time. This is consistent with previous findings (W. V. Liu 2013). Figure 5-65 illustrates the relationship between the 28-day STS and E of different mixes. Figure 5-66 shows a strong relationship between the 28-day STS versus voids of soilcrete mixes. It is clear that as the specimen voids increase, STS decreases.

5.4.8. Moisture content of hardened soilcrete mixes

The moisture content of each soilcrete mix was measured and calculated in three different time periods: three, seven, and 28 days after casting. The results are shown in Table 5-15 and Figure 5-67. Figure 5-68 shows a strong relationship between the 28-day moisture content and 28-day density of soilcrete mixes. As the moisture content from Mix 1 to Mix 5 increases, the specimens' density decreases. At the constant moisture content, the density of wet soilcrete is more than that of the oven-dried soilcrete specimen. This is because water is denser than air. Figure 5-69 shows a relationship between the 28-day moisture content and 28-day UCS of soilcrete specimens in all mixes. As the moisture content increases, the UCS of the soilcrete decreases; however, at the same moisture content, the UCS of oven-dried samples is more than that for the corresponding wet samples. Figure 5-70 and Figure 5-71 present another strong relationship between the 28-day moisture content and 28-day E and STS of soilcrete mixes, respectively. As the moisture content increases, both values decrease. The reason that the soilcrete samples decrease in density, UCS, E, and STS as the moisture content from Mix 1 to Mix 5 increases is that the low-strength, lightweight ELP was replaced with cement and soil material with higher values of strength and density. Figure 5-72 shows a relationship between the 28-day moisture content and volume of permeable pores (voids) of soilcrete mixes, and indicates an increase in the amount of voids when the moisture content increases.

5.4.9. Thermal properties of hardened soilcrete mixes

Table 5-16 illustrates the thermal properties of aggregates used in the laboratory experiment. As with the soil samples, the thermal properties were tested by the Thermal Constants Analyzer TPS 1500, which uses the transient plane heat source method based on the three-dimensional non-steady-state heat conduction in the sample. This test was done after the soilcrete samples were cured for 56 days in the moisture room. The test was conducted in both wet and oven-dried conditions. To simulate the UTES borefield condition after it was fully charged, half of the samples were oven-dried for 56 days, then cut with an electrical chop saw into pieces that were 30 cm wide (Figure 5-73). The other half were cut in wet conditions after being air-dried for 56 days in the moisture room. Table 5-17 shows the laboratory results of the thermal properties test.

5.4.9.1. Thermal conductivity

Figure 5-74 shows that in both wet and dry conditions thermal conductivity decreases as the amount of ELP increases. This occurs because ELP has a porous structure and low thermal conductivity (0.04 Watt/m.K). Figure 5-75 illustrates the percentage of thermal conductivity reduction (improvement) in each mix with respect to the thermal conductivity of in-situ soil and Mix 1 (control mix). For instance, the thermal conductivity of Mix 3 is reduced 83 and 63% in oven-dried and wet conditions, respectively, with respect to in-situ soil thermal conductivity. As discussed previously, thermal conductivity is measure of a material's ability to conduct heat. In other words, the ability of in-situ soil to conduct heat will be reduced 83% if the jet grouting operation is carried out using the new thermal-insulating grout. Figure 5-76 shows a strong relationship between the moisture content and thermal conductivity of the soilcrete in both wet and oven-dried conditions. At the given moisture content, the thermal conductivity in the wet condition is more than that in the dry condition. This is because the thermal conductivity of air (0.026 W/m.K) is a lot lower than that of water (0.58 W/m.K @ 20°C), and also, in the oven-dried condition, the free and structural moisture content was replaced with the low thermal conductivity of air. In Mix 1 to Mix 5, the overall moisture content of the samples increased. However, it is important to remember that from Mix 1 to Mix 5, components with higher values of heat conductivity were replaced with ELP, which had lower values of heat conductivity. This is why, even by increasing the moisture content from Mix 1 to Mix 5, thermal conductivity decreases. Figure 5-77 illustrates the reduction percentage of thermal conductivity from the wet to oven-dried condition. Mix 3 has the greatest reduction value of all the mixes. Figure 5-78 illustrates the relationship between thermal conductivity and the density of soilcrete samples in both oven-dried and wet conditions. Samples with low density have low thermal conductivity values. In the same manner, increasing the percentage of voids in the specimen decreases thermal conductivity (Figure 5-79).

5.4.9.2. Volumetric heat capacity

Figure 5-80 shows the results of the volumetric heat capacity of soilcrete mixes. Volumetric heat capacity tends to decrease as the amount of ELP increases, except in the case of Mix 3. Volumetric heat capacity values in the wet condition are more than those in the oven-dried condition, because of the high value of water's volumetric heat capacity in the wet condition.

Also, as discussed previously, all ELP was replaced by weight with cement. A considerable volume of ELP with very low volumetric heat capacity values was combined with other components in each mixture. Thus, in a given mold with constant volume, the amount of other components was reduced, which decreased the overall volumetric heat capacity of all mixes. However, in Mix 3, the replacement ratio of ELP with cement was not enough to waive the effect of the high volumetric heat capacity of the water ($4.2 \text{ MJ/m}^3 \cdot \text{K}$). As a result, a slight increase was observed in the wet volumetric heat capacity of Mix 3. In the oven-dried condition, all free water and structural water that significantly affect the volumetric heat capacity were dried out, so the volumetric heat capacity gradually decreased as the amount of ELP increased. Figure 5-81 illustrates the improvement percentage of volumetric heat capacity in each mix with respect to in-situ soil and Control Mix 1. For instance, the volumetric heat capacity of Mix 3 increased 11 and 44% in oven-dried and wet conditions, respectively, with respect to the in-situ soil volumetric heat capacity. In other words, to increase soilcrete's unit volume unit temperature, more heat energy is required compared to what is necessary for in-situ soil. Figure 5-82 shows a strong relationship between the moisture content and oven-dried volumetric heat capacity of the soilcrete. In the same manner as thermal conductivity, at a given moisture content, the volumetric heat capacity of the wet condition is more than that of the dry condition. This is because the volumetric heat capacity of air is a lot lower than water, and also because in the oven-dried condition, the free and structural moisture content was replaced with air. Again, as can be seen from Mix 1 to Mix 5, the overall moisture content of samples increased. However, components with higher values of volumetric heat capacity were replaced with ELP with lower values of volumetric heat capacity. Therefore, although from Mix 1 to Mix 5, the overall moisture content increased, the volumetric heat capacity of the soilcrete mixes decreased. Figure 5-83 illustrates the relationship between volumetric heat capacity and the density of soilcrete samples in both oven-dried and wet conditions. Samples with low density have low volumetric heat capacity values. In the same manner, when the percentage of voids in the specimen increases, the volumetric heat capacity decreases (Figure 5-79).

5.4.9.3. Specific heat capacity

Figure 5-85 presents results of the specific heat capacity of all the mixes. Specific heat capacity was calculated by dividing the volumetric heat capacity by the corresponded density of each mix.

Oven-dried specific heat capacity tends to increase when the amount of ELP increases. Specific heat capacity values in oven-dried condition are more than those in wet conditions, because wet densities have higher values. As discussed previously, from Mix 1 to Mix 5, the amount of ELP and other components increased and decreased, respectively. ELP with a higher value of specific heat capacity was replaced with cement and soil material with lower heat capacity values, and the overall specific heat capacity of all mixes increased gradually. Figure 5-86 illustrates the improvement percentage of specific heat capacity in each mix with respect to in-situ soil and Control Mix 1. The specific heat capacity of Mix 3 increased 76 and 55% in oven-dried and wet conditions, respectively, with respect to in-situ soil-specific heat capacity. In other words, more heat energy is required to increase soilcrete's unit mass unit temperature compared to what is needed for in-situ soil.

5.4.9.4. Heat diffusivity

Figure 5-87 presents the results of heat diffusivity for all mixes. Generally, heat diffusivity is a material's ability to adjust its temperature to the surrounding environment. For any thermal-insulating purpose, material with lower heat diffusivity is preferred. Heat diffusivity decreases as the amount of ELP increases. Looking at Figure 5-74 and Figure 5-80 and Equation 5-15, it is easy to spot the decreasing heat diffusivity. As discussed previously, the volumetric heat capacity decreased when the amount of ELP increased. However, the amount of heat conductivity reduction was much greater than the amount of volumetric heat capacity, which reduced the overall value of heat diffusivity. Figure 5-88 illustrates the reduction percentage of heat diffusivity with respect to Control Mix 1 and in-situ soil. The reductions with respect to the in-situ soil thermal properties in oven-dried samples were 84% to 89% in Mix 3 to Mix 5, respectively. The reductions for the wet samples were in range of 73% to 82% in Mix 3 to Mix 5. This indicates that oven-dried samples with a particular amount of moisture content could expect more of a decrease in heat diffusivity than wet samples. Figure 5-89 shows the relationship between the moisture content and heat diffusivity of the soilcrete specimens in both wet and oven-dried conditions. Figure 5-90 illustrates the relationship between heat diffusivity and the density of the soilcrete samples in both oven-dried and wet conditions. Samples with low density have low heat diffusivity values. In the same manner, by increasing the percentage of the voids in the specimen, heat diffusivity decreases (Figure 5-91).

5-5. Conclusions

Based on the aforementioned discussion and test results, in-situ soil properties used in the laboratory experiment are as follows.

<u>Properties</u>	<u>Values</u>	<u>Comments</u>
In-situ moisture content:	15.5%	
Liquid limit:	36.4 %	Inorganic clays of medium plasticity
Plastic limit:	19.57%	
Plasticity index:	16.83%	
UCSC soil classification:	CL	Sandy lean clay
Specific gravity:	2.7	
Optimum moisture content:	14.75%	
Dry density:	1785 kg/m ³	At optimum moisture content
Dry density:	1785 kg/m ³	At in-situ moisture content
Unconfined compression strength:	370 kPa	At in-situ moisture content
Modulus of elasticity:	48 kPa	At in-situ moisture content
Thermal conductivity:	1.41 W/m.K	Based on laboratory and field thermal properties test
Thermal diffusivity:	1.56 mm ² /s	
Volumetric heat capacity:	0.83 MJ/m ³ .K	
Specific heat capacity:	465 J/kg.K	

Based on the results of the physical, mechanical, and thermal properties tests in the laboratory, Mix No. 3 was chosen for the actual jet grouting experiment that will be discussed in Chapter six. Mix No. 3 has the best mechanical and thermal properties with respect to improving the thermal properties of in-situ soil and maintaining enough strength to prevent any settlement and collapse on the surface of the ground. The physical, mechanical, and thermal properties of fresh grout, fresh soilcrete and 28-day hardened soilcrete of Mix 3 are presented as follows.

<u>Properties</u>	<u>Values</u>	<u>Comments</u>	<u>Improvement</u>
Fresh grout density	1501.47 kg/m ³		
Fresh soilcrete density	1765.56 kg/m ³		
28-day hardened soilcrete	1661.53 kg/m ³	Wet	

	1127.39 kg/m ³	Dry	
Bleeding of fresh grout	43.75%		
Marsh Funnel viscosity	22 sec		
Bulk density	1094.3 kg/m ³		
Voids	53.20%		
Unconfined compression strength	1.814 MPa	Wet	390.2 % increase
28-day	1.978 MPa	Dry	435% increase
Modulus of elasticity	222.64 MPa	Wet	463733% increase
28-day	156.43 MPa	Dry	325795% increase
Splitting tensile strength	0.463 MPa	Wet	
28-day	0.324 MPa	Dry	
28-day moisture content	46.55%	Wet	
Thermal conductivity	0.52 W/m.K	Wet	63% reduction
	0.23 W/m.K	Dry	83% reduction
Thermal diffusivity	0.42 mm ² /s	Wet	73% reduction
	0.25 mm ² /s	Dry	84% reduction
Volumetric heat capacity	1.19 MJ/m ³ .K	Wet	44% increase
	0.92 MJ/m ³ .K	Dry	11% increase
Specific heat capacity	719.81 J/kg.K	Wet	55% increase
	819.4 J/kg.K	Dry	76% increase

The literature values of different properties were discussed in Chapter three. Values of fresh grout density as well as UCS and thermal conductivity of hand-mixed soilcrete specimens were verified with the values reported in the literature. Density for a typical grout type in a jet grouting operation (Equation 3-56) is 1500 kg/m³, which is in agreement with the calculated density of the No. 3 grout mixture (1501.47 kg/m³) in the laboratory experiment. The UCS of soilcrete created by different jet grouting systems in different jobsites on clay soil was reported to be 1 to 2.4 MPa (Table 3-1, Table 3-9, Table 3-10, Figure 3-46, Figure 3-62, Figure 3-65, Figure 3-66, and Figure 3-69). The values in wet and dry conditions of hand-mixed soilcrete specimens were 1.814 and 1.978 MPa. It is clear that the calculated values are in agreement with the literature findings. The thermal conductivity of lightweight concrete was reported to be between 0.1 and 0.5 W/m.K (Engineering 2015; Norlite 2015; ASTM:C332-09 2009). Results showed that

thermal conductivity values of hand-mixed soilcrete specimens in wet (0.52 W/m.K) and dry (0.23 W/m.K) conditions were within the same range. Considering the results, the following conclusions have been reached:

- 1) The density of mixes decreased dramatically as the amount of ELP increased.
- 2) Density remains almost the same after the seventh day of curing.
- 3) Fresh grout density decreased and percentage of bleeding increased as the amount of ELP increased.
- 4) The viscosity of fresh grout decreased as the amount of ELP increased.
- 5) Increasing the amount of ELP, decreased and increased, respectively, the bulk density and volume of permeable pore spaces of soilcrete mixes.
- 6) UCS, E, and STS generally decreased as the amount of ELP increased.
- 7) Mix 3 reached a value of UCS that was almost 435% higher than that of in soil after 28-days of mixing.
- 8) UCS, E, and STS decreased as the specimen's density decreased and its voids increased.
- 9) The thermal conductivity of oven-dried mixes decreased 79% to 89% in Mix 2 to Mix 5 with respect to the in-situ soil heat conductivity value. Also the oven-dried thermal conductivity of Mix 3 improved 83%.
- 10) The thermal conductivity of wet mixes decreased 55% to 83% in Mix 2 to Mix 5 with respect to the in-situ soil heat conductivity value. Also the wet thermal conductivity of Mix 3 improved 63%.

- 11) The thermal diffusivity of oven-dried mixes decreased 82% to 88% in Mix 2 to Mix 5 with respect to the in-situ soil heat diffusivity value. Also the oven-dried thermal diffusivity improved 84% in Mix 3.
- 12) The thermal diffusivity of wet mixes decreased 62% to 82% in Mix 2 to Mix 5 with respect to the in-situ soil heat conductivity value. Also the wet thermal conductivity of Mix 3 improved 73%.
- 13) The oven-dried volumetric and specific heat capacity improved 11% and 76% in Mix 3, respectively, with respect to the in-situ soil thermal properties. Also the wet volumetric and specific heat capacity of Mix 3 improved 44% and 55% respectively, with respect to the in-situ soil thermal properties.
- 14) A strong relationship has been found between density, voids, and moisture content versus the UCS, STS, E, thermal conductivity, thermal diffusivity, volumetric and specific heat capacity; STS versus UCS; UCS versus E; STS versus E; bleeding versus fresh grout density; MFV versus fresh grout density; and density versus voids and moisture content.

Table 5-1 Minimum requirement for mass of test specimen, and balance readability (ASTM:D2216-10 2010)

Maximum particle size (100% passing)		Method B, water content recorded to $\pm 0.1\%$	
SI Unit Sieve size	Alternative sieve size	Specimen mass	Balance readability (g)
75.0 mm	3 in	50 kg	10
37.5 mm	1 ½ inch	10 kg	10
19.0 mm	¾ inch	2.5 kg	1
9.50 mm	3/8 inch	500 g	0.1
4.75 mm	No. 4	100 g	0.1
2.00 mm	No. 10	20 g	0.01

Table 5-2 UCS of specimens with different moisture contents

Moisture content, w, %	10.82	12.5	14.92	17.49	20.36
Average UCS, kPa	-	382.39	395.11	216.15	110.14

Table 5-3 Modulus of elasticity of specimens with different moisture contents

Moisture content, w, %	10.82	12.5	14.92	17.49	20.36
Average Modulus of elasticity, kPa	-	196.13	63.86	18.57	7.29

Table 5-4 Thermal properties of the given soil in the experiments using empirical methods

Heat conductivity	Volumetric heat capacity	Thermal diffusivity
Figure 5-32 1.125 (Btu. ft/ft ² . h. F) 1.945 (Watt/m. K)		
Equation 5-18 11.337 (Btu. in/ft ² . h. F) 0.9447 (Btu. ft/ft ² . h. F)	37451 (Btu/ft ³ . °F) 2.51 (MJ/m ³ . K)	0.71 (mm ² /sec)
Equation 5-20 1.635 (Watt/m. K)		

Table 5-5 Results of thermal test on soil core samples (SMPE 2012a; SMPE 2012b)

Depth (m)	Thermal Conductivity (W/mK)	Thermal Diffusivity (mm ² /s)	Specific Heat (MJ/m ³ K)
6.4008	1.422	0.5138	2.767
9.7536	1.13	1.31	0.8624
9.7536	1.029	0.9113	1.129
10.3632	0.4481	1.84	0.2436
12.8016	1.864	1.444	1.291
12.8016	1.894	1.27	1.491
13.4112	0.8654	1.418	0.6105
14.6304	0.4949	1.987	0.2491
15.8496	0.7821	0.9866	0.7928
22.5552	1.289	0.5444	2.368
23.4696	0.1725	3.421	0.1725
25.908	1.386	0.6272	2.21
27.1272	0.8839	1.609	0.5498
28.956	1.101	0.9164	1.202
30.1752	1.41	0.6864	2.054
31.0896	0.6178	3.534	0.1748
32.004	1.03	1.77	0.5818
34.1376	1.515	2.425	0.6245
34.7472	1.051	0.7257	1.448
35.3568	1.357	0.8463	1.604
35.9664	0.3458	1.354	0.2553
39.624	1.468	0.7048	2.083
41.4528	1.594	2.051	0.7769
43.2816	1.767	1.283	1.377
44.5008	0.6496	3.7	0.1756
46.3296	1.333	1.01	1.32
46.9392	1.24	1.386	0.8949
46.9392	0.9215	2.403	0.3826
48.4632	1.695	0.9616	1.763
50.292	0.6241	2.462	0.2535
50.292	0.779	2.645	0.2945
53.0352	0.9631	1.713	0.5621
54.2544	0.6805	1.128	0.6031
56.0832	1.285	0.9819	1.309
63.7032	0.4343	0.5425	0.8005
64.3128	1.092	0.9709	1.125

Table 5-6 Proportions of the aggregates

Aggregates	Combination	Measure	Soilcrete				
			1	2	3	4	5
C.M. ¹	C.M. = ELP + Cement	By weight	0.00	0.15	0.30	0.50	0.70
Grout=Water/C.M.	Grout = Water + C.M.	By volume	1.00	1.00	1.00	1.00	1.00
Water/Grout	Jet Grouting	By volume	0.40	0.40	0.40	0.40	0.40
Grout/Soil=(8/5)	Soilcrete = Grout + Soil	By volume	1.60	1.60	1.60	1.60	1.60

¹ Cementitious Material

Table 5-7 Final proportions of aggregates in the soilcrete body

Aggregates	Measure	Soilcrete				
		1	2	3	4	5
Soilcrete	Lit	21.34	31.02	40.70	53.61	66.52
	kg	30.28	30.28	30.28	30.28	30.28
Amount of ELP in soilcrete	By volume %	0.00	34.04	51.88	65.65	74.07
	By weight %	0.00	4.36	8.72	14.53	20.34
Amount of soil in soilcrete	By volume %	34.25	23.56	17.95	13.63	10.99
	By weight %	43.91	43.91	43.91	43.91	43.91
Amount of cement in soilcrete	By volume %	27.40	16.02	10.05	5.45	2.64
	By weight %	29.06	24.70	20.34	14.53	8.72
Amount of water in Soilcrete	By volume %	38.36	26.39	20.11	15.27	12.30
	By weight %	27.03	27.03	27.03	27.03	27.03

Table 5-8 Unit weight of grout and soilcrete mixes

Density, kg/m ³	Mix No.				
	1	2	3	4	5
Fresh Grout	1871.19	1622.20	1501.47	1350.	1214.76
Fresh Soilcrete	2014.54	1878.735	1765.558	1705.2	1644.83
3 rd Day Hardened Wet	1898.65	1791.96	1697.02	1582.17	1497.04
7 th Day Hardened Wet	1883.79	1793.1	1694.8	1581.59	1499.37
28 th Day Hardened Wet	1896.88	1796.53	1661.53	1577.14	1502.81
3 rd Day Hardened Oven Dry	1396.3	1232.98	1102.27	951.7	830.47
7 th Day Hardened Oven Dry	1482.34	1274.245	1131.17	993.56	939.24
28 th Day Hardened Oven Dry	1504.77	1355.07	1127.39	977.77	912.97

Table 5-9 Expansion and bleed water of grout mixes

Grout mix No.	1	2	3	4	5
Bleeding	-9.375	-18.75	-43.75	-68.75	-72.5
Expansion	9.375	18.75	43.75	68.75	72.5

Table 5-10 Marsh Funnel Viscosity test results

Grout mix No.	1	2	3	4	5
MFV, seconds	29	24	22	19	15

Table 5-11 Density and voids of hardened soilcrete specimens

Mix No.	1	2	3	4	5
Bulk density, dry, kg/m ³	1465.7	1283.2	1094.29	955.52	859.84
Volume of permeable pore spaces (voids), %	37.19	44.94	53.20	57.57	59.88

Table 5-12 UCS test results

Unconfined Compressive Strength, MPa	Mix No.				
	1	2	3	4	5
3rd Day Hardened Wet UCS	3.312	1.766	0.808	0.266	0.082
7th Day Hardened Wet UCS	5.276	2.123	0.846	0.349	0.113
28th Day Hardened Wet UCS	6.571	4.173	1.814	0.755	0.196
3rd Day Hardened Oven Dry UCS	5.638	1.972	0.905	0.288	0.103
7th Day Hardened Oven Dry UCS	5.462	3.115	1.279	0.399	0.201
28th Day Hardened Oven Dry UCS	10.055	4.588	1.978	0.686	0.187

Table 5-13 Modulus of elasticity of soilcrete in different mixes

Modulus of elasticity, MPa	Mix No.				
	1	2	3	4	5
3 rd Day Hardened Wet	158.313	93.873	49.042	15.076	5.261
7 th Day Hardened Wet	465.520	158.330	48.018	22.904	19.867
28 th Day Hardened Wet	1280.322	823.678	222.638	39.668	12.820
3 rd Day Hardened Oven Dry	378.462	102.666	48.321	15.729	4.989
7 th Day Hardened Oven Dry	1056.134	382.942	92.561	20.248	17.482
28 th Day Hardened Oven Dry	1118.043	398.443	156.431	28.210	5.712

Table 5-14 Splitting tensile strength test results

Splitting tensile strength, MPa	Mix No.				
	1	2	3	4	5
3rd Day Hardened Wet	0.906	0.338	0.141	0.057	0.015
7th Day Hardened Wet	-	0.515	0.211	0.063	0.024
28th Day Hardened Wet	1.851	0.952	0.463	0.179	0.053
3rd Day Hardened Oven Dry	-	-	-	-	-
7th Day Hardened Oven Dry	-	0.349	0.113	0.039	0.026
28th Day Hardened Oven Dry	1.910	0.818	0.324	0.135	0.044

Table 5-15 Moisture content of each mix during time

Moisture content, %	Mix No.				
	1	2	3	4	5
3rd Day Hardened	36.31	45.20	54.39	67.09	80.14
7th Day Hardened	27.29	40.69	49.65	60.86	60.41
28th Day Hardened	26.55	32.74	46.55	56.46	59.70

Table 5-16 Thermal properties of aggregates¹

	K, W/m. K	C, MJ/m ³ . K	c, J/kg. K	α , mm ² /sec	γ , kg/m ³
ELP material	0.04	0.06	837	0.67	71.49
Cement	0.29	1.11	740	0.26	1505
Soil ²	1.41	0.83	465	1.56	1785
Free water	0.58	4.2	4200 ³	0.14	1000
Air	0.026	0.0012	1010	20	1.2

Table 5-17 Thermal properties of soilcrete mixes

Thermal properties of 56 th -day Hardened Specimen		Mix No.				
		1	2	3	4	5
Wet	Thermal conductivity, W/m. K	0.77	0.63	0.52	0.30	0.22
	Thermal diffusivity, mm ² /s	0.57	0.58	0.42	0.33	0.28
	Volumetric heat capacity, MJ/m ³ . K	1.38	1.07	1.19	0.92	0.81
	Specific heat capacity, J/kg. K	730.14	599.21	719.81	584.91	544.44
Oven-dried	Thermal conductivity, W/m. K	0.36	0.29	0.23	0.18	0.14
	Thermal diffusivity, mm ² /s	0.31	0.28	0.25	0.22	0.19
	Volumetric heat capacity, MJ/m ³ . K	1.24	1.129	0.92	0.83	0.78
	Specific heat capacity, J/kg. K	826.70	833.65	819.49	857.86	860.81

¹ An approximate thermal property values have been provided for air, cement and water.

² Thermal properties of in situ soil used in laboratory experiment have been provided.

³ Bound water has specific heat capacity of 2200 J/kg. K.



Figure 5-1 Delivered cores samples from GSS Geothermal Ltd



Figure 5-2 Extracted soil sample from core barrels

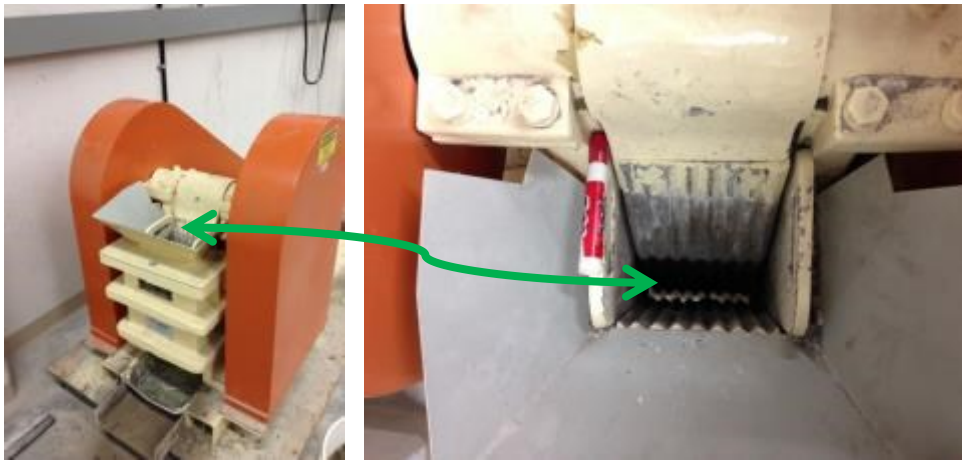


Figure 5-3 Rock crusher machine



Figure 5-4 Maximum particle size of soil after crushing, 2cm

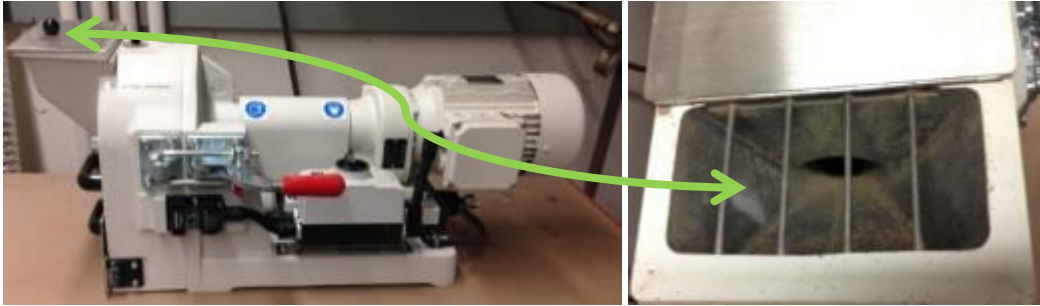


Figure 5-5 Rock grinder machine



Figure 5-6 Maximum particle size passes sieve No.4 after grinding



Figure 5-7 Mixing all grinded soil samples together

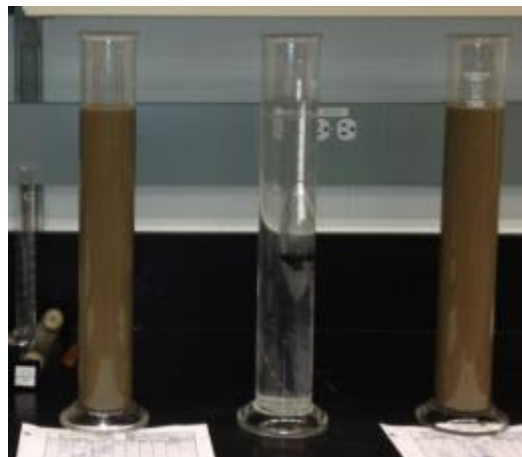


Figure 5-8 Hydrometer test on portion smaller than sieve No. 10

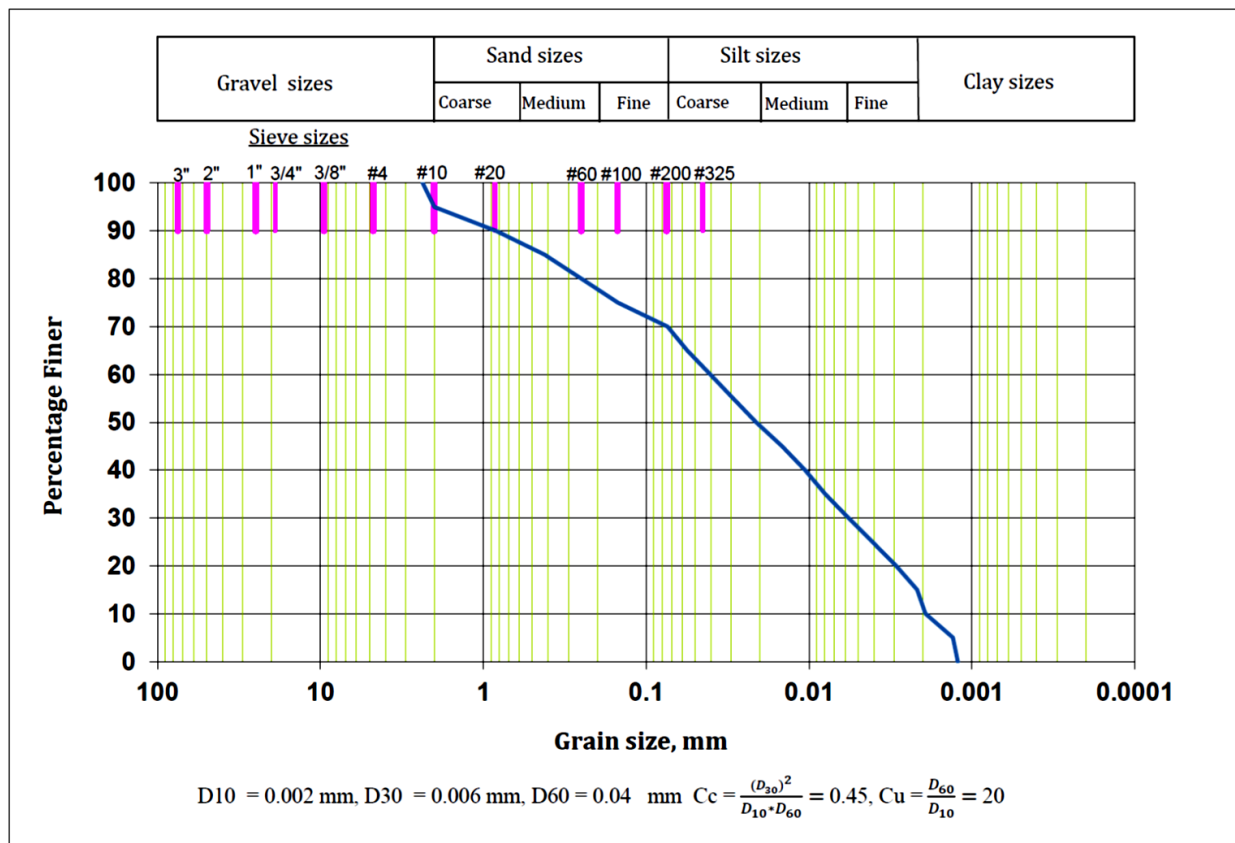


Figure 5-9 Distribution of Particle-Size Analysis

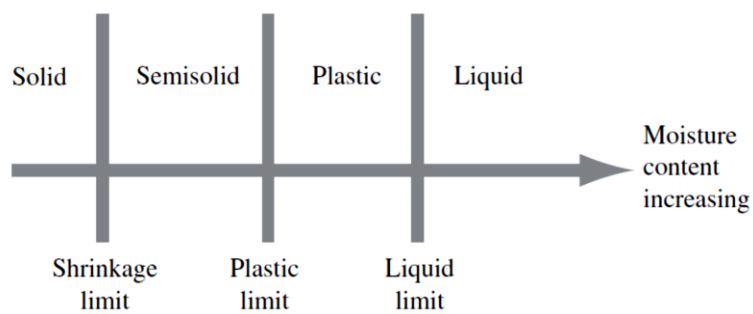


Figure 5-10 Atterberg limits (Das 2008)

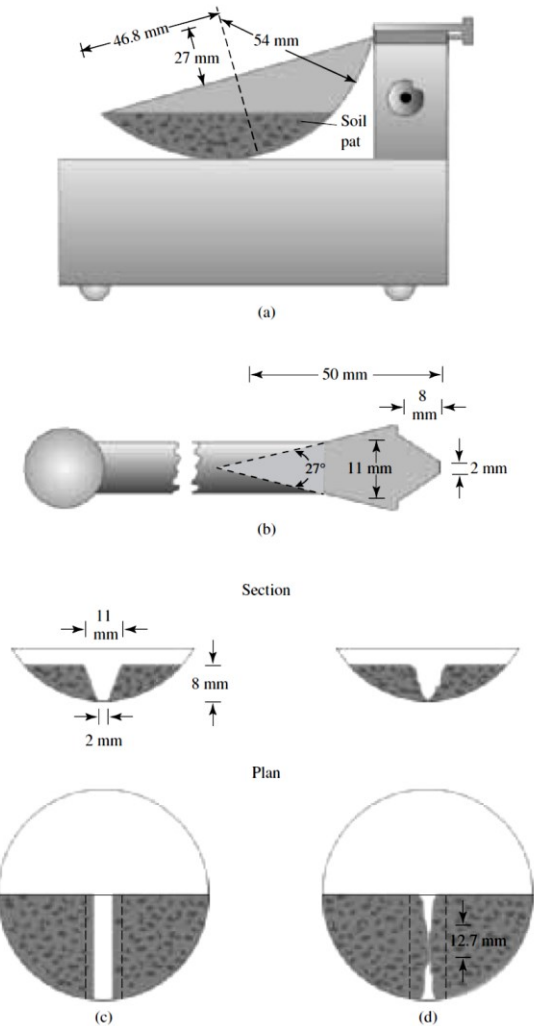


Figure 5-11 Liquid limit test: (a) liquid limit device; (b) grooving tool; (c) soil pas before test; (d) soil pat after test (Das 2008)

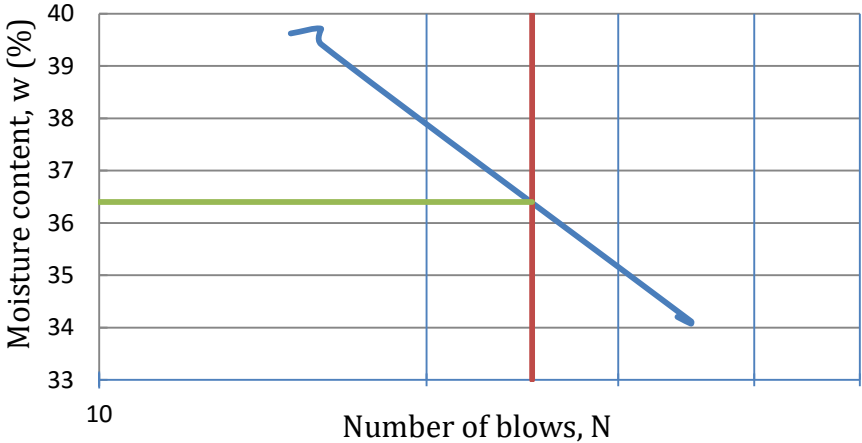


Figure 5-12 Flow curve for liquid limit determination

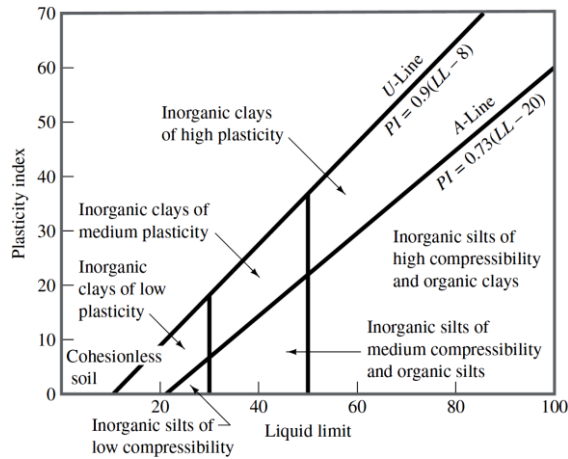


Figure 5-13 Plasticity chart (ASTM:D2487-11 2011; Das 2008)

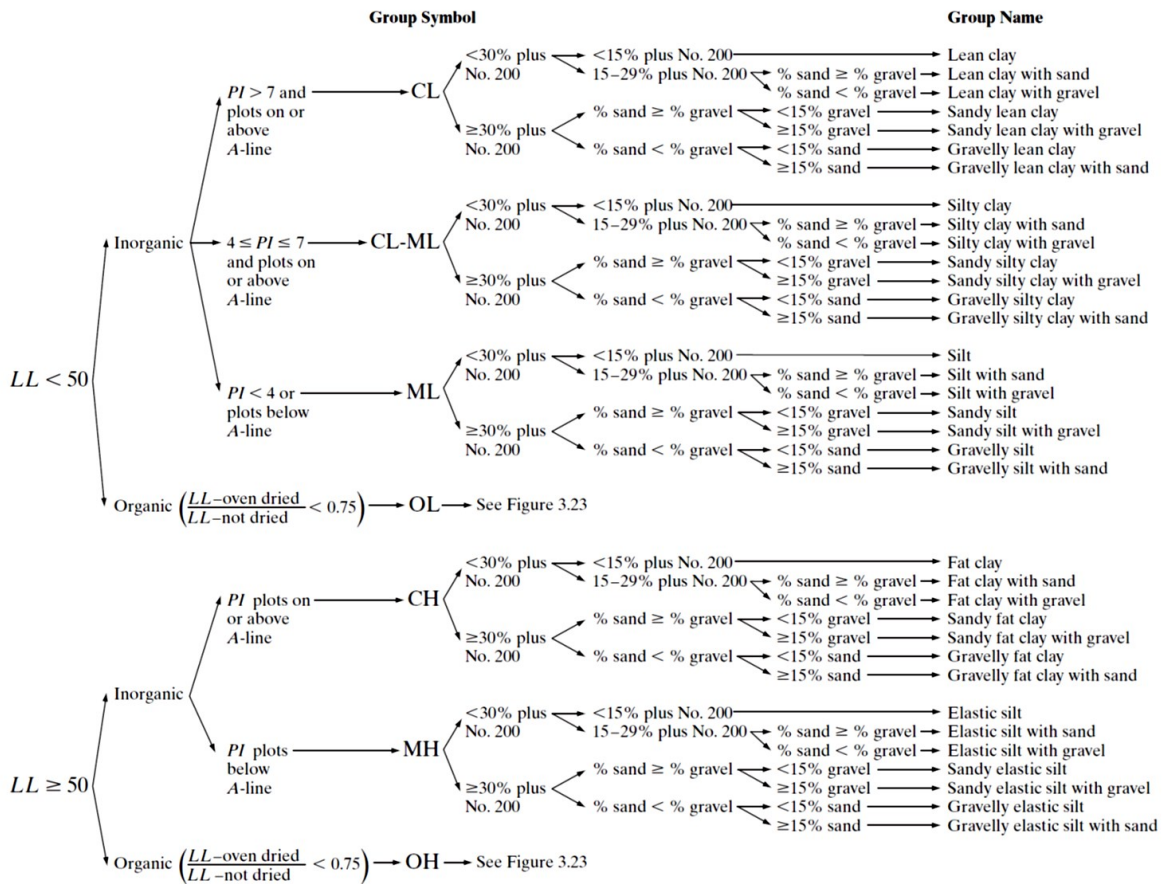


Figure 5-14 Flowchart group names for inorganic silty and clayey soils (Das 2008; ASTM:D2487-11 2011)



Figure 5-15 Specific gravity test

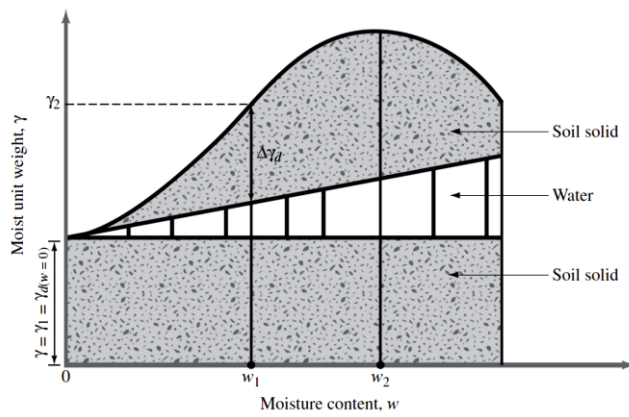


Figure 5-16 Principles of compaction (Das 2008)

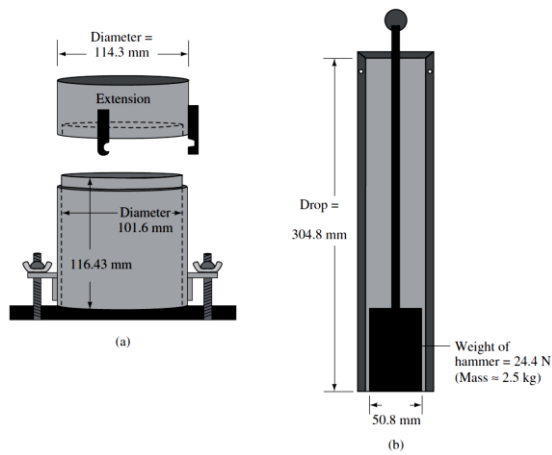


Figure 5-17 Standard Proctor test equipment: (a) mold; (b) hammer (Das 2008)



Figure 5-18 Compacted soil samples

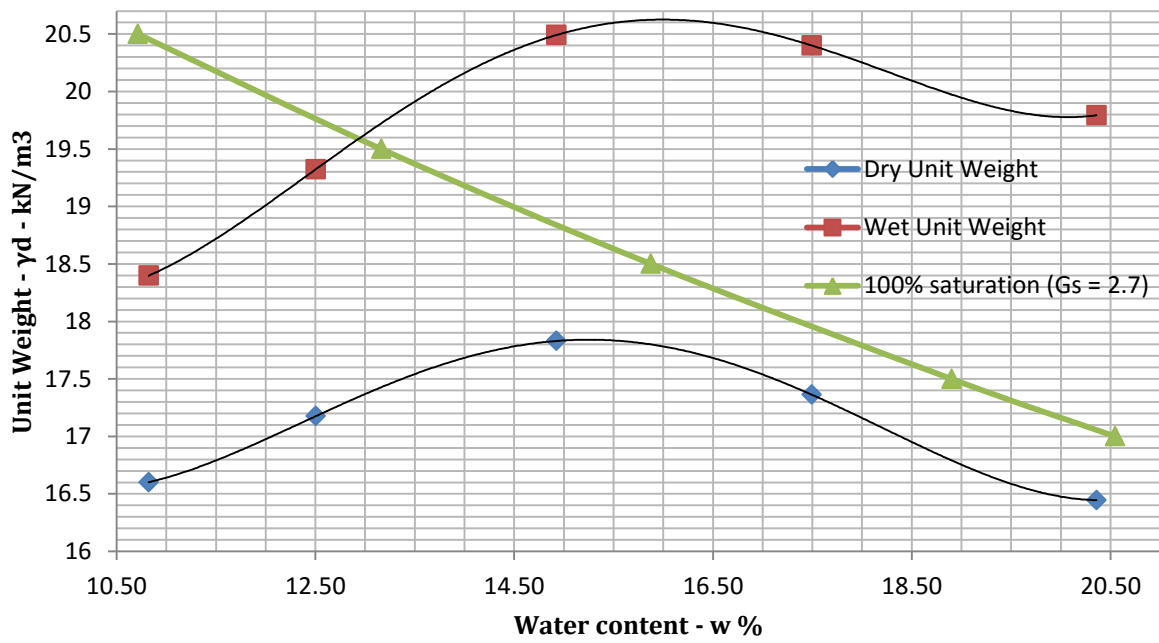


Figure 5-19 Standard Proctor compaction test results for the soil samples



Figure 5-20 Pushing Shelby tubes through remolded soil samples



Figure 5-21 Shelby tubes inside the remolded soil samples



Figure 5-22 Extracting soil samples from Shelby tubes



Figure 5-23 Soil sample for UCS test

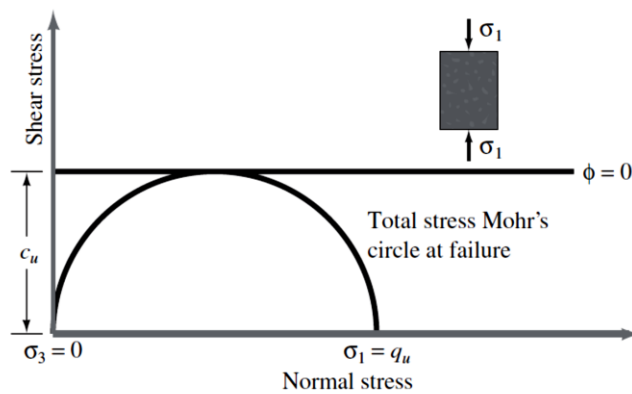


Figure 5-24 Unconfined Compression Strength test (Das 2008)

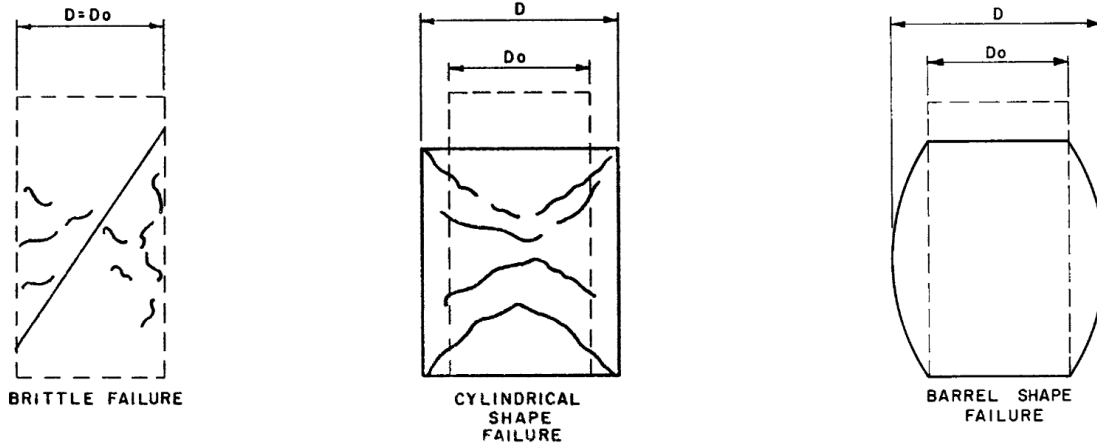


Figure 5-25 Cross-sectional area correction determination (Das 2008)

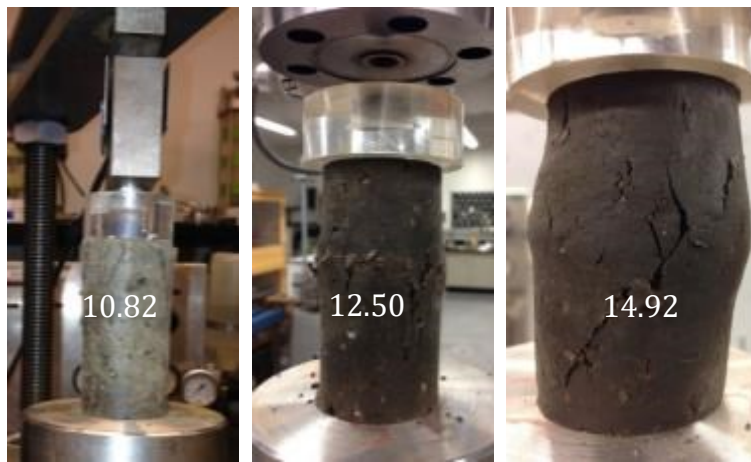


Figure 5-26 Failure of specimens under UCS tests for 10.82%, 12.5%, and 14.92%



Figure 5-27 Failure of specimens under UCS test for 17.49%, 20.36%

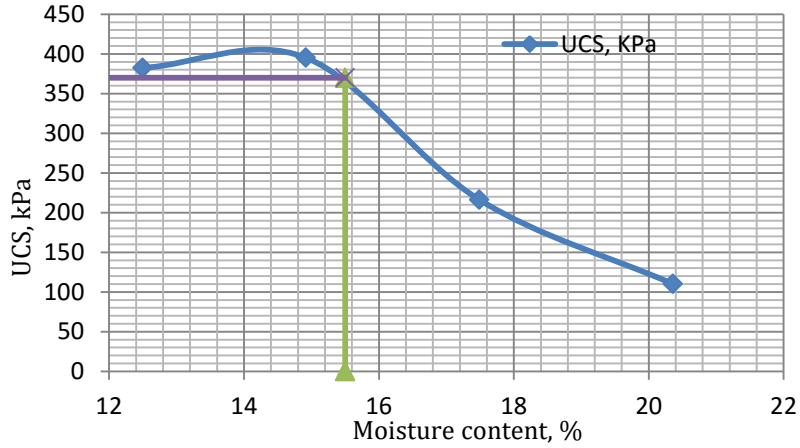


Figure 5-28 UCS of soil specimens versus moisture content

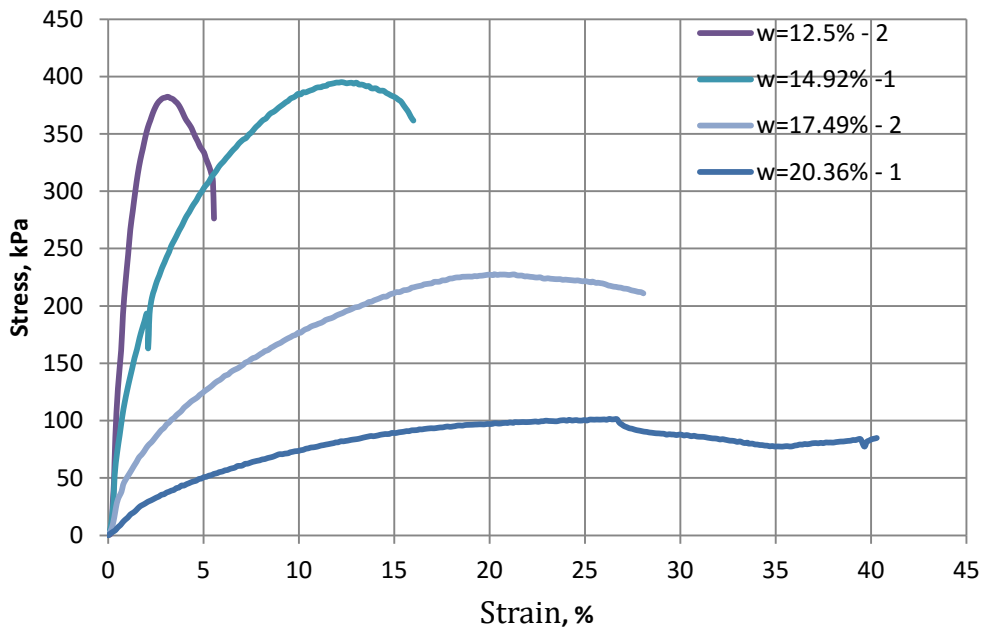


Figure 5-29 Average stress-strain curves for different moisture contents

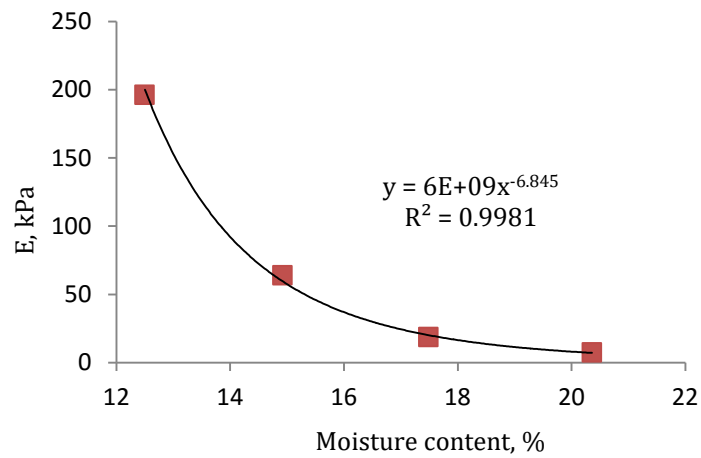


Figure 5-30 Modulus of elasticity of soil specimens with different moisture contents

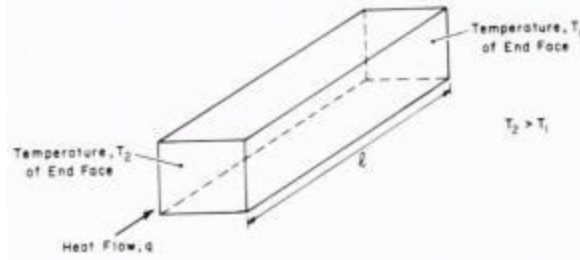


Figure 5-31 Heat flow through an element of soil (Farouki 1986)

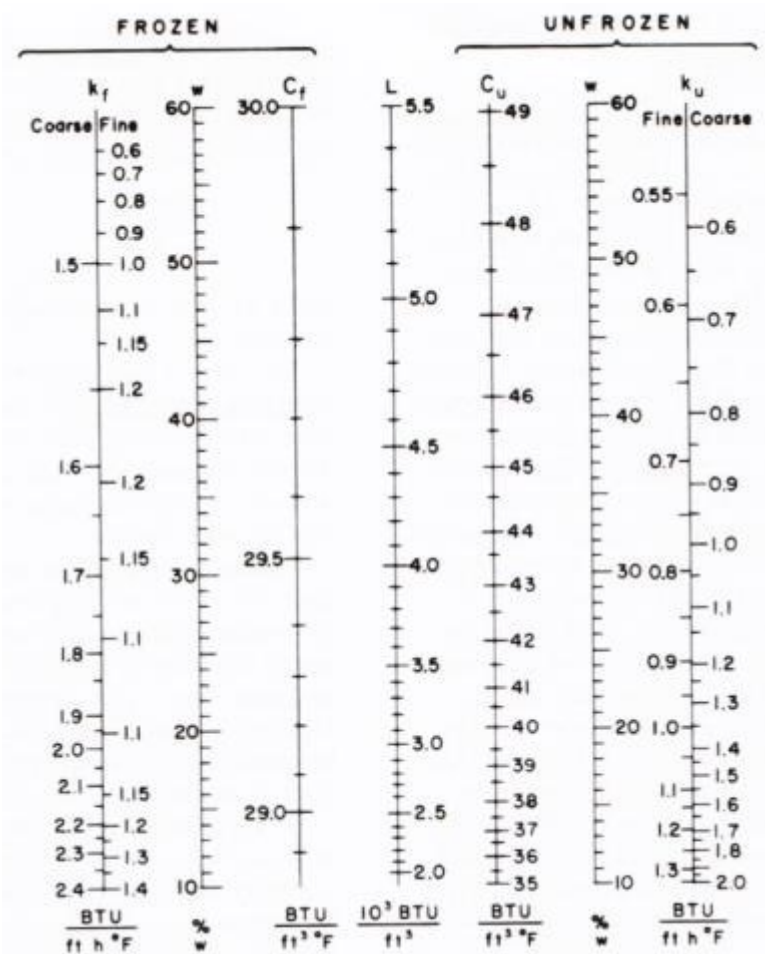


Figure 5-32 Thermal properties and water content for standard soils¹ (Sanger 1968)

¹ $L(Btu/ft^3) = 1.44 \times \gamma_d(lb/ft^3) \times w(\%)$; $C_F = \gamma_d(0.17 + 0.005w)$; $C_U = \gamma_d(0.17 + 0.01w)$. The value C_F is always about 30 in saturated soils and C_U varies between 35 and 50 but is usually 45. The heat capacity of soil can be calculated by multiplying C_U with mass specific heat of water (c_w).

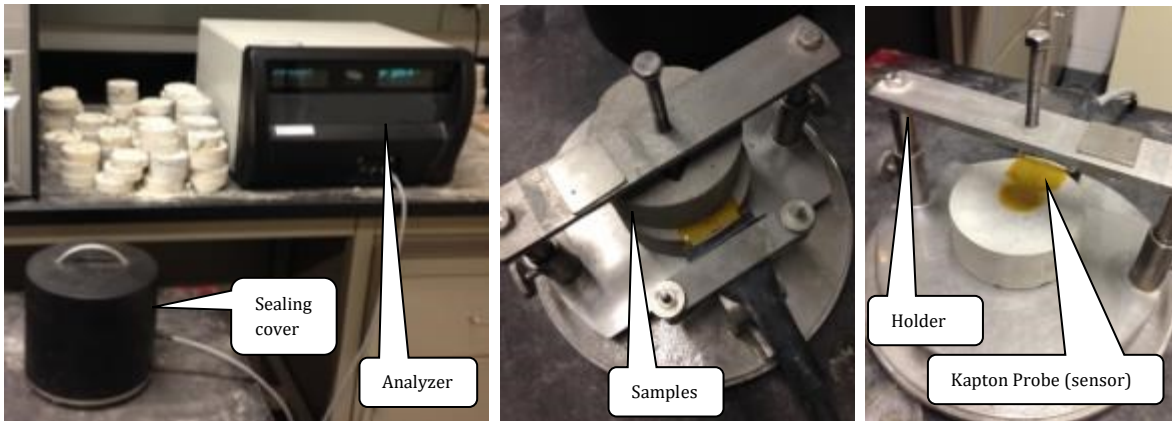


Figure 5-33 TPS 1500 setup in the laboratory



Figure 5-34 Sample preparation (SMPE 2012a; SMPE 2012b)

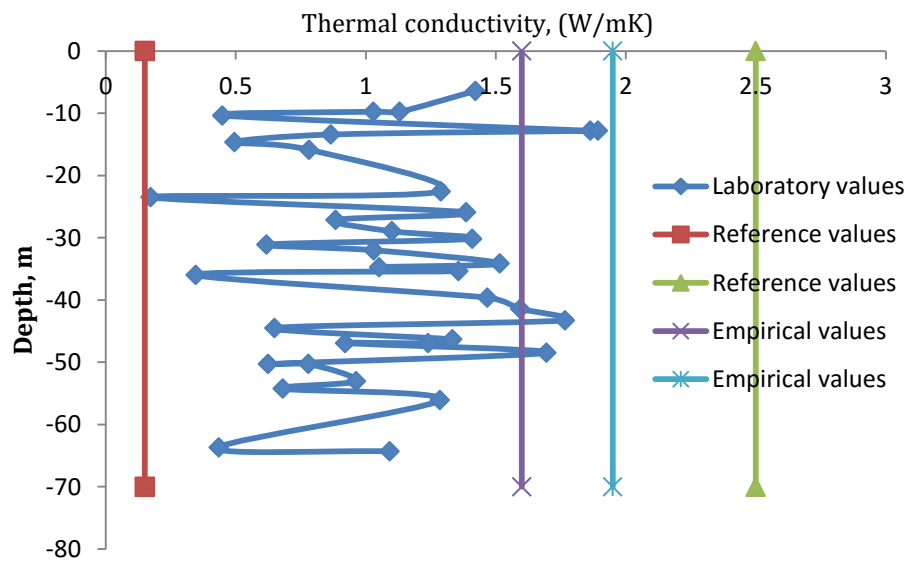


Figure 5-35 Variation of thermal conductivity with depth

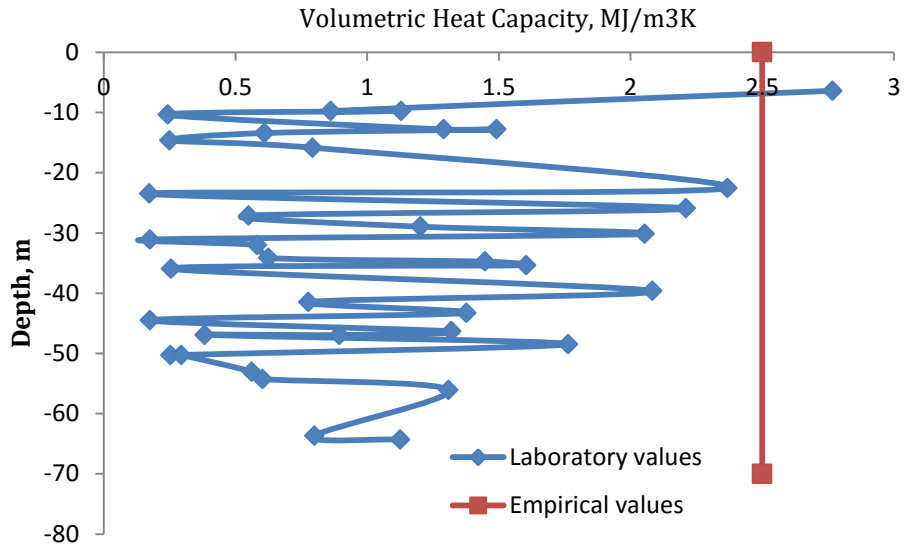


Figure 5-36 Variation of specific heat capacity with depth

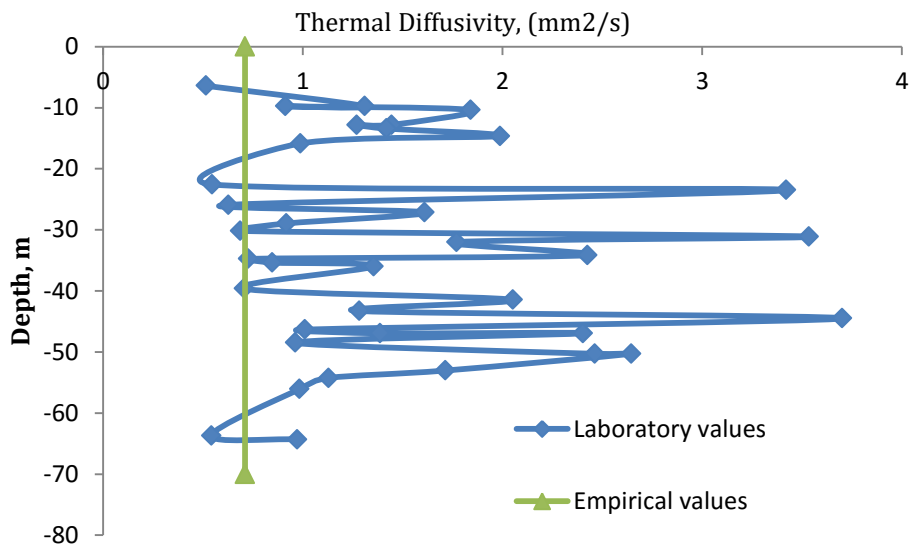


Figure 5-37 Variation of heat diffusivity with depth

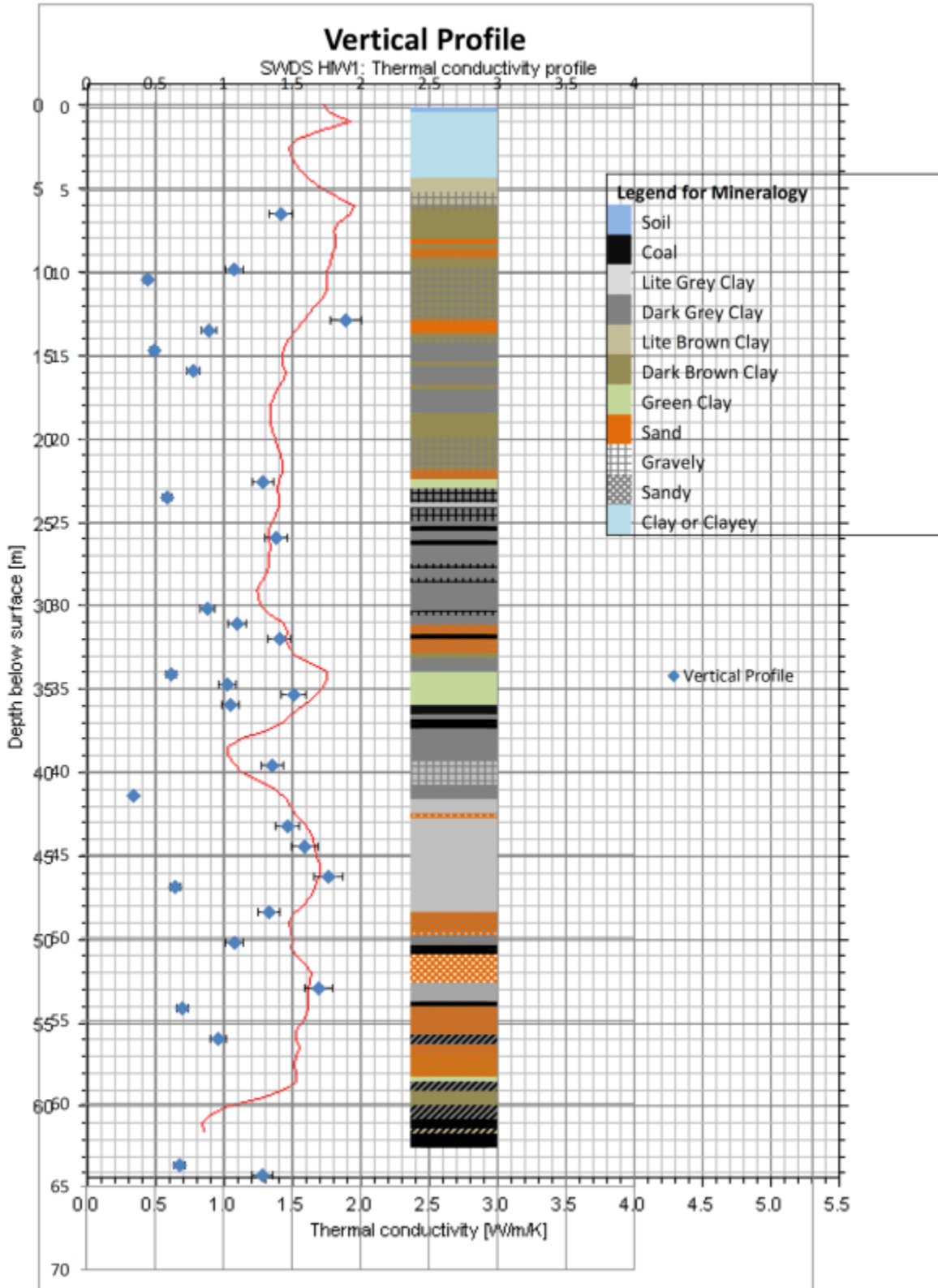


Figure 5-38 Vertical profile of heat conductivity based on laboratory and field thermal tests (SMPE, 2012a, 2012b)

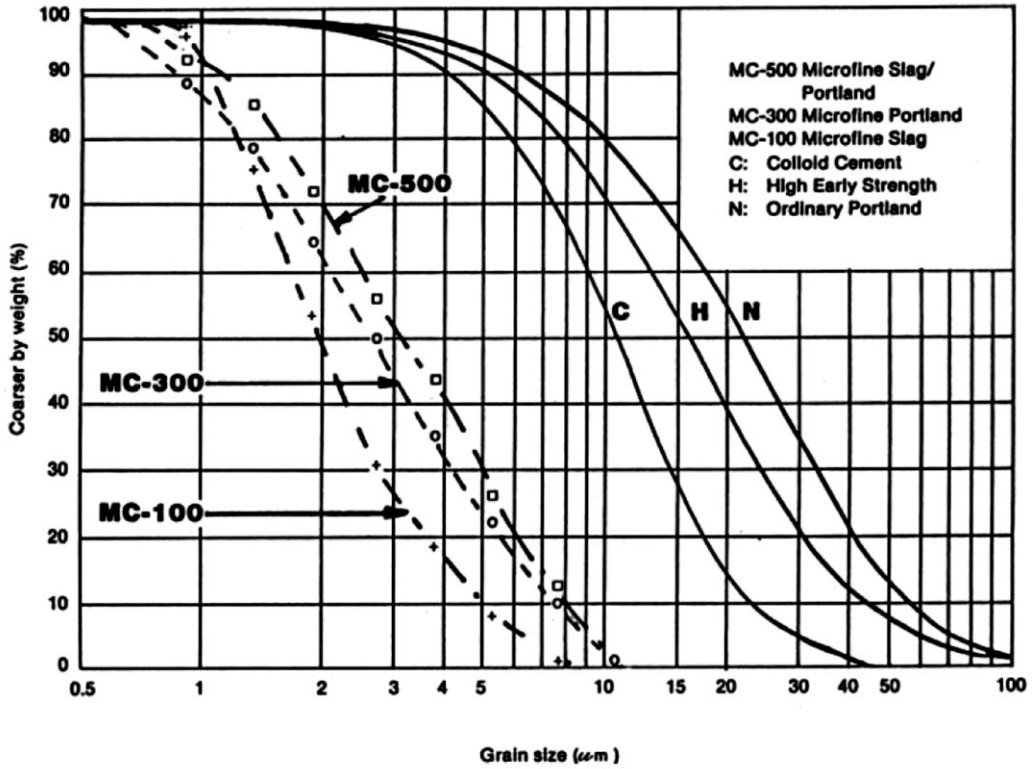


Figure 5-39 Grain size distribution of various cement (Karol 2003)

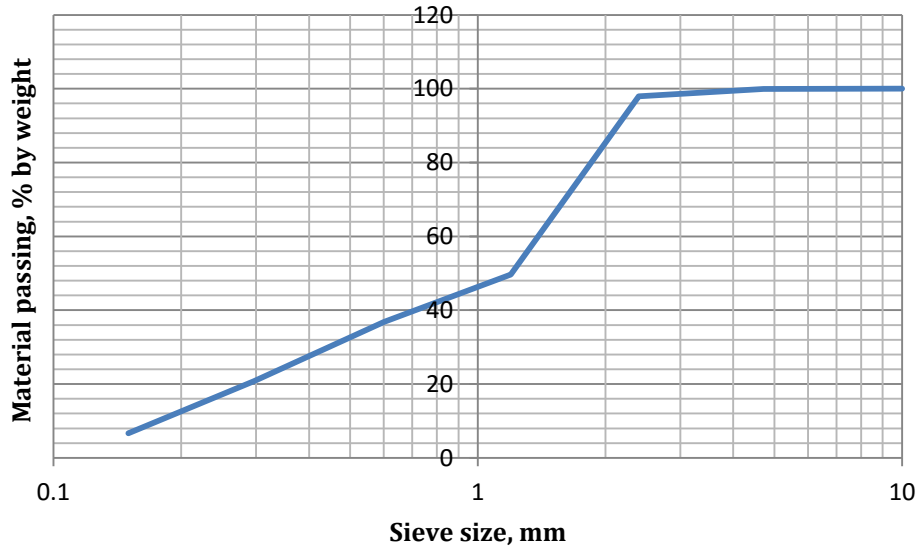


Figure 5-40 Grain size distribution of ELP



Figure 5-41 Grinding the top and bottom of the specimens

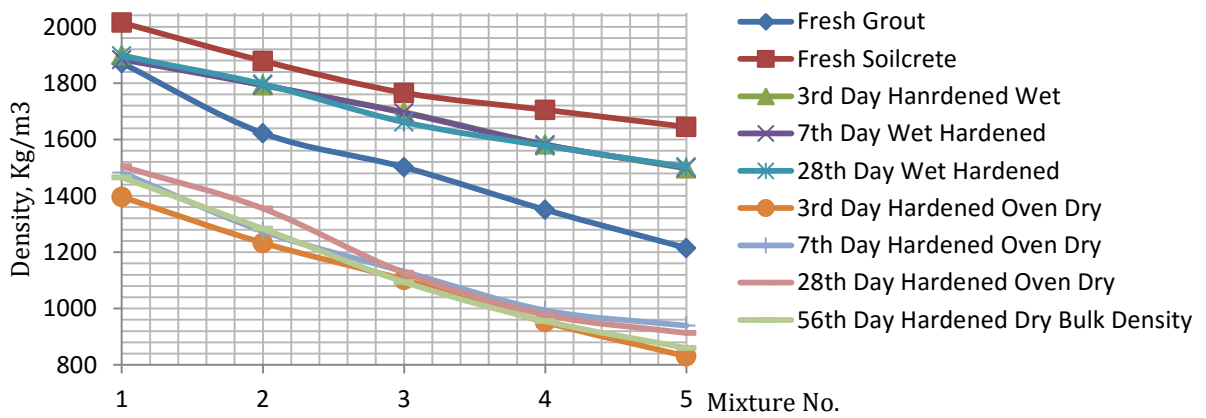


Figure 5-42 Density of fresh grout and soilcrete specimens with different mixtures of ELP

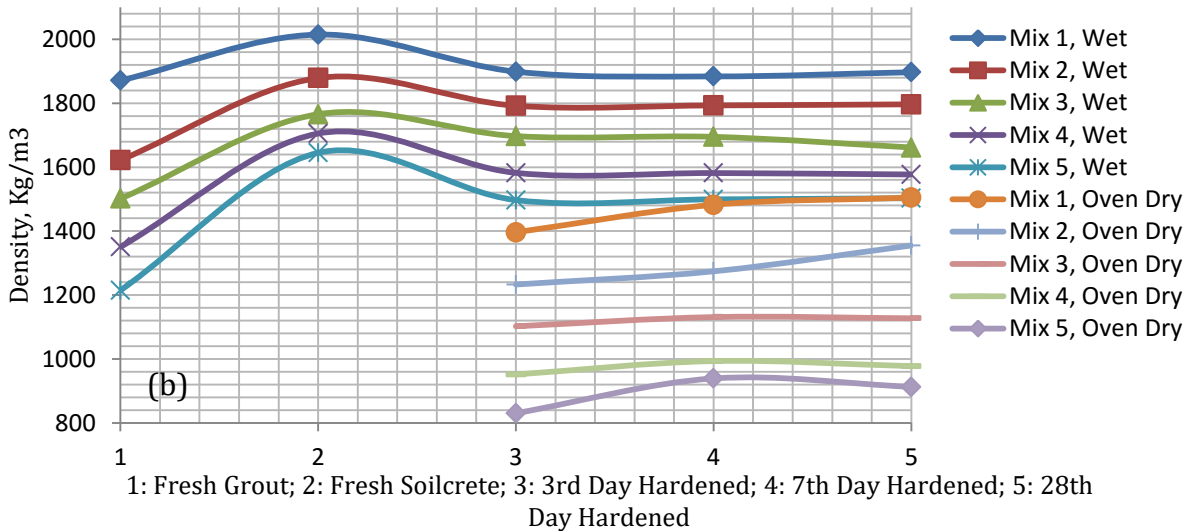


Figure 5-43 Density of fresh grout and soilcrete mixes during curing time

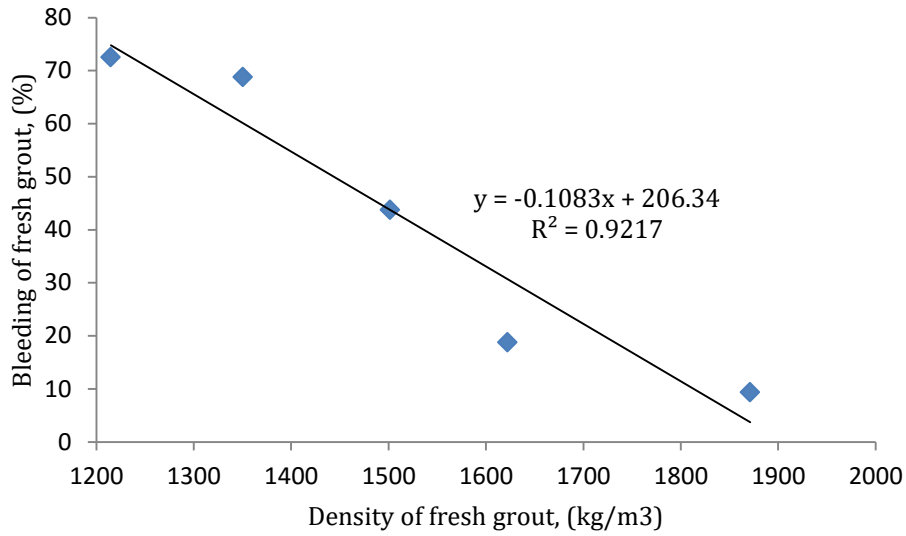


Figure 5-44 Relationship between density of fresh grout and its bleeding in all mixes

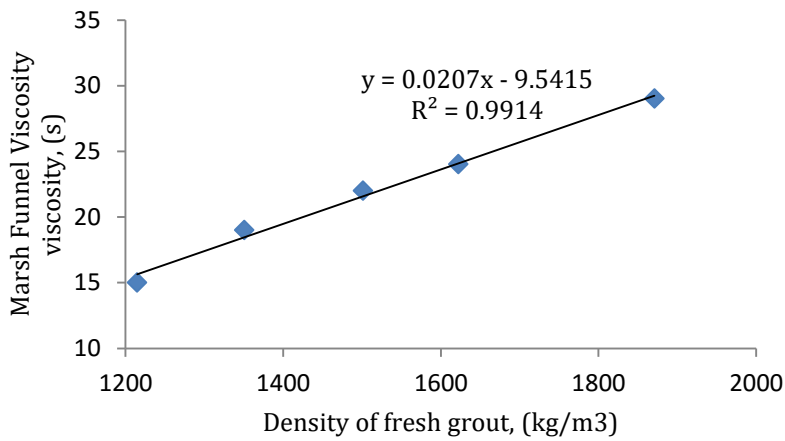


Figure 5-45 Relationship between fresh grout density and Marsh Funnel Viscosity

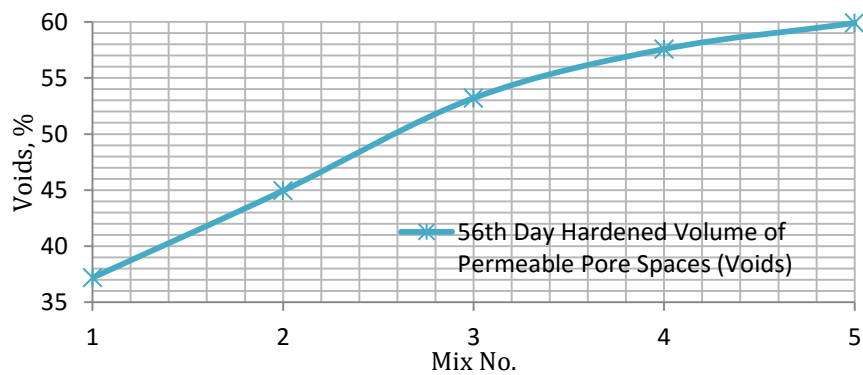


Figure 5-46 56-day volume of permeable pore spaces in different soilcrete mixes

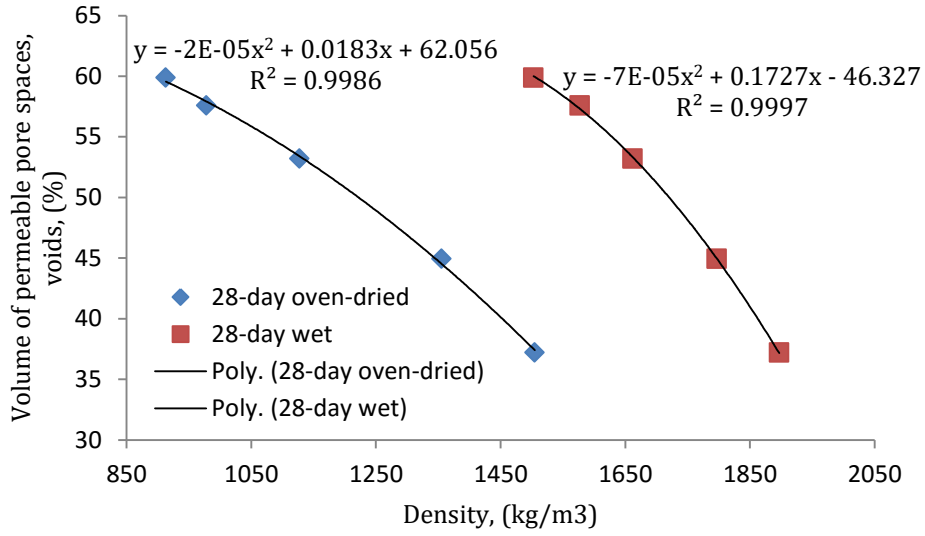


Figure 5-47 Relationship between volume of permeable pore spaces versus 28-day density in soilcrete mixes

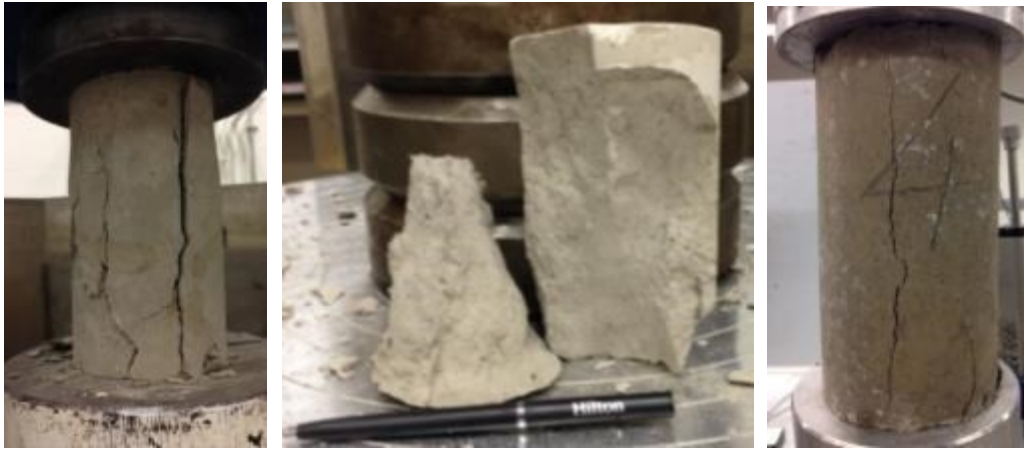


Figure 5-48 UCS test on soilcrete samples

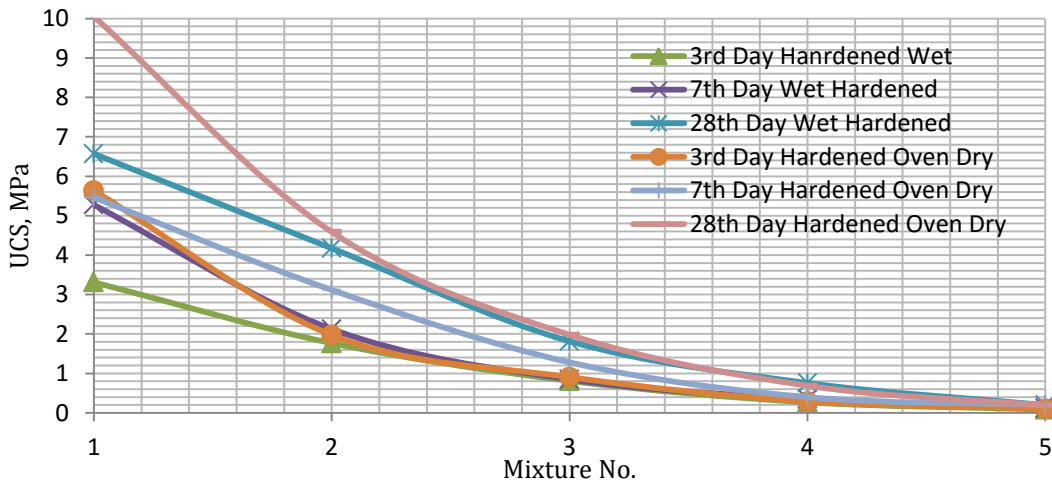
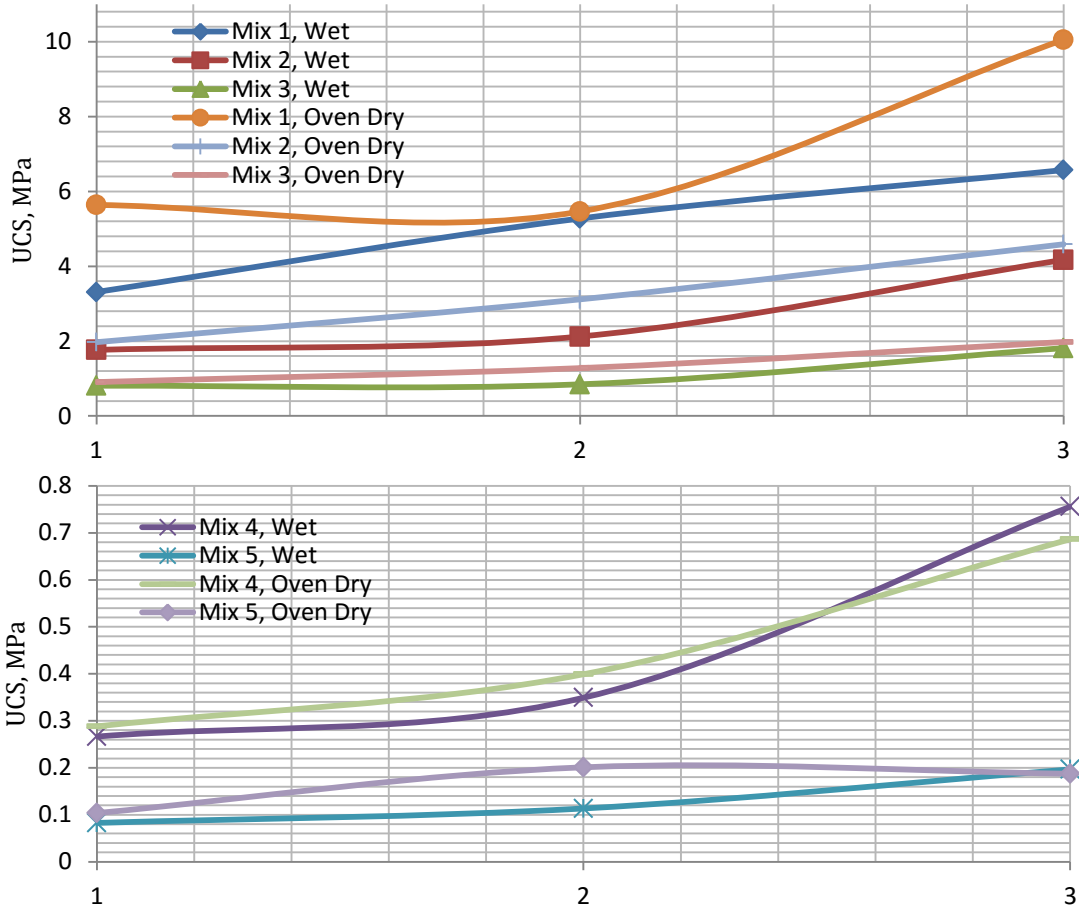


Figure 5-49 UCS of soilcrete specimens with different mixtures of ELP material



1: 3rd Day Hardened; 2: 7th Day Hardened; 3: 28th Day Hardened
 Figure 5-50 UCS of soilcrete specimens during curing times

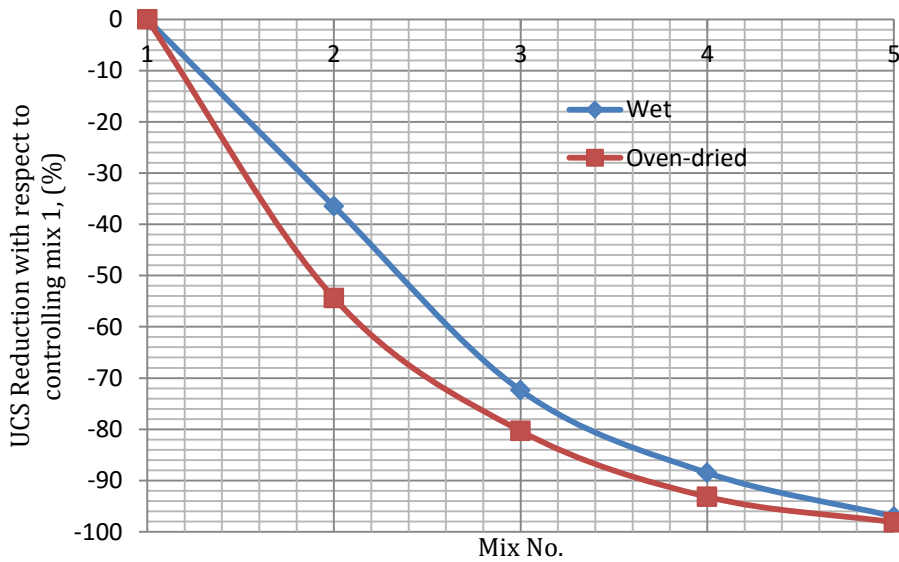


Figure 5-51 UCS reduction with respect to controlling mix 1

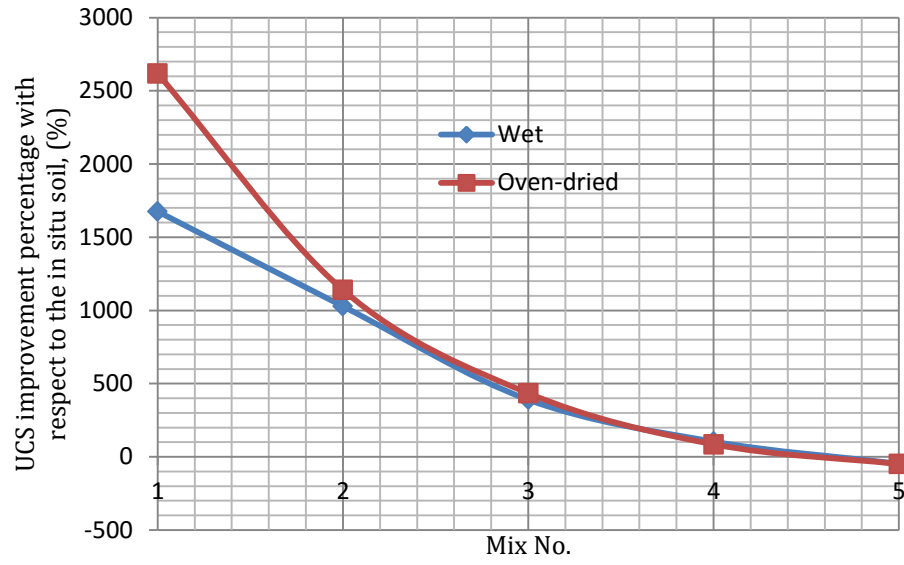


Figure 5-52 UCS improvement percentage with respect to in-situ soil strength (370 kPa)

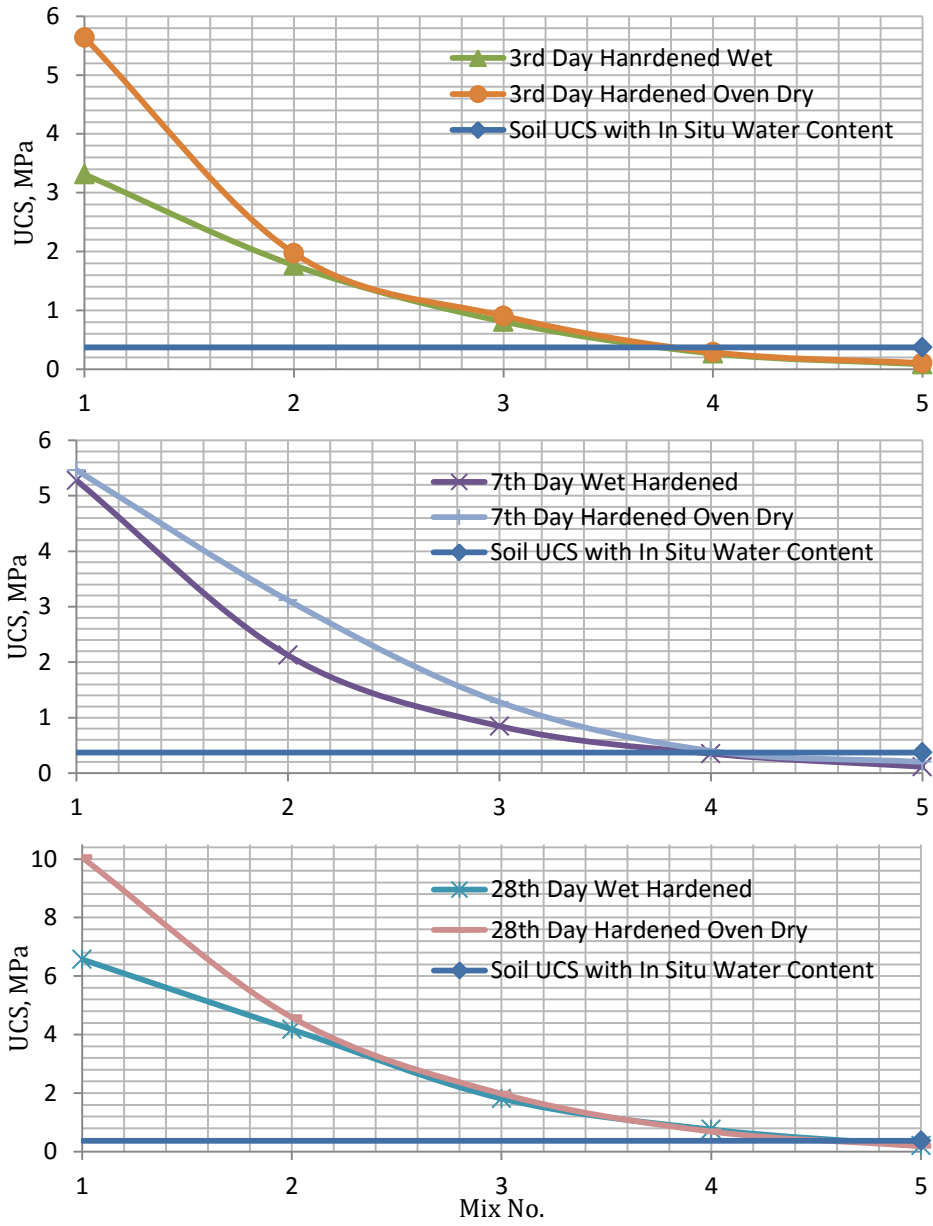


Figure 5-53 Progression of soilcrete mixes during curing time and in-situ soil strength

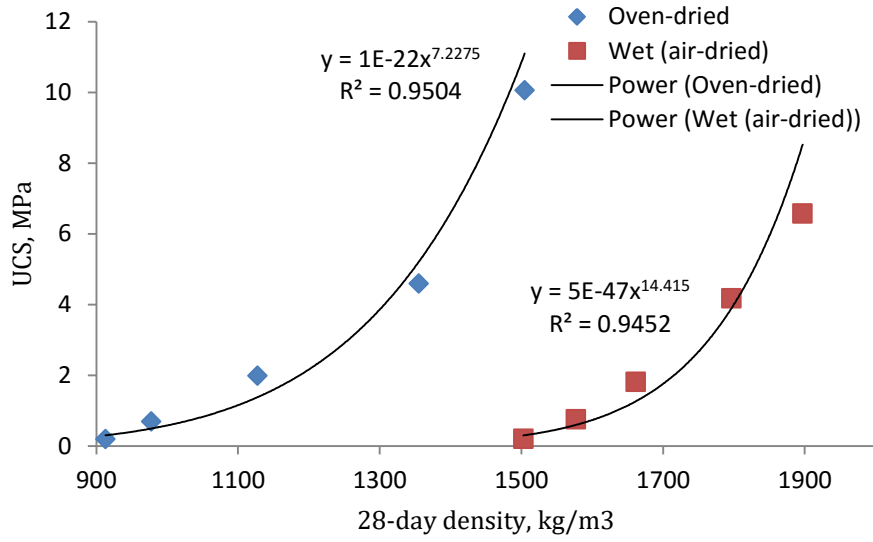


Figure 5-54 28-day UCS of soilcrete mixes versus 28-day density

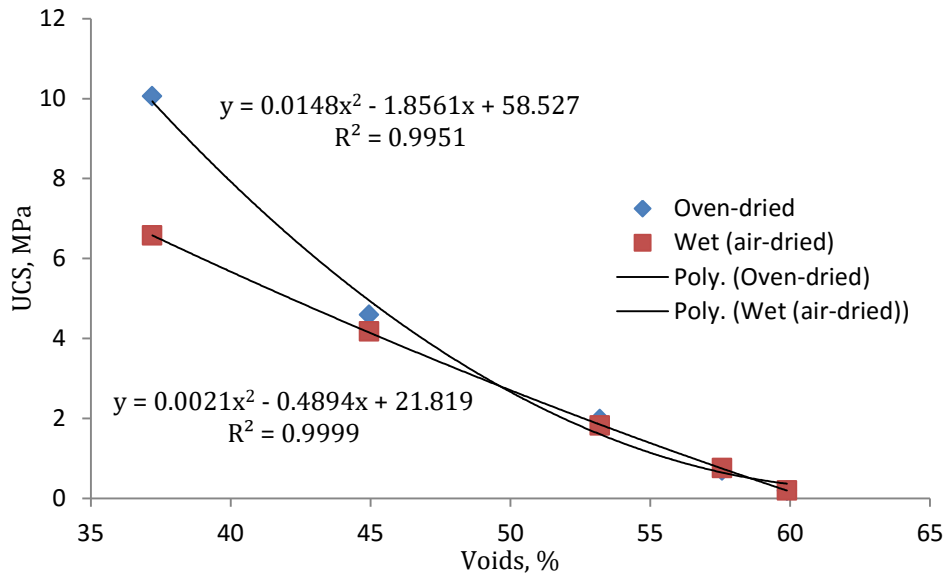


Figure 5-55 28-day UCS of soilcrete mixes versus voids

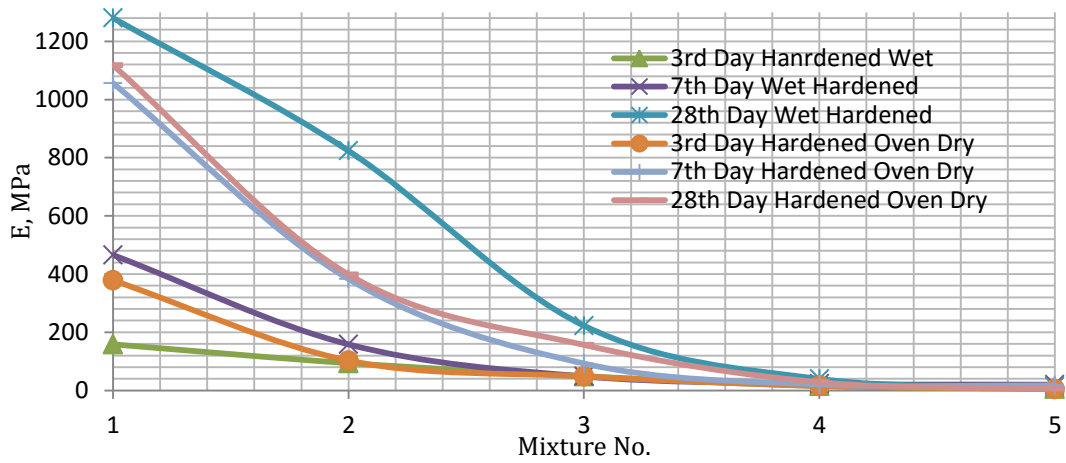


Figure 5-56 Modulus of elasticity of soilcrete specimens with different mixtures of ELP material

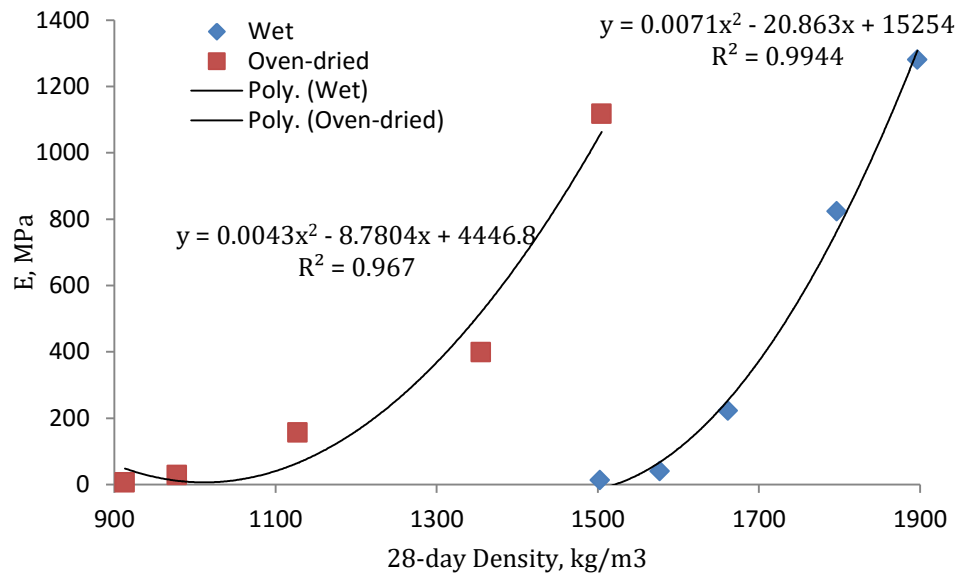


Figure 5-57 Relationship between 28-day density and 28-day modulus of elasticity of soilcrete mixes

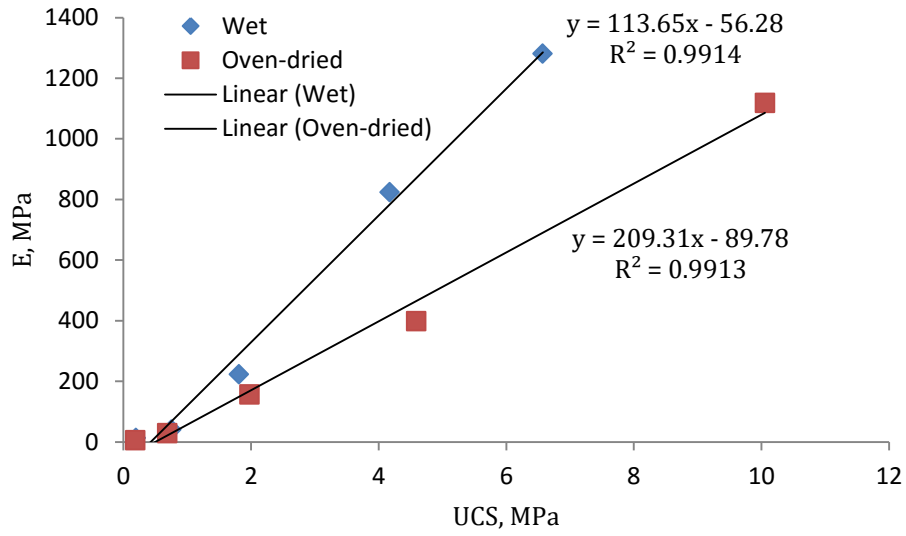


Figure 5-58 Relationship between 28-day UCS and E of soilcrete mixes

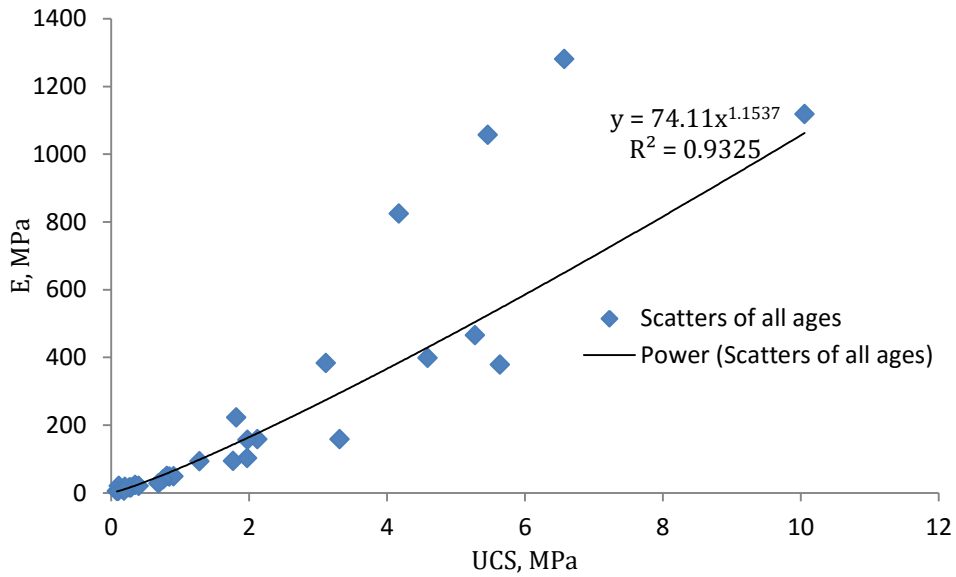


Figure 5-59 Relationship between E and UCS of soilcrete mixes in all ages

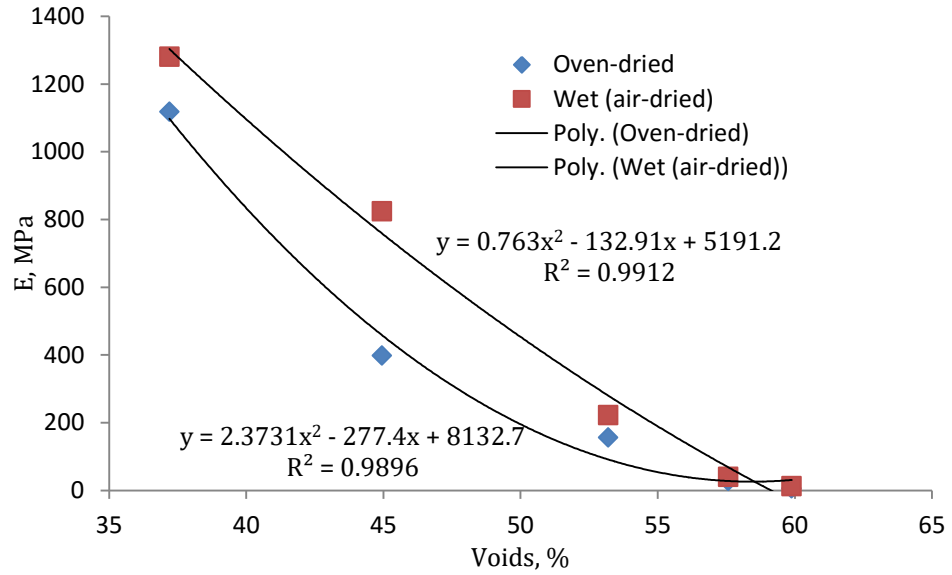


Figure 5-60 Relationship between 28-day E and voids of soilcrete mixes

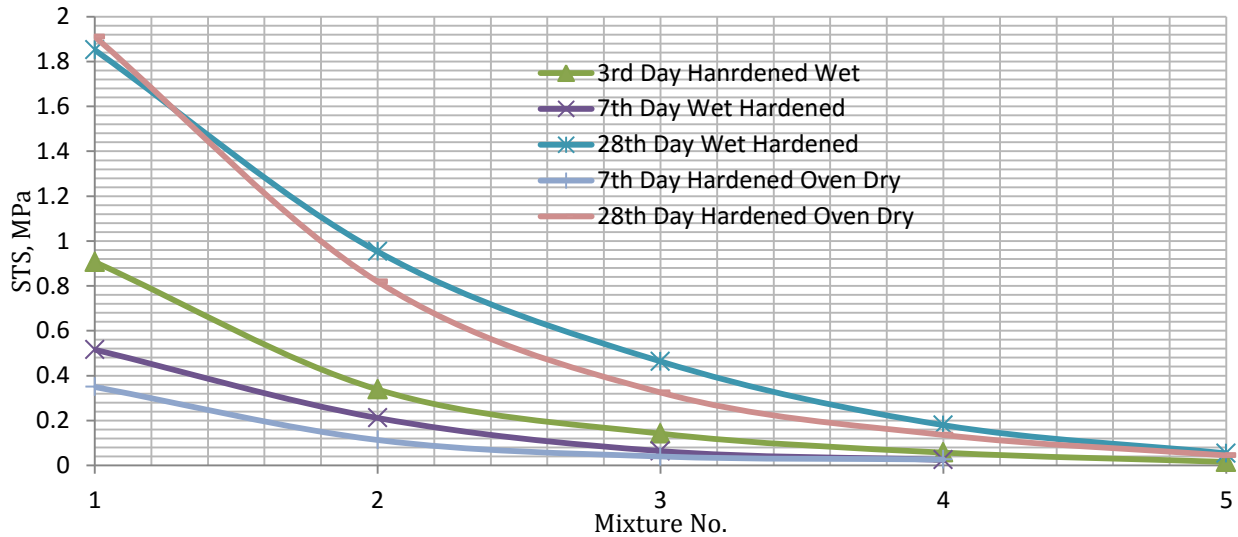


Figure 5-61 Splitting tensile strength of soilcrete specimens with different mixtures of ELP material

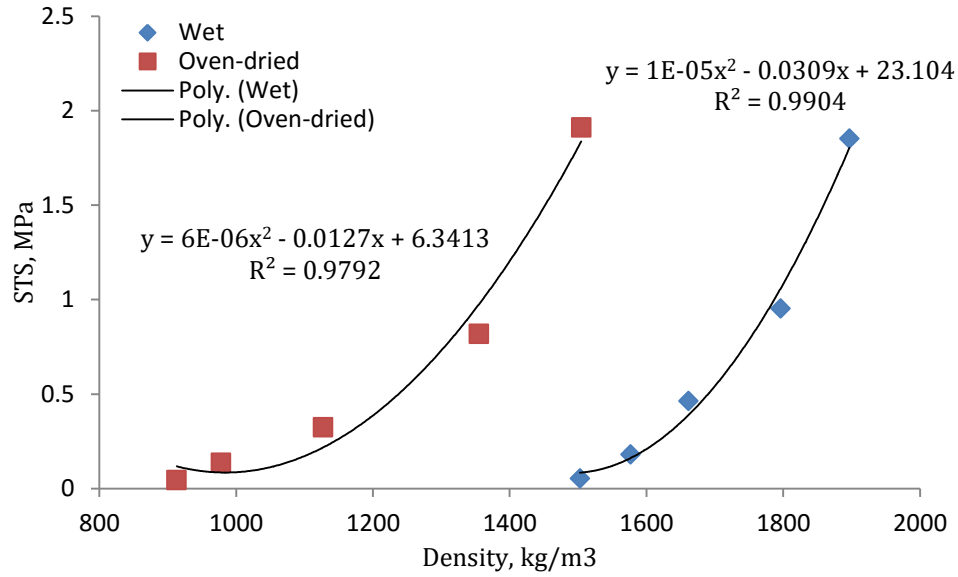


Figure 5-62 Relationship between 28-day STS and 28-day density of soilcrete mixes

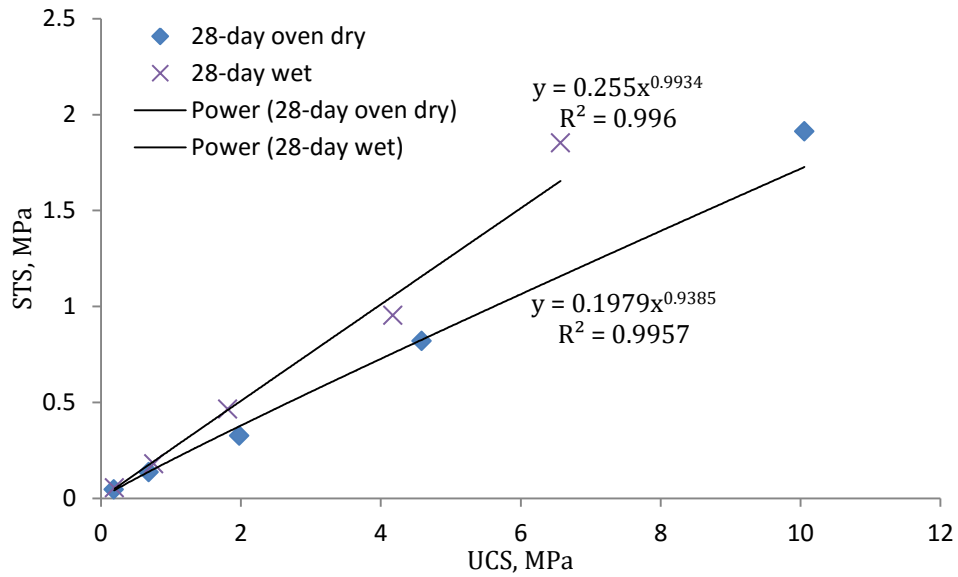


Figure 5-63 Relationship between 28-day STS and 28-day UCS of soilcrete mixes

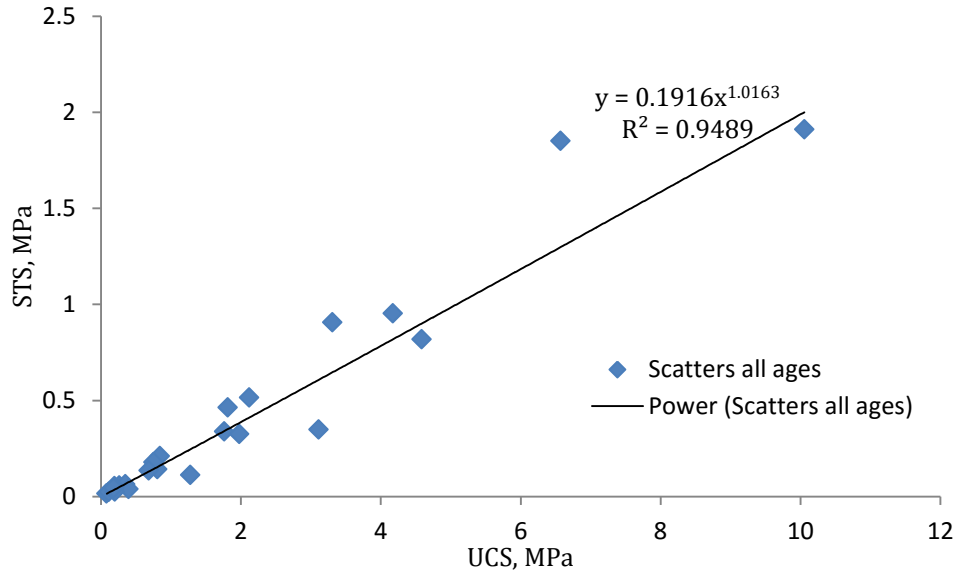


Figure 5-64 Relationship between STS and UCS of soilcrete mixes in all ages

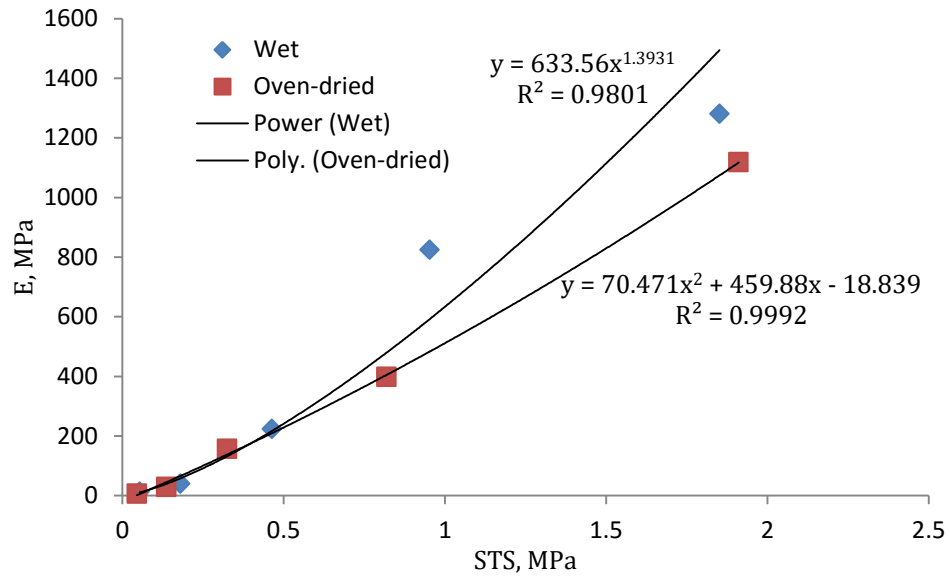


Figure 5-65 Relationship between 28-day STS and 28-day E of soilcrete mixes

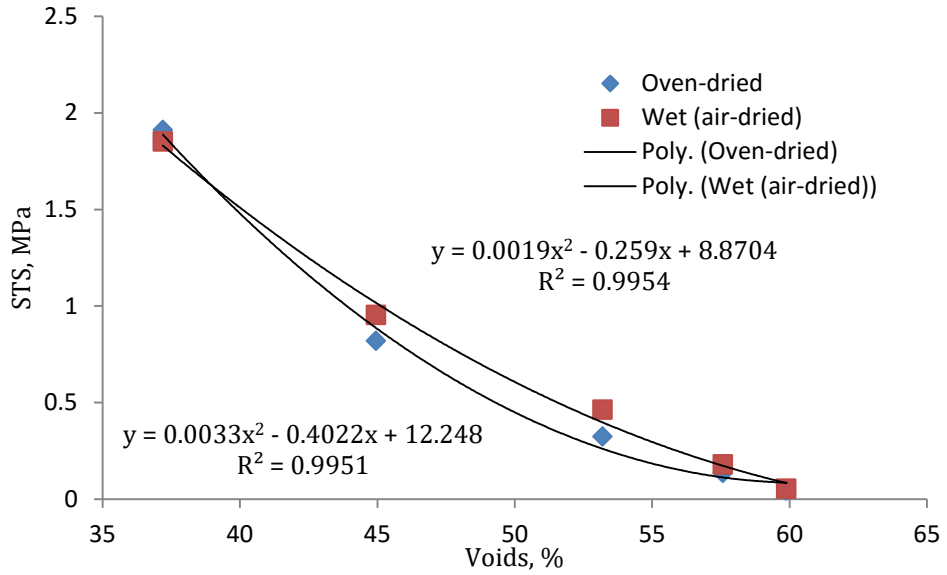


Figure 5-66 Relationship between 28-day STS and voids of soilcrete mixes

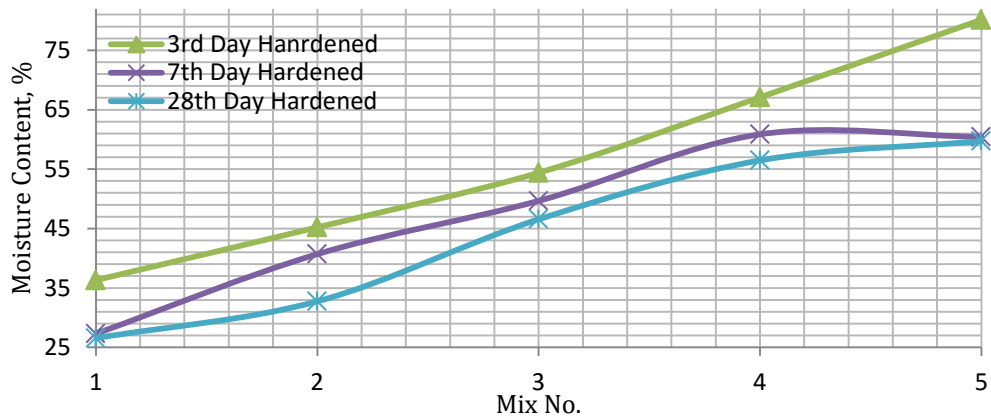


Figure 5-67 Moisture content of soilcrete mixes in different curing times

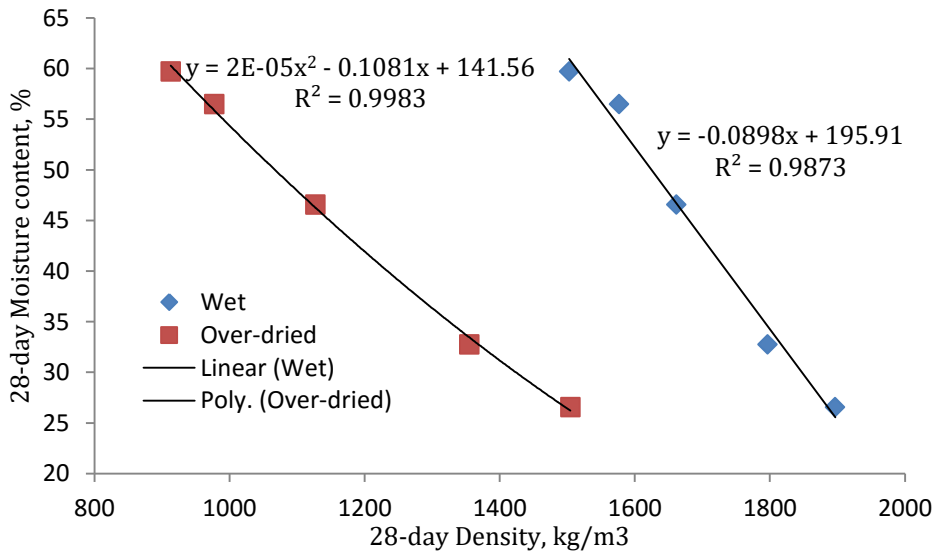


Figure 5-68 Relationship between 28-day moisture content and 28-day density of soilcrete mixes

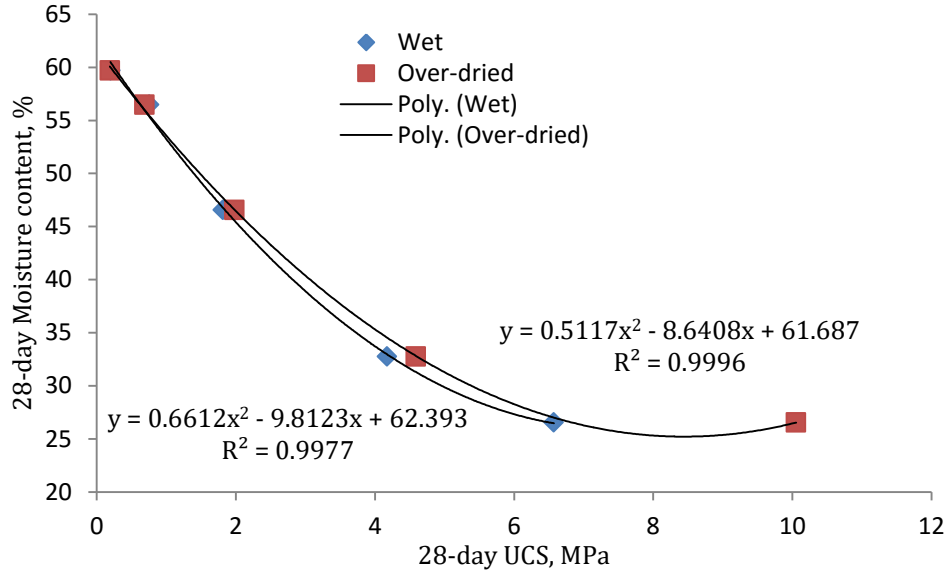


Figure 5-69 Relationship between 28-day moisture content and 28-day UCS of soilcrete mixes

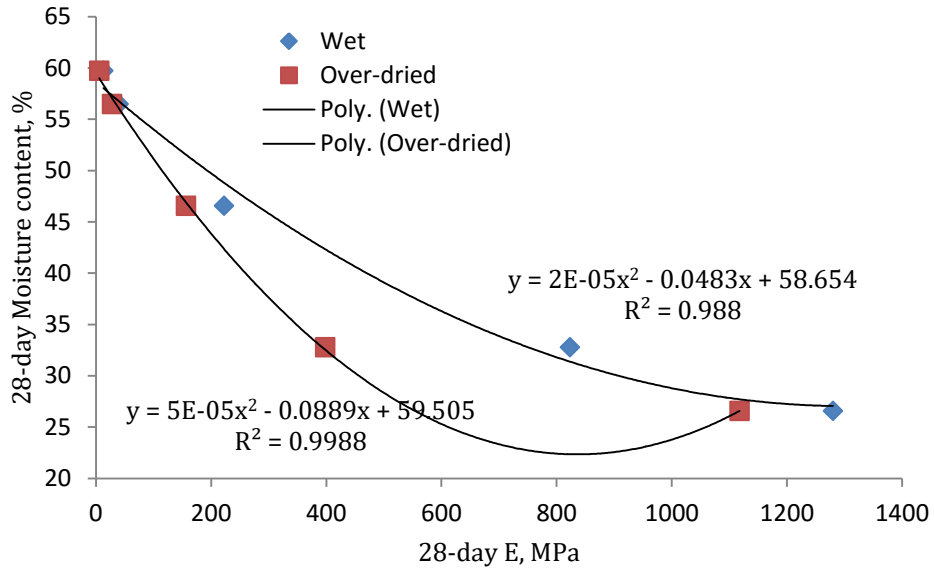


Figure 5-70 Relationship between 28-day moisture content and 28-day E of soilcrete mixes

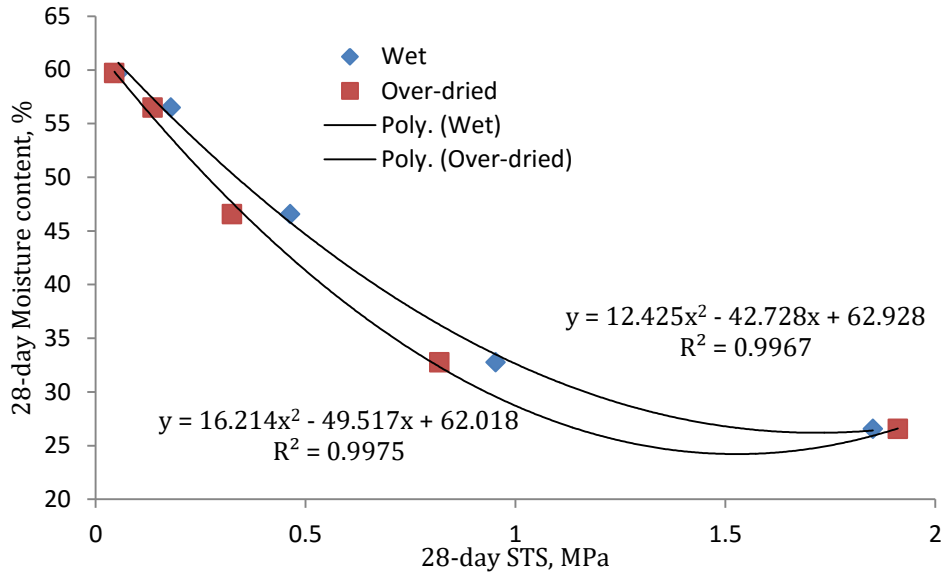


Figure 5-71 Relationship between 28-day moisture content and 28-day STS of soilcrete mixes

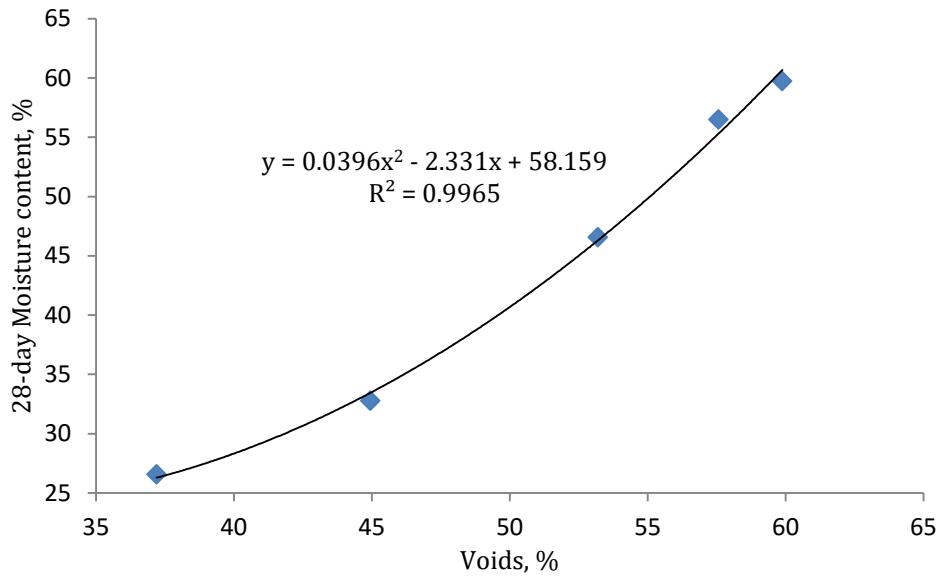


Figure 5-72 Relationship between 28-day moisture content and voids of soilcrete mixes



Figure 5-73 Soilcrete samples for thermal properties test

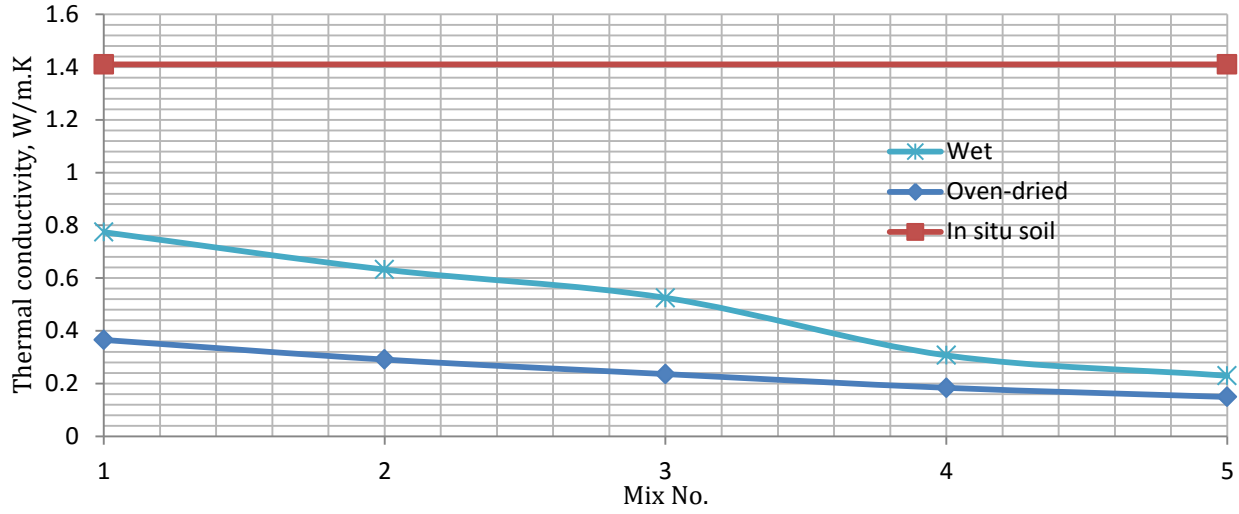


Figure 5-74 Thermal conductivity of soilcrete mixes with increasing ELP material

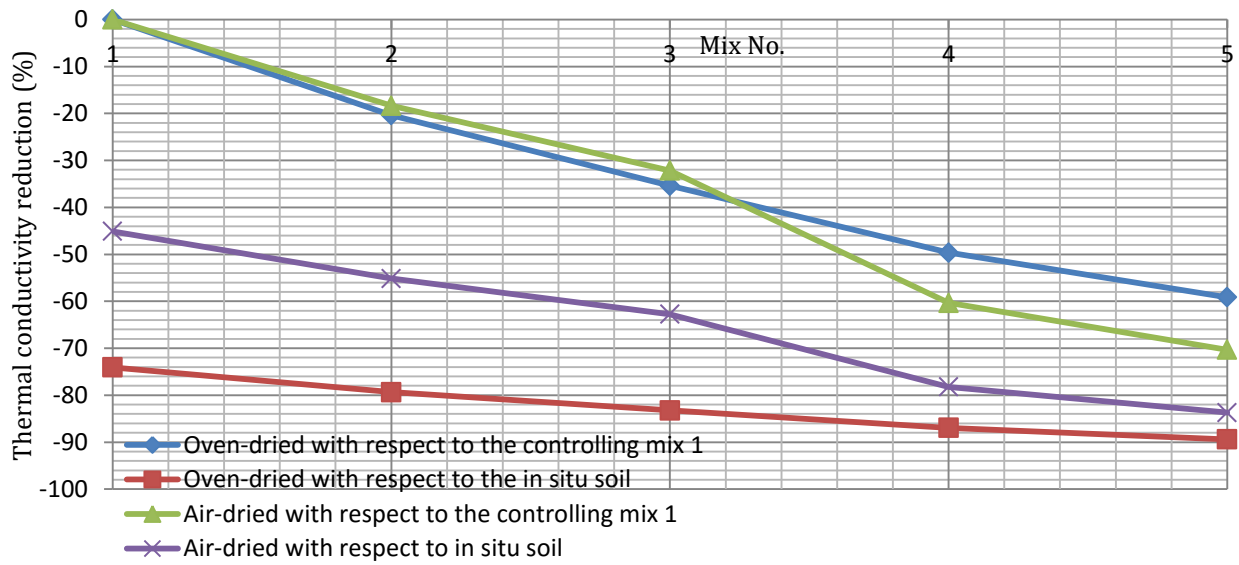


Figure 5-75 Thermal conductivity reduction with respect to controlling mix 1 and in-situ soil thermal properties

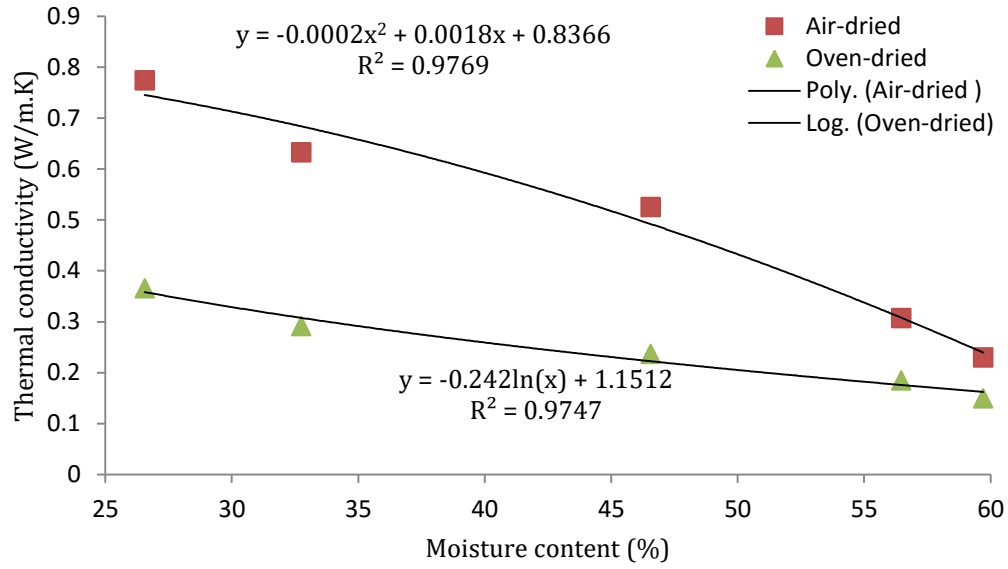


Figure 5-76 Relationship between thermal conductivity and moisture content of soilcrete

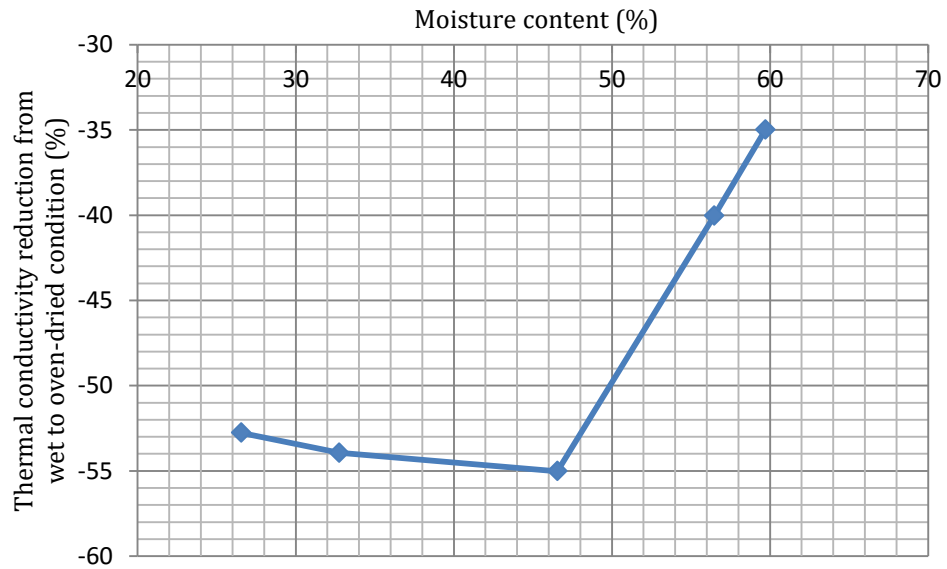


Figure 5-77 Thermal conductivity reduction from wet to oven-dried condition versus moisture content of each mix

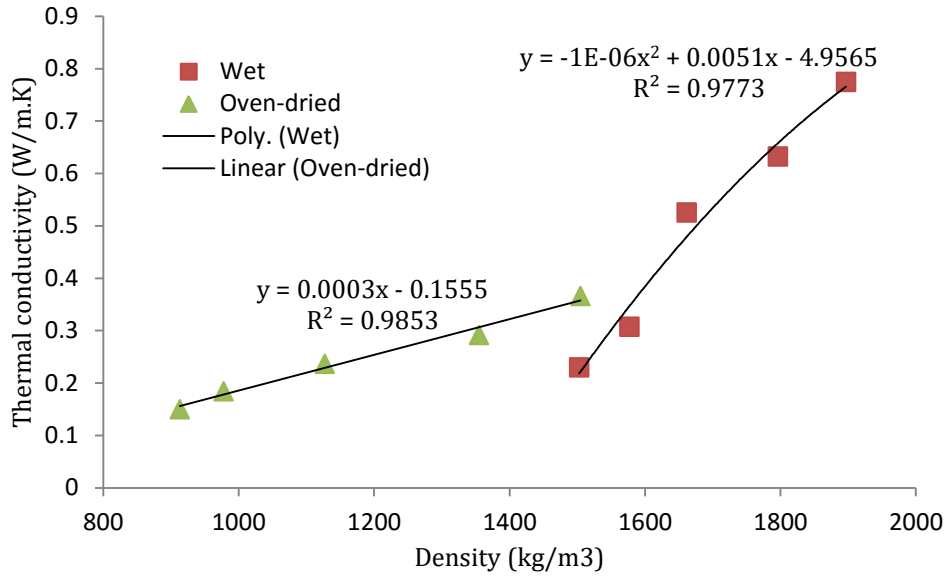


Figure 5-78 Relationship between thermal conductivity and 28-day density of soilcrete

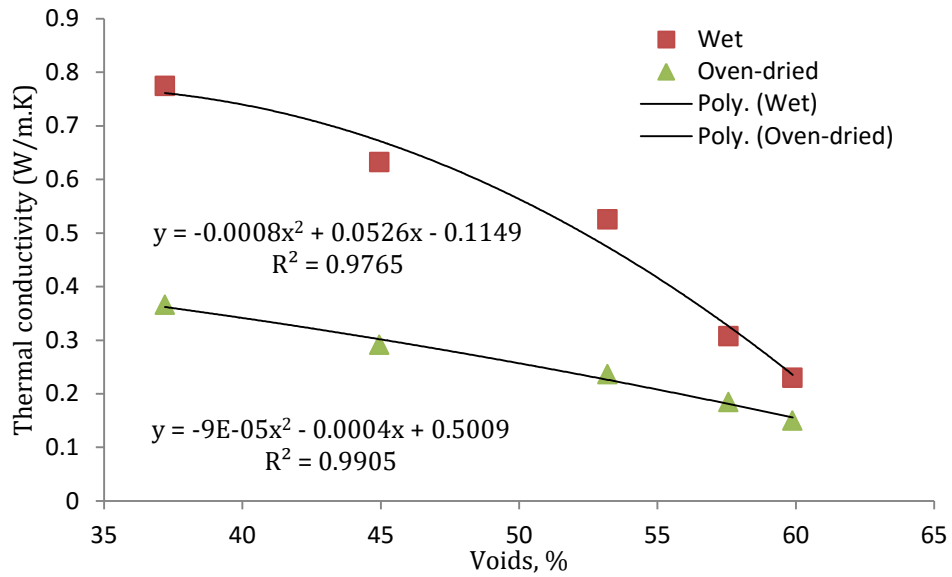


Figure 5-79 Relationship between thermal conductivity and voids of soilcrete

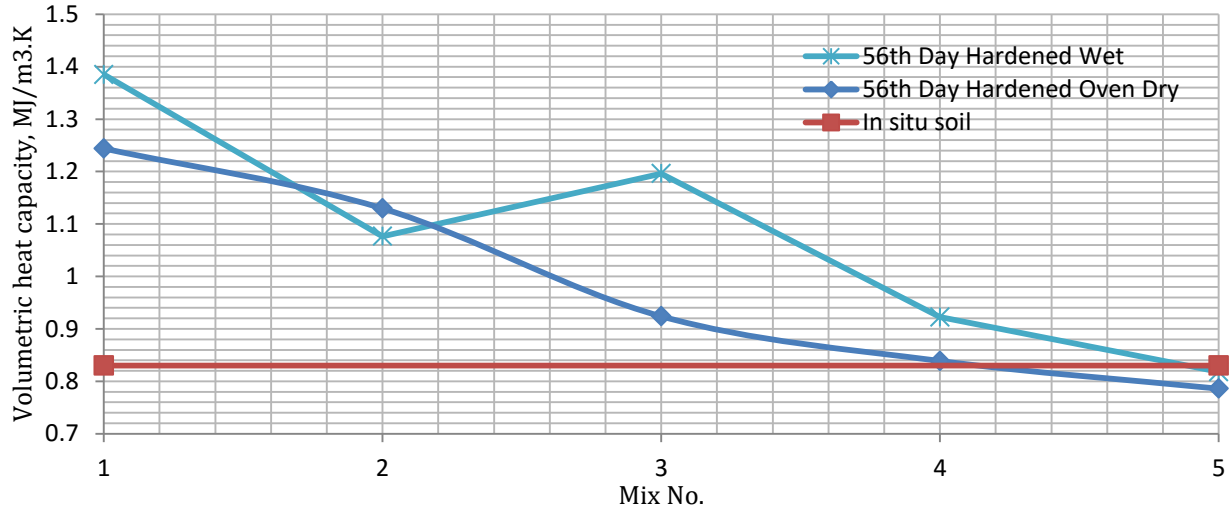


Figure 5-80 Volumetric heat capacity of soilcrete mixes with increasing ELP material

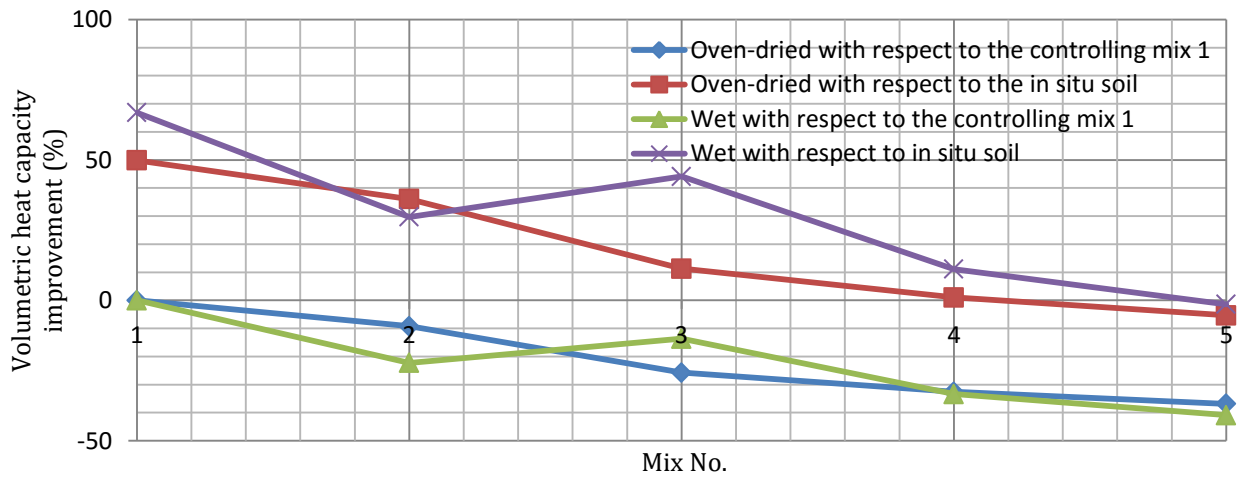


Figure 5-81 Improvement percentage of volumetric heat capacity of soilcrete mixes with respect to in-situ soil and controlling mix 1

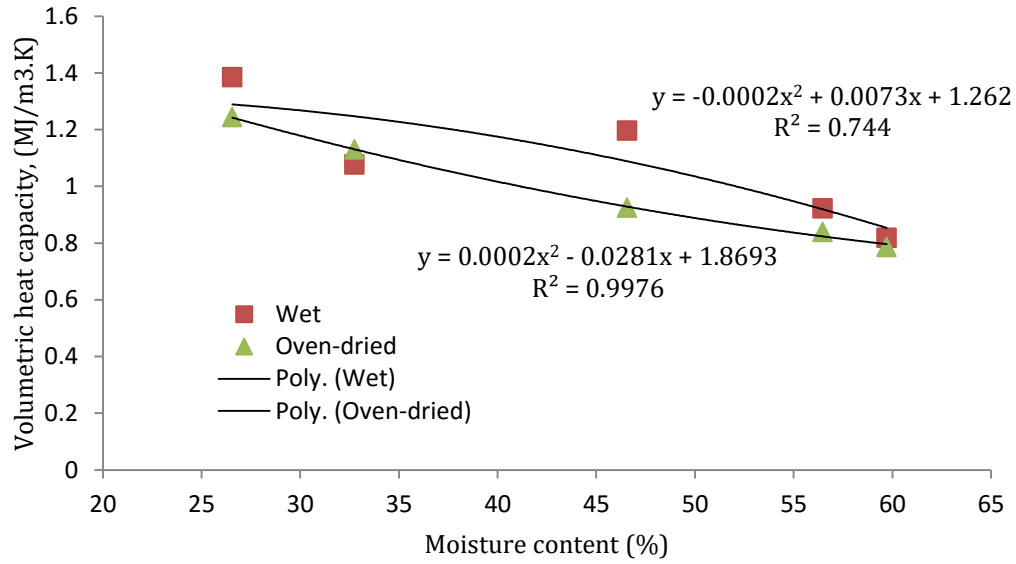


Figure 5-82 Relationship between volumetric heat capacity and moisture content of soilcrete

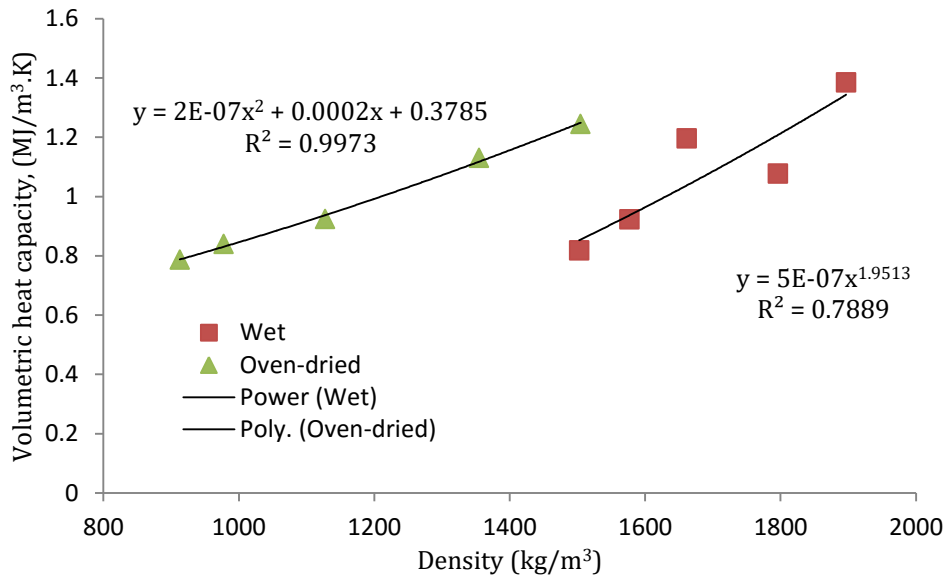


Figure 5-83 Relationship between volumetric heat capacity and 28-day density of soilcrete

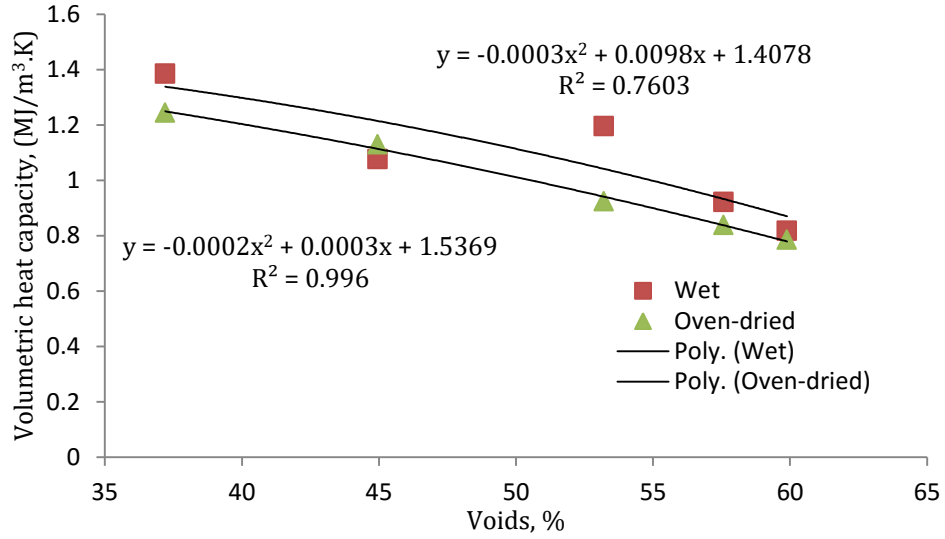


Figure 5-84 Relationship between volumetric heat capacity and voids of soilcrete

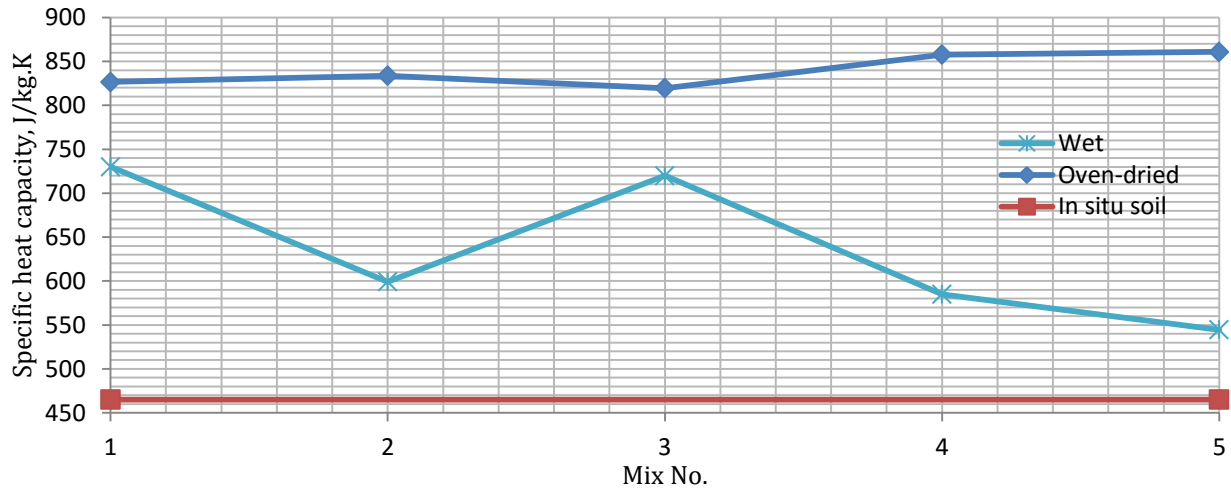


Figure 5-85 Specific heat capacity of soilcrete mixes with increasing ELP material

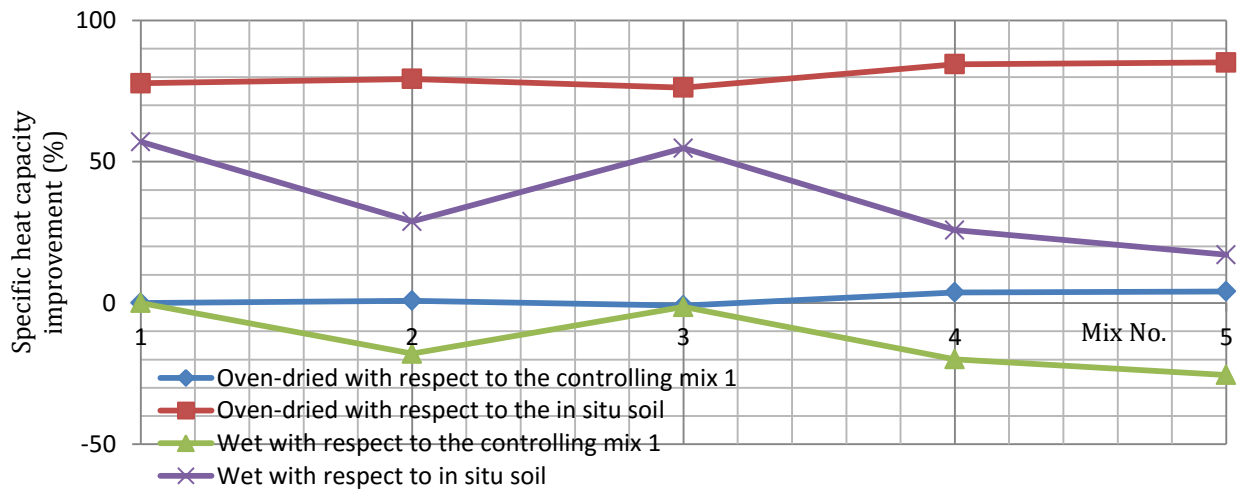


Figure 5-86 Specific heat capacity improvement percentage in all mixes with respect to in-situ soil and controlling mix 1

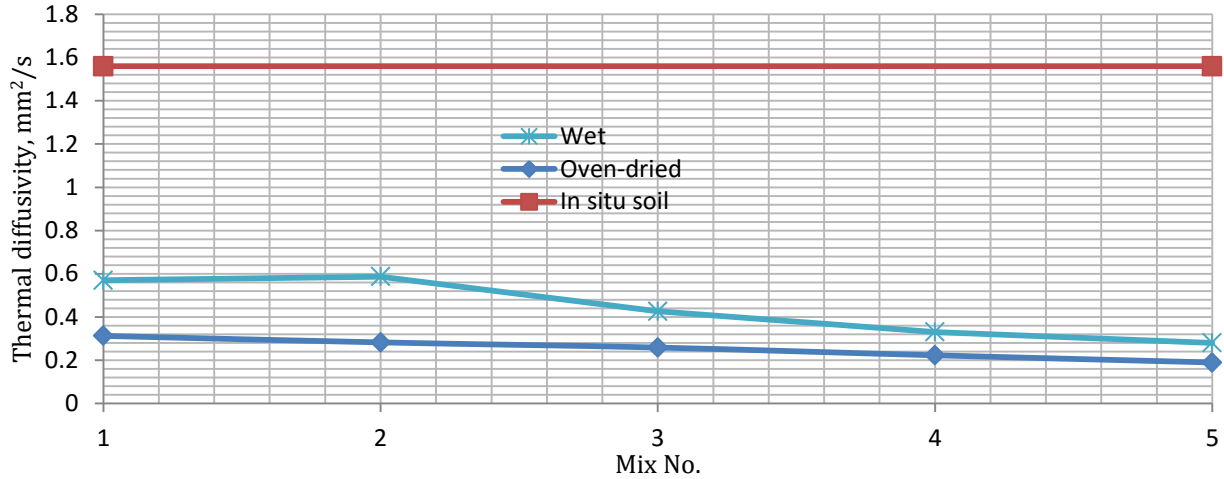


Figure 5-87 Heat diffusivity of soilcrete mixes with increasing ELP material

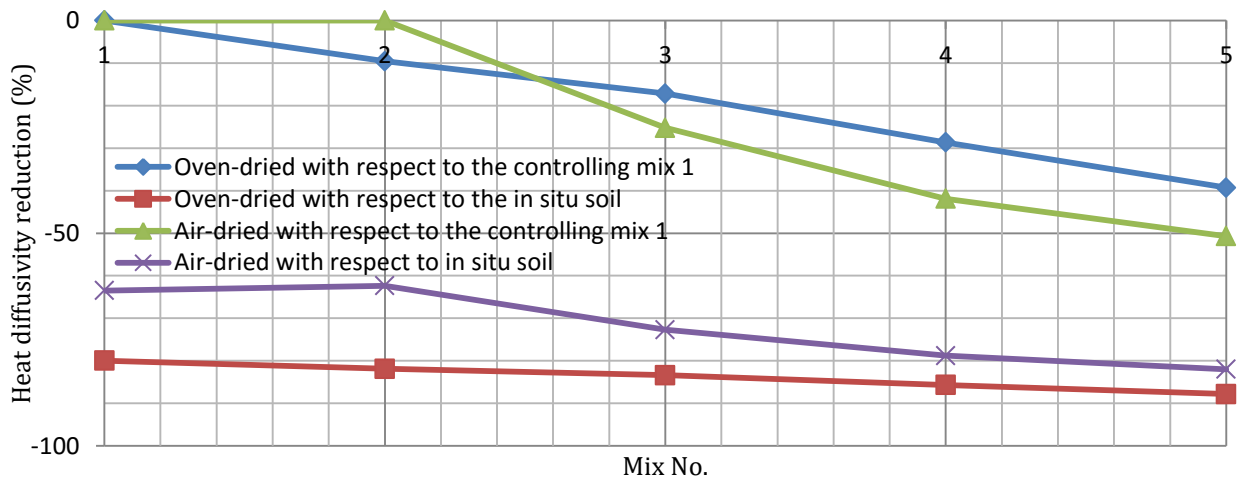


Figure 5-88 Heat diffusivity improvement percentage in all mixes with respect to in-situ soil and controlling mix 1

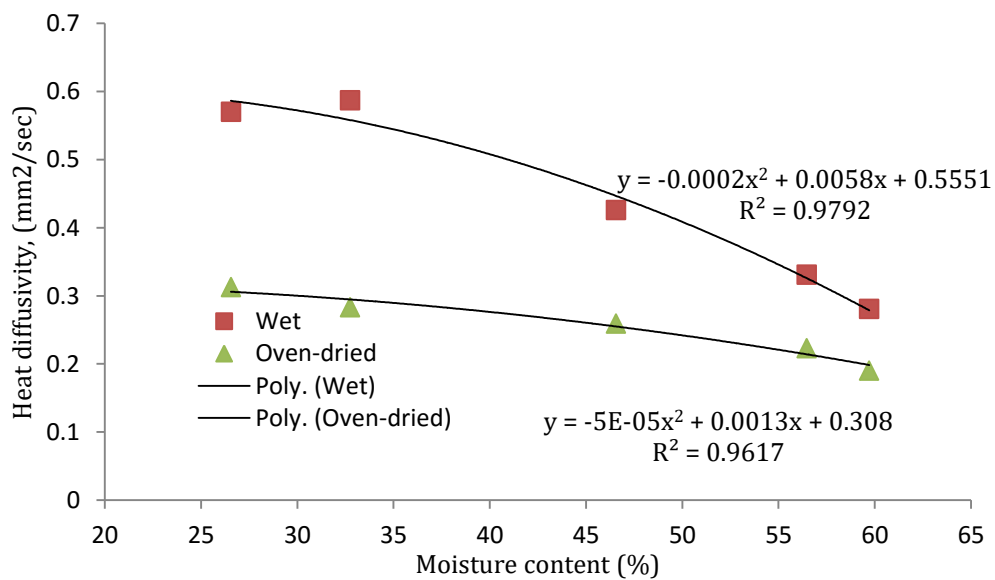


Figure 5-89 Relationship between heat diffusivity and moisture content of soilcrete mixes

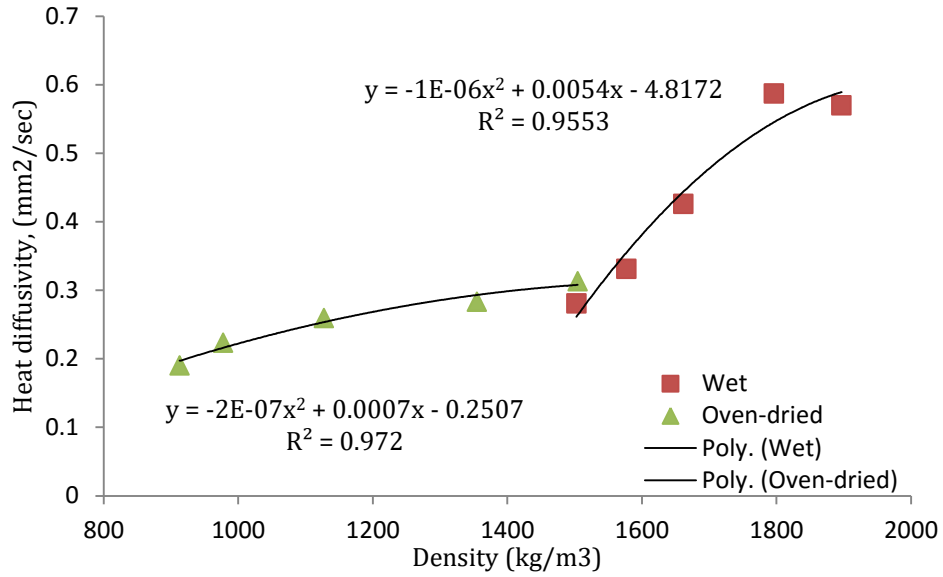


Figure 5-90 Relationship between heat diffusivity and 28-day density of soilcrete mixes

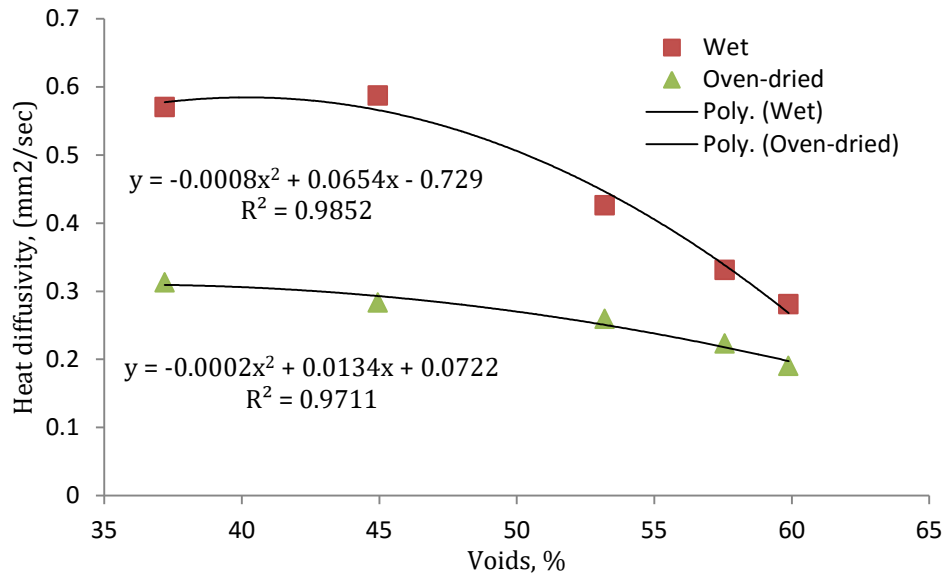









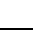
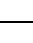




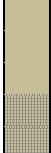
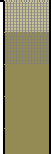


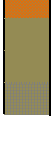


Figure 5-91 Relationship between heat diffusivity and voids of soilcrete mixes

Appendix 5-1 Vertical profile and core logging data sheet (SMPE 2012a)

Column	Description	Legend for Mineralogy
A	Depth, ft (marked on core)	 Soil
B	Depth, inch (measured)	 Coal
C	Mineralogy	 Lite Grey Clay
D	Notes on the core holder	 Dark Grey Clay
E	Comments	 Lite Brown Clay
		 Dark Brown Clay
		 Green Clay
		 Sand
		 Gravelly
		 Sandy
		 Clay or Clayey

A	B	C	D	E
1	12		0-60	62" long, approximately 10" of soil
2	24			
3	36			
4	48			
5	62			
6	72		60-120	54" long, hard clay, softens and dries near 60 end sample taken 28" from the 120 end
7				
8				
9				
10	116		120-180	43" long, hard clay
11				
12				
13				
14				
15	159		180-240	Some loose, broken clay 50" long
16				
17				
18			207-273	67" long, clay is lighter, sample 9" from 207 end
19				
20	209			
21	228			
22	240		273-318	Hard Dark clay 43" long
23	276			
24				
25				
26				
27	319		318-360	42" long some sand Hard Dark clay
28				
29	346			
30	361		NA	29" + 25" = 54" long, dark sandy clay, sample 13" from 360 end
31				
32	415			
33				
34				
35	463		360-420	27" + 19" = 48" long, hard, dark clay, sample 6" from 420 end

36				
37				
38			420 - 480	17" + 39" = 58" long, hard dark gravelly clay
39				
40	521			
41			480-540 3 of 3	48" + 19" = 67" long, hard, dark gravelly clay, sample 36" from 540' end
42				
43	588			Rocks
44			540-600 2 of 3	27" + 40" = 67" long, hard dark gravelly clay, sample 7" from 600 end
45	643			sandy hard dark clay
46				sand
47	655			
48	667		600 - 700 1 of 3	44" long, sand turning to hard brown clay and finally gravel, sample 9" from 600 end and sample 3" from 700 End
49	689			
50	699			
51			600-660 2 of 2	53" long, hard grey clay, turning to soft dark brown clay, sample 16" from 660 end
52				
53				
54	736			
55	752		660-720 1 of 2	65" long, hard grey clay turning to brown clay, sample 17" from 720 end
56				
57				
58				
59	803			
60	817			
61			720-840	19.5" long, grey clay changes to brown
62				
63				
64				
65	830			
66				
67				
68				
69				
70	837			
71			840-900 2 of 2	28" + 35" = 63" long, soft brown gravelly clay/silt, sample 22" from 900 end
72				
73				
74				
75	893		900-960 1 of 2	61" long, brown gravelly, sample 11" from 960 end
76				grey w/fine sand
77	906			Dark/gravelly w/ blue/green tinge
78				
79	950			
80	954		4 of 4	47" long, blue/green clay turning to dark, gravelly clay, sample 8" from 960 End
81	972			
82			960 3 of 4	54" long, dark, gravelly clay w/ 28" of lite grey clay in between, sample 7"
83	1001			
84	1009			
85	1037			
86	1055		960-1020 2 of 4	46" long, dark grey clay w/ gravel and oxidization
87				
88	1101			

89	1137		1020-1080 1 of 4	48" long w/ grey clay, coal, sample 11"
90	1149			
91			1080 - 1200 3 of 3	67" long dark, hard silty clay
92	1184			
93	1216			coal
94			1080 - 1200 2 of 3	57" long, oxidized, more near 1080 end, hard dark clay, sample 30" from 1080 end
95				
96	1273			
97	1280		1080 - 1200 1 of 3	43" long, hard, dark clay w/ gravel for part, sample 7" from 1200 end
98	1288			
99				
100	1316			
101	1328		1200-1320 4 of 4	43" long, grey clay w/ oxidation, some gravel at top sample 6" from 1200 end
102				
103	1359		1200-1320 3 of 4	50" long, grey clay w/ oxidization sample 17" from 1200 end
104				
105	1409		1200-1320 2 of 4	39" long, grey clay
106				
107	1448		1200-1320 1 of 4	68" long gravel towards top, grey clay, sample 14" from 1320 end
108				
109				
110	1516			
111			1320-1440 3 of 3	52" long clay w/ coarse sand sample 19" from 1320 end
112				
113	1568		1320-1440 2 of 3	74" long clay w/ fine sand near top, coarser at bottom samples 19" and 61" from 1440 end
114				
115			1320-1440 1 of 3	49" long, brown clay on top, the rest grey clay, sample 14" from 1320 end
116	1642			
117	1662			
118				
119				
120	1691			
121			1440-1560	57" long green clay (sample @ 117'2" (6" long)) (sample at 120'3" (3" long))
122				
123				
124				
125				
126				
127	1730			coal
128				grey clay (sample @ 126'6" (4" long))
129	1742			below this was measured from the bottom
130	1748			
131	1529		Section starts at 1320	130'10"-127'5" coal
132	1570			
133				139'5" - 130'10" dark grey clay
134				
135				
136				sample @ 136'4" (4.5" long)
137				
138				
139	1673			
140				144'10" - 139'5" light grey clay (gravelly)
141				
142				sample @ 142'5" (6" long)

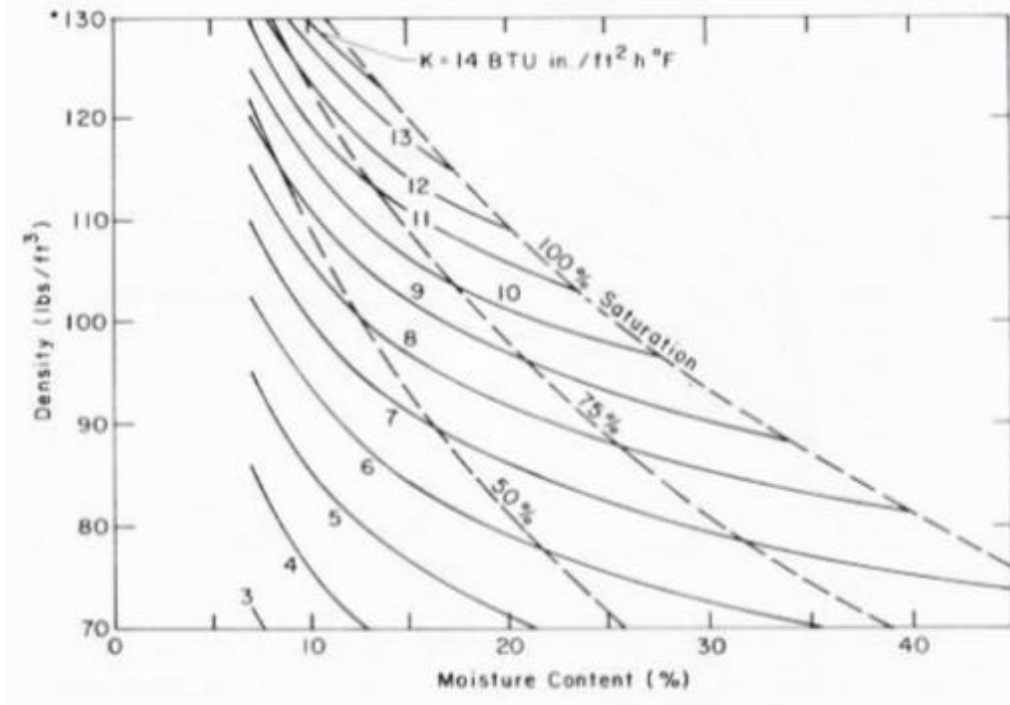
143			
144	1738		
145			146'8"-144'10" dark clay sample @145'7" (4" long)
146			
147	1760		148'0" - 146'8" light grey clay sample @ 147'9" (4" long)
148			
149			
150	1776	Section ends at 150'	
151	1812		151'-148' lite grey sandy clay sample @148'6" (2.5" long)
152	1824		
153	1836		171'-151' grey clay sample @ 153' (6" long)
154	1848		
155	1860		
156	1872		
157	1884		
158	1896		
159	1908		sample @ 159'6" (8" long)
160	1920		
161	1932		
162	1944		
163	1956		
164	1968		
165	1980		sample @ 165' (9.5" long)
166	1992		
167	2004		
168	2016		
169	2028		
170	2040		
171	2052		175' -171' dark, sandy clay w/ coal
172	2064		
173	2076		sample @174'11" (6" long)
174	2088		
175	2100		
176	2112		175'8"-175' hard sand/clay light (rock?) sample @ 175'2.5" (5.5" long)
177	2124		
178	2136		178'2"-175'8" dark clay w/coal sample @176'10"(6" long)
179	2148		180'6"-178'2" coal sample @ 179'8" (3.5" long)
180	2160		
181	2172		185'10"-180'6" sandy dirt
182	2184		
183	2196		
184	2208		sample @183'9" (4.5" long)
185	2220		
186	2232		
187	2244		190'3"-185'10" grey clay sample @ 187'8" (6" long)
188	2256		
189	2268		
190	2280		
191	2292		191-190'3" coal
192	2304		196'2"-191' dark clay/sand
193	2316		
194	2328		
195	2340		
196	2352		
197	2364		197'6"-196'2" clay/coal mixture sample @ 197'4" (4.5" long)
198	2376		

199	2388		200-197'6" dark clay/sand sample @ 198'1" (7.5" long)	
200	2400			
201	2412			205.5'-200' lite brown clay/sand
202	2424			
203	2436			sample 203'3" (5.5" long)
204	2448			
205	2460			
206	2472			205.5'-206.5' green clay sample at 206' (6.5" long)
207	2484			208.5-206.5 clay/coal mixture sample @ 207'1" (7" long)
208	2496			
209	2508			211.5-208.5 brown clay
210	2520			sample @ 211' (4" long)
211	2532			214.5-211.5 clay/coal mixture sample @ 213' (3" long)
212	2544			sample @ 214'5" (4.5" long)
213	2556			216.5-214.5 coal
214	2568			sample @ 215' (1.5" long)
215	2580			217-216.5 coal/lite brown clay mix
216	2592			220-217 coal
217	2604			sample @219'3" (2.5" long)
218	2616			
219	2628			
220	2640			

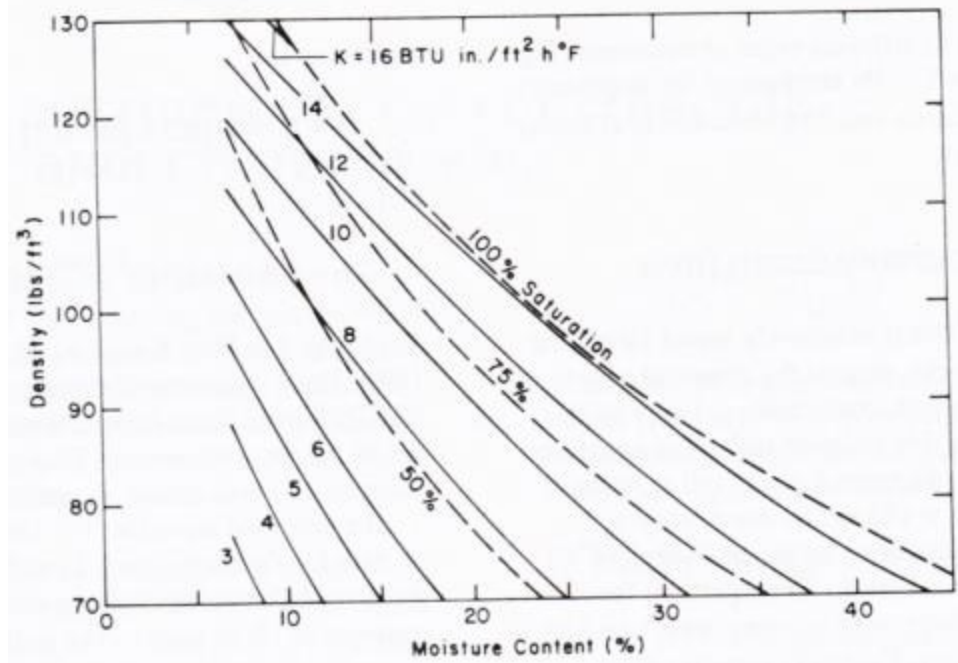
Appendix 5-2 Unit conversion information

British Thermal Unit (BTU) is amount of the energy needed to cool or heat one pound of water by one degree of Fahrenheit at constant pressure of 1 atm. However to convert the BTU to calories, there are several definitions of the BTU exists and that is because the temperature response of water to heat energy is non-linear. Therefore the change in temperature of water mass caused by adding a certain amount of heat to water is function of water's initial temperature. Thus the definition of BTU is based on the different water temperatures and can vary by up to 0.5%. In Thermochemical (Th) aspects, the exact conversion of between calorie and joule $1 \text{ Calorie} = 4.184 \text{ Joules}$ is used where $1 \text{ BTU} = 1054.35 \text{ Joules} = 0.293 \text{ Watt. hour}$. Watt is a unit of power defined by the work required to produce one watt of power for one second which equals to one joule per second and measures rate of energy conversion or transform ($W = J/s = N \cdot m/s = kg \cdot m^2/s^3$). Joule is a unit of energy, work, or amount of heat defined by energy expanded or work done in applying a force of one newton through a distance of one meter ($J = N \cdot m = kg \cdot \frac{m^2}{s^2} = Pa \cdot m^3 = W \cdot s$). Calorie is amount of the energy which equals to exactly 4.18J in thermochemical.

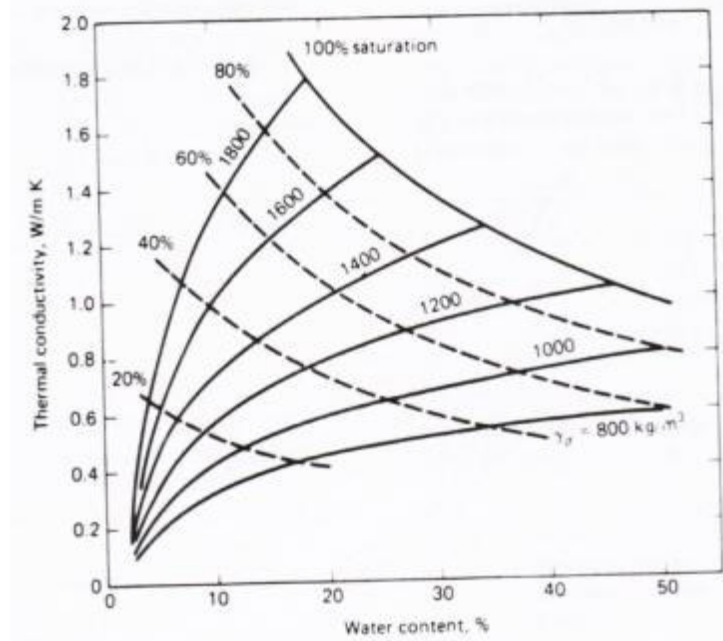
Appendix 5-3 Thermal conductivity of unfrozen silt and clay soils as a function of moisture content and dry density (mean temperature is 40°F). The degree of accuracy is $\pm 25\%$ (after Kersten 1949) (adopted from (Farouki 1986))



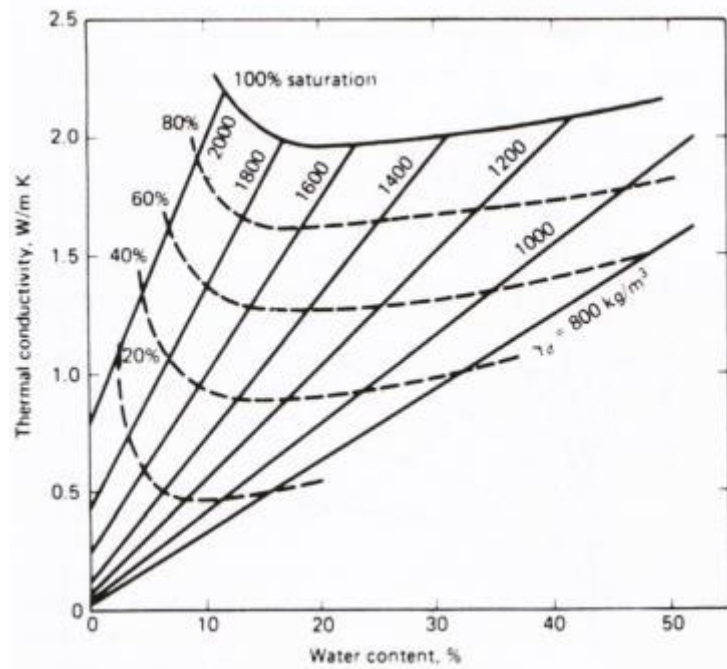
Appendix 5-4 Thermal conductivity of frozen silt and clay soils as a function of moisture content and dry density (mean temperature is 25°F). The degree of accuracy is $\pm 25\%$ (after Kersten 1949) (adopted from (Farouki 1986))



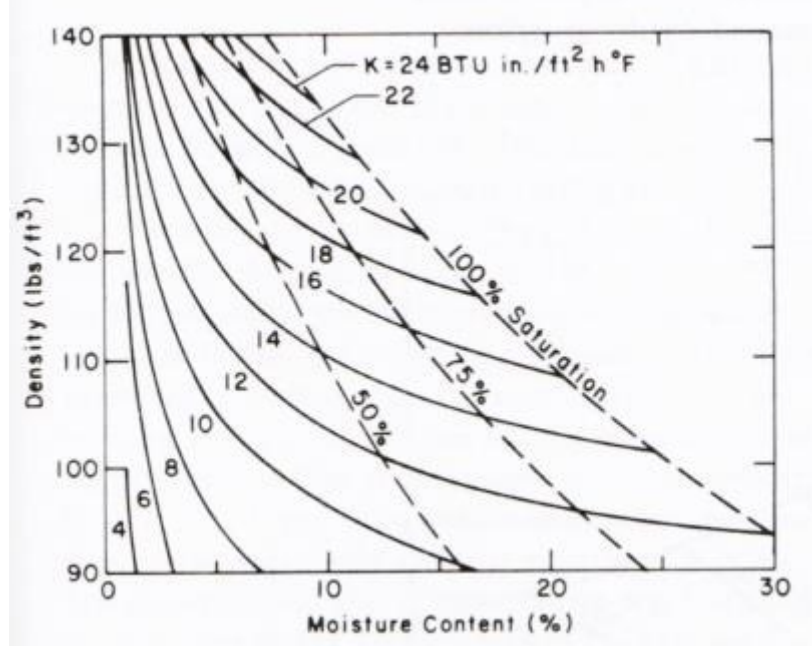
Appendix 5-5 Average thermal conductivity of unfrozen silt and clay soils as a function of moisture content and dry density (Andersland and Anderson 1978) (adopted from (Farouki 1986))



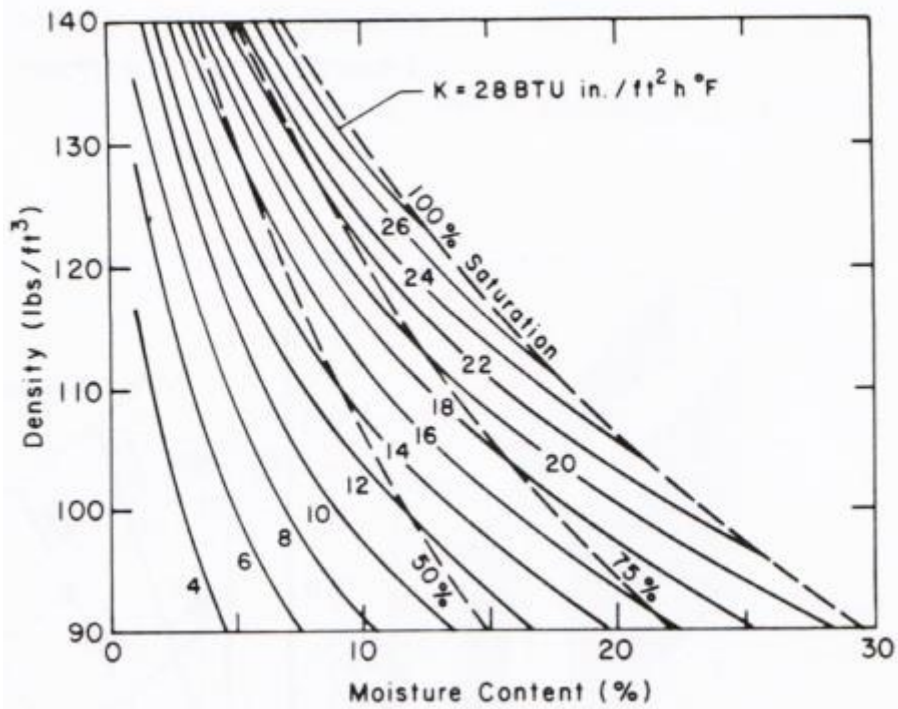
Appendix 5-6 Average thermal conductivity of frozen silt and clay soils as a function of moisture content and dry density (Andersland and Anderson 1978) (adopted from (Farouki 1986))



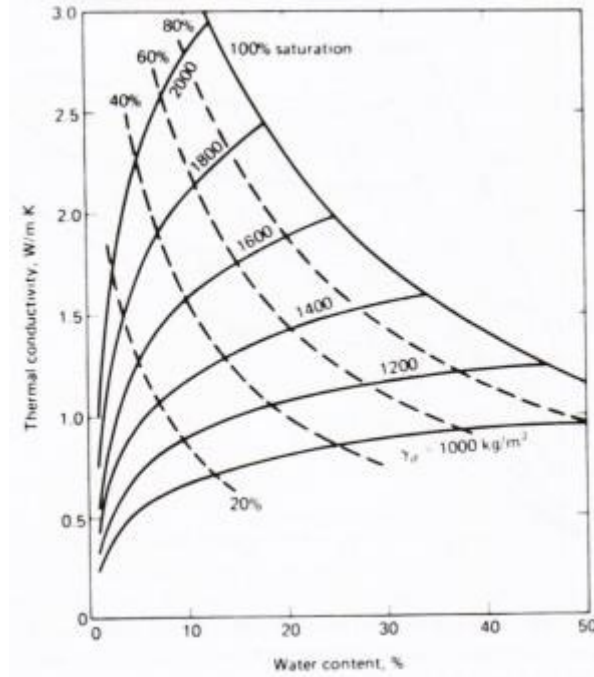
Appendix 5-7 Thermal conductivity of unfrozen sandy soils as a function of moisture content and dry density (mean temperature is 40°F). The degree of accuracy is $\pm 25\%$ (after Kersten 1949) (adopted from (Farouki 1986))



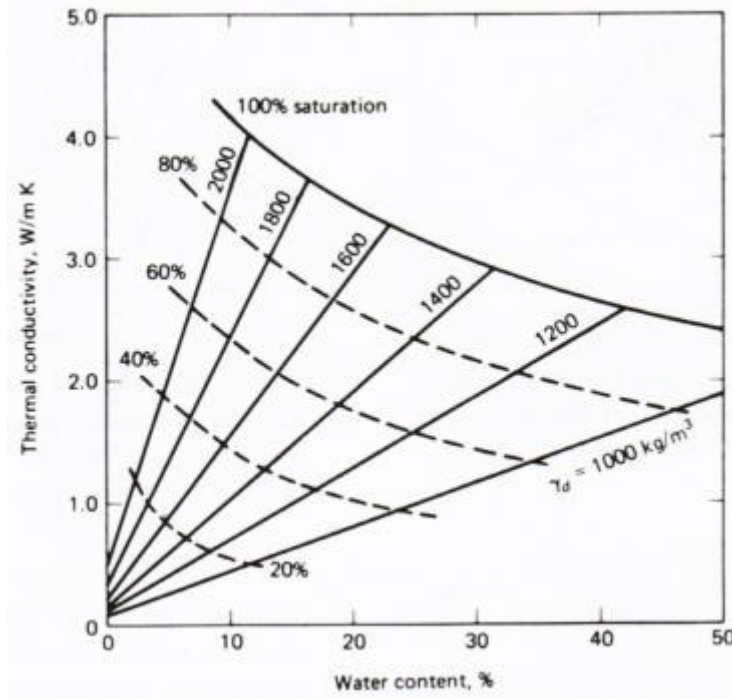
Appendix 5-8 Thermal conductivity of frozen sandy soils as a function of moisture content and dry density (mean temperature is 25°F). The degree of accuracy is $\pm 25\%$ (after Kersten 1949) (adopted from (Farouki 1986))



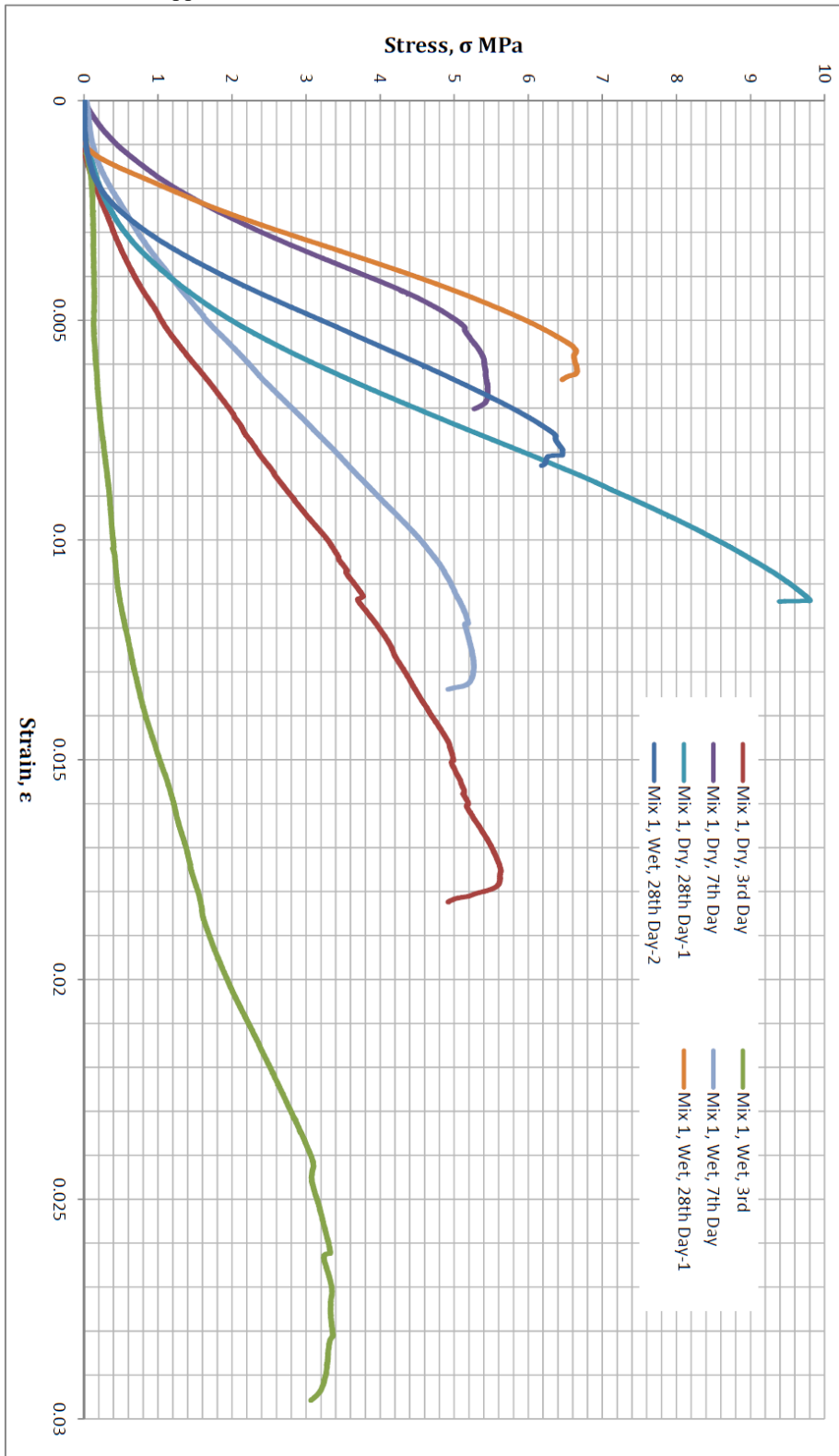
Appendix 5-9 Average thermal conductivity of unfrozen sandy soils as a function of moisture content and dry density (Andersland and Anderson 1978) (adopted from (Farouki 1986))



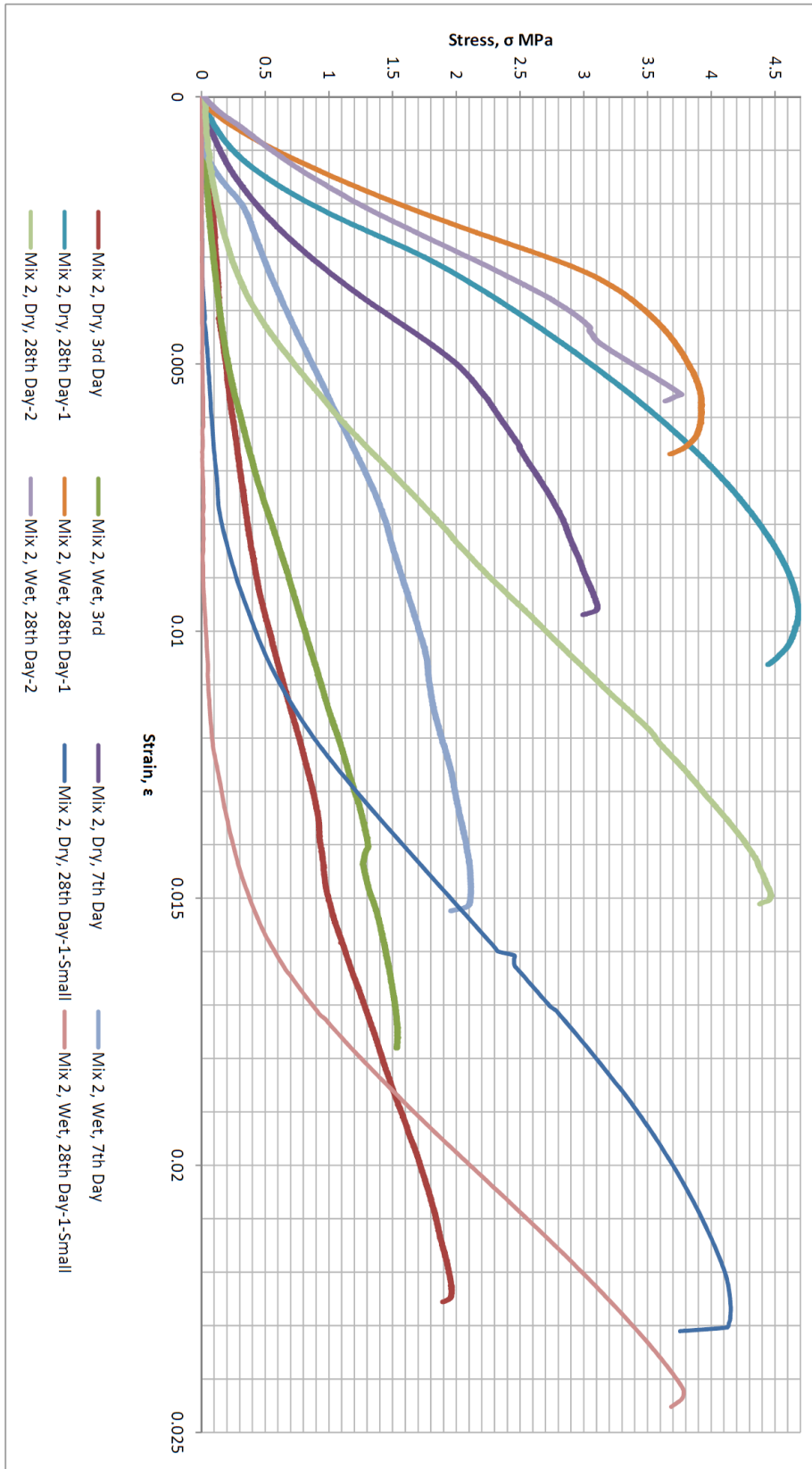
Appendix 5-10 Average thermal conductivity of frozen sandy soils as a function of moisture content and dry density (Andersland and Anderson 1978) (adopted from (Farouki 1986))



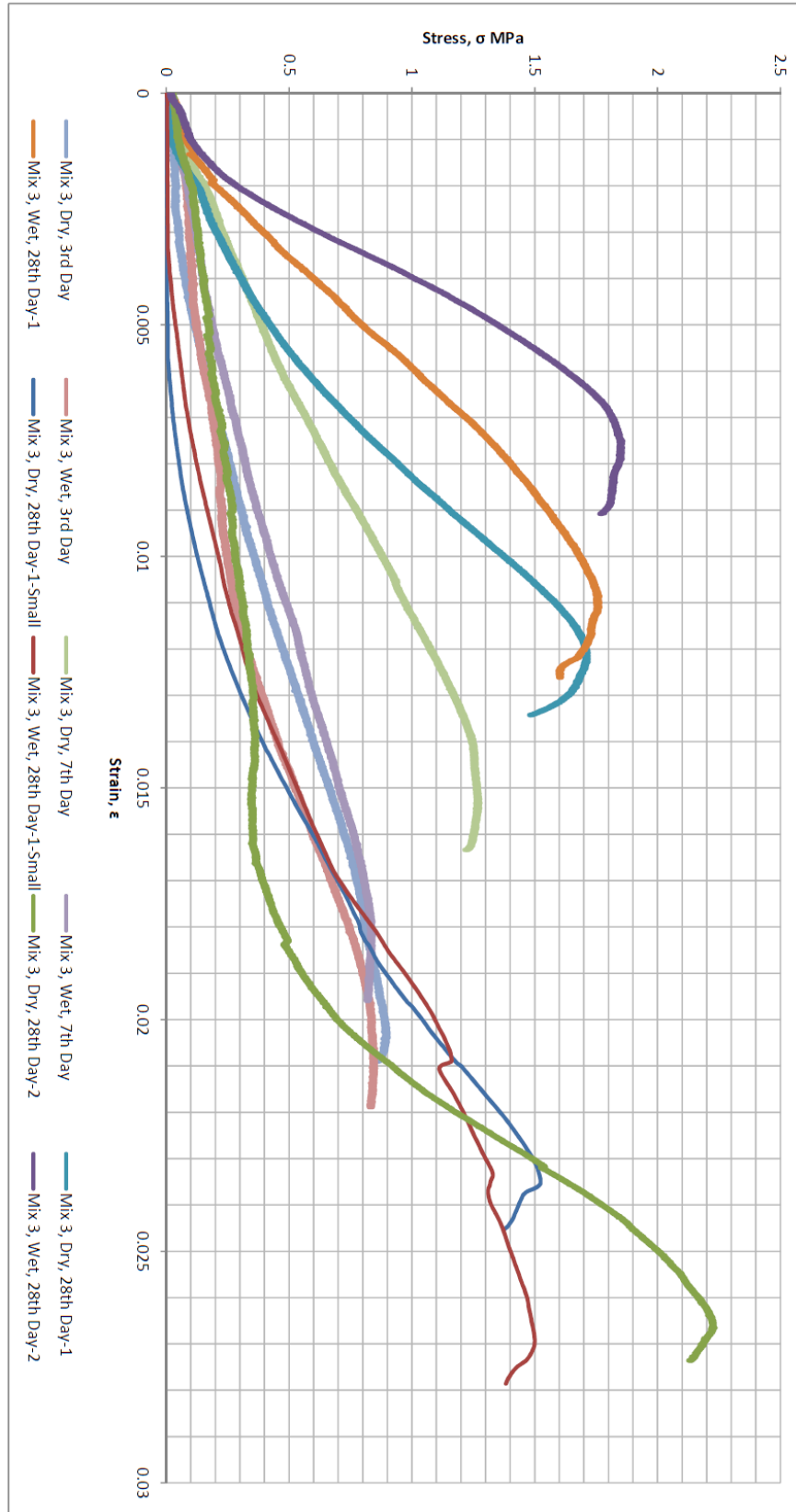
Appendix 5-11 Stress to strain curve of mix 1 soilcrete



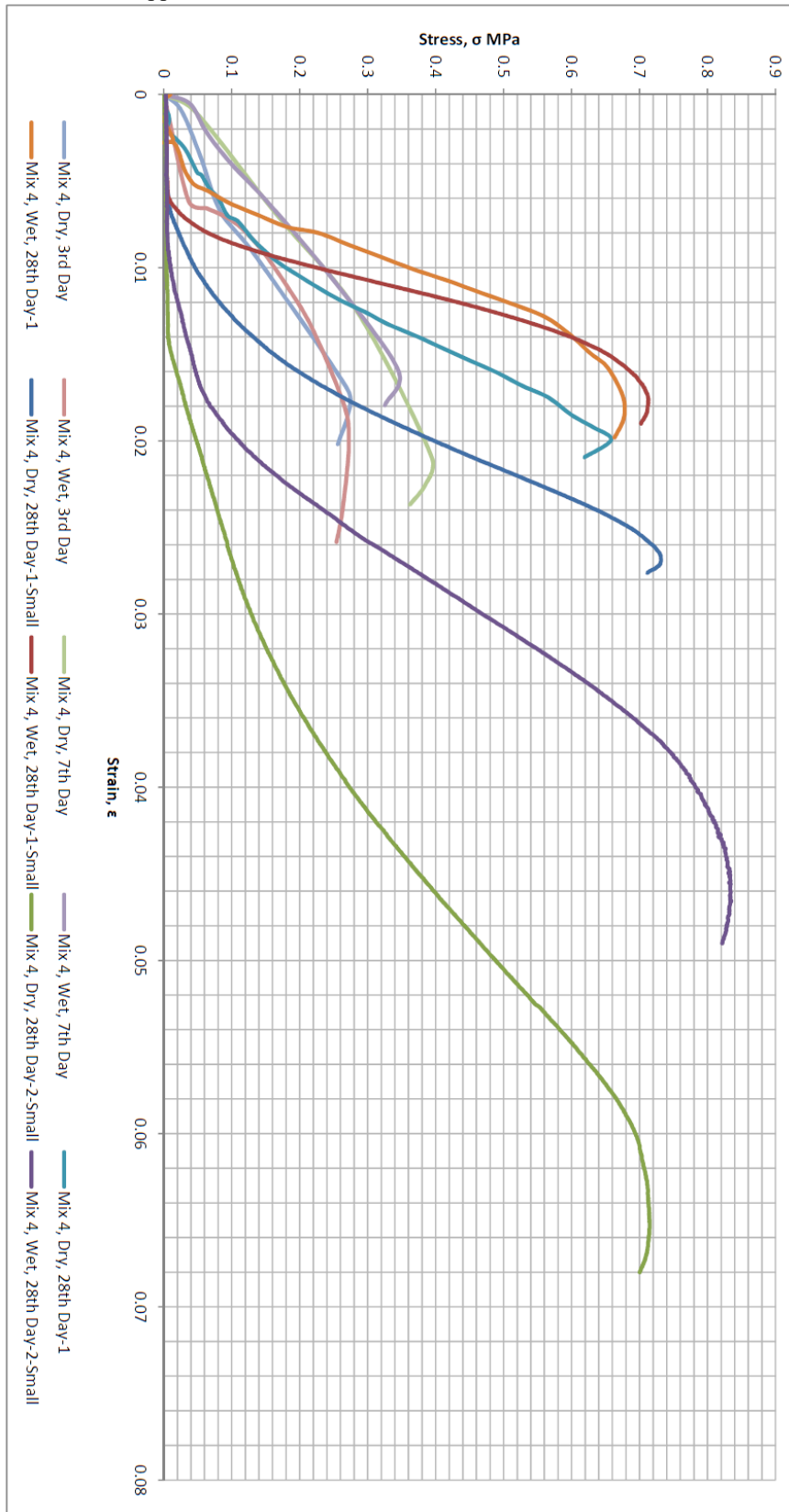
Appendix 5-12 Stress to strain curve of mix 2 soilcrete



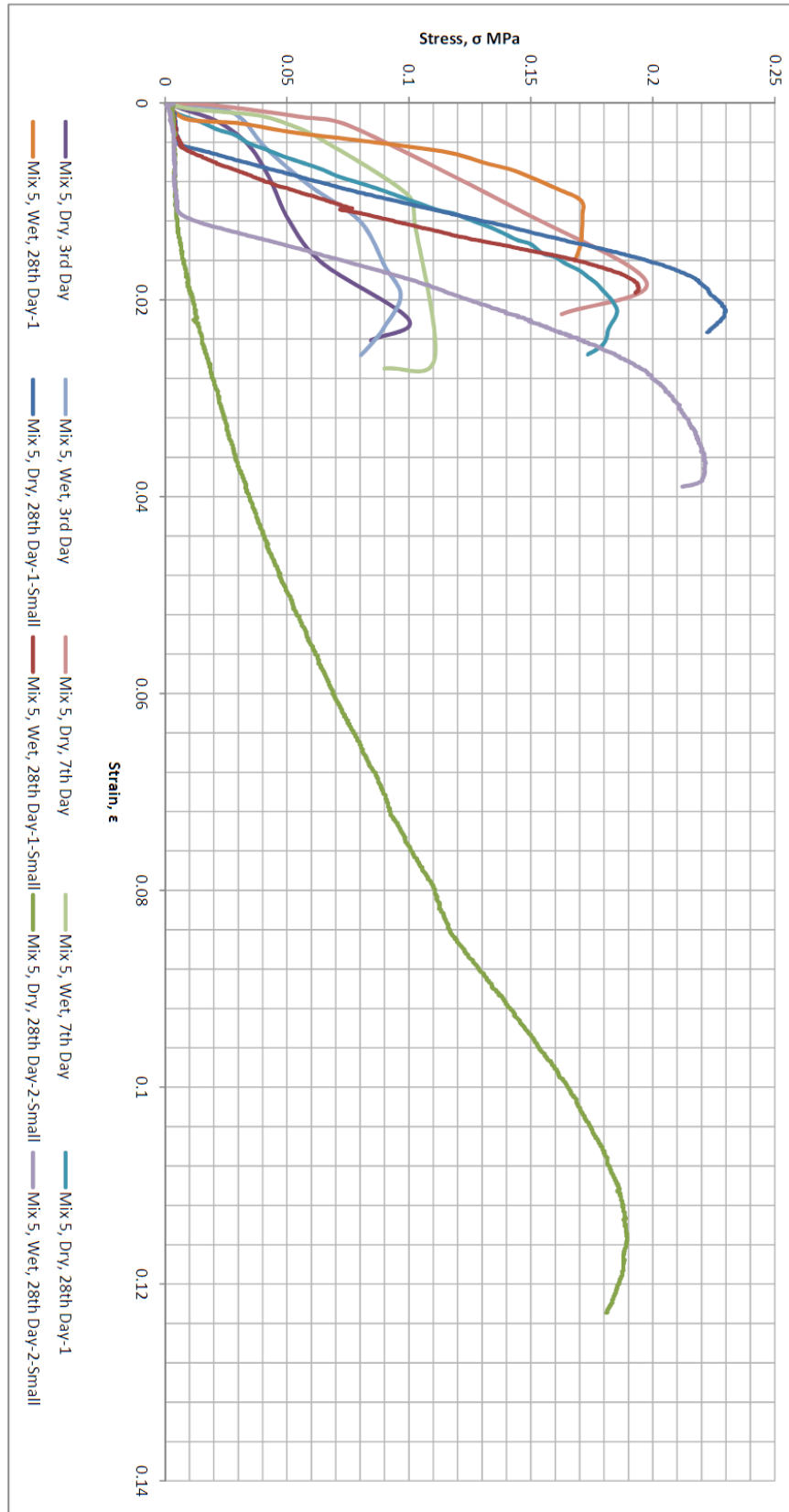
Appendix 5-13 Stress to strain curve of mix 3 soilcrete



Appendix 5-14 Stress to strain curve of mix 4 soilcrete



Appendix 5-15 Stress to strain curve of mix 5 soilcrete



Chapter 6 LABORATORY JET GROUTING EXPERIMENT

This chapter examines the reconstruction procedure of the in-situ soil in the jet grouting tank. It also discusses implementation steps of the laboratory jet grouting operation after the development of the most suitable thermal-insulating grout mixture and the completion of the manufacturing laboratory jet grouting setup. Also, the capability of the manufactured jet grouting setup and the actual laboratory jet grouting experiment results were verified with well-documented literature about jet grouting projects.

6-1. Introduction

A developed thermal-insulating grout (Mix No. 3) can improve in-situ soil's thermal conductivity and mechanical properties. If the developed thermal-insulating grout is injected into the soil using a jet grouting operation, thermal-insulating barriers can be created for underground enclosures. These barriers will keep the heat inside the enclosure from escaping. However, based on the literature, the jet grouting technique has been barely used to improve the thermal-insulating properties of soils. Thus, a laboratory jet grouting operation was implemented with different operational parameters such as jetting pressure and flow rates, withdrawal and rotational rates, and nozzle sizes to validate previous laboratory results and verify the performance of the laboratory jet grouting setup and the groutability of the expanded lightweight perlite (ELP) mixed with grout.

6-2. Reconstructing the in-situ soil ¹

A large-scale creation and reconstruction of soil with the same properties as the in-situ soil is important and challenging. To reconstruct the soil used in the hand-mixed soilcrete samples, the same 67-meters borehole provided by GSS Geothermal Ltd. was used (Figure 6-1). The soil used was sandy lean clay with medium plasticity. Because cohesive soils have low hydraulic conductivity, there was little likelihood of bleeding or permeation into the surrounding area during jet grouting, and the soilcrete boundary could be precisely determined.

The diameter and height of the jet grouting tank were 42 and 40 inches, respectively. After taking into consideration the cap of the tank, which is supposed to model the casing length, there were 22 inches left at the bottom of the tank on which to perform the jet grouting and which must be filled with reconstructed in-situ soil. Based on the dry unit weight of the in-situ soil (1785 kg/m^3) at its initial moisture content of 15.5%, a total weight of at least 900 kg (1984.16 lb) of soil was required to fill the tank.

To reconstruct the in-situ soil in the jet grouting tank, the length of the core barrel was considered to be uniform, with constant physical, mechanical, and thermal properties. However, based on the core logging information discussed in Chapter five, there were layers of coal seam in the provided core which might have affected the thermal properties of the in-situ soil; those layers were taken away from the reconstruction procedure and the total weight of 1000 kg

¹ All tests were done based on the same ASTM methods discussed in Chapter five.

(2204.62 lb) of in-situ soil was used for the soil reconstruction (Figure 6-2). The in-situ moisture content of the soil was calculated in different elevations following the extrusion of soils from the core barrel. Since the total length of soil is considered to be uniform, an average initial moisture content of soil was calculated to be 15.5%. All of the soils were extruded from the core barrel, oven-dried, crushed using the rock crusher machine, and then ground to reduce the maximum particle size to pass a No. 4 sieve. After grinding, all of the soil samples were mixed together to produce a uniform soil for a laboratory jet grouting experiment (Figure 6-3). Next, the whole soil was mixed with its in-situ water content using a concrete mixer (Figure 6-4). Following the mixing, the conditioned soil was poured into the jet grouting tank in layers of five centimeters and was compacted using manual compaction hammers (Figure 6-6). A thick layer of plastic was placed between the jet grouting tank and soil to prevent the soilcrete from sticking to the jet grouting tank after the operation (Figure 6-5). While the soil was being compacted, a five-inch steel cylinder was placed in the center of the tank to simulate the jet grouting borehole in the center of the compacted soil where the jetting monitor is supposed to be lowered down the hole (Figure 6-8). Shelby tubes were pushed into the compacted soil in different layers to extract the soil cores for engineering property tests including moisture content, unconfined compressive strength (UCS), and direct shear strength (Figure 6-7). The Shelby tubes were kept in the steady moisture room until the test day.

6-3. Reconstructed soil test results and discussion

The moisture content of reconstructed soil from 15 specimens in different compaction layers was calculated to be 16%. The uniaxial compressive strength (Figure 6-9) of reconstructed soil and its wet density was calculated to be 350 kPa and 1767 kg/m³, respectively. All three values are in good agreement with the in-situ soil properties measured in Chapter five.

The shear strength of soil is another important property which engineers need to know in order to analyze soil stability and the bearing capacity of foundations and piles. Mohr (1900) presented a theory that material fails because of a critical combination of shear and normal stress and not just because of the failure from exceeding the maximum normal or shear stress alone. Equation 6-1 can be used to express a functional relationship between the normal and shear stress (Das 2008).

Equation 6-1

$$\tau_f = f(\sigma)$$

Where,

τ_f : shear stress on the failure plane

σ : normal stress on the failure plane

The defined relationship in Equation 6-1 is a curve envelope. However, in most soils and geotechnical projects, it is sufficient to define the failure envelope as a linear line (Equation 6-2), the Mohr-Coulomb failure criteria (Figure 6-10) (Das 2008).

Equation 6-2

$$\tau_f = c + \sigma \tan \varphi$$

Where,

c : cohesion (between particles, stress independent component); cementation between sand grains or electrostatic attraction between clay particles

φ : angle of internal friction (between particles, stress dependent component)

The shear strength parameters can be determined using two different laboratory tests: the direct shear test and triaxial test. In the current research, a set of direct shear tests was performed in the laboratory to identify shear strength characteristics of the reconstructed soil (ASTM D3080 2014). Figure 6-11 shows a schematic diagram of the direct shear test apparatus. The size of specimens used in the test is generally 25 cm² across and 25 to 30 mm high. The shear box is split horizontally into halves and a normal force is applied from the top of the shear box. At the same time a shear force is applied by moving the top half of the box relative to other half in order to cause a shear failure in the soil specimen (Das 2008). The test can be either stress-controlled or strain-controlled. In the stress-controlled test, the shear force is applied in equal increments until the soil specimen fails. In the strain-controlled test, a constant rate of horizontal displacement is applied to the top half of the shear box. Either way, the shear failure occurs along the plane of the split of the shear box. In the current direct shear test, the strain-controlled method was used because in this method the peak shear resistance (at failure) as well as lesser

shear resistance (after failure, ultimate strength) can be observed and plotted (Das 2008). The normal and shear stresses were calculated using Equation 6-3 and Equation 6-4, respectively.

Equation 6-3

$$\sigma = \text{normal stress} = \frac{\text{normal force}}{\text{area of cross section of the specimen}}$$

Equation 6-4

$$\tau = \text{shear stress} = \frac{\text{resisting shear force}}{\text{area of cross section of the specimen}}$$

The direct shear test method is suited to relatively rapid determination of consolidated drained strength properties, because the drainage paths through the soil specimen are short, which allows the excess pore pressure to dissipate more quickly than in other drained stress tests. However, the specimen must be sheared at a relatively slow rate; hence, insignificant excess pore pressure exists at failure. An estimated time required for the dissipation of excess pore pressure and amount of deformation required to reach failure are compulsory to determine an appropriate rate of displacement (Equation 6-5) (ASTM D3080 2014).

Equation 6-5

$$R_d = \frac{d_f}{t_f}$$

Where, R_d : displacement rate, in./min [mm/min]
 d_f : estimated relative lateral displacement at failure, inch.
 t_f : total estimated elapsed time to failure, min.

These two factors (d_f and t_f) depend on the type of material and stress history. However, in the absence of soil-specific consolidation data, the time should be based on the soil type (Table 6-1). Also, in the absence of specific experience relative to the test condition, as a guide, an estimated lateral displacement at failure is considered to be 0.5 in. if the material is normally or lightly over-consolidated fine-grained soil. Otherwise, the estimated displacement at failure is 0.2 in. As

discussed previously, based on the unified soil classification system (UCSC), the given soil used in the current experiment falls into the SC category. The time required to failure was estimated to be approximately 200 min and the displacement rate was considered to be 0.002 in./min. Also, six different normal stresses of 0, 100, 150, 200, 250, and 500 kPa were used to carry out the test (Figure 6-12). The results are presented in Table 6-2 and Figure 6-13. Finally, the cohesion and friction angle of the reconstructed soil were calculated to be 81.83 kPa and 7 degrees, respectively, based on Figure 6-14.

As shown in Figure 6-13, in low normal stress, the resisting shear stress increases with the shear displacement until a failure of shear stress is reached. After that point, with any increase of shear displacement, the shear resistance remains constant. However, in high normal stress, the resisting shear stress increases with shear displacement to a point of failure. This point of shear resistance is called Peak Shear Strength. After this point, shear resistance decreases as shear displacement increases, until it finally reaches a constant value which is called Ultimate Shear Strength.

As pointed out earlier, the whole soil in the core barrel is assumed to be uniform with the same properties. Therefore, the thermal properties of soil were considered to be the same, as discussed in Chapter five. Soil thermal conductivity, volumetric thermal capacity, and thermal diffusivity of the given soil were determined to be 1.41W/mK, 0.83 MJ/m³K , and 1.56 mm²/s, respectively.

6-4. Implementation of the laboratory jet grouting

It is important to test the performance of the jet grouting setup before carrying out any operation on the reconstructed soil. For that reason, the performances of water and grout pumps as well as jetting nozzles were tested. Because in triple fluid jet grouting, most of the soil excavation is done using a high velocity water jet, three nozzles with smaller orifice sizes of 1.09, 1.19, and 1.5mm were tested on the water line. However, since the grout mixture included coarse ELP particles, a nozzle with a bigger orifice diameter of 2.5mm was used for the grout line. Based on the results shown in Table 6-3 and Table 6-4, it was determined that PW1/4M0003 and 2.5mm custom nozzles should be used in the water and grout lines, respectively. As discussed in Chapter four, the pressure loss was observed to be less than 10 psi using two pressure gauges installed on top of the supporting frame. The vertical and rotational motions were also calibrated to calculate actual speeds relative to variable speed drive (VSD) settings. The results are shown in Table 6-5

and Table 6-6. Based on the literature review in Chapter three and the jet grouting experience on the same soil type, Table 6-7 short-lists all the jet grouting operational parameters used in the laboratory experiment.

After testing the performance of the jet grouting setup, the thermal-insulating grout was batched in the grout tank. As discussed in Chapter five, the thermal-insulating grout Mix No.3 was able to produce an optimum hand-mixed soilcrete from both the mechanical and thermal properties' aspects. For that reason, Mix No.3 was chosen to be used in the laboratory jet grouting experiment. The mixing procedure was divided into two steps. First, an appropriate amount of pre-soaked ELP was mixed with a calculated amount of water in small buckets. The buckets were emptied into the grout tank while the grout mixer was running. Next, an appropriate amount of Portland cement was slowly added into the grout tank to prevent the sudden settlement of cement at the bottom of the tank. In addition to the grout mixer, another hand drill mixer was used in the upper elevation of the grout tank to prevent an accumulation of ELP on the mixture surface.

Immediately after preparing the grout in the batching plant and mixing it for 30 minutes, the jetting monitor was lowered to the bottom of the tank and the jet grouting operation commenced in incremental steps followed by two minutes of rotation and one minute of a lifting and rotating process. As discussed in Chapter three, an optimal repetition frequency of five was reached with two minutes of rotating only at a speed of 2.5 rpm. All operational parameters were monitored and controlled during the jet grouting operation. Also during the operation, the outlet of the jetting tank was connected to the waste tanks with a four-inch PVC pipe to collect the spoil material return (Figure 6-15). After the jetting operation, the cap was removed and the top portion of the soilcrete was covered with plastic wrap to prevent it from dehydrating during the curing period (Figure 6-16).

In order to test the physical, mechanical, and thermal properties of the soilcrete, it was decided to drill out core samples from the soilcrete body and extract specimens for the required tests. However, three weeks after the laboratory jetting, the soilcrete was too weak to have its diameter visually inspected or to have any core extracted. This condition was the result of having the soilcrete tank wrapped in plastic, which prevented the moisture from escaping and replaced the cementitious material (cement) with low density ELP. However, as was discussed in Chapter three, the UCS value stayed constant after 56 days of curing in all soil types (Figure 3-45 and

Figure 3-46). Consequently, the soilcrete was left at room temperature of 24⁰C for 56 days to cure and gain strength. Then, the plastic wrap and any spoil material on top of the soilcrete were removed in order to perform an examination. Core samples were extracted from the center to the perimeter in all directions using the handheld coring machine with a three-inch diameter diamond drill bit to visually examine the actual soilcrete and its other engineering properties (Figure 6-17).

6-5. Soilcrete and grout test results and discussion¹

As with the previous experiments, all laboratory tests were done under two different conditions of wet and dry. In the wet condition, core specimens were stored in the moisture constant room right after they were extruded from the core-drilling machine until the test day. However, in the dry condition, after being extruded from the core barrel, the specimens were cut and ground into the appropriate size for each test and then oven-dried for 24 hours at 110⁰C before the test day.

6.5.1. Mechanical properties of thermal-insulating grout

After mixing the water, ELP, and cement in the grout tank for 30 minutes, a fresh unit weight of 1450 (kg/m³) grout was measured. That amount is in agreement with the fresh unit weight of grout in Mix No. 3 in the experiment discussed in Chapter five. From this batch, 12 cylinders of 75 mm diameter and 150 mm height were filled with fresh thermal-insulating grout. They were demolded after 72 hours and left in the moisture-constant room for 56 days to cure. Table 6-8 and Figure 6-18 show the mechanical properties of the hardened thermal-insulating grout. Its strength seems to be higher in the wet condition than in the dry condition. This is because of the grout's high water content in the wet condition, which was replaced with a void in the dry condition. For the same reason, the grout's unit weight in the wet condition was almost double its value in the dry condition.

6.5.2. Mechanical properties of soilcrete

The thermal-insulating grout Mix No.3 was used to create a soilcrete column using the laboratory jet grouting setup. The same mechanical and thermal property tests and a direct shear test were conducted on core specimens extracted from the soilcrete column to validate the results

¹ All tests were done based on the ASTM methods discussed in the previous section and chapter.

obtained in a hand-mixed experiment. The soilcrete diameter was measured to be 0.5 meters. All together, 61 specimens were tested to calculate the UCS, splitting tensile strength (STS), thermal properties, and shear strength of soilcrete in both wet and dry conditions. As discussed in Chapter three, the soilcrete properties vary along the radius of the jet grouting column; however, the variations are negligible in small diameter columns such as the 1.0m column. Although core specimens were extracted from the center to the perimeter of the soilcrete in all directions, the average values were considered in the evaluation process since variances between the values were less than 1%.

Table 6-9 illustrates the UCS (Figure 6-19), STS (Figure 6-20), and modulus of elasticity (E) of 56-day-old hardened soilcrete in both wet and oven-dried conditions. Unlike the hardened grout samples, the UCS of hardened soilcrete in the dry condition is more than its value in the wet condition. This is because the soil-cement-ELP particles in the wet condition were surrounded by water, which prevents the particles from moving into a denser state and consequently causes failure; however, in the dry condition, those particles under compression pressure can slip over each other to reach a denser state, which results in more compression resistance before the failure occurs. Figure 6-21 shows the UCS of soilcrete and grout versus soil in wet and dry conditions. Similar to the hand-mixed soilcrete, the UCS of soilcrete in wet and dry conditions reached values that were 198% and 360% higher than those of the tested soil. In grout samples, there are no aggregates such as soil particles that cement can bond with to increase the strength of the specimen. For that reason, the UCS of grout samples is less than that of the soil specimen in both wet and dry conditions.

To calculate the E of soilcrete samples, the longitudinal displacement of specimens during the compression test was measured and recorded. Then, an average slope of the stress-strain curves, which represents the E, was calculated (Table 6-9). An enormous increase of soilcrete E compared to its value in the tested soil is shown in Figure 6-22. This indicates that during the jet grouting the soil structure was modified, replaced, and mixed with cement, which consequently results in soilcrete's elastic behavior.

A direct shear test was also done on the hardened soilcrete specimens to understand the effect of the jet grouting operation on the soil's shear strength characteristics. Normal stresses of 0, 100, 200, 350, and 500 kPa and 0, 150, 350, and 500 kPa were used to carry out the tests on dry and wet soilcrete specimens (Figure 6-23). Table 6-10 and Figure 6-24 show the results for the dry

condition. Table 6-11 and Figure 6-26 show the results for the wet condition. Based on Figure 6-25 and Figure 6-27, the cohesion and friction angle of soilcrete in dry and wet conditions has been calculated to be 287.5 kPa and 26 degrees and 302.5 kPa and 35 degrees, respectively. Figure 6-28 shows a change in height of soilcrete specimens in the dry condition versus shear displacement during the test. Specimens under normal stress of 100 kPa behave like normally consolidated clay (NC), whereas the specimens under higher normal stresses behave like over-consolidated clay (OC)¹. Figure 6-29 shows that soilcrete cohesion in wet and dry conditions increased 270% and 240% compared to the soilcrete's original value in soil. Also, as shown in Figure 6-30, the friction angle of soilcrete in wet and dry conditions increased 400% and 272% compared to the soilcrete's original value in soil. Unlike UCS values in soilcrete wet and dry conditions, shear strength characteristics of soilcrete in the wet condition were greater than those in the dry condition. This may have happened because of cohesion strength or the stickiness of bond water in the high water content of specimens in the wet condition and also the nature of the direct shear and STS test where tensile failure occurred.

6.5.3. Thermal properties of soilcrete

The same Thermal Constants Analyzer TPS 1500 and method were used to determine the thermal properties of soilcrete specimens. Table 6-12 presented all thermal properties of soilcrete specimens in both wet and dry conditions.

Figure 6-31 shows that the thermal conductivity of soilcrete specimens with respect to thermal conductivity of soil was reduced by 56% and 89% in wet and dry conditions, respectively. As discussed earlier, the thermal conductivity is a measure of the material's ability to conduct heat. After the field jet grouting operations, the soil's ability to conduct heat through its structure will reduce by 89% in the dry condition. This is what happens when the borefield has already been injected with thermal energy. Thermal conductivity in the wet condition is higher than in the dry condition, which is caused by the higher thermal conductivity of water in the wet condition compared to its value of air in the dry condition.

Figure 6-32 shows that the volumetric heat capacity of soilcrete specimens was increased by 108% and 10% with respect to the original volumetric heat capacity of soil in wet and dry

¹ The vertical displacement of specimens under other test conditions has not been recorded due to equipment failure during the test.

conditions, respectively. Volumetric heat capacity is the term used to define the amount of heat required to increase the temperature of a unit volume of soil by 1°C; more energy is required to increase the temperature of soilcrete than of in-situ soil. Since the volumetric heat capacity of water in the wet condition is more than air in the dry condition, the volumetric heat capacity of wet soilcrete specimens is higher than that for the dry specimens.

Thermal diffusivity is defined as a material's ability to adjust its temperature to the surrounding environment. For thermal-insulating purposes, material with low heat diffusivity is preferred. As shown in Figure 6-33, the thermal diffusivity of soilcrete specimens was reduced 74% and 86% with respect to in-situ soil in wet and dry condition, respectively. Theoretically, thermal diffusivity is calculated by dividing thermal conductivity by volumetric heat capacity. The thermal conductivity was reduced more in the dry soilcrete specimens than in the wet ones, suggesting that heat diffusivity is greater in wet than dry conditions

6-6. Conclusions

As discussed in Chapters three and five, to create hand-mixed soilcrete specimens, the volumetric percentage of grout retained by soil and the volumetric percentage of soil removed by jet grouting were considered to be 80% and 50%, respectively. Then, five hand-mixed soilcrete compositions of water, cement, soil, and ELP were calculated based on the triple jet grouting system. However, these values are based on the jet grouting literature and jet grouting experience on different soil types using the steady lifting method. In the laboratory jet grouting experiment, considering the practical pressures of water and grout jet, steady and incremental lifting methods were used together to increase the jetting specific energy per unit length of the borehole and to reach the most optimal soilcrete properties. It was discussed in Chapter three that the reconstructed soil was sandy clay. The clay soil is difficult to erode and is generally eroded in chunks. Hence, the two lifting methods were used to increase the cutting performance of the water jet and the percentage of the soil replacement with grout material. These two lifting methods also help to smooth the spoil material retune. However 30% to 40% more water was used during jet grouting than what was used for the hand-mixed experiment.

Of all the thermal and mechanical parameters of soilcrete, UCS and thermal conductivity were chosen as the major improvement criteria for designing thermal-insulating soilcrete. Table 6-13 presents variations between important soilcrete properties created by the laboratory jet grouting

setup and those properties measured in the hand-mixed experiment. Considering the results presented in Table 6-13, the following statements can be made:

- 1) As anticipated, the higher water content affected the soilcrete UCS that was created by the jet grouting. The UCS of soilcrete created by jet grouting operation was reduced by 39% and 14% in wet and dry conditions relative to its value in the hand-mixed experiment. In the dry condition, the particles moved to a denser state during compression and reached more compression resistance before failure; therefore there was less reduction in the UCS. However, the jet grouting operation still improved in-situ soil strength by 198% and 360% in wet and dry condition, respectively.
- 2) The thermal conductivity of soilcrete created by the jet grouting operation increased by 19% in the wet condition relative to the wet thermal conductivity of soilcrete in the hand-mixed soilcrete. This occurred because the jet grouting samples had a higher water content than the hand-mixed samples. However, the thermal conductivity of the dry soilcrete was reduced by 33% relative to its value in the hand-mixed soilcrete which was caused by the very low thermal conductivity of air replaced by the water content.
- 3) The volumetric heat capacity of soilcrete increased (improved) by 44% over the value of the hand-mixed soilcrete. The volumetric heat capacity improved for the same reason that the thermal conductivity of soilcrete increased in the wet condition
- 4) The thermal conductivity of soilcrete was greatly improved compared to its value in the insulating shotcrete developed by Liu (2013). Table 6-14 shows that even by replacing 100% of the ELP with sand aggregate in the insulating shotcrete, the thermal conductivity of the created soilcrete was reduced 146.7% compared to the insulating shotcrete in the dry condition.

The performance of the laboratory jet grouting setup was also verified with the values reported in Chapter three for soilcrete diameter and its strength properties. Theoretically, the soilcrete diameter created by the triple jet grouting system at different jobsites with clay soils has been reported to be 0.9 to 2m (Table 3-1, Table 3-7, Table 3-12, Table 3-14, Figure 3-58, Figure 3-59,

Figure 3-60, and etc.). That range of reported diameter was created by a typical triple fluid jet grouting system with an average specific jetting energy of 35 MJ/m. However, in the current laboratory jet grouting, the specific jetting energy is calculated to be 16 MJ/m. The expected soilcrete diameter based on Figure 3-31, Figure 3-36, Figure 3-50, Figure 3-51, and Equation 3-10 is estimated to be in the range of 0.38 to 0.5m. As reported previously, the diameter of the soilcrete was observed to be 50 cm after implementing the laboratory jet grouting operation, which is in perfect agreement with the reported values in the literature. As discussed in Chapter five, the UCS of soilcrete created by different jet grouting systems at different jobsites on clay soil ranges from 1 to 2.4 MPa. Also B Nikbakhtan & Osanloo (2009) and B. Nikbakhtan & Ahangari (2010) reported case histories of triple fluid jet grouting operations on the clay soil. Based on the results in Figure 3-66 and Figure 3-69, the UCS of soilcrete created by the laboratory jet grouting setup is estimated to be 1.25 to 1.7 MPa. Hence, the performance of the laboratory jet grouting setup was verified with calculated values of soilcrete UCS. Those values were 1.1 and 1.7 MPa in wet and dry conditions, respectively.

Table 6-15 concluded improvement percentages of soilcrete properties created by both the jet grouting operation and the hand-mixed experiment in wet and dry conditions. It is recommended to consider dry condition values in underground thermal energy storage projects where this condition represents a situation where thermal energy has already been injected into the borefield area.

To address the complexity of the jet grouting process and the design procedure of soilcrete properties, Equation 6-6 and Equation 6-7 are proposed to estimate actual soilcrete properties in the field based on the hand-mixed soilcrete experiments in the laboratory.

Equation 6-6

$$\aleph_{S,v,A} = \aleph_{S,v,H} \times \beta$$

Equation 6-7

$$\vartheta_{\text{actual soilcrete}} = \vartheta_{\text{in-situ soil}} + [(\vartheta_{\text{hand-mixed soilcrete}} - \vartheta_{\text{in-situ soil}}) \times \beta]$$

Where, $\aleph_{S,v,H}$: improvement percentage of soil particular property relative to the same property of hand-mixed soilcrete

$\aleph_{S.v.A}$: improvement percentage of soil particular property relative to the same property of actual soilcrete

ϑ : particular property of soil or soilcrete in both wet and dry condition (UCS, thermal conductivity, volumetric heat capacity, and thermal diffusivity)

β : field factor of safety for each particular property presented in Table 6-16.

Table 6-1 Minimum time required for failure in direct shear test (ASTM D3080 2014)

UCSC Classification	Minimum Time to failure, t_f
SW, SP (<5% fines)	10 min
SW,-SM, SP-SM, SM (>5% fines)	60 min
SC, ML, CL, SP-SC	200 min
Mh, CH	24 hours

Table 6-2 Direct shear test results on reconstructed soil specimens

Normal stress, kPa	Shear stress, kPa
0	75.46
100	96.39
150	100.99
200	104.01
250	123.48
500	138.08

Table 6-3 Water pump performance test

Nozzle	Orifice Size	Pressure (psi)	Flow (GPM)
1.5mm Custom	1.5mm	850	3
PW1/4M0004	0.047" (1.19mm)	2200	2.9
PW1/4M0003	0.043" (1.09mm)	2500	2.25

Table 6-4 Grout pump performance test

Nozzle	Orifice Size	Pressure (psi)	Flow (GPM)
2.5mm Custom	2.5mm	170	3.1

Table 6-5 Vertical motion calibration

Speed Setting	speed (cm/min)
19%	3.00
20%	5.00
22%	16.41
24%	29.17
26%	45.65
30%	59.66

Table 6-6 Rotational motion calibration

Speed Setting	Speed (rpm)
18%	2.22
20%	3.75
30%	10.00

Table 6-7 Jet grouting operational parameters

Parameter	Water pressure (psi)	Water flow rate (GPM)	Grout pressure (psi)	Grout flow rate (GPM)	Lifting speed (cm/min)	Rotating speed (rpm)
Value	2500	2.25	170	3.1	3	2.5

Table 6-8 56 day old thermal-insulating grout samples

Condition	Wet	Dry
Unit weight, kg/m ³	758.32	373.25
UCS, kPa	127	77
E, MPa	5.32	4.6
STS, kPa	22	7

Table 6-9 UCS, E, and STS of 56 day hardened soilcrete

Condition	Wet	Dry
UCS, MPa	1.10	1.70
E, MPa	87.50	130.00
STS, kPa	270.00	73.00

Table 6-10 Direct shear test results on dry soilcrete specimens

Normal stress, kPa	Shear stress, kPa
0	294.70
100	324.25
200	336.36
350	481.24
500	515.18

Table 6-11 Direct shear test results on wet soilcrete specimens

Normal stress, kPa	Shear stress, kPa
0	315.80
150	417.81
350	478.79
500	697.40

Table 6-12 Thermal properties of soilcrete specimens in both dry and wet condition

Condition	Thermal conductivity w/mK	Thermal diffusivity mm ² /s	Volumetric heat capacity MJ/m ³ . K
dry soilcrete	0.154	0.224	0.91
wet soilcrete	0.621	0.402	1.73

Table 6-13 Variation of important soilcrete properties created by jet grouting relative to hand-mixed experiment

Condition	Parameter	Jet grouting (1)	Hand-mixed experiment (2)	In-situ soil	Variation 1 & 2 %
Wet	UCS, MPa	1.100	1.814	0.370	39
	Thermal conductivity, w/mK	0.621	0.520	1.410	-19
	Volumetric heat capacity, MJ/m ³ . K	1.730	1.196	0.830	-44
Dry	UCS, MPa	1.700	1.978	0.370	14
	Thermal conductivity, w/mK	0.154	0.230	1.410	33
	Volumetric heat capacity, MJ/m ³ . K	0.910	0.924	0.830	1.5

Table 6-14 Thermal conductivity of insulating shotcrete developed by (W. V. Liu 2013)

Parameter	Replacement ratio of ELP material with sand aggregate, %	Wet	Dry
Thermal conductivity w/mK	100	0.6852	0.3799
	75	1.1565	0.7351
	50	1.7532	1.1830
Soilcrete created by laboratory jet grouting setup		0.621	0.154
Improvement percentage relative to soilcrete created by laboratory jet grouting	100	10.33	146.7
	75	86.2	377.3
	50	182.3	668.2

Table 6-15 Improvement percentage of soilcrete properties versus in-situ soil¹

Condition	Parameter	In-situ soil Versus Actual S.C. ²	In-situ soil Versus Hand-mixed S.C.
Wet	UCS, MPa	+197	+390
	Thermal conductivity, w/mK	-56	-63
	Thermal diffusivity, mm ² /s	-74	-73
	Volumetric heat capacity, MJ/m ³ .K	+108	+44
Dry	UCS, MPa	+359	+435
	Thermal conductivity, w/mK	-89	-84
	Thermal diffusivity, mm ² /s	-86	-84
	Volumetric heat capacity, MJ/m ³ .K	+10	+11

Table 6-16 Recommended safety factor to calculate actual soilcrete properties based on hand-mixed specimens

Condition	Parameter	Recommended correction factor
Wet	UCS, MPa	0.50
	Thermal conductivity, w/mK	0.90
	Thermal diffusivity, mm ² /s	1.00
	Volumetric heat capacity, MJ/m ³ .K	2.50
Dry	UCS, MPa	0.83
	Thermal conductivity, w/mK	1.05
	Thermal diffusivity, mm ² /s	1.00
	Volumetric heat capacity, MJ/m ³ .K	0.85

¹ Positive and negative signs mean increase and decrease, respectively.

² Soilcrete



Figure 6-1 In-situ cores used to create reconstructed soil in laboratory



Figure 6-2 Excluding coal layers during crushing in-situ core samples



Figure 6-3 Crushed in-situ soil



Figure 6-4 Conditioning oven dried and crushed soil with its in-situ moisture content



Figure 6-5 Jet grouting tank wrapped with thick plastic



Figure 6-6 Compacting soil in different layers in jet grouting tank



Figure 6-7 Extracting soil samples from reconstructed and compacted soil



Figure 6-8 Reconstructed soil with a center jetting hole in jet grouting tank



Figure 6-9 Uniaxial compression strength on reconstructed soil specimens

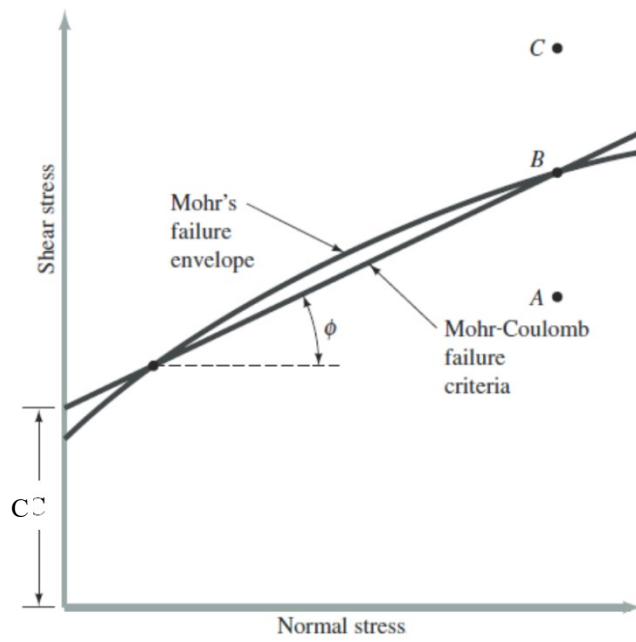


Figure 6-10 Mohr's failure envelope and Mohr-Coulomb failure envelope (Das 2008)

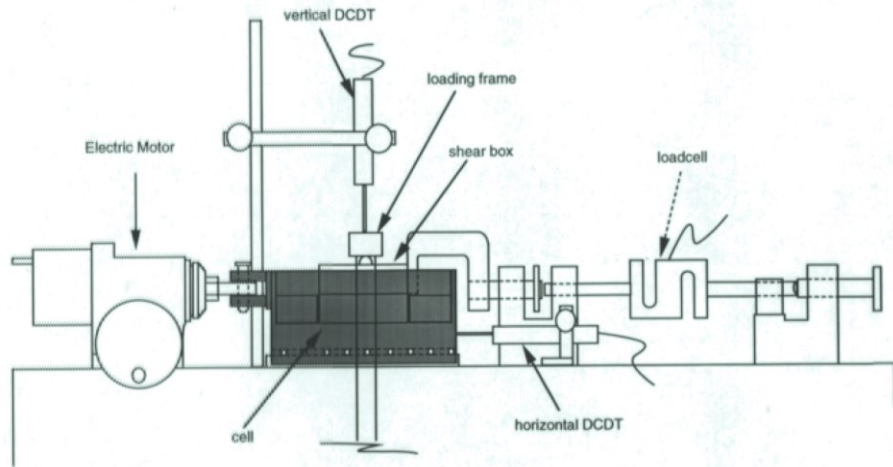


Figure 6-11 Schematic drawing of direct shear apparatus (Olson 2004)



Figure 6-12 Direct shear test on reconstructed soil specimens

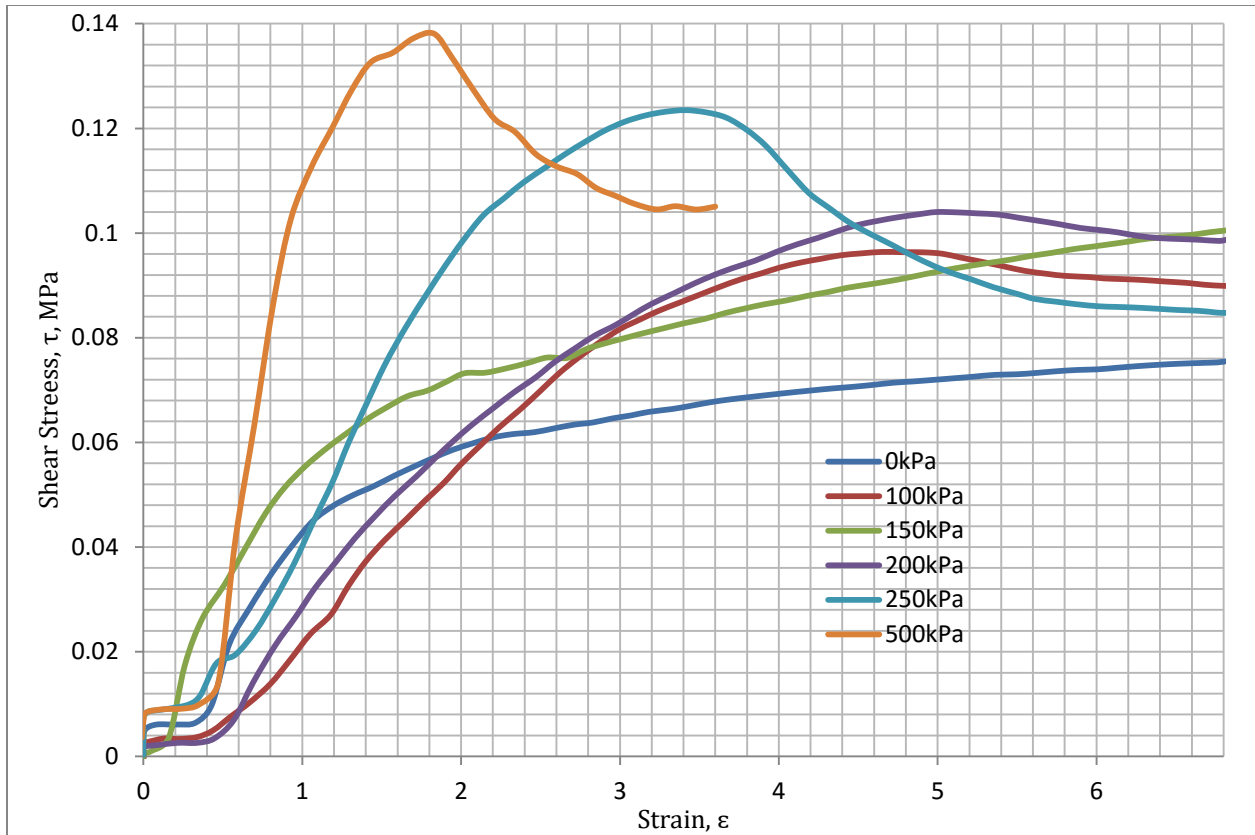


Figure 6-13 Shear stress versus shear strain in direct shear test on reconstructed soil specimens

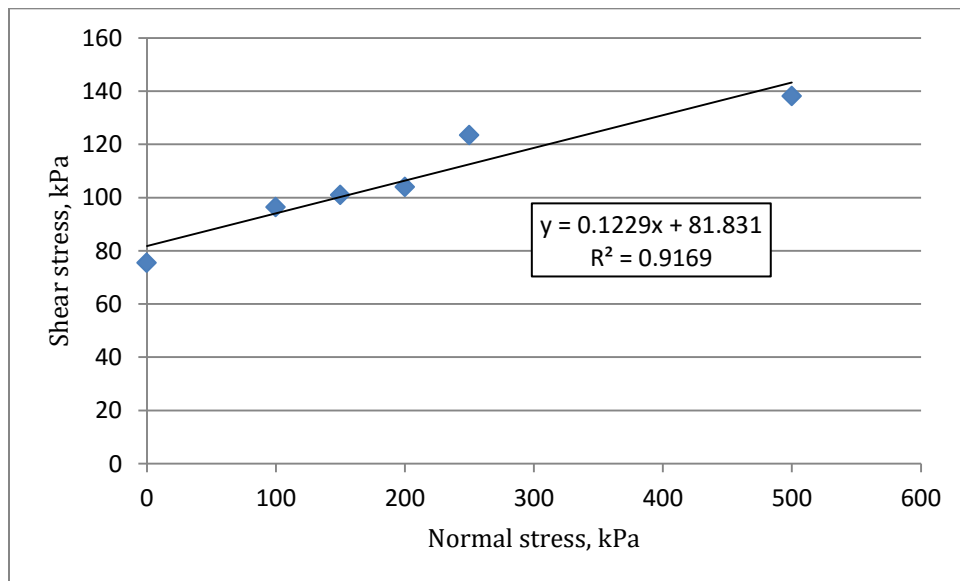


Figure 6-14 shear stress vs normal stress in direct shear test on reconstructed soil specimens



Figure 6-15 Laboratory jet grouting operation



Figure 6-16 Soilcrete mixture in laboratory jet grouting tank



Figure 6-17 Cores extracted from soilcrete body in jet grouting tank

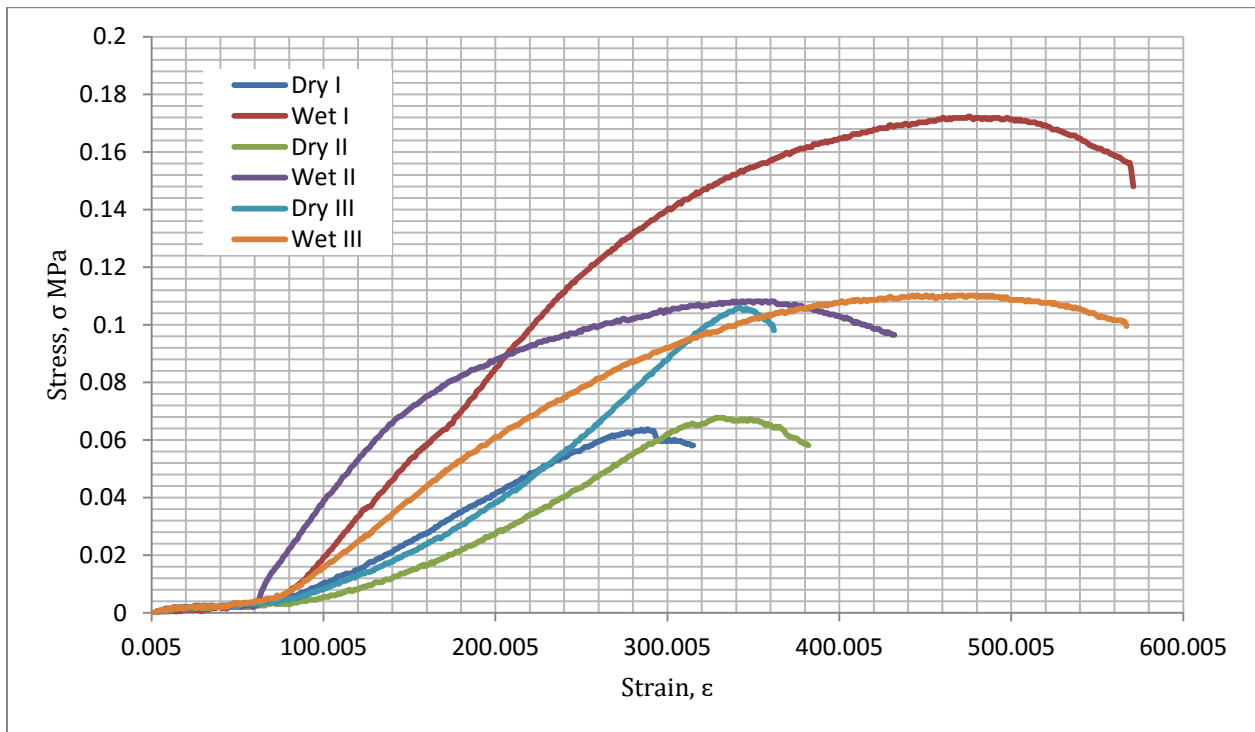


Figure 6-18 UCS of 56 day hardened thermal-insulating grout

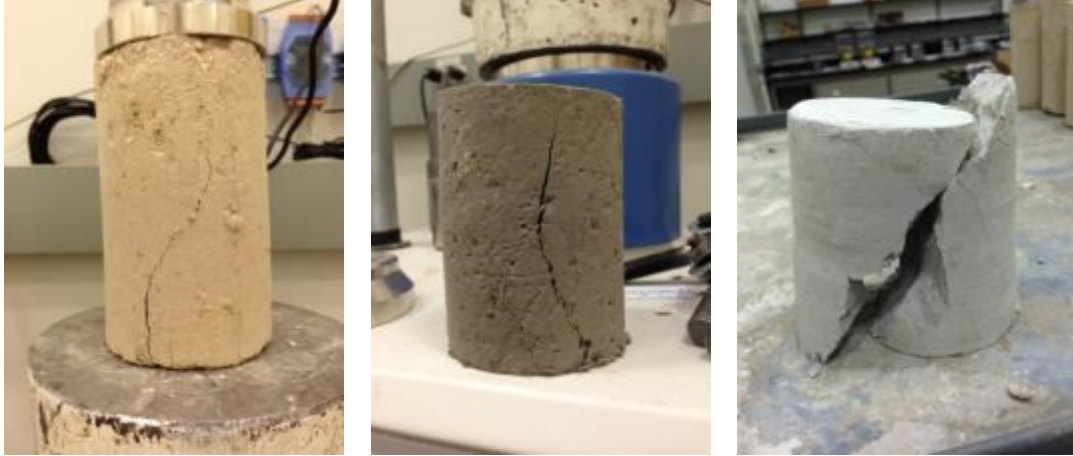


Figure 6-19 Unconfined compressive strength test on soilcrete cores



Figure 6-20 STS test on soilcrete cores

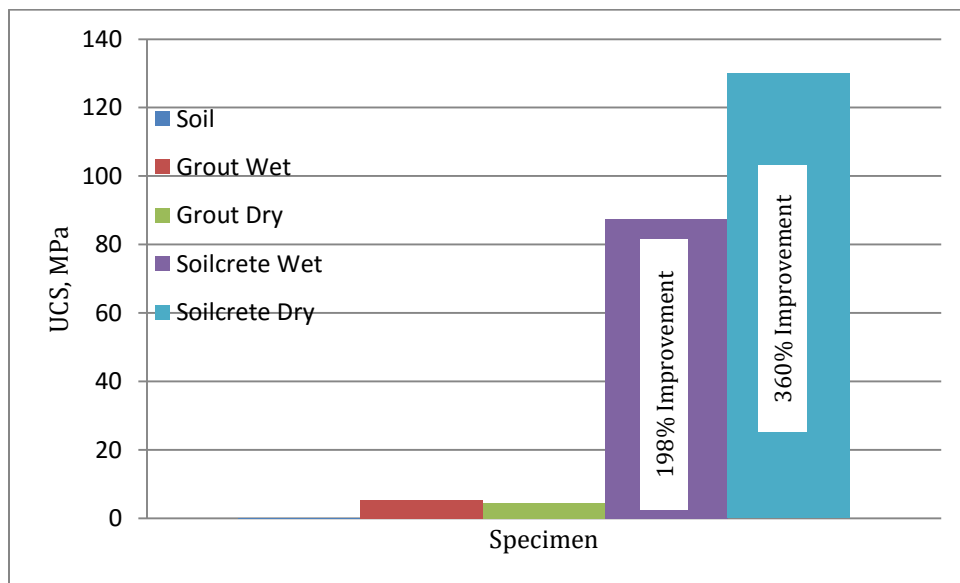


Figure 6-21 UCS of soilcrete and grout versus soil

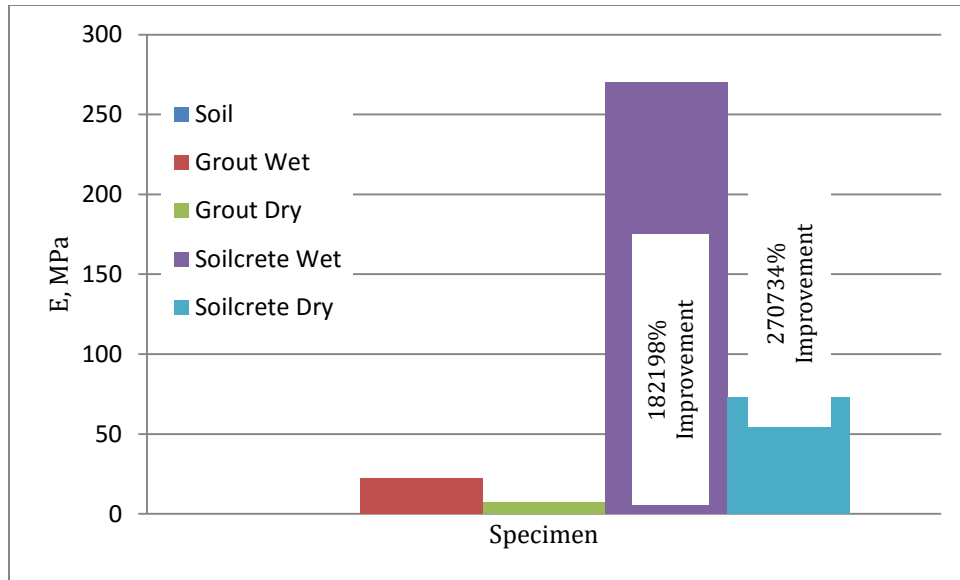


Figure 6-22 Modulus of elasticity of soilcrete and grout versus soil



Figure 6-23 Direct shear test on soilcrete cores

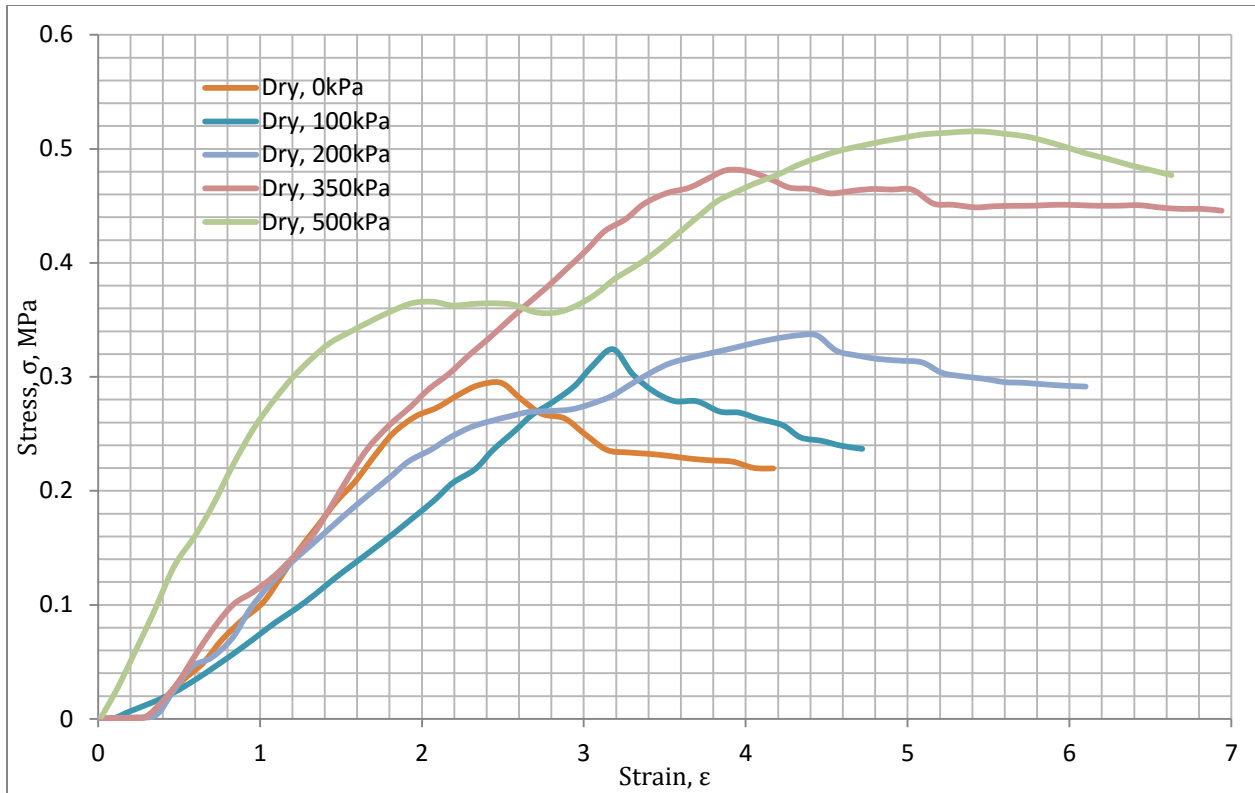


Figure 6-24 Shear stress versus shear strain in direct shear test on soilcrete specimens in dry condition

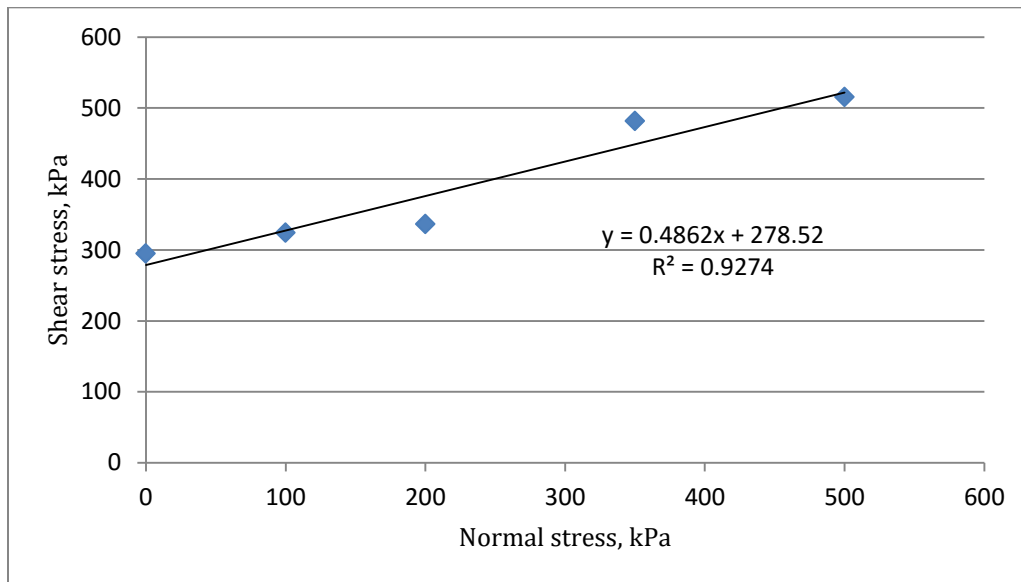


Figure 6-25 shear stress vs normal stress in direct shear test on soilcrete specimens in dry condition

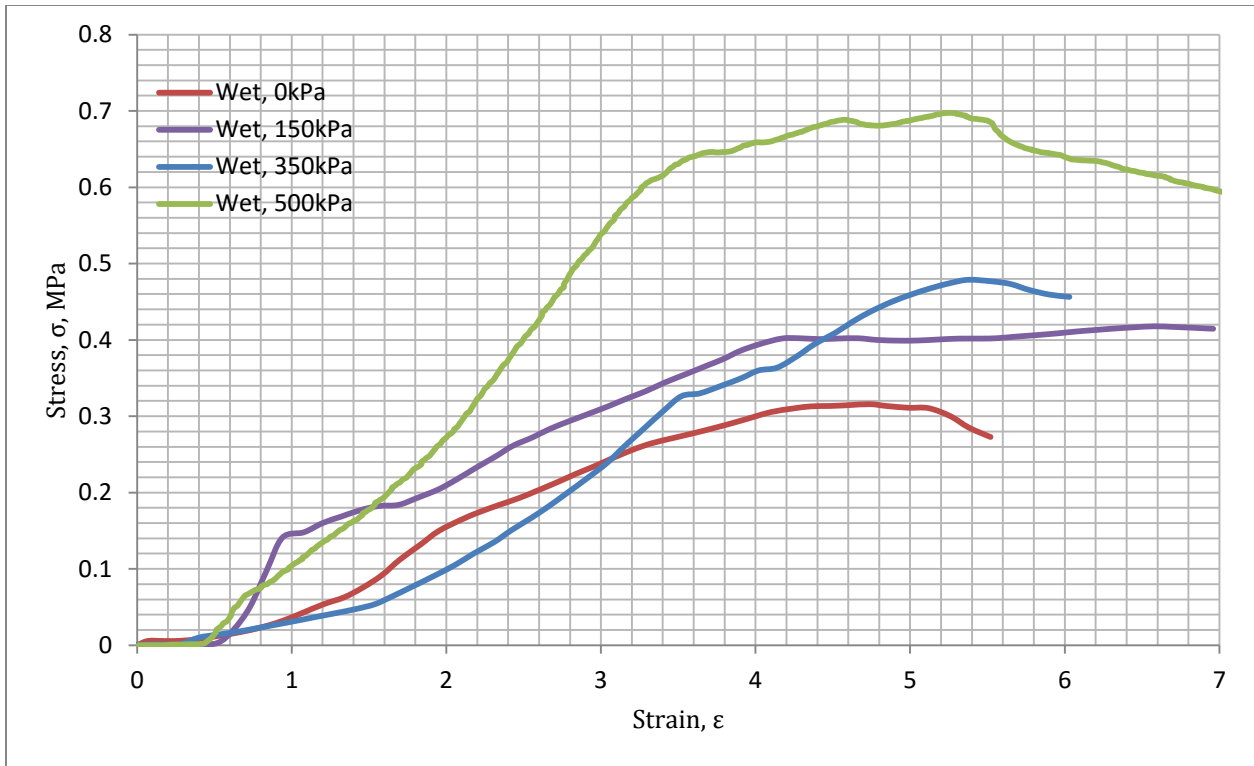


Figure 6-26 Shear stress versus shear strain in direct shear test on soilcrete specimens in wet condition

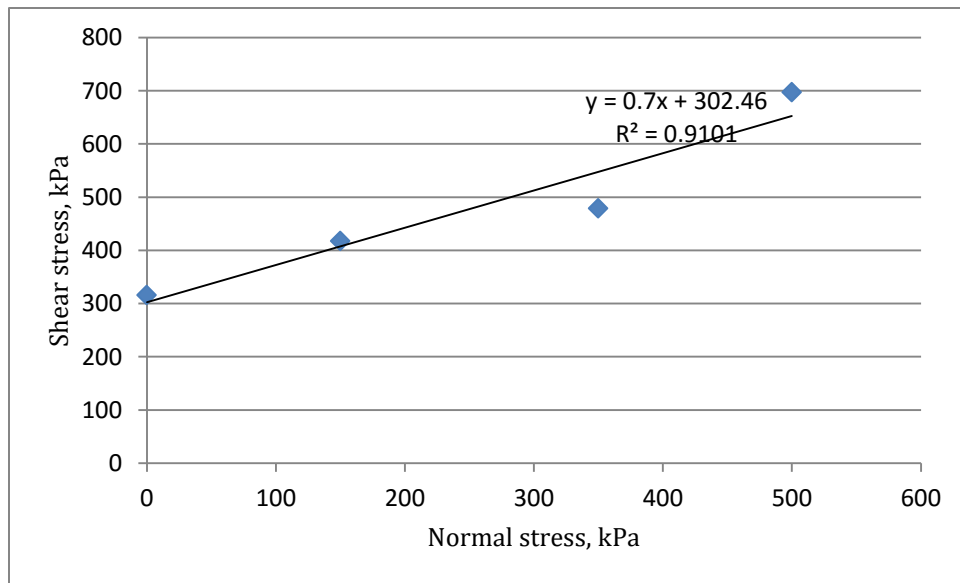


Figure 6-27 shear stress vs normal stress in direct shear test on soilcrete specimens in wet condition

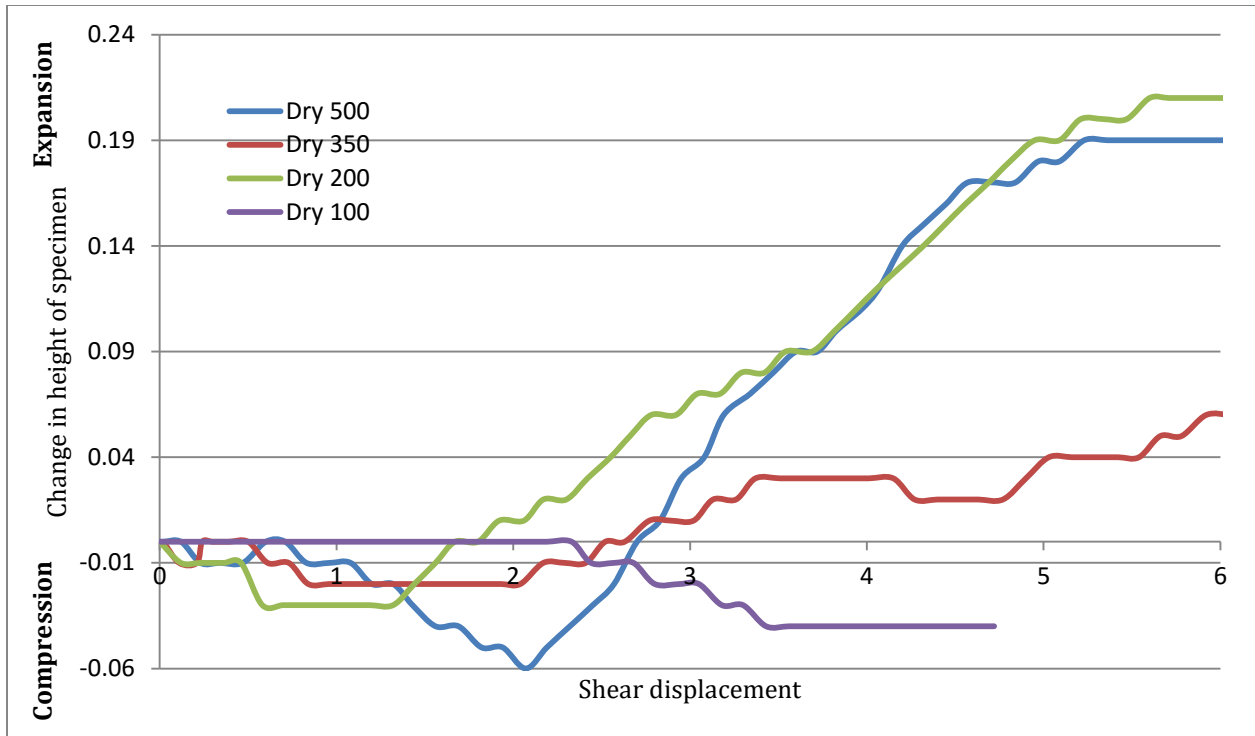


Figure 6-28 Shear displacement versus change in height of the soilcrete specimen in dry condition

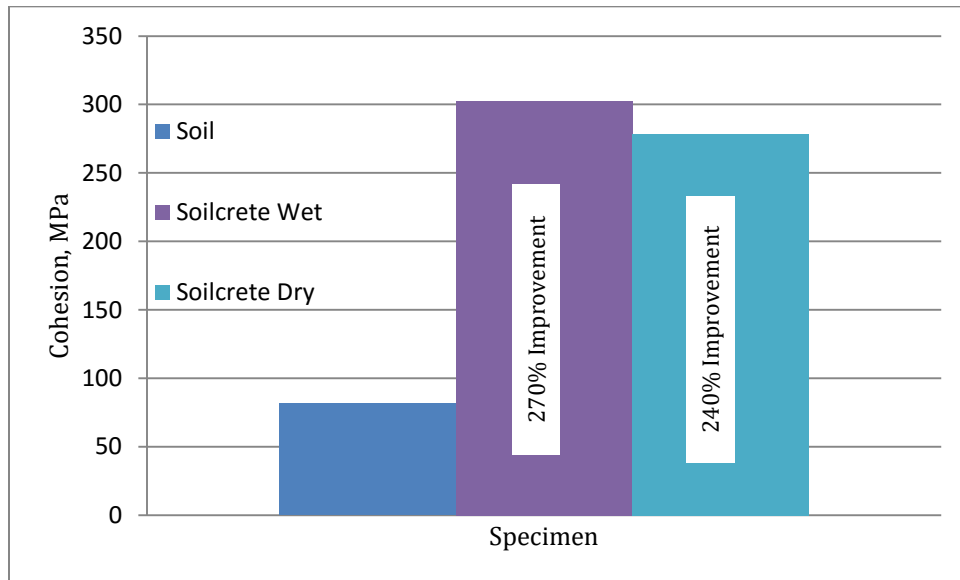


Figure 6-29 Cohesion of soil versus soilcrete in wet and dry condition

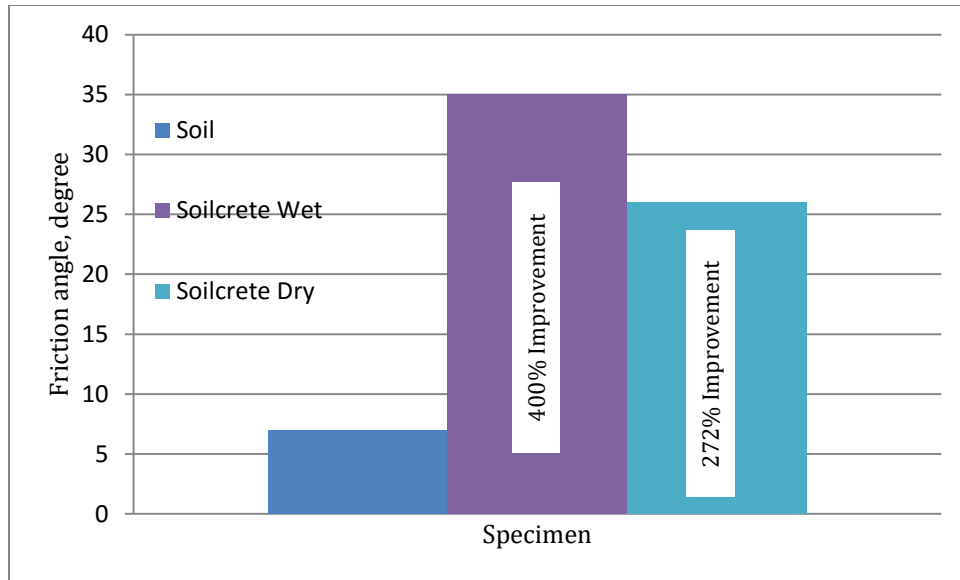


Figure 6-30 Friction angle of soil versus soilcrete in wet and dry condition

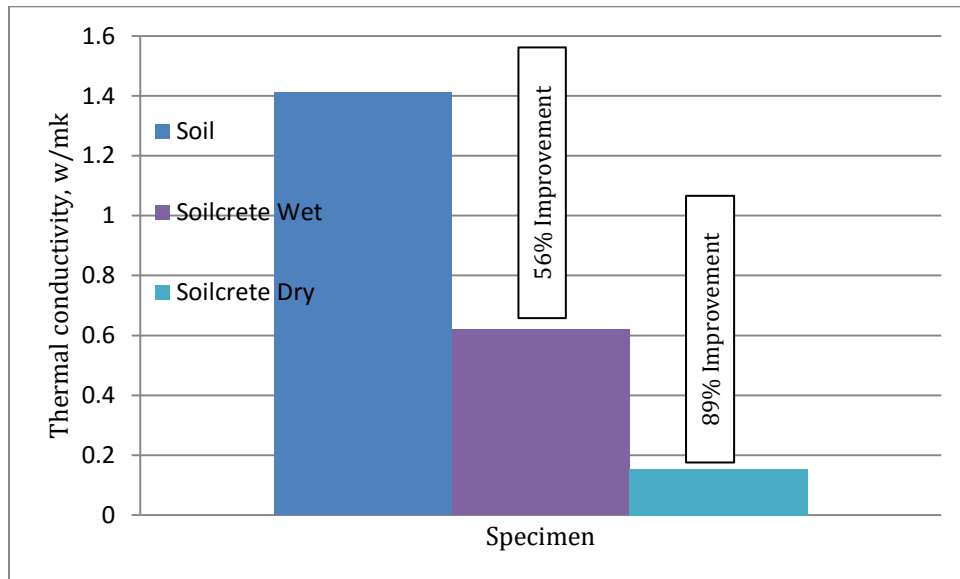


Figure 6-31 Thermal conductivity of soil versus soilcrete in wet and dry condition

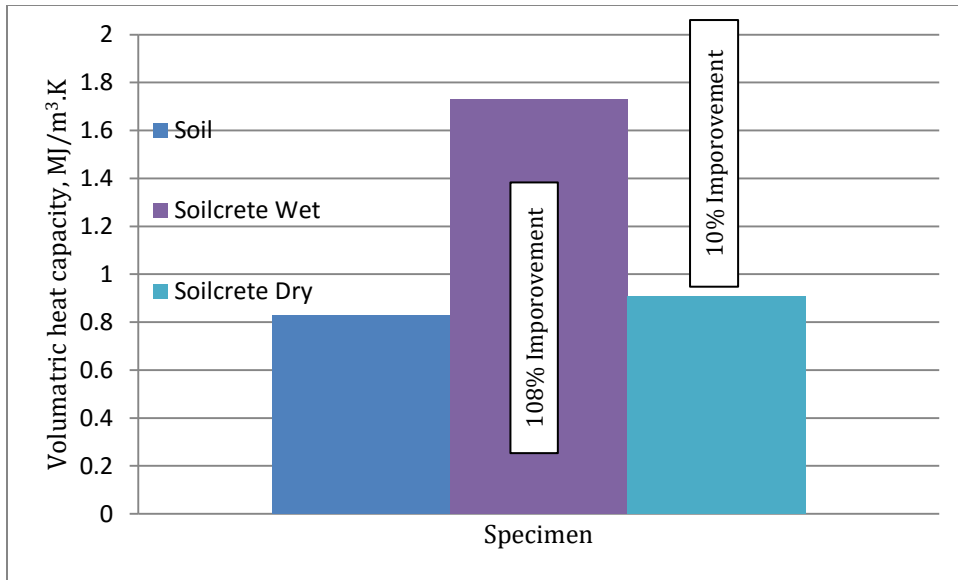


Figure 6-32 Volumetric heat capacity of soil versus soilcrete in wet and dry condition

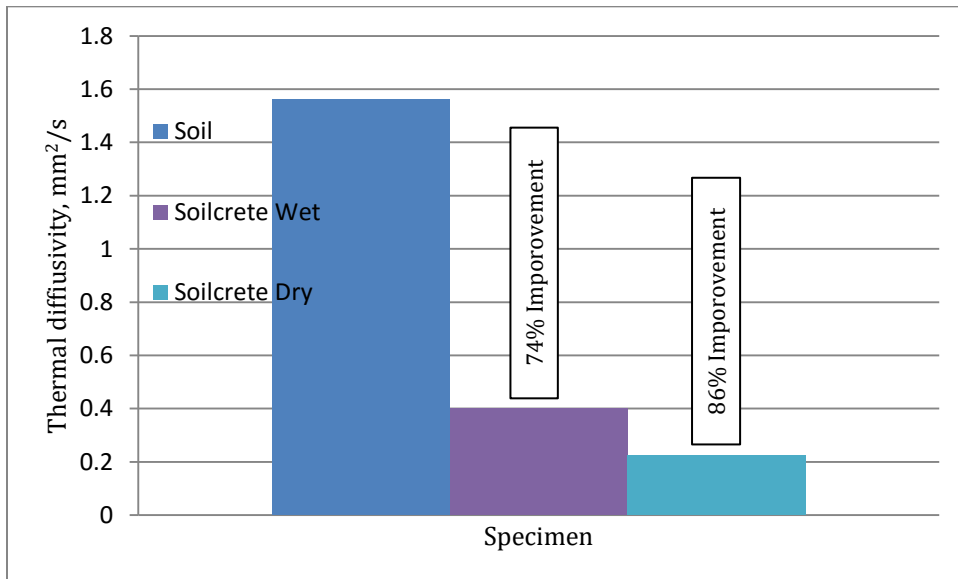


Figure 6-33 Thermal diffusivity of soil versus soilcrete in wet and dry condition

Chapter 7 CONCLUSION

This chapter contains the summary of the research and its contributions, as well as concluding statements and recommendations for future research in both jet grouting technique and its thermal-insulating concept.

7-1. Research summary

One of the obstacles preventing the wide usage of underground thermal energy storage (UTES) technology is that many soils exhibit high thermal conductivity. Generally, having soil with high thermal conductivity is an advantage to charge the borefield enclosure in borehole thermal energy storage (BTES) at early stages of a project. However, high thermal conductive soil will accelerate the amount of heat that escapes from the borefield enclosure. Consequently, most of the heat injected into the borefield will escape from the borefield enclosure. To increase the performance of the UTES, the amount of heat that flows into the surrounding media must be reduced. The current research was designed to create thermal-insulating barriers for underground energy enclosures in UTES projects. The barriers will keep the heat inside the enclosure and increase the UTES performance. A main goal of the research was to use the jet grouting technique to develop thermal-insulating soilcrete that would have lower thermal conductivity and greater strength than in-situ soil.

Chapter two and three looked at the basics of the UTES and the jet grouting technique, respectively. It is necessary to conduct a field trial operation to investigate the performance of jet grouting. However, trial field jet grouting operations can be time-consuming and expensive, and don't always lead to desired results. Therefore, in Chapter four, a proposal was made to design and manufacture a laboratory jet grouting setup with almost the same performance ability as the field equipment but with reduced footprint and cost.

Chapter five details the steps taken to hand-mixed the thermal-insulating soilcrete. Five thermal-insulating grouts were mixed with different proportions of water, cement and expanded light perlite (ELP). Thermal-insulating grouts were mixed and cast with appropriate proportions of the soil, based on the theoretical definition of the jet grouting technique. Extensive laboratory tests were conducted on the physical, mechanical, and thermal properties of the hand-mixed soilcrete to select an optimal thermal-insulating grout. The laboratory results were verified using literature values and findings.

Chapter six describes the jet grouting test that was implemented on reconstructed in-situ soil in the jet grouting tank to validate the results of hand-mixed soilcrete in Chapter five. The performance of the laboratory jet grouting setup were verified using well-documented literature about jet grouting projects in Chapter three.

7-2. Conclusions

Although detailed conclusions were discussed in each chapter, more general conclusions are summarized here:

- 1) An optimal thermal-insulating grout was developed with different proportions of ELP, water and cement. Thermal-insulating soilcrete was created by injecting thermal-insulating grout into the reconstructed soil using laboratory jet grouting setup. The mechanical and thermal properties of the soilcrete were improved significantly with respect to in-situ soil.
- 2) The values of the fresh grout density as well as the unconfined compression strength (UCS) and thermal conductivity of hand-mixed and actual soilcrete specimens were in agreement with the values reported in the literature.
- 3) The thermal conductivity of actual soilcrete with respect to its value in soil was improved 56% and 89% in wet and dry conditions, respectively.
- 4) Field jet grouting operations are implemented around the perimeter of the borefield and heat is injected into the borefield enclosure. This led to a dry condition for the laboratory experiments. The effect on the soil was that its ability to conduct heat through its structure is reduced by 89% and consequently the performance of the UTES will be improved. Also, the improvement ratios of volumetric heat capacity and heat diffusivity indicated that increasing the temperature of soilcrete required more energy than increasing the temperature of in-situ soil.
- 5) The UCS of the actual soilcrete in wet and dry conditions was 198% and 360% more than its value in soil. The modulus of elasticity (E) of actual soilcrete compared to its value in soil indicated a structural change from the soil state into more elastic behavior in soilcrete. Also, the cohesion and friction angle of soilcrete in dry conditions increased 240% and 272% compared to its original value in soil.

- 6) The thermal and strength properties of hand-mixed soilcrete specimens were validated with actual soilcrete properties with a maximum variance of 14% in dry conditions.
- 7) The performance of laboratory jet grouting setup was verified using literature values about soilcrete diameter. Also, the strength of the actual soilcrete was in agreement with the value reported in the literature.
- 8) A theoretical equation was proposed to calculate the actual soilcrete properties based on the experiment using hand-mixed soilcrete. However, the equation must be validated if any other jet grouting system or grout mixture is to be used in the future. Also, it is strongly recommended to carry out an actual jet grouting operation either in the laboratory with real soil properties and ground conditions, or a trial jet grouting where the trial is applicable.

7-3. Contributions

There are four main outcomes of the current research that will have an enormous impact on jet grouting and the UTES industry: the complete design approach of the jet grouting procedure to calculate engineering properties of soilcrete; laboratory setup of the jet grouting equipment; development of the thermal-insulating grout mixture; and development of thermal-insulating soilcrete elements. The following two sections describe the most important contributions of the research:

- 1) In municipal areas where there is neither space to carry out trial jet grouting, nor a budget for a feasibility study, a laboratory setup with jet grouting equipment can be used as an in-situ trial operation. Such a setup would make it possible to answer a variety of questions about the effectiveness of the system in achieving particular criteria and soil treatment effectiveness in terms of physical, mechanical, and/or thermal properties of soilcrete. It would also provide information about operational parameters to achieve specific column diameter, effectiveness of spoil material return, and costing.

- 2) The UTES system is an integral component required to increase the use of renewable fuels and energy for decentralized utilities. Many communities in Canada will be producing their own energy by harvesting solar, wind or other renewable energies and storing the excess underground for later use. Improving the efficiency of the UTES systems will also improve the reliability of renewable energy sources. Creating thermal-insulating soilcrete elements by implementing field jet grouting around the perimeter of a borefield using an optimal thermal-insulating grout mixture will increase efficiency of UTES systems. The heat that flows into the surrounding ground will be reduced and the system's charging time with a particular energy source will be accelerated. This technology will reduce Canada's reliance on fossil fuels and its carbon footprint.

7-4. Availability of similar equipment around the world

Based on the literature review, there are only two laboratory jet grouting setups in the world which simulate the single fluid jet grouting system. They were designed and manufactured by the Massachusetts Institute of Technology in 2005 and the University of Cambridge in 2008. Many simplifications in comparison with actual field single fluid system were considered in those setups. In Cambridge, for instance, a two-dimensional setup was used to inject only water in one direction without rotating. At MIT, the operational parameters were less than the field values and only rotational or vertical displacement was possible at the same time.

7-5. Recommendations for future research

Alberta has an incredibly rich oil reserve of 171.3 billion barrels which is valued by the Province, Canada and the world ("Oil Sands Economic Benefits" 2011). There is enough oil in Alberta's oil sands to meet Canada's current oil demand for almost 400 years. These oil reserves play an important role in the Canadian and global economy by supplying stable and reliable energy to the world. It is estimated that every dollar invested in Alberta's oil sands creates about \$9 of economic activity ("Alberta's Oil Sands: The Facts" 2011). The Canadian Energy Research Institute estimates that oil sands will create more than \$307 billion in tax revenue across Canada over the next 25 years ("Oil Sands Economic Benefits" 2011). Currently, oil sands are extracted by surface and in-situ mining methods (Gosselin et al. 2010). Surface mining techniques require mine wastes to be stored. Currently, storage is implemented by pumping tailings mixed with

water into large settling basins called tailings ponds (“Alberta’s Oil Sands: The Facts” 2011). On many occasions, the failure of tailing ponds or dykes has had a tremendous impact on the environment and human lives. Sometimes the failure of tailing pond or dykes is caused by a failure of the foundations on which these structures are built. An example of a base-metal tailings dam failure due to weak foundations occurred at Los Frailes, Spain, in 1998. The failure allowed acidic tailings water and sulphide-rich tailings solids to flow rapidly through the breach and downstream towards a national park and the ocean (Figure 7-1) (Mech 2011). The failure was caused by the foundation movement and was not related to earthquakes, blasting, acid drainage, etc. (Mech 2011).

In-situ mining is used where oil sands deposits are more than 150 meters deep (Gosselin et al. 2010). Compared to surface mining, this method recovers less bitumen, requires more energy to create steam, and contributes greatly to greenhouse gas emissions (GHG) (Gosselin et al. 2010). Underground mining is another method for extracting oil sands. It has more advantages than other methods. It requires less energy than in-situ methods and does not disturb the land as much as surface mining does. As most oil sands reserves are located at depths greater than 150 meters, underground mining will become a preferred method in the near future to recover oil sands (“Alberta’s Oil Sands: opportunity. balance,” 2008). However, oil sands should be recovered in such a manner that the disturbed land can be reclaimed and risks to people and the environment are minimized. To excavate oil sands using underground mining methods, soil layers located at the planned roofs of underground excavations must be solidified. To use surface mining methods, dykes enveloping tailing ponds should be stabilized and must prevent tailings from leaking into the environment.

Jet grouting has great potential to be used in Alberta in various mining and civil engineering applications. It can be used in various soil types, from the finest to the coarsest grained soils as well as oil sands; it can be used to strengthen the foundations underneath the tailings dykes; and/or it can be used to strengthen the unstable weak roofs in oil sands underground mining. However, although jet grouting has been used in civil engineering projects where the ground properties are fairly well understood, oil sands materials have different mechanical and physical properties than well-known materials such as clays, sands, and silts. Also, the types of grout used in civil engineering projects are designed for most common soils. Before applying jet grouting in the oil sands industry, it is necessary to develop methods to reduce the cost and understand the

parameters of jet grouting operations. Investigating the following parameters on different properties of soilcrete will contribute to a fundamental understanding of jet grouting, which can be applied in the oil sands mining industries: the effect of air pressure around grout nozzles; effect of air pressure around water; effect of rotational and withdrawal rates; and effect of jet grouting on different soil types. Designing the most suitable grouts for different types of oil sands materials can be another objective of future research. Designing the most suitable jet grouting nozzle for breaking oil sands structures to inject the bonding medium can be also an objective of future research. With the current setup, a laboratory experiment can be carried out to investigate the effect of various jetting parameters and grout types on different soils and oil sands, and consequently determine the engineering properties of the soilcrete. This will make it possible to compute the volume of grout needed to build up the soilcrete columns by determining the diameter, which will increase the understanding of the parameters in jet grouting operations, increase oil sands operations safety and decrease the overall costs of civil and oil sands projects. Implementing jet grouting around tailing dams will also help to protect the Canadian environment from tailing pond failures.

Regarding the thermal-insulating soilcrete, a 3D finite element model is being developed by the author's colleague at the Department of Civil and Environmental Engineering (University of Alberta) under the supervision of Dr. D. Apel to study the improvement performance of the BTES using the developed thermal-insulating soilcrete in the current study.



Figure 7-1 Los Frailes tailing dam failure (Mech 2011)

BIBLIOGRAPHY

- “Alberta’s Oil Sands: Opportunity. Balance.” 2008. *JWP Publishing, Joey Podlubny, Alberta, Canada.* Developments in Environmental Science. Elsevier.
- “Alberta’s Oil Sands: The Facts.” 2011. *Government of Alberta, Canada.* www.oilsands.alberta.ca
- Alsayedahmad, Mohammad Taha. 1992. “Properties of Cement Based Grouts and Soilcrete and Applications of Jet Grouting.”
- Alzamora, Daniel, Mark H Wayne, and Jie Han. “PERFORMANCE OF SRW SUPPORTED BY GEOGRIDS AND.” *PERFORMANCE CONFIRMATION OF CONSTRUCTED FACILITIES, ASCE:* 456–466.
- Andromalos, K.B., and H.N. Gazawy. 1986. “Jet Grouting: Snail’s Pace of Adoption.” *Civil Engineering:* 40–43.
- Andromalos, Kenneth B, and Eric W Bahner. 2003. “The Application of Various Deep Mixing Methods for Excavation Support Systems.” In *Proceedings of the Third International Conference: Grouting And Ground Treatment, February 10, 2003 - February 12, 2003*, 120 I, 515–526. New Orleans, LA, United states: American Society of Civil Engineers.
- Andromalos, Kenneth B, and Herff N Gazaway. 1989. “Jet Grouting to Construct a Soilcrete Wall Using a Twin Stem System.” In *Foundation Engineering: Current Principles and Practices, June 25, 1989 - June 29, 1989*, 301–312. Evanston, IL, USA: Publ by ASCE.
- “Application of Ground Improvement : Jet Grouting:” 1–7. [http://www.scribd.com/doc/133977927/Asoc-Japonesa-Del-Jet-Grouting.](http://www.scribd.com/doc/133977927/Asoc-Japonesa-Del-Jet-Grouting)
- Arora, S, and J Kinley. 2011. “Jet Grouting for the Re-Support of Pier 11A in San Diego, CA.” In *2011 Conference on Coastal Engineering Practice, August 21, 2011 - August 24, 2011*, 56–63. San Diego, CA, United states: American Society of Civil Engineers (ASCE). doi:10.1061/41190(422)6.
- ASCE. 2009. “JET GROUTING GUIDELINE.”
- Aschieri, F., M. Jamiolkowski, and R. Tornaghi. 1983. “Case History of a Cut-off Wall Executed by Jet Grouting.” In *Proceedings of 8th European Conference on Soil Mechanics and Foundation Engineering, Helsinki 23-26 May*, Vol 1, 121–126.
- ASTM D3080. 2014. “Standard Test Method for Direct Shear Test of Soils Under Consolidated Drained.” *ASTM Geotechnical Testing Journal:* 1–9. doi:10.1520/D3080.
- ASTM:C138/C138M-13. 2013. “Standard Test Method for Density (Unit Weight), Yield, and Air Content (Gravimetric).” *ASTM International:* 23–26. doi:10.1520/C0138.
- ASTM:C192/C192M-13. 2013. “Standard Practice for Making and Curing Concrete Test Specimens in the Laboratory.” *ASTM International:* 1–8. doi:10.1520/C0192.
- ASTM:C332-09. 2009. “Standard Specification for Lightweight Aggregates for Insulating Concrete.” *ASTM International:* 9–11. doi:10.1520/C0332-09.2.
- ASTM:C39/C39M-12a. 2012. “Standard Test Method for Compressive Strength of Cylindrical Concrete Specimens.” *ASTM International:* 1–7. doi:10.1520/C0039.

- ASTM:C469/C469M-10. 2010. "Standard Test Method for Static Modulus of Elasticity and Poisson' S Ratio of Concrete in Compression." *ASTM International*: 1–5. doi:10.1520/C0469.
- ASTM:C496/C496-11. 2011. "Standard Test Method for Splitting Tensile Strength of Cylindrical Concrete Specimens." *ASTM International*. doi:10.1520/C0496.
- ASTM:C642-13. 2013. "Standard Test Method for Density, Absorption, and Voids in Hardened Concrete." *ASTM International*: 4–6. doi:10.1520/C0642-13.5.
- ASTM:C702/C702M-11. 2011. "Standard Practice for Reducing Samples of Aggregate to Testing Size." *ASTM International*: 1–5. doi:10.1520/C0702.
- ASTM:C939-10. 2010. "Standard Test Method for Flow of Grout for Preplaced-Aggregate Concrete (Flow Cone Method)." *ASTM International*: 9–11. doi:10.1520/C0939-10.2.
- ASTM:C940-10a. 2010. "Standard Test Method for Expansion and Bleeding of Freshly Mixed Grouts for Preplaced-Aggregate Concrete in the Laboratory." *ASTM International*: 1–3. doi:10.1520/C0940-10a.2.
- ASTM:D2166/D2166M-13. 2013. "Standard Test Method for Unconfined Compressive Strength of Cohesive Soil 1." *ASTM International*: 1–7. doi:10.1520/D2166.
- ASTM:D2216-10. 2010. "Standard Test Methods for Laboratory Determination of Water (Moisture) Content of Soil and Rock by Mass." *ASTM International2*: 1–7. doi:10.1520/D2216-10.2.
- ASTM:D2487-11. 2011. "Standard Practice for Classification of Soils for Engineering Purposes (Unified Soil Classification System)." *ASTM International*. doi:10.1520/D2487-11.
- ASTM:D421-85. 2007. "Standard Practice for Dry Preparation of Soil Samples for Particle-Size Analysis and Determination of Soil Constants." *ASTM International*.
- ASTM:D422-63. 2007. "Standard Test Method for Particle-Size Analysis of Soils." *ASTM International*: 1–8.
- ASTM:D4318-10. 2010. "Standard Test Methods for Liquid Limit, Plastic Limit, and Plasticity Index of Soils." *ASTM International*. doi:10.1520/D4318-10.
- ASTM:D5102-09. 2009. "Standard Test Methods for Unconfined Compressive Strength of Compacted Soil-Lime Mixtures." *ASTM International*: 1–7. doi:10.1520/D5102-09.the.
- ASTM:D6910/D6910M-09. 2009. "Standard Test Method for Marsh Funnel Viscosity of Clay Construction Slurries." *ASTM International*. doi:10.1520/D6910.
- ASTM:D698-12. 2012. "Standard Test Methods for Laboratory Compaction Characteristics of Soil Using Standard Effort." *ASTM International*: 1–13. doi:10.1520/D0698-12.1.4.
- ASTM:D7263-09. 2009. "Standard Test Methods for Laboratory Determination of Density (Unit Weight) of Soil Specimens." *ASTM International*: 1–7. doi:10.1520/D7263-09.2.
- ASTM:D75/D75M-09. 2009. "Standard Practice for Sampling Aggregates." *ASTM International*: 1–6.
- ASTM:D854-10. 2010. "Standard Test Methods for Specific Gravity of Soil Solids by Water Pycnometer." *ASTM International*. doi:10.1520/D0854-10.2.

- Atwood, M.j., and R. Lambrechts. 1995. "A Test Program to Verify Grouting Applicability for Boston's Central Artery Tunnel." *Verification of Geotechnical Grouting, ASCE Geotechnical Special Publication 57*: 42–55.
- Ayoubian, Alireza, and Verya Nasri. 2004. "Design of Jet Grout Plugs for Base Stability and Groundwater Control." In *Geotechnical Engineering for Transportation Projects: Proceedings of Geo-Trans 2004, July 27, 2004 - July 31, 2004*, 126 II, 1905–1914. Los Angeles, CA, United states: American Society of Civil Engineers.
- Barker, C. R., and B. P. Selberg. 1978. "Water Jet Nozzle Performance Tests." In *Proceedings of the Fourth International Symposium on Jet Cutting Technology, Canterbury, UK*, A1–1–A1–20.
- Baumann, V. 1984. "On the Excution of Soil Improvement Method Utilizing Water Jet." In *Proceedings of the International Symposium on Water Jet Technology, Tokyo, Japan, Dec 6th*.
- Bedenis, Timothy H, Larry P Jedele, and Steve Maranowski. 2005. "Underpinning of Drilled Shafts Using Jet Grouting." In *Geo-Frontiers 2005, January 24, 2005 - January 26, 2005*, 130th–142nd ed., 1751–1760. Austin, TX, United states: American Society of Civil Engineers.
- Bell, F G. 1993. *Engineering Treatment of Soils*. London ; New York : E & FN Spon, 1993.
- Bergado, D.T., L.R. Anderson, N. Miura, and A.S. Balasubramaniam. 1996. "Soft Ground Improvement in Lowland and Other Environments." *ASCE Press, New York*: 234–304.
- Berry, G.l., J.n. Shirlaw, K. Hayata, and S.h. Tan. 1988. "A Review of Grouting Techniques Utilised for Bored Tunnelling with Emphasis on the Jet Grouting Method." *CONSTRUCTION & BUILDING MATERIALS 2* (1): 34–41.
- Boehm, Dennis W. 2004. "The Utilization of Jet Grouting and Soil Mixing Methods to Repair and Support Bulkhead Structures." In *Port Development in the Changing World, PORTS 2004, Proceedings of the Conference, May 23, 2004 - May 26, 2004*, 947–956. Houston, TX, United states: American Society of Civil Engineers.
- Boehm, Dennis W., and Thomas A. Posey. 2003. "Super Jet Grouting Repairs and Extends the Life of Ailing Coastal Front Structure." *Grouting 2003, ASCE*: 330–341.
- Bolen, W. P. 2004. "Perlite." *U.S. Geological Survey*.
- Botto, G. 1985. "Developments in the Techniques of Jet Grouting." In *XII Ciclo Di Conferenze Di Geotecnica, Torino, Reprint by Trevi*.
- Bottomley, P. 1985. "The Reduction in Heat Flow due to the Insulation of Rock Surfaces in Mine Airways." In *2nd US Mine Ventilation Symposium. Reno, NV*.
- Brandstatter, C, R Lackner, and H A Mang. 2005. "In Situ Temperature Measurements Provide New Insight into the Performance of Jet Grouting." *Ground Improvement 9* (4): 163–167. doi:10.1680/grim.2005.9.4.163.
- Bregola, Andrew F, and Bradford W Roberts. 2003. "Jet Grout Foundations to Resist Compressive, Uplift and Lateral Loads at an Operational Power Plant." In *Proceedings of the Third International Conference: Grouting And Ground Treatment, February 10, 2003 - February 12, 2003*, 120 I, 428–439. New Orleans, LA, United states: American Society of Civil Engineers.
- Brill, Gary T, George K Burke, and Alan R Ringen. 2003. "A Ten-Year Perspective of Jet Grouting: Advancements in Applications and Technology." In *Proceedings of the Third International Conference: Grouting And*

- Ground Treatment, February 10, 2003 - February 12, 2003*, 120 I, 218–235. New Orleans, LA, United states: American Society of Civil Engineers.
- Broid, I.J., M.F. Khasin, L.I. Malyshev, Y.V. Alecsandrovsky, V.V. Burenkova, and V.S. Istomina. “Jet Grout Method and Cut-off Walls Stability.” In *Proceedings of the 10th International Conference on Soil Mechanics and Foundation Engineering, Stockholm*, vol 1, 397–399.
- Brouk, J. J. 1949. “Perlite Aggregate: Its Properties and Uses.” *Journal of the American Concrete Institute* 46: 185–190.
- Bruce, D.A., and M.E.C. Bruce. 2003. “The Practitioner’s Guid to Deep Mixing.” In *Proceedings of Rapid Excavation and Tunneling Conference*, 474–488.
- Bruce, Donald A, Dennis L Boley, and Francesco Gallavresi. 1987. “NEW DEVELOPMENTS IN GROUND REINFORCEMENT AND TREATMENT FOR TUNNELLING.” In *Proceedings of Rapid Excavation and Tunneling Conference*, 2:811–835. Proceedings - Rapid Excavation and Tunneling Conference. Nicholson Construction Co., Bridgeville, PA, USA, Nicholson Construction Co, Bridgeville, PA, USA: Soc of Mining Engineers of AIME.
- BSEN12716:2001. 2001. “Execution of Special Geotechnical Works - Jet Grouting, The European Standard.”
- Burke, G K. 2007. “Vertical and Horizontal Groundwater Barriers Using Jet Grout Panels and Columns.” In *Geo-Denver 2007: New Peaks in Geotechnics, February 18, 2007 - February 21, 2007*, 168th ed. Denver, CO, United states: American Society of Civil Engineers. doi:10.1061/40912(231)8.
- Burke, G K, D M Cacoilo, and K R Chadwick. 2000. “SuperJet Grouting: New Technology for in Situ Soil Improvement.” *Transportation Research Record* (1721): 45–53.
- Burke, G.k. 1992. “In Situ Containment Barriers and Collection Systems for Environmental Applications.” In *Symposium on Design and Construction of Slurry Walls, Canadian Geotechnical Society, Toronto*.
- . 1995. “Applying Jet Grouting Techniques to Construct Vertical and Horizontal Barriers.” *International Containment Technology Workshop, Baltimore, MD*.
- Burke, G.K., and G.t. Brill. 1992. “Foundation Stabilization Systems Using Jet Grouting Techniques.” In *Proceedings of the Ohio River Valley Seminar XXIII, Louisville, KY*.
- Burke, G.k., and G.t. Brill. 1993. “Anchored Cutoff Design and Construction.” In *Proceedings of the Third International Conference on Case Histories in Geotechnical Engineering, University of Missouri-Rolla*, 1313–1318.
- Burke, G.K., R.A. Heller, and L.F. Johnsen. 1989. “Jet Grouting for Underpinning: The Cutting Edge.” *Geotechnical News* 7 (1): 25–28.
- Burke, G.k., and M.a. Koelling. 1995. “Special Applications for Jet Grouting: Underpinning, Excavation Support and Gropundwater Control.” In *Proceedings of 48th Canadian Geotechnical Conference, Vancouver, BC*, 89–97.
- Burke, G.K., and D.A. Meffe. 1991. “Fixing Foundations.” *Civil Engineering*: 63–65.
- Burke, G.K., J.H. Peterson, and M.L. Smith. “Superjet Grouting and the Quality of Its Product.” *Grouting and Ground Modification*: 111–125.

- Burke, George K. 2004. "Jet Grouting Systems: Advantages and Disadvantages." In *GeoSupport 2004 - Drilled Shafts, Micropiling, Deep Mixing, Remedial Methods, and Specialty Foundation Systems, Proceedings of Sessions of the Geosupport Conference: Innovation and Cooperation in the Geoindustry, January 29, 2004 - January 31, 2004*, 124th ed., 875–886. Orlando, FL, United states: American Society of Civil Engineers.
- Burke, George K, Lawrence F Johnsen, and Robert A Heller. 1989. "Jet Grouting for Underpinning and Excavation Support." In *Foundation Engineering: Current Principles and Practices, June 25, 1989 - June 29, 1989*, 291–300. Evanston, IL, USA: Publ by ASCE.
- Burson, B., A. Baker, B. Jones, and J. Shailer. 1997. "Developing and Installing a Vertical Containment System." *Geotechnical Fabrics Report* 15 (3): 39– 44.
- Bzówka, Joanna. 2004. "COMPUTATIONAL MODEL FOR JET-GROUTING PILE – SOIL INTERACTION." *Studia Geotechnica et Mechanica* XXVI (3): 1–44.
- Carletto, Marcos Francisco Wosgrau. 2009. "Jet Grouting (Sistema Monofluide): UM MÉTODO TEÓRICO SIMPLIFICADO PARA A PREVISÃO DO DIÂMETRO DAS COLUNAS." Escola Politecnica da Universidade de Sao Paulo, Sao Paulo, Brasil, Agosto.
- Carreto, J. R. 2000. "Jet Grouting. Uma Tecnica Em Desenvolvimento." In *VII Congresso Nacional de Geotecnia*, 1043–1054.
- Carroll, J O, R Flanagan, N Loganathan, and D Ratty. 2004. "A Correlation between Energy Input and Quality for Jet Grouting in Marine Clay." *Tunnelling and Underground Space Technology* 19 (4-5) (July): 502. doi:10.1016/j.tust.2004.02.099.
- Carter, Ernie, and Frank Webber. 2007. "Jet Grouting with Molten Wax for in-Situ Encapsulation of Radioactive Beryllium Waste." In *Geo-Denver 2007: New Peaks in Geotechnics, February 18, 2007 - February 21, 2007*, 168th ed. Denver, CO, United states: American Society of Civil Engineers. doi:10.1061/40912(231)9.
- Casagrande. 2012. "Improvement of the Mechanical Characteristics of Soils by Jet Grouting." www.casagrandegroup.com.
- CEB-FIP. 1991. "Model Code 1990. Comite Euro-International Du Beton, Vienna,."
- CEN. 2004. "CEN. Eurocode 2: Design of Concrete Structures - Part 1-1: General Rules and Rules for Buildings." *European Committee for Standardization, Brussels*.
- Chen, John Y L, Robin M Lim, and Kyle Furuhashi. 2011. "Jet-Grouting in Cohesive Soils for Ground Improvement in Hawaii." In *GeoRisk 2011: Geotechnical Risk Assessment and Management, June 26, 2011 - June 28, 2011*, 224 GSP, 578–585. Atlanta, GA, United states: American Society of Civil Engineers (ASCE). doi:10.1061/41183(418)57.
- Chernyakov, a. V. 2009. "Evaluation of Dynamic Loads on Underground Structures during Horizontal Jet Grouting of a Saturated Soil." *Soil Mechanics and Foundation Engineering* 46 (3) (August 20): 108–116. doi:10.1007/s11204-009-9055-y.
- Ciullo, P. A. 1996. "The Industrial Minerals." In *Industrial Minerals and Their Uses: A Handbook and Formulary*. Westwood, New Jersey, Noyes Publication.
- Collotta, Tiziano, Andrea Frediani, and Vittorio Manassero. 2004. "Features and Results of a Jet-Grouting Trial Field in Very Soft Peaty Soils." In *GeoSupport 2004 - Drilled Shafts, Micropiling, Deep Mixing, Remedial Methods, and Specialty Foundation Systems, Proceedings of Sessions of the Geosupport Conference*:

- Innovation and Cooperation in the Geoindustry, January 29, 2004 - January 31, 2004*, 124th ed., 887–901. Orlando, FL, United states: American Society of Civil Engineers.
- Cong-jiao, Zhang, Zhang Shi-bao, and Fan Feng-shan. 2011. “Application of High Pressure Jet Grouting Technology in the Seepage Control of Earth Dam Reinforcement.” *Advanced Materials Research* 291-294: 3259–3263. doi:10.4028/www.scientific.net/AMR.291-294.3259.
- Coomber, D. B. 1985. “Tunneling and Soil Stabilization by Jet Grouting.” In *Proceeding of Symposium on Tunneling, Brighton, England, IMM*, paper 22.
- Coulter, S, and C D Martin. 2006. “Single Fluid Jet-Grout Strength and Deformation Properties.” *Tunnelling and Underground Space Technology* 21 (6): 690–695. doi:10.1016/j.tust.2005.12.136.
- Coulter, S., and C.D. Martin. 2006. “Effect of Jet-Grouting on Surface Settlements above the Aeschertunnel, Switzerland.” *Tunnelling and Underground Space Technology* 21 (5) (September): 542–553. doi:10.1016/j.tust.2005.07.005.
- Coulter, Steven, and C Derek Martin. 2004. “Ground Deformations Above a Large Shallow Tunnel Excavated Using Jet Grouting.” In *Proceeding of ISRM Regional Symposium EUROCK 2004 and 53rd Geomechanics Colloquy. Edited by W. Schubert*, 1:155–160.
- Coulter, Steven Ninian Patrick. 2004. “Influence of Tunnel Jet-Grouting on Ground Deformations at the Aeschertunnel, Switzerland.” University of Alberta.
- Cristelo, Nuno, Stephanie Glendinning, and Amandio Teixeira Pinto. 2011. “Deep Soft Soil Improvement by Alkaline Activation.” *Proceedings of the Institution of Civil Engineers: Ground Improvement* 164 (2): 73–82. doi:10.1680/grim.900032.
- Croce, P, and A Flora. 2000. “Analysis of Single-Fluid Jet Grouting.” *Geotechnique* 50 (6): 905–906.
- Croce, P, and G Modoni. 2007. “Design of Jet-Grouting Cut-Offs.” *Ground Improvement* 11 (1): 11–19. doi:10.1680/grim.2007.11.1.11.
- Croce, P., A. Chisari, and T. Merletti. 1990. “Indagini Sui Trattamenti Dei Terreni Mediante Jet-Grouting per Le Fondazioni Di Alcuni Viadotti Autostradali (in Italian).” *Rassegna Dei Lavori Pubblici* 1 (12): 249–260.
- Croce, P., and A. Flora. 1998. “Jet Grouting Effects on Pyroclastic Soil.” *Revista Italiana Di Geotecnica* 2: 5–14.
- Croce, P., A. Flora, and G. Modoni. 2001. “Experimental Investigations of Jet Grouting.” *Geotechnical Special Publication* 113: 245–252.
- Croce, P., A. Gaio, L. Mongiovì, and A. Zaninetti. 1994. “Una Verifica Sperimentale Degli Effetti Della Gettiniezione.” In *Rivista Italiana Di Geotecnica, XXVIII, No. 2., (in Italian)*, 91 – 101.
- Croce, Paolo, Giuseppe Modoni, and Giacomo Russo. 2004. “Jet-Grouting Performance in Tunnelling.” *GeoSupport 2004* (January 23): 910–922. doi:10.1061/40713(2004)78.
- CSA:A23.1-09/A23.2-09. 2009. “Concrete Materials and Methods of Concrete construction/Test Methods and Standard Practices for Concrete.” *Canadian Standards Association*.
- Dabbagh, Ali Asghar, Alcibiades Serrano Gonzalez, and Antonio Soriano Pena. 2002. “Soil Erosion by a Continuous Water Jet.” *Soils and Foundations* 42 (5): 1–13.

- Das, Braja M. 2008. *Fundamentals of Geotechnical Engineerin*. Stamford, CT. : Cengage Learning, c2008.
- Dash, Umakant, Thomas S Lee, and Randy Anderson. 2003. “Jet Grouting Experience at Posey Webster Street Tubes Seismic Retrofit Project.” In *Proceedings of the Third International Conference: Grouting And Ground Treatment, February 10, 2003 - February 12, 2003*, 120 I, 413–417. New Orleans, LA, United states: American Society of Civil Engineers.
- Davie, John, Mehmet Piyal, Armagan Sanver, and Bahattin Tekinturhan. 2003. “Jet Grout Columns Partially Support Natural Draft Cooling Tower.” In *Proceedings of the Third International Conference: Grouting And Ground Treatment, February 10, 2003 - February 12, 2003*, 120 I, 365–376. New Orleans, LA, United states: American Society of Civil Engineers.
- Davie, John R, Mehmet Piyal, Armagan Sanver, and Bahattin Tekinturhan. 2003. “Jet Grout Columns Support Major Power Plant Structures.” In *12th PanAmerican Conference on Soil Mechanics and Geotechnical Engineering, ASCE GeoInstitute, Cambridge, MA*.
- Day, Steven R, Stephen J Zarlinski, and Peter Jacobson. 1997. “Stabilization of Cadmium-Impacted Soils Using Jet-Grouting Techniques.” In *Proceedings of the 1997 ASCE Annual Fall National Convention, October 5, 1997 - October 8, 1997*, 71st ed., [d]388–402. Minneapolis, MN, USA: ASCE.
- De Paoli, Battista, Renato Tornaghi, and Donald A Bruce. 1989. “Jet Grout Stabilization of Peaty Soils under a Railway Embankment in Italy.” In *Foundation Engineering: Current Principles and Practices, June 25, 1989 - June 29, 1989*, 272–290. Evanston, IL, USA: Publ by ASCE.
- “Difficult Foundation Problems Solved by Jet Grouting:” 1–4.
- DLSC. 2015. “Drake Landing Solar Community.” [Http://dlsc.ca/data/DLSC48.swf](http://dlsc.ca/data/DLSC48.swf).
- Drooff, Eric R, Allen J Furth, and Jessee A Scarborough. 1995. “Jet Grouting to Support Historic Buildings.” In *Proceedings of the Conference of the Geotechnical Engineering Division of the ASCE in Conjunction with the ASCE Convention, October 22, October 26*, 42–55. Geotechnical Special Publication. Hayward Baker Inc, Odenton, United States: ASCE.
- Druss, David L. 2003. “Guidelines for Design and Installation of Soil-Cement Stabilization.” In *Proceedings of the Third International Conference: Grouting And Ground Treatment, February 10, 2003 - February 12, 2003*, 120 I, 527–539. New Orleans, LA, United states: American Society of Civil Engineers.
- Durgunoglu, H T, H F Kulac, K Oruc, R Yildiz, J Sickling, I E Boys, T Altugu, and C Emrem. 2003. “A Case History of Ground Treatment with Jet Grouting against Liquefaction, for a Cigarette Factory in Turkey.” In *Proceedings of the Third International Conference: Grouting And Ground Treatment, February 10, 2003 - February 12, 2003*, 120 I, 452–463. New Orleans, LA, United states: American Society of Civil Engineers.
- Durgunoglu, H T, H F Kulac, S Yilmaz, and D Kocak. 2003. “Case History for Soil Improvement of SETAT 2002 High Rise Residential by Jet Grouting in Istanbul.” In *Proceedings of the Third International Conference: Grouting And Ground Treatment, February 10, 2003 - February 12, 2003*, 120 I, 377–388. New Orleans, LA, United states: American Society of Civil Engineers.
- Duzceer, Rasin, and Alp Gokalp. 2003. “Construction and Quality Control of Jet Grouting Applications in Turkey.” In *Proceedings of the Third International Conference: Grouting And Ground Treatment, February 10, 2003 - February 12, 2003*, 120 I, 281–293. New Orleans, LA, United states: American Society of Civil Engineers.
- Edgerton, W.w., D.j. Berti, and M.m. Wong. 1995. “San Francisco CSO.” *Civil Engineering* 68-71.

- Engineering, T. 2015. "The Engineering Toolbox." *Http://www.engineeringtoolbox.com/thermal-Conductivity-d_429.html*.
- Essler, R. D. 1995. "Applications of Jet Grouting in Civil Engineering." *Geological Society, London, Engineering Geology Special Publications* 10 (1) (January 1): 85–93. doi:10.1144/GSL.ENG.1995.010.01.06.
- Essler, R., and H. Yoshida. 2004. "Chapter Jet Grouting." In *Taylor & Francis, Second Edition*, 160–196.
- Fang, Y S, C C Kao, J Chou, K F Chain, D R Wang, and C T Lin. 2006. "Jet Grouting with the Superjet-Midi Method." *Ground Improvement* 10 (2): 69–76.
- Fang, Yung-Show, Lin-Yao Kuo, and Da-Rong Wang. 2004. "Properties of Soilcrete Stabilized with Jet Grouting." In *The Fourteenth International Offshore and Polar Engineering Conference - ISOPE 2004, May 23, 2004 - May 28, 2004*, 696–702. Toulon, France: International Society of Offshore and Polar Engineers.
- Fang, Yung-Show, Jyh-Jong Liao, and Shaw-Chi Sze. 1994. "An Empirical Strength Criterion for Jet Grouted Soilcrete." *Engineering Geology* 37 (3-4): 285–293.
- Farouki, Omar T. "Thermal Properties of Soils Relevant to Ground Freezing, Design Echniques for Their Estimation." *Department of Civil Engineering, Queen's University*: 139–146.
- . 1986. *Thermal Properties of Soils*. Series on Rock and Soil Mechanics: 11. Clausthal-Zellerfeld: Trans Tech, 1986.
- Flick, Loren D, Nigel B R Osborn, A.E.'Ted' Graham, Michael J Marasa, and Frank T Tobey III. 1992. "Minipile Milestone in Memphis." *Civil Engineering* 62 (9): 46–49.
- Flora, A, G P Lignola, and G Manfredi. 2007. "A Semi-Probabilistic Approach to the Design of Jet Grouted Umbrellas in Tunnelling." *Ground Improvement* 11 (4): 207–217. doi:10.1680/grim.2007.11.4.207.
- Foundations, Bilfinger Berger. 2012. "Jet Grouting." *Bilfinger Berger Foundations*. www.foundation-engineering.bilfingerberger.com.
- Frank, J. N., D. E. Fogelson, and J. W. Chester. 1972. "Hydraulic Mining in the USA." In *Proceedings of the First International Symposium on Jet Cutting Technology, Coventry, UK*, E4–45–E4–60.
- Franz, Raymond J, and Kyle E Camper. 2003. "Jet Grout Columns in Mixed Profile to Control Foundation Settlement Gerald Ratner Athletics Center." In *Proceedings of the Third International Conference: Grouting And Ground Treatment, February 10, 2003 - February 12, 2003*, 120 I, 389–400. New Orleans, LA, United states: American Society of Civil Engineers.
- Furth, Allen, Bob Gordon, and Dan Dobbels. 2003. "Hard Rock Tunneling Stabilization Using Jet Grouting Techniques." In *Rapid Excavation and Tunneling Conference*, 494–499. United states: Society for Mining, Metallurgy and Exploration.
- Gainé, Kenneth, and Aidan Duffy. 2010. "A Life Cycle Cost Analysis of Large-Scale Thermal Energy Storage Technologies for Buildings Using Combined Heat and Power." In *Zero Emission Buildings - Proceedings of Renewable Energy Conference*, 49–60. Trondheim, Norway A.
- GALLAVRESI, F. 1992. "GROUTING IMPROVEMENT OF FOUNDATION SOILS." In *Proceedings of the 1992 ASCE Specialty Conference on Grouting, Soil Improvement and Geosynthetics*, 1:1–38.

- Ganeshan, V., and J.Y. Yang. 2009. "Jet Grouting and Its Applications." In *Ground Improvement Technologies and Case Histories, ISGI09 Techn. Session; December 9-11, Singapore, Geotechnical Society of Singapore*, 209–220.
- Garner, S.J., M.k. Lee, B.I. Kilpatrick, and J.k. Lou. 1989. "The Application of Flexible Jet Grout for a Cutoff at John Hart Dam." In *Proceedings of the 42nd Canadian Geotechnical Conference*, 249–256.
- Gazaway, herff n., and Brian h. Jasperse. 1992. "Jet Grouting in Contaminated Soils." In *Proceedings of the 1992 ASCE Specialty Conference on Grouting, Soil Improvement and Geosynthetics, February 25, 1992 - February 28, 1992*, 30th ed., 1:206–214. New Orleans, LA, USA: Publ by ASCE.
- Gazzarrini, Paolo, Matt Kokan, and Stephen Jungaro. 2005. "Case History of Jet-Grouting in British Columbia. Underpinning of CN Rail Tunnel in North Vancouver." *Geotechnical News* 23 (4): 47–54.
- Gemmi, Bruno, Gianfranco Morelli, and F A Bares. 2003. "Geophysical Investigations to Assess the Outcome of Soil Modification Work." In *Proceedings Of The Third International Conference: Grouting And Ground Treatment, February 10, 2003 - February 12, 2003*, 120 II, 1490–1506. New Orleans, LA, United states: American Society of Civil Engineers.
- Gens, A, A Di Mariano, J M Gesto, and H Schwarz. 2006. "Ground Movement Control in the Construction of a New Metro Line in Barcelona." In *5th International Conference of TC28 of the International Society for Soil Mechanics and Geotechnical Engineering, ISSMGE, June 15, 2005 - June 17, 2005*, 389–395. Amsterdam, Netherlands: Taylor & Francis - Balkema.
- "GeoEng Consultants." *GeoEng Consultants, Specialist Civil and Geotechnical Consulting Engineers*. [http://www.geoss.sg/documents/seminar/GeoSS Event Seminar 30 june 2009_slide.pdf](http://www.geoss.sg/documents/seminar/GeoSS%20Event%20Seminar%2030%20june%202009_slide.pdf).
- Godfrey, K.A., and JR. 1987. "Water Jets: Concrete Yes, Tunneling Maybe." *Civil Engineering Magazine*.
- Gosaburo, M. 1985. "The Newest Techniques on Chemical Grouting and Jet Grouting." In *Symposium on Recent Developments in Ground Improvement Techniques, Bangkok, 29 Nov. - 3Dec.*, 279–288.
- Gosselin, Pierre, Steve E. FRSC (Chair) Hrudey, M. Anne Naeth, André Plourde, René Therrien, Glen Van Der Kraak, and Zhenghe Xu. 2010. "The Royal Society of Canada Expert Panel: Environmental and Health Impacts of Canada's Oil Sands Industry."
- Greenwood, D. 1987. "Underpinning by Grouting." *Ground Engineering Magazine*.
- Gronauer, R. W. 1972. "High Pressure Plunger Pumps." In *Proceedings of the First International Symposium on Jet Cutting Technology, Coventry, UK, C2–13–C2–20*.
- Grosso Sembenelli, P, and G Sembenelli. 1999. "Deep Jet-Grouted Cut-Offs in Riverine Alluvia for Ertan Cofferdams." *Journal of Geotechnical and Geoenvironmental Engineering* 125 (2): 142–153. doi:10.1061/(asce)1090-0241(1999)125:2(142).
- GSS. 2012. "Borehole Thermal Energy Storage Economic Value Analysis."
- Guatteri, G. "Advances in the Construction and Design of Jet Grouting Methods in South America." In *Proceedings of the Second International Conference on Case Histories in Geotechnical Engineering, St. Louis, MO*.
- Guatteri, G., R. koshima, A. lopes, A. Ravaglia, and M.R. Pieroni. 2009. "Historical Cases and Use of Horizontal Jet Grouting Solutions with 360 ° Distribution and Frontal Septum to Consolidate Very Weak and Saturated

Soils.” *Geotechnical Aspects of Underground Construction in Soft Ground – Ng, Huang & Liu (eds)*: 287–293.

Haider, Tarek F, and Michael J Byle. 2000. “Verification of Jet Grouting for Structure Rehabilitation.” In *ASCE Geo-Institute Specialty Conference on Performance Confirmation of Constructed Geotechnical Facilities - Performance Confirmation of Constructed Geotechnical Facilities, GSP 94, April 9, 2000 - April 12, 2000*, 300:441–454. Amherst, MA, United states: American Society of Civil Engineers. doi:10.1061/40486(300)30.

Harris, D., C.e. Wooden, and G.p. Motl. 1992. “Application of Jet Grouting as an Insitu Technology for the White Oak Creek Embankment Time Critical Rempval Action.” In *Proceedings of Eighth Annual Oak Ridge Model Conference on Waste Management and Environmental Resoation, Oak Ridge, TN*.

Hashimoto, T., B. Ye, and G.I. Ye. 2009. “Construction Method , Ground Treatment , and Conditioning for Tunneling.” *Geotechnical Aspects of Underground Construction in Soft Ground – Ng, Huang & Liu (eds)*: 99–107.

HBI. 2004. “Jet Grouting.” *Hayward Baker Inc.* www.HaywardBaker.com.

HBI, D B Coomber, Reporter A L Bell, Bilfinger Berger Foundations, and D.a. Bruce. 1994. “Jet Grouting.” *Ground Control and Improvement, Xanthakos, Abramson and Bruce, Eds, John Wiley and Sons, Inc., New York, N.Y.* www.foundation-engineering.bilfingerberger.com.

Ho, C E, and S Hu. 2006. “Numerical Analysis of Jet Grout Elements for Braced Excavation in Soft Clay.” In *GeoCongress 2006, February 26, 2006 - March 1, 2006*, 2006:260. Atlanta, GA, United states: American Society of Civil Engineers. doi:10.1061/40803(187)260.

Ho, C E, C H Lim, and C G Tan. 2002. “Characteristics of Bored Piles Installed through Jet Grout Layer.” *Journal of Performance of Constructed Facilities* 16 (4): 160–168. doi:10.1061/(asce)0887-3828(2002)16:4(160).

Ho, C. E. 2008. “Investigation of Parameter Variability on Jet Grout Column Formation.” In *2nd BGA International Conference on Foundations, Dundee*, 1357–1368.

Ho, C. E., C. G. Tan, and C. H. Lim. 2001. “Strength Increase in Soft Clay Surrounding Jet Grouted Soil Mass.” *Geotechnical Special publication* 2 113: 395–409.

Ho, C.e. 1995. “An Instrumented Jet Grouting Trial in Soft Marine Clay.” *ASCE Geotechnical Special Publication* 57: 101–115.

———. 2010. “Jet Grout Dike for Temporary Excavation Support in Soft Clay.” In *2010 Earth Retention Conference (ER2010)*, 400–407.

Ho, Chu E. 2007. “Fluid-Soil Interaction Model for Jet Grouting.” *Geo-Denver: New Peaks in Geotechnics, Grouting for Ground Improvement, ASCE*: 1–10.

———. 2011. “Evaluation of Jet Grout Formation in Soft Clay for Tunnel Excavation.” In *Geo-Frontiers 2011: Advances in Geotechnical Engineering, March 13, 2011 - March 16, 2011*, 211 GSP, 3391–3400. Dallas, TX, United states: American Society of Civil Engineers (ASCE). doi:10.1061/41165(397)347.

Ho, Chu Eu. 2005. “Turbulent Fluid Jet Excavation in Cohesive Soil with Particular Application to Jet Grouting.” Massachusetts Institute of Technology.

———. 2009. “Analysis of Deep Jet Grouting Field Trial in Clay.” In *International Foundation Congress and Equipment Expo*, 233–240. ASCE.

- Ho, Chu Eu, Ching Heng Lim, and Chin Gee Tan. 2005. "Jet Grouting Applications for Large-Scale Basement Construction in Soft Clay." In *Geo-Frontiers 2005, January 24, 2005 - January 26, 2005*, 130th–142nd ed., 1695–1709. Austin, TX, United states: American Society of Civil Engineers.
- Ho, Chu Eu, and Chin Gee Tan. 2003. "Stabilization of Deep Open Excavations in Soft Soil by Jet Grouting." In *Proceedings of the Third International Conference: Grouting And Ground Treatment, February 10, 2003 - February 12, 2003*, 120 I, 269–280. New Orleans, LA, United states: American Society of Civil Engineers.
- Hong, Won-Pyo, Dong-Wook Kim, Mun-Ku Lee, and Geu-Guwen Yea. 2002. "Case Study on Ground Improvement by High Pressure Jet Grouting." In *Proceedings of the Twelfth (2002) International Offshore and Polar Engineering Conference, May 26, 2002 - May 31, 2002*, 12:610–615. Kitakyushu, Japan: International Society of Offshore and Polar Engineers.
- Horpibulsuk, S., N. Miura, and TS Nagaraj. 2003. "Assessment of Strength Development in Cement-Admixed High Water Content Clays with Abrams' Law as a Basis." *Geotechnique* 53 (4): 439–444.
- Houlsby, A. C. 1990. *Construction and Design of Cement Grouting, a Guide to Grouting in Rock Foundations*. John Wiley & Sons, Inc.
- Hsieh, Hsii-Sheng, Chien-Chih Wang, and Chang-Yu Ou. 2003. "Use of Jet Grouting to Limit Diaphragm Wall Displacement of a Deep Excavation." *Journal of Geotechnical and Geoenvironmental Engineering* 129 (2): 146–157. doi:10.1061/(asce)1090-0241(2003)129:2(146).
- Hurley, Thomas M. 2004. "Jet Grout Bottom Seal for Cut and Cover Tunnel." *North American Tunneling 2004, Ozdemir (ed) © Taylor & Francis Group, London, ISBN 90 5809 669 6*: 265–270.
- Hurley, Tom, and Richard Crockford. 2010. "Innovative Use of Jet Grouting for Earth Retention, Underpinning and Water Control." In *2010 Earth Retention Conference - Earth Retention Conference 3, August 1, 2010 - August 4, 2010*, 208 GSP, 384:417–428. Bellevue, WA, United states: American Society of Civil Engineers. doi:10.1061/41128(384)43.
- ISO22007-2. 2008. "Plastics — Determination of Thermal Conductivity and Thermal Diffusivity — Part 2: Transient Plane Heat Source (hot Disc) Method." *International Organization for Standardization*.
- Jefferis, S A. 1994. *Fresh Properties of Portland Cement Grouts*. Chapman & Hall 1994. Chapman & Hall.
- "Jet Grouting." *Cementation Foundation Skanska*. www.skanska.co.uk.
- Ji, Heng. 2008. "Physical Modelling of Jet Grouting Process." University of Cambridge.
- JJGA. 2005. "Japanese Jet Grout Association." *Jet Grout Design Manual , 13th Edition, Japan* (6th editi.
- Jongpradist, Pornkasem, Narongrit Jumlongrach, Sompote Youwai, and Somchai Chucheepsakul. 2010. "Influence of Fly Ash on Unconfined Compressive Strength of Cement-Admixed Clay at High Water Content." *Journal of Materials in Civil Engineering* 22 (1): 49–58. doi:10.1061/(asce)0899-1561(2010)22:1(49).
- Kamon, M., and D.T. Bergado. 1992. "Ground Improvement Techniques." In *Proceedings of 9th Asian Regional Conference on Soil Mechanics and Foundation Engineering, Bangkok*, Vol. 2, 526–546.
- Kanematsu, H. 1980. "High Pressure Jet Grouting Method." *Civil Construction* 21 (13).

- Kantrowitz, Ted, and Bruce McFarlane. 2012. "Canada's Heat Pump Association Congratulates an Alberta Integrated Energy Leader." Vol. 34. www.geoexchange.ca.
- Karol, R H. 2003. *Chemical Grouting and Soil Stabilization*. Civil and Environmental Engineering: 12. New York : M. Dekker, c2003.
- Kasai, A., K. Yamagishi, K. Komazawa, H. Ito, and A. Nunomura. 1979. "Fire-Retardant Boards Made of Pulp Sludge and Perlite, 5: The Effect of Thickness and Rock-Wool Fiber on the Flammability and Bending Strength of the Boards." *Journal of the Hokkaido Forest Products Research Institute*.
- Kauschinger, J.L., Rachid S M Hankour, E.B. B Perry, L Kauschinger, and M Joseph. 1992. "Methods to Estimate Composition of Jet Grout Bodies." *Grouting, Soil Improvement, and Geosynthetics: Proceeding of the Conference (geotechnical Special Publication) 1* (30). Geotechnical Special Publication: 194–205.
- Kauschinger, J.L., E.B. Perry, and R. Hankour. 1992. "Jet Grouting: State of the Practice." In *Proceedings of the 1992 ASCE Specialty Conference on Grouting, Soil Improvement and Geosynthetics*, 1:169–181.
- Kauschinger, J.L., and J.P. Welsh. 1989. "Jet Grouting for Urban Construction." *Geotechnical Lecture Series: Design Construction and Performance of Earth Support Systems, Boston Society of Civil Engineering, Massachusetts Institute of Technology, Cambridge, MA*.
- Kazemian, Sina, and Bujang B K Huat. 2009. "Assessment and Comparison of Grouting and Injection Methods in Geotechnical Engineering." *European Journal of Scientific Research* 27 (2): 234–247.
- Kazemian, Sina, and Bujang B K Huat. 2010. "Assessment of Stabilization Methods for Soft Soils by Admixtures." In *2010 International Conference on Science and Social Research, CSSR 2010, December 5, 2010 - December 7, 2010*, 118–121. Kuala Lumpur, Malaysia: IEEE Computer Society. doi:10.1109/cssr.2010.5773714.
- Kazemian, Sina, Bujang B K Huat, Arun Prasad, and Maassoumeh Barghchi. 2010. "A Review of Stabilization of Soft Soils by Injection of Chemical Grouting." *Australian Journal of Basic and Applied Science* 4 (12): 5862–5868.
- Kee, W. R., and M. C. Kurko. 1972. "Development of Jet Cutting Machine System." In *Proceedings of the First International Symposium on Jet Cutting Technology, Coventry, UK*, G5–49–G5–60.
- Keller. "The Soilcrete - Jet Grouting Process." *Keller Ground Engineering Pty Ltd*. doi:67-03E. www.kellerholding.com.
- Kersten, M. S. 1949. "The Thermal Properties of Soils." *Bulletin 28, Engineering Experiment Station, University of Minnesota, Minneapolis, Minn.*
- Khasin, M F. 1996. "Jet Geotechnology in Construction." *Hydrotechnical Construction (English Translation of Gidrotekhnicheskoe Stroitel'stvo)* 30 (8): 471.
- Klein, Eric M, Kenneth B Andromalos, and Jennifer L Trimble. 2006. "SOIL NAIL AND JET GROUTED EXCAVATION SUPPORT WALL AT PEIRCE MILL DAM." In *31st Annual Conference On Deep Foundations Washington, D. C. ? 2006 Conference Proceedings*, 1–13.
- Kochen, R. 1992. "Pre - Supported Soft Ground Tunnels." *Canadian Tunnelling*: 1–16.
- Koelling, M.A., and A.R. Ringen. 1992. "Jet Grouting - Soil Improvement Case Histories." In *Proceedings of the 28th Symposium on Engineering Geology and Geotechnical Engineering, Boise, Idaho*.

- Kramar, D., and V. Bindiganavile. 2010. "Mechanical Properties and Size Effects in Lightweight Mortars Containing Expanded Perlite Aggregate." *Material and Structures* 44: 735–748.
- Kwong, James, and Mathew Francis. 2003. "Microtunneling and HDD Performance in Jet Grouted Soil." *Grouting 2003, ASCE*: 303–317.
- Kwong, James, Kealohi Sandefur, and Reyn Hashiro. 2010. "Case Histories on Design and Construction of Jet Grouted Ground for Trenchless Projects." In *International Symposium on Ground Improvement Technologies and Case Histories, ISGI'09, December 9, 2009 - December 12, 2009*, 605–614. Singapore, Singapore: Research Publishing Services. doi:10.3850/gi079.
- Labus, T. J. 2001. "High Pressure Equipment and Systems." *An Overview of Waterjet Fundamentals and Applications* (ed T. J. Labus and G. A. Savanick), Waterjet Technology Association, Missouri, US.
- Lai, Peter, Michael McVay, David Bloomquist, and Heath Forbes. 2010. "An Innovative Prefabricated Pile Installation Method Utilizing Jetting and Pressure Grouting." In *GeoFlorida 2010: Advances in Analysis, Modeling and Design Conference, February 20, 2010 - February 24, 2010*, 1592–1601. West Palm Beach, FL, United states: American Society of Civil Engineers (ASCE). doi:10.1061/41095(365)161.
- "Lake Placid's Luge Run Undergoes Jet Grouting." 1990. *Civil Engineering, News Section*.
- Laloui, Lyesse, Mathieu Nuth, and Laurent Vulliet. 2006. "Experimental and Numerical Investigations of the Behaviour of a Heat Exchanger Pile." *International Journal for Numerical and Analytical Methods in Geomechanics* 30 (8) (July): 763–781. doi:10.1002/nag.499.
- Lamarche, Louis, and Benoit Beauchamp. 2007a. "A Fast Algorithm for the Simulation of GCHP Systems." Vol. 113.
- . 2007b. "A New Contribution to the Finite Line-Source Model for Geothermal Boreholes." *Energy and Buildings* 39 (2) (February): 188–198. doi:10.1016/j.enbuild.2006.06.003.
- Langbehn, W.K. 1986. "The Jet Grouting Method: Applications in Slope Stabilization and Landslide Repair." *Master of Engineering Report, Department of Civil Engineering, University of California, Berkeley, CA*.
- Lawrence, B., and M. Gruner. 1999. "Jet Grouting in Cohesive Soil." In *Geo Engineering for Underground Facilities Conference*, 1016–1026.
- Leach, S. J., and G. L. Walker. 1966. "Some Aspects of Rock Cutting by High Speed Water Jets." *Phil. Trans., Royal Society of London* 206 (A): 295–308.
- Lee, Fook Hou, Yeong Lee, Soon-Hoe Chew, and Kwet-Yew Yong. 2005. "Strength and Modulus of Marine Clay-Cement Mixes." *Journal of Geotechnical and Geoenvironmental Engineering* 131 (2): 178–186. doi:10.1061/(asce)1090-0241(2005)131:2(178).
- Lee, Kun Sang. 2008. "Performance of Open Borehole Thermal Energy Storage System under Cyclic Flow Regime." *Geosciences Journal* 12 (2) (July 11): 169–175. doi:10.1007/s12303-008-0018-5.
- Lee, Thomas S, Rod Murray, and Marcia Kiese. 2005. "Jet Grouting at Posey Tube, Oakland, California." In *Geo-Frontiers 2005, January 24, 2005 - January 26, 2005*, 130th–142nd ed., 1711–1725. Austin, TX, United states: American Society of Civil Engineers.

- Lewis, Dwayne A, and Martin G Taube. 2003. "North Airfield Drainage Improvement at Chicago-O'Hare International Airport: Soil Stabilization Using Jet Grouting." In *Rapid Excavation and Tunneling Conference*, 325–334. United states: Society for Mining, Metallurgy and Exploration.
- Li, Jin, and Peng Hu. 2010. "Numerical Simulation of Large Diameter Bored Pile of High Pressure Jet Grouting." In *44th US Rock Mechanics Symposium and the 5th US/Canada Rock Mechanics Symposium, June 27, 2010 - June 30, 2010*, American Rock Mechanics Association. Salt Lake City, UT, United states: Omnipress.
- Lianwei, Ren, and Wang Guangyong. 2011. "Practical Variational Analysis on Vertical Behavior of Jet Grouting Soil-Cement-Pile Strengthened Pile." In *2011 GeoHunan International Conference - Advances in Pile Foundations, Geosynthetics, Geoinvestigations, and Foundation Failure Analysis and Repairs, June 9, 2011 - June 11, 2011*, 220 GSP, 126–134. Hunan, China: American Society of Civil Engineers (ASCE). doi:10.1061/47631(410)15.
- Lignola, G P, A Flora, and G Manfredi. 2008. "Simple Method for the Design of Jet Grouted Umbrellas in Tunneling." *JOURNAL OF GEOTECHNICAL AND GEOENVIRONMENTAL ENGINEERING, ASCE* (December): 1778–1791.
- Liu, S. Y., D. W. Zhang, Z. B. Liu, and Y. F. Deng. 2008. "Assessment of Unconfined Compressive Strength of Cement Stabilized Marine Clay." *Marine Georesourse and Geotechnology* 26 (1): 19–35.
- Liu, W V, D B Apel, and V Bindiganavile. 2011. "Thermal Characterisation of a Lightweight Mortar Containing Expanded Perlite for Underground Insulation." *International Journal of Mining and Mineral Engineering* 3 (1): 55–71.
- Liu, Wei Victor. 2013. "Development and Testing of Insulating Shotcrete for the Application in Underground Tunnels." University of Alberta.
- Lloret, A, E E Alonso, A Gens, and J Suriol. 1991. "Horizontal Load Tests on Jet-Grouted Columns." In *Proceedings of the 10th European Conference on Soil Mechanics and Foundation Engineering, May 26, 1991 - May 30, 1991*, 2:471–474. Florence, Italy: Publ by A.A. Balkema.
- Loomis, Guy G, and Jim J Jessmore. 2003. "Contamination Control During In Situ Jet Grouting For Application In A Buried Transuranic Waste Site." *Idaho National Engineering and Environmental Laboratory (INEEL/CON-02-01530)*: 1–15.
- Lunardi, P. 1997. "Ground Improvement by Means of Jet-Grouting Examined :." *Ground Improvement* 1: 65–85.
- Malinin, A G, and I L Gladkov. 2011. "Investigation of the Diameter of Soil-Cement Columns under Various Soil Conditions." *Soil Mechanics & Foundation Engineering* 48 (3): 121–126. doi:10.1007/s11204-011-9138-4.
- Malinin, A G, and P A Malinin. 2007. "Jet-Grouting in Underground Construction." *Underground Space - the 4th Dimension of Metropolises -Bartak, Hrdina, Romancov & Ziamal*, 17 (2): 327–330.
- Malinin, Alexey, Ilya Gladkov, and Dmitriy Malinin. 2010. "Experimental Research of Jet-Grouting Parameters in Different Soil Conditions." In *GeoShanghai International Conference 2010, June 3, 2010 - June 5, 2010*, 206 GSP, 49–54. Shanghai, China: American Society of Civil Engineers.
- Martin Ii, James R, C Guney Olgun, James K Mitchell, and H Turan Durgunoglu. 2004. "High-Modulus Columns for Liquefaction Mitigation." *Journal of Geotechnical and Geoenvironmental Engineering* 130 (6): 561–571. doi:10.1061/(asce)1090-0241(2004)130:6(561).

- Massoudi, Nasser. 2008. "Jet Grouting for Support of Excavations near Historic Structures." In *GeoCongress 2008: Geosustainability and Geohazard Mitigation, March 9, 2008 - March 12, 2008*, 178th ed., 955–959. New Orleans, LA, United states: American Society of Civil Engineers. doi:10.1061/40971(310)119.
- Mcclenahan, Doug, John Gusdorf, John Kokko, Jeff Thornton, and Bill Wong. 2006. "Okotoks: Seasonal Storage of Solar Energy for Space Heat in a New Community." *ACEEE Summer Study on Energy Efficiency in Buildings*: 121–132.
- Mcgonagle, K. A., R. S. Cheng, R. J. Micciche, J. P. Geraci, and S. A. Benedict. 2011. "Recent Advances in Computerized Large-Diameter Jet Grouting Technology in the Santa Clara Valley Basin Formation San Fra." In *2011 Rapid Excavation and Tunneling Conference Proceedings*, 644–653.
- Mech, Michelle. 2011. "A Comprehensive Guide to the Alberta Oil Sands."
- Meyers, John, Tim Myers, and Kerry Petrasic. 2003. "Jet Grout Stabilization of Steeply Excavated Soil Slope." In *Proceedings of the Third International Conference: Grouting And Ground Treatment, February 10, 2003 - February 12, 2003*, 120 I, 318–329. New Orleans, LA, United states: American Society of Civil Engineers.
- Mihalis, I K, G Tsiambaos, and A Anagnostopoulos. 2004. "Jet Grouting Applications in Soft Rocks: The Athens Metro Case." *Proceedings of the Institution of Civil Engineers: Geotechnical Engineering* 157 (4): 219–228. doi:10.1680/geng.157.4.219.51831.
- Mihalis, I. K. 1999. "Jet Grouting: A Method to Control Ground Settlements and Overbreak Failures Caused by Tunneling in Weak Rock Conditions." *Proceedings of the European Conference on Soil Mechanics and Geotechnical Engineering* 12, Vol 1: 65–70.
- Miki, G. 1985. "Soil Improvement by Jet Grouting." In *Proc. 3rd Int. Geotechnical Seminar on Soil Improvement Methods, Singapore*, 45 – 52.
- Miki, G., and W. Nakanishi. 1984. "Technical Progress of the Jet Grouting Method and Its Newest Type." In *Proceedings of International Conference on in Situ Soil and Rock Reinforcement, Paris*, Vol 1, 195–200.
- Mitchell, J.K, T.S. Veng, and C.L. Monismith. 1974. "Behavior of Stabilized Soils under Repeated Loading."
- Mitchell, J.K. 1981. "Soil Improvement: State of the Art Report." In *Proceeding of the 10th International Conference on Soil Mechanics and Foundation Engineering, Stockholm, 15-19 June*, 509–565.
- Miyasaka, G. 1992. "Jet Grouting for a Seld Standing Wall." *Grouting, Soil Improvement and Geosynthetics, ASCE Geotechnical Special Publication* 1 (30): 144–155.
- Modoni, G, P Croce, and L Mongiovi. 2006. "Theoretical Modelling of Jet Grouting." *Geotechnique* 56 (5): 335–347. doi:10.1680/geot.2006.56.5.335.
- Momber, A. W. 1998a. "Introductory Aspects of Water Jet Technology in the Construction Industry." *Waterjet Application in Construction Engineering* (ed. A. W. Momber), A. A. Balkema, Rotterdam, Netherland.
- . 1998b. "On-Site Abrasive Water Jet Equipment for Demolition: Basics and Experience." *Water Jet Applications in Construction Engineering* (ed. A. W. Momber), A. A. Balkema, Rotterdam, Netherlands.
- Mondoni, G, P Croce, and L Mongiovi. 2008. "Theoretical Modelling of Jet Grouting (Discussion)." *Geotech* 58 (6): 533–535. doi:10.1680/geot.2008.D.004.

- Mongioli, L., P. Croce, and A. Zaninetti. 1991. "Analisi Sperimentale Di Un Intervento Di Consolidamento Mediante Gettiniezione." In *Il Convegno Nazionale Dei Ricercatori Del Gruppo Di Coordinamento Degli Studi Di Ingegneria Geotecnica Del CNR, Ravello (in Italian)*.
- Morey, J, and D W Campo. 1999. "Quality Control of Jet Grouting on the Cairo Metro." *Grou* 3: 67–75.
- Morey, J., and R. R. W. Harris. 1995. "Jet Grouting in Construction." *Geological Society, London, Engineering Geology Special Publications* 10 (1) (January 1): 105–114. doi:10.1144/GSL.ENG.1995.010.01.08.
- Moseley, M.p. 1993. *Ground Improvement*. CRC press inc., boca raton, FI.
- Muller, Miklos. 2003. "Foundation Strengthening and Grouting by Means of Jet Piles for a 9+1-Storey Building with Strengthened-Concrete Framing." *Periodica Polytechnica: Civil Engineering* 47 (2): 145–168.
- Munfakh, G.A. 1987. "In Situ Ground Reinforcement, Soil Improvement-a Ten Year Update." *Geotechnical Special Publications, ASCE Convention, Atlantic City, NJ* No.2: 43–55.
- Mussger, K., J. Koinig, and St. Reischl. 1987. "Jet Grouting in Combination with NATM." In *Proceedings of the Rapid Excavation and Tunneling Conference, Society of Mining Engineers of AIME, Littleton, Co, USA*, 292–308.
- Mustapha, Akchiche, and Bahar Ramdan. 2008. "Some Algiers Experience on Measurement and Evaluation of Settlement around Urbane Tunnel Reinforced with Jet Grouting ." *International Journal of Theoretical and Applied Mechanics* 3 (1): 1–16.
- Nagaraj, T.S., and N. Miura. 1996. "Induced Cementation of Soft Ground - a Parametric Assessment." In *Proceedings of the International Symposium on Lowland Technology, Saga, Japan*, 85–97.
- Narendra, B.S., P.V. Sivapullaiah, S. Suresh, and S.N. Omkar. 2006. "Prediction of Unconfined Compressive Strength of Soft Grounds Using Computational Intelligence Techniques: A Comparative Study." *Computers and Geotechnics* 33 (3): 196–208.
- Nikbakhtan, B. 2007. "Application of Jet Grouting to Ground Improvement in Downstream of Cofferdam at Shahriar Dam (in Persian)." In *6th Conference of Mining Engineering, AmirKabir University, Tehran, Iran*, 363–368.
- Nikbakhtan, B, K Ahangari, A Norzad, K Ghoshtasbi, and S. Litkahi. 2009. "Soil Improvement by Jet Grouting (in Persian)." *Journal of Engineering Geology* 2 (2228-6837): 757–772.
- Nikbakhtan, B, K Ahangari, and N Rahmani. 2010. "Estimation of Jet Grouting Parameters in Shahriar Dam, Iran." *Mining Science and Technology (China)* 20 (3) (May): 472–477. doi:10.1016/S1674-5264(09)60228-3.
- Nikbakhtan, B, and K Ghoshtasbi. 2008. "APPLICATION OF JET GROUTING IN GROUND IMPROVEMENT OF SHAHRIYAR DAM SITE-IRAN." In *Indo-Korean Joint International Symposium on GEO-SCIENCE AND TECHNOLOGY: Utilization of Geo-Space as a Solution for Energy and Environment (GTEE), Kharagpur, India*, 150–158.
- Nikbakhtan, B, and M Osanloo. 2009. "Effect of Grout Pressure and Grout Flow on Soil Physical and Mechanical Properties in Jet Grouting Operations." *International Journal of Rock Mechanics and Mining Sciences* 46 (3) (April): 498–505. doi:10.1016/j.ijrmms.2008.10.005.

- Nikbakhtan, B, and Y Pourrahimian. 2006. "Application of Jet Grouting in Ground Improvement (in Persian)." In *Proceedings of the Secondary Conference of Mine and Related Science, Tabas University, Tabas, Iran*, 351–358.
- . 2007. "Assessment Operation of Jet Grouting in Soil Improvement (in Persian)." In *Proceeding of the 13th Student Conference on Civil Engineering, Kerman, Iran*, 570.
- Nikbakhtan, B, Y Pourrahimian, and H Aghababaei. 2007a. "The Effects of Jet Grouting on Slope Stability at Shahriar Dam , Iran." In *1st Canada-US Rock Mechanics Symposium, Vancouver, Canada*, 1075–1081.
- . 2007b. "Investigation of Jet Grouting Effect on Slope Stability- A Case Study at the Shahriar Dam, Iran." In *20th International Mining Congress and Exhibition of Turkey-IMCET2007, Ankara, Turkey*, 229–238.
- Nikbakhtan, B., H. Aghababaei, and Y. Pourrahimian. 2007. "EFFECTS OF JET GROUTING ON EXCAVATED SLOPES IN SHAHRIAR DAM'S FOUNDATION, IRAN." In *Geo-Changsha An International Conference on Geotechnical Engineering, Hunan, China*, 503–510.
- Nikbakhtan, B., and K. Ahangari. 2010. "Field Study of the Influence of Various Jet Grouting Parameters on Soilcrete Unconfined Compressive Strength and Its Diameter." *International Journal of Rock Mechanics and Mining Sciences* 47 (4) (June): 685–689. doi:10.1016/j.ijrmms.2010.03.004.
- Nikbakhtan, B., D. Apel, and K. Ahangari. 2014a. "Jet Grouting: Using Artificial Neural Networks to Predict Soilcrete Column Diameter – Part II." *International Journal of Mining and Mineral Engineering* Accepted (1): 1–11. doi:10.1504/IJMME.2015.067951.
- . 2014b. "Jet Grouting: Mathematical Model to Predict Soilcrete Column Diameter – Part I." *International Journal of Mining and Mineral Engineering* Accepted (1): 1–8. doi:10.1504/IJMME.2015.067950.
- Nikbakhtan, Babak, and Nader Nikbakhtan. 2008. "STABILIZATION OF ALLUVIAL LAYERS IN FOUNDATION OF SHAHRIAR DAM USING JET-GROUTING TECHNIQUE , IRAN." In *Indo-Korean Joint International Symposium on GEO-SCIENCE AND TECHNOLOGY: Utilization of Geo-Space as a Solution for Energy and Environment (GTEE), Kharagpur, India*, 57–62.
- Nikbakhtan, S., B. Nikbakhtan, and N. Rahmani. 2008. "OPERATION ASSESMENT OF JET GROUTING AS A NEW METHOD FOR GROUND REINFORCEMENT." In *Indo-Korean Joint International Symposium on GEO-SCIENCE AND TECHNOLOGY: Utilization of Geo-Space as a Solution for Energy and Environment (GTEE), Kharagpur, India*, 221–226.
- Nikonov, B. P., and S. S. Shavlovsky. 1961. "Gornye Mashiny: Avtomatika." *Nauchno-Tekh. Sb.* 1 (18): 5.
- Nishimatsu, Y. 1972. "The Mechanics of Rock Cutting." *International Journal of Rock Mechanics and Mining Science* 9: 261–270.
- Norlite. 2015. "Norlite Lightweight Aggregate." [Http://www.norliteagg.com/structuralconcrete/insulation.asp](http://www.norliteagg.com/structuralconcrete/insulation.asp).
- "Oil Sands Economic Benefits." 2011. *Government of Alberta, Canada*. www.oilsands.alberta.ca.
- Olgun, Guney C, and James R Martin. 2008. "Effectiveness of Jet-Grout Columns for Mitigation of Liquefaction during Earthquakes." In *2nd International Conference on Geotechnical Engineering for Disaster Mitigation and Rehabilitation, GEDMAR08, May 30, 2008 - June 2, 2008*, 768–773. China: Springer-Verlag GmbH and Co. KG.
- Olson, Roy. 2004. "Direct Shear Testing."

- Osborne, Nick, and David Ng Chew Chiat. 2010. "Jet Grouting (JGP) for Deep Excavation - The Importance of Quality Control." *Ground Improvement Technologies and Case Histories*, Edited by C. F. Leung, J. Chu and R. F. Shen. Published by Research Publishing Services by Geotechnical Society of Singapore: 721–728.
- Oteo, C, and L Sopena. 1991. "Use of Jet Grouting to Improve Loose Fills." In *Proceedings of the 10th European Conference on Soil Mechanics and Foundation Engineering, May 26, 1991 - May 30, 1991*, 2:903–906. Florence, Italy: Publ by A.A. Balkema.
- Ozgulrel, H Gurkan, and Cumaraswamy Vipulanandan. 2005. "Effect of Grain Size and Distribution on Permeability and Mechanical Behavior of Acrylamide Grouted Sand." *Journal of Geotechnical and Geoenvironmental Engineering* 131 (12): 1457–1465. doi:10.1061/(asce)1090-0241(2005)131:12(1457).
- Padura, A B, J B Sevilla, J G Navarro, E Y Bustamante, and E P Crego. 2009. "Study of the Soil Consolidation Using Reinforced Jet Grouting by Geophysical and Geotechnical Techniques: La Normal" Building Complex (Granada)." *Construction & Building Materials* 23 (3): 1389–1400. doi:10.1016/j.conbuildmat.2008.07.011.
- Palla, Reinhold, and Stefan Leitner. 2009. "Application of Jet Grouting on the Various Contracts in the Lower Inn Valley." *Geomechanik Und Tunnelbau* 2 (6) (December): 693–708. doi:10.1002/geot.200900059.
- Parry-Davies, R, R M H Bruin, G Hardie, and N G Nixon. 1992. "Stabilization of Pier Foundation Using Jet Grouting Techniques." In *Proceedings of the 1992 ASCE Specialty Conference on Grouting, Soil Improvement and Geosynthetics, February*, 1:156–168. Geotechnical Special Publication. R. Perry-Davies and Associates, Bryanston, South Africa: Publ by ASCE.
- Passlick, Thomas, and Karsten Doerendahl. 2006. "Quality Assurance in Jet Grouting for a Deep Seated Slab in Amsterdam." In *Piling and Deep Foundations Conference, Amsterdam*, 1–11.
- Pavlovic, Milija N, Demetrios M Cotsovos, Milan M Dedic, and Anastasia Savidu. 2010a. "Reinforced Jet-Grouted Piles. Part 2: Materials and Tolerances." *Proceedings of the Institution of Civil Engineers: Structures and Buildings* 163 (5): 309–315. doi:10.1680/stbu.2010.163.5.309.
- . 2010b. "Reinforced Jet-Grouted Piles. Part 1: Analysis and Design." *Proceedings of the Institution of Civil Engineers: Structures and Buildings* 163 (5): 299–308. doi:10.1680/stbu.2010.163.5.299.
- Pearlman, S. 1998. "Jet Grouting: New Directions." *Civil Engineering* 68 (8): 44–47.
- Pettit, Paul, and Clayton C Wooden. 1988. "Jet Grouting: The Pace Quickens." *Civil Engineering* 58 (8): 65–68.
- Pichler, Christian, Roman Lackner, Lothar Martak, and Herbert a. Mang. 2004. "Optimization of Jet-Grouted Support in NATM Tunnelling." *International Journal for Numerical and Analytical Methods in Geomechanics* 28 (78) (June 16): 781–796. doi:10.1002/nag.366.
- Pichler, Christian, Roman Lackner, Yvonne Spira, Herbert A Mang, and F Asce. 2003. "Thermochemomechanical Assessment of Ground Improvement by Jet Grouting in Tunneling." *Journal of Engineering Mechanics, ASCE* 129 (8): 951–962.
- Pinto, Alexandre, Joao Falcao, Carlos Barata, Sandra Ferreira, Duilio Cebola, and Joana Pacheco. 2003. "Case Histories of Ground Treatment with Vertical Jet Grouting Solutions." In *Proceedings of the Third International Conference: Grouting And Ground Treatment, February 10, 2003 - February 12, 2003*, 120 I, 401–402. New Orleans, LA, United states: American Society of Civil Engineers.

- Plescan, Costel, and Ancuta Rotaru. 2010. "ASPECTS CONCERNING THE IMPROVEMENT OF SOILS AGAINST LIQUEFACTION." *Bulletin of the Polytechnic Institute of Iasi - Construction & Architecture Section, Gheorghe Asachi Technical University*: 39–45.
- Poh, Teoh Yaw, and Ing Hieng Wong. 2001. "A Field Trial of Jet-Grouting in Marine Clay." *Canadian Geotechnical Journal* 38 (2) (April): 338–348. doi:10.1139/t00-093.
- "Process and Device for the Decontamination of Contaminated Sites." *Soil Washing U.S. Patent No. 5,098,224*.
- Raines, G.L., and J.k. Honke. 1996. "Honolulu's Street Relief." *Civil Engineering*.
- Raju, Vegesna Ranganadha, and Hari Krishna Yandamuri. 2010. "Ground Improvement for Infrastructure Projects in Malaysia." *Proceedings of the Institution of Civil Engineers: Ground Improvement* 163 (4): 251–263. doi:10.1680/grim.2010.163.4.251.
- Rollins, Kyle M, Mark Herbst, Matthew Adsero, and Dan Brown. 2010. "Jet Grouting and Soil Mixing for Increased Lateral Pile Group Resistance." In *GeoFlorida 2010: Advances in Analysis, Modeling and Design Conference, February 20, 2010 - February 24, 2010*, 199th ed., 1563–1572. West Palm Beach, FL, United states: American Society of Civil Engineers (ASCE). doi:10.1061/41095(365)158.
- Rollins, Kyle M., Matthew E. Adsero, and Dan a. Brown. 2009. "Jet Grouting to Increase Lateral Resistance of Pile Group in Soft Clay." *International Foundation Congress and Equipment Expo* (March 10): 265–272. doi:10.1061/41023(337)34.
- Roppelt, Mike. 2011. "Report on Modelling of Ground Heat Exchangers (GHX) for Contract with Natural Resources Canada." Edmonton, AB.
- Rosenbaum, D.B. 1989. "Sugar Sands Stabilized Safely." *Engineering News Record*: 18.
- Roth, Kurt, and James Brodrick. 2009. "Seasonal Energy Storage." *ASHRAE Journal* (January): 41–43.
- "Safety Issue Boosts Record Soft Ground Jet Grouting Job." 1994. *Civil Engineering, New Features*: 18–19.
- Saglam, Ahmet, Rasin Duzceer, Alp Gokalp, and Elif Yilmaz. 2002. "Ground Improvement by Jet Grout Columns for the Foundations of an Automobile Plant in Turkey." In *Deep Foundations Congress 2002 - International Perspective on Theory, Design, Construction, and Performance*, February 14, 2002 - February 16, 2002, 116 I, 559–569. Orlando, FL, United states: American Society of Civil Engineers.
- Sakai, T. & Nagao, S. 1985. "Twenty-Eight Week Toxicity Study of Perlite Powder in Mice." *The Journal of Toxicological Sciences* 10 (83).
- Samtani, Naresh C, and Douglas E Alexander. 2005. "Remediation of a Failing MSE Wall by Jet Grouting." In *Geo-Frontiers 2005, January 24, 2005 - January 26, 2005*, 130th–142nd ed., 1913–1927. Austin, TX, United states: American Society of Civil Engineers.
- Sanger, Frederick J. 1968. "GROUND FREEZING IN CONSTRUCTION." *American Society Of Civil Engineers. Soil Mechanics & Foundation Division. Journal*: 131–158.
- Satio, S, T Kawasaki, S Niia, R Babasaki, and T Miyata. 1980. "Research on Deep Mixing Method Using Cementitious Agents (part 10) - Engineering Properties of Treated Soils (3)." In *15th Soil Engineering Research Conference*, 717–720.

- Saurer, E, and M Lesnik. 2011. "Grid Space Optimization of Jet Grouting Columns Optimisation de La Distance Entre Les Colonnes de Sols Cimentés." In *Proceedings of the 15th European Conference on Soil Mechanics and Geotechnical Engineering A. Anagnostopoulos et Al. (Eds.)*, 1055–1060.
- Scarborough, J.a., D.w. Boehm, and G.t. Brill. 1993. "The Use of Jet Grouting for Underpinning and Temporary Excavation Support of a Historic Building." In *Proceedings of the Ohio River Valley Soils Seminar XXIV, Cincinnati, Ohio*.
- Schaefer, Vernon R. 1997. *Ground Improvement, Ground Reinforcement, Ground Treatment Developments 1987-1997*. Geotechnical Special Publication: No. 69. New York, N.Y. : American Society of Civil Engineers, c1997.
- Schorr, Claus- P, Reinhold Traegner, and Romano J Micciche. 2007. "Evaluating in-Situ Jet Grout Column Diameters Utilizing Wave Analysis." In *Geo-Denver 2007: New Peaks in Geotechnics, February 18, 2007 - February 21, 2007*, 168th ed. Denver, CO, United states: American Society of Civil Engineers. doi:10.1061/40912(231)12.
- Senapathy, H., J.r. Davie, and D. Bohem. 2003. "Improving Deep-Seated Soft Clay Using Super-Jet Grouting." *Grouting 2003, ASCE*: 440–451.
- Sepehri, Mohammadali. 2011. "Underground Thermal Energy Storage Methods."
- Shao, Lisheng, and Ken Ivanetich. 2010. "Heavy Structures Supported by Soil-Cement Columns." In *GeoShanghai International Conference 2010, June 3, 2010 - June 5, 2010*, 207 GSP, 125–130. Shanghai, China: American Society of Civil Engineers.
- Sheen, M S. 2001. "Grouting Pressure and Damaged Adjacent Buildings . Part 1: Behaviour Analysis." *Ground Improvement* 5 (4): 155–162.
- Shen, S L, C Y Luo, Y H Kim, and S J Peng. 2009. "Instant Solidification of Soft Ground Horizontally Using Jet-Grouting." In *International Foundation Congress and Equipment expo2*, 257–264. ASCE.
- Shen, S. L., Y. S. Xu, J. Han, and J.M. Zhang. 2010. "A Ten Review on the Development of Soil Mixing Technologies in China."
- Shibazaki, M. 1991. "The State of Art in Jet Grouting." In *Proceedings of the Symposium on Soil and Rock Improvement in Underground Works, SocietaÁ Italiana Gallerie*, 19 – 46.
- Shibazaki, M., and S. Ohta. 1982. "A Unique Underpinning of Soil Solidification Utilizing Super High Pressure Liquid Jet." In *Proceedings of the Conference on Grouting in Geotechnical Engineering, New Orleans, Louisiana, 10-12 Feb*, 680–693.
- Shibazaki, M., and H. Yoshida. 1997. "Constructing Bottom Barriers with Jet Grouting." In *In International Containment Techology Conference and Exhibition*.
- Shibazaki, M., H. Yoshida, and Y. Matsumoto. 1996. "Development of a Soil Improvement Method Utilizing Cross Jet." In *Proceedings of IS-Tokyo 96: The Second International Conference on Ground Improvement Geosystems, Tokyo*, 707–710.
- Shibazaki, Mitsuhiro. 2003. "State of Practice of Jet Grouting." *Grouting, ASCE*: 198–217.

- Shibazaki, Mitsuhiro, Mitsuru Yokoo, and Hiroshi Yoshida. 2003. "Development Oversized Jet Grouting." In *Proceedings of the Third International Conference: Grouting And Ground Treatment, February 10, 2003 - February 12, 2003*, 120 I, 294–302. New Orleans, LA, United states: American Society of Civil Engineers.
- Shibazaki, Mitsuhiro, Hiroshi Yoshida, Kenji Yoshida, Kiyoshi Horii, and Isao Kataoka. 2005. "Analyses Hydrodynamic Structure of Cross Water Jet and Its Performance of Soil Improvement." In *2005 ASME Fluids Engineering Division Summer Meeting, FEDSM2005, June 19, 2005 - June 23, 2005*, 2005:2149–2155. Houston, TX, United states: American Society of Mechanical Engineers.
- Shirlaw, J. Nick. 2003. "Jet Grouting Soft Clays for Tunnelling and Deep Excavations - Design and Construction Issues." In *Grouting 2003, ASCE*, 257–268.
- Smith, Alex.W., and H. Borden, roy. 2007. "Jet Grouting Induced Changes in Soldier Pile Loads and Pile Deflections." In *FMGM 2007: Seventh International Symposium on Field Measurements in Geomechanics, ASCE*, 1–6.
- SMPE. 2012a. "Core Logging and Thermal Properties Tests."
- . 2012b. "Determination of Thermal Properties of Soil Samples."
- Soranzo, M., and P. Mazzalai. 1986. "Underpinning a Deep Foundation - a Case History." In *International Conference on Deep Foundations, Beijing, China*, 4.50–4.55.
- Spagnoli, Giovanni. 2008. "Theoretical Evaluations of Liquefaction Mitigation through Jet Grouting." *Geotechnical News* 26 (3): 41–45.
- "Specialist Grouting." *Keller Ground Engineering Pty Ltd*. www.kellerge.com.
- Stark, Timothy D, Paul J Axtell, Justin R Lewis, John C Dillon, B Empson, Joseph E Topi, and C Francke. 2009. "Soil Inclusions in Jet Grout Columns." *DFI Journal* 3 (1): 44–55.
- Stavridakis, Evangelos I. 2006. "A Solution to the Problem of Predicting the Suitability of Silty-Clayey Materials for Cement-Stabilization." *Geotechnical and Geological Engineering* 24 (2): 379–398. doi:10.1007/s10706-004-7934-6.
- Steiner, Walter, Ernst Schneider, and Manfred Cartus. 1992. "Soilcrete Cut-off Wall for Undercrossing a Busy Rail Line." In *Proceedings of the 1992 ASCE Specialty Conference on Grouting, Soil Improvement and Geosynthetics*, 1:384–397. Geotechnical Special Publication. Partner Balzari Schudel AG, Bern, Switzerland: Publ by ASCE.
- Stella, By C., G. Cepl, E. D'Appolonia, C Stella, G Ceppi, and E. D'Appolonia. 1990. "TEMPORARY TUNNEL SUPPORT USING JET-GROUTED CYLINDERS." *Journal of Construction Engineering and Management* 116 (1): 35–53.
- Suer, Pascal, Niklas Hallberg, Christel Carlsson, David Bendz, and Goran Holm. 2009. "Biogrouting Compared to Jet Grouting: Environmental (LCA) and Economical Assessment." *Journal of Environmental Science and Health - Part A Toxic/Hazardous Substances and Environmental Engineering* 44 (4): 346–353. doi:10.1080/10934520802659679.
- Summers, D. A. 1995. *Water Jetting Technology*. E & FN Spon, London, UK. E & FN Spon, London, UK.
- Superjet, Association. 2004. "Superjet Technology (Superjet-Midi & Superjet)." *Japan, in Japanese*.

- Tanaka, T, and T Yokoyama. 2006. "Effects of Jet Grouting under Sheet Piles on Seepage Failure Stability of Soil." In *5th International Conference of TC28 of the International Society for Soil Mechanics and Geotechnical Engineering, ISSMGE, June 15, 2005 - June 17, 2005*, 923–929. Amsterdam, Netherlands: Taylor & Francis - Balkema.
- Tarnawski, V. R., and W. H. Leong. 2000. "Thermal Conductivity of Soils at Very Low Moisture Content and Moderate Temperatures." *Transport in Porous Media* 41: 137–147.
- Tarricone, Paul. 1994. "Jet Grouting Gains." *Civil Engineering* 64 (12): 40–43.
- Tinoco, J. 2012. "Application of Data Mining Techniques to Jet Grouting Columns Design." Universidade do Minho Escola de Engenharia.
- Tinoco, J, A Gomes Correia, and P Cortez. 2011a. "Application of Data Mining Techniques in the Estimation of the Uniaxial Compressive Strength of Jet Grouting Columns over Time." *Construction and Building Materials* 25 (3): 1257–1262. doi:10.1016/j.conbuildmat.2010.09.027.
- . 2011b. "Using Data Mining Techniques to Predict Deformability Properties of Jet Grouting Laboratory Formulations over Time." In *Progress in Artificial Intelligence. 15th Portuguese Conference on Artificial Intelligence, EPIA 2011, 10-13 Oct. 2011*, 491–505. Berlin, Germany: Springer-Verlag. doi:10.1007/978-3-642-24769-9_36.
- . 2012. "Jet Grouting Mechanicals Properties Prediction Using Data Mining Techniques." In *Grouting and Deep Mixing*, 2082–2091.
- Tonon, Fulvio. 2011. "ADECO Full-Face Tunnel Excavation of Two 260m² Tubes in Clays with Sub-Horizontal Jet-Grouting under Minimal Urban Cover." *Tunnelling and Underground Space Technology* 26 (2) (March): 253–266. doi:10.1016/j.tust.2010.09.006.
- Tornaghi, R. 1989. "Trattamento Colonnare Dei Terreni Mediante Gettiniezione (jet-Grouting)." In *XVII Convegno Nazionale Di Geotecnica, Taormina (in Italian)*, 193 –203.
- "Trevi Brochure." 2010. *Trevi Group*. www.trevispa.com.
- Tsuboi, H, H Fukada, M Ootsuka, H Nitao, S Isoya, S Higashi, F Kusakabe, and T Matsui. 2007. "Quality Characteristics of Improved Soil Columns by New Type Jet Grout Mixing Method." In *17th 2007 International Offshore and Polar Engineering Conference, ISOPE 2007, July 1, 2007 - July 6, 2007*, 1276–1281. Lisbon, Portugal: International Society of Offshore and Polar Engineers.
- "Underground Thermal Energy Storage for Efficient Heating and Cooling of Buildings." 2013. www.iftech.co.uk.
- USBM. 1994. "Insulating Shotcrete for Heat Abatement in Deep Mines." *Technology News* 434.
- Van hoesen, S.d. 1992. "White Oak Creek Embankment Sediment Retention Structure: The Oak Ridge Model in Action." In *Proceedings of Eighth Annual Oak Ridge Model Conference on Waste Management and Environmental Resoation, Oak Ridge, TN*.
- Vardar, Mahir, Halil Karaoglan, Kenan Kaya, and Riza Mucukgil. 2005. "Jet-Grout Application at Sarayköy Tunnel Interval Portals." In *Proceedings of the International World Tunnel Congress and the 31st ITA General Assembly*, 347–352. Istanbul, Turkey. doi:10.1201/NOE0415374521.ch53.

- Vià, A Da, M Marotta, and G Peach. 2005. "High Pressure Jet Grouting in Tunnels – a Case Study." In *Proceedings of the International World Tunnel Congress and the 31st ITA General Assembly*, 477–483. Istanbul, Turkey. doi:10.1201/NOE0415374521.ch72.
- "Victoria Station Upgrade Supplementary Environmental Statement: Technical Appendix G – Jet Grouting Trials Report." 2008. http://www.tfl.gov.uk/assets/downloads/vsu-14-ses-technical_appendix-jet-grouting-trials-report.pdf.
- Vijay, M. M. 2001. "Fluid Mechanics of Jets." *An Overview of Waterjet Fundamentals and Applications* (ed T. J. Labus and G. A. Savanick), Waterjet Technology Association, Missouri, US.
- Viner, R.L., and C. Wooden. 1990. "Jet Grout Underpinning of the New Jersey Avenue Sewer." In *Proceeding of the International Symposium on Unique Underground Structures, Denver, CO*, 89–1 to 89–19.
- Wang, Huajun, and Chengying Qi. 2008. "Performance Study of Underground Thermal Storage in a Solar-Ground Coupled Heat Pump System for Residential Buildings." *Energy and Buildings* 40 (7) (January): 1278–1286. doi:10.1016/j.enbuild.2007.11.009.
- Wang, J G, B Oh, S W Lim, and G S Kumar. 1998. "Studies on Soil Disturbance Caused by Grouting in Treating Marine Clay." In *2nd International Conference on Ground Improvement Techniques*, 521–528.
- Wang, J L, D F Wang, and J W Wang. 2009. "State of Jet Grouting in Shanghai." In *Contemporary Topics in Ground Modification, Problem Soils, and Geo-Support - 2009 International Foundation Congress and Equipment Expo, March 15, 2009 - March 19, 2009*, 187th ed., 179–188. Orlando, FL, United states: American Society of Civil Engineers. doi:10.1061/41023(337)20.
- Wang, J.G., B Oh, S.W. Lim, and G.S. Kumar. 1999. "Effect of Different Jet-Grouting Installations on Neighboring Structures." In *Proceedings of the 5th International Symposium Field Measurements in Geomechanics*, 511–516.
- Wang, Zhi Feng, Shui Long Shen, and Jun Yang. 2012. "Estimation of the Diameter of Jet-Grouted Column Based on Turbulent Kinematic Flow Theory." In *Grouting and Deep Mixing*, 2044–2051.
- Warner, James. 2004. *Practical Handbook of Grouting: Soil, Rock, and Structures*. Hoboken, N.J.: John Wiley & Sons, c2004.
- Wei, Meijiu. "A SHEETPILE RETAINING WALL AND JGP IMPROVEMENT SYSTEM FOR EXCAVATION IN SOFT MARINE CLAY."
- Welsh, J P. 1998. "State of the Art of Grouting in North America." *Ground Improvement* 2: 11–15.
- Welsh, Joseph P, and George K Burke. 1995. "Vertical Cutoffs and Bottom Sealing by Jet Grouting." In *Proceedings of the Specialty Conference on Geotechnical Practice in Waste Disposal. Part 1 (of 2), February 24, 1207–1221*. Geotechnical Special Publication. Hayward Baker Inc, Odenton, United States: ASCE.
- Welsh, joseph p., and george k. Burke. 1991. "Jet Grouting - Uses for Soil Improvement." In *Proceedings of the Geotechnical Engineering Congress, June 10 - June 12*, 334–345. Hayward Baker Inc, Odenton, United States.
- WJA. 2002. "Code of Practice for the Use of High Pressure and Ultra High Pressure Water Jetting Equipment." *Water Jetting Association, Sawtry, UK*.

- Wong, Ing Hieng, and Teoh Yaw Poh. 2000. "Effects of Jet Grouting on Adjacent Ground and Structures." *Journal of Geotechnical and Geoenvironmental Engineering*: 247–256.
- Wong, W P, J L Mcclung, J P Kokko, and A L Snijders. "First Large-Scale Solar Seasonal Borehole Thermal Energy Storage in Canada."
- X-Jet, Association. 2002. "X-Jet Technology." *Japan, in Japanese*.
- Yahiro, T., and H. Yoshida. 1973. "Induction Grouting Method Utilizing High Speed Water Jet." In *Proceedings of the Eighth International Conference on Soil Mechanics and Foundation Engineering*, 402–404.
- . 1974. "On the Characteristics of High Speed Water Jet in the Liquid and Its Utilization on Induction Grouting Method." In *2nd International Symposium on Jet Cutting Technology, 2-4 Apr*, G4–41 to G4–63.
- Yahiro, T., H. Yoshida, and K. Nishi. 1975. "The Development and Application of a Japanese Grouting System." *Water Power and Dam Construction* 83: 56–59.
- . 1982. "Soil Improvement Method Utilizing High Speed Water and Air Jet on the Development and Application of Columnar Solidified Construction Method (column Jet Method)." In *Proceedings of the 6th International Symposium on Jet Cutting Technology, 6-8 Apr.*, 397–427.
- Yamadera, A., T.S. Nagaraj, and N. Miura. 1997. *Prediction of Strength Development in Cement Stabilized Marine Clay*, In Short C 141–153.
- Yang, Haibo, Thiam Soon Tan, and Chun Fai Leung. 2011. "Mass Behaviour of Embedded Improved Soil Raft in an Excavation." *Proceedings of the ICE - Geotechnical Engineering* 164 (1) (February 1): 11–25. doi:10.1680/geng.9.00078.
- Yilmaz, Davut, Fatih Babuccu, Serhat Batmaz, and Fatih Kavruk. 2008. "Liquefaction Analysis and Soil Improvement in Beydag Dam." *Geotechnical and Geological Engineering* 26 (2): 211–224. doi:10.1007/s10706-007-9158-z.
- Yoshida, H., R. Asano, H. Kubo, S. Jinbo, and S. Uesawa. 1991. "Effect of Nozzle Traverse Rate and Number of Passes on Soft Ground Cutting by Water Jet." In *Proceeding of 6th American Water Jet Conference, Houston, WJTA*, 381–392.
- Yoshida, H., M. Shibazaki, H. Kubo, S. Jimbo, and M. Sakakibara. 1989. "The Effect of Pressure and Flow Rate on Cutting Soil Utilizing Water Jet for Wider Application." In *5th American Water Jet Conference, 29-31 August, Toronto, Canada*, 297–305.
- Yoshida, Hiroshi, Kennosuke Uemura, Kenji Yoshida, and Isao Kataoka. 2007. "Visual Observation and Analysis of Hydrodynamic Structure of Water Jet in Application to Jet Grouting." In *2007 5th Joint ASME/JSME Fluids Engineering Summer Conference, FEDSM 2007, July 30, 2007 - August 2, 2007, PART B, 1 SYMPOSIA:1891–1897*. San Diego, CA, United states: American Society of Mechanical Engineers.
- Yoshitake, Isamu, Takashi Mitsui, Tadashi Yoshikawa, Akihiko Ikeda, and Koji Nakagawa. 2004. "An Evaluation Method of Ground Improvement by Jet-Grouting." *Tunelling and Underground Space Technology* 19: 496–497.
- Yourman, Jr., Allen M., Christopher M. Diaz, and Gary K. Gilbert. 2006. "Jet Grouted Settlement Isolation Wall at the Henry Ford Avenue Grade Separation." In *GeoCongress*, 1–6. Reston, VA: American Society of Civil Engineers. doi:10.1061/40803(187)266.

YuLiang, Qiu, Zheng WanKun, Shi BaoTong, and Huang Rui. 2011. "Research on Grouting Experiment in Aeolian Sand Tunnel." In *2011 International Conference on Advanced Research on Advanced Structure, Materials and Engineering (ASME 2011)*, 24-25 Dec. 2011, 382:316–320. Switzerland: Trans Tech Publications Ltd. doi:10.4028/www.scientific.net/AMR.382.316.

Yung-Show, Fang, Jyh Jong Liao, and Lin Ta-King. 1994. "Mechanical Properties of Jet Grouted Soilcrete." *Quarterly Journal of Engineering Geology* 27 (pt 3): 257.